

Library Declaration Form



University of Otago Library

Author's full name and year of birth: Simon Thomas Kelly,
(for cataloguing purposes) 24 February 1992

Title of thesis: A Bioinformatics Approach to Synthetic Lethal Interactions in Breast Cancer with Gene Expression Data

Degree: Doctor of Philosophy

Department: Department of Biochemistry

Permanent Address: 710 Cumberland Street, Dunedin, NZ

I agree that this thesis may be consulted for research and study purposes and that reasonable quotation may be made from it, provided that proper acknowledgement of its use is made.

I consent to this thesis being copied in part or in whole for

- i) a library
- ii) an individual

at the discretion of the University of Otago.

Signature:

Date:

A Bioinformatics Approach to
Synthetic Lethal Interactions in
Breast Cancer with Gene
Expression Data

S. Thomas Kelly

a thesis submitted for the degree of
Doctor of Philosophy
at the University of Otago, Dunedin,
New Zealand.

17 June 2017

Abstract

Background

Synthetic lethal genetic interactions are re-emerging in the post-genomics era due to their potential for precision medicine against cancers. Synthetic lethal drug design exploits the functional redundancy of genes disrupted in cancers (including tumour suppressors) to develop specific treatments against them. *CDH1*, which encodes [E-cadherin](#), is a tumour suppressor gene with loss of function in breast and stomach cancers. Experimental screens have identified candidate synthetic lethal interactions for drug target triage, which can be further supported with bioinformatics analysis. Furthermore, gene expression data enables investigation of synthetic lethal pathways and graph structure of synthetic lethal genes within them.

Approach

A computational methodology, the Synthetic Lethal Prediction Tool ([SLIPT](#)) has been developed to detect synthetic lethal interactions in gene expression data. This methodology was demonstrated on interactions with *CDH1* in breast and stomach cancer data from The Cancer Genome Atlas ([TCGA](#)) project. Synthetic lethal genes and pathways were further investigated with unsupervised clustering, gene set over-representation analysis, metagenes, and permutation resampling. In particular, analyses focused on comparing [SLIPT](#) gene candidates to an experimental [siRNA](#) screen [Telford et al. \(2015\)](#). Network analysis methods were applied to the most supported pathways to test for pathway structure among between synthetic lethal candidates. Simulation and modelling was used to assess the statistical performance of [SLIPT](#), including simulated data with correlation structures derived from graph stuctures.

Findings

Many candidate synthetic lethal partners of *CDH1* were detected in both [TCGA](#) breast cancer. These genes clustered into several distinct groups, with distinct biological functions and elevated expression in different clinical subtypes. While the number of genes detected by both approaches was not significant, these contained significantly enriched pathways. In particular, $G_{\alpha i}$ signalling, cytoplasmic microfibres, and extracellular fibrin clotting were robustly supported by both approaches, which is consistent with the known cytoskeletal and cell signalling roles of [E-cadherin](#) and validation of [GPCR](#) pathways performed by [Telford et al. \(2015\)](#). Many of these pathways were replicated in stomach cancer data. The pathways supported only by [SLIPT](#) included regulation of immune signalling and translational elongation which were not expected to be detected in an isogenic cell line model but are still candidates for further investigation.

Synthetic lethal candidates detected by [SLIPT](#) and [siRNA](#) were compared within graph structures of the candidate synthetic lethal pathways. These genes did not differ with respect to network metrics of importance or connectivity in the pathway. There was little support, across pathways, that [SLIPT](#) gene candidates were consistently upstream or downstream of [siRNA](#) gene candidates with pathways.

A model of synthetic lethality was used to simulate gene expression data with synthetic lethal partners of a gene. The [SLIPT](#) methodology had high statistical performance, detecting few synthetic lethal partners, which diminished with more synthetic lethal partners or lower sample size. The [SLIPT](#) methodology performed better than Pearson correlation or the χ^2 -test. In particular, it performed well with high specificity for datasets containing thousands of genes or genes positively correlated with the query gene (as expected to occur in expression data). [SLIPT](#) was robust across correlation structures, including those derived from complex pathway structures and often distinguished synthetic lethal genes from those positively or negatively correlated with them. Therefore [SLIPT](#) is appropriate to identify synthetic lethal genes within pathways and use candidate synthetic lethal genes (and their correlates) to identify synthetic lethal pathways.

Summary

Thus my thesis has developed, evaluated, and refined a bioinformatics approach to discovery of synthetic lethal genes solely from gene expression data. This approach has been demonstrated to detect biologically informative and clinically relevant candidate partners for *CDH1* in breast and stomach cancers. These investigations have also involved the development of network analysis and simulation procedures which may be more widely applicable.

Research Contributions During Candidature

Publications

Kelly, S. T. and Spencer, H. G. (2017) Population-Genetics Models of Sex-Limited Genomic Imprinting. *Theoretical Population Biology* **115**:35-44
doi:[10.1016/j.tpb.2017.03.004](https://doi.org/10.1016/j.tpb.2017.03.004)

Manuscripts Submitted

Kelly, S. T., Single, A. B., Telford, B. J., Beetham, H. G, Godwin, T. D., Chen, A., Black, M., A., and Guilford, P. J. (2017) Towards HDGC chemoprevention: vulnerabilities in E-cadherin-negative cells identified by genomic interrogation of isogenic cell lines and whole tumors. Submitted to *Cancer Prevention Research*.

Kelly, S. T., Chen, A., Guilford, P. J., and Black, M. A. (2017) Synthetic lethal interaction prediction of target pathways in E-cadherin deficient breast cancers. Submitted to *BMC Genomics*.

Conference Presentations

Consortium of Biological Sciences 2017 (Kobe) December TBC

eResearch 2017 (Queenstown) February 20th-22nd

Research Bazaar 2016 (Dunedin) February 2nd-4th

eResearch 2016 (Queenstown) February 9th-11th

Genetics Otago Symposium 2016 (Dunedin) March 7th-8th

DunDead: Zombie Science and Culture Festival 2014 (Dunedin) August 16th-17th

eResearch 2014 (Hamilton) June 30th-July 2nd (Supported by Google)

Poster Presentations

Next Generation Sequencing Asia 2016 (Singapore) October 11th-12th (Supported by the University of Otago Division of Health Sciences; Maurice and Phyllis Paykel Trust)

Research Bazaar 2015 (Melbourne) February 16th-18th (Supported by the New Zealand eScience Infrastructure)

Otago School of Medical Sciences Postgraduate Symposium 2015 (Dunedin) April 28th-29th

QMB Cancer Drugs Satellite 2014 (Queenstown) August 24th-25th

Seminar Presentations

University of Otago Department of Biochemistry 2017 (Dunedin) November TBC

Tōhoku University 2016 (Sendai) November 11th

Okinawa Institute of Science and Technology 2016 (Onna) November 1st

Sōkendai Graduate University 2016 (Hayama) October 25th

Tōkyō University Institute of Medical Science 2016 (Shirokanedai) October 24th

National Institute of Genetics 2016 (Mishima) October 21st

RIKEN Division of Genomic Technologies 2016 (Yokohama) October 20th

Software Packages

Software packages in the R language have been released. Please refer to the appropriate GitHub repository for more information (including documentation, vignettes, and installation instructions), on the following account:
<https://github.com/TomKellyGenetics>

- `slipt` to accompany the synthetic lethal publication above and release SLIPT (Synthetic Lethal Interaction Prediction Tool)
- `vioplotx` to provide enhanced violin plots
- `heatmap.2x` to provide annotated heatmaps
- `igraph.extensions` metapackage for the packages for iGraph objects:
 - `plot.igraph` to provide plotting for directed graphs
 - `info.centrality` to compute network analysis metrics
 - `pathway.structure.permutation` for resampling within pathways
 - `graphsim` to simulate expression (`mvtnorm`) from pathway structures

The `slipt-app` GitHub repository also hosts an application for Synthetic Lethal Interaction Prediction Tool (SLIPT) developed in the R `shiny` environment as part of a related project. There is a digital copy of this thesis, including high resolution full-colour figures, hosted at:

<https://github.com/TomKellyGenetics/thesis/blob/master/thesis.pdf>

Acknowledgements

I thank my supervisors A/Prof. Mik Black and Prof. Parry Guilford for their support and guidance throughout this my postgraduate studies. It has been a great experience, I look forward to seeing what your research groups produce in the future, may this not be the end for us.

I am also thankful for the guidance and mentorship of Prof. Hamish Spencer for career advice throughout my studies and time in his research group.

I am also grateful to the past and current members of these research groups, and my peers at the laboratory benches and computers across campus. The peer support, camaraderie, and guidance of newer students has been an incredible part of my time at Otago and has made my thesis studies not just easier but possible at all. The postgraduate community is very special here and I have truly made some lifelong friends from all over the world. You are talented researchers and amazing people. May we meet again some day. Where-ever you may end up, its small world and there's always time to catch up. I'd be delighted to host some visits while working abroad.

I cannot thank my friends, flatmates, family, and diligent proofreaders enough for their patience and support during such as massive, challenging, and (I'm sure you've heard too often) stressful undertaking during both my PhD and the study leading up to it. There are too many of you to name everyone here without leaving someone out, so thank you all for everything you've done, both the good times and the tough. Thank you for at least pretending to understand complex math oft brought up at the wrong moment. Thank you for checking my writing or slides, even when sprung on you last minute. Thank for your time when what I really needed was a chat, a walk, a drink with "the guys", or a moment to think clearly.

I thank the various organisations that supported this research project:

- This thesis was supported by the Postgraduate Tassell Scholarship in Cancer Research, a University of Otago Doctoral Scholarship.
- The New Zealand eScience Infrastructure (NeSI) provided access to the Intel Pan high-performance computing cluster, support, and training to use it effectively. Various aspects of this thesis would not have been possible without access to such an incredible national resource.
- The Health Research Council (HRC) of New Zealand provided funding for experimental research in the Cancer Genetics Laboratory. Some aspects of this project would not have been possible without access to the data and findings funded by this grant.
- The Allan Wilson Centre and Otago School of Biomedical Sciences provided funding for summer research placements which was a valuable opportunity to gain experience and training used in this thesis project.

I thank the following organisations for support towards presenting findings in this thesis at conference and seminars:

- Google (eResearch 2014, Hamilton)
- NeSI (Software Carpentry training and Research Bazaar 2015, Melbourne)
- REANNZ, NZGL, and NeSI (eResearch 2016, Queenstown)
- Otago Division of Health Sciences, Oxford Global, and Maurice and Phyllis Paykel Trust (NGS Asia 2016, Singapore)
- RIKEN Division of Genomic Technologies and the Okinawa Institute of Science and Technology (seminar visits in Japan)

Thanks most of all to my fianceé, Dr Yui Kawagishi, you've been an inspiration. Thank you for your support and encouragement, every day, even from afar: it has always made a difference. It's been incredible to see you flourish in your career and I look forward to joining you again soon. May the next chapter of our adventures involve a bit less Skype across timezones.

どうもありがとうございます。また来月。頑張った！行きます！

Contents

| | |
|---|-------------|
| Glossary | xxi |
| Acronyms | xxvi |
| 1 Introduction and Literature Review | 1 |
| 1.1 Cancer Research in the Post-Genomic Era | 1 |
| 1.1.1 Cancer is a Global Health Issue | 2 |
| 1.1.1.1 The Genetics and Molecular Biology of Cancers | 3 |
| 1.1.2 The genomic Revolution in Cancer Research | 4 |
| 1.1.2.1 High-Throughput Technologies | 4 |
| 1.1.2.2 Bioinformatics and Genomic Data | 6 |
| 1.1.3 Genomics Projects | 6 |
| 1.1.3.1 The Cancer Genome Project | 6 |
| 1.1.3.2 The Cancer Genome Atlas Project | 7 |
| 1.1.4 Genomic Cancer Medicine | 9 |
| 1.1.4.1 Cancer Genes and Driver Mutations | 9 |
| 1.1.4.2 Precision Cancer Medicine | 10 |
| 1.1.4.3 Molecular Diagnostics and Pan-Cancer Medicine | 10 |
| 1.1.4.4 Targeted Therapeutics and Pharmacogenomics | 10 |
| 1.1.5 Systems and Network Biology | 11 |
| 1.1.5.1 Network Medicine and Polypharmacology | 13 |
| 1.2 A Synthetic Lethal Approach to Cancer Medicine | 14 |
| 1.2.1 Synthetic Lethal Genetic Interactions | 14 |
| 1.2.2 Synthetic Lethal Concepts in Genetics | 15 |
| 1.2.3 Synthetic Lethality in Model Systems | 16 |
| 1.2.3.1 Synthetic Lethal Pathways and Networks | 16 |
| 1.2.3.2 Evolution of Synthetic Lethality | 17 |
| 1.2.4 Synthetic Lethality in Cancer | 18 |
| 1.2.5 Clinical Impact of Synthetic Lethality in Cancer | 19 |
| 1.2.6 High-throughput Screening for Synthetic Lethality | 21 |
| 1.2.6.1 Synthetic Lethal Screens | 22 |
| 1.2.7 Computational Prediction of Synthetic Lethality | 25 |
| 1.2.7.1 Bioinformatics Approaches to Genetic Interactions | 25 |
| 1.2.7.2 Comparative Genomics | 26 |
| 1.2.7.3 Analysis and Modelling of Protein Data | 29 |
| 1.2.7.4 Differential Gene Expression | 31 |

| | | |
|----------|---|-----------|
| 1.2.7.5 | Data Mining and Machine Learning | 32 |
| 1.2.7.6 | Mutually Exclusive Bimodality | 35 |
| 1.2.7.7 | Rationale for Further Development | 36 |
| 1.3 | E-cadherin as a Synthetic Lethal Target | 36 |
| 1.3.1 | The <i>CDH1</i> gene and its Biological Functions | 36 |
| 1.3.1.1 | Cytoskeleton | 37 |
| 1.3.1.2 | Extracellular and Tumour Micro-environment | 37 |
| 1.3.1.3 | Cell-Cell Adhesion and Signalling | 37 |
| 1.3.2 | <i>CDH1</i> as a Tumour (and Invasion) Suppressor | 38 |
| 1.3.2.1 | Breast Cancers and Invasion | 38 |
| 1.3.3 | Hereditary Diffuse Gastric Cancer and Lobular Breast Cancer | 38 |
| 1.3.4 | Cell Line Models of <i>CDH1</i> Null Mutations | 40 |
| 1.4 | Summary and Research Direction of Thesis | 40 |
| 1.4.1 | Thesis Aims | 42 |
| 2 | Methods and Resources | 43 |
| 2.1 | Bioinformatics Resources for Genomics Research | 43 |
| 2.1.1 | Public Data and Software Packages | 43 |
| 2.1.1.1 | Cancer Genome Atlas Data | 44 |
| 2.1.1.2 | Reactome and Annotation Data | 45 |
| 2.2 | Data Handling | 45 |
| 2.2.1 | Normalisation | 45 |
| 2.2.2 | Sample Triage | 46 |
| 2.2.3 | Metagenes and the Singular Value Decomposition | 46 |
| 2.2.3.1 | Candidate Triage and Integration with Screen Data . . | 48 |
| 2.3 | Techniques | 49 |
| 2.3.1 | Statistical Procedures and Tests | 49 |
| 2.3.2 | Gene Set Over-representation Analysis | 50 |
| 2.3.3 | Clustering | 50 |
| 2.3.4 | Heatmap | 50 |
| 2.3.5 | Modeling and Simulations | 51 |
| 2.3.5.1 | Receiver Operating Characteristic (Performance) . . | 52 |
| 2.3.6 | Resampling Analysis | 52 |
| 2.4 | Pathway Structure Methods | 53 |
| 2.4.1 | Network and Graph Analysis | 53 |
| 2.4.2 | Sourcing Graph Structure Data | 54 |
| 2.4.3 | Constructing Pathway Subgraphs | 54 |
| 2.4.4 | Network Analysis Metrics | 55 |
| 2.5 | Implementation | 56 |
| 2.5.1 | Computational Resources and Linux Utilities | 56 |
| 2.5.2 | R Language and Packages | 57 |
| 2.5.3 | High Performance and Parallel Computing | 60 |

| | |
|---|------------|
| 3 Methods Developed During Thesis | 62 |
| 3.1 A Synthetic Lethal Detection Methodology | 62 |
| 3.2 Synthetic Lethal Simulation and Modelling | 65 |
| 3.2.1 A Model of Synthetic Lethality in Expression Data | 65 |
| 3.2.2 Simulation Procedure | 69 |
| 3.3 Detecting Simulated Synthetic Lethal Partners | 72 |
| 3.3.1 Binomial Simulation of Synthetic Lethality | 72 |
| 3.3.2 Multivariate Normal Simulation of Synthetic Lethality | 74 |
| 3.3.2.1 Multivariate Normal Simulation with Correlated Genes | 77 |
| 3.3.2.2 Specificity with Query-Correlated Pathways | 84 |
| 3.3.2.3 Importance of Directional Testing | 84 |
| 3.4 Graph Structure Methods | 86 |
| 3.4.1 Upstream and Downstream Gene Detection | 86 |
| 3.4.1.1 Permutation Analysis for Statistical Significance | 87 |
| 3.4.1.2 Hierarchy Based on Biological Context | 88 |
| 3.4.2 Simulating Gene Expression from Graph Structures | 89 |
| 3.5 Customised Functions and Packages Developed | 93 |
| 3.5.1 Synthetic Lethal Interaction Prediction Tool | 93 |
| 3.5.2 Data Visualisation | 94 |
| 3.5.3 Extensions to the iGraph Package | 97 |
| 3.5.3.1 Sampling Simulated Data from Graph Structures | 97 |
| 3.5.3.2 Plotting Directed Graph Structures | 97 |
| 3.5.3.3 Computing Information Centrality | 98 |
| 3.5.3.4 Testing Pathway Structure with Permutation Testing | 98 |
| 3.5.3.5 Metapackage to Install iGraph Functions | 99 |
| 4 Synthetic Lethal Analysis of Gene Expression Data | 100 |
| 4.1 Synthetic Lethal Genes in Breast Cancer | 101 |
| 4.1.1 Synthetic Lethal Pathways in Breast Cancer | 103 |
| 4.1.2 Expression Profiles of Synthetic Lethal Partners | 104 |
| 4.1.2.1 Subgroup Pathway Analysis | 107 |
| 4.2 Comparing Synthetic Lethal Gene Candidates | 110 |
| 4.2.1 Primary siRNA Screen Candidates | 110 |
| 4.2.2 Comparison with Correlation | 110 |
| 4.2.3 Comparison with Primary Screen Viability | 112 |
| 4.2.4 Comparison with Secondary siRNA Screen Validation | 114 |
| 4.2.5 Comparison to Primary Screen at Pathway Level | 116 |
| 4.2.5.1 Resampling Genes for Pathway Enrichment | 118 |
| 4.2.6 Integrating Synthetic Lethal Pathways and Screens | 121 |
| 4.3 Metagene Analysis | 123 |
| 4.3.1 Pathway Expression | 124 |
| 4.3.2 Somatic Mutation | 126 |
| 4.3.3 Synthetic Lethal Pathway Metagenes | 130 |
| 4.3.4 Synthetic Lethality in Breast Cancer | 131 |
| 4.4 Replication in Stomach Cancer | 132 |
| 4.5 Discussion | 133 |

| | | |
|----------|--|------------|
| 4.5.1 | Strengths of the SLIPT Methodology | 133 |
| 4.5.2 | Synthetic Lethal Pathways for E-cadherin | 134 |
| 4.5.3 | Replication and Validation | 136 |
| 4.5.3.1 | Integration with short interfering RNA (siRNA) Screening | 136 |
| 4.5.3.2 | Replication across Tissues | 137 |
| 4.6 | Summary | 137 |
| 5 | Synthetic Lethal Pathway Structure | 139 |
| 5.1 | Synthetic Lethal Genes in Reactome Pathways | 139 |
| 5.1.1 | The PI3K/AKT Pathway | 140 |
| 5.1.2 | The Extracellular Matrix | 142 |
| 5.1.3 | G Protein Coupled Receptors | 145 |
| 5.1.4 | Gene Regulation and Translation | 145 |
| 5.2 | Network Analysis of Synthetic Lethal Genes | 146 |
| 5.2.1 | Gene Connectivity and Vertex Degree | 147 |
| 5.2.2 | Gene Importance and Centrality | 148 |
| 5.2.2.1 | Information Centrality | 148 |
| 5.2.2.2 | PageRank Centrality | 150 |
| 5.3 | Relationships between Synthetic Lethal Genes | 152 |
| 5.3.1 | Hierarchical Pathway Structure | 152 |
| 5.3.1.1 | Contextual Hierarchy of PI3K | 152 |
| 5.3.1.2 | Testing Contextual Hierarchy of Synthetic Lethal Genes | 152 |
| 5.3.2 | Upstream or Downstream Synthetic Lethality | 156 |
| 5.3.2.1 | Measuring Structure of Candidates within PI3K . . . | 156 |
| 5.3.2.2 | Resampling for Synthetic Lethal Pathway Structure . | 158 |
| 5.4 | Discussion | 160 |
| 5.5 | Summary | 162 |
| 6 | Simulation and Modeling of Synthetic Lethal Pathways | 164 |
| 6.1 | Synthetic Lethal Detection Methods | 165 |
| 6.1.1 | Performance of SLIPT and χ^2 across Quantiles | 165 |
| 6.1.1.1 | Correlated Query Genes affects Specificity | 169 |
| 6.1.2 | Alternative Synthetic Lethal Detection Strategies | 171 |
| 6.1.2.1 | Correlation for Synthetic Lethal Detection | 171 |
| 6.1.2.2 | Testing for Bimodality with BiSEp | 173 |
| 6.2 | Simulations with Graph Structures | 174 |
| 6.2.1 | Performance over Graph Structures | 175 |
| 6.2.1.1 | Simple Graph Structures | 175 |
| 6.2.1.2 | Constructed Graph Structures | 177 |
| 6.2.2 | Performance with Inhibitions | 180 |
| 6.2.3 | Synthetic Lethality across Graph Structures | 185 |
| 6.2.4 | Performance within a Simulated Human Genome | 189 |
| 6.3 | Simulations in More Complex Graph Structures | 193 |
| 6.3.1 | Simulations over Pathway-based Graphs | 194 |
| 6.3.2 | Pathway Structures in a Simulated Human Genome | 197 |

| | | |
|---------------------|--|------------|
| 6.4 | Discussion | 200 |
| 6.4.1 | Simulation Procedure | 200 |
| 6.4.2 | Comparing Methods with Simulated Data | 201 |
| 6.4.3 | Design and Performance of SLIPT | 202 |
| 6.4.4 | Simulations from Graph Structures | 204 |
| 6.5 | Summary | 205 |
| 7 | Discussion | 207 |
| 7.1 | Synthetic Lethality and <i>CDH1</i> Biology | 207 |
| 7.1.1 | Established Functions of <i>CDH1</i> | 208 |
| 7.1.2 | The Molecular Role of <i>CDH1</i> in Cancer | 208 |
| 7.2 | Significance | 209 |
| 7.2.1 | Synthetic Lethality in the Genomic Era | 209 |
| 7.2.2 | Clinical Interventions based on Synthetic Lethality | 211 |
| 7.3 | Future Directions | 212 |
| 7.4 | Conclusions | 214 |
| Bibliography | | 216 |
| A | Sample Quality | 240 |
| A.1 | Sample Correlation | 240 |
| A.2 | Replicate Samples in The Cancer Genome Atlas (TCGA) Breast | 243 |
| B | Software Used for Thesis | 247 |
| C | Mutation Analysis in Breast Cancer | 256 |
| C.1 | Synthetic Lethal Genes and Pathways | 256 |
| C.2 | Synthetic Lethal Expression Profiles | 259 |
| C.3 | Comparison to Primary Screen | 262 |
| C.3.1 | Resampling Analysis | 264 |
| C.4 | Compare SLIPT genes | 266 |
| C.5 | Metagene Analysis | 268 |
| C.6 | Expression of Somatic Mutations | 269 |
| C.7 | Metagene Expression Profiles | 272 |
| D | Intrinsic Subtyping | 275 |
| E | Expression Analysis in Stomach Cancer | 277 |
| E.1 | Synthetic Lethal Genes and Pathways | 277 |
| E.2 | Comparison to Primary Screen | 282 |
| E.2.1 | Resampling Analysis | 284 |
| E.3 | Metagene Analysis | 286 |
| F | Synthetic Lethal Genes in Pathways | 287 |
| G | Pathway Connectivity for Mutation SLIPT | 295 |

| | |
|--|------------|
| H Information Centrality for Gene Essentiality | 299 |
| I Pathway Structure for Mutation SLIPT | 302 |
| J Performance of SLIPT and χ^2 | 305 |
| J.1 Correlated Query Genes affects Specificity | 311 |
| K Graph Structures | 317 |
| K.1 Simulations from Simple Graph Structures | 317 |
| K.1.1 Simulations from Inhibiting Graph Structures | 319 |
| K.2 Simulation across Graph Structures | 322 |
| K.3 Simulations from Complex Graph Structures | 326 |
| K.3.1 Simulations from Complex Inhibiting Graphs | 329 |
| K.4 Simulations from Pathway Graph Structures | 335 |

List of Tables

| | | |
|-----|---|-----|
| 1.1 | Methods for predicting genetic interactions | 26 |
| 1.2 | Methods for predicting synthetic lethality in cancer | 27 |
| 1.3 | Methods used by Wu <i>et al.</i> (2014) | 28 |
| 2.1 | Excluded samples by batch and clinical characteristics. | 46 |
| 2.2 | Computers used during thesis | 56 |
| 2.3 | Linux utilities and applications used during thesis | 57 |
| 2.4 | R installations used during thesis | 58 |
| 2.5 | R Packages used during thesis | 58 |
| 2.6 | R packages developed during thesis | 60 |
| 4.1 | Candidate synthetic lethal gene partners of <i>CDH1</i> from SLIPT | 102 |
| 4.2 | Pathways for <i>CDH1</i> partners from SLIPT | 104 |
| 4.3 | Pathways for clusters of <i>CDH1</i> partners from SLIPT | 108 |
| 4.4 | ANOVA for synthetic lethality and correlation with <i>CDH1</i> | 112 |
| 4.5 | Comparing SLIPT genes against secondary siRNA screen | 115 |
| 4.6 | Pathways for <i>CDH1</i> partners from SLIPT and siRNA | 117 |
| 4.7 | Pathways for <i>CDH1</i> partners from SLIPT | 120 |
| 4.8 | Pathways for <i>CDH1</i> partners from SLIPT and siRNA primary screen | 122 |
| 4.9 | Candidate synthetic lethal metagenes against <i>CDH1</i> from SLIPT | 131 |
| 5.1 | ANOVA for synthetic lethality and vertex degree | 148 |
| 5.2 | ANOVA for synthetic lethality and information centrality | 150 |
| 5.3 | ANOVA for synthetic lethality and PageRank centrality | 152 |
| 5.4 | ANOVA for synthetic lethality and PI3K hierarchy | 155 |
| 5.5 | Resampling for pathway structure of synthetic lethal detection methods | 159 |
| B.1 | R packages used during thesis | 247 |
| C.1 | Candidate synthetic lethal gene partners of <i>CDH1</i> from mtSLIPT | 257 |
| C.2 | Pathways for <i>CDH1</i> partners from mtSLIPT | 258 |
| C.3 | Pathways for clusters of <i>CDH1</i> partners from mtSLIPT | 261 |
| C.4 | Pathways for <i>CDH1</i> partners from mtSLIPT and siRNA | 263 |
| C.5 | Pathways for <i>CDH1</i> partners from mtSLIPT | 264 |
| C.6 | Pathways for <i>CDH1</i> partners from mtSLIPT and siRNA primary screen | 265 |
| C.7 | Candidate synthetic lethal metagenes against <i>CDH1</i> from mtSLIPT | 268 |
| D.1 | Comparison of intrinsic subtypes | 275 |

| | | |
|-----|--|-----|
| E.1 | Synthetic lethal gene partners of <i>CDH1</i> from SLIPT in stomach cancer | 278 |
| E.2 | Pathways for <i>CDH1</i> partners from SLIPT in stomach cancer | 279 |
| E.3 | Pathways for clusters of <i>CDH1</i> partners in stomach SLIPT | 281 |
| E.4 | Pathways for <i>CDH1</i> partners from SLIPT and siRNA | 283 |
| E.5 | Pathways for <i>CDH1</i> partners from SLIPT in stomach cancer | 284 |
| E.6 | Pathways for <i>CDH1</i> partners from SLIPT in stomach and siRNA | 285 |
| E.7 | Synthetic lethal metagenes against <i>CDH1</i> in stomach cancer | 286 |
| G.1 | ANOVA for synthetic lethality and vertex degree | 298 |
| G.2 | ANOVA for synthetic lethality and information centrality | 298 |
| G.3 | ANOVA for synthetic lethality and PageRank centrality | 298 |
| H.1 | Information centrality for genes and molecules in the Reactome network | 300 |
| I.1 | ANOVA for synthetic lethality and PI3K hierarchy | 302 |
| I.2 | Resampling for pathway structure of synthetic lethal detection methods | 304 |

List of Figures

| | | |
|------|--|-----|
| 1.1 | Synthetic genetic interactions | 15 |
| 1.2 | Synthetic lethality in cancer | 19 |
| 2.1 | Read count density | 47 |
| 2.2 | Read count sample mean | 47 |
| 3.1 | Framework for synthetic lethal prediction | 63 |
| 3.2 | Synthetic lethal prediction adapted for mutation | 64 |
| 3.3 | A model of synthetic lethal gene expression | 66 |
| 3.4 | Modeling synthetic lethal gene expression | 67 |
| 3.5 | Synthetic lethality with multiple genes | 68 |
| 3.6 | Simulating gene function | 70 |
| 3.7 | Simulating synthetic lethal gene function | 70 |
| 3.8 | Simulating synthetic lethal gene expression | 71 |
| 3.9 | Performance of binomial simulations | 73 |
| 3.10 | Comparison of statistical performance | 73 |
| 3.11 | Performance of multivariate normal simulations | 75 |
| 3.12 | Simulating expression with correlated gene blocks | 78 |
| 3.13 | Simulating expression with correlated gene blocks | 79 |
| 3.14 | Synthetic lethal prediction across simulations | 80 |
| 3.15 | Performance with correlations | 81 |
| 3.16 | Comparison of statistical performance with correlation structure | 82 |
| 3.17 | Performance with query correlations | 83 |
| 3.18 | Statistical evaluation of directional criteria | 84 |
| 3.19 | Performance of directional criteria | 85 |
| 3.20 | Simulated graph structures | 89 |
| 3.21 | Simulating expression from a graph structure | 91 |
| 3.22 | Simulating expression from graph structure with inhibitions | 92 |
| 3.23 | Demonstration of violin plots with custom features | 95 |
| 3.24 | Demonstration of annotated heatmap | 95 |
| 3.25 | Simulating graph structures | 98 |
| 4.1 | Synthetic lethal expression profiles of analysed samples | 106 |
| 4.2 | Comparison of SLIPT to siRNA | 110 |
| 4.3 | Compare SLIPT and siRNA genes with correlation | 111 |
| 4.4 | Compare SLIPT and siRNA genes with correlation | 112 |
| 4.5 | Compare SLIPT and siRNA genes with viability | 113 |

| | | |
|------|--|-----|
| 4.6 | Compare SLIPT genes with siRNA viability | 114 |
| 4.7 | Resampled intersection of SLIPT and siRNA candidates | 118 |
| 4.8 | Pathway metagene expression profiles | 125 |
| 4.9 | Expression profiles for constituent genes of PI3K | 127 |
| 4.10 | Expression profiles for estrogen receptor related genes | 128 |
| 4.11 | Somatic mutation against the PI3K metagene | 129 |
| 5.1 | synthetic lethality in the PI3K cascade | 141 |
| 5.2 | synthetic lethality in Elastic Fibre Formation | 143 |
| 5.3 | Synthetic lethality in Fibrin Clot Formation | 144 |
| 5.4 | Synthetic lethality and vertex degree | 147 |
| 5.5 | Synthetic lethality and centrality | 150 |
| 5.6 | Synthetic lethality and PageRank | 151 |
| 5.7 | Hierarchical structure of PI3K | 153 |
| 5.8 | Hierarchy score in PI3K against synthetic lethality in PI3K | 154 |
| 5.9 | Structure of synthetic lethality in PI3K | 156 |
| 5.10 | Structure of synthetic lethality resampling in PI3K | 157 |
| 6.1 | Performance of χ^2 and SLIPT across quantiles | 167 |
| 6.2 | Performance of χ^2 and SLIPT across quantiles with more genes | 168 |
| 6.3 | Performance of χ^2 and SLIPT across quantiles with query correlation . | 169 |
| 6.4 | Performance of χ^2 and SLIPT across quantiles with query correlation and more genes | 170 |
| 6.5 | Performance of negative correlation and SLIPT | 172 |
| 6.6 | Simple graph structures | 175 |
| 6.7 | Performance of simulations on a simple graph | 176 |
| 6.8 | Performance of simulations is similar in simple graphs | 178 |
| 6.9 | Performance of simulations on a pathway | 179 |
| 6.10 | Performance of simulations on a simple graph with inhibition | 181 |
| 6.11 | Performance is higher on a simple inhibiting graph | 182 |
| 6.12 | Performance of simulations on a constructed graph with inhibition . . . | 183 |
| 6.13 | Performance is affected by inhibition in graphs | 185 |
| 6.14 | Detection of synthetic lethality within a graph structure | 187 |
| 6.15 | Performance of simulations including a simple graph | 190 |
| 6.16 | Performance on a simple graph improves with more genes | 191 |
| 6.17 | Performance on an inhibiting graph improves with more genes | 193 |
| 6.18 | Performance of simulations on the PI3K cascade | 196 |
| 6.19 | Performance of simulations including the PI3K cascade | 198 |
| 6.20 | Performance on pathways improves with more genes | 199 |
| A.1 | Correlation profiles of removed samples | 241 |
| A.2 | Correlation analysis and sample removal | 242 |
| A.3 | Replicate excluded samples | 243 |
| A.4 | Replicate samples with all remaining | 244 |
| A.5 | Replicate samples with some excluded | 245 |
| C.1 | Synthetic lethal expression profiles of analysed samples | 260 |

| | | |
|------|--|-----|
| C.2 | Comparison of mtSLIPT to siRNA | 262 |
| C.3 | Compare mtSLIPT and siRNA genes with correlation | 266 |
| C.4 | Compare mtSLIPT and siRNA genes with correlation | 266 |
| C.5 | Compare mtSLIPT and siRNA genes with siRNA viability | 267 |
| C.6 | Somatic mutation against PIK3CA metagene | 269 |
| C.7 | Somatic mutation against PI3K protein | 270 |
| C.8 | Somatic mutation against AKT protein | 271 |
| C.9 | Pathway metagene expression profiles | 272 |
| C.10 | Expression profiles for p53 related genes | 273 |
| C.11 | Expression profiles for BRCA related genes | 274 |
| E.1 | Synthetic lethal expression profiles of stomach samples | 280 |
| E.2 | Comparison of SLIPT in stomach to siRNA | 282 |
| F.1 | Synthetic lethality in the PI3K/AKT pathway | 287 |
| F.2 | Synthetic lethality in the PI3K/AKT pathway in cancer | 288 |
| F.3 | Synthetic lethality in the Extracellular Matrix | 289 |
| F.4 | Synthetic lethality in the GPCRs | 290 |
| F.5 | Synthetic lethality in the GPCR Downstream | 291 |
| F.6 | Synthetic lethality in the Translation Elongation | 292 |
| F.7 | Synthetic lethality in the Nonsense-mediated Decay | 293 |
| F.8 | Synthetic lethality in the 3' UTR | 294 |
| G.1 | Synthetic lethality and vertex degree | 295 |
| G.2 | Synthetic lethality and centrality | 296 |
| G.3 | Synthetic lethality and PageRank | 297 |
| H.1 | Information centrality distribution | 301 |
| I.1 | Synthetic lethality and heirarchy score in PI3K | 302 |
| I.2 | Heirarchy score in PI3K against synthetic lethality in PI3K | 303 |
| I.3 | Structure of synthetic lethality in PI3K | 303 |
| I.4 | Structure of synthetic lethality resampling | 304 |
| J.1 | Performance of χ^2 and SLIPT across quantiles | 305 |
| J.2 | Performance of χ^2 and SLIPT across quantiles | 307 |
| J.3 | Performance of χ^2 and SLIPT across quantiles with more genes | 309 |
| J.4 | Performance of χ^2 and SLIPT across quantiles with query correlation | 311 |
| J.5 | Performance of χ^2 and SLIPT across quantiles with query correlation | 313 |
| J.6 | Performance of χ^2 and SLIPT across quantiles with query correlation and more genes | 315 |
| K.1 | Performance of simulations on a simple graph | 318 |
| K.2 | Performance of simulations on an inhibiting graph | 319 |
| K.3 | Performance of simulations on a constructed graph with inhibition | 320 |
| K.4 | Performance of simulations on a constructed graph with inhibition | 321 |
| K.5 | Detection of synthetic lethality within a graph structure | 322 |
| K.6 | Detection of synthetic lethality within an inhibiting graph | 324 |

| | | |
|------|--|-----|
| K.7 | Detection of synthetic lethality within an inhibiting graph | 325 |
| K.8 | Performance of simulations on a branching graph | 326 |
| K.9 | Performance of simulations on a complex graph | 327 |
| K.10 | Performance of simulations on a large graph | 328 |
| K.11 | Performance of simulations on a branching graph with inhibition | 329 |
| K.12 | Performance of simulations on a branching graph with inhibition | 330 |
| K.13 | Performance of simulations on a complex graph with inhibition | 331 |
| K.14 | Performance of simulations on a complex graph with inhibition | 332 |
| K.15 | Performance of simulations on a large constructed graph with inhibition | 333 |
| K.16 | Performance of simulations on a large constructed graph with inhibition | 334 |
| K.17 | Performance of simulations on the $G_{\alpha i}$ signalling pathway | 335 |
| K.18 | Performance of simulations including the $G_{\alpha i}$ signalling pathway | 336 |

Glossary

| | |
|------------------------|---|
| allele | A gene variant with a specific sequence and phenotype |
| bioinformatics | Statistical or computational approaches to biological data or research tools |
| Bisulfite-Seq | Epigenomic data from sequencing bisulfite treated DNA |
| cancer | A class of diseases, formally “malignant neoplasm”, of abnormal cellular growth and spread to other organs |
| cancer gene | A gene which is involved in the malignancy of some cancers, encompassing oncogenes and tumour suppressors , which have molecular aberrations in cancer or variants which predispose individuals to cancer |
| centrality | A network metric which identifies important vertices |
| chemoprevention | The use of cytotoxic drugs to prevent early-stage cancers, generally applied to high-risk mutation carriers |
| chemotherapy | The use of cytotoxic drugs to treat cancers, in combinations, generally applied to advanced stage cancers |
| compound screen | A high-throughput screen performed using a library of chemical compounds |
| computational biology | Applying computational or mathematical modelling to understanding biological systems and relationships |
| copy number | The number of copies of DNA, typically two copies for diploid organisms but subject to variation |
| <i>de novo</i> | A bioinformatics sequence assembly conducted entirely from raw genomics data without a reference sequence |
| diagnosis | The identification of disease by clinical, cellular, and molecular characteristics |
| driver mutation | A mutation which promotes cancer growth |
| E-cadherin | Epithelial cadherin (calcium-dependent adhesion), a cell-adhesion protein encoded by <i>CDH1</i> |
| edge or link | A relationship connecting a pair of elements of a graph structure or network, may be weighted or directional |
| epigenome | An analysis of epigenetic modifications of all genes in the genome |
| epistasis (biological) | The effects of a gene modifying or masking the phenotype of another gene |

| | |
|-------------------------|---|
| epistasis (statistical) | A divergence of the observed double mutant phenotype from that expected based on the respective phenotypes of single mutant (Fisher, 1919) |
| essential | A gene which is required to be functional or expressed for a cell or organism to be viable, grow or develop |
| exome | A sequencing approach designed to generate data enriched for coding genes within the genome |
| familial | A trait recurrently occurring in families, not necessarily with a genetic cause |
| functional redundancy | Genes which perform a common function, also known as genetic redundancy |
| gene expression | A measure of the relative expression of each gene from the mRNA extracted from (pooled) cells |
| genetic robustness | A system of biological pathways which (has evolved to) continue to function as a whole under various conditions, including the inactivation of various individual genes |
| genome | An analysis of all of the DNA sequence in the genome |
| genomic | An approach or technology designed to generate or use data from all genes in the genome |
| genomic medicine | The use of genomic information to tailor medicine treatment to the genetics of an individual |
| germline mutation | A mutation that occurred in germline cells and is passed between generation |
| graph or network | A mathematical structure modelling or depicting the relationships between elements |
| hallmark of cancer | An underlying characteristic of cancer as part of a rational approach devised by (Hanahan and Weinberg, 2000) |
| hereditary | A trait or disease which has a genetic cause and is inherited from family members |
| high-throughput screen | An experimental procedure to perform a large scale series of chemical, genetic, or pharmacological tests |
| hub | A central or highly connected component of a network |
| <i>in silico</i> | An investigation conducted using computations, typically simulations or analyses |
| <i>in vivo</i> | An investigation conducted using in the context of a biological cell or organism, including pre-clincal models and clinical trials |
| induced essentiality | A gene becoming essential to viability under certain conditions, including inactivation of a synthetic lethal partner |
| information centrality | A network centrality metric which uses the impact of removing a vertex or node on connections in the network |

| | |
|------------------------|--|
| intrinsic subtype | Distinguishing cancer by molecular and genetic features |
| MCF10A cell line | A non-tumorigenic epithelial cell line derived from breast tissue |
| metagene | A consistent signal of expression for a collection of genes such as a biological pathway, derived from singular value decomposition |
| metastasis | A secondary growth of a tumour or spread of cancer to other organs |
| microarray | A high-throughput technique to measure presence or abundance of nucleic acid sequences from binding to probes |
| microRNA | Short RNA molecules generally regarded to regulate gene expression by binding to mRNA |
| molecular profile | A combination of genetic and biochemical measures which identifies characteristic traits of a tumour |
| molecular subtype | A classification of cancers based on an identification using molecular properties |
| mutant | A variant or dysfunctional phenotype arising from a mutation in a gene |
| mutation | A change in DNA sequence that disrupts gene function |
| network biology | The application mathematical and computational approaches to networks in understanding biological relationships |
| network medicine | The use of network biology to understand, prevent, or treat diseases |
| non-oncogene addiction | The dependence of a cancer cell on functioning non-mutant genes |
| 'omics | A combination of approaches to generating biological data with high-throughput procedures such as genomics, proteomics or metabolomics |
| oncogene | A gene that potentially causes cancer, typically by over-expression or mutant gene variants |
| oncogene addiction | The dependence of a cancer cell on a specific oncogenic pathway |
| PageRank centrality | A network centrality metric which uses eigenvectors with a scaling factor (Brin and Page, 1998) |
| pan cancer | A focus on the molecular and genetic features across cancers in different tissues |
| passenger mutation | A mutation that occurs in cancers but does not affect the growth of cancers |
| pathway | A series of biomolecules that produces a particular product or biological function |

| | |
|-------------------------|---|
| pleiotropy | A gene which has multiple biological functions |
| polypharmacology | The design of drugs to target multiple molecular targets or biological pathways |
| precision medicine | The application of prevention and treatment measures to target diseases by molecular and genetic features |
| prognosis | The estimation of disease progression and patient outcome |
| proto-oncogene | The non-mutant variant or precursor to a mutant oncogene |
| recurrent mutation | The repeated occurrence of mutations in a particular gene across cancers |
| RNAi screen | A high-throughput screen performed using a RNA interference (RNAi) |
| RNA-Seq | Transcriptome data from sequencing RNA |
| scale-free | A property of a network which has a power law vertex degree distribution, that is several highly connected hub genes and many with very few connections |
| shortest path | A path with the fewest possible edges which connects two particular vertices |
| small world | A property of a network which is highly connected and has a low characteristic path length, derived from the mean shortest path length across all pairs of nodes |
| somatic mutation | A mutation that occurs in somatic cells, during a patient's lifespan |
| sporadic cancer | Cancers which do occur in patients with a family history or carry a high-risk genetic variant |
| synergy | When multiple drugs have more effect than expected from the effect of each separately |
| synthetic dosage lethal | A synthetic genetic interaction (SGI) analogous to synthetic lethality where one gene is inactivated and the other over-expressed |
| synthetic lethal | Genetic interactions where inactivation of multiple genes is inviable (or deleterious) which are viable if inactivated separately |
| synthetic lethal screen | A high-throughput screen performed on isogenic cell lines to detect genes for which inhibition specifically deleterious to the null mutant genotype |
| synthetic rescue | A synthetic genetic interaction when the combined mutations restores the wild-type phenotype of one of the mutations |
| synthetic sick | Genetic interactions where inactivation of multiple genes is deleterious which are viable if inactivated separately |
| synthetic suppression | A synthetic genetic interaction when the combined mutations (partially) suppresses the mutant phenotype of one of the mutations |

| | |
|-------------------------|--|
| targeted therapy | Cancer treatment that specifically acts against a molecular target, in contrast to standard chemotherapy |
| transcriptome treatment | An analysis of all of the genes expressed in the genome |
| tumour | Medical procedures for a disease to improve patient outcomes |
| | An abnormal lump of tissue or growth of cells, may be cancerous |
| tumour suppressor | A gene potentially causes cancer, typically by disruption of functions which protect the cell from cancer |
| vertex degree | A network metric of connectivity of vertices which uses the number of edges connected to each vertex or node |
| vertex or node | An element of a graph structure or network |
| wild-type | A natural phenotype of a trait or the normally functional allele which encodes it |

Acronyms

| | |
|----------|---|
| ADP | Adenosine Diphosphate |
| AMP | Adenosine Monophosphate |
| AMPK | AMP -activated Protein Kinase |
| ANOVA | Analysis of Variance |
| AUROC | Area Under the Receiver Operating Characteristic (curve) |
| BioPAX | Biological Pathway Exchange |
| BiSEp | Bimodal Subsetting Expression |
| BMP | Bone Morphogenic Protein |
| cAMP | Cyclic AMP |
| CCLE | Cancer Cell Line Encyclopaedia |
| cDNA | Complementary DNA (from mRNA) |
| CGP | Cancer Genome Project |
| CNV | Copy Number Variation |
| COSMIC | Catalogue Of Somatic Mutations In Cancer |
| CpG | 5'-C-phosphate-G-3' |
| CRAN | comprehensive R archive network |
| CXCR | Chemokine Receptor |
| DAISY | Data Mining Synthetic Lethal Identification Pipeline |
| DNA | Deoxyribonucleic Acid |
| EMT | Epithelial-Mesenchymal Transition |
| ER | Estrogen Receptor |
| FDR | False Discovery Rate |
| GO | Gene Ontology |
| GPCR | G Crotein Coupled Receptor |
| HDAC | Histone Deacetylase |
| HDGC | Hereditary Diffuse Gastric Cancer |
| HLRCC | Hereditary Leiomyomatosis and Renal Cell Carcinoma |
| HPC | High Performance Computing |
| JAK | Janus Kinase |
| microRNA | Micro RNA |
| mRNA | Messenger RNA |
| MSI | Microsatellite Instability |
| mtSLIPT | Synthetic Lethal Interaction Prediction Tool (against mutation) |

| | |
|------------------|---|
| NeSI | New Zealand eScience Infrastructure |
| NGS | Next-Generation Sequencing |
| NMD | Nonsense-Mediated Decay |
| PAM50 | Prediction Analysis of Microarray 50 |
| PARP | Poly- ADP -Ribose Polymerase |
| PCR | Polymerase Chain Reaction |
| PDE | Phosphodiesterase |
| PI3K | Phosphoinositide 3-kinase |
| PIP ₂ | Phosphatidylinositol-(4,5)-bisphosphate |
| PIP ₃ | Phosphatidylinositol-(3,4,5)-trisphosphate |
| PPI | Protein-Protein Interaction |
| PR | Progesterone Receptor |
| RGS | G-protein Signalling |
| RHO | Ras Homolog Family |
| RNA | Ribonucleic Acid |
| RNAi | RNA Interference |
| ROC | Reciever Operating Characteristic (curve) |
| RSEM | RNA-Seq by Expectation Maximization (normalisation) |
| SGA | Synthetic Gene Array (technique) |
| SGI | Synthetic Genetic Interaction |
| shRNA | Short Hairpin RNA |
| siRNA | Short Interfering RNA |
| SL | Synthetic Lethal |
| SLIPT | Synthetic Lethal Interaction Prediction Tool |
| Slurm | Simple Linux Utility for Resource Management |
| SNP | Single Nucleotide Polymorphism |
| SR | Synthetic Rescue (or viability) |
| SS | Synthetic Suppression |
| SSL | Synthetic Sick |
| TCGA | The Cancer Genome Atlas (genomics project) |
| TGF β | Transforming Growth Factor β |
| UCSC | University of California, Santa Cruz |
| UTR | Untranslated Region (of mRNA) |
| WNT | Wingless-Related Integration Site |

Chapter 1

Introduction and Literature Review

The thesis presents research into genetic interactions using [genomics](#) data and [bioinformatics](#) approaches. This chapter introduces the recent developments in [genomics](#) and [bioinformatics](#), particularly in their application to [cancer](#) research. Studies of [synthetic lethal](#) interactions, which have fundamental importance in genetics in both model organisms and renewed relevance in [cancer](#) biology specifically, will be discussed and reviewed in detail. A bioinformatic approach to [synthetic lethal](#) interactions enables a wider exploration of the function of genes and proteins in [cancer](#) cells, in contrast with candidate gene and experimental screening approaches. [Synthetic lethal](#) drug design aims to develop [treatments](#) with specificity against loss of function [mutations](#) in [tumour suppressor](#) genes, such as *CDH1* (which encodes [E-cadherin](#)) and was the focus of the analysis in this thesis. The role of *CDH1* in cellular and [cancer](#) biology is therefore also briefly reviewed.

1.1 Cancer Research in the Post-Genomic Era

[Genomic](#) technologies could significantly impact on the clinical [treatment](#) of [cancers](#) along with wider applications of genetics ([Goodwin et al., 2016](#); [Roychowdhury and Chinnaiyan, 2016](#)). These technologies enable focused genetics investigations on candidates selected from [bioinformatics](#) analysis of [genomics](#) data. Facilitated by rapidly developing technologies, large-scale projects have investigated populations ([1000 Genomes, 2010](#)), [cancers](#) ([Dickson, 1999](#); [Zhang et al., 2011](#)), and functional [genomics](#) ([Kawai et al., 2001](#); [ENCODE, 2004](#)). However, genomic technologies have yet to be widely adopted in healthcare or oncology ([Roychowdhury and Chinnaiyan, 2016](#); [Waldron, 2016](#)). [bioinformatics](#) analysis for interpretation of [genomic](#) data is one of the main approaches to address this disparity ([Goodwin et al., 2016](#)) . Here, I outline

the [cancer genomics](#) projects and findings which have led to availability of [genomics](#) data used in this thesis and recent findings in [cancer](#) research which demonstrates the potential applications of using this data.

1.1.1 Cancer is a Global Health Issue

Cancers are diseases of malignant cellular growth which typically involve [tumour](#) formation, invasion of tissues and spread to other organs. Cancers are the second leading cause of death globally ([WHO, 2017](#)), with an estimated annual incidence of 14.1 million cases and annual mortality of 8.2 million people ([Ferlay et al., 2015](#)). Breast and stomach [cancers](#) are among the most prevalent [cancers](#). Breast cancer is the most common [cancer](#) in women and has an estimated annual incidence of 1.6 million cases and mortality of 520,000 people. Stomach cancer has an estimated annual incidence of 950,000 cases and a mortality of 723,000 people. Cancer is also a major health concern here in New Zealand, with 19,100 people (including 2500 cases of breast cancer and 370 cases of stomach cancer) [diagnosed](#) annually ([Hanna, 2003](#)), near the highest incidence (age-standardised per capita) of [cancer](#) in the world ([Ferlay et al., 2015](#)).

While environmental factors often also have a role, genetics has an important role in cancer risk. Most [cancers](#) occur more frequently with age and family history. Cancers arise from dysregulated cellular growth or differentiation from stem cells. These can occur through genetic [mutations](#) or alterations in gene regulation or [expression](#) which generally accumulate as the disease develops. Therefore, early [diagnosis](#) is important to ensure patient survival and quality of life. Identification of patients with genetic variants or family histories at a high-risk of particular cancers is an important health issue. These high-risk individuals are regularly monitored for some cancers are sometimes offered preventative surgery or [treatment](#) for pre-cancerous tissue ([Guilford et al., 2010](#); [Scheuer et al., 2002](#)).

[Chemotherapy](#) is a [treatment](#) for many advanced stage cancer, designed to inhibit rapidly growing cells. However, this approach often has severe adverse effects, a narrow therapeutic window, and is not suitable for [chemopreventative](#) application in many cases ([Kaelin, Jr, 2009](#)). Patients at high-risk of cancers, are offered surveillance and preventative surgery but these approaches are not completely effective at preventing cancers and may impact on quality of life ([Guilford et al., 2010](#)). Alternative [chemoprevention](#) and [treatment](#) strategies based on molecular biology and other fields are being investigated, including targeted molecular therapeutics ([Bozovic-Spasojevic et al., 2012](#); [Kelly et al., unpublished](#)).

1.1.1.1 The Genetics and Molecular Biology of Cancers

Cancers involve dysregulation of genes including **mutations** which occur during a patient's lifetime and **hereditary mutations** which predispose them to high-risk cancers (American Cancer Society, 2017; Guilford *et al.*, 1998; NCI, 2015). Due to these **familial** cancer syndromes, **hereditary** risk factors, and the molecular changes occurring in cancers, they are in part a genetic disease involving many **cancer genes** Stratton *et al.* (2009); Vogelstein *et al.* (2013). The **mutations** increase the risk of **cancer** with age. An association of cancer incidence with the stem cell divisions in which **mutations** could occur across tissue types, suggests that cancers may be inseparably coupled with aging (Tomasetti and Vogelstein, 2015).

Hanahan and Weinberg (2000) propose the “**hallmarks** of cancer”, molecular and cellular traits shared across cancers. These form the basis of a rational approach to the complex changes that occur in **cancer**. These traits include limitless replication potential, signals for indefinite growth, and invasive or metastatic capabilities. **Cancers** also evade apoptosis, the immune system, and sustain angiogenesis and energy metabolism (Hanahan and Weinberg, 2011). To achieve this, **cancer** cells change their **genomes** and the **tumour** microenvironment. **Genomic** instability has a role in the survival and proliferation of **cancer** cells and the progression of disease, as these malignant characteristics are acquired. Identifying the genetic mechanisms involved in the acquisition of these traits is important for understanding and effectively inhibiting **cancer**.

Gene expression can be used to characterise breast cancers. The “**intrinsic subtypes**” identified were characterised by estrogen receptor, *HER2*, and basal, epithelial signalling (Perou *et al.*, 2000). The **expression** profiles were similar across independent samples of the same tumour or the same patient and therefore represent the molecular state of a **tumour**. The molecular **intrinsic subtypes** “luminal A”, “luminal B”, “*HER2*-enriched”, “basal-like”, and “normal-like” have been replicated across **microarray** studies (Hu *et al.*, 2006), with their relevance to **prognosis** demonstrated, and a 50-gene subtype predictor developed (Parker *et al.*, 2009; Sørlie *et al.*, 2001). Despite specific differences in subtyping, there is widespread agreement that distinguishing luminal, *HER2*-enriched, and triple negative **tumours** has prognostic importance for patients (Dai *et al.*, 2015). The “**pan cancer**” The Cancer Genome Atlas project (discussed in Section 1.1.3.2) demonstrates the importance of molecular similarities and differences between cancers across cancer tissue types (Weinstein *et al.*, 2013).

Gatza *et al.* (2010) used gene signatures for 18 cellular **pathways** in breast cancer to define subtypes with distinct molecular **pathway** activity. A “**metagene**” is a measure

pathway activation (derived from eigenvectors or principal components) which gives a consistent signal of gene expression (Anjomshoaa *et al.*, 2008; Huang *et al.*, 2003; Nagalla *et al.*, 2013). Unsupervised hierarchical clustering defined subtypes with common pathway activity, despite variation in mutations. These subtypes intrinsic subtypes and provide finer molecular stratification with a functional basis (Gatza *et al.*, 2014; Parker *et al.*, 2009). The subtypes with shared pathway activity have similar molecular characteristics (such as DNA copy number) and clinical properties including prognosis.

1.1.2 The genomic Revolution in Cancer Research

Genomic technologies have transformed genetics research, including the study of health and disease (Goodwin *et al.*, 2016; Lander, 2011). Genomics enables systematic, unbiased studies across all of the genes in the genomes. Cancer genomics investigations have been widely applied to different tissues across molecular profiles (Bamford *et al.*, 2004; Weinstein *et al.*, 2013; Zhang *et al.*, 2011). Genomes sequencing technologies continue to improve and become feasible in a wider range of applications.

Genomics has been used in many investigations (Goodwin *et al.*, 2016) but relatively few of the potential applications in healthcare have been realised yet (Roychowdhury and Chinnaiyan, 2016; Tran *et al.*, 2012). Cancer genomics, in particular, could have numerous benefits across diagnostics, prognosis, management, and treatment (Roychowdhury and Chinnaiyan, 2016). While direct impact of genomic on the clinic has been limited thus far, the cancer genes and therapeutic targets identified have begun to be introduced in the clinic (Stratton *et al.*, 2009).

1.1.2.1 High-Throughput Technologies

Microarray are a high-throughput molecular technique, reducing the cost, time, and labour required to study genes at the “genome” scale (Schena, 1996). Microarray can detect genotype or expression across many genes, making it feasible to perform on a statistically informative number of samples. Microarray are manufactured with probes which measure binding of nucleotides which either detect the presence of a sequence such as a single nucleotide polymorphism (SNP) or quantify sequences for DNA copy number, gene expression, or DNA CpG dinucleotide (CpG) methylation. In addition to being more versatile with higher-throughput than polymerase chain reaction (PCR) based techniques, microarrays are considered cost-effective, particularly when scaled up to a large number of probes. These remained popular, especially in large-scale projects, during the introduction of newer technologies due to reliability and relatively lower cost for testing processing samples.

The introduction of massively parallel sequencing technologies has further expanded high-throughput molecular studies and the availability of genomics data. This “Next-Generation Sequencing” (NGS) enables rapid *de novo* genomes and transcriptome sequencing, in addition to gene expression studies (Goodwin *et al.*, 2016). However, the cost of sequencing for gene expression or DNA methylation studies is still considerably higher than a microarray study, limiting feasible sample sizes, and NGS studies have large compute requirements to handle the raw data. In many cases, the benefits of NGS technologies outweigh the additional cost. NGS technologies have the advantage of greater potential accuracy and sensitivity than microarrays. NGS has a wider dynamic range than microarrays and are not limited to genes with an already characterised sequence or functions.

NGS is highly adaptable to different applications, including DNA sequencing (whole genome or exome), DNA methylation (Bisulfite-Seq), or RNA-Seq (Goodwin *et al.*, 2016; Tran *et al.*, 2012; Waldron, 2016). RNA-Seq of the transcriptome is a common adaptation where RNA is reverse transcribed and sequenced from the resulting complementary DNA (cDNA). This is utilised to quantify the levels of RNA and identify which regions of DNA are expressed. Similarly, bisulfite treatment converts cytosine residues to uracil, sparing methylated cytosine enabling them to be distinguished with Bisulfite-Seq for detection of epigenetic modifications to generate an epigenome. Subsets of the nucleic acid may be extracted for sequencing such as the coding regions of DNA (for the “exome”), mRNA(RNA-Seq), micro RNA (microRNA), or capturing variable regions for DNA (“genotyping by sequencing”) and methylation studies (“reduced-representation bisulfite sequencing). These “omics” technologies (Roychowdhury and Chinnaiyan, 2016; Waldron, 2016) are applicable across a wide range of biomolecules to generate “” of a cell or sample (Perou *et al.*, 2000).

NGS technologies continue to be refined (Goodwin *et al.*, 2016) with Illumina (the platform used to generate data in this project) and competitors continuing to improve products and decrease costs. As such, RNA-Seq for examining transcriptomes or expression studies is a growing field and will continue to be generated for a range of samples. The technology may yet improve (Goodwin *et al.*, 2016) with developments in speed and accuracy (such as Ion Torrent platforms) or long reads, single molecules sequences (such as Pacific Biosciences, Oxford Nanopore, and Quantum Biosystems Japan). Due to the benefits of sequencing and the availability of public data, this thesis has focused on gene expression data generated by RNA-Seq. RNA-Seq data is

publicly available from large-scale cancer genomics projects and the methods developed for RNA-Seq data could be applied to future genomics technologies.

1.1.2.2 Bioinformatics and Genomic Data

Genomic technologies have generated data at a scale which requires computational, mathematical, and statistical expertise to handle this data effectively (Markowetz, 2017; Tran *et al.*, 2012), in addition to an understanding of the biological context and research questions. The interdisciplinary field of “bioinformatics”, which draws upon these skills, focuses specifically on making inferences from genomics data or developing the tools to do so. Gene expression analysis is the focus of many bioinformatics research groups, drawing upon statistical approaches to appropriately handle microarray and RNA-Seq data along with making biological inferences from a large number of statistical tests.

This is often confused with the broader field “computational biology” (Markowetz, 2017), which focuses on modelling and simulating aspects of biology and is not necessarily limited to genetics or data analysis. In practice, many researchers identify with both bioinformatics and computational biology or use techniques in both fields. This thesis uses many of these approaches, mainly in bioinformatics, to address biological research questions pertaining to synthetic lethal interactions.

1.1.3 Genomics Projects

Genomic projects have also been applied to various organisms, functional genetics (Kawai *et al.*, 2001; ENCODE, 2004), and human populations focusing on variability between individuals and health or disease risk (HapMap, 2003; 1000 Genomes, 2010). International projects and consortiums have begun to release data gathered using common agreed upon protocols across laboratories. These include many genomics projects including cancer genomics projects discussed below. The quality, consistency, and accessibility of these international projects is appealing, particularly for gene expression datasets where the more recent, larger projects have switched from microarray to RNA-Seq technologies.

1.1.3.1 The Cancer Genome Project

The Cancer Genome Project (CGP) was among the first genomics investigations into cancer (Dickson, 1999), using the human genomes sequence (Collins and Barker, 2007; Lander *et al.*, 2001), the cancer research literature, and sequencing the genes of cancers themselves. The main aim of the Cancer Genomes Project was to discover “cancer

genes”, which are frequently mutated in cancers by comparing cancer and normal tissue samples. These include both “oncogenes” and “tumour suppressors” which are functionally activated and inactivated in cancers respectively. This project is ongoing and the continues to maintain the Catalogue Of Somatic Mutations In Cancer (COSMIC), a database of cancer genes (COSMIC, 2016). It includes 1,257,487 samples with 4,175,8787 gene mutations curated from 23,870 publications, including 29,112 whole genomes (COSMIC, 2016).

1.1.3.2 The Cancer Genome Atlas Project

The Cancer Genome Atlas (TCGA) network initially set out to demonstrate a pilot project on brain (McLendon *et al.*, 2008), ovarian (Bell *et al.*, 2011), and squamous cell lung (Hammerman *et al.*, 2012) cancers. The project then expanded, aiming to analyse 500 samples each for 20-25 **tumour** tissue types. They have since exceeded that goal, with data available for 33 cancer types including 10 “rare” cancers, a total of over 10,000 samples (TCGA, 2017). The TCGA projects set out to generate a molecular “profile” of the **tumour** (and some matched normal tissue) samples: the genotype, somatic mutation mutations, gene expression, DNA copy number, and RNA methylation levels. Data which cannot be used to identify the patients are publicly available

The Cancer Genome Atlas pilot projects (Bell *et al.*, 2011; Hammerman *et al.*, 2012; McLendon *et al.*, 2008) serve to demonstrate the power of applying genomic technologies to cancer research at such as scale. TCGA demonstrated the potential discovery of the molecular basis of cancer with these tissues, including the describing recurrently mutated genes in each cancer, identifying differentially methylated regions, and proposing transcriptional subtypes for ovarian cancers. The molecular aberrations in each cancer represent potential therapeutic targets in some cases and some were shown to have an impact on patient survival.

The TCGA breast cancer analysis (TCGA, 2012) consisted of 802 samples with exomes, copy number variants, RPPA protein quantification, and DNA methylation, mRNA, and microRNA arrays with 97 whole genomes sequenced. Four main molecular classes were identified to subtype the samples, despite considerable heterogeneity between samples. Recurrent mutations across more than 10% of samples were identified in *TP53*, *PIK3CA*, and *GATA*. TCGA further suggests subtypes by HER2 and EGFR protein levels. In a further analysis of 817 breast cancer samples including 127 invasive lobular breast and 88 mixed type samples (Ciriello *et al.*, 2015), 3 molecular subtypes

of lobular breast cancer were identified. Lobular breast cancer was also characterised by [recurrent mutations](#) in *CDH1*, *PTEN*, *TBX2*, and *FOXA1*.

The TCGA stomach cancer analysis of 295 samples ([Bass et al., 2014](#)) identified 4 [molecular subtypes](#) of stomach cancers characterised by: the Epstein-Barr virus, microsatellite instability ([MSI](#)), genomic instability, and chromosomal instability. Aberrations in *PD-L1*, *PIK3CA*, and *JAK2* were also identified in stomach cancers which may present therapeutic targets.

[TCGA](#) have identified various genes as recurrent, [driver mutations](#) across cancer types which are likely to have a role in driving the proliferation of these cancers and present a molecular target that could be applied across tissue types. In addition to disregarding the tissue-based distinction between colon and rectal cancers based on molecular similarity ([Muzny et al., 2012](#)), the [TCGA](#) project have observed differences within tumour types and proposed [molecular subtyping](#) for breast, clear cell renal, papillary renal, stomach, skin, bladder, and prostate cancers ([Abeshouse et al., 2015](#); [Akbani et al., 2015](#); [Bass et al., 2014](#); [Ciriello et al., 2015](#); [Creighton et al., 2013](#); [Hamerman et al., 2012](#); [Linehan et al., 2016](#); [Muzny et al., 2012](#); [TCGA, 2012](#); [Weinstein et al., 2014](#)).

The “pan cancer” project ([Hoadley et al., 2014](#); [Weinstein et al., 2013](#)) analysed 3527 samples across 12 tissue types. This project was performed a comprehensive analysis of molecular data across cancer types to identify molecular similarities and differences. These included recurrent *TP53*, *BRCA1* and *BRCA2* [mutations](#), HER2 over-expression, and [MSI](#) across cancer types. The [pan cancer](#) project ([Hoadley et al., 2014](#)) has identified 11 [molecular subtypes](#) across these tissues, with only 5 of these corresponding to tissue cancer types due to molecular similarities shared across cancer types. This project further supports the [genomic](#) stratification of cancer patients, demonstrated in breast cancer ([Parker et al., 2009](#); [Pereira et al., 2016](#); [Perou et al., 2000](#)), and there being core molecular characteristics across cancers ([Hanahan and Weinberg, 2000, 2011](#)).

While these findings contribute to further understanding cancer biology within and across tissue types, the main objective of such projects is to publicly release data to analyse in future investigations ([McLendon et al., 2008](#); [TCGA, 2017](#); [Weinstein et al., 2013](#)). These serve as a vast resource of common and rare cancer types and are publicly available for further analysis ([cBioPortal, 2017](#); [TCGA, 2017](#); [Zhang et al., 2011](#)).

1.1.4 Genomic Cancer Medicine

Cancer genomics has significant potential for impacts in cancer medicine: from diagnosis to treatment (Roychowdhury and Chinnaiyan, 2016; Tran *et al.*, 2012). Beyond direct use of genomes or RNA-Seq in clinical laboratories, genomic studies also generate the biomarkers and inform development of treatments. These are likely to have a more immediate patient benefit considering the cost of routine genomes sequencing for diagnostics.

1.1.4.1 Cancer Genes and Driver Mutations

There are two main classes of “cancer genes” (Futreal *et al.*, 2001). Oncogenes are activated in cancers either by gain of function mutations in proto-oncogenes, amplification of DNA, or elevated gene expression. Their normal functions are typically to regulate stem cells or to promote cellular growth and recurrent mutations are typically concentrated to particular gene regions. Conversely, tumour suppressor genes are those inactivated in cancer either by loss of function mutations, deletion of DNA copies, or reduced of gene expression, including hypermethylation. Their normal functions are typically to regulate cell division, DNA repair, and cell signalling.

Detecting these cancer genes has accelerated with genomic technologies, as demonstrated by COSMIC and TCGA (COSMIC, 2016; Weinstein *et al.*, 2013). Recurrent mutations, or DNA copy number variants and differential gene expression or DNA methylation are all indicative of cancer genes (Mattison *et al.*, 2009), which can be detected in genomics data (Pereira *et al.*, 2016; Weinstein *et al.*, 2013). However, many cancer genes have been identified or replicated in genomics data.

Distinguishing important “driver” mutations in cancer genes from “passenger mutation” mutations is challenging due to patient variation, tumour heterogeneity, and genomic instability producing many variant gene sequences (Stratton *et al.*, 2009; Tran *et al.*, 2012). Driver mutations can be identified by whether they co-occur or are mutually exclusive with mutations in other genes in cancers, are recurrently mutated across a significant proportion of samples for a specific tissue type, or if mutations are recurrent across different cancer tissue types (cBioPortal, 2017; Pereira *et al.*, 2016; COSMIC, 2016; Weinstein *et al.*, 2013; Zhang *et al.*, 2011). Approximately 140 driver mutations have been identified, including many novel genes in particular cancers from genomic studies, with 2–8 in typically occurring in each tumour usually affecting cell fate, survival, or genomes maintenance (Vogelstein *et al.*, 2013). There need to trans-

late the identification of many **cancer genes** and **driver mutations** to patient benefit by repurposing or designing of **therapeutic interventions** against these molecular targets.

1.1.4.2 Precision Cancer Medicine

The importance of **genomics** is emphasised in translational cancer research in contrast with current strategies of healthcare based on what works well for the most of the population. Cancers could eventually be treated by their **genomic** features (Roychowdhury and Chinnaiyan, 2016), particularly grouping patients by the **mutation**, **expression**, or **DNA methylation** profiles of their cancers, which is already done in part (Parker *et al.*, 2009). Identifying actionable molecular targets is a key aspect of “precision medicine”, the rationale to target **molecular subtypes** with separate treatment strategies (Glaire *et al.*, 2017). To this end many driver mutations and gene expression signatures for distinguishing cancers have been identified. Some oncogenic **driver mutations** have effective pharmacological inhibitors designed against them but there remain many **cancer genes** and **mutations**, particularly **tumour suppressors**, for which there is not yet a targeted therapy.

1.1.4.3 Molecular Diagnostics and Pan-Cancer Medicine

Molecular features such as **mutations** or **gene expression** signatures have been proposed to **diagnose** tumour subtypes. In breast cancer, several distinct “**intrinsic subtypes**” have been identified, distinguished by molecular mechanisms, with differences in malignancy and patient outcome (Parker *et al.*, 2009; Perou *et al.*, 2000). Conversely, common molecular mechanisms may be shared between cancers across tissue types as discovered by the **TCGA** “pan cancer” project, which combined **molecular profiles** across tissue types Weinstein *et al.* (2013). **Molecular subtypes** could feasibly be included in clinical testing as a panel of biomarkers for **diagnosis**, monitoring drug response, or predicting risk of recurrence. Having identified these **molecular subtypes** and genetic aberrations specific to cancers, there is clear need for further development of **treatments** that target them.

1.1.4.4 Targeted Therapeutics and Pharmacogenomics

Targeted therapies with specificity against a molecular target are examples of **precision cancer medicine**. Molecular targets can be tested in laboratory conditions with **RNA interference (RNAi)** or pharmacological agents. Identification of molecular targets is important for developing novel anti-cancer **treatments** along with validation and drug testing. For oncogenic **mutations**, the recurrent **mutant** variant or over-expressed gene is directly inhibited using structure-aided drug design or compound screening.

However, **oncogenes** with high homology to other genes or **tumour suppressor** genes are not amenable to direct targeting (Kaelin, Jr, 2009).

Targeted therapeutics have been applied as monoclonal antibodies against **oncogenes** (such as *HER2*) with relative success in clinical trials (Miles, 2001). Such targeted therapies have potential applications across tissue types and specificity against tumour cells (even in advanced disease or as a **chemopreventative** in high-risk individuals), with wide therapeutic windows and use in combination therapies. However, they have already begun to manifest problems with resistance, recurrence, tissue specificity, and design of inhibitors specific to oncogenic variants. Targeted anticancer therapeutics can exploit complex interactions to distinguish normal and cancerous cells which may benefit from studies of gene regulation or interaction networks.

The unexpected **synergy** between inhibitors of the **oncogenes** *BRAF^{V600E}* and *EGFR* in colorectal cancer is an example of such a system Prahallad *et al.* (2012). Despite successful application of vemurafenib against *BRAF^{V600E}* in melanomas Dienstmann and Tabernero (2011); Ravnan and Matalka (2012), colorectal cancers with *BRAF^{V600E}* mutations have poor **prognosis** and lack drug response. Prahallad *et al.* (2012) used an **RNAi** screen and found that *EGFR* inhibition is **synergistic** with vemurafenib against *BRAF^{V600E}* in colon cell lines and xenografts due to feedback activation of *EGFR*. Vemurafenib induced rapid reactivation of MAPK/ERK signalling via *EGFR* in colorectal cell lines in a tissue-specific manner Corcoran *et al.* (2012) and may be relevant to acquired resistance in melanoma Sun *et al.* (2014). Thus combination therapies against several molecular **pathways** may be necessary to anticipate acquired resistance Ravnan and Matalka (2012) and **targeted therapeutic** may be further refined from understanding the **pathway** structure and functional interactions across cancer cells.

1.1.5 Systems and Network Biology

Driver **mutations** in **oncogenes** and **tumour suppressor** genes do not occur in isolation. The genetic interactions, regulatory and cellular signalling, and metabolic reactions are inter-related and may each be perturbed by aberrations in gene function occurring in **cancers**. These relationships can be represented by **biological networks** of connected pairs of genes with a relationship. Due to the complexity of a cell, these molecular networks are very large consisting of thousands of **nodes** comprised by genes or proteins.

The properties of large **networks** were first studied by constructing random **networks** by randomly linking a fixed number of **nodes** (Erdős and Rényi, 1959, 1960). Despite the random nature of these **networks**, properties such as their connectivity were well

characterised. The **vertex** degree (number of partners for each **node**) of random **network** follows a Poisson distribution, however this property does not hold in nature. Thus natural **networks** are non-random or not formed in this way Barabási and Oltvai (2004).

This work formed the foundation for studying complex **networks** (van Steen, 2010), which model features of observed **networks** not found in Erdő and Rényi's random **networks** (Erdős and Rényi, 1959, 1960). The **small world** property, made popular by findings in social **networks** (Travers and Milgram, 1969), is the remarkably short path lengths between any **nodes** in a **small world network**. A **small world network** is well-connected with a characteristic path length (the average length of **shortest paths** between all pairs of **nodes**) proportional to the logarithm of the number of **nodes**. Watts and Strogatz (1998) developed a model of random rewiring of a regular **network** to construct random **networks** with the **small world** property and a high clustering coefficient. While these properties are more representative of **networks** occurring in nature, their model is limited by the degree distribution which converges to a Poisson distribution as it is rewired Barrat and Weigt (2000). The **vertex** degree distribution of naturally occurring **networks** often follows a power law distribution with most **nodes** having far fewer connections than average and a small subset of highly connected network 'hubs' Barabási and Albert (1999).

Barabási and Albert (1999) constructed a **network** model in an entirely different way to randomly generate **scale-free networks** which have a power law degree distribution. They constructed random **networks** by preferential attachment, modelling growth of a **network** by sequentially adding **nodes** with **links** to existing **nodes**. The **scale-free** nature of the random **networks** was ensured by adding new **nodes** with an increasing probability of attachment to an existing **node** if it has higher degree. These **networks** successfully capture the **scale-free** nature of many observed **networks** with short characteristic path length and low eccentricity resulting in super **small worlds** Barabási and Albert (1999). Scale-free **networks** are limited by a low clustering coefficient and lack of modular structure; however, they have enabled the study of **scale-free** network topology and served as a basis for modified **scale-free** models (Dorogovtsev and Mendes, 2003; Holme and Kim, 2002).

High-throughput technologies such as **siRNA** screens, two-hybrid screens, **microarrays** and massively parallel sequencing have generated **genomes-scale** data and enabled analysis of biological **networks**. Many types of molecular networks can be constructed, depending on the biological application. Genetic interactions are relatively unexplored within molecular networks and may lead to better understanding of the role

of gene functions in cellular function and disease. High-throughput screens in humans, mammals, and non-model organisms are costly and labour-intensive. Computational approaches with effective predictive models are therefore a more feasible alternative to study the connectivity of a biological network in a complex metazoan cell at the genomes-scale.

1.1.5.1 Network Medicine and Polypharmacology

Molecular networks are biological networks consisting of biological molecules including genes, transcripts (with non-coding and microRNAs), or proteins related by known interactions and gene regulatory or metabolic pathways. Targeted therapeutics have had some success for drug discovery, particularly in anticancer applications, including exploiting these molecular networks by designing combination therapies and applying a network pharmacology framework Hopkins (2008). Rational design of drugs selective to a single target has often failed to deliver clinical efficacy. Many existing effective drugs modulate multiple proteins, having been selected for biological effects or clinical outcome rather than molecular targets. Proponents of network biology and polypharmacology (specific binding to multiple targets) recommend developing drugs with a desired target profile designed for the target topology Barabási and Oltvai (2004); Hopkins (2008). Multi-target treatments aim to achieve a clinical outcome through modulation of molecular networks since the genetic robustness of a cell often compensates for loss of a single molecular target.

While multi-target drugs may be more difficult to design, they are faster to test clinically than drug combinations which are usually required to be tested separately first Hopkins (2008). Synthetic lethal treatments for cancer, drug combinations and multi-target drugs to combat resistance to chemotherapy and antibiotics can be informed by biological networks Barabási and Oltvai (2004); Hopkins (2008). Further optimisation of timing and dosing of drug combinations may increase efficacy of treatments with low efficacy applied separately. Low doses and drug holidays are other counter intuitive approaches which may increase clinical efficacy, reduce adverse effects, and reduce drug resistance (Sun *et al.*, 2014; Tsai *et al.*, 2012).

A molecular map of the interactions and pathways in the mammalian cellular network has the potential to impact upon drug design and clinical practice, particularly in treatment of cancer and infectious disease. Characterisation of the target system and impact of existing treatments, such as *BRAF*^{V600E} and *EGFR* inhibitors, enable wider application of the mechanisms for such interventions exploiting genetic interactions or pathways. This could lead to development of more effective treatment interventions

for these systems and prediction of similar molecular systems for development of novel drug targets and combinations.

1.2 A Synthetic Lethal Approach to Cancer Medicine

Synthetic lethality has vast potential to improve cancer medicine by expanding application of targeted therapeutic to include inactivation of tumour suppressors and genes that are difficult to target directly. Synthetic lethal interactions are also studied for gene function and drug mode-of-action in model organisms. This section introduces the concept of synthetic lethality as it was originally conceived and how it has been adopted conceptually in cancer research. Detecting these interactions at scale and interpreting them is the focus of this thesis, hence we start with an overview of the concepts involved, initial work on the interaction, and the rationale for applications to cancer. Specific investigations into synthetic lethality in cancer, detection by experimental screening, and prediction by computational analysis will then be reviewed.

1.2.1 Synthetic Lethal Genetic Interactions

Genetic interactions are a core concept of molecular biology, discovered among earliest investigations of Mendelian genetics, and have received revived interest with new technologies and potential applications. Biological epistasis is the effect of an allele at one locus “masking” the phenotype of another locus (Bateson and Mendel, 1909). Statistical epistasis is where there is significant disparity between the observed and expected phenotype of a double mutant, compared to the respective phenotypes of single mutant and the wild-type (Fisher, 1919). Fisher’s definition lends itself to quantitative traits and more broadly encompasses synthetic genetic interactions. These have become popular for studies in yeast genetics and cancer drug design (Boone *et al.*, 2007; Kaelin, Jr, 2005).

SGIs are substantial deviations of growth or viability from the expected null mutant phenotype (of an organism or cell) assuming additive (deleterious) effects of the single mutant. The double mutant does not necessarily have either single mutant phenotype (as shown for cellular growth phenotypes in Figure 1.1). Most SGIs are more viable than either single mutant or less viable than the expected double mutant. Mutations are “synergistic” in negative SGI with more deviation from the wild-type than expected. Formally, “synthetic sick” (SSL) and “synthetic lethal” (SL) interactions are negative SGIs giving growth inhibition and complete inviability respectively. In cancer research,

synthetic lethality more broadly describes any negative **SGI** with specific inhibition of a **mutant** cell, including **SSL** interactions. Mutations are “alleviating” in positive **SGI** with less deviation from the **wild-type** than expected. For viability, “**suppression**” (**SS**) and “**rescue**” (**SR**) are positive **SGIs** giving at least partial restoration of **wild-type** growth from single **mutant** with growth impairment and lethal phenotypes respectively. Negative **SGIs** were markedly more common than positive **SGIs** in a number of studies in model systems Boucher and Jenna (2013); Tong *et al.* (2004).

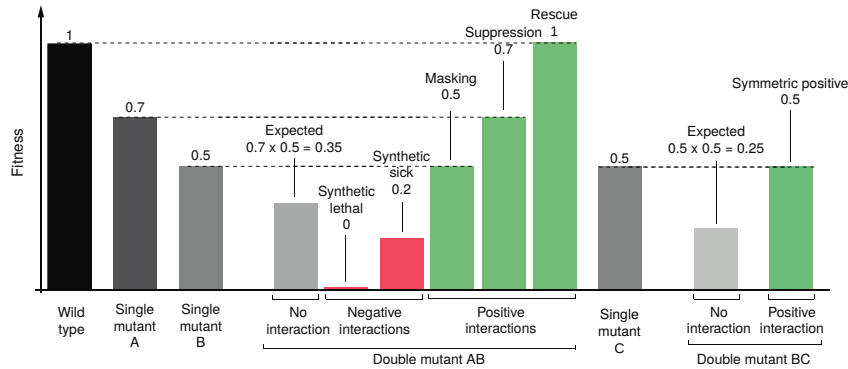


Figure 1.1: **Synthetic genetic interactions.** Impact of various negative and positive **SGIs**: negative interactions involve deleterious (sick) or inviable (lethal) phenotypes whereas positive interactions involve restoring viability by masking or suppressing the other **mutation** or complete rescue of the wildtype phenotype. Figure adapted from (Costanzo *et al.*, 2011) concerning growth viability fitness in yeast.

1.2.2 Synthetic Lethal Concepts in Genetics

Synthetic lethal genes are generally regarded to arise due to **functional redundancy**. Due to the functional level of **SGIs**, synthetic lethal genes do not need to directly interact, nor be expressed in the same cell or at the same developmental stage: serving related functions is sufficient to affect cell (or organism) viability and be relevant to drug-mode-of-action cancer biology. Combined loss of genes performing an **essential** or important function in a cell are therefore deleterious. Synthetic lethal gene pairs are therefore pairwise **essential** with “**induced essentiality**”: each synthetic lethal gene becomes **essential** to the cell upon loss of the other.

Since synthetic lethal gene partners can be affected by extracellular stimuli such as chemicals, essentiality of synthetic lethal genes can be induced by the environment of a cell. An environmental stress condition may inhibit one or the other synthetic lethal gene, such as exposure to chemicals, in which case the synthetic lethal partner gene is

“conditionally essential” (Hillenmeyer, 2008). Thus the evolutionary rationale for the abundance of SGIs (compared to the surprisingly low number of essential genes) in a Eukaryotic genomes can be attributed to genetic functional redundancy and network robustness of a cell which are advantageous to survival.

Biological functions are typically performed by a pathway of genes (or their products). Synthetic lethal genes occur within the same biological pathway and between them (Boone *et al.*, 2007; Costanzo *et al.*, 2010; Kelley and Ideker, 2005). Many genes of the same pathway may be functionally interchangeable, synthetic lethal partners of a particular gene. Therefore biological pathways can exhibit induced essentiality with loss of the synthetic lethal partner gene and synthetic lethality may occur at pathway level or in a gene regulation network.

1.2.3 Synthetic Lethality in Model Systems

Genetic high-throughput screens have identified unexpected, functionally informative, and clinically relevant synthetic lethal interactions; including synthetic lethal partners of genes recurrently mutated in cancer or attributed to familial early-onset cancers. While screening presents an appealing strategy for synthetic lethal discovery, computational approaches are becoming popular as an alternative or complement to experimental methods to overcome inherent bias and limitations of experimental screens. An array of recently developed computational methods (Jerby-Arnon *et al.*, 2014; Lu *et al.*, 2015; Tiong *et al.*, 2014; Wang and Simon, 2013; Wappett, 2014) show the need for synthetic lethal discovery in the fundamental genetics and translational cancer research community. However, existing computational methods are not suitable for queries of genomic data for interacting partners of a particular gene: they have been applied pairwise across the genomes, do not have software released to apply the methodology, or lack statistical measures of error for further analysis. A robust prediction of gene interactions is an effective and practical approach at a scale of the entire genomes for ideal translational applications, analysis of biological systems, and constructing functional gene networks.

1.2.3.1 Synthetic Lethal Pathways and Networks

SGIs are common in genomes, 4× more interactions were detected with synthetic gene array (SGA) mating screens than protein-protein interactions detected with yeast-2-hybrid (Tong *et al.*, 2004). The SGI network is scale-free with power-law vertex degree distribution and low average shortest path length (3.3), as expected for a complex biological network (Barabási and Oltvai, 2004). Highly connected “hub” genes with the

highest number of **links** (**vertex degree**) are functionally important with many negative **SGI** hubs involved in cell cycle regulation and many positive **SGI** hubs involved in translation (Baryshnikova *et al.*, 2010b; Costanzo *et al.*, 2010). Negative **SGIs** were far more common than positive **SGIs**, with synthetic gene loss being more likely to be deleterious to cell than advantageous which indicates that **synthetic lethality** may be comparably easier to detect than other **SGIs**.

Essential pathways are highly buffered with $5\times$ more interactions than other **SGIs**, consistent with strong selection for survival, as found with conditional and partial **mutations** in **essential** genes (Davierwala *et al.*, 2005). This **SGI** network had **scale-free** topology and rarely shared interactions with the protein-protein interaction network. These networks are related by an “orthogonal” relationship: shared partners in one network tend to be themselves connected directly in the other network. Essential genes were likely to have closely related functions, whereas non-**essential** networks were relatively more inclined to have **SGIs** between distinct biological **pathways**.

1.2.3.2 Evolution of Synthetic Lethality

There is poor conservation of specific **SGIs** between *S. cerevisiae* and *S. pombe* with 29% of the interactions tested in both distantly related species being conserved between them (Dixon *et al.*, 2008). The remaining interactions show high species-specific differences; however, many of the species-specific interactions were still conserved between biological **pathways**, protein complexes, or protein-protein interaction modules. Similarly, conservation of **pathway** redundancy was also found between Eukaryotes (*S. cerevisiae*) and prokaryotes (*E. coli*) (Butland *et al.*, 2008). Negative **SGIs** were more likely to be conserved between biological **pathways**, whereas positive **SGIs** were more likely to be conserved within a **pathway** or protein complex (Roguev *et al.*, 2008).

A modest 5% of interactions were conserved between unicellular (*S. cerevisiae*) and multicellular (*C. elegans*) organisms. However, the nematode **SGI** network had similar **scale-free** topology and modularity despite differences in methodology: metazoan **synthetic lethal** screens with **RNA interference (RNAi)** are incomplete knockouts, whereas screening null **mutations** is feasible in yeast (Bussey *et al.*, 2006). The nematode **SGI** screen identified network hubs with important interactions to orthologues of known human disease genes (Lehner *et al.*, 2006). Despite the lack of direct conservation of **SGIs** between yeasts and nematode worms, **genetic redundancy** was consistent with an “**induced essentiality**” model of **SGIs** where gene functions are conserved with network restructuring over evolutionary change (Tischler *et al.*, 2008).

While nematode models are more closely related to human cells which are also screened with **RNAi**, cancer cells can present growth and viability phenotypes more comparable to yeast models. Therefore findings from both **SGA** and **RNAi** models are relevant to understanding human and cancer cells. **RNAi** has also been applied to human and mouse cancer cells with **short interfering RNA (siRNA)** in cell culture and genetic screening experiments. These findings suggest that **SGI** network “rewiring” is a concern for identifying specific **synthetic lethal** interactions in cancer as specific **synthetic lethal** genes may vary between genetic backgrounds. Thus it is expected at a **pathway** approach will be more robust in the context of evolution, patient variation, tumour heterogeneity, or disease progression.

1.2.4 Synthetic Lethality in Cancer

Loss of function occurs in many genes in cancers including **tumour suppressors** and yet few interventions target such **mutations** compared to targeted therapies for gain of function **mutation** in **oncogenes** (Kaelin, Jr, 2005). **Synthetic lethality** is a powerful design strategy for therapies selective against loss of gene function with potential for application against a range of genes and diseases (Fece de la Cruz *et al.*, 2015; Kaelin, Jr, 2009). When genes are disrupted in cancers, the **induced essentiality** of **synthetic lethal** partners presents a vulnerability that may be exploited for anti-cancer therapy. Since **synthetic lethality** affects cellular viability by indirect functional relationships between genes, it is suitable for indirectly targeting **mutations** in cancers via **synthetic lethal** partners with **targeted therapeutic**. These have could be highly specific against cancer cells (with the target **mutation**) over non-cancer cells (with a functional compensating gene). Analogous to “**oncogene addiction**”, where cancer cells adapt to particular oncogenic growth signals and become reliant on them to remain viable (Luo *et al.*, 2009; Weinstein, 2000), **synthetic lethal** partners of inactivated **tumour suppressors** are required to maintain cancer cell viability and proliferation. As such cancers are subject to “**non-oncogene addiction**” and are feasible anti-cancer drug targets.

The synthetic lethal approach to cancer medicine is most amenable to loss of function **mutations** in **tumour suppressor** genes, where it would feasibly be effective against any loss of function **mutation** across the **tumour suppressor** with a viable **synthetic lethal** partner gene (as shown in Figure 1.2). However, the approach may also be suitable for cases where cancer cells have **mutations** where the normal function of the gene is disrupted such as if it were over-expressed (“**synthetic dosage lethality**”) or if an oncogenic **mutation** interfered with the function of the **proto-oncogene**. Thus **synthetic**

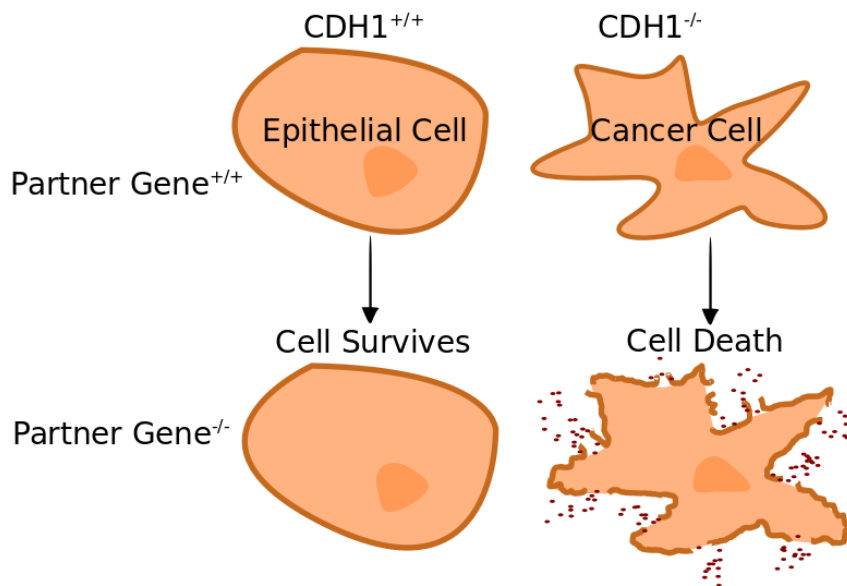


Figure 1.2: **Synthetic lethality in cancer.** Rationale of exploiting synthetic lethality for specificity against a **tumour suppressor** gene (e.g., *CDH1*) while other cells are spared under the inhibition of a partner gene.

lethality makes it feasible to target a range of cancer-specific mutations with **targeted therapeutic**, including inactivated **tumour suppressor** genes. **synthetic lethality** may also enable distinguishing highly homologous **oncogenes** by functional differences by targeting their **synthetic lethal** partners.

1.2.5 Clinical Impact of Synthetic Lethality in Cancer

The **synthetic lethal** interaction of *BRCA1* or *BRCA2* with *PARP1* in breast cancer is an example of how gene interactions are important in cancer, including translation to the clinic. These genetic interactions enable specific targeting of **mutations** in *BRCA1* or *BRCA2* **tumour suppressor** genes with **Poly-ADP-ribose polymerase (PARP)** inhibitors by inducing **synthetic lethality** in breast cancer (Farmer *et al.*, 2005). PARP inhibitors are one of the first **targeted therapeutic** against a **tumour suppressor mutation** with success in clinical trials.

BRCA1 or *BRCA2* and *PARP1* genes demonstrate the application of the **synthetic lethal** approach to cancer therapy (Ashworth, 2008; Kaelin, Jr, 2005). *BRCA1* and *BRCA2* are homologous **DNA** repair genes, widely known as **tumour suppressors**; **mutation** carriers have substantially increased risk of breast (risk by age 70 of 57% for *BRCA1* and 59% for *BRCA2*) and ovarian cancers (risk by age 70 of 40% for

BRCA1 and 18% for *BRCA2*) (Chen and Parmigiani, 2007). The *BRCA1* or *BRCA2* genes, which usually repair DNA or destroy the cell if it cannot be repaired, have inactivating somatic mutation mutations in some familial and sporadic cancers. Poly-ADP-ribose polymerase (PARP) genes are tumour suppressor genes involved in base excision DNA repair. Loss of PARP activity results in single-stranded DNA breaks. However, *PARP1*^{-/-} knockout mice are viable and healthy indicating low toxicity from PARP inhibition (Bryant *et al.*, 2005).

Bryant *et al.* (2005) showed that *BRCA2* cells were sensitive to PARP inhibition by siRNA of *PARP1* or drug inhibition (which targets *PARP1* and *PARP2*) using Chinese hamster ovary cells, MCF7 and MDA-MB-231 breast cell lines. This effect was sufficient to kill mouse tumour xenografts and showed high specificity to *BRCA2* deficient cells in culture and xenografts. Farmer *et al.* (2005) replicated these results in embryonic stem cells and showed that *BRCA1* cells were also sensitive to PARP inhibition relative to the wild-type with siRNA and drug experiments in cell culture and drug activity against *BRCA1* or *BRCA2* deficient embryonic stem cell mouse xenografts. They found evidence that PARP inhibition causes DNA lesions, usually repaired in wild-type cells, which lead to chromosomal instability, cell cycle arrest, and induction of apoptosis in *BRCA1* or *BRCA2* deficient cells. Therefore, the pathways cooperate to repair DNA giving a plausible mechanism for combined loss as an effective anti-cancer treatment.

Thus PARP inhibitors have potential for clinical use against *BRCA1* or *BRCA2* mutations in hereditary and sporadic cancers (Ashworth, 2008; Kaelin, Jr, 2005). PARP inhibition has been found to be effective in cancer patients carrying *BRCA1* or *BRCA2* mutations and some other ovarian cancers, suggesting synthetic lethality between PARP and other DNA repair pathways (Ström and Helleday, 2012). This supports the potential for PARP inhibition as a chemo-preventative alternative to prophylactic surgery for high-risk individuals with *BRCA1* or *BRCA2* mutations (Ström and Helleday, 2012). Hormone-based therapy has also been suggested as a chemo-preventative in such high-risk individuals and aromatase inhibitors have completed phase I clinical trials for this purpose (Bozovic-Spasojevic *et al.*, 2012). Ström and Helleday (2012) also postulate increased efficacy of PARP inhibitors in the hypoxic DNA-damaging tumour micro-environment.

A PARP inhibitor, olaparib, showed fewer adverse effects than cytotoxic chemotherapy and anti-tumour activity in various clinical trials against *BRCA1* or *BRCA2* deficient familial or sporadic breast, ovarian, and prostate cancers (Audeh *et al.*, 2010;

Fong *et al.*, 2009, 2010; Tutt *et al.*, 2010). This treatment has a favourable therapeutic window and similarly low toxicity between **mutation** carriers of *BRCA1* or *BRCA2* mutations and sporadic cases. These PARP inhibitors have been FDA approved for some cancers McLachlan *et al.* (2016), are effective against **germline mutation** and sporadic *BRCA1* or *BRCA2* mutations, and are a potential prevention alternative to prophylactic surgery for high-risk **mutation** carriers Ström and Helleday (2012).

This demonstrates the clinical impact of a well characterised system of **synthetic lethality** with known cancer risk genes. Synthetic lethality has the benefit of being effective against inactivation of **tumour suppressor** genes by any means, broader than targeting a specific oncogenic **mutation** (Kaelin, Jr, 2005). The **targeted therapy** is effective in both sporadic and **hereditary** *BRCA1* or *BRCA2* deficient **tumours** acting against an oncogenic molecular aberration across several tissues.

1.2.6 High-throughput Screening for Synthetic Lethality

RNA interference (RNAi) technologies have enabled extensive investigations of **genetic redundancy** in mammalian experimental models including testing experimentally for **synthetic lethality** (Fraser, 2004). Synthetic lethal RNAi screens are performed, using **short interfering RNA** (siRNA) or **short hairpin RNA** (shRNA) to target specific genes in isogenic cells. Identifying **synthetic lethality** is crucial to study gene function, drug mechanisms, and design novel therapies (Lum *et al.*, 2004). Candidate selection of **synthetic lethal** gene pairs relevant to cancer has shown some success but is limited because interactions are difficult to predict; they can occur between seemingly unrelated **pathways** in model organisms (Costanzo *et al.*, 2011). While biologically informed hypotheses have had some success in **synthetic lethal** discovery (Bitler *et al.*, 2015; Bryant *et al.*, 2005; Farmer *et al.*, 2005), interactions occurring indirectly between distinct pathways would be missed (Boone *et al.*, 2007; Costanzo *et al.*, 2011). Scanning the entire **genomes** for interactions against a clinically relevant gene is an emerging strategy being explored with **high-throughput** screens (Fece de la Cruz *et al.*, 2015) and computational approaches (Boucher and Jenna, 2013; van Steen, 2012).

Experimental **screening** for **synthetic lethality** is an appealing strategy for wider discovery of functional interactions *in vivo* despite many potential sources of error which must be considered. The **synthetic lethal** concept has both genetic and pharmacological screening applications to cancer research. Genetic screens, with **RNAi** to discover the specific genes involved, inform development of targeted therapies with a known mode of

action, anticipated mechanisms of resistance, and biomarkers for treatment response. RNAi is a transient knockdown of gene expression more similar to the effect of drugs than complete gene loss and is more representative of disease than model organisms (Bussey *et al.*, 2006). The RNAi gene knockdown process has inherent toxicity to some cells, potential off-target effects, and issues with a high false positive rate. Therefore, it is important to validate any candidates in a secondary screen and replicate knockdown experiments with a number of independent shRNAs. Genetic screens have potential for quantitative gene disruption experiments to selectively target over-expressed genes in cancer via synthetic dosage lethality. While powerful for understanding fundamental cellular function, analysis of isogenic cell lines is inherently limited by assuming only a single mutation differs between them despite susceptibility to “genetic drift” and cannot account for diverse genetic backgrounds or tumour heterogeneity (Fece de la Cruz *et al.*, 2015). Genetic screens thus identify targets to develop or repurpose targeted therapies for disease but alone will not directly identify a lead compound to develop for the market or clinical translation.

Chemical screens are immediately applicable to the clinic by directly screening for selective lead compounds with suitable pharmacological properties. However chemical screens lack a known mode of action, may affect many targets, and screen a narrow range of genes with existing drugs. With either approach there are many challenges translating candidates into the clinic such as finding targets relevant to a range of patients, validation of targets, accounting for a range of genetic (and epigenetic) contexts or tumour micro-environment, identifying effective synergistic combinations, enhancers of existing radiation or cytotoxic treatments, avoiding inherent or acquired drug resistance, and developing biomarkers for patients which will respond to synthetic lethal treatment, including integrating these into clinical trials and clinical practice. Identifying specific target genes is an effective way to anticipate such challenges, which can be approached with genetic screens, so we will focus on these and computational alternatives. Screening methods have proven a fruitful area of research, despite being costly, laborious, and having many different sources of error. These limitations suggest a need for complementary computational approaches to synthetic lethal discovery.

1.2.6.1 Synthetic Lethal Screens

Overexpression of genes is another suitable application for synthetic lethality since over-expressed genes cannot be distinguished from the wild-type by direct sequence specific targeted therapy. Overexpression of oncogenes, such as EGFR, MYC, and PIM1, has been found to drive many cancers. PIM1 is a candidate for synthetic lethal drug de-

sign in lymphomas and prostate cancers, where it interacts with *MYC* to drive cancer growth. van der Meer *et al.* (2014) performed an RNAi screen for synthetic lethality between *PIM1* over-expression and gene knockdown in RWPE prostate cancer cell lines. *PLK1* gene knockdown and drug inhibition was effective as a specific inhibitor of *PIM1* over-expressing prostate cells in cell culture and mouse tumour xenografts. *PLK1* inhibition reduced *MYC* expression in pre-clinical models, consistent with expression in human tumours in which *PIM1* and *PLK1* are co-expressed and correlated with tumour grade. Thus RNAi screening was valuable to identify therapeutic targets and biomarkers for patient response as demonstrated with the finding of *PLK1* as a candidate drug target against prostate cancer progression.

Heredity leiomyomatosis and renal cell carcinoma (HLRCC) is a cancer syndrome of predisposition to benign tumours in the uterus and risk of malignant cancer of the kidney attributed to inherited mutations in fumarate hydratase (*FH*). Boettcher *et al.* (2014) performed an RNAi screen on HEK293T renal cells for synthetic lethality with *FH*. They found enrichment of haem metabolism (consistent with the literature) and adenylate cyclase pathways (consistent with cyclic AMP (cAMP) dysregulation in *FH* mutant cells). Synthetic lethality between *FH* mutation and adenylate cyclases were validated with gene knockdown, drug experiments, and replicated across both HEK293T renal cells and VOK262 cells derived from a HLRCC patient, suggesting new therapeutic targets against the disease.

Similarly, hereditary diffuse gastric cancer (HDGC) is a cancer syndrome of predisposition to early-onset malignant stomach and breast cancers attributed to mutations in E-cadherin (*CDH1*). Telford *et al.* (2015) performed an RNAi screen on MCF10A cell line breast cells for synthetic lethality with *CDH1*. They found enrichment of G protein coupled receptors and cytoskeletal gene functions. The results were consistent with a concurrent drug compound screen with several candidates validated by lentiviral shRNA gene knockdown and drug testing including inhibitors of Janus kinase (JAK), histone deacetylase (HDAC), phosphoinositide 3-kinase (PI3K), aurora kinase, and tyrosine kinases. Therefore the synthetic lethal strategy has potential for clinical impact against HDGC, with an interest in interventions with low adverse effects for chemo-prevention, including repurposing existing approved drugs for activity against *CDH1* deficient cancers.

RNAi screening for synthetic lethality is also useful for functional genetics to understand drug sensitivity. Aarts *et al.* (2015) screened the WiDr colorectal cell line for synthetic lethality between *WEE1* inhibitor treatment and an RNAi library of 1206

genes with functions known to be amenable to drug treatment or important in cancer such as kinases, phosphatases, tumour suppressors, and DNA repair (a pathway *WEE1* regulates). Screening identified several synthetic lethal candidates including genes involved in cell cycle regulation, DNA replication, repair, homologous recombination, and Fanconi anaemia. Synthetic lethality with cell-cycle and DNA repair genes was consistent with the literature and validation in a panel of breast and colorectal cell lines supported checkpoint kinases, Fanconi anaemia, and homologous recombination as synthetic lethal partners of *WEE1*. These results show that synthetic lethality can be used to improve drug sensitivity as a combination treatment, especially to exploit genomic instability and DNA repair, which are known to be clinically applicable from previous results with *BRCA1* or *BRCA2* genes and PARP inhibitors (Lord *et al.*, 2015). Therefore, *WEE1* inhibitors are an example of treatment which could be repurposed with the synthetic lethal strategy. Similar findings would be valuable to clinicians as a source of biomarkers and novel treatments. While using a panel of cell lines to replicate findings across genetic background is a promising approach to ensure wide clinical application of validated synthetic lethal partners, a computational approach may be more effective as it could account for wider patient variation than scaling up intensive experiments on a wide array of cell lines and could screen beyond limited candidates from an RNAi library.

Chemical genetic screens are also a viable strategy to identify therapeutically relevant synthetic lethal interactions. Bitler *et al.* (2015) investigated *ARID1A* mutations, aberrations in chromatin remodelling known to be common in ovarian cancers, for drug response. Ovarian RMG1 cells were screened for drug response specific to *ARID1A* knockdown cells. They used *ARID1A* gene knockdown for consistent genetic background, with control experiments and 3D cell culture to ensure relevance to drug activity in the tumour micro-environment. Screening a panel of commercially available drugs targeting epigenetic regulators found *ESH2* methyltransferase inhibitors effective and specific against *ARID1A* mutation with validation in a panel of ovarian cell lines. Synthetic lethality between *ARID1A* and *ESH2* was supported by decreases in H3K27me3 epigenetic marks and markers of apoptosis in response to *ESH2* inhibitors. This was mechanistically supported with differential expression of *PIK3IP1* and association of both synthetic lethal genes with the *PIK3IP1* promoter identifying the phosphoinositide 3-kinase (PI3K)-AKT signalling pathway as disrupted when both genes were inhibited.

This successfully demonstrates the importance of **synthetic lethality** in epigenetic regulators, identifies a therapeutically relevant **synthetic lethal** interaction, and shows that chemical genetic screens could model drug response and combination therapy in cancer cells. However, this approach is limited to finding **synthetic lethal** interactions between genes with known similar function, which may not be the most suitable for **treatment**. Further limiting experiments to genes with existing targeted drugs reduces the number of **synthetic lethal** interactions detected and assumes the specificity of drugs to a particular target.

The examples above show that high-throughput screens are an effective approach to discover **synthetic lethality** in cancer with a wide range of applications. Screens are more comprehensive than hypothesis-driven candidate gene approaches and successfully find known and novel **synthetic lethal** interactions with potential for rapid clinical application. They have the power to test mode of action of drugs, find unexpected **synthetic lethal** interactions between **pathways**, or identify effective **treatment** strategies without needing a clear mechanism. However, **synthetic lethal** screens are costly, labour-intensive, error-prone, and biased towards genes with effective **RNAi** knockdown libraries. Limited genetic background, lethality to **wild-type** cell during gene knockdown, off-target effects, and difficulty replicating **synthetic lethality** across different cell lines, tissues, laboratories, or conditions stems from a high false positive rate and a lack of standardised thresholds to identify **synthetic lethality** in a high-throughput screen. Therefore there is a need for replication, validation, and alternative approaches to identify **synthetic lethal** candidates. Varied conditions between experimental screens and differences between **RNAi** and drug screens renders meta-analysis ineffective.

Genome-scale **synthetic lethal** experiments (across gene pairs) are not feasible, even in model organisms, and they typically focus on specific gene candidates or the partners of a gene of interest (such as importance in health). Therefore a computational approach is more suitable for this task and may further augment experimental screening to replicate screen candidates beyond experimental models.

1.2.7 Computational Prediction of Synthetic Lethality

1.2.7.1 Bioinformatics Approaches to Genetic Interactions

Prediction of gene interaction networks is a feasible alternative to high-throughput screening with biological importance and clinical relevance. There are many existing methods to predict gene networks, as reviewed by [van Steen \(2012\)](#) and [Boucher and Jenna \(2013\)](#) and summarised in Table 1.1. However, many of these methods have

limitations including the requirement for existing SGI data, several data inputs, and reliability of gene function annotation. Many of the existing methods also assume conservation of individual interactions between species, which has been found not to hold in yeast studies (Dixon *et al.*, 2008). Tissue specificity is important in gene regulation and gene expression, which are used as predictors of genetic interaction. However, tissue specificity of genetic interactions cannot be explored in yeast studies and has not been considered in many studies of multicellular model organisms, human networks, or cancers. Similarly, investigation into tissue specificity of PPIs , an important predictor of genetic interactions, is difficult given that high-throughput two-hybrid screens occur out of cellular context for multicellular organisms.

Table 1.1: Methods for predicting genetic interactions

| Method | Input Data | Species | Source | Tool Offered |
|--------------------------------|--|---|--|----------------|
| Between Pathways Model | PPI, SGI | <i>S. cerevisiae</i> | Kelley and Ideker (2005) | |
| Within Pathways Model | PPI, SGI | <i>S. cerevisiae</i> | Kelley and Ideker (2005) | |
| Decision Tree | PPI, expression, phenotype | <i>S. cerevisiae</i> | Wong <i>et al.</i> (2004) | 2 Hop |
| Logistic Regression | SGI, PPI, co-expression, phenotype | <i>C. elegans</i> | Zhong and Sternberg (2006) | Gene Orienteer |
| Network Sampling | SGI, PPI, GO | <i>S. cerevisiae</i> | Le Meur and Gentleman (2008) Le Meur <i>et al.</i> (2014) | SLGI(R) |
| Random Walk | GO, PPI, expression | <i>S. cerevisiae</i> <i>C. elegans</i> | Chipman and Singh (2009) | |
| Shared Function | Co-expression, PPI, text mining, phylogeny | <i>C. elegans</i> | Lee <i>et al.</i> (2010b) | WormNet |
| Logistic Regression | Co-expression, PPI, phenotype | <i>C. elegans</i> | Lee <i>et al.</i> (2010a) | GI Finder |
| Jaccard Index | GO, SGI, PPI, phenotype | Eukarya | Hoehndorf <i>et al.</i> (2013) | |
| Machine Learning | | | Pandey <i>et al.</i> (2010) | MNMC |
| Machine Learning Meta-Analysis | | | Wu <i>et al.</i> (2014) | MetaSL |
| Flux Variability Analysis | | | | |
| Flux Balance Analysis | Metabolism | <i>E. coli</i> <i>M. pneumoniae</i> | Güell <i>et al.</i> (2014) | |
| Network Simulation | | | | |

There are existing computational methods for predicting synthetic lethal gene pairs in humans with a specific interest in cancer (as summarised in 1.2). While these demonstrate the power and need for predictions of synthetic lethality in human and cancer contexts, limitations of previous methods could be met with a different approach. Existing computational approaches to synthetic lethal prediction are often difficult to interpret, replicate for new genes, or are reliant on data types not available for a wider range of genes to test.

1.2.7.2 Comparative Genomics

A comparative genomic approach by Deshpande *et al.* (2013) used the results of well characterised high-throughput mutation screens in *S. cerevisiae* as candidates for synthetic lethality in humans (Baryshnikova *et al.*, 2010a; Costanzo *et al.*, 2010, 2011; Tong

Table 1.2: Methods for predicting synthetic lethality in cancer

| Method | Input Data | Source | Tool Offered |
|---|---|--|---------------------------------------|
| Network Centrality | protein-protein interactions | Kranthi <i>et al.</i> (2013) | |
| Differential Expression | Expression Mutation | Wang and Simon (2013) | |
| Comparative Genomic Chemical-Genomic | Yeast synthetic gene interactions Homology | Heiskanen and Aittokallio (2012) | |
| Comparative Genomic | Yeast synthetic gene interactions Homology | Deshpande <i>et al.</i> (2013) | |
| Machine Learning | | Discussed by Babyak (2004) and Lee and Marcotte (2009) | |
| Differential Expression | Expression | Tiong <i>et al.</i> (2014) | |
| Literature Database | | Li <i>et al.</i> (2014) | Syn-Lethality |
| Meta-Analysis | Meta-Analysis Machine Learning | Wu <i>et al.</i> (2014) | MetaSL |
| Pathway Analysis | | Zhang <i>et al.</i> (2015) | |
| Protein Domains | Homology | Kozlov <i>et al.</i> (2015) | |
| Data-Mining | Expression | Jerby-Arnon <i>et al.</i> (2014) | |
| Machine Learning | Somatic mutation and DNA CNV siRNA in cell lines | Ryan <i>et al.</i> (2014) Crunkhorn (2014) Lokody (2014) | DAISY (method) |
| Genome Evolution | Expression | Lu <i>et al.</i> (2013) | |
| Hypothesis Test | DNA CNV | Lu <i>et al.</i> (2015) | |
| Machine Learning | Known SL | | |
| Bimodality | Expression DNA CNV Somatic Mutation | Wappett (2014) Wappett <i>et al.</i> (2016) | BiModal Subsetting ExPression (BiSEp) |
| Directional Chi-Square | Expression (microarray) Somatic mutation | Kelly, S. T., Guilford, P. J., and Black, M. A. Dissertation (Kelly, 2013) and developed here | SLIPT |

et al., 2001, 2004). Yeast synthetic lethal partners were compared to human orthologues to find cancer relevant synthetic lethal candidate pairs with direct therapeutic potential. Proposed as a complementary approach to siRNA screens, approximately 24,000 of the 116,000 negative SGI in yeast (Costanzo *et al.*, 2011) were matched to human orthologues, with over 500 involving a cancer gene (Futreal *et al.*, 2004). Under strict criteria of one-to-one orthologues, large effect size and significant interaction in yeast data ($\epsilon < -0.2$, $p < 0.05$), 1522 interactions were identified with 70 involving cancer genes. Of the 21 gene interactions tested with pairs of siRNA in IMR1 fibroblast cells, 6 exhibited synthetic lethal effects. The two strongest interactions (*SMARCB1* with *PSMA4* and *ASPSCR1* with *PSMC2*) were successfully validated by protein analysis of human cells and replication with tetrad analysis for yeast orthologues.

Another approach to systematic synthetic lethality discovery specific to human cancer (in contrast to the plethora of yeast synthetic lethality data) was to build a database as done by Li *et al.* (2014). In their relational database, called “Syn-lethality”, they have curated both known experimentally discovered synthetic lethal pairs in humans (113 pairs) from the literature and those predicted from synthetic lethality between orthologous genes in *S. cerevisiae* yeast (1114 pairs). This knowledge-based database

is the first dedicated to human cancer [synthetic lethal](#) interactions and integrates gene function annotation, [pathway](#) and molecular mechanism data with experimental and predicted [synthetic lethal](#) gene pairs. This combination of data sources is intended to tackle the trade-off between more conclusive [synthetic lethal](#) experiments in yeast and more clinically relevant [synthetic lethal](#) experiments in human cancer models, such as [RNAi](#), especially when high-throughput screens are costly and prone to false positives in either system and difficult to replicate across gene backgrounds. This database centralises a wealth of knowledge scattered in the literature including cancer relevant genes , including the previously mentioned interactions of *BRCA1* and *BRCA2* with *PARP1* and *TP53* with *WEE1* and *PLK1*, although the computational methodology was not released and was limited to 647 human genes. Their future directions were promising, such as constructing networks of known [synthetic lethality](#), applying known [synthetic lethality](#) to cancer [treatment](#), data mining, replicating the approach for [synthetic lethality](#) in model organisms, signalling pathways, and developing a complete global network in human cancer or yeast (both of which are still incomplete with experimental data), some of which has been implemented in “SynLethDB” ([Guo et al., 2016](#)).

Table 1.3: Machine Learning Methods used by [Wu et al. \(2014\)](#)

| Method | Source | Tool Offered |
|---|--------------------------------------|--------------|
| Random Forest | Breiman (2001) | |
| Random Forest | | |
| J48 (decision tree) | | |
| Bayes (Log Regression) | | |
| Bayes (Network) | Hall et al. (2009) | WEKA |
| PART (Rule-based) | | |
| RBF Network | | |
| Bagging / Bootstrap | | |
| Classification via Regression | | |
| Support Vector Machine (Linear) | Vapnik (1995) | |
| Support Vector Machine (RBF – Gaussian) | Joachims (1999) | |
| Multi-Network Multi-Class (MNMC) | Pandey et al. (2010) | |
| MetaSL (Meta-Analysis) | Wu et al. (2014) | MetaSL |

Machine learning approaches have also been explored for [synthetic lethal](#) discovery ([Babyak, 2004; Lee and Marcotte, 2009](#)). Due to concerns that these may be subject

to overfitting or noise, Wu *et al.* (2014) developed a meta-analysis method (based on the machine learning methods in Table 1.3). They focused on synthetic lethal gene pairs relevant to developing selective drugs against human cancer, building upon their previous database (Li *et al.*, 2014). Their “metaSL” approach utilises genomic, proteomic and annotation data and had a high statistical performance in yeast data with an area under receiver operating characteristic (ROC) (AUROC) of 0.871. They predicted orthologous synthetic lethal partners in human data were not experimentally validated but some were relevant to cancer such as *EGFR* with *PRKCZ*.

Computational approaches scale-up across the genomes at lower cost than experimental screen (Wu *et al.*, 2014). Wu *et al.* (2014) provided their most supported interactions online but the method is not available for analysis of other genes. Syn-Lethality (Li *et al.*, 2014) and MetaSL (Wu *et al.*, 2014) demonstrate the value of computational approaches to synthetic lethality but omit many genes of importance in cancer, such as *CDH1*. Accordingly, there remains a need to enable biological researchers to query further genes and do so in a particular tissue or genetic background.

There is also concern for analyses based on yeast data that many synthetic lethal interactions may not be conserved between species Dixon *et al.* (2009), although interactions between pathways may be more comparable. It is unsurprising that many of the interactions identified were not experimentally validated. There have been many gene duplications in the separate evolutionary histories of humans and yeast which may lead to differences in genetic redundancy. Yeast are not an ideal human cancer model because they do not have tissue specificity, multicellular gene regulation, or orthologues to several known cancer genes such as p53. Although these studies have tried to anticipate these issues with stringent criteria such as requiring one-to-one orthologues, there remains the possibility that changes in gene function may affect whether these are solely redundant such as if functions had co-evolved without sequence homology. Many genes will also be excluded since they lack homologues in yeast, the corresponding experimental data, or having paralogues in either species. Thus conservation of yeast interactions is not an ideal strategy and analysis of human data directly for comparison with human experimental data will be the focus of this thesis.

1.2.7.3 Analysis and Modelling of Protein Data

Kranthi *et al.* (2013) took a network approach to discovery of synthetic lethal candidate selection applying the concept to “centrality” to a human PPI network involving interacting partners of known cancer genes. The effect of removing pairs of genes on connectivity of the network was used as a surrogate for viability which is supported by

observations that the PPI and synthetic lethal networks are orthogonal in *S. cerevisiae* studies (Tong *et al.*, 2004). They showed that the human cancer protein interaction network (of 1539 proteins and 6471 interactions) exhibits the power law distribution expected of a scale-free synthetic lethal network with high connectivity (average vertex degree of 23.67 and network efficiency of 0.2952). Their top 100 candidate interactions included interactions of the tumour suppressor *TP53* with *BRCA1*, *CDKNA1*, *CDKNA2*, *MET*, and *RB1* which have been detected by prior studies. The gene pairs were often observed to be in the same or a plausible compensatory pathway. Thus the network structure is important in the biological functions of cancers and could be exploited for targeting *TP53* loss of function mutations.

However, their approach was limited to known cancer genes and is not applicable to genes that do not have PPI data. Other nucleotide sequencing data types are more commonly available for cancer studies at a genomic scale. Of further concern is that the results were enriched for p53 synthetic lethal partners which is relevant to many cancer researchers but this genomes-wide approach did not detect many other cancer genes due to multiple testing. This enrichment may be due to the known drastic effect of removing p53 itself from the network as a master regulator, cancer driving tumour suppressor gene, and highly connected network “hub”. The focus on cancer genes is useful for translation into therapeutics but does not account for variable genetic backgrounds or effect of protein removal on the cellular network.

Focusing on the potential for synthetic lethality to be an effective anti-cancer drug target, Zhang *et al.* (2015) used modelling of signalling pathways to identify synthetic lethal interactions between known drug targets and cancer genes by simulating gene knockdowns. A computational approach was applied to avoid the limitations of experimental RNAi screens such as scale, instability of knockdown, and off-target effects. This ‘hybrid’ method of a data-driven model and known signalling pathways showed potential to predict cell death in single and combination gene knockouts. They used time series protein phosphorylation data (Lee *et al.*, 2012) for 28 signalling proteins and Gene Ontology (GO) pathways Ashburner *et al.* (2000); Blake *et al.* (2015). This approach successfully detected many known essential genes in the human gene essentiality database, known synthetic lethal partners in the Syn-Lethality database (Li *et al.*, 2014), and predicted novel synthetic lethal gene pairs.

These novel results contained many *TP53* and AKT synthetic lethal partners (Zhang *et al.*, 2015), genes known to be important in many cancers. However these also have a severe impact on the signalling pathways in their essentiality analysis of single

gene disruptions and large phenotypic changes in cancer. This approach is amenable to detect functionally related pathways and protein complexes across the molecular function, cellular component, and biological process annotations provided by GO. The results were consistent with the experimental results in the literature but the novel synthetic lethal interactions have yet to be validated. While the mathematical reasoning and algorithms are given, the code was not released to replicate the findings or apply the methodology beyond the signalling pathways analysed by Zhang *et al.* (2015). While this is an interesting approach, the analysis of this thesis will focus on gene expression and RNAi data which is available to test a wider range of candidate gene pairs.

1.2.7.4 Differential Gene Expression

Differential gene expression has been explored to predict synthetic lethal pairs in cancer which would be widely applicable due to the availability of public gene expression data for many samples and cancer types. Wang and Simon (2013) found differentially expressed genes (by the t-test, adjusted by False discovery rate (FDR)) between tumours with or without functional p53 mutations in TCGA (McLendon *et al.*, 2008) and Cancer Cell Line Encyclopaedia (CCLE) (Barretina *et al.*, 2012) RNA-Seq gene expression data as candidate synthetic lethal partner pathways of p53. They identified 2, 8, and 21 candidate synthetic lethal partner genes in 3 microarray datasets from the NCI60 cell lines, 31 partner genes from the CCLE RNA-Seq data (Barretina *et al.*, 2012), and 50 in TCGA RNA-Seq data (Muzny *et al.*, 2012). *PLK1* was replicated across 4 of these analyses and 17 other genes were replicated across 2 analyses (including *MTOR*, *PLK4*, *MAST2*, *MAP3K4*, *AURKA*, *BUB1* and 6 CDK genes) with many playing a role in cell cycle regulation. This was supported by a drug sensitivity experiment on the NCI60 cell lines which found that cells which lacked functional p53 were more sensitive to paclitaxel (which targets *PLK1*, *AURKA*, and *BUB1*). This demonstrated the potential of gene expression as a surrogate for gene function and use of public genomic data to predict synthetic lethal gene pairs in cancer. Wang and Simon (2013) advocated for pre-screening of expression profiles to augment future RNAi screens. However, the analyses were limited to kinase genes and focused on currently druggable genes, lacking wider application of synthetic lethal prediction methodology. This approach may not be feasible or applicable in cancer genes with a lower mutation rate than p53.

Tiong *et al.* (2014) also investigated gene expression as a predictor of synthetic lethal pairs with colorectal cancer microarrays from a Han Chinese population with a

sample size of 70 tumour and 12 normal tissue samples. Simultaneously differentially expression of “tumour dependent” gene pairs (which includes co-expression) between cancer and normal tissue was used to rank 663 candidate synthetic lethal interactions identified in cell line siRNA experiments. Of the top 20 genes, 17 were tested for differential expression at the protein level with immunohistochemistry staining and correlation with clinical characteristics, with 11 pairs exhibiting synergistic effects. Some of the predicted synthetic lethal pairs were consistent with the literature (including TP53 with S6K1 and partners of KRAS, PTEN, BRCA1, and BRCA2) and two novel synthetic lethal interactions (TP53 with CSNK1E and CTNNB1) were validated in pre-clinical models. This serves a valuable proof-of-concept for integration of *in silico* approaches to synthetic lethal discovery in cancer demonstrating its utility to triage and identify synthetic lethal partners of p53 applicable to colorectal tissues. Although the experimental work was the focus of the paper, these findings show that bioinformatics synthetic lethal candidates can be validated in patient tissue samples to find those applicable to colorectal cancers (including in a non-Caucasian population) .

1.2.7.5 Data Mining and Machine Learning

Recognising the utility of synthetic lethality to drug inhibition and specificity of anti-cancer treatments, Jerby-Arnon *et al.* (2014) also saw the need for effective prediction of gene essentiality and synthetic lethality to augment experimental studies of SL. They developed the DAData mIning SYnthetic lethal identification pipeline (DAISY), a data-driven approach for genomes-wide analysis of synthetic lethality in public cancer genomics data from TCGA and CCLE (Barretina *et al.*, 2012). DAISY is intended to predict the candidate synthetic lethal partners of a query gene such as genes recurrently mutated in cancer.

Jerby-Arnon *et al.* (2014) combined a computational approach to triage candidates with a conventional RNAi screen to validate synthetic lethal partners. They screened a selection of computationally predicted candidates and randomly selected genes with RNAi against VHL loss of function mutation in RCC4 renal cell lines. The computational method had a high AUROC of 0.779 and predictions were enriched 4× for validated RNAi hits over randomly selected genes. This approach detected known synthetic lethal pairs such as BRCA1 or BRCA2 genes with PARP1 and MSH2 with DHFR. The synthetic lethal candidates identified with both RNAi screening and computational prediction formed an extensive network of 2077 genes with 2816 synthetic lethal interactions and similar network of 3158 genes with 3635 synthetic dosage lethal interactions (for synthetic lethality with over-expression). Each network was scale-free

as expected of a biological network and was enriched for known cancer genes, essential genes in mice, and could be harnessed for predicting prognosis and drug response. While demonstrating the feasibility of combining experimental and computational approaches to synthetic lethality in cancer, there remain challenges in predicting synthetic lethal genes, novel drug targets, and translation into the clinic.

The DAISY methodology (Jerby-Arnon *et al.*, 2014) compares the results of analysis of several data types to predict synthetic lethality, namely: DNA copy number and somatic mutation mutation for TCGA patient samples and CCLE cell lines. The cell lines were also analysed with gene expression and gene essentiality (shRNA screening) profiles. Genes were classed as inactivated by copy number deletion, somatic mutation loss of function mutation, or low expression and tested for synthetic lethal gene partners which are either essential in screens or not deleted with copy number variants. Co-expression is also used for synthetic lethality prediction based on studies in yeast (Costanzo *et al.*, 2010; Kelley and Ideker, 2005). Copy number, gene expression and, essentiality analyses are stringently compared by adjusting each for multiple tests with Bonferroni correction and only taking candidates identified in all analyses. This methodology was also adapted for synthetic dosage lethality by testing for partner genes where genes are overactive with high copy number or expression. As discussed above, the predictions performed well and an RNAi screen for the example of *VHL* in renal cancer validated predicted synthetic lethal partners of *VHL* demonstrating the feasibility of combining approaches to synthetic lethal discovery in cancer and using computational predictions to enable more efficient high-throughput screening. DAISY performs well statistically with a AUROC of 0.779 on a set of gene pairs with experimental screen data, although co-expression and shRNA functional examination contributes much less of this than the mutation and copy number analysis (AUROC 0.683 alone). However, this methodology is very stringent, missing potentially valuable synthetic lethal candidates, may not be applicable to genes of interest to other groups and the software for the procedure has not been publicly released for replication.

Although the DAISY procedure performs well and has been well received by the scientific community (Crunkhorn, 2014; Lokody, 2014; Ryan *et al.*, 2014), showing a need for such methodology, there is no indication of adoption of the methodology in the community yet. The co-expression analysis may not be the most effective way to test gene expression for directional synthetic lethal interactions (where inverse correlation would be expected). In the interests of a large sample size, tissue types were not tested separately despite tissue-specific synthetic lethality being likely since gene function (and

by extension [expression](#), isoforms, and clinical characteristics) in cancers may often be tissue-dependent. Some data forms and analyses used, such as gene essentiality, may not be available for all cancers, genes, or tissues, and may not be reproduced.

[Lu et al. \(2015\)](#) critique the assumption of co-expression in the [DAISY](#) methodology and propose an alternative computational prediction of [synthetic lethality](#) based on machine learning methods and a “cancer [genomes](#) evolution” hypothesis. Using [DNA copy number](#) and [gene expression](#) data from [TCGA](#) patient samples, a cancer [genomes](#) evolution model assumes that [synthetic lethal](#) gene pairs behave in two distinct ways in response to an inactive [synthetic lethal](#) partner gene, either a “compensation” pattern where the other [synthetic lethal](#) partner is overactive or a “co-loss underrepresentation” pattern where the other [synthetic lethal](#) partner is less likely to be lost, since loss of both genes would cause death of the cancer cell. During the [genomes](#) evolution of cancers, the cell becomes addicted to the remaining [synthetic lethal](#) partner due to induced gene essentiality. These patterns would explain why [DAISY](#) detects only a small number of [synthetic lethal](#) pairs, compared to the large number expected based on model organism studies ([Boone et al., 2007](#)), and the disparity between screening and computationally predicted [synthetic lethal](#) candidates due to testing different classes of [synthetic lethal](#) gene pairs.

[Lu et al. \(2015\)](#) compared a [genomes](#)-wide computational model of [genomes](#) evolution and [gene expression](#) patterns to the experimental data of [Vizeacoumar et al. \(2013\)](#) and [Laufer et al. \(2013\)](#). This simpler model performing well with an [AUROC](#) of 0.751 but was less than [DAISY](#), although it did not rely on data from cell lines which may not represent patient disease. They predict a larger comprehensive list of 591,000 human [synthetic lethal](#) partners with a probability score threshold of 0.81, giving a precision of 67% and 14 \times enrichment of [synthetic lethal](#) true positives compared to randomly selected gene pairs. Discovery of such a vast number of cancer-relevant [synthetic lethal](#) interactions in humans would not be feasible experimentally and is a valuable resource for research and clinical applications. These predictions are not limited by assuming co-expression of [synthetic lethal](#) partners or evolutionary conservation with model organisms enabling wider [synthetic lethal](#) discovery. However, there remains a lack of basis for an expectation of how many [synthetic lethal](#) partners a particular gene will have, how many pairs there are in the human [genomes](#), and whether [pathways](#) or correlation structure would influence predicted [synthetic lethal](#) partners.

Large scale, computational approaches have yet to determine whether [synthetic lethal](#) interactions are tissue-specific since [Lu et al. \(2015\)](#) used pan-cancer data for

14136 patients with 31 cancer types. Experimental data used for comparison was a small training dataset specific to colorectal cancer, and based on screens for other phenotypes, which may limit performance of the model or application to other cancers. Proposed expansion of the computational approach to **mutation**, **microRNA**, or epigenetic modulation of gene function and tumour micro-environment or heterogeneity suggests that **synthetic lethal** discovery could be widely applied to the current challenges in cancer **genomics**. This approach was also based on machine learning methodology and not supported by a software release for the community to develop, contribute to, or reproduce beyond the gene pairs given in the supplementary results.

1.2.7.6 Mutually Exclusive Bimodality

Wappett *et al.* (2016) demonstrate a multi-omic approach to identification of **synthetic lethality** in cancer with a strategy to detect bimodal patterns in **molecular profiles**. They released this solution as the **BiSEp** R package Wappett (2014) which aims to detect subtle bimodal and non-normal patterns in **expression** data. Since loss of gene function is not consistently genetic. Wappett *et al.* (2016) advocate the use of **gene expression** (loss of **mRNA**) and deletion (loss of **copy number**) data in addition to **mutation**. The **BiSEp** procedure was demonstrated on an analysis of 881 cell lines from **CCLE** (Barretina *et al.*, 2012), 442 cell lines from **COSMIC** (Forbes *et al.*, 2015), and **RNA-Seq by Expectation Maximization (RSEM)** normalised **RNA-Seq** data for 178 **TCGA** lung patient samples (Collisson *et al.*, 2014). **BiSEp** was demonstrated to have significant enrichment of validated **tumour suppressor**, **synthetic lethal** gene pairs (detecting 76 experimentally supported gene pairs) and was improved (detecting 420) with **expression** data rather than relying on detecting loss of gene function by **mutation** or deletion. They identified interactions with genes relevant to cancer with support in experimental screens including *ERCC4* with *XRCC1*, *BRCA1* with *PARP3*, and *SMARCA1* with *SMARCA4*.

Wappett *et al.* (2016) demonstrated that analysis of **genomics** data, particularly **expression** data, is relevant to augment the identification of **synthetic lethal** interactions with screening experiments. They further show that this is applicable in both genetically homogeneous cell lines and heterogeneous cell population from patient samples. This approach is limited however to genes which exhibit bimodal **expression** patterns which do not commonly occur, particularly in normalised **gene expression** data, and other approaches may need to be considered for gene such as *CDH1* which were not identified by **BiSEp**.

1.2.7.7 Rationale for Further Development

Many of the approaches discussed here aimed to identify the strongest synthetic lethal pairs across the yeast or human genomes (Deshpande *et al.*, 2013; Lu *et al.*, 2015; Wappett *et al.*, 2016; Wu *et al.*, 2014), which may not be an ideal strategy to identify interactions in particular functions or relevance to particular cancers. These demonstrate a need for computational approaches to prioritise candidate gene pairs for validation but this thesis will focus on the interactions with *CDH1* with importance in breast and stomach cancers, although these partners may be applicable in other cancers. As such, this thesis presents a query-based method, amenable to identification of candidate partners for a selected gene of functional or translational importance such as *CDH1*.

1.3 E-cadherin as a Synthetic Lethal Target

E-cadherin is a transmembrane protein (encoded by *CDH1*) with several characterised functions in the cytoskeleton and cell-to-cell signalling. Here we outline the characterised functions of E-cadherin and its importance in cancer biology. *CDH1* is a tumour suppressor gene, with loss of function occurring in both familial (germline mutation mutations) and sporadic (somatic mutation mutations) cancers. As such, *CDH1* inactivation is a prime example of a genetic event that could be targeted by synthetic lethality for anti-cancer treatments. Most notably this includes patients at risk of developing hereditary breast and stomach cancers for which conventional surgical or cytotoxic chemotherapy is not ideal and who have a known genetic aberration in their familial syndromic cancers. Effective treatments against *CDH1* inactivation would also benefit patients with sporadic diffuse gastric cancers since they often present with symptoms at a late stage.

1.3.1 The *CDH1* gene and its Biological Functions

The tumour suppressor gene *CDH1* is implicated in hereditary and sporadic lobular breast cancers (Berx *et al.*, 1996; Berx and van Roy, 2009; De Leeuw *et al.*, 1997; Masciari *et al.*, 2007; Semb and Christofori, 1998; Vos *et al.*, 1997). The *CDH1* gene encodes the E-cadherin protein and is normally expressed in epithelial tissues, where it has also been identified as an invasion suppressor and loss of *CDH1* function has been implicated in breast cancer progression and metastasis (Becker *et al.*, 1994; Berx *et al.*, 1995; Christofori and Semb, 1999).

1.3.1.1 Cytoskeleton

The primary function of *CDH1* is cell-cell adhesion forming the adherens junction, maintaining the cytoskeleton and mediating molecular signals between cells. The function of the adherens complex is particularly important for cell structure and regulation because it interacts with cytoskeletal actins and microtubules. The cytoskeletal role of **E-cadherin** maintains healthy cellular viability and growth in epithelial tissues including cellular polarity (Jeanes *et al.*, 2008). **E-cadherin** is not essential to cellular viability but loss in epithelial cells does lead to defects in cytoskeletal structure and proliferation. In addition to a central role in the adherens complex, **E-cadherin** is involved in many other cellular functions and thus *CDH1* is regarded as a highly pleiotropic gene (Kroepil *et al.*, 2012).

1.3.1.2 Extracellular and Tumour Micro-environment

As a transmembrane signalling protein **E-cadherin** also interacts with the extracellular environment and other cells, most notably forming tight junctions between cells (Chen *et al.*, 2014; Tunggal *et al.*, 2005). These junctions serve to both regulate movement of ion signals between cells and separate membrane proteins on the apical and basal surfaces of a cell, maintaining cell polarity. Thus **E-cadherin** is an important regulator of epithelial tissues by intercellular communication (Jeanes *et al.*, 2008). It also has important roles in the extracellular matrix, including fibrin clot formation. The role of intercellular interactions and the tissue micro-environment are important themes in cancer research, being a potential mechanism for cancer progression and malignancy in addition to its potential for specifically targeting tumour cells.

1.3.1.3 Cell-Cell Adhesion and Signalling

The signals mediated by tight junctions are also passed on to intracellular signalling pathways and thus **E-cadherin** also has a role in maintaining cellular function and growth. One such example is the regulation of β -catenin which interacts with both the actin cytoskeleton and acts as a transcription factor via the Wingless-related integration site (WNT) pathway (Jeanes *et al.*, 2008). Similarly, the Hippo and PI3K/AKT pathways are implicated in being mediated by **E-cadherin** (De Santis *et al.*, 2009; Kim *et al.*, 2011), having roles in promoting cell survival, proliferation, and repressing apoptosis. **E-cadherin** shares several downstream pathways with signalling pathways such as integrins and thus indirectly interacts with them, particularly since feedback loops may occur in such pathways. Conversely, the multifaceted roles of **E-cadherin** have been shown with over-expression in ovarian cells promoting tumour growth, while it

maintains healthy cellular functions in other cells (Brouxhon *et al.*, 2014; Dong *et al.*, 2012).

1.3.2 *CDH1* as a Tumour (and Invasion) Suppressor

E-cadherin has key roles in maintaining cellular structure and regulating growth, consistent with *CDH1* being a tumour suppressor gene. Loss of *CDH1* in epithelial tissues leads to disrupted cell polarity, differentiation, and migration. E-cadherin loss has been identified as a recurrent driver tumour suppressor mutation in sporadic cancers of many tissues including breast, stomach, lung, colon, and pancreas tissue.

1.3.2.1 Breast Cancers and Invasion

E-cadherin loss in breast cancers has been shown to cause increased proliferation, lymph node invasion, and metastasis with poor cell-cell contact. Thus *CDH1* gene has also been implicated as an invasion suppressor, with a key role in the epithelial-mesenchymal transition (EMT), an established mechanism of cancer progression (Hanahan and Weinberg, 2011). The epithelial-mesenchymal transition is important during development and wound healing but such changes in cellular differentiation also occur in cancers. If *CDH1* is inactivated by mutation or DNA methylation (Berx *et al.*, 1996; Guilford, 1999; Machado *et al.*, 2001), it is likely that EMT will drive growth of E-cadherin deficient cancers (Berx and van Roy, 2009; Graziano *et al.*, 2003; Polyak and Weinberg, 2009). While loss of E-cadherin is not sufficient to cause EMT or tumorigenesis, it is an important step in this mechanism of tumour progression and a potential therapeutic intervention may therefore also impede cancer progression and have activity against advanced stage cancers.

1.3.3 Hereditary Diffuse Gastric Cancer and Lobular Breast Cancer

CDH1 loss of function mutations also causes familial cancers, including diffuse gastric cancer and lobular breast cancer (Graziano *et al.*, 2003; Guilford *et al.*, 2010, 1999; Oliveira *et al.*, 2009). Individuals carrying a null mutation in *CDH1* have a syndromic predisposition to early-onset these cancers, known as hereditary diffuse gastric cancer (HDGC) (Guilford *et al.*, 1998). Due to the loss of an allele, these individuals are prone to carcinogenic lesion in the breast and stomach when the other allele is inactivated, occurring much more frequently and thus younger than in individuals without a second functional allele of *CDH1*. The loss of the second allele is most often hypermethylation suppressing expression rather than mutation (Grady *et al.*, 2000; Machado *et al.*, 2001;

Oliveira *et al.*, 2009), although loss of heterozygosity may also occur (Guilford *et al.*, 2010). Therefore HDGC is an autosomal dominant cancer syndrome with incomplete penetrance. The “lifetime” (until age 80 years) risk for mutation carriers of diffuse gastric cancer is 70% in males and 56% in females (Hansford *et al.*, 2015; van der Post *et al.*, 2015). In addition, the lifetime risk of lobular breast cancer is 42% in female mutation carriers.

HDGC affects less than 1 in a million people globally (Ferlay *et al.*, 2015) and less than 1% of gastric cancers. However, HDGC is documented to affect several hundred families globally. E-cadherin mutations in the germline mutation is implicated in 1-3% of gastric cancers presenting with a family history, varying between high and low incidence populations. E-cadherin is also mutated in 13% of sporadic gastric cancers.

While diagnostic testing for *CDH1* genotype has enabled more effective management of HDGC and improved patient outcomes, there are still limited options for clinical interventions (Guilford *et al.*, 2010). Individuals with a family history of HDGC are recommended to be tested for *CDH1* mutations in late adolescence and are offered prophylactic stomach surgery before the risk of developing cancers increases with age. Another option is annual endoscopic screening to diagnose early stage stomach cancers with surgical intervention once they are detected (Oliveira *et al.*, 2013). However, these early stage cancers are difficult to detect and may be missed in regular screening. Thus patients carrying *CDH1* mutations either have surgical interventions with a significant impact on quality of life and risk of complications or remain at risk of developing advanced stage stomach cancers. Due to the lower mortality rate due to stomach cancers, there is increasing concerns among these HDGC families on the elevated risk of lobular breast cancers for women later in life.

The current clinical management of HDGC still has significant risks for patients and therefore a greater understanding of the molecular and cellular function of *CDH1* is important for its role in these cancers. Such studies may lead to alternative treatment strategies such as pharmacological treatments with specificity against *CDH1* null cells, once they lose the second allele. While a loss of gene function cannot be targeted directly, designing a treatment with specificity against *CDH1* may also have activity in sporadic cancers in a range of epithelial cancers. Thus an effective treatment against *CDH1* mutant cancers would potentially have significant therapeutic and preventative applications in a large number of patients.

1.3.4 Cell Line Models of *CDH1* Null Mutations

Previous work our research group has published used a model of homozygous *CDH1*^{-/-} null mutation in non-malignant MCF10A cell line breast cells to show that loss of *CDH1* alone was not sufficient to induce EMT with compensatory changes in the expression of other cell adhesion genes occurring (Chen *et al.*, 2014). However, *CDH1* deficient cells did manifest changes in morphology, migration, and weaker cell adhesion (Chen *et al.*, 2014).

This *CDH1*^{-/-} MCF10A cell line model has been used in a genomes-wide screen of 18,120 genes using siRNA and a complementary drug screen using 4057 compounds to identify synthetic lethal partners to E-cadherin (Telford *et al.*, 2015). One of the strongest candidate pathways identified by Telford *et al.* (2015) were the G protein coupled receptor (GPCR) signalling cascades, which were highly enriched by GO analysis of the candidate synthetic lethal partners the primary siRNA screen. This was supported by validation with Pertussis toxin, known to target G_{αi} signalling (Clark, 2004), as were various candidate cytoskeletal pathways by inhibition of Janus kinase (JAK) and aurora kinase. The drug screen also produced candidates in histone deacetylase (HDAC) and PI3K which were supported by validation and time course experiments.

1.4 Summary and Research Direction of Thesis

Genomic technologies and the data available from them have immense potential for understanding of genetics and improving healthcare, including identification of genes altered in cancer for molecular diagnosis, prognostic biomarkers, and therapeutic targets. This has been demonstrated with the identification of cancer genes in many cancers, distinguishing tumour subtypes by expression profiles, and the development of targeted therapies against oncogenes (such as *BRAF*) and tumour suppressors (such as *BRCA1*). Synthetic lethality is an important genetic interaction to study fundamental cellular functions and exploit them for biomarkers and cancer treatment. They present a means to target loss of function mutations and genetic dysregulation in tumour suppressor genes by identifying interacting partners with redundant or compensating molecular functions.

CDH1 (encoding E-cadherin) is an example of a tumour suppressor gene implicated in sporadic breast and stomach cancers. Germline mutations in *CDH1* are also found in many patients with familial early onset cancers (HDGC). Discovery of synthetic lethal partners would contribute to an understanding on the molecular mechanisms driving the growth of *CDH1* deficient tumours and identification of potential therapeutic

targets or **chemopreventative** agents for management of **HDGC**. The clinical potential of the **synthetic lethal** approach has been demonstrated with the application of olaparib against *BRCA1* and *BRCA2* mutations Lord *et al.* (2015) but there remains the need to systematically identify **synthetic lethal** partner genes for other **tumour suppressors** such as *CDH1*. A **synthetic lethal** screen has been conducted on breast cell lines Telford *et al.* (2015) but computational approaches to identification of **synthetic lethal** partners of *CDH1* remains to be done.

While there are a wide range of experimental and computational approaches to **synthetic lethal** discovery, many are limited to particular applications, prone to false positives, inconsistent across independent approaches, or enriched for particular genes of interest. Therefore **synthetic lethal** interactions are difficult to replicate or apply in the clinic. Computational approaches to **synthetic lethality** are not widely adopted by the cancer research community and experimental approaches cannot be combined to study **synthetic lethality** at a **genomes-wide** scale. However, these show interest in **synthetic lethal** discovery in the community and the need for robust predictions of **synthetic lethal** interactions in cancer and human tissues.

Effective screening, prediction, and analysis of **synthetic lethal** interactions are a crucial part of developing next generation anti-cancer strategies. Therefore, we propose developing a computational statistical procedure to identify **synthetic lethal** interactions and construct gene networks. This will enable the development of personalised medicine targeted to particular molecular aberrations. Genetic tests and **genomic** have the potential to revolutionise cancer screening, **diagnosis**, and prognostics; **targeted therapeutic**, similarly, have applications in prevention and therapy of **sporadic** or **hereditary** cancers with known molecular properties.

To address the concerns raised by recent computational approaches to **synthetic lethal** discovery in cancer (Jerby-Arnon *et al.*, 2014; Lu *et al.*, 2015; Wappett *et al.*, 2016), I present similar analysis using solely **gene expression** data which is widely available for a large number of samples in many different cancers. This uses a statistical methodology the **SLIPT** developed for this purpose. To further determine the limitations and implications of **synthetic lethal** predictions, modelling and simulation was performed upon the statistical behaviour of **synthetic lethal** gene pairs in **genomics** data. Comparison of **synthetic lethal** gene candidates from public data analysis and experimental candidates, pathway analysis, and networks structure will also be presented to investigate the relationships between **synthetic lethal** candidates. Release of R codes used for simulation, prediction, and analysis will enable adoption of the methodology

in the cancer research community and comparison to existing methods. Therefore my thesis aims to develop such predictions for **synthetic lethal** partner genes with a focus on the example of **E-cadherin** to compare to the findings of **Telford et al.** (2015), develop of network approaches for **pathway** structure, and simulate **gene expression** on **pathway** structure with the **bioinformatics** and **computational biology** investigations.

1.4.1 Thesis Aims

Understanding **synthetic lethality** is important in cancers, having shown an impact clinical practice and patient outcomes for certain genes already. Thus this thesis aims to identify **synthetic lethal** gene pairs using public **gene expression** data. Accordingly, chapter **3** aims to develop the methods to do so including a **synthetic lethal** detection methodology (**SLIPT**) and its release as an R software package. This chapter also serves to document the original simulation and network analysis procedures developed to support the use of **SLIPT** and perform analyses in throughout this thesis.

This thesis also aims to demonstrate **SLIPT** methodology for analysis of **RNA-Seq** **gene expression** data. Chapter **4** aimed to do so by performing an analysis to identify candidate **synthetic lethal** gene partners of **CDH1** in public breast and stomach cancer data (**Bass et al.**, 2014; **TCGA**, 2012). Chapter **4** also aimed to demonstrate the biological relevance of these candidate **synthetic lethal** partners by identifying **synthetic lethal** pathways and comparing them with the results of an experimental **siRNA** screen (**Telford et al.**, 2015).

Pathway analysis was extended with **graph** structures in chapter **5** which aimed to assess the importance of **synthetic lethal** genes within **pathway** structures. Chapter **5** also aimed to use **pathway** structure to identify directional relationships between **SLIPT** and **siRNA synthetic lethal** candidates and explore the disparity between them. The **SLIPT** methodology was also supported by simulations investigations in chapters **3** and **6** which aimed to evaluate the **SLIPT** method on detecting known **synthetic lethal** genes in simulated data. Graph structures were also used in chapter **6** which also aimed to determine the effect of **pathway** structures of **synthetic lethal** detection with **SLIPT** in simulated data and ascertain that the simulation results were comparable to **expression** data with contains complex correlation structures within biological pathways.

Chapter 2

Methods and Resources

In this Chapter, I will outline the various existing resources and methods utilised throughout this project. This includes public data repositories, stable and development releases of software packages (mostly for the R programming environment), and implementation of [bioinformatics](#) methods and statistical concepts with Shell or R scripts developed for this purpose. Methods and packages developed specifically for this project will be covered in more detail along with preliminary data to demonstrate and support their use in Chapter 3.

2.1 Bioinformatics Resources for Genomics Research

2.1.1 Public Data and Software Packages

Various [bioinformatics](#) resources, such as databases and methods, have become integral parts of genetics and [genomics](#) research. Reference [genomes](#), genotyped variants, [gene expression](#), and epigenetics profiles are among the most commonly used resources. [Gene expression](#) data in particular is widely available from many [microarray](#) and [RNA-Seq](#) studies, from repositories such as Gene Expression Omnibus (GEO) (Clough and Barrett, 2016), caArray (Heiskanen *et al.*, 2014), and ArrayExpress (Rustici *et al.*, 2013). Such profiles are excellent resources to examine the changes of [gene expression](#) occurring in cancers and the variation between samples. These [microarray](#) initiatives have set a precedent for data sharing, data mining, and the wider benefits of publicly available data for enabling the scientific community to further utilise the data rather than a single research group or consortium (Rung and Brazma, 2013). The practice of integrating findings from publicly available [genomics](#) data with the research questions and experimental results of individual research groups has carried over into [RNA-Seq](#)

datasets including the large-scale cancer genomics projects (Zhang *et al.*, 2011). This thesis is one such example of an investigation enabled by this wider movement and tools developed in various disciplines to generate, process, and disseminate genomic-scale data.

Along with databases, it is also becoming common practice for bioinformatics researchers to release their code as open-source or provide a software package to enable replication of the findings or further applications of the methods (Stajich and Lapp, 2006). This is part of a wider movement in software and data analysis with many tools to facilitate such work being released for use in Linux or the R programming environment (R Core Team, 2016). In addition to the R packages hosted on comprehensive R archive network (CRAN) (CRAN, 2017), the Bioconductor repositories (Gentleman *et al.*, 2004) also contain many packages specifically for applications in bioinformatics, and the GitHub site hosts many packages in various stages of development and early release. Packages from these various sources have been used throughout this project and cited where-ever possible. Several R packages have been developed during this thesis project and either publicly released on GitHub or prepared to accompany a publication.

2.1.1.1 Cancer Genome Atlas Data

Molecular profile data from normal and tumour samples was downloaded from publicly available sources, using the TCGA (TCGA, 2012) and the International Cancer Genomes Consortium (ICGC) web portals (Zhang *et al.*, 2011). These include gene expression (RNA-Seq), somatic mutation mutations, and anonymous clinical data. These versions downloaded were on the 6th of August 2015 (Release 19) and the 2nd of May 2016 (Release 20) for breast and stomach cancer respectively via the ICGC data portal (<https://dcc.icgc.org/>).

Performing a genomic alignment in remains a challenge in bioinformatics and methods to do so may yet be improved (Chen and Tompa, 2010). However, the statistical and biological aspects of bioinformatics are the focus of this thesis, comparing alignment methods is outside the scope of these investigations. The TCGA project (TCGA, 2012) used widely adopted tools: “Bowtie” for alignment (Langmead *et al.*, 2009), “mapsplice” to detect splice sites (Wang *et al.*, 2010), and the Reads Per Kilobase per Million mapped reads (RPKM) approach to qualify reads per transcript as a measure of gene expression (Mortazavi *et al.*, 2008). These are widely acceptable tools for processing RNA-Seq data which were used to produce the raw counts of mapped reads (tier 1) and normalised expression data (tier 3) publicly available from TCGA.

Raw count and RSEM normalised TCGA expression data from Illumina RNA-Seq protocols were available from 1177 breast samples (113 normal, 1057 primary tumour, and 7 metastases) for 20,501 genes. TCGA breast somatic mutation mutation data for 981 samples (976 primary tumours and 5 metastases) across 25,836 genes were available including 969 samples (964 primary tumours and 5 metastases) with corresponding RNA-Seq expression data and 19,166 genes mapped from Ensembl identifiers to gene symbols, of which 16,156 had corresponding gene expression information. Unless otherwise stated, the raw counts were used for further processing rather than the RSEM normalised data (provided by TCGA tier 3). For the purposes of this analysis somatic mutation mutations were reported if they were detected to non-synonymous substitutions, frameshifts, or truncations (by premature stop codons) which would likely disrupt the wild-type gene function.

Raw count TCGA expression data (TCGA tier 1) from Illumina RNA-Seq was also available for 450 stomach samples (35 normal, 415 primary tumour) for 20,501 genes. TCGA stomach mutation data was also available for 289 samples across 25807 genes, corresponding to 19436 genes with expression data.

2.1.1.2 Reactome and Annotation Data

Unless otherwise specified, pathway analysis was performed for human pathway annotation from the Reactome database (version 52) with pathway gene sets derived from the reactome.db R package. Entrez identifiers were mapped to gene symbols or aliases to match to TCGA expression and mutation data using the org.Hs.eg.db R package. Further pathway analysis used breast cancer gene signatures from Gatza and colleagues (Gatza *et al.*, 2011; Gatza *et al.*, 2014). These gene symbols were matched to the relevant dataset and used to construct a matrix of category membership using the safe R package (Barry, 2016).

2.2 Data Handling

2.2.1 Normalisation

Apart from the Prediction Analysis of Microarray 50 (PAM50) subtyping procedure (Parker *et al.*, 2009), which required RSEM normalised data (J.S. Parker personal communication), the analysis of the RNA-Seq data presented here was based on raw read count data. Raw read counts were log-scaled; samples removed for consistency (based on a Euclidean distance correlation matrix as described in Section 2.2.2); and the final dataset was TMM normalised (Robinson and Oshlack, 2010) then processed

using the `voom` function (Law *et al.*, 2014) in the `limma` R package (Ritchie *et al.*, 2015). Protein expression data generated from RPPA was normalised to dilution curves using the `SuperCurve` R package (Ju *et al.*, 2015; Neeley *et al.*, 2009).

2.2.2 Sample Triage

The `TCGA` breast RNA-Seq data were assessed for batch effects using a correlation matrix of the log-transformed raw counts for which a heatmap (Euclidean distance, complete linkage) is shown in Figure A.2. While no major batch effects were detectable between the samples, 9 samples were excluded due to poor correlation with the remaining samples, as detailed in Table 2.1. These samples showed unusual density plots compared to the rest of the dataset, and exhibited low mean read count in Figures 2.1 and 2.2. A heatmap showing key clinical properties of these excluded samples and their correlation with the remainder of the samples is shown in Figure A.1, and a full correlation heatmap (Figure A.2) shows these samples as relatively poorly correlated outliers in the bottom rows and left columns. In addition to the clustering analysis (in Appendix A.1), replicate tumour samples were also examined for sample quality in Appendix A.2. After removal of these samples, the `TCGA` dataset used for analysis consisted of the remaining 1168 samples (from 1040 patients): 1049 tumour samples, 112 normal tissue for matched samples, and 7 metastases.

Table 2.1: Excluded samples by batch and clinical characteristics.

| Tissue Source | Type | Batch | Plate | Patient | Samples | p53 | Subtype | Treatment (History) | Clinical Subtypes (Stage) |
|------------------|--------|-------|-------|---------|---------|----------|-----------|--|---|
| A7 Christiana | Tumour | 47 | A227 | A0DB | 1 of 3 | NA | Luminal A | Mastectomy (no) | Estrogen receptor (ER) ⁺ Ductal (2) |
| A7 Christiana | Tumour | 96 | A220 | A13D | 1 of 3 | Wildtype | Luminal A | Mastectomy (no) | ER ⁺ Ductal (2) |
| A7 Christiana | Tumour | 96 | A227 | A13E | 1 of 3 | NA | Basal | Lumpectomy (no) | ER ⁻ Ductal (2) |
| A7 Christiana | Tumour | 142 | A277 | A26E | 1 of 3 | NA | Basal | Lumpectomy (no) | ER ⁺ Ductal (2) |
| A7 Christiana | Tumour | 47 | A277 | A0DC | 1 of 2 | NA | Luminal A | Mastectomy (yes) | ER ⁺ Lobular (3) |
| A7 Christiana | Tumour | 142 | A220 | A26I | 1 of 2 | Mutant | Basal | Lumpectomy (yes) | ER ⁻ Ductal (2) |
| AC Intl Genomics | Tumour | 177 | A18M | A2QH | 2 of 2 | Mutant | Basal | Radical Mastectomy (no) | ER ⁻ Metaplastic (2) |
| AC Intl Genomics | Tumour | 177 | A220 | A2QH | 2 of 2 | Mutant | Basal | Radical Mastectomy (no) | ER ⁻ Metaplastic (2) |
| GI ABS IUPUI | Normal | 177 | A16F | A2C8 | 1 of 1 | NA | Luminal A | Radical Mastectomy and Neoadjuvant (no) | ER ⁺ Ductal (2) |

Similarly, a correlation matrix of log-transformed raw counts was used to evaluate sample quality for `TCGA` stomach RNA-Seq. A tumour sample (patient 4294) was removed due to similar quality concerns leaving a final dataset for 449 samples (from 417 patients): 414 tumour samples and 35 normal tissue samples.

2.2.3 Metagenes and the Singular Value Decomposition

A “metagene” offers a consistent signal of pathway (expression) activation or inactivation by dimension reduction of a matrix, avoiding negatively correlated genes averaging out the signal of a mean-based centroid (Huang *et al.*, 2003). Constructing these path-

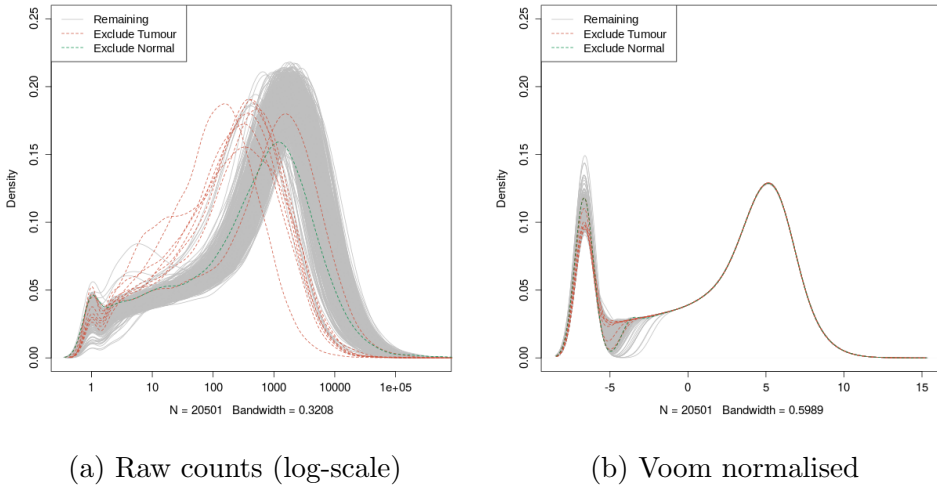


Figure 2.1: **Read count density.** Sample density plots of raw counts on log-scale and voom normalised showing samples removed due to quality concerns.

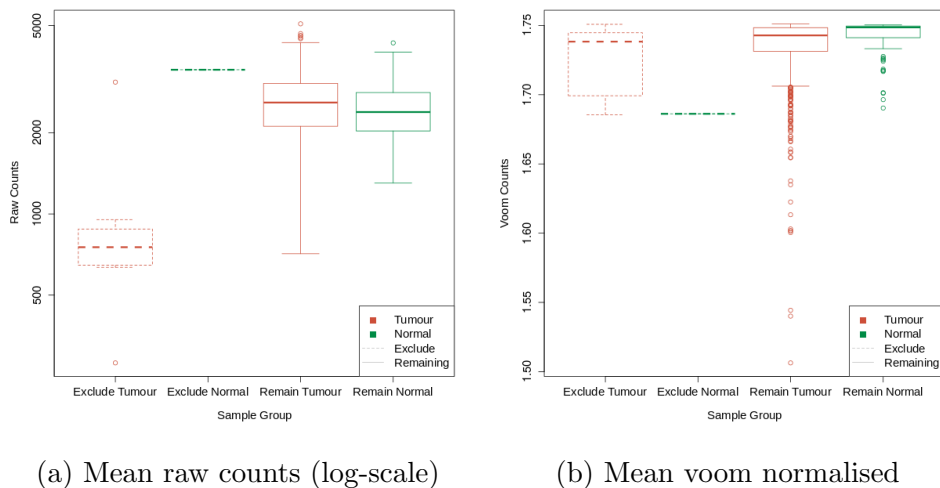


Figure 2.2: **Read count sample mean.** Boxplots of sample means for raw counts on log-scale and voom normalised show removed tumour samples with low mean read count.

way metagenes used gene sets for Reactome and Gatzka signatures (Gatzka *et al.*, 2011, 2014) as specified above (see Section 2.1.1.2). The singular-value decomposition was performed ($X = U^T DV$ where X is the data matrix of the gene set with genes \times samples) and the leading eigenvector (first column of V) corresponding to the largest singular value was used as a metagene for the pathway gene set. To ensure consistent directionality of metagene signals, the median of the gene set in each sample was calculated and correlated against the metagene with the (arbitrary) metagene sign adjusted as needed to conform with the majority of the gene set (i.e., positive correlation between metagene and the median-based centroid). To ensure that genes and pathways were weighted equally, metagenes were derived from a z-transformed dataset of gene expression and samples were scaled (by fractional ranking) for each metagene so that they were comparable on a [0, 1] scale.

2.2.3.1 Candidate Triage and Integration with Screen Data

Candidate triage in combination with the experimental data was intended to integrate findings of the SLIPT analysis with an ongoing experiment project (Chen *et al.*, 2014; Telford *et al.*, 2015). The first procedure to compare the SLIPT gene candidates for *CDH1* with an siRNA experimental screen (Telford *et al.*, 2015) was a direct comparison of the overlapping candidates, presented in a Venn diagram and tested with the χ^2 test. Since these candidates modestly overlapped at the gene level (even when excluding genes not contained in both datasets), further gene set over-representation analysis was performed for pathways specific to each detection approach and the intersection of the two.

The pathway composition of the intersection was further verified by a permutation resampling analysis (as described in Section 2.3.6): the same number of genes detected by SLIPT were sampled randomly from the universe of genes tested by both approaches. These samplings were performed over 1 million iterations and the pathway over-representation was compared for each of the 1652 reactome pathways. These over-representation scores (χ^2) were compared the observed over-representation in the intersection of the SLIPT candidates, with the proportion of resamplings with higher χ^2 values used for empirical p-values of pathway composition. The χ^2 test was used as an appropriation of Fisher's exact test on a hypergeometric distribution for resampling to computationally scale pathway over-representation tests across iterations. Pathways for which no resamplings were occurred as high as the observed were reported as $p < 10^{-6}$. These empirical p-values were adjusted for multiple comparisons (FDR). Intersection size was not assumed to be constant across resamplings so similarly with

the proportion of resamplings with higher or lower intersection size were used to evaluate significance of enrichment or depletion respectively (of **siRNA** candidate among **SLIPT** candidate genes).

2.3 Techniques

Various statistical, computational, and **bioinformatics** techniques were performed throughout this thesis. This section describes these techniques and gives the parameters used unless otherwise specified. Where relevant, the R package implementation which provided the technique will be acknowledged.

2.3.1 Statistical Procedures and Tests

As described in sections 2.3.4 and 2.2.3, the z-transform has been used to generate z-scores in various analyses in this thesis. Each row of dataset (x) is transformed into a scores (z) using the mean (μ) and standard deviation (σ) of the data such that:

$$z = \frac{x - \mu(x)}{\sigma(x)}$$

This generates data where each row (gene) has a mean of 0 and standard deviation of 1. Where plotted as a heatmap, any data more than 3 standard deviations above or below the mean is plotted as 3 or -3 respectively.

Empirical Bayes differential **expression** analysis was performed using the **limma** R package (Ritchie *et al.*, 2015). Where specified, the Fisher's exact test, χ^2 test, and correlation were used to measure associations between variables (as implemented in the **stats** R package (R Core Team, 2016)). Unless otherwise specified, Pearson correlation was used for correlation analyses (r) and coefficient of determination (R^2). Where these comparisons are discussed in more detail, Fisher's exact test and χ^2 tests are supported by a table or Venn diagram, rendered with the **limma** R package (Ritchie *et al.*, 2015). In some analyses, correlation is further supported by a scatter plot and a line of best fit derived by least squares linear regression.

The **t.test** function (R Core Team, 2016) has also been used to implement the t-test to compare pairs of data. Where relevant, an **analysis of variance (ANOVA)** has been performed to report significance of multivariate predictors of outcomes, or least squares linear regression performed for the adjusted coefficient of determination (R^2) and F-statistic p-value to evaluate the fit of the predictor variables. For some analyses these are supported by boxplot or violinplot visualisation (rendered in R).

Multiple comparisons are adjusted by the Benjamini-Hochberg procedure to control the **FDR** unless otherwise specified (Benjamini and Hochberg, 1995). This procedure

adjusts p-values to achieve an average of the proportion of false-positives among significant tests below a threshold, α . The more stringent Holm-Bonferroni (Holm) procedure (Holm, 1979) was also applied in some cases to adjust for multiple comparisons and control the family-wise error rate which adjusts p-values so that the probability that any one of the tests is a false-positive (type-1 error) below a threshold, α .

2.3.2 Gene Set Over-representation Analysis

Gene set enrichment over-representation was performed to test whether there is an enrichment of a gene set (e.g., a biological [pathway](#)) among a group of input genes. Such input genes may be predicted [synthetic lethal](#) candidates or a subset defined by clustering (in Section 2.3.3) or comparison with experimental candidates (see Section 2.2.3.1). Initially, these tests were performed using the GeneSetDB web tool (Araki *et al.*, 2012) hosted by the University of Auckland on the Reactome [pathways](#) (Croft *et al.*, 2014). Since the GeneSetDB tool used an older version of Reactome (version 40), it was difficult to directly compare with the results of other analysis (see sections 2.2.3.1 and 2.3.6) performed on version 52 (as described in Section 2.1.1.2). Thus an implementation of the hypergeometric test in R (R Core Team, 2016) was used to test for over-representation against Reactome (version 52) [pathways](#). Pathways containing less than 10 genes or more than 500 (as performed in GeneSetDB by Araki *et al.*, 2012) were excluded before adjusting for multiple comparisons.

2.3.3 Clustering

Clustering analysis when performed uses unsupervised hierarchical clustering with complete linkage (distance calculated from the furthest possible pairing). For correlation matrices or multivariate normal parameters (e.g., Σ), the distance metric used was Euclidean distance. For empirical or simulated gene and [pathway expression](#) data correlation distance was used, calculated by $distance = 1 - cor(t(x))$ where cor is Pearson correlation and $t(x)$ is the transpose of the [expression](#) matrix.

2.3.4 Heatmap

Standardised z-scores of the data were used to plot heatmaps on an appropriate scale. Raw (log-scale) read counts or voom normalised counts per gene (as specified) were plotted as normalised z-scores on a $[-3, +3]$ blue-red scale. Similarly, correlations were plotted on a $[-1, +1]$ blue-red scale. These heatmaps were performed using the linkage and distance specified for the clustering performed in Section 2.3.3. The `gplots` R package (Warnes *et al.*, 2015) was used to generate many of the heatmaps throughout

this thesis, along with a customised heatmap function (released as `heatmap.2x`). Where clearly specified, data have been split into subsets with clustering performed separately on each subset with these plotted alongside each other.

2.3.5 Modeling and Simulations

Statistical modeling and simulations have been used to test various **synthetic lethal** detection procedures on simulated data. This involves constructing a statistical model of how **synthetic lethality** would appear in (continuous normally distributed) **gene expression** data. Where presented (in Section 3.2.1), the assumptions of the model are stated clearly. The model allows sampling from a multivariate normal distribution (using the `mvtnorm` R package (Genz and Bretz, 2009; Genz *et al.*, 2016)) to generate simulated data with known underlying **synthetic lethal** partners (detailed in Section 3.2.2). We can test whether statistical procedures, including those developed in this thesis (presented in Section 3.1), are capable of detecting them upon this simulated data. This multivariate normal simulation procedure also enables the inclusion of correlation structure which is either given as correlated blocks of genes or derived from **pathway** structures (as detailed in Section 3.4.2).

If this multivariate normal distribution was sampled once and the procedure to add known **synthetic lethal** partners was performed, it generates a simulated dataset. Performing this simulation procedure and testing with a **synthetic lethal** detection procedure iteratively, these simulations can be used to assess the statistical performance of the detection procedure. The number of iterations (`Reps`) will be given for each simulation result. Typically, these are performed 1000 or 10,000 times depending on computational feasibility of doing so on larger datasets.

Several measures of statistical performance were used to assess the simulations. The following measures used the final classification of the detection procedure, statistical significance for χ^2 , significance and directional criteria met for **SLIPT** (see Section 3.1), and an arbitrary threshold: < -0.2 and $> +0.2$ for negative correlation and correlation respectively. Sensitivity (or “true positive rate”) was measured as the proportion of known **synthetic lethal** partners predicted to be **synthetic lethal**. Specificity (or “true negative rate”) was measured as the proportion of known non-synthetic lethal partners predicted not to be **synthetic lethal**. The “false positive rate” was measured here as the proportion of known non-synthetic lethal partners out of all putative partners predicted by the detection procedure. Statistical “accuracy” is the proportion of true predictions

for a detection procedure, which is both the correctly predicted known synthetic lethal partners and correctly negative known non-synthetic lethal partners.

2.3.5.1 Receiver Operating Characteristic (Performance)

A more general procedure to measure the statistical performance of a simulation is the Receiver Operating Characteristic (ROC) curve which does not assume a threshold for classification of synthetic lethality but demonstrates the trade-off of sensitivity and specificity (Akobeng, 2007; Fawcett, 2006; Zweig and Campbell, 1993). These curves (implemented with the `ROCR` R package (Sing *et al.*, 2005)) plot the True Positive Rate (sensitivity) against the False Positive Rate (1–specificity) as the prediction threshold is varied. An ideal detection method will have a true positive rate of 1 and a false positive rate of 0, hence the Area Under the ROC curve (AUC or AUROC) is a measure of statistical performance for a detection procedure accounting for this trade-off. AUROC values are typically range from 0.5 the value expected by random chance to 1 for an optimal detection method, however it is possible for an AUROC below 0.5 for a poor detection method that performs worse than random chance. In cancer biology, an AUROC of approximately 0.8 is a predictive biomarker suitable for publication (Hajian-Tilaki, 2013) but predictors with lower AUROC values may still be informative depending on the context. In this thesis, the AUROC values varies widely across simulation parameters and a primarily used for comparisons across these parameters, although they can also be used to refine thresholds for optimal classification.

2.3.6 Resampling Analysis

Resampling analyses (e.g., “permutation” analysis) are used to statistically test the significance of an observation without assuming the underlying distribution of expected test statistics Collingridge (2013). Instead these are derived from randomly shuffling test statistics or randomly sampling predicted candidates. For the purposes of this thesis, this involved randomly sampling genes from those tested to be analysed as putative synthetic lethal candidates. This was performed both for testing the significance of pathway composition in the intersection with experimental gene candidates (Section 2.2.3.1) and for assessing the significance of pathway structure among synthetic lethal candidates (Section 3.4.1.1).

These were analysed to compare the observed synthetic lethal genes against values derived from randomly sampling the same number of genes as observed by synthetic lethal from among the genes tested. Sampling iteratively across many resampling procedures, these resampling-based values form a null distribution that would be observed

if the null hypothesis were true. Thus the proportion of resampling-based values across these iterations that are greater than or equal to that observed, forms an empirically derived p-value to test significance.

Resampling was performed for comparison (in Section 2.2.3.1) with fixed experimental screen candidates (Telford *et al.*, 2015) both resampling the number of genes overlapping with the screen candidates and test statistics for pathway enrichment. Resampling analysis was also applied to shortest paths and network metrics (in Section 3.4.1.1) to test significance of directional relationships between synthetic lethal candidate genes within pathway structures.

The number of iterations determines the accuracy of these p-values. For pathway composition (in Section 2.2.3.1), a million iterations were performed using high performance computing (as detailed in Section 2.5.3) to provide sufficient accuracy after adjusting for multiple comparisons across pathways. For the purposes of network analysis (in Section 3.4.1.1), a thousand iterations were sufficient to reject the null hypothesis for the majority of pathways tested before adjusting for multiple comparisons, and thus further iterations were not performed.

2.4 Pathway Structure Methods

2.4.1 Network and Graph Analysis

Networks are important in considering the structure of relationships in molecular biology, including gene regulation, kinase cellular signalling, and metabolic pathways (Barabási and Oltvai, 2004). Network theory is an interdisciplinary field which combines the approaches of computer science with the metrics and fundamental principles of graph theory, an area of pure mathematics dealing with relationships between sets of discrete elements. The vast amounts of molecular and cellular data from high-throughput technologies have enabled the application of network-based and genomes-wide bioinformatics analysis to examine the complexity of a cell at the molecular level and understand aberrations in cancer. This thesis uses various metrics and analysis procedures developed in Graph and Network theory to analyse graph structure of biological pathways. Where feasible, these have been implemented using the igraph R package with such procedures described below (Csardi and Nepusz, 2006). Custom R functions to perform more complex analysis and visualisation of iGraph data objects will be described later.

Graph theory is a branch of pure mathematics which deals with the properties of sets of discrete objects (referred to as a ‘node’ or ‘vertex’) with some pairs are joined (by a ‘link’ or an ‘edge’). While a seemingly reductionist abstraction to mathematically study relationships, graph theory serves has applications in a wide range of studies including life sciences. Network theory is the sub-discipline of graph theory which deals with networks which has become popular due to the vast potential for applications of networks (van Steen, 2010).

Applications vary depending on the situation modelled, particularly in how the edges between vertices are defined, whether they are directed or weighted, and whether multiple redundant edges between a pair of vertices (referred to as ‘parallel edges’) or edges connecting a vertex to itself (referred to as ‘loops’) are permitted in the model. Networks are defined such that the edges represent a relationship between the vertices and may be directed, weighted, or contain parallel edges or loops depending on the application (van Steen, 2010). Unless otherwise stated, graph structures and networks in thesis will be unweighted and have no parallel edges or loops. Where a directional relationship is known or modelled, it will be represented with a directed edge in a directed graph.

2.4.2 Sourcing Graph Structure Data

Pathway Commons interaction data was sourced using Biological pathway exchange (BioPAX) with the paxtools-4.3.0 Java application on October 6th 2015 (Cerami *et al.*, 2011; Demir *et al.*, 2013). This utility was used to source ‘sif’ format interaction data into R (R Core Team, 2016), from which the human Reactome (version 52) dataset of interactions was imported (Croft *et al.*, 2014), matching those used for pathway enrichment analysis. These interactions were used to construct an adjacency matrix for the Reactome network and subnetworks corresponding to each relevant biological pathway.

2.4.3 Constructing Pathway Subgraphs

Subgraphs for each relevant pathway were constructed by matching the nodes in the complete Reactome network to the pathway gene sets (as derived in Section 2.1.1.2). A subgraph with adjacent nodes was constructed by adding nodes which have an edge with a gene in the pathway gene set. The pathways these adjacent nodes belong to were added to form a “meta-pathway” to account for the possibility for nodes within the pathway being linked by the surrounding graph structure.

2.4.4 Network Analysis Metrics

The existing network analysis measures applied in this thesis (as described below) used an implementation in the `igraph` R package where it was available (Csardi and Nepusz, 2006). Otherwise, custom features were developed for analysis of iGraph objects in R and released as `igraph.extensions` (as described in Section 3.5.3).

Vertex degree is the number of `edges` a `node` has and is a fundamental measure of the importance and connectivity of a network (van Steen, 2010). More connected `nodes`, such as network hubs, will have a higher `vertex` degree relative to other `nodes`. For the purposes of this thesis, `vertex` degree ignored `edge` direction with loops (edges with itself) and double `edges` to the same `node` excluded.

A fundamental concept in network analysis is a “`shortest path`”, that is the shortest route via `edges` between any two particular `nodes` in a network. These are computed by Dijkstra’s algorithm (Dijkstra, 1959) in the `igraph` R package (Csardi and Nepusz, 2006). Where applicable paths will only use directed `edges` in a particular direction. Shortests paths are a useful measure of how close `nodes` are in a network. This is used to compute `information centrality`, and for further analysis of `pathway` structure (as described in Section 3.4.1).

Network `centrality` is an alternative measure of the importance or influence of a `node` to the `graph` structure (Borgatti, 2005). Various strategies are used to derive centrality, typically based on how connected the `node` is or the impact of `node` removal on the connectivity of the network. One of the most notable is the “`PageRank`” algorithm, a refinement of eigenvector `centrality` based on the eigenvectors of the adjacency matrix (Brin and Page, 1998). This is implemented in the `igraph` R package (Csardi and Nepusz, 2006).

Another network `centrality` measure that has been previously applied to biological protein interaction networks (Kranthi *et al.*, 2013) is the “`information centrality`”. The `information centrality` of a `node` is the relative impact on efficiency (transmission of information via shortest paths) of the network when the `node` is removed. That is the `centrality` (C) (Kranthi *et al.*, 2013) for `node` n in graph G is defined as:

$$C_n = \frac{E(G) - E(G')}{E(G)}$$

where G' is the subgraph with the `node` removed and E is the efficiency (Latora and Marchiori, 2001) derived from `shortest paths` (d_{ij} between `nodes` i and j) as:

$$E(G) = \frac{2}{N(N-1)} \sum_{i < j \in G} \frac{1}{d_{ij}}$$

The efficiency of the network can be derived from [shortest paths](#) implemented in the [igraph](#) R package and the iterative network [centrality](#) computation of each [node](#) has been released as an R package ([info.central](#)) and included in the [igraph.extensions](#) package.

2.5 Implementation

2.5.1 Computational Resources and Linux Utilities

Several computers were used to process and store data during this thesis (as summarised in Table 2.2), running different versions of Linux operating systems, including a personal laptop computer, laboratory desktop machine, departmental server, and the New Zealand eScience Infrastructure Intel Pan high-performance computing cluster (a supercomputer based at the University of Auckland). Each of these systems support a 64-bit architecture. Current workflows on local machines use Elementary OS (based on the Ubuntu versions given in Table 2.2) and interacting with these via ZSH shell. However, Ubuntu OS and the Bourne Again SHell (bash) were used at the inception of this project and bash is continues to be used for running scripts. Various Linux applications and command-line utilities were used on these machines (as summarised in Table 2.3). As such, the workflows developed in this project should be backwards-compatible with Ubuntu Linux (and other derivatives). The majority of novel methodology and implementations were performed in R which is a cross-platform language, packages developed in R will be available for users of Linux, Mac, and Windows machines.

Table 2.2: Computers used during thesis

| | Viao Laptop | Lab Machine | Biochem Server | NeSI Pan Cluster |
|-----------------------|------------------------------|----------------------------|---------------------------------|----------------------------|
| Operating System (OS) | Elementary OS Freya 0.3.2 | Elementary OS Loki 0.4 | Red Hat Enterprise Maipo 7.2 | Cent OS Final 6.4 |
| Upstream OS | Ubuntu LTS Trusty 14.04 | Ubuntu LTS Xenial 16.04 | | |
| Linux Kernel | 3.19.0-65-generic | 4.4.0-36-generic | 3.10.0-327.36.2.el7.x86_64 | 2.6.32-504.16.2.el6.x86_64 |
| Shell: bash | 4.3.11(1) | 4.3.46(1) | 4.2.46(1) | 4.2.1(1) |
| Shell: zsh | 5.0.2 | 5.1.1 | 5.0.2 | 5.2 |

Table 2.3: Linux utilities and applications used during thesis

| | | Viao Laptop | Lab Machine | Biochem Server | NeSI Pan Cluster |
|------------------|---|------------------------------|---------------------------|---------------------------------|----------------------------|
| | OS | Elementary OS Freya 0.3.2 | Elementary OS Loki 0.4 | Red Hat Enterprise Maipo 7.2 | Cent OS Final 6.4 |
| | Linux Kernel | 3.19.0-65-generic | 4.4.0-36-generic | 3.10.0-327.36.2.el7.x86_64 | 2.6.32-504.16.2.el6.x86_64 |
| Scripting | Shell bash | 4.3.11(1) | 4.3.46(1) | 4.2.46(1) | 4.2.1(1) |
| | Shell zsh | 5.0.2 | 5.1.1 | 5.0.2 | 5.2 |
| Programming | Python | 2.7.6 | 2.7.12 | 2.7.5 | |
| | Java | 1.8.0_101 | 9-ea | 1.8.0_101 | |
| | C++ | 4.8.4 | 5.4.0 | 4.8.5 | 4.4.7 |
| Text Editor | nano | 2.2.6 | 2.5.3 | 2.3.1 | 2.0.9 |
| | kile (L ^A T _E X) | 2.1.3 | 2.1.3 | | |
| Version Control | git | 1.9.1 | 2.11.0 | 1.7.1 | 1.8.3.1 |
| Shell Utilities | sed | 4.4.2 | 4.4.2 | 4.4.2 | 4.4.1 |
| | grep | 2.16-1 | 2.25-1 | 2.20 | 2.6.3 |
| | nohup | 8.21 | 8.25 | 8.22 | 8.4 |
| Typesetting | TeX | 3.1415926 | 3.14159265 | | |
| | TeXLive (L ^A T _E X) | 2013 | 2015 | | |
| | PDFTeX | 2.5-1 | 2.6 | | |
| | pandoc | 1.12.2.1 | 1.16.0.2 | | |
| Remote Computing | Slurm scheduler | | | | 16.05.6 |
| | OpenSSH | 7.2p2 | 7.2p2 | 6.6.1 | 5.3p1 |
| | OpenSSL | 1.0.2g | 1.0.2g | 1.0.01e-fips | 1.0.01e-fips |
| | rsync | 3.1.0p31 | 3.1.1p31 | 3.0.9p30 | |
| | Globus Online Transfer | | | 3.1 | 3.1 |
| | Cisco AnyConnect VPN | | 3.1.05170 | | |
| Image Processing | Inkscape | 0.48.4 | 0.91 | | |
| | GIMP | 2.8.10 | 2.8.16 | | |
| | ImageMagick | 6.7.7.10-6 | | | |

2.5.2 R Language and Packages

The R programming language has been used for the majority of this thesis. Current R installations across the machines used are given in Table 2.4. Local machines currently run the latest version of the R (at the time of writing) and remote machines run the versions and modules as managed by the system administrator.

Various scripts and packages in this thesis were developed or run in previous versions of RStudio and R but these run without error in the current version of R (and the older versions on remote machines). The R packages which were used throughout this thesis (as detailed in Table 2.5 with versions specified) were installed from the [comprehensive R archive network \(CRAN\)](#) ([CRAN, 2017](#)), Bioconductor ([Gentleman *et al.*, 2004](#), version 3.4; BiocInstaller 1.24.0), or GitHub. These packages were not updated when they would change the functionality of scripts or functions in packages, in particular imported data from annotation packages (used to define gene sets) have been saved as local files to continue using stable versions of these [pathway](#) data (across machines).

This is a summary of the key packages which (in addition to their dependencies) have been used throughout this project. Where a package implementation has been central to the methods applied, they are described in more detail in the relevant section. A full table of packages used in this thesis can be found in Appendix B (Table B.1). The R packages developed during this thesis are given in Table 2.6 with the relevant sections describing their implementation and use where appropriate, in addition to further details on these functions in Section 3.5.

Table 2.4: R installations used during thesis

| | | Viao Laptop | Lab Machine | Biochem Server | NeSI Pan Cluster |
|-------------|---------|------------------------------|---------------------------|---------------------------------|----------------------|
| | OS | Elementary OS Freya 0.3.2 | Elementary OS Loki 0.4 | Red Hat Enterprise Maipo 7.2 | Cent OS Final 6.4 |
| Programming | R | 3.3.2 | 3.3.2 | 3.3.1 | 3.3.0-intel (module) |
| Development | RStudio | 1.0.136 | 1.0.136 | 1.0.136 (server) | |

Table 2.5: R Packages used during thesis

| Package | Version Used | Built | Repository |
|--------------|--------------|-------|--------------|
| colorspace | 1.3-2 | 3.3.1 | CRAN |
| curl | 2.3 | 3.3.1 | CRAN |
| data.table | 1.9.6 | 3.3.1 | CRAN |
| dendextend | 1.4.0 | 3.3.2 | CRAN |
| DBI | 0.5-1 | 3.3.1 | CRAN |
| devtools | 1.12.0 | 3.3.1 | CRAN |
| dplyr | 0.5.0 | 3.3.1 | CRAN |
| ggplot2 | 2.2.1 | 3.3.1 | CRAN |
| git2r | 0.18.0 | 3.3.1 | CRAN |
| gplots | 3.0.1 | 3.3.1 | CRAN |
| gtools | 3.5.0 | 3.3.1 | CRAN |
| igraph | 1.0.1 | 3.3.1 | CRAN |
| matrixcalc | 1.0-3 | 3.3.1 | CRAN |
| mclust | 5.2.2 | 3.3.1 | CRAN |
| mvtnorm | 1.0-6 | 3.3.1 | CRAN |
| org.Hs.eg.db | 3.1.2 | 3.1.2 | Bioconductor |
| openssl | 0.9.6 | 3.3.1 | CRAN |
| plyr | 1.8.4 | 3.3.1 | CRAN |
| purrr | 0.2.2 | 3.3.1 | CRAN |

| | | | |
|--------------|---------|-------|----------------------|
| reactome.db | 1.52.1 | 3.2.1 | Bioconductor |
| RColorBrewer | 1.1-2 | 3.3.1 | CRAN |
| Rcpp | 0.12.9 | 3.3.1 | CRAN |
| ROCR | 1.0-7 | 3.3.1 | CRAN |
| roxygen2 | 6.0.1 | 3.3.2 | CRAN |
| shiny | 1.0.0 | 3.3.1 | CRAN |
| snow | 0.4-2 | 3.3.1 | CRAN |
| testthat | 1.0.2 | 3.3.2 | CRAN |
| tidyverse | 1.1.1 | 3.3.2 | GitHub (hadley) |
| sm | 2.2-5.4 | 3.3.1 | CRAN |
| Unicode | 9.0.0-1 | 3.3.2 | CRAN |
| vioplot | 0.2 | 3.3.1 | CRAN |
| viridis | 0.3.4 | 3.3.2 | CRAN |
| xml2 | 1.1.1 | 3.3.2 | CRAN |
| xtable | 1.8-2 | 3.3.1 | CRAN |
| zoo | 1.7-14 | 3.3.1 | CRAN |
| graphics | 3.3.2 | 3.3.2 | base |
| grDevices | 3.3.2 | 3.3.2 | base |
| cluster | 2.0.5 | 3.3.1 | base |
| graphics | 3.3.2 | 3.3.2 | base |
| grDevices | 3.3.2 | 3.3.2 | base |
| Matrix | 1.2-8 | 3.3.1 | base |
| stats | 3.3.2 | 3.3.2 | base |

Table 2.6: R packages developed during thesis

| Package Name | Description and GitHub Repository | Section |
|--------------------|---|---------|
| <code>slipt</code> | Synthetic lethal detection by SLIPT (to accompany publication) https://github.com/TomKellyGenetics/slipt | 3.1 |
| visualisation | <code>vioplotx</code> Customised violin plots (based on <code>vioplot</code>) https://github.com/TomKellyGenetics/vioplotx | 3.4 |
| | <code>heatmap.2x</code> Customised heatmaps (based on <code>gplots</code>) https://github.com/TomKellyGenetics/heatmap.2x | |
| igraph.extensions | <code>igraph.extensions</code> Meta-package to install the follow iGraph functions https://github.com/TomKellyGenetics/igraph.extensions | 3.5.3 |
| | <code>plot.igraph</code> Custom plotting of directed graphs https://github.com/TomKellyGenetics/plot.igraph | 2.4.4 |
| | <code>info.centrality</code> Computing information centrality from network efficiency https://github.com/TomKellyGenetics/info.centrality | 3.4.2 |
| | <code>pathway.structure.permutation</code> Testing pathway structure with resampling analysis https://github.com/TomKellyGenetics/pathway.structure.permutation | 3.4.1.1 |
| | <code>graphsim</code> Generating simulated expression from graph structures https://github.com/TomKellyGenetics/graphsim | 3.4.2 |

2.5.3 High Performance and Parallel Computing

Another enabling technology for bioinformatics is parallel computing, performing independent operations in separate cores: this “multithreading” is widely used to increase the time to compute results. Bioinformatics is particularly amenable to this since performing multiple iterations of a simulation or testing separate genes is often “embarrassingly parallel”, being completely independent of the results of each other. As such parallel computing is offered by many high-performance “supercomputers” including national research infrastructure.

The New Zealand eScience Infrastructure (NeSI) is a High Performance Computing (HPC) organisation providing the Intel Pan cluster hosted by the University of Auckland (NeSI, 2017). The Pan cluster used throughout this thesis project to optimise and perform computations which would have otherwise been infeasible in the timeframe of thesis. Such technological developments and infrastructure initiatives have enabled bioinformatics research including this project. High performance computing on the Pan cluster was used extensively in this project including for resampling analysis (in sections 2.3.6 and 3.4.1.1), calculating information centrality (in Section 2.4.4), and in simulations (in sections 2.3.5, 3.2, and 3.4.2)

Scripts and data were transferred between the Pan cluster and University of Otago computing resources by `rsync` or the Globus file transfer service (Globus, 2017). R scripts (R Core Team, 2016) were run in parallel with the “simple network of workstations” `snow` R package Tierney *et al.* (2015). This utilised the “message passing interface” (Yu, 2002) when it was feasible with memory requirements to run in par-

allel across multiple compute [nodes](#), otherwise SOCKS was used to access multiple cores within an instance of R and pass input data to them. R jobs were submitted to queue for available resources and run on the Pan cluster via the [Simple Linux Utility for Resource Management \(Slurm\)](#) workload manager ([Slurm, 2017](#)). When running R scripts across many parameters or for memory-intensive jobs, Slurm array job submission and independent submission of different parameters via shell commands with arguments passed to R. In some cases, this submission was automated across a range of parameters with Bash scripts.

Chapter 3

Methods Developed During Thesis

In this Chapter, I will outline the rationale and development of various methods used throughout this thesis to examine [synthetic lethality](#) in gene expression data, graph structures, models and simulations. First by describing the [Synthetic Lethal Interaction Prediction Tool \(SLIPT\)](#), a [bioinformatics](#) approach to triage of synthetic lethal candidate genes. This is considered one of the main research outputs of the thesis, which is supported by comparisons to an experimental screen from a related project and performance on simulated data. These supporting data will be covered in further chapters but preliminary data to support the use and design of [SLIPT](#) are provided alongside description of the method. This includes the construction of a statistical model of [synthetic lethality](#) in (continuous multivariate Gaussian) gene expression data, which enables testing [SLIPT](#) upon simulated data with known [synthetic lethal](#) partners. Another key component of the simulation pipeline used later is the generation of simulated data from a known [graph](#) structure or simulated biological pathway. The development of this simulation procedure and other statistical [treatment](#) of graph and [network](#) structures will also be covered. Various R packages have been developed to support this project, most notably the [slipt](#) package to implement the [SLIPT](#) methodology. The additional R packages for handling [graph](#) structures, simulations, and custom plotting features will also be described as research outputs of this thesis, methods applied throughout, and contributions to the open-source software community that made this project feasible.

3.1 A Synthetic Lethal Detection Methodology

The [SLIPT](#) methodology identifies [gene expression](#) patterns consistent with [synthetic lethal](#) interactions between a query gene and a panel of candidate interacting partners.

Gene expression is called low, medium, or high by separating samples into tertiles (3-quantiles) for each gene. Genes with insufficient expression across all samples were excluded by requiring that the first tertile of raw counts is above zero. Then a χ^2 test is performed between the query gene and each candidate partner, with the p-values for the χ^2 test being corrected for multiple testing using FDR error control to reduce false positives for large candidate gene panels (Benjamini and Hochberg, 1995). Significance was called only if FDR adjusted p-values were below the threshold $p < 0.05$. A synthetic lethal interaction is predicted (as shown in Figure 3.1) when (i) the χ^2 test is significant; (ii) observed low-query, low-candidate samples are less frequent than expected; and (iii) observed low-query, high-candidate and high-query, low-candidate samples are more frequent than expected.

The synthetic lethal prediction procedure has also been adapted to utilise somatic mutation data for the query gene. This is intended to utilise a query gene known to be recurrently mutated in the disease (and dataset), with the majority of mutations inactivating gene function (e.g., null or frameshift mutations). A synthetic

| | | Candidate Gene | | |
|-----------------------------------|--------|-----------------------------|--------|-----------------------------|
| | | Low | Medium | High |
| Query Gene (e.g. <i>CDH1</i>) | Low | Observed less than expected | | Observed more than expected |
| | Medium | | | |
| | High | Observed more than expected | | |

Figure 3.1: **Framework for synthetic lethal prediction.** SLIPT was designed to identify candidate interacting genes from gene expression data using the χ^2 test against a query gene. Samples are sorted into low, medium, and high expression quantiles for each gene to test for a directional shift. A sample being low in both genes of a synthetic lethal pair is unlikely, since loss of both genes will be deleterious, and is expected to be statistically under-represented in a gene expression dataset. We expect a corresponding (symmetric) increase in frequency of sample with low-high gene pairs. Synthetic lethal candidate (exprSL) partners of a gene are identified by running this procedure on all possible partner genes, selecting those with an FDR-adjusted χ^2 p-value of $p < 0.05$, and meeting the directional criteria. Since synthetic lethal genes are partners of each other commutatively, the symmetric direction criteria are all required such that synthetic lethal genes will be predicted to be partners of each other.

| | | Candidate Gene | | |
|-----------------------------------|-----------|-----------------------------|--------|-----------------------------|
| | | Low | Medium | High |
| Query Gene (e.g. <i>CDH1</i>) | Mutation | Observed less than expected | | Observed more than expected |
| | Wild-type | Observed more than expected | | |

Figure 3.2: **Synthetic lethal prediction adapted for mutation.** SLIPT was also adapted to identify candidate interacting genes using (somatic mutation) mutation data of the query gene in the χ^2 test. Samples are sorted into low, medium, and high expression quantiles for each candidate gene and tested for a directional shift against mutation status of the query gene. A sample having low expression or mutation for the synthetic lethal pair is expected to be unlikely with a corresponding increase in frequency of sample with mutant-high or wild-type-low gene pairs. Synthetic lethal candidate (mtSL) partners of a gene are identified by running this procedure on all possible partner genes, selecting those with an FDR-adjusted χ^2 p-value of $p < 0.05$, and meeting the directional criteria.

lethal interaction is predicted (as shown in Figure 3.2) when (i) the χ^2 test is significant; (ii) observed mutant-query, low-candidate samples are less frequent than expected; and (iii) observed mutant-query, high-candidate and wild-type-query, low-candidate samples are more frequent than expected. Unless otherwise specified, computationally predicted synthetic lethal gene candidates from SLIPT used expression data (exprSL) for both genes (as shown in Figure 3.1) rather than mutation data (mtSL) for the query gene (as shown in Figure 3.2).

The SLIPT methodology is amenable for use on expression data including pathway metagenes (as generated in Section 2.2.3). The suitability of the SLIPT methodology to application on public gene expression data will further be supported by simulation results in Section 3.3 and Chapter 6, including comparison to other statistical methods. SLIPT results for *CDH1* will also compare experimental screen results in a breast cell line (Telford *et al.*, 2015), primary screen results are discussed in Section 4.2 and secondary (validation) screen results are presented in Appendix 4.2.4.

3.2 Synthetic Lethal Simulation and Modelling

A statistical model of Synthetic Lethality was developed to generate simulated data to test the **SLIPT** procedure. This section will describe the **synthetic lethal** model and the simulation procedure for generating **gene expression** data with known **synthetic lethal** partners. Some preliminary results to support usage of the **SLIPT** methodology throughout this thesis will be presented here. The simulation procedure will be applied in more depth in Chapter 6, including in combination with simulations from **graph structures**.

3.2.1 A Model of Synthetic Lethality in Expression Data

A conceptual model of **synthetic lethality** was constructed (see Figure 3.3), which will be used to build a statistical model of **synthetic lethal gene expression** from which to simulate **expression** data to on which test SLIPT and various potential **synthetic lethal** prediction methods. In the model, **synthetic lethality** arises between genes with related functions as a cell death phenotype when these functions are removed.

This model suggests that **synthetic lethality** is detectable in measures of gene inactivation across a sample population, namely **mutation**, **DNA copy number**, **DNA methylation**, and suppression of **expression**. While any of these mechanisms of gene inactivation could lead to **synthetic lethality**, **expression** data is readily available and changes in these alternative mechanisms are likely to impact on the amount of expressed (functional) **RNA** or protein detectable. There are several ways that functional relationships between genes could manifest in **expression** data, including coexpression, mutual exclusivity and directional shifts. Co-expression is overly simplistic and has previously performed poorly as a predictor of **synthetic lethality** (Jerby-Arnon *et al.*, 2014), although this will still be tested with correlation measures in later simulations. Here the alternative hypothesis is that **synthetic lethality** will lead to a detectable directional shift in the number of samples exhibiting low or high **expression** of either gene. This model does not preclude mutual exclusivity (Wappett *et al.*, 2016), compensating **expression** or co-loss under-representation (Lu *et al.*, 2015) as previously postulated to occur between **synthetic lethal** genes.

The first condition of the **synthetic lethal** model is that if there are only two **synthetic lethal** genes (e.g., *CDH1* and one SL partner), then they will not both be non-functional in the same sample (in an ideal model). Gene function is thus determined for each sample in a model of **synthetic lethal** with the proportion of samples with a functional or non-functional gene being arbitrary. Whether a gene is functional can

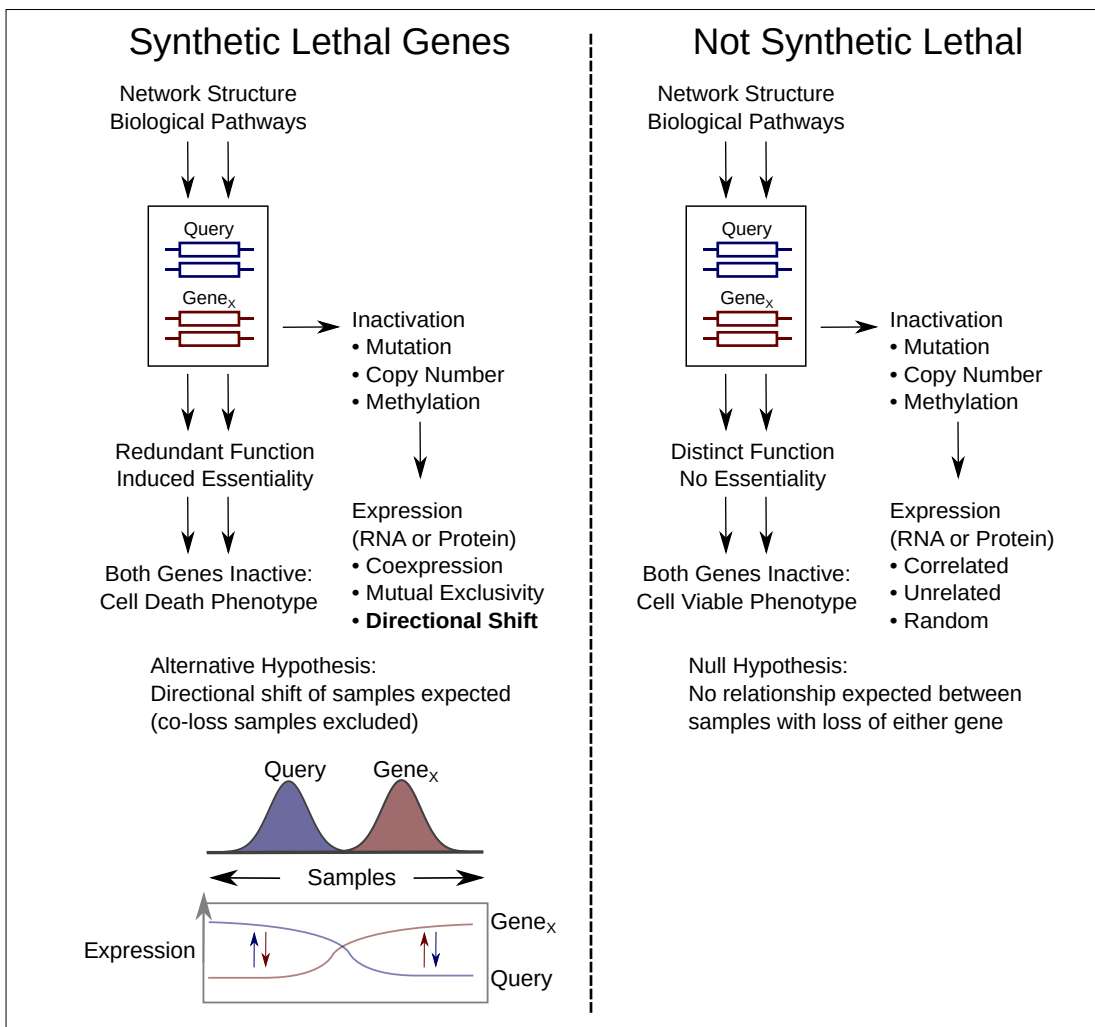


Figure 3.3: **A model of synthetic lethal gene expression.** A conceptual model of synthetic lethal interactions between a Query gene and partner gene (G_X). Genes that are synthetic lethal may not both be non-functional in the same sample without another gene compensating for the loss of function. This is most likely to be detectable as low gene expression, whether they are lost by mutation, deletion, DNA methylation, or suppressing regulatory signals. This could manifest as coexpression, mutual exclusivity, or directional shifts in sample frequency. Thus the alternative hypothesis (H_A) is that synthetic lethal genes will have a reduced frequency of co-loss samples while the null hypothesis (H_0) is that non-synthetic lethal gene pairs would show no such relationship, even if they may be correlated for other means such as pathway relationships. In this model synthetic lethal genes may compensate for the loss of each other but this is not assumed, only that loss of both is unfavourable to cell viability and probability of detecting samples with combined gene loss.

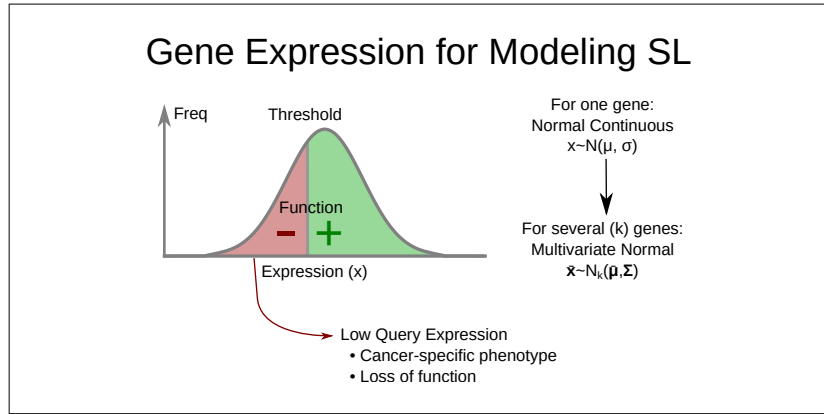


Figure 3.4: **Modeling synthetic lethal gene expression.** When modeling **synthetic lethal** interactions between a Query gene with partner genes (G_X and G_Y) above, cellular viability requires that at least one of genes is not inactivated. Expression below a threshold is used as a model of loss of function, where genes are regarded as non-functional for the purposes of modelling **synthetic lethality**. Tumour suppressor genes with loss of function also have cancer specific phenotypes (although these thresholds are not necessarily the same). Expression is modeled by a normally (Gaussian) distributed continuous data such as (log-scale) data from RNA (microarray or RNA-Seq), protein, or pathway **metagenes**. This rationale generalises for several genes on a multivariate normal distribution.

similarly be modelled by an arbitrary threshold of continuous and normally distributed **gene expression** data to define gene function (as shown in Figure 3.4). For the purposes of modeling **synthetic lethality** in breast cancer **expression** data, a threshold of the 30th percentile of the **expression** levels was used because approximately 30% of samples analysed had *CDH1* inactivation. This was generalised for a model of the proportion of samples inactivated for each gene. In this ideal case, no samples lowly expressing both of these genes are expected to be observed. While this is not observed, that is to be expected as it is unlikely that only 2 genes will have an exclusive **synthetic lethal** partnership. The threshold of the 0.3 quantile was used in simulations derived from this model throughout this thesis.

A **synthetic lethal** pair of genes is unlikely to act in isolation, therefore higher-order **synthetic lethal** interactions (i.e., 3 or more genes) must be considered in the model as shown in Figure 3.5. Even when testing pairwise interactions, modelling higher level interactions that may interfere is important. If there are additional **synthetic lethal** partners, there are two possibilities for adding these: 1) that they are independent partners of the query genes interacting pairwise (and not with each other) or 2) that

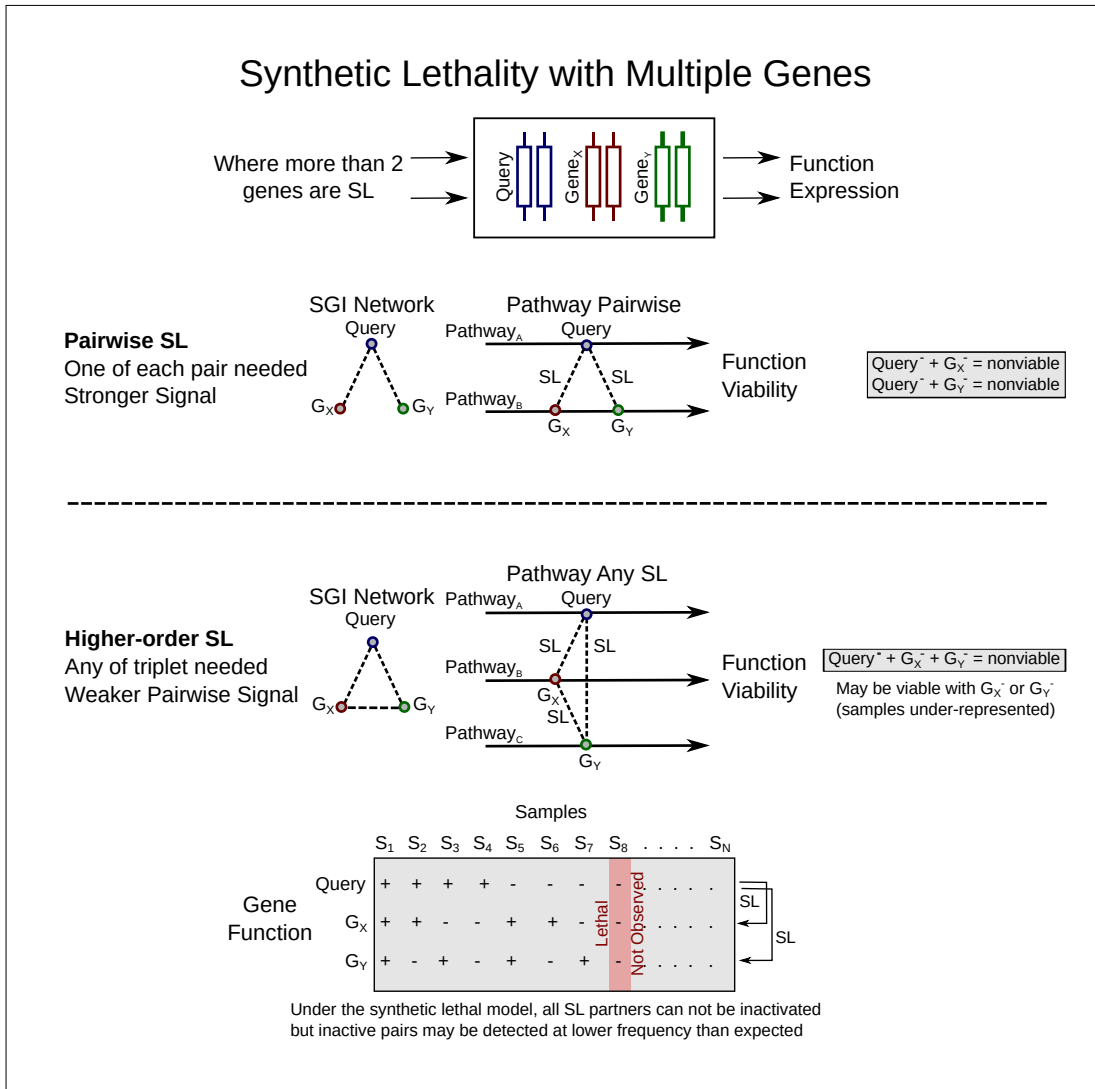


Figure 3.5: **Synthetic lethality with multiple genes.** Higher order synthetic lethal interactions may occur between 3 or more genes, affecting the simulated expression (or synthetic lethal predictions) even if undetected when observed pairwise. Consider interactions between a Query gene and two partner genes (G_x and G_y). They may interact with the Query pairwise (inviolate when either gene pair is lost) or form a higher-order interaction such as the “synthetic lethal triplet” if any of the genes provide an essential function (inviolate only when all are lost). Either is plausible with the potential pathway structures. A synthetic lethal triple has 8 potential combinations of gene functional but one is not expected to be observed (due to inviability) but pairwise inactivation may be observed if additional partner genes are functional. The proportion of these combinations vary depending on the functional threshold.

an addition partner gene interacts with both of the **synthetic lethal** genes already in the system and any of the three (or more) are required to be functional for the cell to survive.

The signal (in terms of **gene expression** data) will be weaker for this latter case and this model has the more stringent assumption that all **synthetic lethal** partner genes interact with each other: that only one of these must be expressed to satisfy the model of **synthetic lethality**. In this model any of the **synthetic lethal** genes in a higher-order interaction is able to provide the missing function of the others, allowing for higher-level **synthetic lethal** partners to compensate for loss a **synthetic lethal** gene pair. While samples expressing low levels of the **synthetic lethal** gene pairs will be under-represented, they may not be completely absent from the dataset due to these higher-level interactions.

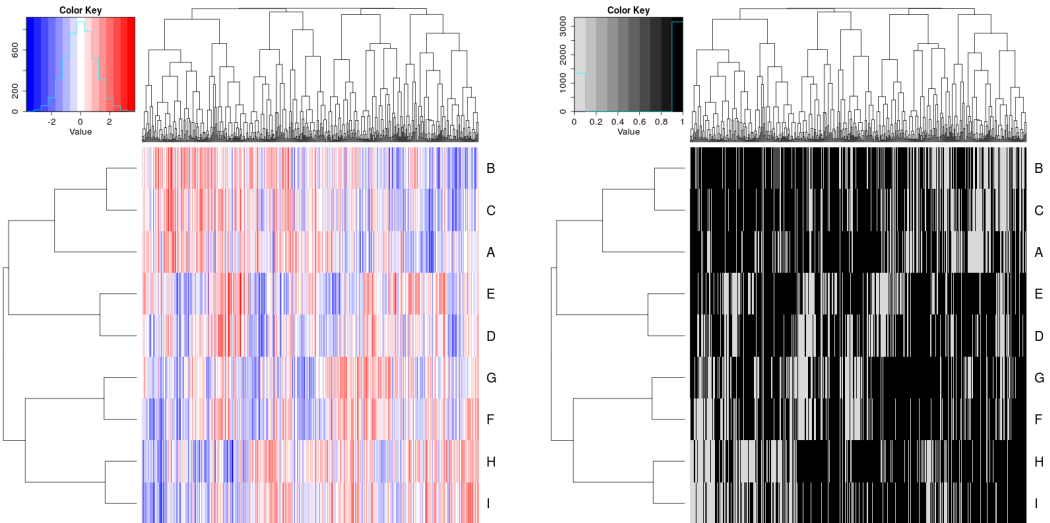
In the example of 3 **synthetic lethal** genes 3.5, only one of genes involved in the higher-order **synthetic lethal** interaction is required for cell viability. For **synthetic lethal** pairs, only a subset of these samples will be inviable (i.e., removed from simulated data), leading to an under-representation.

In practice, samples are not removed from a simulated dataset, rather the **expression** and function of the query gene is generated across samples separately from the pool of potential partner genes. The query gene data is matched to simulated samples (as shown in Figure 3.7), satisfying the **synthetic lethal** condition with the procedure described in Section 3.2.2. This is performed to maintain a comparable samples size across simulations and the preserve the assumed (multivariate) normal distribution of the data.

3.2.2 Simulation Procedure

Simulations were developed to simulate normal distributions of **expression** data and define function with a threshold cut-off. This is the reverse to the procedure of **SLIPT** to predict **synthetic lethal** partners (although the threshold is assumed to be unknown when testing upon simulated data). While gene function is used as an intermediary step in modelling **synthetic lethal** genes in **expression** data, the normal distribution is sampled for simulated data to represent normalised empirical **gene expression** data for which **SLIPT** (and other methods) will be applicable.

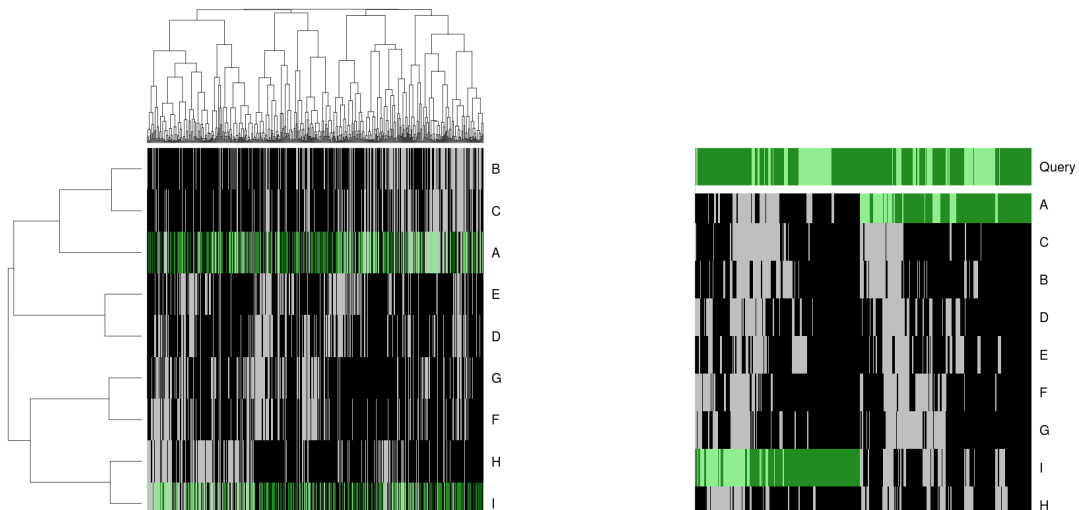
Sampling a distribution for **expression** profiles has the added advantage of being amenable to simulating correlation structures with the multivariate normal distribution (using the **mvtnorm** R package (Genz and Bretz, 2009; Genz *et al.*, 2016)). The



(a) Simulated expression matrix

(b) Corresponding gene function calls

Figure 3.6: **Simulating gene function.** A simulated dataset with samples (columns) and genes A–H (rows) is transformed from a continuous (coloured blue–red) scale to a discrete matrix of gene function (black for functional levels and grey for non-functional).



(a) Simulated gene function with SL genes (b) Query gene added with SL condition

Figure 3.7: **Simulating synthetic lethal gene function.** In a discrete simulated gene function dataset (shaded for functional levels and pale otherwise) with samples (columns) and genes (rows), genes A and I are SL partners of a “Query” gene. A partner is selected (highlighted in green) randomly in each sample for simulating synthetic lethality, then ordered such that the query gene or an SL partner are functional in each sample.

parameter Σ is a covariance matrix defines the correlation structure between simulated genes being sampled. With a diagonal of one, this Σ matrix simulates genes with a standard deviation of one and the covariance parameters between them are the correlations between each gene. In Figure 3.6, an example of such a simulated multivariate normal dataset is shown with the functional threshold applied.

Once we have generated a simulated dataset, the samples are compared by gene function (as derived from a functional threshold). Known underlying synthetic lethal partners are selected within the dataset and a query gene is generated by sampling from the normal distribution. These are matched (as shown for 2 synthetic lethal partners in Figure 3.7) such that the synthetic lethal condition is met: that at least one of the synthetic partner genes and the query gene are functional in any particular cell. The samples are ordered by functional data (without assuming correlation of underlying expression values) with the query gene in one direction and the remaining dataset ordered by the selected synthetic lethal partner.

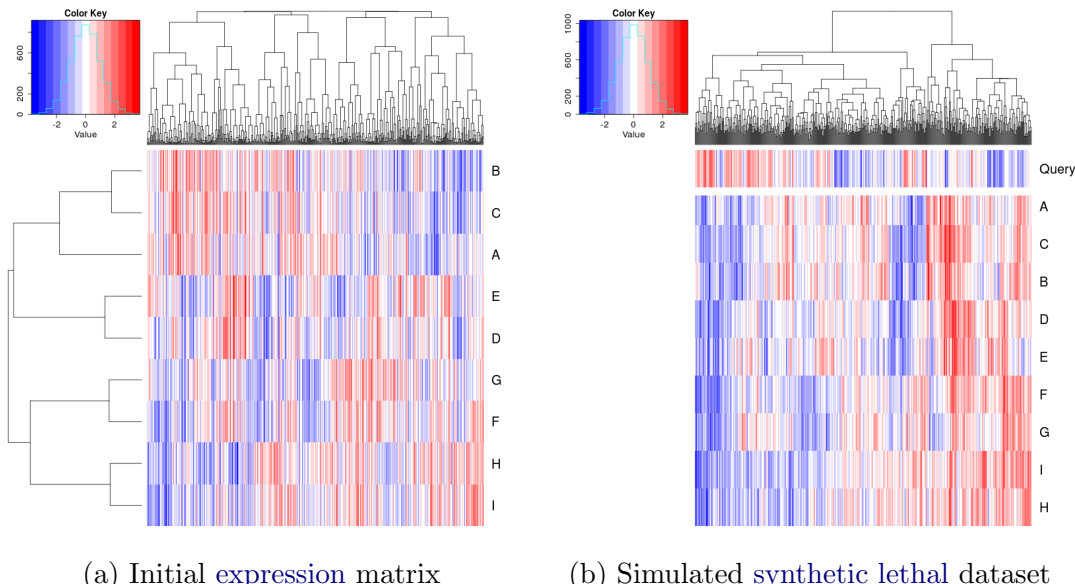


Figure 3.8: **Simulating synthetic lethal gene expression.** A simulated continuous expression dataset (blue–red scale) with samples (columns) and genes (rows) is matched to a query gene such that at least one synthetic lethal partner is above a functional threshold when the query gene is below it satisfying the synthetic lethal model.

This results a simulated dataset where samples with non-functional query gene have at least one functional partner gene. Similarly, the query gene is functional in all samples where all of the synthetic lethal partner genes are non-functional. Therefore a

dataset has been generated with known [synthetic lethal](#) partners (see Figure 3.8) by as few assumptions about the relationships between the each [synthetic lethal](#) pair as possible (and allowing compensating functions from higher-order interactions). This has been designed to have the most stringent (least detectable) [synthetic lethal](#) relationships where higher-order interactions are possible for the purposes of testing pairwise detection procedures such as [SLIPT](#).

3.3 Detecting Simulated Synthetic Lethal Partners

The [synthetic lethal](#) detection methodology ([SLIPT](#)), as described in Section 3.1, was tested on simulated data with known [synthetic lethal](#) partners, generated using the procedure described in Section 3.2.2. This section will present basic simulations to demonstrate the methodology and support its use throughout this thesis. These will be performed with sampling from basic statistical distributions as described, including multivariate normal distribution with correlated blocks of genes, with the Σ matrix show in the plots where relevant. A more complex multivariate normal sampling procedure based on pathway [graph](#) structures, as described in section 3.4.2, will be applied in Chapter 6.

3.3.1 Binomial Simulation of Synthetic Lethality

A previous version of the [synthetic lethal](#) simulation procedure (described in Section 3.2.2), used gene function sampled directly from a binomial distribution using the binomial probability of observing functional gene levels ($p = 0.3$) in one observation ($n = 1$) for each samples:

$$X \sim \text{Bin}(n, p)$$

Once a query gene consistent with [synthetic lethality](#) has been added, these functional levels were passed directly into [SLIPT](#) as “low” and “high” categories.

The simulation procedure was performed with 20,000 total genes (as feasible in the human [genomes](#) and [expression](#) datasets) with a variable number of true [synthetic lethal](#) partners and sample sizes of 500, 1000, 2000, and 5000. Each [ROC](#) curve was derived from the results of 10,000 replicate simulations. The statistical performance (as shown in Figure 3.9) of such an approach based on the χ^2 p-value declines towards random predictions (an [AUROC](#) of 0.5) with an increasing number of underlying true [synthetic lethal](#) partners to detect. However, increased sample size mitigates this decline to some extent, as expected with a statistical predictor, particularly for moderate numbers of [synthetic lethal](#) partners.

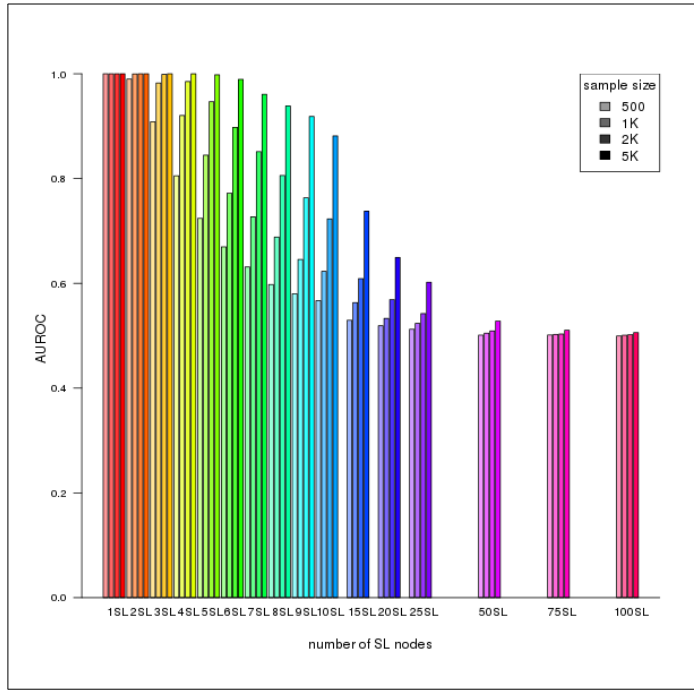


Figure 3.9: **Performance of binomial simulations.** Gene function was simulated by binomial sampling and tested for synthetic lethal genes. Statistical performance declines with additional known synthetic partners but this is mitigated by increased sample sizes.

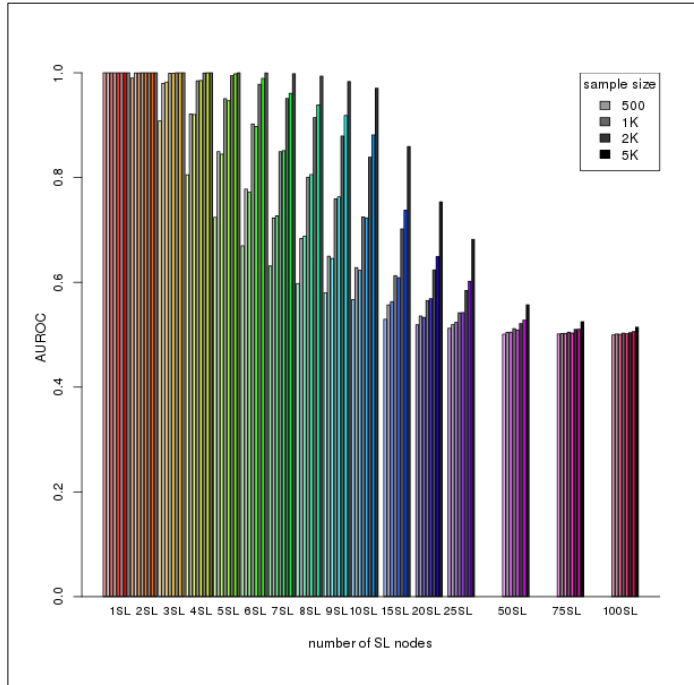


Figure 3.10: **Comparison of statistical performance.** Binomial simulation of synthetic lethality (in colour) is compared (in greyscale) to multivariate normal simulations (detailed below) which consistently outperforms binomial simulation across parameters.

Simulations based on a simple binomial model of **synthetic lethality** are limited but form a basis for building a more complex model including **expression** and correlation structures. While this does not represent the data that **SLIPT** will be applied to, binomial simulations do demonstrate that **SLIPT** is able to distinguish small numbers of **synthetic lethal** partners in a simplistic simulated system with behaviour expected with respect to sample size. This supported further development of the **synthetic lethal** model and simulation pipeline (as described in Section 3.2) using the multivariate normal distribution.

The multivariate normal simulation procedure is more representative of the (normalised) **expression** data **SLIPT** is intended for and enables the prediction procedure to be tested without changes to the methodology (presented in more detail in Section 3.3.2). Sampling continuous **expression** values from a normal distribution allows the **expression** threshold for gene function to differ from the categorical “low” and “high” **expression** binning performed by **SLIPT** (as discussed in Section 3.2.1) which represents that the **SLIPT** procedure does not assume a known threshold for **expression** but rather uses **expression** as an estimate of gene function. This functionality can be included in the multivariate normal simulation without compromising the statistical performance of the **SLIPT**, rather the performance estimates (shown in Figure 3.10) were a marked improvement over the binomial simulation procedure across simulation parameters in an equivalent simulation (without correlation structure). This improvement may be due to binomial model defining the **synthetic lethal** condition in a way that, while ensuring at least one **synthetic lethal** partner is active in query deficient samples, disrupts the number of samples with functional **synthetic lethal** genes compared to other genes affecting the expected sample proportions of χ^2 test.

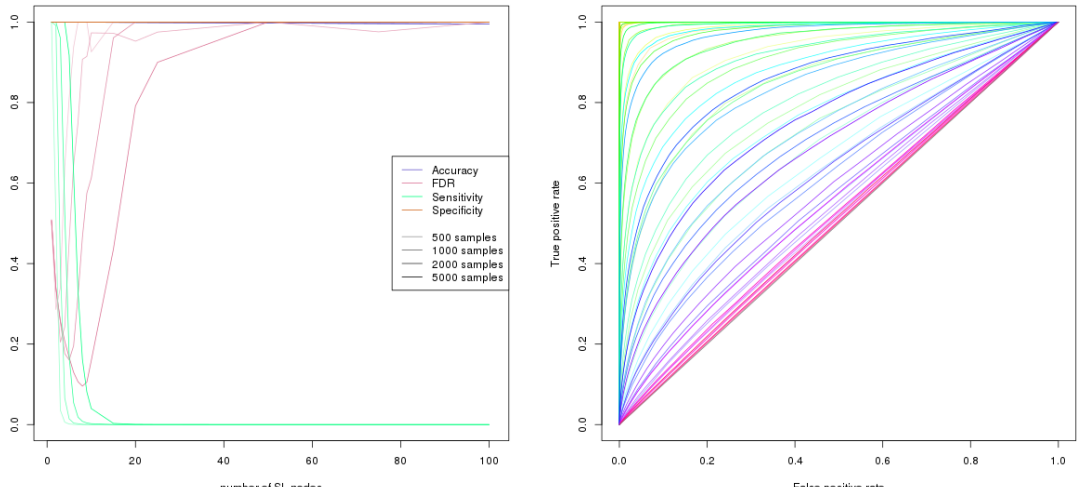
3.3.2 Multivariate Normal Simulation of Synthetic Lethality

The multivariate normal simulation procedure was initially performed using the **mvtnorm** R package (Genz and Bretz, 2009; Genz *et al.*, 2016) (as described in Section 3.2) without correlation structure.

Expression is sampled from multivariate normal distribution with a mean ($\mu = 0$), standard deviation ($\sigma = 1$), and no correlation between genes ($r = 0$):

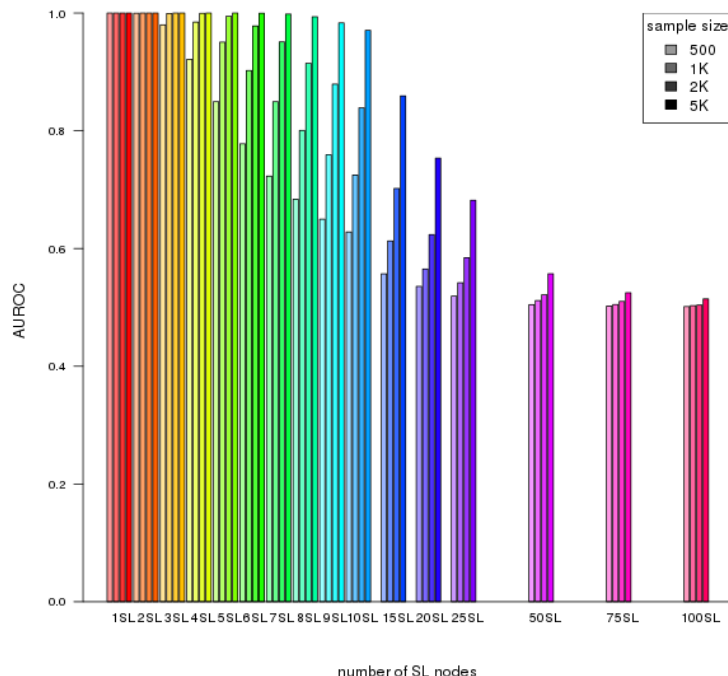
$$X \sim N(\bar{\mu}, \Sigma)$$

Once a query gene consistent with **synthetic lethality** has been added, the simulated **expression** values are tested by **SLIPT** exactly as described in Section 3.1.



(a) Statistical evaluation

(b) Receiver operating characteristic



(c) Statistical performance

Figure 3.11: **Performance of multivariate normal simulations.** Simulation of synthetic lethality was performed sampling from a multivariate normal distribution (without correlation structure). Performance of **SLIPT** declines for more synthetic partners but this is mitigated by increased sample sizes (in darker colours). This generally occurs as the sensitivity decreases for a greater number of true positives to detect, leading to a trade off in accuracy as seen in a trough for false positive rate and the **ROC** curves.

As shown in Figure 3.11a, the statistical accuracy of **SLIPT** as a binary classifier is considerably high across simulations of a full human dataset of 20,000 genes. However, with the χ^2 p-value as a threshold for prediction, this is largely to desirable specificity: the majority of non-SL genes are distinguished from the few underlying **synthetic lethal** genes. In this regard, the **SLIPT** methodology generally performs better with larger datasets with more expected negatives and thus the results of simulations of smaller numbers of genes (e.g., the **graph** structures analysed in Chapter 6) can be applied to larger datasets where they are expected to perform comparably or better with a lower false negative rate. Accordingly, key results will be supported by replication with larger numbers of non-SL genes added to the simulations.

However, with higher numbers of **synthetic lethal** genes to detect, the sensitivity (in Figure 3.11a) of **SLIPT** as a binary classifier of **synthetic lethality** declines, although this is somewhat mitigated by higher sample sizes (shown in darker colours). Thus the minority of true **synthetic lethal** partners are more difficult to distinguish when there are more of them (and a weaker **expression** signal from each). While a reasonable reduction of the false positive rate can be achieved for moderate numbers of underlying **synthetic lethal** partners, we can not be sure how many partners are expected to be detected in analyses of **expression** data. However this simulation procedure is amenable to assessing the performance of **SLIPT** across simulation parameters, **graph** structures and comparisons to other approaches (presented in more detail in Chapter 6).

Not all of the genes detected by **SLIPT** will be true **synthetic lethal** genes but these will be among the strongest candidates and it performs better with fewer underlying **synthetic lethal** genes to detect. This supports a focus on pathway analyses, in particular detecting pathways for further investigation. Since individually gene candidates are not necessarily gene **synthetic lethal** themselves, pathway over-representation analysis will be performed to detect functional groups recurrently detected by **SLIPT** as these detection of functionally related genes further support their role in **synthetic lethal** relationships in addition to being biologically informative. Alternatively, pathway **meta-genes** will reduce the number of underlying **synthetic lethal** to identify **synthetic lethal** pathways. Both of these approaches will be applied in Chapter 4 to identify and replicate synthetic pathways of *CDH1*. Pathways are also more likely to replicate across experimental models as demonstrated by Dixon *et al.* (2008).

The receiver operating characteristic curves (in Figure 3.11b) demonstrate that **SLIPT** is subject to near equal trade-off between sensitivity and specificity across threshold values. The lower sensitivity and higher specificity with a binary classification

(in Figure 3.11a) stems from stringent testing by **SLIPT** with (FDR) p-values adjusted for multiple tests. The area under these curves is also used to compare statistical performance (in Figure 3.11c), with declining performance across increased underlying synthetic lethal partners and increased performance with sample size in multivariate normal simulations.

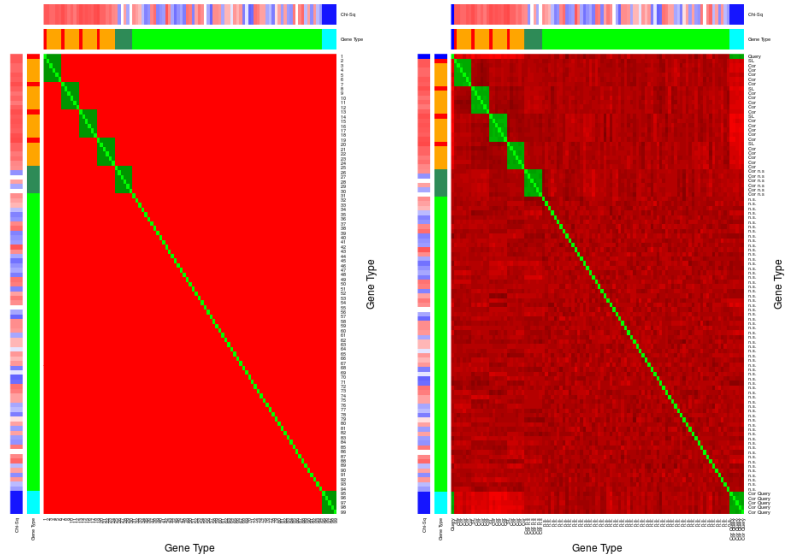
3.3.2.1 Multivariate Normal Simulation with Correlated Genes

Correlation structures can be added to the simulation procedure (as discussed in Section 3.2), starting with simple correlated blocks of genes as the Σ parameter depicted in Figure 3.12a. These correlated blocks represent genes with correlated expression such as that expected by coregulation or biological pathways. Figure 3.12 gives an example of 4 synthetic lethal genes (out of 100), each with 5 correlated genes that are not themselves synthetic lethal partners of the query gene. This serves to test whether synthetic lethal genes are distinguishable from correlated partners. This Σ matrix produces a similar correlation structure (Figure 3.12b) in the resulting expression profiles (Figure 3.12c) where apart from correlated blocks of genes ($r = 0.8$), the remaining genes have only slight variations due to random sampling. The structure of the dataset, particularly between synthetic lethal genes and the query, is shown at the gene expression (Figure 3.12c) and function (Figure 3.12d). These are ordered by the **SLIPT** results and the synthetic lethal genes are ranked high, with the majority of them being distinguishable from highly correlated genes.

The use of correlation structures generalises to larger datasets, such as 1000 genes shown in Figure 3.13. Synthetic lethal genes are highly ranked by **SLIPT** and still largely distinguishable from correlated genes. As previously discussed in Section 3.3.2, these synthetic lethal genes are still detectable among a larger number of true negatives and the **SLIPT** methodology performs better on such datasets.

These plots (Figures 3.12 and 3.13) also show similar correlated blocks with a non-synthetic lethal gene (true negative) and the query gene (which is not synthetic lethal with itself). Neither of these should be synthetic lethal (or detected to be) but they may impact upon the performance of the model, particularly the specificity as correlated negative genes may be distinguishable from true synthetic lethal genes. The non-synthetic lethal correlated block has no impact on synthetic lethal detection but the impact of query correlated genes will be discussed in Section 3.3.2.2 and Chapter 6.

These simulations (on 100 genes) were repeated to examine the variation between detection on different samples and varying the number of underlying synthetic lethal partners, in simulated gene expression data with correlations structure. A small number



(a) Input Σ matrix parameter (b) Simulated correlation matrix

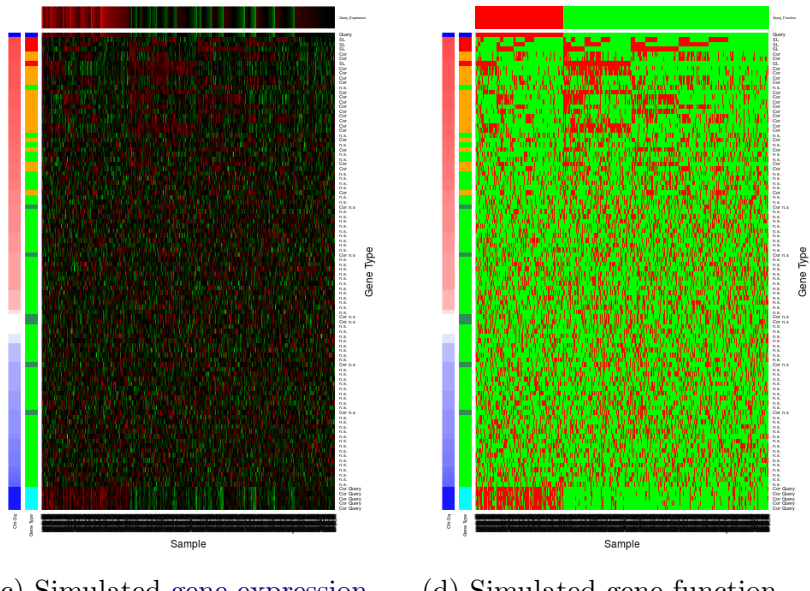


Figure 3.12: **Simulating expression with correlated gene blocks.** A Σ matrix (a) is used to generate a multivariate normal distribution with 100 genes in correlated blocks of genes (correlated by 0.8) with a comparable structure (b) to the input Σ , as shown by correlation on a red–green scale. The annotation bars for genes give the χ^2 (in blue if the direction of **SLIPT** is met or red otherwise) and the gene category (blue for query, cyan for query-correlated, red for SL, orange for SL-correlated, forest green for non-SL-correlated, and green for non-SL). The simulated **gene expression** (c) and function (d) generated are ordered by χ^2 showing the functional structure of **synthetic lethal** genes and that they are among the strongest **SLIPT** results.

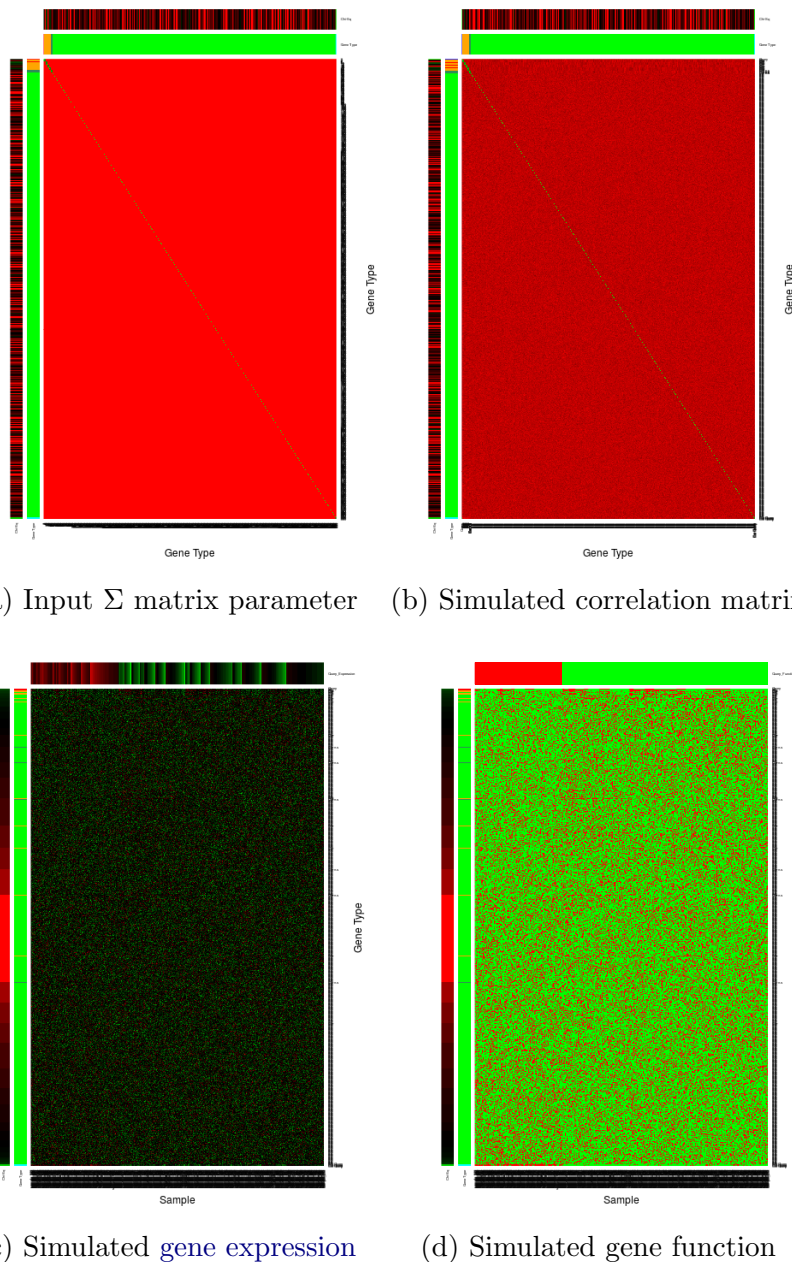


Figure 3.13: **Simulating expression with correlated gene blocks.** Using the (a) Σ matrix, sampling from a multivariate normal distribution with of 1000 genes produced (b) correlated blocks of genes (correlated by 0.8) on a red-green scale. The simulated gene expression (c) and function (d) generated are ordered by χ^2 and SLIPT direction show that synthetic lethal genes are among the strongest SLIPT results with high specificity against many potential false positives. These are annotated for χ^2 (on a red-green scale) and category (blue for query, cyan for query-correlated, red for SL, orange for SL-correlated, forest green for non-SL-correlated, and green for non-SL) for each gene.

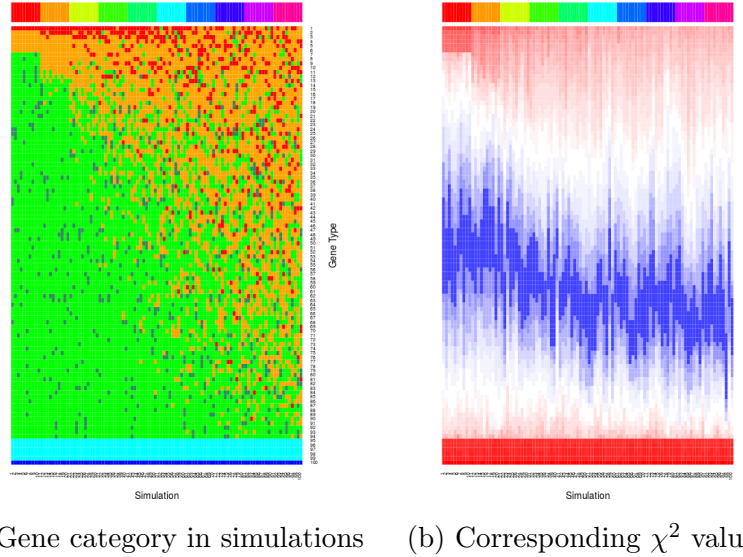
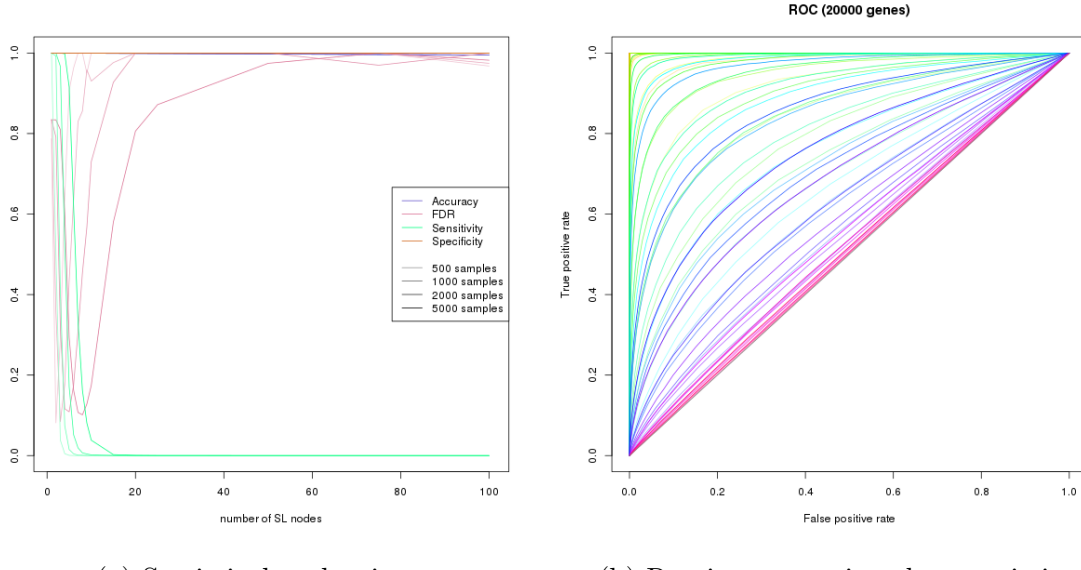


Figure 3.14: Synthetic lethal prediction across simulations. The gene category (blue for query, cyan for query-correlated, red for SL, orange for SL-correlated, forest green for non-SL-correlated, and green for non-SL) ordered by χ^2 signed by the [SLIPT](#) directional condition is shown across simulations. For each of 1–10 SL partners, 10 simulations demonstrate that the increasing numbers of SL partners become harder detect. The χ^2 values show a clear threshold for SL and correlated genes when there are fewer of them, distinguishable from correlated genes in this case.

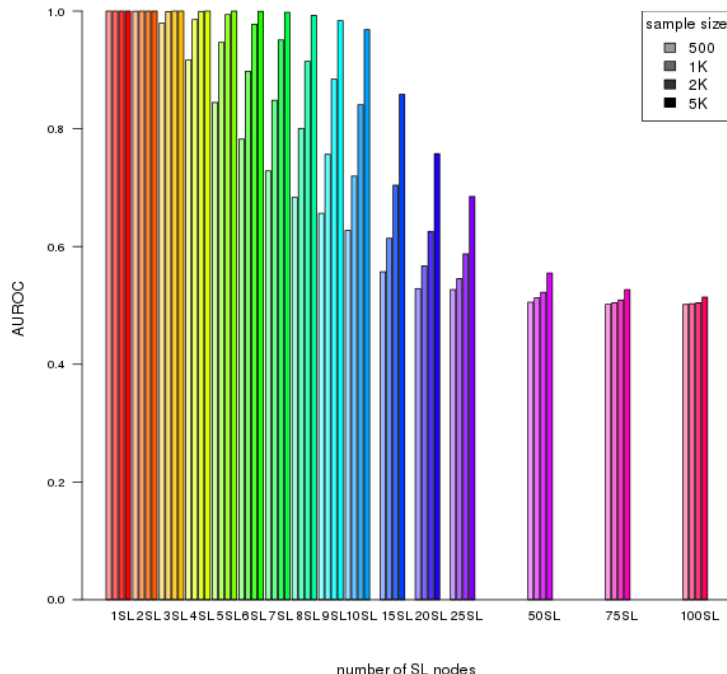
(10 for each) simulations are shown in Figure 3.14 to demonstrate the variation between replicate simulations, with iterative sampling from the same multivariate normal distribution. These simulations show [synthetic lethal](#) genes are not only highly ranked by [SLIPT](#) when there are few of them but also that they are fairly consistent across replicate simulations. Whereas they become less consistent for increasing numbers of true [synthetic lethal](#) partners to detect and thus more difficult to distinguish from other genes, particularly those correlated with them. Similarly, the χ^2 values show a marked stepwise increase with clear thresholds for SL and correlated genes in simple simulations, whereas these become less evident for higher numbers of SL partners.

Whether the [synthetic lethal](#) genes detected in simple simulations (in Figure 3.14) are robustly detectable across greater number of simulations, in addition to further comparisons, was tested with a supporting [ROC](#) analysis. These results (in Figure 3.15) are very similar to simulations without correlation structure, with [SLIPT](#) as a binary classifier having a poor sensitivity with increasing numbers of [synthetic lethal](#) partners to detect but high specificity in a total of 20,000 genes with the vast majority being true



(a) Statistical evaluation

(b) Receiver operating characteristic



(c) Statistical performance

Figure 3.15: Performance with correlations. Simulation of synthetic lethality was performed sampling from a multivariate normal distribution (with correlation structure). Performance of **SLIPT** declines for more synthetic partners but this is mitigated by increased sample sizes (darker colours). This generally occurs as the sensitivity decreases for a greater number of true positives to detect, leading to a trade off in accuracy as seen in a trough for false positive rate and the **ROC** curves.

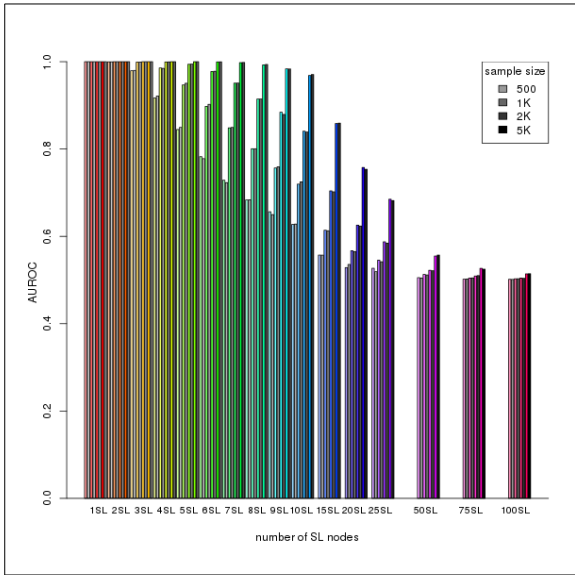
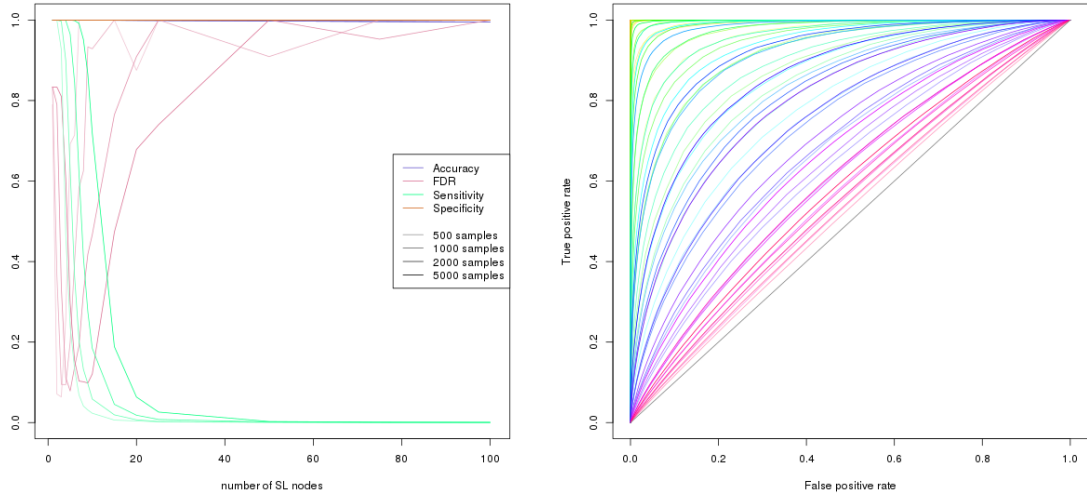


Figure 3.16: **Comparison of statistical performance with correlation structure.** Multivariate simulation of [synthetic lethality](#) with correlation structure (in colour) has comparable performance to simulation without correlations (in greyscale) with known synthetic partners across parameters.

negatives. This is reflected in a similar decline in statistical performance for increasing numbers of [synthetic lethal](#) partners and a compensating increase in performance with higher sample size. Overall, the statistical performance is very similar to simulations without correlation structure (as shown in Figure 3.16).

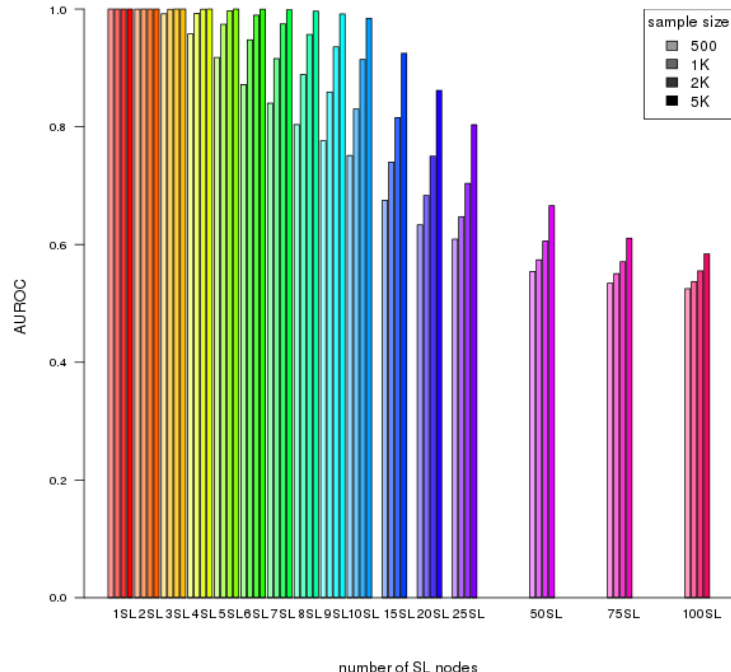
Thus **SLIPT** is robust across correlation structures and applicable to real gene expression data where [pathway](#) structures and correlations are a consideration. These correlation structures are not intended to model specific biological pathways or represent them, rather they serve to test the impact of correlation structure on the performance of **SLIPT** with an extreme example of closely correlated ($r = 0.8$) gene blocks. More complex correlation structures, such as genes positively correlated with the query gene and derived from pathway [graph](#) structures (as described in 3.4.2) will be examined below (in Section 3.3.2.2) and in Chapter 6 respectively.

In particular, genes correlated with true [synthetic lethal](#) genes have little impact on the performance of **SLIPT** detection: [synthetic lethal](#) genes are as distinguishable from true negative genes as without correlated genes. [Synthetic lethal](#) correlated genes will not interfere detect of true [synthetic lethal](#), although they may be ranked next below them and be biologically informative with related gene functions.



(a) Statistical evaluation

(b) Receiver operating characteristic



(c) Statistical performance

Figure 3.17: Performance with query correlations. Simulation of synthetic lethality was performed sampling from a multivariate normal distribution (with correlation structure including correlated genes with non-SL and query genes). As before, performance of **SLIPT** declines for more synthetic partners and is mitigated by increased sample sizes (darker colours) but the sensitivity remains higher for a greater number of true positives with corresponding improvements in **ROC** curves.

3.3.2.2 Specificity with Query-Correlated Pathways

Another consideration for correlation structures is positively correlated genes with the query that are not *synthetic lethal*. As described in Section 3.3.2.1, 5 highly correlated ($r = 0.8$) with the query gene were added. These simulations perform similarly to before (in Figure 3.17) with a higher specificity and a lower false positive rate being feasible (as shown in Figure 3.17a).

3.3.2.3 Importance of Directional Testing

It is important to notice here that the directional criteria of the **SLIPT** procedure is enhancing its performance, particularly in distinguishing positively correlated true negatives. The multivariate normal simulation results, with 20,000 genes including all of the correlation structures discussed (SL, non-SL, and query correlated genes), are compared here for **SLIPT** with and without (χ^2) directional testing. There is a marked improvement in statistical performance with directional criteria, particularly with increased sensitivity and lower false positive rate (as shown in Figure 3.18).

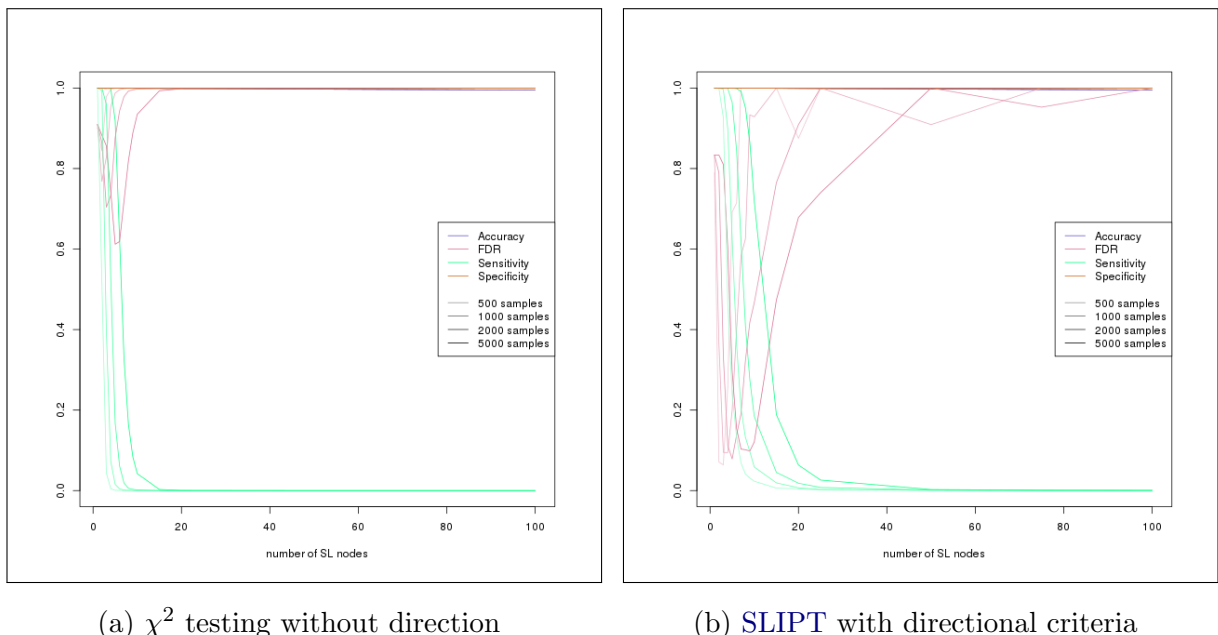
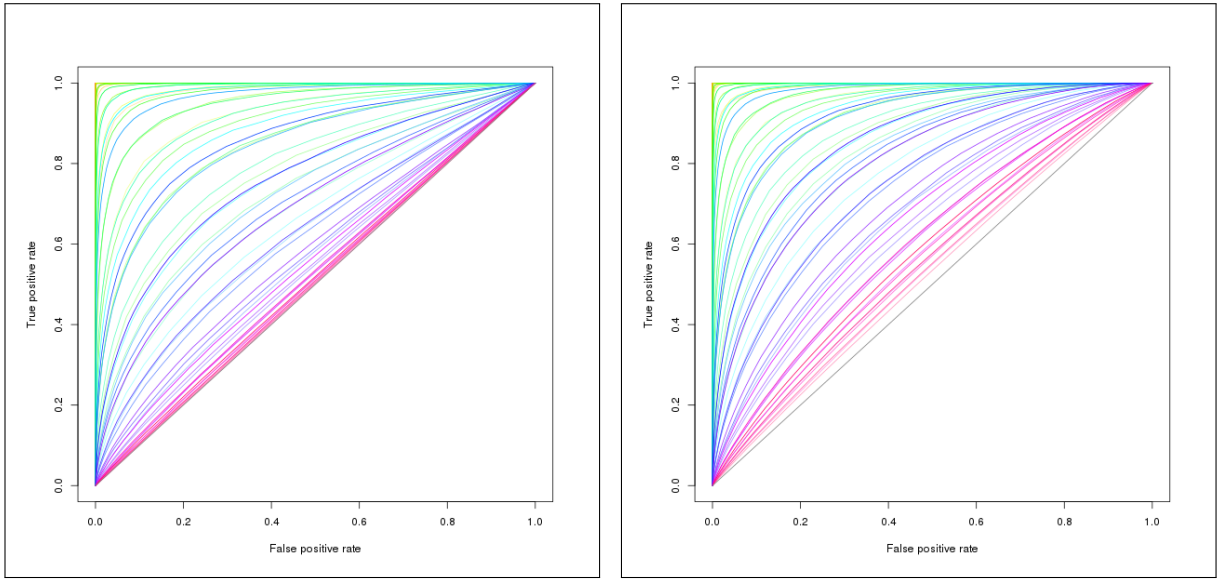
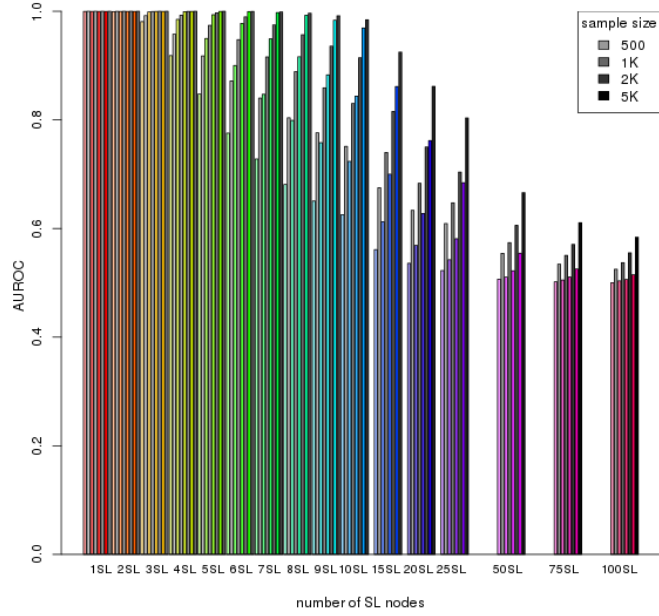


Figure 3.18: **Statistical evaluation of directional criteria.** A simulated multivariate normal dataset of 20,000 genes with correlation structures was tested by **SLIPT** with the directional condition and the equivalent χ^2 test without. **SLIPT** exhibited a consistently higher sensitivity and lower false positive rate.



(a) χ^2 testing without direction

(b) SLIPT with directional criteria



(c) Statistical performance

Figure 3.19: **Performance with directional criteria.** A simulated multivariate normal dataset of 20,000 genes with correlation structures was tested by **SLIPT** with the directional condition and the equivalent χ^2 test without. **SLIPT** has higher performance across simulation parameters, clearly differing from random (grey diagonal) in ROC curves up to 100 SL genes (b). The performance (c) of **SLIPT** (in greyscale) was consistently higher than the χ^2 test (in color).

This is encouraging for the application of **SLIPT** to empirical **expression** datasets as positively correlated genes are likely to occur and the directional condition robustly improves the performance of **SLIPT** across simulation parameters. Without assuming the underlying number of **synthetic lethal** genes, **SLIPT** will perform better than the χ^2 test alone at detecting them. This is further supported irrespective of significance threshold for the χ^2 test by the **ROC** analysis in Figure 3.19. The directional **SLIPT** methodology outperforms the ordinary χ^2 test at detecting **synthetic lethal** partners with some predictive power (above random and **AUROC** of 0.5) even up to 100 **synthetic lethal** genes.

Together these simulation results support the application of the **SLIPT** methodology as it has been performed throughout Chapter 4 and 5. However, the methodology and simulation procedure will explored in more detail in Chapter 6, with the inclusion of **graph** structures and comparison to other **synthetic lethal** detection approaches.

3.4 Graph Structure Methods

Graph structures have been used in several ways in this project with novel approaches to analysis and simulations. Procedures were developed for statistical and network analysis of gene states in **pathway** structures. Specifically, the relationships between **siRNA** and **SLIPT** genes were tested within biological pathways in Chapter 5. These **graph** structures were also used in Chapter 6 for the simulation of **synthetic lethality** to derive correlation structure between simulated **gene expression** profiles in manner that resembles biological pathways.

3.4.1 Upstream and Downstream Gene Detection

Comparison of experimental and computational candidate **synthetic lethal** partner genes within **pathway** structures arose from the hypothesis that these sets of genes were related by **pathway** structure. Due to differences in how these candidates were generated, it should not be expected that they detect the identical genes within the candidate biological pathways, rather they may be related by being upstream or downstream of each other.

Using the Reactome version 52 data (Croft *et al.*, 2014) as described in Section 2.4.2, genes identified by each **synthetic lethal** discovery approach were mapped to the **graph** structure for the candidate pathways identified in Chapter 4 (with subgraphs defined as described in Section 2.4.3). To test whether **siRNA** candidate genes were upstream of **SLIPT** candidate genes, **shortest paths** were traced between each potential pair of

these genes in a directed network. The number of genes where the **siRNA** candidate was upstream were scored “up” and where the **siRNA** candidate was downstream were scored “down”. This procedure enabled counting the total number of **shortest paths** which supported **siRNA** genes being upstream or downstream of the **SLIPT** genes and measuring the difference between these to determine if there is an imbalance in a particular direction. While this difference is indicative of the number of paths between the gene candidate groups in either direction, alone it is not sufficient to statistically support structure or relationships between **siRNA** and **SLIPT** genes. However, it may be combined with a permutation resampling procedure (as described in Section 3.4.1.1) to test for directional relationships in either direction.

The original version of this procedure excluded gene detected by both approaches since they would count in both directions. Upon further consideration, the intersection genes were restored to being accounted for by the **shortest paths** counts since they may count unequally to being upstream or downstream of each gene set if there are unequal numbers above or below them in the **pathway** structure.

3.4.1.1 Permutation Analysis for Statistical Significance

A permutation procedure was developed to randomly assign members of the pathway to **siRNA** and/or **SLIPT** groups, with the same number of each candidate partner gene set as observed in the pathway. These permuted genes are measured for **pathway** structure between the permuted gene groups as performed for the observed candidates (as performed in Section 3.4.1). A distribution of **pathway** structure relationships expected by chance is generated by permuting iteratively over these pathways. This null distribution can be compared to the observed counts of relationships (in either direction), which yields a permutation p-value as the proportion of permutations in which had value or greater or more extreme magnitude than the observed value.

The null hypothesis is that there is no relationship between these gene groups that would not have occurred had the genes been selected at random. Thus we can test both the alternate hypothesis that the **siRNA** genes were upstream of the **SLIPT** genes or that they are downstream of them.

The permutation procedure does not assume the underlying distribution of the data under the null hypothesis and accounts for the total number of **nodes**, **edges**, **siRNA**, and **SLIPT** genes in each pathway **network** structure. The intersection size of the **siRNA** and **SLIPT** genes was originally not accounted for under the **shortest path** counts procedure that excluded them. A refined version of this procedure ensured that

the number of intersecting genes was equal to the number observed to test for pathway structure without changing the intersection size, the subject of prior analyses.

3.4.1.2 Hierarchy Based on Biological Context

An alternative approach to pathway structure was performed based on the biological context that genes at the upstream and downstream ends of a pathway perform different functions, such as a kinase signalling cascade receiving signals from external stimuli and passes these on ribosomes or the nucleus. The genes were assigned to a hierarchy to determine if genes of either candidate group (or those with stronger support for either group) performed upstream or downstream functions disproportionately.

A network-based approach was used to determine the pathway hierarchy of genes in a computationally rational way when applied to different biological pathways with a directed graph structure, G (without loops). The diameter of the network (i.e., the length of longest possible shortest path between the most distant genes) was used to identify a gene (z) at the downstream end of the pathway (at the end of a diameter spanning shortest path), assigned a hierarchy of:

$$\text{hierarchy}(z) = 1 + \text{diameter}(G)$$

Having identified the downstream end of the pathway, genes upstream (e.g., gene i) of this are assigned a hierarchy by the length of their shortest path (d) to this gene, z .

$$\text{hierarchy}(i) = \text{hierarchy}(z) - d_{iz}$$

The remaining unassigned genes (e.g., gene j) gain the hierarchy of the length of the shortest path downstream from the nearest assigned gene if possible.

$$\text{hierarchy}(j) = \text{hierarchy}(i) + d_{ij}$$

This process may be performed iteratively to fill in pathway hierarchy but it was not necessary to perform further iterations for the candidate synthetic lethal pathways investigated (amenable to this procedure) which exhibited clear directional structure and the small world property (with a low diameter). Thus genes in a pathway graph structure were assigned integer valued hierarchy upstream to downstream by this procedure:

$$\text{hierarchy} \in \{1, 2, 3, \dots, 1 + \text{diameter}(G)\}$$

This hierarchy of pathway directionality (e.g., that shown in Figure 5.7) can be used for comparison with measures of the number of genes of each candidate group and the support for being synthetic lethal partners with either approach.

3.4.2 Simulating Gene Expression from Graph Structures

A further refinement of the simulation procedure generated [expression](#) data with correlation structure, derived from a known [graph](#) structure. This enables modelling of synthetic lethal partners within a biological pathway and the investigation of impact of [pathway](#) structure on [synthetic lethal](#) prediction. A simulated pathway is first constructed as a [graph](#) structure, with the [igraph](#) R package [Csardi and Nepusz \(2006\)](#), with the added annotation of the state of the [edges](#) (i.e, whether they activate or inhibit downstream pathway members). This simulation procedure was intended for biological pathway members with correlated [gene expression](#) (higher than the background of genes in other pathways) but it may also be applicable to modelling protein levels (in a kinase regulation cascade) or substrates and products (in a metabolic pathway).

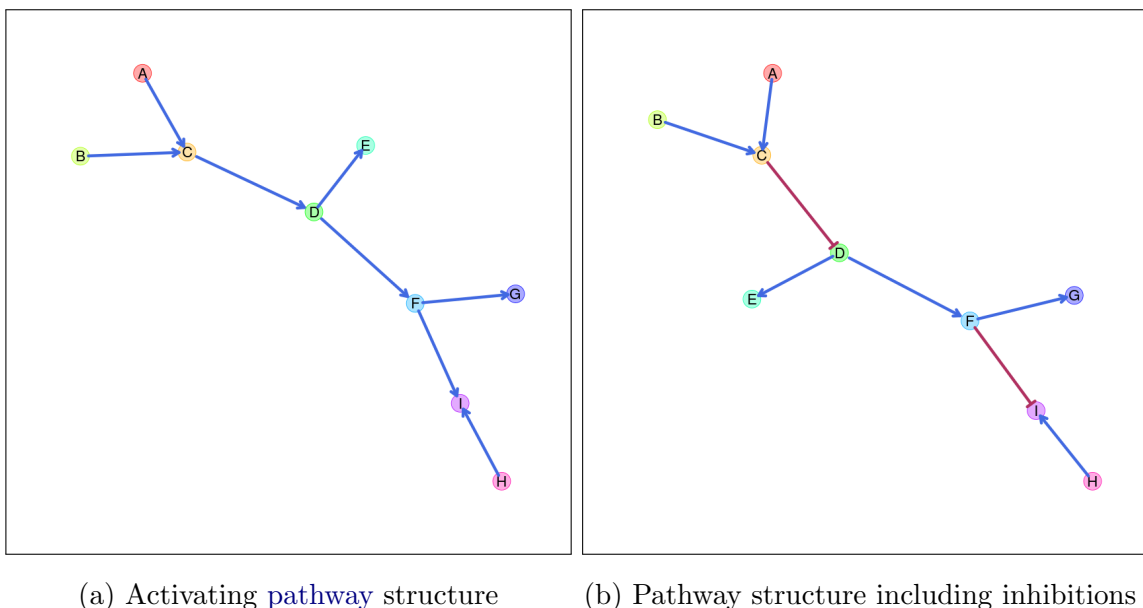


Figure 3.20: **Simulated graph structures.** A constructed [graph](#) structure used as an example to demonstrate the simulation procedure. Activating [links](#) are denoted by blue arrows and inhibiting [links](#) by red edges.

First, the [graph](#) structure is constructed for simulated data to be generated from (by sampling from a multivariate normal distribution using the [mvtnorm](#) R package ([Genz and Bretz, 2009; Genz et al., 2016](#))). Throughout this section, the simulation procedure will be demonstrated with the relatively simple constructed [graph](#) structure shown in Figure 3.20. This [graph](#) structure visualisation was specifically developed for (directed) iGraph objects in R and has been released in the [plot.igraph](#) package and

`igraph.extensions` library (see Table 2.6 and Section 3.5.3). The `plot_directed` function allows customisation of plot parameters for each `node` or `edge` and mixed (directed) `edge` types for indicating activation or inhibition. These inhibition `links` (which often occur in biological pathways) are demonstrated in Figure 3.20b.

The simulation procedure is designed to use such `graph` structures to inform development of a “Sigma” variance-covariance matrix (Σ) for sampling from a multivariate normal distribution (using the `mvtnorm` R package). Given a `graph` structure (or adjacency matrix), such as Figure 3.21a, a relation matrix is calculated based on distance such that nearer `nodes` are given higher weight than farther `nodes`. For the purposes of this thesis a geometrically decreasing (relative) distance weighting is used, with each more distant `node` being related by $1/2$ compared to the next nearest as shown in Figure 3.21b. However, an arithmetically decreasing (absolute) distance weighting is also available in the `graphsim` R package release of this procedure.

A Σ matrix is derived from this distance weighting matrix, creating a matrix (with a diagonal of 1) where each `node` has a variance and standard deviation of 1. Thus covariances between adjacent `nodes` are assigned by a correlation parameter and the remaining matrix based on weighting these correlations with by the distance matrix (or the nearest “positive definite” matrix). For the purposes of this thesis, the correlation parameter is 0.8 unless otherwise specified (as used for the example in Figure 3.21c). This Σ matrix is used to sample from a multivariate normal distribution with each gene having a mean of 0, standard deviation 1, and covariance within the range [0, 1] such that they are correlations. This procedure generates a simulated (continuous normally distributed) `expression` profile for each `node` (as shown in Figure 3.21e) with corresponding correlation structure (Figure 3.21d). The simulated correlation structure closely resembles the expected correlation structure (Sigma in 3.21c) even for the relatively modest sample size ($N = 100$) illustrated in 3.21. Once a simulated `gene expression` dataset has been generated (as in Figure 3.21e), then a discrete matrix of gene function can be constructed with a functional threshold quantile to simulate functional relationships of `synthetic lethality` (as shown in Figure 3.4). For the purposes of this thesis, this threshold is the 0.3 quantile (as discussed in Section 3.2.1) which generates functional discrete matrices such as those used for `synthetic lethal` simulation in Section 3.2.2 (as shown Figure 3.21f)

The simulation procedure (depicted in Figure 3.21) is amenable to pathways containing inhibition `links` (as shown in Figure 3.22) with several refinements. With the inhibition `links` (as shown in Figure 3.22a), distances are calculated in the same manner

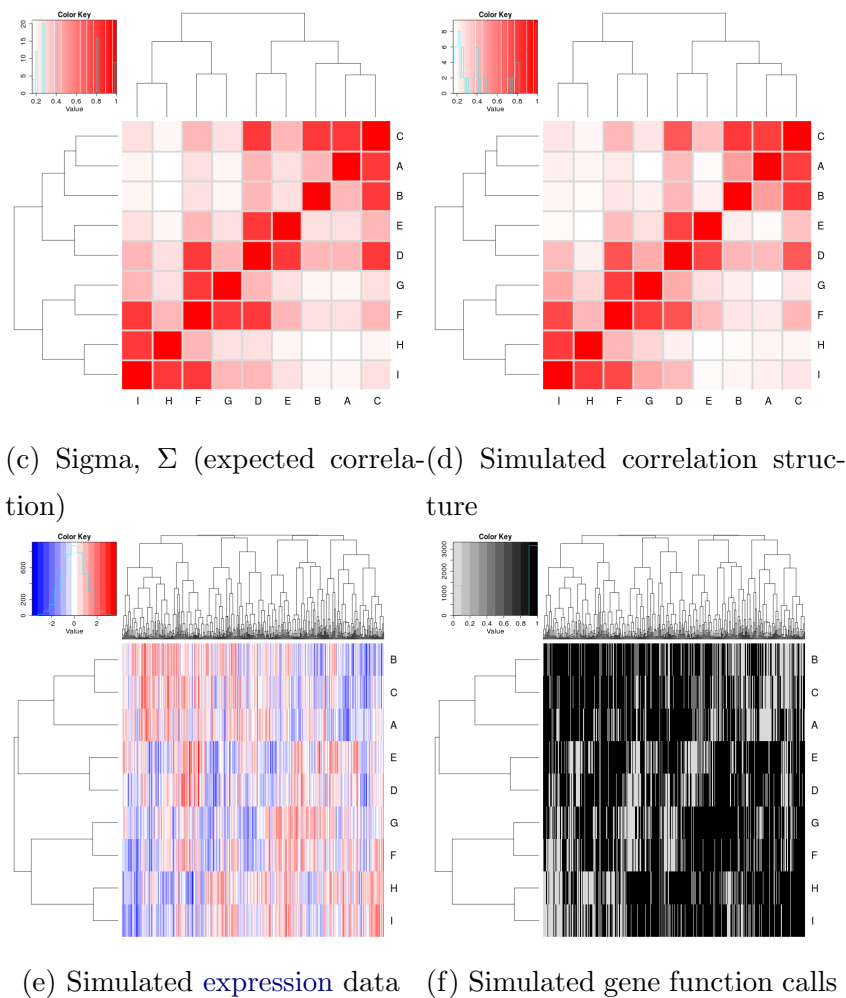
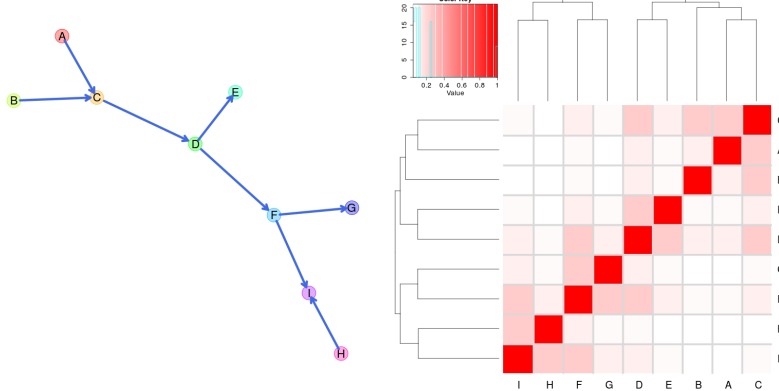


Figure 3.21: **Simulating expression from a graph structure.** An example graph structure is used to derive a correlation structure from the relative distances between nodes and simulate continuous gene expression with sampling from the multivariate normal distribution.

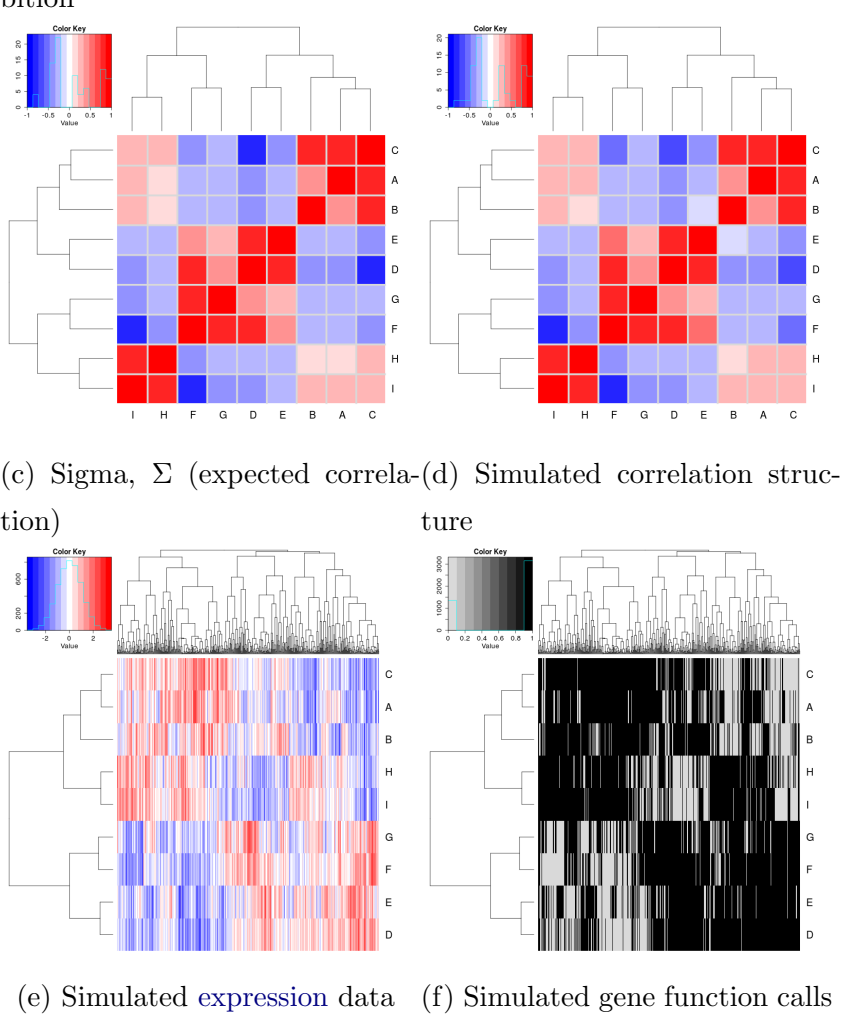
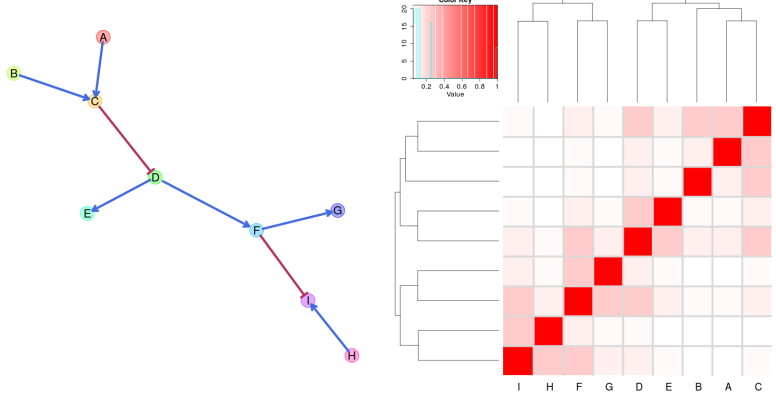


Figure 3.22: **Simulating expression from graph structure with inhibitions.** An example graph structure is used to derive a correlation structure from the relative distances between nodes and simulate continuous gene expression with sampling from the multivariate normal distribution.

as before (Figure 3.22b) with inhibitions accounted for by iteratively multiplying downstream `nodes` by -1 to form blocks of negative correlations (as shown in Figures 3.22c and 3.22d). As before, a multivariate normal distribution with these negative correlations can be sampled to generate simulated data (as shown in Figures 3.22e and 3.22f).

These simulated datasets are amenable to simulating synthetic lethal partners of a query gene within a graph network. The query gene is assumed to be separate from the graph network pathway and is added to the dataset using the procedure in Section 3.2.2. Thus we can simulate known synthetic lethal partner genes within a synthetic lethal partner pathway structure.

3.5 Customised Functions and Packages Developed

[Move to Appendix?]

Various R packages have been developed throughout this thesis using `devtools` (Wickham and Chang, 2016) and `roxygen` (Wickham *et al.*, 2017) to enable reproducibility of customised analysis and visualisation. Many of these have the added benefit of the functions being documented, demonstrated in example vignettes, and released on GitHub to enable the research community to access utilise them in their own analysis. These are summarised in Table 2.6, along with the corresponding urls for their GitHub repository which contains a README file with instructions for installation with the `devtools` R package (Wickham and Chang, 2016) and links to the relevant vignette(s) where available.

3.5.1 Synthetic Lethal Interaction Prediction Tool

The statistical methodology for detection of synthetic lethality in gene expression data (**SLIPT**) is one of the main novel procedures developed in this thesis, as described in Section 3.1. The `slipt` R package has been prepared for release to accompany a publication demonstrating the applications of the methodology for identifying candidate interacting genes and pathways with *CDH1* in breast cancer (TCGA, 2012).

SLIPT is amenable to analysis of any effectively continuous measure of gene activity (e.g., microarray, RNA-Seq, protein abundance, or pathway metagenes). Executing `slipt` is straightforward: the `prep_data_for_SL` function scores samples as “low”, “medium”, or “high” for each gene, then the `detect_SL` function tests a given query gene against all potential partners by performing the chi-squared test and directional conditions. This function returns a table summarising the observed and expected sample numbers used for the directional criteria, the χ^2 values, and corresponding p-values

including adjusting for multiple comparisons. The `count_of_SL` and `table_of_SL` functions serve to facilitate summary and extraction of the positive **SLIPT** hits, respectively, from the table of predictions of **synthetic lethal** partners.

The **SLIPT** methodology in this package release has been used in later analyses rather than the corresponding source R code, including use on remote machines and upon simulated data. In particular, the functions in the package facilitate alterations to parameters, such as the proportion of samples called as exhibiting low or high gene activity. This release support reproducibility and enables wider use of **SLIPT** in future investigations into other disease genes.

3.5.2 Data Visualisation

Customisations to existing data visualisations in R have been developed to present data throughout this thesis. The `vioplotx` and `heatmap.2x` packages are enhancements of the `vioplot` package (Adler, 2005) and `heatmap.2` provided by the `gplots` package (Warnes *et al.*, 2015).

The `vioplotx` package provides an alternative visualisation (of continuous variables against categories) to the more familiar boxplot, showing variability of the data by the width of the plots. As demonstrated in Figure 3.23, the customised version enables separate plotting parameters for each violin with vector inputs for colour, shape, and size of various elements of the median point, central boxplot, borders, and fill colour for the violin. Scaling violin width to adjust violin area and splitting data by a second categorical variable is also enabled. This function is intended to be backwards compatible with the inputs of `vioplot` (applying scalar inputs across all violins) and `boxplot` (by enabling formula inputs as an S3 method). Each of these features is demonstrated with examples in respective vignettes on the package [GitHub repository](#).

The `heatmap.2x` provides extensions for annotation colour bars for both the rows and columns (as shown in Figure 3.24). Multiple bars are enabled on both axes with matrix inputs (rather than single vector for `heatmap.2`) which facilitates additional plotting of gene and sample characteristics for comparison with correlation matrices, `expression` profiles, or pathway `metagenes`. Annotation bar inputs correspond to their orientation on the plot, each colour bar is provided as a column for the row annotation on the left of the heatmap and as a row for the column annotation on top of the heatmap. Row and column annotation bars are labelled with the column or row names respectively. Additional parameters enable resizing of these annotation bar labels and control of reordering columns for if samples are ordered in advance (e.g., ranked by a

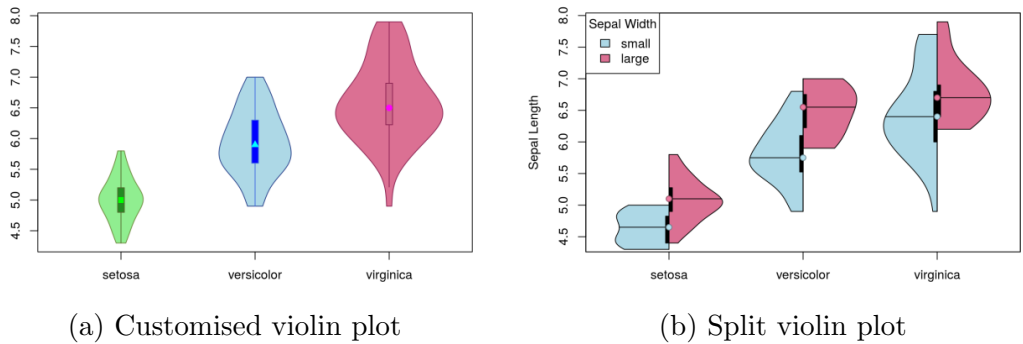


Figure 3.23: **Demonstration of violin plots with custom features.** An example of the *iris* dataset is plotted to show the custom features of the `vioplotx` package including a) individual colour, shape and size parameters of each violin, scaling violin widths by area, and b) splitting violins to compare subsets of data.

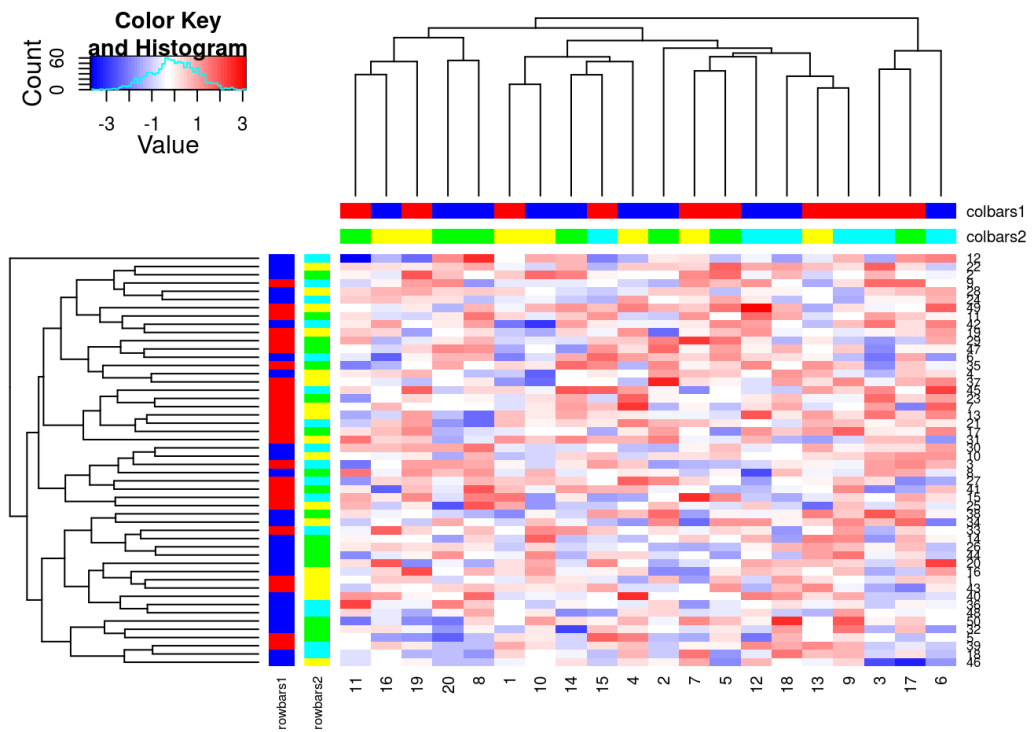


Figure 3.24: **Demonstration of annotated heatmap.** The example heatmap depicts the additional row and column annotation bars enabled by `heatmap.2x`, extending the features of `gplots` with backwards compatible inputs.

`metagene` or split into groups clustered separately). These features were used through this thesis and are provided in a package [GitHub repository](#).

3.5.3 Extensions to the iGraph Package

The following features were developed during this thesis using “iGraph” data objects, building upon the `igraph` package (Csardi and Nepusz, 2006). These have been released as separate packages for each respective procedure and can be installed together as a collection of extensions to the `igraph` package.

3.5.3.1 Sampling Simulated Data from Graph Structures

The `graphsim` package implements the procedure for simulating gene expression from `graph` structures (as described in Section 3.4.2). By default, this derives a matrix with a geometrically decreasing weighting by distance (by `shortest paths`) between each pair of `nodes` with. An absolute decreasing weighting is also available with the option of to derive correlation structures from adjacency matrices or the number of `links` common partners (i.e., size of the shared “neighbourhood” (Hell, 1976)) between each pair of `nodes`. Functions to compute these are called directly by passing parameters to them when running the `generate_expression` or `make_sigma_mat` commands. This package enables simulating `expression` data directly from a `graph` structure (with the intermediate steps automated) or generating Σ parameters for `mvtnorm` from `graph` structures or matrices derived from them. These functions support assigning activating or inhibiting to each `edge` (with a `state` parameter).

3.5.3.2 Plotting Directed Graph Structures

The `plot.igraph` package provides the `plot_directed` function specifically developed for directed `graph` structures and to plot activating or inhibiting for each `edge` (as described in Section 3.4.2). As shown in Figure 3.25, this function supports separate plotting parameters for each `node`, `node` label, and `edge`. This includes colours of `node` fill, border, label text, and `edges` and size of `nodes`, `edge` widths, arrowhead lengths, and font size of labels. The `state` parameter for assigning activating or inhibiting to each `edge` determines whether `edges` are depicted with 30° or 90° arrowheads. Colours are assigned separately and so they may be customised. Vectorised parameters are applied across each `node` or `edge`, whereas scalar parameters apply the same plotting parameters across them. The default layout function is `layout.fruchterman.reingold` but any layout function supported by `plot` function in `igraph` (Csardi and Nepusz, 2006) is compatible such as `layout.kamada.kawai` used to implement the Kamada–Kawai algorithm (Kamada and Kawai, 1989) for graph plots throughout this thesis.

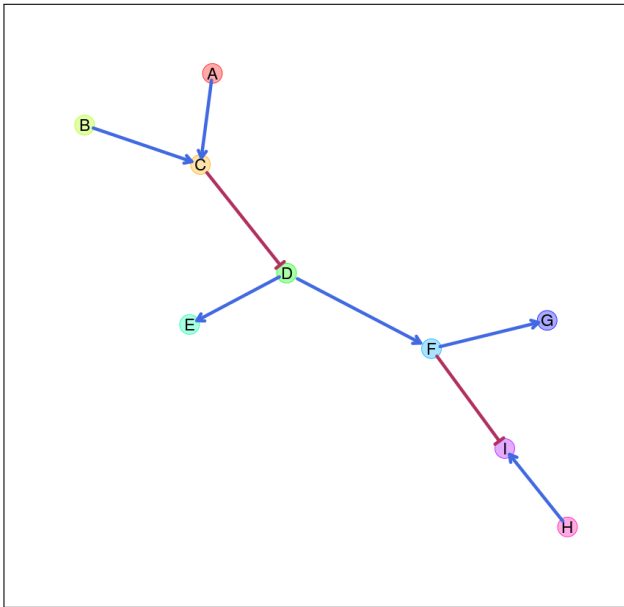


Figure 3.25: **Simulating graph structures.** An example graph structure which will be used throughout demonstrating the simulation procedure from graph structures. Here activating links are denoted by blue arrows and inhibiting links by red edges.

3.5.3.3 Computing Information Centrality

The shortest paths of a network are computed by the `igraph` package Csardi and Nepusz (2006) which can be extended to calculate the network efficiency but is not provided by the package itself (as described in Section 2.4.4). The “information centrality” of a vertex is computed as the relative change in the network efficiency when the vertex is removed. Information centrality is calculated iteratively for each node and the sum of information centrality for each vertex is the information centrality for the network. These metrics are provided by the `info.centrality` package.

3.5.3.4 Testing Pathway Structure with Permutation Testing

A network-based procedure developed was used for comparison of siRNA and SLIPT candidate genes in a pathway structure. Such pathway structure relationships were tested by computing the number of shortest paths between two different groups of nodes in either direction within a graph. This pathway relationship metric was implemented in the `pathway.structure.permutation` package with permutation testing (as described in sections 3.4.1 and 3.4.1.1).

3.5.3.5 Metapackage to Install iGraph Functions

These features may be installed together with `igraph.extensions` which can be accessed from a [GitHub repository](#). This meta-package installs `igraph` ([Csardi and Nepusz, 2006](#)) and the packages described in Section 3.5.3 including their dependencies for matrix operations and statistical procedures: `Matrix`, `matrixcalc`, and `mvtnorm` ([Bates and Maechler, 2016](#); [Genz and Bretz, 2009](#); [Genz *et al.*, 2016](#); [Novomestky, 2012](#)).

Chapter 4

Synthetic Lethal Analysis of Gene Expression Data

Having developed a statistical synthetic lethal detection methodology, **SLIPT**, it was then applied to publicly available cancer gene expression datasets. The analysis focuses on breast cancer for which TCGA expression data (TCGA, 2012) from a patient cohort and siRNA screen data (Telford *et al.*, 2015) from experiments conducted in MCF10A cell line cells were available. Stomach cancer data (Bass *et al.*, 2014) was used to replicate findings in an independent dataset, with this cancer chosen because it also occurs in syndromic HDGC patients. The TCGA data also has the advantages of other clinical and molecular profiles including somatic mutation mutation across many of the same samples, in addition to a considerable sample size for RNA-Seq expression data generated with a common TCGA procedures to minimise batch effects.

Synthetic lethal candidate partners for *CDH1* were identified at both the gene and pathway level. **SLIPT** gene candidates were analysed by cluster analysis for common expression profiles across samples and relationships with clinical factors and mutations in key breast cancer genes. These genes will also be compared to the gene candidates from a primary and secondary (validation) screens conducted by Telford *et al.* (2015) on isogenic cell lines. For comparison, the **SLIPT** methodology was also applied using mutation data for *CDH1* against expression of candidate partners (as described in Section 3.1) which may better represent the null mutations in HDGC patients and the experiment cell model (Chen *et al.*, 2014). Pathways were analysed by over-representation analysis (with resampling for comparisons with siRNA data) and supported by a metagene analysis of pathway gene signatures. The pathway metagene expression profiles were used to replicate known relationships between clinical and molecular characteris-

tics for breast cancer and to demonstrate application of **SLIPT** directly on **metagenes** to detect **synthetic lethal** pathways.

Together these results demonstrate the wide range of applications for **SLIPT** analysis and examine the **synthetic lethal** partners of *CDH1* in breast and stomach cancer. These **synthetic lethal** genes and pathways were identified both in the context of the functional implications of novel **synthetic lethal** relationships and as potential actionable targets against *CDH1* deficient tumours, in addition to replication of established functions of **E-cadherin**. In particular, these analyses focused on comparisons with experimental screening data to explore the potential for **SLIPT** to augment triage of candidate partners and support further experimental investigations. The key **synthetic lethal** partner pathways for *CDH1*, supported by both approaches, will be examined in more detail at the gene and **pathway** structure level in Chapter 5.

4.1 Synthetic Lethal Genes in Breast Cancer

The **SLIPT** methodology (as described in Section 3.1) was applied to the normalised **TCGA** breast cancer **gene expression** dataset ($n = 1168$). As shown in Table 4.1, the most significant genes had strong evidence of **expression-based association** with *CDH1* (high χ^2 values) with fewer samples exhibiting low **expression** of both genes than expected statistically. Eukaryotic translation genes were among the highest scoring gene candidates, including initiation factors, elongation factors, and ribosomal proteins. These are clearly necessary for cancer cells to grow and proliferate, with sustained **gene expression** needed to maintain growth signalling pathways and resist apoptosis or immune factors translation may be subject to **non-oncogene addiction** for *CDH1*-deficient cells.

While these are among the strongest **synthetic lethal** candidates, translational genes are crucial to the viability of healthy cells and dosing for a selective **synthetic lethal** effect against these may be difficult compared to other biological functions which may also be supported among the **SLIPT** candidate genes. Furthermore, few known biological functions of *CDH1* were among the strongest SL candidates, so the remaining candidate genes may also be informative since they are likely to contain these expected functions in addition to novel relationships for *CDH1*. Thus further pathway level analyses were also conducted to examine biological functions over-represented among synthetic candidate genes and to identify **synthetic lethal** pathways.

The modified **mtSLIPT** methodology (as described in Section 3.1) was also applied to the normalised **TCGA** breast cancer **gene expression** dataset, against **somatic muta-**

Table 4.1: Candidate [synthetic lethal](#) gene partners of *CDH1* from SLIPT

| Gene | Observed | Expected | χ^2 value | p-value | p-value (FDR) |
|------------------|----------|----------|----------------|------------------------|---------------------------------|
| <i>TRIP10</i> | 62 | 130 | 162 | 5.65×10^{-34} | 1.84×10^{-31} |
| <i>EEF1B2</i> | 56 | 130 | 158 | 3.10×10^{-33} | 9.45×10^{-31} |
| <i>GBGT1</i> | 61 | 131 | 156 | 1.08×10^{-32} | 3.14×10^{-30} |
| <i>ELN</i> | 81 | 130 | 149 | 3.46×10^{-31} | 8.82×10^{-29} |
| <i>TSPAN4</i> | 78 | 130 | 146 | 1.63×10^{-30} | 3.79×10^{-28} |
| <i>GLIPR2</i> | 72 | 130 | 146 | 1.68×10^{-30} | 3.86×10^{-28} |
| <i>RPS20</i> | 73 | 131 | 145 | 1.89×10^{-30} | 4.28×10^{-28} |
| <i>RPS27A</i> | 80 | 130 | 143 | 5.53×10^{-30} | 1.18×10^{-27} |
| <i>EEF1A1P9</i> | 63 | 130 | 141 | 1.91×10^{-29} | 3.74×10^{-27} |
| <i>C1R</i> | 73 | 130 | 141 | 2.05×10^{-29} | 3.97×10^{-27} |
| <i>LYL1</i> | 73 | 130 | 140 | 2.99×10^{-29} | 5.74×10^{-27} |
| <i>RPLP2</i> | 71 | 130 | 139 | 4.88×10^{-29} | 9.07×10^{-27} |
| <i>C10orf10</i> | 73 | 130 | 138 | 6.72×10^{-29} | 1.20×10^{-26} |
| <i>DULLARD</i> | 74 | 131 | 138 | 9.29×10^{-29} | 1.61×10^{-26} |
| <i>PPM1F</i> | 64 | 130 | 136 | 1.61×10^{-28} | 2.65×10^{-26} |
| <i>OBFC2A</i> | 69 | 130 | 136 | 2.49×10^{-28} | 3.93×10^{-26} |
| <i>RPL11</i> | 70 | 130 | 136 | 2.56×10^{-28} | 3.97×10^{-26} |
| <i>RPL18A</i> | 70 | 130 | 135 | 3.08×10^{-28} | 4.70×10^{-26} |
| <i>MFNG</i> | 76 | 131 | 133 | 7.73×10^{-28} | 1.12×10^{-25} |
| <i>RPS17</i> | 77 | 131 | 133 | 8.94×10^{-28} | 1.29×10^{-25} |
| <i>MGAT1</i> | 73 | 130 | 132 | 1.44×10^{-27} | 2.03×10^{-25} |
| <i>RPS12</i> | 72 | 130 | 128 | 8.57×10^{-27} | 1.12×10^{-24} |
| <i>C10orf54</i> | 73 | 130 | 127 | 1.37×10^{-26} | 1.75×10^{-24} |
| <i>LOC286367</i> | 72 | 130 | 126 | 2.20×10^{-26} | 2.70×10^{-24} |
| <i>GMFG</i> | 70 | 130 | 126 | 2.20×10^{-26} | 2.70×10^{-24} |

Strongest candidate SL partners for *CDH1* by [SLIPT](#) with observed and expected numbers of [TCGA](#) breast cancer samples with low [expression](#) of both genes.

tion loss of function [mutations](#) in *CDH1*. As shown in Table C.1, the most significant genes also had strong evidence of [expression](#) associated with *CDH1 mutations* (high χ^2 values) with fewer samples with *CDH1* exhibiting low [expression](#) each candidate gene than expected statistically. These genes were not strongly supported as the [expression](#) analysis (in Table 4.1), however, nor were as many genes detected. This is perhaps unsurprising due to the lower sample size with matching [somatic mutation](#) data and the lower frequency of *CDH1 mutations* compared to low [expression](#) defined by $1/3$ quantiles.

The [mtSLIPT](#) candidates had more genes involved in cell and gene regulation, particularly [DNA](#) and [RNA](#) binding factors. The strongest candidates also included

microtubule (*KIF12*), microfibril (*MFAP4*), and cell adhesion (*TENC1*) genes consistent with the established cytoskeletal role of *CDH1*. The elastin gene (*ELN*) was notably strongly supported by both expression and mutation SLIPT analysis of *CDH1* supporting interactions with extracellular proteins and the tumour microenvironment.

4.1.1 Synthetic Lethal Pathways in Breast Cancer

Translational pathways were strongly over-represented in SLIPT partners, as shown in Table 4.2. These include ribosomal subunits, initiation, peptide elongation, and termination. Regulatory processes involving mRNA including 3' untranslated region (UTR) binding, L13a-mediated translational silencing, and nonsense-mediated decay were also implicated. These are consistent with protein translation being subject to “non-oncogene addiction” (Luo *et al.*, 2009), as a core process that is dysregulated to sustain cancer proliferation and survival (Gao and Roux, 2015).

Immune pathways, including the adaptive immune system and responses to infectious diseases were also strongly implicated as synthetic lethal with loss of E-cadherin. This is consistent with the alterations of immune response being a hallmark of cancer Hanahan and Weinberg (2000), since evading the immune system is necessary for cancer survival. Either of these systems are potential means to target *CDH1* deficient cells, although these were not detected in an isolated cell line experimental screen (Telford *et al.*, 2015) and the differences between the findings in patient data are described in more detail in Section 4.2.5.

It is also notable that the pathways over-represented in SLIPT candidate genes have strongly significant over-representation of Reactome pathways from the hypergeometric test (as described in Section 2.3.2). Even after adjusting stringently for multiple tests, biologically related pathways were supported together. These pathways are further supported by testing for synthetic lethality against *CDH1* mutations (mtSLIPT) with many of these pathways also among the most strongly supported in this analysis (shown in Table C.2). This mutation-based analysis more closely represents the null *CDH1* mutations in HDGC (Guilford *et al.*, 1998) and the experimental MCF10A cell line cell model (Chen *et al.*, 2014). There was still support for translational and immune pathways not detected in the isolated experimental system. GPCRs also among the most strongly supported pathways, supporting the experimental findings of Telford *et al.* (2015) for these intracellular signalling pathways already being targeted for other diseases.

Table 4.2: Pathways for *CDH1* partners from SLIPT

| Pathways Over-represented | Pathway Size | SL Genes | p-value (FDR) |
|---|--------------|----------|------------------------|
| Eukaryotic Translation Elongation | 86 | 81 | 1.3×10^{-207} |
| Peptide chain elongation | 83 | 78 | 5.6×10^{-201} |
| Eukaryotic Translation Termination | 83 | 77 | 1.2×10^{-196} |
| Viral mRNA Translation | 81 | 76 | 1.2×10^{-196} |
| Formation of a pool of free 40S subunits | 93 | 81 | 3.7×10^{-194} |
| Nonsense Mediated Decay independent of the Exon Junction Complex | 88 | 77 | 5.3×10^{-187} |
| L13a-mediated translational silencing of Ceruloplasmin expression | 103 | 82 | 9.6×10^{-183} |
| 3' -UTR-mediated translational regulation | 103 | 82 | 9.6×10^{-183} |
| GTP hydrolysis and joining of the 60S ribosomal subunit | 104 | 82 | 1.9×10^{-181} |
| Nonsense-Mediated Decay | 103 | 80 | 6.2×10^{-176} |
| Nonsense Mediated Decay enhanced by the Exon Junction Complex | 103 | 80 | 6.2×10^{-176} |
| Adaptive Immune System | 412 | 167 | 6.5×10^{-174} |
| Eukaryotic Translation Initiation | 111 | 82 | 5.7×10^{-173} |
| Cap-dependent Translation Initiation | 111 | 82 | 5.7×10^{-173} |
| SRP-dependent cotranslational protein targeting to membrane | 104 | 79 | 2.0×10^{-171} |
| Translation | 141 | 91 | 6.1×10^{-170} |
| Infectious disease | 347 | 146 | 1.6×10^{-166} |
| Influenza Infection | 117 | 81 | 1.9×10^{-163} |
| Influenza Viral RNA Transcription and Replication | 108 | 77 | 1.9×10^{-160} |
| Influenza Life Cycle | 112 | 77 | 2.5×10^{-156} |

Gene set over-representation analysis (hypergeometric test) for Reactome pathways in SLIPT partners for *CDH1*.

4.1.2 Expression Profiles of Synthetic Lethal Partners

Due to the sheer number of gene candidates, investigations proceeded into correlation structure and pathway over-representation. These analyses also examined expression patterns of synthetic lethal gene candidates. This serves to explore the functional similarity of the synthetic lethal partners of *CDH1*, with the eventual aim to assess their utility as drug targets. As shown in Figure 4.1 (which clusters *CDH1* lowly expressing samples separately), there were several large clusters of genes among the expression profiles of the *CDH1* synthetic lethal candidate partners. The clustering suggests co-regulation of genes or pathway correlation between partner gene candidates. A number of candidates from an experimental RNAi screen study performed by Telford *et al.* (2015) were also identified by this approach. In addition, we identified novel gene candidates, which had not been observed affect viability in isogenic cell line experiments.

In these expression profiles, a gene with a moderate or high signal across samples exhibiting low *CDH1* expression would represent a potential drug target. However, it appears that several molecular subtypes of cancer have elevation of different clusters of synthetic lethal candidates in samples with low *CDH1*. This clustering suggests

that different targets (or combinations) could be effective in different patients, suggesting potential utility for stratification. In particular, estrogen receptor negative, basal-like subtype, and “normal-like” tumours (Dai *et al.*, 2015; Eroles *et al.*, 2012; Parker *et al.*, 2009) have elevation of genes specific to particular clusters, indicative of some **synthetic lethal** interactions being specific to a particular molecular subtype or genetic background. Thus **synthetic lethal** drug therapy against these subtypes may be ineffective if it were designed against genes in another cluster.

A similar correlation structure was observed among the candidates tested against *CDH1* **mutation** (**mtSLIPT**), as shown in Figure C.1. This clustering analysis similarly identified several major clusters of putative **synthetic lethal** partner genes. In this case, many partner genes had consistently high **expression** across most of the (predominantly lobular subtype) *CDH1* breast cancer samples. However, a major exception to this in the *CDH1* **expression** analysis were the normal samples which were excluded from the **mutation** data (as they were not tested for tumour-specific genotypes). This supports **synthetic lethal** interventions being more applicable to *CDH1* **mutant** tumours. There was still considerable correlation structure, particularly among *CDH1* wildtype samples, sufficient to distinguish gene clusters. In contrast to the **expression** analysis the (predominantly ductal *CDH1* wildtype) basal-like subtype and estrogen receptor negative samples had depleted **expression** among most candidate **synthetic lethal** partners. This is consistent with **synthetic lethal** interventions only being effective in lobular estrogen receptor positive breast cancers in which they are a more common, as recurrent (**driver**) **mutation**. However, the remaining samples are still informative for **synthetic lethal** analysis (by **SLIPT**) as it requires highly expressing *CDH1* samples for comparison.

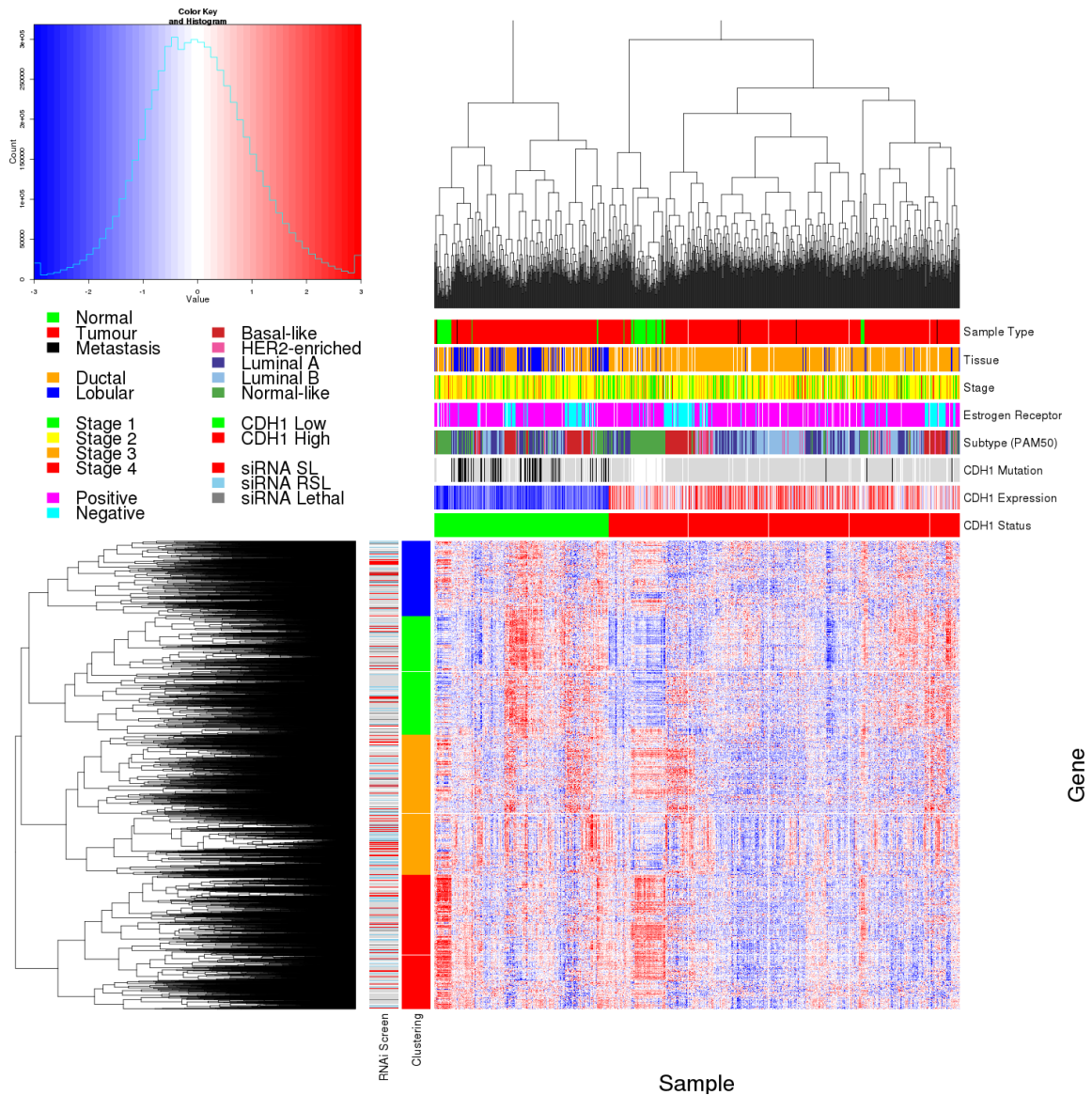


Figure 4.1: Synthetic lethal expression profiles of analysed samples. Gene expression profile heatmap (correlation distance, complete linkage) of all samples (separated by the 1/3 quantile of *CDH1* expression) analysed in TCGA breast cancer dataset for gene expression of 5165 candidate partners of E-cadherin (*CDH1*) from SLIPT prediction (with FDR adjusted $p < 0.05$). Deeply clustered, inter-correlated genes form several main groups, each containing genes that were SL candidates or lethal in an siRNA screen (Telford *et al.*, 2015). Screen results for synthetic lethal (SL), the reverse effect (RSL), or lethal cell viability are shown as reported by Telford *et al.* (2015). Clusters had different sample groups highly expressing the synthetic lethal candidates in *CDH1* low samples, notably ‘normal-like’, ‘basal-like’, and estrogen receptor negative samples have elevated expression in one or more distinct clusters showing complexity and variation among candidate synthetic lethal partners. *CDH1* low samples also contained most of samples with *CDH1* mutations (shown in black). Negative values for mutation and screen data are shown in light grey with missing data in white.

The *CDH1* mutant samples (in Figure 4.1) were predominantly among the low *CDH1* expressing samples and distributed throughout *CDH1* samples with clustering analysis. Thus the molecular profiles of *CDH1* low samples were indistinguishable from *CDH1* mutant samples, with the exception of normal samples (that do not have somatic mutation mutation data available). Conversely, many of the *CDH1* mutant samples (in Figure C.1) had among the lowest *CDH1* expression, and some of the synthetic lethal partners were also highly expressed in low expressing *CDH1* wildtype samples, despite these not being considered as “inactivated” by mtSLIPT analysis.

Together these results support the use of low *CDH1* expression as a strategy for detecting *CDH1* inactivation. This has the benefit of increasing sample size (including samples such as normal tissue which do not have somatic mutation mutation data available) and increasing the expected number of mutually inactive (low-low) samples for the directional criteria of (mt)SLIPT which enabling it to better distinguish significant deviations below this (as discussed in Section 6.1). This also circumvents the assumption that all (detected) mutations are inactivating (although synonymous mutations were excluded from the analysis), which may not be the case for several highly expressing *CDH1* mutant samples that do not cluster together in Figures 4.1 or C.1. One of these exhibits among the lowest expression for many predicted synthetic lethal partners and would not be vulnerable to inactivation of these genes. As such correctly genotyping inactivating mutations will be essential in clinical practice for synthetic lethal targeting tumour suppressor genes, particularly for other genes such as *TP53* where oncogenic and tumour suppressor mutations (with different molecular consequences) are both common in cancers. Using expression as a measure of gene expression also avoids the assumptions that mutations are somatic mutation rather than germline mutation and that gene inactivation is by detectable mutations rather than other mechanisms such as epigenetic changes which is supported by many lowly expressing *CDH1* wildtype samples clustering with similar profiles to mutant samples.

4.1.2.1 Subgroup Pathway Analysis

Synthetic lethal gene candidates for *CDH1* from SLIPT analysis of RNA-Seq gene expression data were also used for pathway over-representation analyses (as described in Section 2.3.2). The correlation structure in the expression of candidates synthetic lethal genes in *CDH1* low tumours (lowest 1/3rd quantile of expression) was examined for distinct biological pathways in subgroups of genes elevated in different clusters of samples. These genes were highly expressed in different samples with their clinical

Table 4.3: Pathways for clusters of *CDH1* partners from SLIPT

| Pathways Over-represented in Cluster 1 | Pathway Size | Cluster Genes | p-value (FDR) |
|--|--------------|---------------|------------------------|
| Collagen formation | 67 | 10 | 4.0×10^{-11} |
| Extracellular matrix organisation | 238 | 21 | 1.8×10^{-9} |
| Collagen biosynthesis and modifying enzymes | 56 | 8 | 1.8×10^{-9} |
| Uptake and actions of bacterial toxins | 22 | 5 | 9.5×10^{-9} |
| Elastic fibre formation | 37 | 6 | 1.9×10^{-8} |
| Muscle contraction | 62 | 7 | 2.4×10^{-7} |
| Fatty acid, triacylglycerol, and ketone body metabolism | 117 | 10 | 4.9×10^{-7} |
| XBP1(S) activates chaperone genes | 51 | 6 | 6.6×10^{-7} |
| IRE1alpha activates chaperones | 54 | 6 | 1.2×10^{-6} |
| Neurotoxicity of clostridium toxins | 10 | 3 | 1.3×10^{-6} |
| Retrograde neurotrophin signalling | 10 | 3 | 1.3×10^{-6} |
| Assembly of collagen fibrils and other multimeric structures | 40 | 5 | 1.9×10^{-6} |
| Collagen degradation | 58 | 6 | 2.0×10^{-6} |
| Arachidonic acid metabolism | 41 | 5 | 2.1×10^{-6} |
| Synthesis of PA | 26 | 4 | 3.0×10^{-6} |
| Signalling by NOTCH | 80 | 7 | 3.3×10^{-6} |
| Signalling to RAS | 27 | 4 | 3.7×10^{-6} |
| Integrin cell surface interactions | 82 | 7 | 4.2×10^{-6} |
| Pathways Over-represented in Cluster 2 | Pathway Size | Cluster Genes | p-value (FDR) |
| Eukaryotic Translation Elongation | 86 | 75 | 1.1×10^{-181} |
| Viral mRNA Translation | 81 | 72 | 9.8×10^{-179} |
| Peptide chain elongation | 83 | 72 | 1.9×10^{-175} |
| Eukaryotic Translation Termination | 83 | 72 | 1.9×10^{-175} |
| Formation of a pool of free 40S subunits | 93 | 75 | 1.9×10^{-171} |
| Nonsense Mediated Decay independent of the Exon Junction Complex | 88 | 72 | 9.9×10^{-168} |
| L13a-mediated translational silencing of Ceruloplasmin expression | 103 | 75 | 3.0×10^{-159} |
| 3' -UTR-mediated translational regulation | 103 | 75 | 3.0×10^{-159} |
| Nonsense-Mediated Decay | 103 | 75 | 3.0×10^{-159} |
| Nonsense Mediated Decay enhanced by the Exon Junction Complex | 103 | 75 | 3.0×10^{-159} |
| SRP-dependent cotranslational protein targeting to membrane | 104 | 75 | 3.2×10^{-158} |
| GTP hydrolysis and joining of the 60S ribosomal subunit | 104 | 75 | 3.2×10^{-158} |
| Eukaryotic Translation Initiation | 111 | 75 | 4.5×10^{-151} |
| Cap-dependent Translation Initiation | 111 | 75 | 4.5×10^{-151} |
| Influenza Infection | 117 | 75 | 1.4×10^{-145} |
| Influenza Viral RNA Transcription and Replication | 108 | 72 | 5.7×10^{-145} |
| Translation | 141 | 81 | 8.0×10^{-143} |
| Influenza Life Cycle | 112 | 72 | 2.3×10^{-141} |
| Pathways Over-represented in Cluster 3 | Pathway Size | Cluster Genes | p-value (FDR) |
| Adaptive Immune System | 412 | 90 | 6.1×10^{-61} |
| Chemokine receptors bind chemokines | 52 | 27 | 6.7×10^{-56} |
| Generation of second messenger molecules | 29 | 21 | 6.5×10^{-55} |
| Immunoregulatory interactions between a Lymphoid and a non-Lymphoid cell | 64 | 29 | 6.5×10^{-55} |
| TCR signalling | 62 | 27 | 8.9×10^{-51} |
| Peptide ligand-binding receptors | 161 | 40 | 1.5×10^{-45} |
| Translocation of ZAP-70 to Immunological synapse | 16 | 14 | 3.1×10^{-43} |
| Costimulation by the CD28 family | 51 | 22 | 4.0×10^{-43} |
| PD-1 signalling | 21 | 15 | 4.0×10^{-41} |
| Class A/1 (Rhodopsin-like receptors) | 258 | 50 | 6.7×10^{-41} |
| Phosphorylation of CD3 and TCR zeta chains | 18 | 14 | 1.3×10^{-40} |
| Interferon gamma signalling | 74 | 24 | 5.0×10^{-39} |
| GPCR ligand binding | 326 | 57 | 1.8×10^{-38} |
| Cytokine Signalling in Immune system | 268 | 48 | 8.9×10^{-37} |
| Downstream TCR signalling | 45 | 18 | 1.8×10^{-35} |
| G _{αi} signalling events | 167 | 33 | 2.2×10^{-33} |
| Cell surface interactions at the vascular wall | 99 | 21 | 1.3×10^{-26} |
| Interferon Signalling | 164 | 28 | 1.7×10^{-26} |
| Pathways Over-represented in Cluster 4 | Pathway Size | Cluster Genes | p-value (FDR) |
| Extracellular matrix organisation | 238 | 48 | 8.0×10^{-41} |
| Class A/1 (Rhodopsin-like receptors) | 258 | 47 | 2.8×10^{-36} |
| GPCR ligand binding | 326 | 54 | 2.1×10^{-34} |
| G _{αs} signalling events | 83 | 22 | 1.4×10^{-31} |
| GPCR downstream signalling | 472 | 68 | 1.1×10^{-29} |
| Haemostasis | 423 | 61 | 3.3×10^{-29} |
| Platelet activation, signalling and aggregation | 180 | 31 | 7.1×10^{-28} |
| Binding and Uptake of Ligands by Scavenger Receptors | 40 | 14 | 9.9×10^{-27} |
| RA biosynthesis pathway | 22 | 11 | 2.5×10^{-26} |
| Response to elevated platelet cytosolic Ca ²⁺ | 82 | 19 | 3.0×10^{-26} |
| Developmental Biology | 420 | 57 | 3.5×10^{-26} |
| G _{αi} signalling events | 167 | 28 | 7.3×10^{-26} |
| Platelet degranulation | 77 | 18 | 1.6×10^{-25} |
| Gastrin-CREB signalling pathway via PKC and MAPK | 171 | 28 | 2.5×10^{-25} |
| Muscle contraction | 62 | 16 | 4.7×10^{-25} |
| G _{αo} signalling events | 150 | 25 | 3.2×10^{-24} |
| Retinoid metabolism and transport | 34 | 12 | 5.0×10^{-24} |
| Phase 1 - Functionalisation of compounds | 67 | 16 | 6.5×10^{-24} |

Pathway over-representation analysis for Reactome pathways with the number of genes in each pathway (Pathway Size), number of genes within the pathway identified (Cluster Genes), and the pathway over-representation p-value (adjusted by FDR) from the hypergeometric test.

factors including estrogen receptor status and [intrinsic subtypes](#), from the [PAM50](#) procedure ([Parker *et al.*, 2009](#)) shown in Figure 4.1.

As shown by the most over-represented pathways in Table 4.3, each correlated cluster of candidate [synthetic lethal](#) partners of *CDH1* contains functionally different genes. Cluster 1 contains genes with less evidence of over-represented pathways than other clusters, corresponding to less correlation between genes within the cluster, and to it being a relatively small group. While there is some indication that collagen biosynthesis, microfibril elastic fibres, extracellular matrix, and metabolic pathways may be over-represented in Cluster 1, these results are mainly based on small pathways containing few [synthetic lethal](#) genes. Genes in Cluster 2 exhibited low [expression](#) in normal tissue samples compared to tumour samples (see Figure 4.1) and show compelling evidence of over-representation of post-transcriptional gene regulation and protein translation processes. Similarly, Cluster 3 has over-representation of immune signalling pathways (including chemokines, secondary messenger, and TCR signalling) and downstream intracellular signalling cascades such as [GPCR](#) and $G_{\alpha i}$ signalling events. While pathway over-representation was weaker among genes in Cluster 4, they contained intracellular signalling pathways and were highly expressed in normal samples (in contrast to Cluster 2). Cluster 4 also involved extracellular factors and stimuli such as extracellular matrix, platelet activation, ligand receptors, and retinoic acid signalling.

Based on these results, potential [synthetic lethal](#) partners of *CDH1* include processes known to be dysregulated in cancer, such as translational, cytoskeletal, and immune processes. Intracellular signalling cascades such as the [GPCRs](#) and extracellular stimuli for these pathways were also implicated in potential [synthetic lethality](#) with *CDH1*.

Similar translational, cytoskeletal, and immune processes were identified among [SLIPT](#) partners with respect to *CDH1* [mutation](#), shown in Table C.3. While [GPCR](#) signalling was replicated in [mtSLIPT](#) analysis, there was also stronger over-representation for NOTCH, ERBB2, and PI3K/AKT signalling in [mutation](#) analysis consistent with these signals being important for proliferation of *CDH1* deficient tumours. The GPCR and PI3K/AKT pathways are of particular interest as pathways with oncogenic [mutations](#) that can be targeted and downstream effects on translation (a strongly supported process across analyses). Extracellular matrix pathways (e.g., elastic fibre formation) were also supported across analyses (in Tables 4.3 and C.3) consistent with the established cell-cell signalling role of *CDH1* and the importance of the tumour microenvironment for cancer proliferation.

4.2 Comparing Synthetic Lethal Gene Candidates

4.2.1 Primary siRNA Screen Candidates

Gene candidates were compared between computational ([SLIPT](#) in [TCGA](#) breast cancer data) and experimental (the primary [siRNA](#) screen performed by [Telford et al. \(2015\)](#)) approaches in Figure 4.2. The number of genes detected by both methods did not produce a significant overlap but these may be difficult to compare due to vast differences between the detection methods. There were similar issues in the comparison of [mtSLIPT](#) genes tested against [CDH1 mutations](#) (in Appendix Figure ??), despite excluding genes not tested by both methods in either test. However, these intersecting genes may still be functionally informative or amenable to drug triage as they were replicated across both methods and pathway over-representation differed between the sections of the Venn diagram (see Figure 4.2).

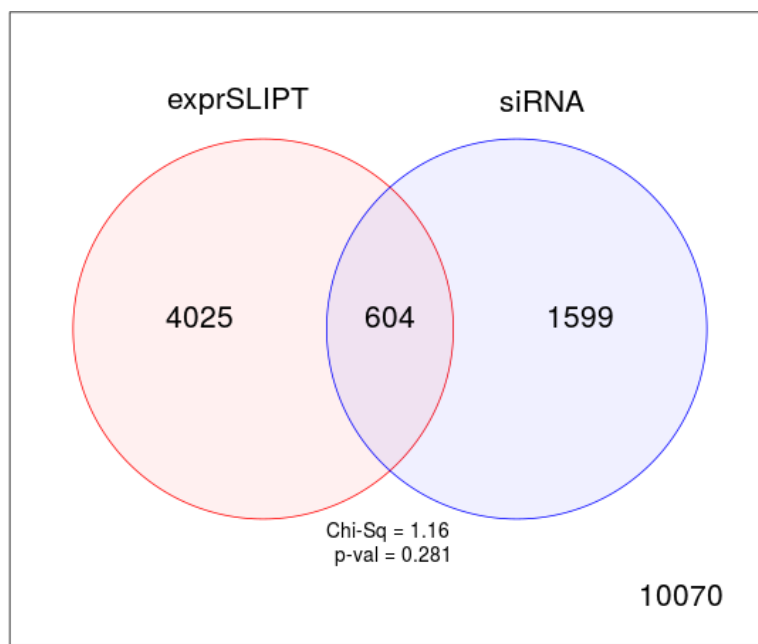


Figure 4.2: **Comparison of SLIPT to siRNA.** Testing the overlap of gene candidates for [E-cadherin synthetic lethal](#) partners between computational ([SLIPT](#)) and experimental screening ([siRNA](#)) approaches. The χ^2 test suggests that the overlap is no more than would be expected by chance ($p = 0.281$). Only genes tested by both methods were included.

4.2.2 Comparison with Correlation

Another potential means to triage drug target candidates is by correlation of [expression](#) profiles with [CDH1](#). Correlation with [CDH1](#) was compared to [SLIPT](#) and [siRNA](#)

results in Figure 4.3. The genes not detected by **SLIPT** (including **siRNA** candidates) had included gene with insignificant **SLIPT** p-values. As expected, these genes were distributed around a correlation of zero and genes with higher correlation with *CDH1* (either direction) were more significant, although there were exceptions to this trend and larger positive correlations than negative correlations. The majority of **SLIPT** candidates had negative correlations, particularly genes detected by both approaches, although these were typically weak correlations and are unlikely to be sufficient to detect such genes on their own. This is supported by simulation results in Section 6.1.

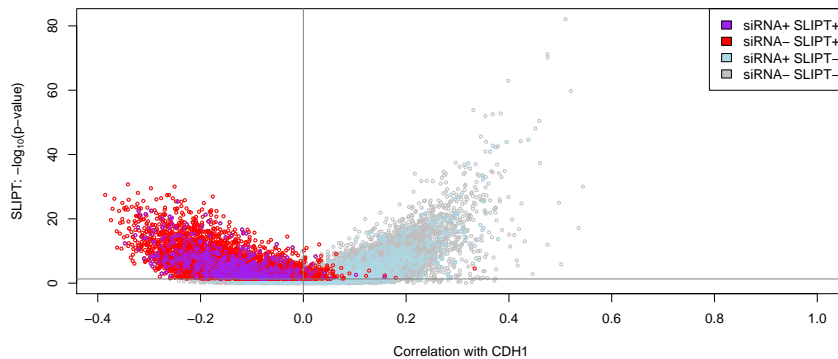


Figure 4.3: Compare **SLIPT and **siRNA** genes with correlation.** The χ^2 p-values for genes tested by **SLIPT** (in TCGA breast cancer) expression analysis were compared against Pearson's correlation of gene expression with *CDH1*. Genes detected by **SLIPT** or **siRNA** are coloured according to the legend.

There were not strong positive correlations with *CDH1* among **siRNA** candidates, consistent with previous findings that co-expression is not predictive of synthetic lethality (Jerby-Arnon *et al.*, 2014; Lu *et al.*, 2015). Negative correlation may not be indicative of synthetic lethality either as many **siRNA** candidates also had positive correlations. The **SLIPT** methodology has shown to detect genes with both positive and negative correlations, although it does appear to preferentially detect negatively correlated genes to some extent. These findings were replicated with the **mtSLIPT** approach against *CDH1* mutation (in Figure C.3), although the range of the χ^2 p-values differ due to lower sample size for mutation analysis.

The apparent tendency for genes detected by **SLIPT** or **siRNA** to have negative correlations with *CDH1* expression is not due to the smaller number of genes in these groups. The distribution of *CDH1* correlations differed across these gene groups (as

shown by Figures 4.4 and C.4), specifically lower in **SLIPT** candidates (as supported by **ANOVA** in Table 4.4). However, these are relatively weak correlations and further triage of gene candidates by correlation is not suitable, nor is use of correlation itself to predict **synthetic lethal** partners in the first place.

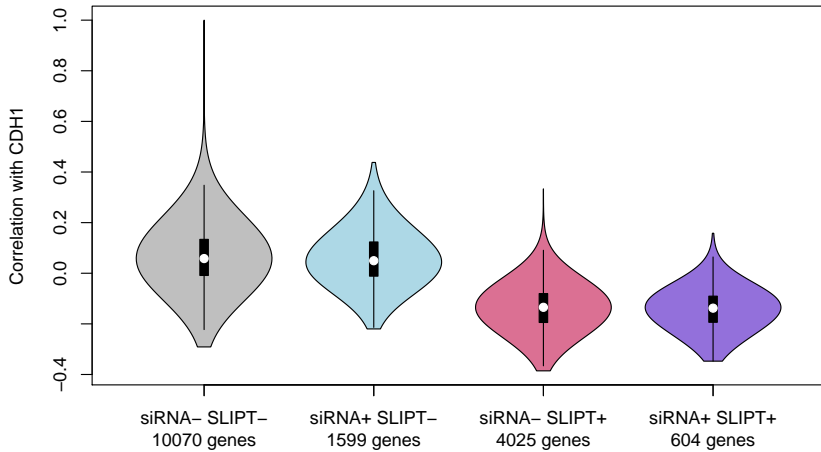


Figure 4.4: **Compare SLIPT and siRNA genes with correlation.** Genes detected as candidate **synthetic lethal** partners by **SLIPT** (in TCGA breast cancer) **expression** analysis and experimental screening (with **siRNA**) were compared against Pearson's correlation of **gene expression** with *CDH1*. There were no differences in correlation between gene groups detected by either approach.

Table 4.4: **ANOVA** for synthetic lethality and correlation with *CDH1*

| | DF | Sum Squares | Mean Squares | F-value | p-value |
|-------------|----|-------------|--------------|------------|---------|
| siRNA | 1 | 0.027 | 0.027 | 2.8209 | 0.09306 |
| SLIPT | 1 | 134.603 | 134.603 | 14115.9824 | <0.0001 |
| siRNA×SLIPT | 1 | 0.000 | 0.000 | 0.0073 | 0.93212 |

Analysis of variance for correlation with *CDH1* against **synthetic lethal** detection approaches (with an interaction term). Only genes tested by both methods were included in this analysis.

4.2.3 Comparison with Primary Screen Viability

A similar comparison of **SLIPT** results was made with the viability ratio (of *CDH1* mutant to wildtype) in the primary **siRNA** screen performed by Telford *et al.* (2015).

The significance and viability thresholds used for **SLIPT** and **siRNA** detection of synthetic lethal candidate partners of *CDH1* are shown in Figure 4.5. However, not all of the genes below the viability thresholds were necessarily selected to be candidate partners, as additional criteria were used in each case: directional criteria as for **SLIPT** (see Section 3.1) and minimum wildtype viability for **siRNA** (Telford *et al.*, 2015).

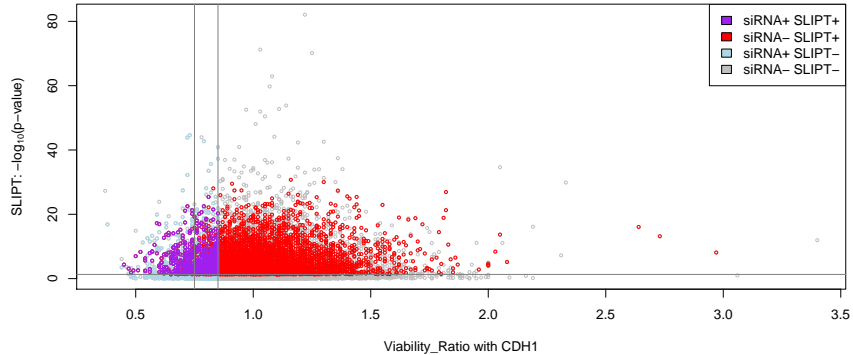


Figure 4.5: **Compare SLIPT and siRNA genes with viability.** The χ^2 p-values for genes tested by **SLIPT** (in TCGA breast cancer) expression analysis were compared (on a log-scale) against the viability ratio of *CDH1* mutant and wildtype cells in the primary **siRNA** screen. Genes detected by **SLIPT** or **siRNA** are coloured according to the legend.

There does not appear to be a clear relationship between **SLIPT** and **siRNA** candidates. Many genes not detected by both approaches were numerous in Figures 4.2 and C.2. These genes detected by either are not necessarily near the thresholds for the other. In this respect the **SLIPT** approach with patient data and cell line experiments are independent means to identify synthetic lethal candidates. While genes detected by both approaches were not necessarily more strongly supported by either, the genes with a viability closer to 1 (no synthetic lethal effect) in **siRNA** included those with more significant **SLIPT** p-values whereas more extreme viability ratios tended to be less significant (as shown by Figure 4.5). However, it should be noted that genes with more moderate viability ratios were more common and **SLIPT** was capable (despite adjusting for multiple testing) of detecting significant genes with extreme viability ratios, particularly those considerably lower than 1.

However, there was not little support for **SLIPT** candidates having considerably different viability ratios (as shown in Figures 4.6 and C.5). While the viability thresholds used by Telford *et al.* (2015) to detect synthetic lethal candidates in the primary

screen, the genes identified by **SLIPT** had a higher mean viability ratio (by t-test: $t = 2.1553$, $p = 0.03117$). However, the effect size was small (mean SLIPT⁻ 1.029, mean SLIPT⁺ 1.037) and the vast majority of **SLIPT** candidate genes did not have different viability in the primary screen to genes not identified by **SLIPT**.

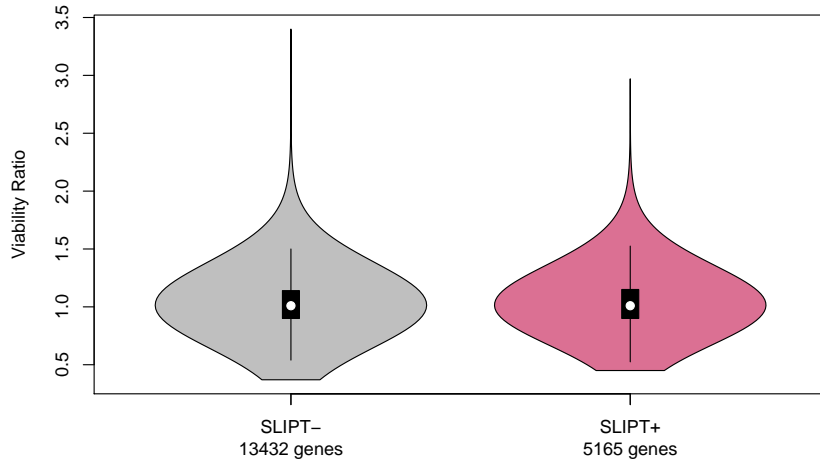


Figure 4.6: Compare **SLIPT genes with siRNA viability.** Genes detected as candidate synthetic lethal partners by **SLIPT** (in TCGA breast cancer) expression analysis were compared against the viability ratio of *CDH1* mutant and wildtype cells in the primary siRNA screen. There were clear no differences in viability between genes detected by **SLIPT** and those not with the differences being primarily due to viability thresholds being used to detect synthetic lethality by Telford *et al.* (2015).

4.2.4 Comparison with Secondary siRNA Screen Validation

However, it should be noted that genes with a lower viability ratio were not necessarily the most strongly supported by experimental screening. The primary screen (with 4 pooled siRNAs) has been used for the majority of comparisons in this thesis because the genomes-wide panel of target genes screened enables a large number of genes to be compared with **SLIPT** results from gene expression and somatic mutation analysis. A secondary screen was also performed by Telford *et al.* (2015) on the isogenic MCF10A cell line breast cell lines to validate the individual (i.e., non-pooled) siRNAs separately, with the strongest candidates being those exhibiting synthetic lethal viability ratios replicated across independently targeting siRNAs. The strongest candidates from a primary screen were subject to a further secondary screen for validation by in-

dependent replication with 4 gene knockdowns with different targeting **siRNAs**. This was performed for the top 500 candidates (with the lowest viability ratio) from the primary screen and the 482 of these genes also tested by **SLIPT** in breast cancer.

The secondary screen results show that **SLIPT** candidate genes were more significantly ($p = 7.49 \times 10^{-3}$ by Fisher's exact test) more likely to be validated in the secondary screen and are thus informative of more robust partner genes, in addition to providing support that these interactions are consistent with **expression** profiles from heterogeneous patient samples across genetic backgrounds. As shown in Table 4.5, there is significant association between **SLIPT** candidates and stronger validations of **siRNA** candidates. Since there were more **SLIPT-** genes among those not validated and more **SLIPT+** genes among those validated with several **siRNAs**, this supports the use of **SLIPT** as a **synthetic lethal** discovery procedure which may augment such screening experiments.

Table 4.5: Comparing **SLIPT** genes against secondary **siRNA** screen

| | | Secondary Screen | | | | | Total | |
|---------------|----------|------------------|-----|-----|-----|-----|--------------|-----|
| | | 0/4 | 1/4 | 2/4 | 3/4 | 4/4 | | |
| SLIPT+ | Observed | 70 | 46 | 31 | 8 | 2 | 157 | |
| | Expected | 85 | 44 | 10 | 4 | 2 | | |
| SLIPT- | Observed | 190 | 90 | 31 | 10 | 4 | 325 | |
| | Expected | 175 | 91 | 42 | 12 | 4 | | |
| | | Total | 280 | 136 | 52 | 18 | 6 | 482 |

While the individual genes detected by either approach do not necessarily match (and are potentially false-positives), the biological functions important in *CDH1* deficient cancers and potential mechanisms for specific targeting of them can be further supported by pathway analysis of the gene detected by either method. The genes detected by both approaches may therefore be more informative at the pathway level, where it is unlikely for a pathway to be consistently detected by chance. As the **SLIPT** candidates differ from the **siRNA** candidates (and are more likely to be validated), they can provide additional mechanisms by which *CDH1* deficient cancers proliferate and vulnerabilities that may be exploited against them by using the **synthetic lethal** pathways.

4.2.5 Comparison to Primary Screen at Pathway Level

These pathway over-representation analyses (performed as described in Section 2.3.2) correspond to genes separated into **SLIPT** or **siRNA** screen candidates unique to either method or detected by both (Table 4.6). The **SLIPT**-specific gene candidates were involved most strongly with translational and immune regulatory pathways, although extracellular matrix pathways were also supported. These pathways were largely consistent with those identified in Table 4.2 and in the clustering analysis (Table 4.3). The genes detected only by the **siRNA** screen had over-representation of cell signalling pathways, including many containing genes known to be involved in cancer (e.g., MAPK, PDGF, ERBB2, and FGFR), with the detection of Class A GPCRs supporting the independent analyses by Telford *et al.* (2015). The intersection of computational and experimental **synthetic lethal** partners of *CDH1* had stronger evidence for over-representation of **GPCR** pathways and more specific subclasses, such as visual phototransduction ($p = 6.9 \times 10^{-10}$) and $G_{\alpha s}$ signalling events ($p = 1.7 \times 10^{-7}$), than other signalling pathways.

The pathway analysis for **mtSLIPT** against *CDH1* mutations (in Table C.4) had concordant results for both **mtSLIPT**-specific and **siRNA**-specific pathways. While the specific pathway composition of the intersection of these analyses differed from **SLIPT** against low *CDH1* expression, signalling pathways including **GPCRs**, NOTCH, EERB2, PDGF, and SCF-KIT. These findings indicate the signalling pathways are among the most suitable vulnerability to exploit in targeting *CDH1* deficient tumours as they can be detected in both a patient cohort (with **TCGA expression** data) and tested in a laboratory system. However, it is possible that the isolated experimental system is set up to preferentially detect kinase singalling pathways (which are amenable to pharmacological inhibition and translation to the clinic) and the other pathways identified by **SLIPT** may still be informative of the role of *CDH1* loss of function in cancers or mechanisms by which further gene loss leads to specific inviability.

Table 4.6: Pathways for *CDH1* partners from SLIPT and siRNA

| Predicted only by SLIPT (4025 genes) | Pathway | Size | Genes Identified | p-value (FDR) |
|---|---------|------|------------------|------------------------|
| Eukaryotic Translation Elongation | | 80 | 75 | 1.5×10^{-182} |
| Peptide chain elongation | | 77 | 72 | 2.9×10^{-176} |
| Viral mRNA Translation | | 75 | 70 | 4.9×10^{-172} |
| Eukaryotic Translation Termination | | 76 | 70 | 5.9×10^{-170} |
| Formation of a pool of free 40S subunits | | 87 | 74 | 9.5×10^{-166} |
| Nonsense Mediated Decay independent of the Exon Junction Complex | | 81 | 70 | 1.2×10^{-160} |
| L13a-mediated translational silencing of Ceruloplasmin expression | | 97 | 75 | 3.8×10^{-155} |
| 3' -UTR-mediated translational regulation | | 97 | 75 | 3.8×10^{-155} |
| GTP hydrolysis and joining of the 60S ribosomal subunit | | 98 | 75 | 6.0×10^{-154} |
| Nonsense-Mediated Decay | | 96 | 73 | 5.2×10^{-150} |
| Nonsense Mediated Decay enhanced by the Exon Junction Complex | | 96 | 73 | 5.2×10^{-150} |
| SRP-dependent cotranslational protein targeting to membrane | | 97 | 73 | 7.8×10^{-149} |
| Eukaryotic Translation Initiation | | 105 | 75 | 4.7×10^{-146} |
| Cap-dependent Translation Initiation | | 105 | 75 | 4.7×10^{-146} |
| Translation | | 133 | 83 | 4.0×10^{-142} |
| Influenza Viral RNA Transcription and Replication | | 102 | 71 | 2.9×10^{-137} |
| Influenza Infection | | 111 | 74 | 3.7×10^{-137} |
| Influenza Life Cycle | | 106 | 71 | 2.3×10^{-133} |
| Infectious disease | | 326 | 125 | 4.2×10^{-120} |
| Extracellular matrix organisation | | 189 | 77 | 5.4×10^{-95} |

| Detected only by siRNA screen (1599 genes) | Pathway | Size | Genes Identified | p-value (FDR) |
|---|---------|------|------------------|-----------------------|
| Class A/1 (Rhodopsin-like receptors) | | 282 | 44 | 1.3×10^{-27} |
| GPCR ligand binding | | 363 | 52 | 5.8×10^{-26} |
| G _{aq} signalling events | | 159 | 26 | 6.7×10^{-23} |
| Gastrin-CREB signalling pathway via PKC and MAPK | | 180 | 27 | 2.0×10^{-21} |
| G _{ai} signalling events | | 184 | 27 | 5.3×10^{-21} |
| Downstream signal transduction | | 146 | 23 | 7.6×10^{-21} |
| Signalling by PDGF | | 172 | 25 | 4.0×10^{-20} |
| Peptide ligand-binding receptors | | 175 | 25 | 8.5×10^{-20} |
| Signalling by ERBB2 | | 146 | 22 | 1.3×10^{-19} |
| DAP12 interactions | | 159 | 23 | 2.6×10^{-19} |
| DAP12 signalling | | 149 | 22 | 2.7×10^{-19} |
| Organelle biogenesis and maintenance | | 264 | 33 | 5.5×10^{-19} |
| Signalling by NGF | | 266 | 33 | 8.2×10^{-19} |
| Downstream signalling of activated FGFR1 | | 134 | 20 | 1.1×10^{-18} |
| Downstream signalling of activated FGFR2 | | 134 | 20 | 1.1×10^{-18} |
| Downstream signalling of activated FGFR3 | | 134 | 20 | 1.1×10^{-18} |
| Downstream signalling of activated FGFR4 | | 134 | 20 | 1.1×10^{-18} |
| Signalling by FGFR | | 146 | 21 | 1.3×10^{-18} |
| Signalling by FGFR1 | | 146 | 21 | 1.3×10^{-18} |
| Signalling by FGFR2 | | 146 | 21 | 1.3×10^{-18} |

| Intersection of SLIPT and siRNA screen (604 genes) | Pathway | Size | Genes Identified | p-value (FDR) |
|--|---------|------|------------------|-----------------------|
| Visual phototransduction | | 54 | 9 | 6.9×10^{-10} |
| G _{as} signalling events | | 48 | 7 | 1.6×10^{-7} |
| Retinoid metabolism and transport | | 24 | 5 | 1.7×10^{-7} |
| Acyl chain remodelling of PS | | 10 | 3 | 6.5×10^{-6} |
| Transcriptional regulation of white adipocyte differentiation | | 51 | 6 | 6.5×10^{-6} |
| Chemokine receptors bind chemokines | | 22 | 4 | 6.5×10^{-6} |
| Signalling by NOTCH4 | | 11 | 3 | 6.9×10^{-6} |
| Defective EXT2 causes exostoses 2 | | 11 | 3 | 6.9×10^{-6} |
| Defective EXT1 causes exostoses 1, TRPS2 and CHDS | | 11 | 3 | 6.9×10^{-6} |
| Platelet activation, signalling and aggregation | | 146 | 12 | 6.9×10^{-6} |
| Phase 1 - Functionalisation of compounds | | 41 | 5 | 1.3×10^{-5} |
| Amine ligand-binding receptors | | 13 | 3 | 1.7×10^{-5} |
| Acyl chain remodelling of PE | | 14 | 3 | 2.4×10^{-5} |
| Signalling by GPCR | | 300 | 23 | 2.4×10^{-5} |
| Molecules associated with elastic fibres | | 29 | 4 | 2.6×10^{-5} |
| DAP12 interactions | | 128 | 10 | 2.6×10^{-5} |
| Cytochrome P ₄₅₀ - arranged by substrate type | | 30 | 4 | 3.2×10^{-5} |
| GPCR ligand binding | | 147 | 11 | 3.8×10^{-5} |
| Acyl chain remodelling of PC | | 16 | 3 | 4.0×10^{-5} |
| Response to elevated platelet cytosolic Ca ²⁺ | | 66 | 6 | 4.2×10^{-5} |

4.2.5.1 Resampling Genes for Pathway Enrichment

Comparisons of genes between experimental screen candidates and prediction from TCGA expression data were less consistent than comparisons of pathways. However, this is not unexpected, since synthetic lethal pathways are more robustly conserved (Dixon *et al.*, 2008) and the computational approach using patient samples from complex tumour microenvironment has considerably different strengths to an experimental screen (Telford *et al.*, 2015) based on genetically homogenous cell line models in an isolated laboratory environment. For instance, it is unlikely for immune signalling to be detected in an isolated cell culture system.

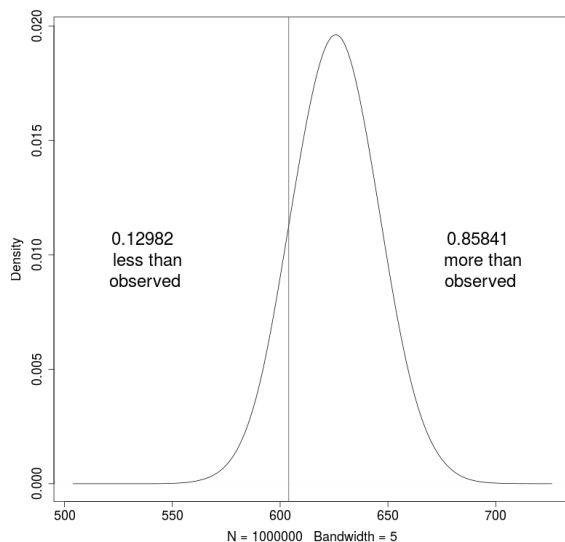


Figure 4.7: **Resampled intersection of SLIPT and siRNA candidates.** Resampling analysis of intersect size from genes detected by SLIPT and siRNA screening approaches over 1 million replicates. The proportion of expected intersection sizes for random samples below or above the observed intersection size respectively, lacking significant over-representation or depletion of siRNA screen candidates within the SLIPT predictions for *CDH1*.

The overlap between synthetic lethal candidates from bioinformatics SLIPT predictions and siRNA screening has raised other questions, including whether the pathways over-represented would be expected by chance. This of particular concern since the siRNA candidate genes themselves are highly over-represented for particular pathways (e.g., GPCRs) so selecting any intersect with them could be enriched for these pathways. Another pathway-based approach is to test whether pathways are over-represented in randomly sampled genes, comparing many “resamplings” or “permutations” of these genes to the enrichment statistics observed for these pathways in the

SLIPT candidates and their intersection with the **siRNA** hits shows whether we detect these pathways more than we expect by chance (as described in Section 2.3.6).

Of particular concern are the over-represented pathways in genes detected by both methods. Pathway over-representation alone does not detect whether **SLIPT** predicted genes or **siRNA** candidates are enriched within each other. This resampling analysis therefore detects whether over-represented pathways were detected by **SLIPT** independently of their over-representation among **siRNA** candidates (without assuming an underlying test statistic distribution).

A resampling approach is also applicable to testing whether the number of genes detected by each approach significantly intersected. As shown in Figure 4.7, resampling did not find evidence of significant depletion or over-representation for experimental **synthetic lethal** candidate genes in the computationally predicted **synthetic lethal** partners of *CDH1*, and thus the observed overlap may be due to chance. This is consistent with previous findings (see Figure 4.2) and does not preclude pathway relationships being supported by resampling.

A permutation analysis was performed to resample the genes tested by both approaches to investigate whether the observed pathway over-representation could have occurred in a randomly selected sample of genes from the experimental candidates, that is, whether the pathway predictions from **SLIPT** could be expected by chance (as described in Sections 2.2.3.1 and 2.3.6). While the number of **siRNA** candidate genes also detected by **SLIPT** was not statistically significant ($p = 0.281$), this may be due to the vastly different limitations of the approaches and the correlation structure of **gene expression** not being independent (as assumed for multiple testing procedures). The intersection may still be functionally relevant to *CDH1*-deficient cancers, such as the pathway data in Table 4.6. The resampling analysis for pathways was compared to the pathway over-representation for **SLIPT** predicted **synthetic lethal** partners in Table 4.7. Similarly, the pathway resampling for intersection between **SLIPT** predictions and experimental screen candidates was compared to pathway over-representation in Table 4.8 for intersection with **siRNA** data.

The pathway resampling approach for **SLIPT**-specific gene candidates (Table 4.7) replicates the gene set over-representation analysis for all **SLIPT** genes, detecting evidence of **synthetic lethal** pathways for *CDH1* in translational, immune, and cell signalling pathways including $G_{\alpha i}$ signalling, GPCR downstream signalling, and chemokine receptor binding. While the immune and signal transduction pathways were not significantly over-represented in the resampling analysis, the results for the two approaches

were largely consistent for translation and post-transcriptional gene regulation, supporting gene set over-representation of the **SLIPT**-specific pathways in Table 4.7. In particular, some of the most significantly over-represented pathways had higher observed χ^2 values than any of the 1 million random permutations. Similar pathways were also replicated by permutation analysis for mt**SLIPT** candidate partners against *CDH1* mutation (shown in Table C.5). This shows that many of the pathways detected specifically by **SLIPT** are replicated by permutation procedures and that the permutation approach is capable of detecting many of the most strongly over-represented pathways.

Table 4.7: Pathways for *CDH1* partners from **SLIPT**

| Reactome Pathway | Over-representation | Permutation |
|--|------------------------|--------------------------|
| Eukaryotic Translation Elongation | 1.3×10^{-207} | $< 1.241 \times 10^{-5}$ |
| Peptide chain elongation | 5.6×10^{-201} | $< 1.241 \times 10^{-5}$ |
| Viral mRNA Translation | 1.2×10^{-196} | $< 1.241 \times 10^{-5}$ |
| Eukaryotic Translation Termination | 1.2×10^{-196} | $< 1.241 \times 10^{-5}$ |
| Formation of a pool of free 40S subunits | 3.7×10^{-194} | $< 1.241 \times 10^{-5}$ |
| Nonsense Mediated Decay independent of the Exon Junction Complex | 5.3×10^{-187} | $< 1.241 \times 10^{-5}$ |
| L13a-mediated translational silencing of Ceruloplasmin expression | 9.6×10^{-183} | $< 1.241 \times 10^{-5}$ |
| 3' -UTR-mediated translational regulation | 9.6×10^{-183} | $< 1.241 \times 10^{-5}$ |
| GTP hydrolysis and joining of the 60S ribosomal subunit | 1.9×10^{-181} | $< 1.241 \times 10^{-5}$ |
| Nonsense-Mediated Decay | 6.2×10^{-176} | $< 1.241 \times 10^{-5}$ |
| Nonsense Mediated Decay enhanced by the Exon Junction Complex | 6.2×10^{-176} | $< 1.241 \times 10^{-5}$ |
| Adaptive Immune System | 6.5×10^{-174} | 0.15753 |
| Eukaryotic Translation Initiation | 5.7×10^{-173} | $< 1.241 \times 10^{-5}$ |
| Cap-dependent Translation Initiation | 5.7×10^{-173} | $< 1.241 \times 10^{-5}$ |
| SRP-dependent cotranslational protein targeting to membrane | 2.0×10^{-171} | $< 1.241 \times 10^{-5}$ |
| Translation | 6.1×10^{-170} | $< 1.241 \times 10^{-5}$ |
| Infectious disease | 1.6×10^{-166} | 0.23231 |
| Influenza Infection | 1.9×10^{-163} | $< 1.241 \times 10^{-5}$ |
| Influenza Viral RNA Transcription and Replication | 1.9×10^{-160} | $< 1.241 \times 10^{-5}$ |
| Influenza Life Cycle | 2.5×10^{-156} | $< 1.241 \times 10^{-5}$ |
| <i>Extracellular matrix organisation</i> | 1.1×10^{-152} | 0.071761 |
| GPCR ligand binding | 1.1×10^{-143} | 0.55801 |
| Class A/1 (Rhodopsin-like receptors) | 1.5×10^{-142} | 0.58901 |
| <i>GPCR downstream signalling</i> | 7.6×10^{-140} | 0.098357 |
| Haemostasis | 1.9×10^{-134} | 0.27059 |
| Developmental Biology | 2.0×10^{-123} | 0.52737 |
| Metabolism of lipids and lipoproteins | 3.3×10^{-120} | 0.724 |
| Cytokine Signalling in Immune system | 2.6×10^{-119} | 0.39661 |
| Peptide ligand-binding receptors | 3.7×10^{-109} | 0.61102 |
| <i>G_{αi} signalling events</i> | 8.9×10^{-100} | $< 1.241 \times 10^{-5}$ |

Over-representation (hypergeometric test) and Permutation p-values adjusted for multiple tests across pathways (**FDR**). Significant pathways are marked in bold (**FDR** < 0.05) and italics (**FDR** < 0.1).

The permutation approach was then also applied to the intersection between computational and experimental candidates. The permutation analysis is testing for consistent detection of pathways was independent of their pre-existing status as experimental candidates. The pathway results for these candidate partners (in Table 4.8) differed between over-representation and resampling analyses.

Namely, many of the over-represented pathways were not significant in the resampling analysis, including visual phototransduction and retinoic acid signalling, and were likely over-represented in the intersection due to over-representation in the **siRNA** candidates rather than additional support from **SLIPT**. In contrast, pathways involving defective *EXT1* or *EXT2* genes approach significance after **FDR** adjustment for multiple tests in resampling. Of the highest over-represented pathways in the intersection, only $G_{\alpha s}$ signalling events were supported by both over-representation and resampling analyses. Other pathways supported by both analyses were cytoplasmic elastic fibre formation, associated HS-GAG protein modification pathways, energy metabolism, and the fibrin clotting cascade.

Many of the pathways supported in the intersection by permutation analysis were also replicated in the **mtSLIPT** analysis of partners tested with *CDH1* mutation (in Table C.6), including $G_{\alpha s}$, elastic fibres, HS-GAG, and energy metabolism. While there were differences between the pathways identified by over-representation analysis, those replicated by permutation were highly concordant, supporting the combined use of these pathway approaches to identify **synthetic lethal** gene functions and targets.

While this indicates that $G_{\alpha s}$ and **GPCR** class A/1 signalling events were significantly detected by both approaches, **GPCR** signalling pathways overall were not. It is likely that **GPCRs** were primarily over-represented in the intersection with the experimental candidates due to strong over-representation of these pathways in experimental candidates, rather than detection by **SLIPT**, which may be driven by these more specific constituent pathways.

However, several pathways, including some immune functions and neurotransmitters, were supported by the resampling analysis (in Tables 4.8 and C.6) when the initial pathway over-representation test was not significant. These functions appear to have been detected by both approaches more than expected by chance but must be interpreted with caution since they were still not common enough to be detected in pathway over-representation analysis.

4.2.6 Integrating Synthetic Lethal Pathways and Screens

Based on these results, it appears that computational and experimental approaches to **synthetic lethal** screening for *CDH1* lead to a broader functional characterisation, and many candidate partners, when combined, despite different strengths and limitations. Compared to candidate gene approaches, experimental **genomes-wide** screens are an appealing unbiased strategy for identifying **synthetic lethal** interactions. Since these

Table 4.8: Pathways for *CDH1* partners from SLIPT and siRNA primary screen

| Reactome Pathway | Over-representation | Permutation |
|---|-----------------------|-------------|
| Visual phototransduction | 6.9×10^{-10} | 0.91116 |
| G_{as} signalling events | 1.6×10^{-7} | 0.012988 |
| Retinoid metabolism and transport | 1.7×10^{-7} | 0.20487 |
| Transcriptional regulation of white adipocyte differentiation | 6.5×10^{-6} | 0.38197 |
| Acylic chain remodelling of PS | 6.5×10^{-6} | 0.58485 |
| Chemokine receptors bind chemokines | 6.5×10^{-6} | 0.97255 |
| <i>Defective EXT2 causes exostoses 2</i> | 6.9×10^{-6} | 0.056437 |
| <i>Defective EXT1 causes exostoses 1, TRPS2 and CHDS</i> | 6.9×10^{-6} | 0.056437 |
| Signalling by NOTCH4 | 6.9×10^{-6} | 0.15497 |
| Platelet activation, signalling and aggregation | 6.9×10^{-6} | 0.53358 |
| Phase 1 - Functionalisation of compounds | 1.3×10^{-5} | 0.24836 |
| Amine ligand-binding receptors | 1.7×10^{-5} | 0.3195 |
| Acylic chain remodelling of PE | 2.4×10^{-5} | 0.7307 |
| Signalling by GPCR | 2.4×10^{-5} | 0.9939 |
| Molecules associated with elastic fibres | 2.6×10^{-5} | 0.0072929 |
| DAP12 interactions | 2.6×10^{-5} | 0.78273 |
| Cytochrome P ₄₅₀ - arranged by substrate type | 3.2×10^{-5} | 0.87019 |
| GPCR ligand binding | 3.8×10^{-5} | 0.99417 |
| Acylic chain remodelling of PC | 4.0×10^{-5} | 0.65415 |
| Response to elevated platelet cytosolic Ca ²⁺ | 4.2×10^{-5} | 0.55461 |
| <i>Arachidonic acid metabolism</i> | 4.4×10^{-5} | 0.060298 |
| Defective B4GALT7 causes EDS, progeroid type | 4.9×10^{-5} | 0.15497 |
| Defective B3GAT3 causes JDSSDHD | 4.9×10^{-5} | 0.15497 |
| Elastic fibre formation | 4.9×10^{-5} | 0.0019227 |
| HS-GAG degradation | 6.2×10^{-5} | 0.017747 |
| Bile acid and bile salt metabolism | 6.2×10^{-5} | 0.15497 |
| Netrin-1 signalling | 7.1×10^{-5} | 0.95056 |
| Integration of energy metabolism | 7.1×10^{-5} | 0.0019287 |
| DAP12 signalling | 7.9×10^{-5} | 0.67835 |
| GPCR downstream signalling | 8.1×10^{-5} | 0.88678 |
| Diseases associated with glycosaminoglycan metabolism | 8.7×10^{-5} | 0.017747 |
| Diseases of glycosylation | 8.7×10^{-5} | 0.017747 |
| Signalling by Retinoic Acid | 8.7×10^{-5} | 0.13592 |
| Signalling by Leptin | 8.7×10^{-5} | 0.15497 |
| Signalling by SCF-KIT | 8.7×10^{-5} | 0.73399 |
| Opioid Signalling | 8.7×10^{-5} | 0.99417 |
| Signalling by NOTCH | 0.0001 | 0.26453 |
| Platelet homeostasis | 0.0001 | 0.55912 |
| Signalling by NOTCH1 | 0.00011 | 0.13797 |
| Class B/2 (Secretin family receptors) | 0.00011 | 0.4659 |
| Diseases of Immune System | 0.00013 | 0.15497 |
| Diseases associated with the TLR signalling cascade | 0.00013 | 0.15497 |
| A tetrasaccharide linker sequence is required for GAG synthesis | 0.00013 | 0.33566 |
| Nuclear Receptor transcription pathway | 0.00016 | 0.22735 |
| Formation of Fibrin Clot (Clotting Cascade) | 0.00016 | 0.0054639 |
| Syndecan interactions | 0.00016 | 0.3974 |
| Class A/1 (Rhodopsin-like receptors) | 0.00016 | 0.99454 |
| HS-GAG biosynthesis | 0.0002 | 0.37199 |
| Platelet degranulation | 0.0002 | 0.39003 |
| EPH-ephrin mediated repulsion of cells | 0.00021 | 0.6193 |

Over-representation (hypergeometric test) and Permutation p-values adjusted for multiple tests across pathways (**FDR**). Significant pathways are marked in bold (**FDR** < 0.05) and italics (**FDR** < 0.1).

screens are costly, laborious, and specific to genetic background, computational analysis can augment candidate triage to either reduce the initial panel of screened genes or prioritise validation.

GPCR pathways were detected among both computational and experimental synthetic lethal candidates, with more support in the experimental screen (Table 4.8). The homogeneous cell line model may be more likely to detect particular pathways. For instance, SLIPT identified immune pathways, not expected to be detected in isolated cell culture. GPCR signalling was supported in experimental models Telford *et al.* (2015) with some of these pathways replicated in varied genetic backgrounds of patient samples. These pathways require further investigation such as identification of more specific pathways, higher order interactions, and modes of resistance.

The pathway composition across computational and experimental synthetic lethal candidates was informative with over-representation (Table 4.6) and supported by resampling analysis (Table 4.8), despite a modest intersection of genes between them (Figure 4.2). Either approach may be significant for a pathway in this intersection without being supported by the other: resampling analysis may support pathways that were not over-represented due to small effect sizes, thus both tests are required for a candidate pathway. The pathways detected by both over-representation and resampling are the strongest candidates for further investigation, such as $G_{\alpha s}$ signalling, a strong candidate in prior analyses with a role in the regulation of translation in cancer Gao and Roux (2015), another function supported by SLIPT analysis.

The predicted synthetic lethal partners occurred across functionally distinct pathways, including characterised functions of *CDH1*. This diversity is consistent with the wide ranging role of *CDH1* in cell-cell adhesion, cell signalling, and the cytoskeletal structure of epithelial tissues. Pathway structure may be relevant to identifying potential drug targets from gene expression signatures, indicating downstream effector genes and mechanisms leading to cell inviability. These distinct synthetic lethal gene clusters and pathways may further lead to the elucidation of drug resistance mechanisms.

4.3 Metagene Analysis

The gene signatures (Gatza *et al.*, 2011, 2014) were used to demonstrate the utility of the metagene approach for use on a wider range of pathways as was performed with the Reactome (Croft *et al.*, 2014) pathways as an alternative approach to identification of synthetic lethal pathways. metagene serve as a summary of activity for each pathway. The direction of metagenes (derived by the singular value matrix decomposition) is

generally arbitrary but care has been taken to ensure that these occur in a direction which reflect overall activation of the pathway (as described in Section 2.2.3). metagene were derived for well characterised gene signatures in breast cancer (Gatza *et al.*, 2011, 2014) to verify that that these pathway signatures are consistent with expected molecular properties of each molecular subtype (Parker *et al.*, 2009; Perou *et al.*, 2000). This was performed by examining the pathway expression of these breast cancer gene signatures in TCGA expression data. These metagenes were also compared to somatic mutation mutation to evaluate mutation as a measure of gene activity in comparison to gene and protein expression.

The gene signatures (Gatza *et al.*, 2011, 2014) were used to demonstrate to utility of the metagene approach for use on a wider range of pathways. Having established that metagenes generated with this procedure reflect gene activity, the metagene procedure (in Section 2.2.3) was then applied to the Reactome pathways (Croft *et al.*, 2014). These Reactome metagenes were used for synthetic lethal analysis of pathways with SLIPT, directly using pathway activity for identifying synthetic lethal pathways with *CDH1*.

4.3.1 Pathway Expression

Pathway metagenes (generated as described in Section 2.2.3) for gene signatures of key processes in breast cancer (Gatza *et al.*, 2011) were used to check that metagenes were generated in the correct direction to indicate pathway activation. Some of these gene signatures are plotted in Figure 4.8 for comparison with clinical factors and somatic mutation mutations. The “intrinsic subtypes” was computed by performing the PAM50 procedure Parker *et al.* (2009) for RNA-Seq data which was highly concordant ($\chi^2 = 1305.9$, $p = 2.73 \times 10^{-268}$) with the subtypes provided by University of California, Santa Cruz (UCSC) (UCSC, 2012) for TCGA samples (TCGA, 2012) previously analysed by microarrays (as shown in Appendix D). Somatic mutation mutations were reported for glslinkrecurrent mutationrecurrently mutated genes in breast cancer, as reported by TCGA (TCGA, 2012), related genes, and those previously discussed to be important in hereditary breast cancers (*BRCA1*, *BRCA2*, and *CDH1*).

These gene signatures reflect intrinsic subtypes as expected. In particular, the estrogen and progesterone receptor signatures are low in the predominantly ER⁻ and Progesterone receptor (PR)⁻ basal-like subtype tumours. These tumours also had the highest frequency of *TP53* mutations and a corresponding reduction of p53 metagene activity, as expected for loss of a tumour suppressor. The luminal A and luminal B

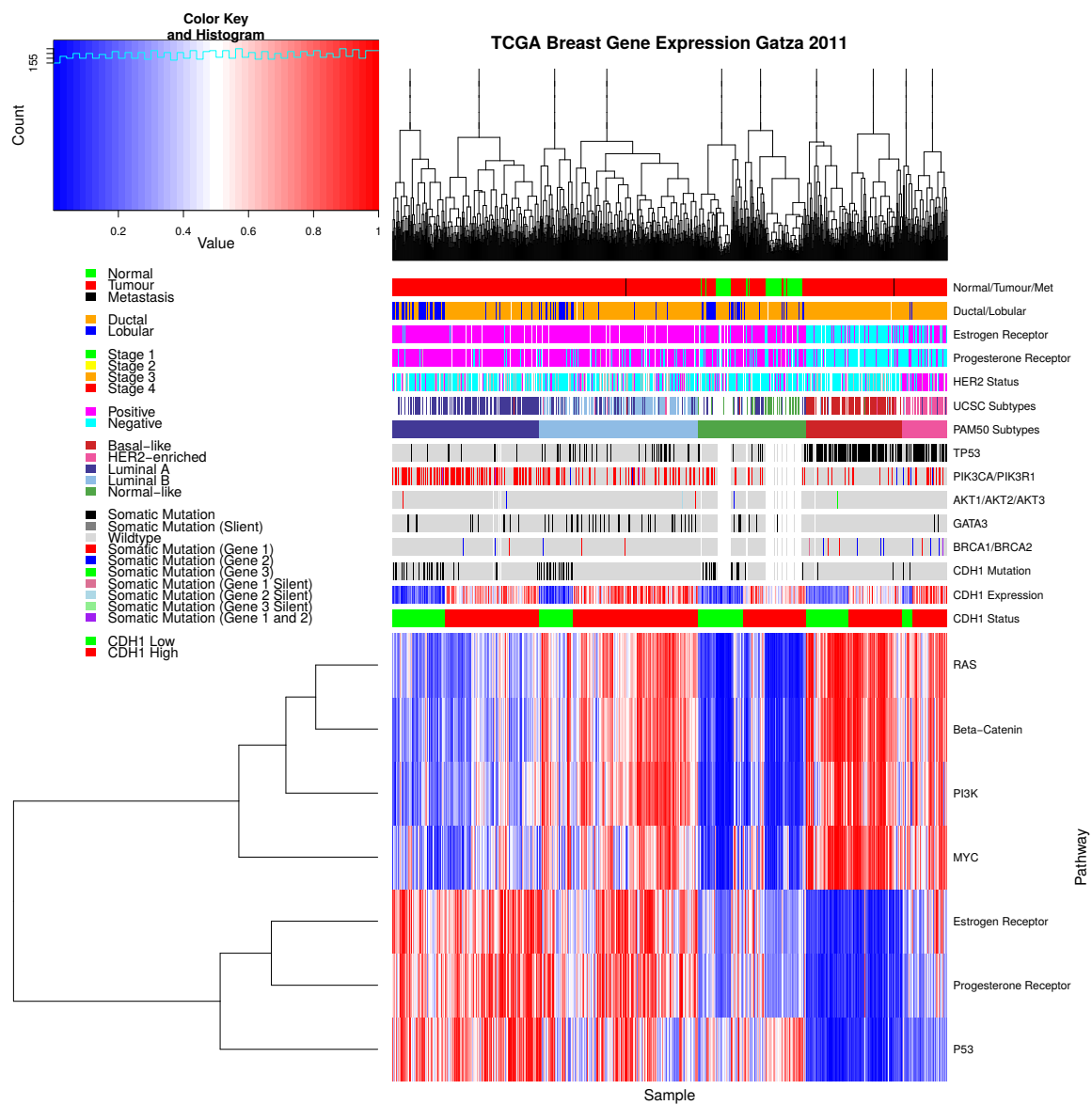


Figure 4.8: **Pathway metagene expression profiles.** Expression profiles for **metagene** signatures from [Gatza et al. \(2011\)](#) in **TCGA** breast data, annotated for clinical factors (with sample types and histological results coloured according to the legend) and cancer gene mutations (Negative values for **mutation** are light grey with missing data in white). Intrinsic subtypes are shown as derived from microarray (UCSC) and RNA-Seq (PAM50) data ([Parker et al., 2009; TCGA, 2012](#)). Samples were clustered independently for each **intrinsic subtypes** and by **CDH1 expression** status. Pathway **expression** signatures are consistent with **mutations** and clinical subgroups.

tumour subtypes are the most similar, which is reflected in these [metagenes](#) signatures, although they are distinguishable molecular subtypes as shown by elevated [PI3K](#), [AKT](#), [RAS](#), and β -catenin signalling in luminal B tumours. However, these pathways were also elevated in basal-like and HER2-enriched subtypes and lowly expressed in the “normal-like” subtype (which contained the normal samples). These [intrinsic subtypes](#) specific gene signature profiles were further supported with [metagenes](#) for an extended set of signatures ([Gatza et al., 2014](#)), as shown in Figure C.9.

[TP53 mutations](#) were the most frequent and more common in the basal-like subtype. Similarly, [GATA3 mutations](#) were more common in luminal subtype tumours. [PI3K mutations](#) were more frequent across breast tumours, although these were less common in the basal-like subtype despite an elevated [metagene](#) (this discrepancy will be discussed further in Section 4.3.2). [CDH1 mutations](#) similarly occurred across molecular subtypes with the exception of the basal-like subtype (as observed in [gene expression](#) with Figure 4.1). [CDH1](#) low samples occurred in all subtypes but were predominantly of the lobular histological subtype. Apart from these genes, [mutations](#) did not show clear specificity to a particular subtype and the variation between samples reflects the range of molecular cascades that can result in tumours with similar molecular profiles, supporting the use of [gene expression](#) data for cancer diagnostics and identification of molecular targets.

The direction of each [metagene](#) was consistent with the clinical characteristics, which formed a consensus of gene activity as shown for the [PI3K](#) and [ER](#) signatures ([Gatza et al., 2011](#)) in Figures 4.9 and 4.10, respectively. Supporting data for p53 and BRCA [metagenes](#) ([Gatza et al., 2011, 2014](#)) are given in the Appendix (Figures C.10 and C.11). In each of the examples for gene signatures, the [expression](#) of the majority of the genes were highly concordant with the [metagene](#), being either positively or negatively correlated. These were generally consistent with established clinical and molecular subtypes of breast cancer and the [recurrent mutations](#) shown. However, the [PIK3CA](#) and [PIK3R1](#) [mutant](#) samples did not necessarily have elevated [PI3K](#) pathway [metagene](#) activity (as shown in Figure 4.9).

4.3.2 Somatic Mutation

It should be noted that [metagenes](#), while consistent with the consensus of constituent expressed genes, were not necessarily reflecting the [somatic mutation](#) [mutation status](#). The [PI3K](#) ([Gatza et al., 2011](#)) [metagene](#) levels in particular, were not statistically significantly varying between [mutant](#) and wildtype [PIK3CA](#) samples (shown in Figure 4.11).

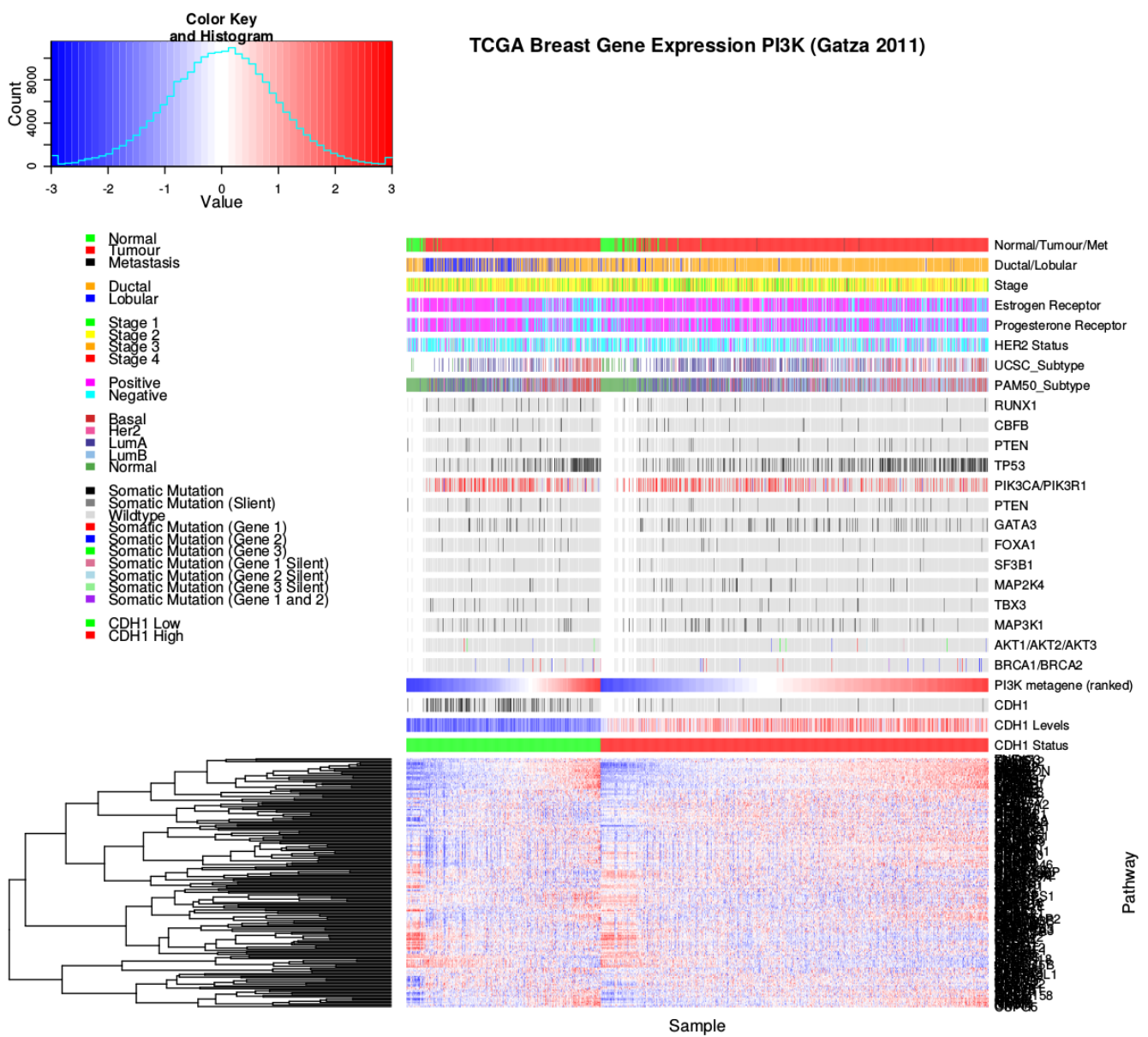


Figure 4.9: **Expression profiles for constituent genes of PI3K.** Expression profiles the genes contained in the PI3K gene signature from Gatza *et al.* (2011) in TCGA breast data, annotated for clinical factors and cancer gene mutations. Samples are separated by *CDH1* expression status and sorted by the metagene. In both cases, the majority of genes were consistent with the direction of the PI3K metagene, although considerable proportion were inversely correlated with the metagene. Normal samples had low PI3K metagene expression and *TP53* mutant samples had high PI3K expression. Although, oncogenic *PIK3CA* and tumour suppressor *PIK3R1* mutations across samples including those with low metagene response.

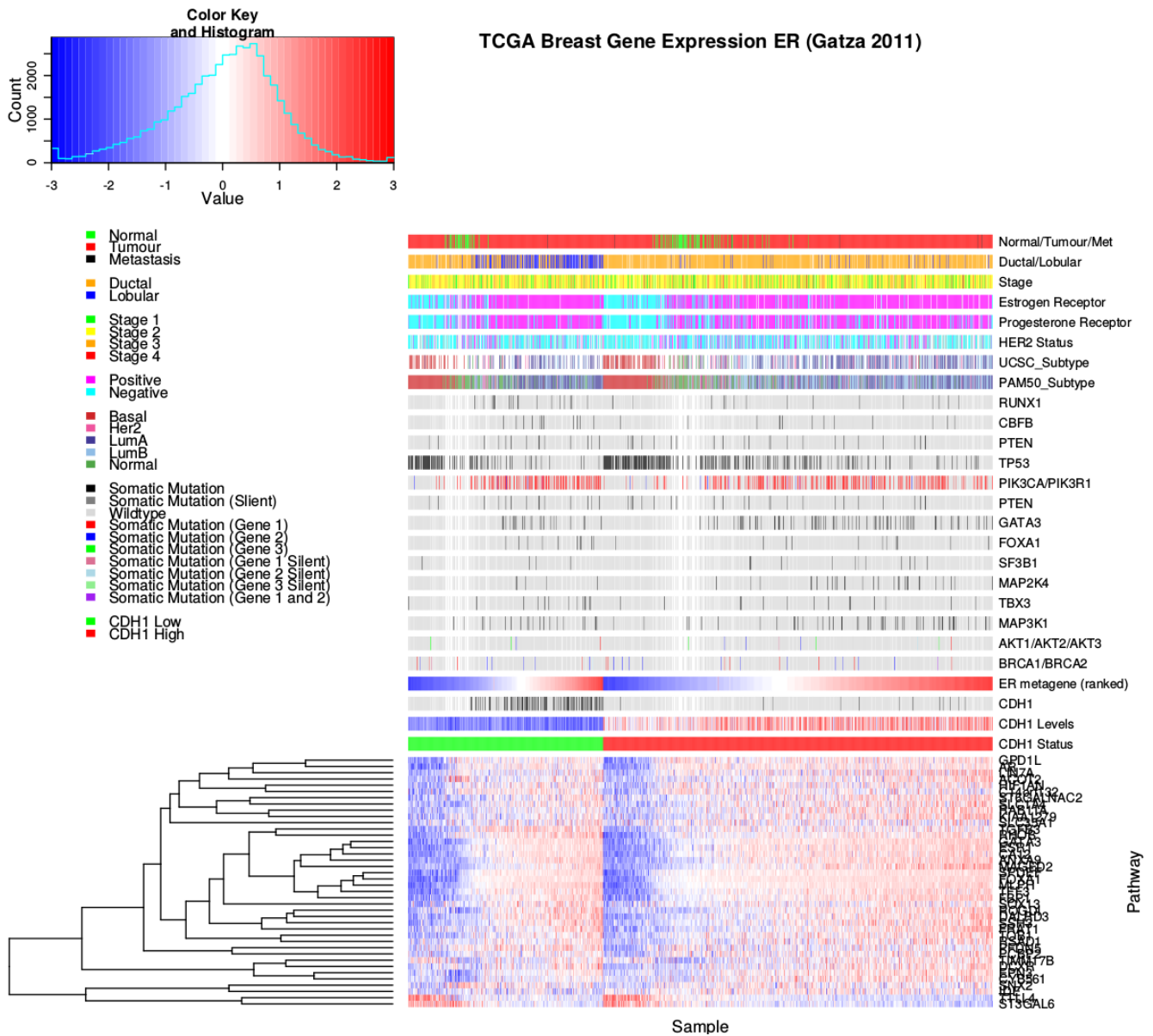


Figure 4.10: **Expression profiles for estrogen receptor related genes.** Expression profiles the genes contained in the estrogen receptor (ER) gene signature from [Gatza et al. \(2011\)](#) in TCGA breast data, annotated for clinical factors and cancer gene [mutations](#). Samples are separated by *CDH1* expression status and sorted by the [metagene](#). In both cases, the majority of genes were consistent with the direction of the [metagene](#), with very few exceptions being inversely correlated. Estrogen receptor (by antibody staining) negative samples had low metagene expression, as expected. These were more likely to be ductal and basal subtypes, lacking *CDH1* or *PIK3CA* mutations.

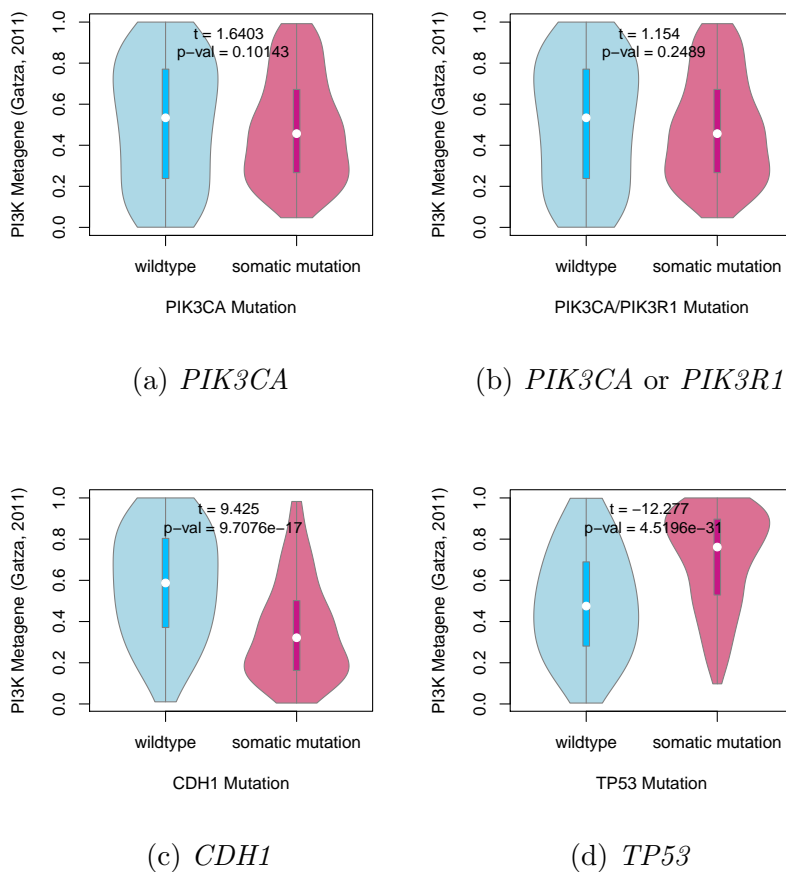


Figure 4.11: **Somatic mutation against the PI3K metagene.** Mutations in *PIK3CA*, *PIK3R1*, *CDH1*, and *TP53* were examined in TCGA breast cancer for their association with the PI3K (Gatza *et al.*, 2011) pathway metagene. The tumour suppressors *CDH1* and *TP53* showed an increase and decrease in the metagene respectively, whereas *PIK3CA* and *PIK3R1* mutations had little effect on the metagene levels.

However, the PI3K metagene differed across *CDH1* and *TP53* mutations, remarkably in opposite directions considering that PI3K is an oncogenic growth pathway and these are both most frequently tumour suppressors inactivated in cancers. This shows that *CDH1* and *TP53* deficient tumours have distinct molecular growth pathways and that synthetic lethal interventions against loss of *CDH1* function may not be applicable to other cancers with driver mutations such as *TP53*, although these were kept in the analysis for comparison. These differences may be related to these mutations being more frequent in tumours with difference clinical characteristics (as observed in Section 4.3.1). Thus mutations do not necessarily have corresponding changes in pathway

[expression](#), particularly for [oncogenes](#) which may change in function rather than being upregulated.

While the more specific *PIK3CA* ([Gatza et al., 2014](#)) [metagene](#) showed significant differences with *PIK3CA* and *PIK3R1* [mutations](#) (as shown in Figure C.6), this [metagene](#) replicated stronger differences for *CDH1* and *TP53*. These differences were less pronounced in the protein levels of p110 α (enocded by *PIK3CA*) and the downstream AKT gene (shown in Figures C.7 and C.8 respectively). However, this may be due to this regulatory cascade (kinases) being transmitted as a change in protein state (phosphorylation) rather than changes in [expression](#) levels. Another consideration is that [mutations](#) at different loci have different effects on protein function, particularly for [oncogenes](#).

4.3.3 Synthetic Lethal Pathway Metagenes

Pathway [metagenes](#) for Reactome pathways (generated as described in Section 2.2.3) were also used for testing [synthetic lethal](#) partner pathways with *CDH1* by [SLIPT](#). Since the [metagenes](#) have are higher when the pathway as a whole is activated, they are amenable to [SLIPT](#) analysis using low [metagene](#) levels for inactivated pathways. These [synthetic lethal metagenes](#) differed to the over-represented pathways among [synthetic lethal](#) gene candidates. However, there were some similarities to previous findings, as shown in Tables 4.9. In particular, translational pathways were replicated as observed in Table 4.2. While the specific pathways differ, immune pathways (e.g., NF- κ B) were also supported by [metagene synthetic lethal](#) analysis.

Signalling pathways were more strongly supported by [mtSLIPT](#) analysis of [metagene](#) pathway [expression](#) against *CDH1* [mutation](#), as shown in Table C.7, although these results were generally less statistically significant than [expression](#) analyses. Signalling pathways detected as [synthetic lethal metagenes](#) include G $_{\alpha z}$, insulin-related growth factor (IGF), GABA receptor, G $_{\alpha s}$, S6K1 and various toxin responses mediated by [GPCRs](#). Metabolic processes including processing of carbohydrates and fatty acids were also implicated across these analyses.

The [metagene](#) analyses differ more between expression and *CDH1* [mutation](#) than previous analyses, with more specific signalling pathways identified in the [mutation](#) analysis. This supports the usage of a complete null [mutant](#) model in experimental testing for [synthetic lethality](#) of signalling pathways against *CDH1* inactivation rather than a knockdown in [expression](#). However, low [expression](#) of partners has been used in either case to be applicable to dose-dependent pharmacological inhibition and across

Table 4.9: Candidate synthetic lethal metagenes against *CDH1* from SLIPT

| Pathway | ID | Observed | Expected | χ^2 value | p-value | p-value (FDR) |
|--|---------|----------|----------|----------------|------------------------|------------------------|
| Glycogen storage diseases | 3229121 | 68 | 130 | 176 | 6.62×10^{-37} | 1.82×10^{-34} |
| Myoclonic epilepsy of Lafora | 3785653 | 68 | 130 | 176 | 6.62×10^{-37} | 1.82×10^{-34} |
| Diseases of carbohydrate metabolism | 5663084 | 68 | 130 | 176 | 6.62×10^{-37} | 1.82×10^{-34} |
| Arachidonic acid metabolism | 2142753 | 81 | 130 | 157 | 8.13×10^{-33} | 1.49×10^{-30} |
| Translation initiation complex formation | 72649 | 70 | 130 | 152 | 7.08×10^{-32} | 1.17×10^{-29} |
| Synthesis of 5-eicosatetraenoic acids | 2142688 | 68 | 130 | 151 | 1.25×10^{-31} | 1.88×10^{-29} |
| SRP-dependent cotranslational protein targeting to membrane | 1799339 | 69 | 130 | 150 | 2.01×10^{-31} | 2.76×10^{-29} |
| L13a-mediated translational silencing of Ceruloplasmin expression | 156827 | 72 | 130 | 148 | 5.91×10^{-31} | 6.44×10^{-29} |
| 3' -UTR-mediated translational regulation | 157279 | 72 | 130 | 148 | 5.91×10^{-31} | 6.44×10^{-29} |
| Activation of the mRNA upon binding of the cap-binding complex and eIFs, and subsequent binding to 43S | 72662 | 70 | 130 | 147 | 1.14×10^{-30} | 9.28×10^{-29} |
| Formation of the ternary complex, and subsequently, the 43S complex | 72695 | 70 | 130 | 147 | 1.14×10^{-30} | 9.28×10^{-29} |
| Ribosomal scanning and start codon recognition | 72702 | 70 | 130 | 147 | 1.14×10^{-30} | 9.28×10^{-29} |
| Eukaryotic Translation Elongation | 156842 | 72 | 130 | 146 | 1.19×10^{-30} | 9.28×10^{-29} |
| Nonsense Mediated Decay independent of the Exon Junction Complex | 975956 | 71 | 130 | 146 | 1.24×10^{-30} | 9.28×10^{-29} |
| Viral mRNA Translation | 192823 | 70 | 130 | 146 | 1.51×10^{-30} | 1.04×10^{-28} |
| Eukaryotic Translation Termination | 72764 | 70 | 130 | 146 | 1.51×10^{-30} | 1.04×10^{-28} |
| NF-kB is activated and signals survival | 209560 | 71 | 130 | 145 | 1.90×10^{-30} | 1.19×10^{-28} |
| Peptide chain elongation | 156902 | 72 | 130 | 145 | 1.91×10^{-30} | 1.19×10^{-28} |
| Influenza Life Cycle | 168255 | 70 | 130 | 145 | 1.95×10^{-30} | 1.19×10^{-28} |
| Formation of a pool of free 40S subunits | 72689 | 73 | 130 | 145 | 2.01×10^{-30} | 1.19×10^{-28} |
| Nonsense-Mediated Decay | 927802 | 71 | 130 | 145 | 2.44×10^{-30} | 1.34×10^{-28} |
| Nonsense Mediated Decay enhanced by the Exon Junction Complex | 975957 | 71 | 130 | 145 | 2.44×10^{-30} | 1.34×10^{-28} |
| GTP hydrolysis and joining of the 60S ribosomal subunit | 72706 | 72 | 130 | 145 | 2.58×10^{-30} | 1.37×10^{-28} |
| Influenza Viral RNA Transcription and Replication | 168273 | 72 | 130 | 144 | 4.01×10^{-30} | 2.07×10^{-28} |
| Signalling by NOTCH1 HD Domain Mutants in Cancer | 2691230 | 79 | 130 | 143 | 5.99×10^{-30} | 2.82×10^{-28} |

Strongest candidate SL partners for *CDH1* by SLIPT with observed and expected numbers of TCGA breast cancer samples with low expression of both *CDH1* and the metagene.

genes where mutations have different functional consequences, including variants of unknown significance.

These results show an independent pathway-based approach to detecting synthetic lethal gene functions interacting with *CDH1*. The use of synthetic lethal metagenes replicates support for these pathways independent of pathway size (as genes are weighted equally). Along with the verifying that the direction of metagenes recapitulates the activity of a pathway, these demonstrate that many of the pathways previously identified from over-represented synthetic lethal genes (detected by SLIPT) are synthetic lethal pathways with their activity dependent on synthetic lethal genes rather than containing synthetic lethal genes as inhibitors or peripheral regulators of the pathways.

4.3.4 Synthetic Lethality in Breast Cancer

The synthetic lethal analysis against low *CDH1* expression supports prior findings in translational and immune pathways even if they were not able to be detected in an experimental screen (Telford *et al.*, 2015). Together these findings support the role of *CDH1* loss in cancer disrupting cell signalling with wider effects on protein translation and metabolism necessary for the proliferation of cancer cells. This is consistent with

the GPCR pathways such as $G_{\alpha s}$ signalling being supported by SLIPT gene candidates and the experimental primary siRNA screen, as shown by resampling in Section 4.2.5.1.

4.4 Replication in Stomach Cancer

CDH1 is also important in stomach cancer biology as a driver tumour suppressor gene, including as a germline mutation mutation in many cases of hereditary diffuse gastric cancer. The synthetic lethal analysis of genes and pathways (previously identified for TCGA breast cancer data) was replicated in TCGA stomach cancer. The accompanying data for SLIPT analysis against *CDH1* expression is provided in Appendix E.

While the sample size was lower for TCGA stomach cancer (particularly for mutations), these results serve to support the findings in breast cancer in an independent patient cohort and tissue samples. The molecular profiling, including RNA-Seq expression, were performed by TCGA using the sample procedures as for breast cancer and the findings reported here were performed used data analysis techniques identical to those presented previously. These procedures should ensure as close comparison as feasible across cancer types for those relevant to HDGC and recurrent *CDH1* mutations.

The strongest SLIPT genes for stomach cancer (shown in Table E.1) did not necessarily directly correspond to those observed in breast cancer (shown in Table 4.1). However, several gene functions were replicated in stomach cancer. Together, these gene candidates indicate widespread functions of *CDH1* and strongly detectable synthetic lethality with many genes from a strategy that can be applied across cancer types. More specifically, the signalling genes included GPCR signalling genes, which was one of the most supported synthetic lethal pathways in breast cancer analysis, the experimental screen (Telford *et al.*, 2015). These findings were further supported by the pathways over-represented in SLIPT candidates from TCGA stomach cancer (shown in Table E.2) which replicated the translational and immune pathways observed in TCGA breast cancer (shown in Table 4.2) and further supported GPCR signalling pathways, including the class A/1 receptors. The extracellular matrix was also detected at the pathway level in stomach cancer, including elastic fibres, glycosylation, collagen, and integrin cell-surface interactions. While fewer pathways were supported by resampling for the intersection of SLIPT and experimental screen (Telford *et al.*, 2015) candidate partners in stomach cancer than breast cancer, many of those detected (shown in Table E.6) replicate those detected in breast cancer (shown in Table 4.8). The pathways detected by both permutation and over-representation were more likely to be replicated across stomach and breast cancer than those detected by over-representation

alone, supporting the use of this procedure to detect **synthetic lethal** pathways applicable across cancer types. These include $G_{\alpha s}$ signalling and elastic fibre formation as discussed for breast cancer (in Section 4.2.5.1).

4.5 Discussion

4.5.1 Strengths of the SLIPT Methodology

Synthetic lethal discovery with **SLIPT** used established statistical procedures to identify putative partner genes from **gene expression** data. Such use of the χ^2 -value is amenable to pathway or permutation analyses and could feasibly be applied to other disease gene or pair-wise across the **genomes**, although **genomes-wide** approaches were unable to find informative candidate genes for **E-cadherin** (Lu *et al.*, 2015). **Synthetic lethal** discovery in cancer has focused on genes with severe cellular **mutant** phenotypes, such as **essential** genes or the **oncogenes** *TP53* and *AKT* (Lu *et al.*, 2015; Tiong *et al.*, 2014; Wang and Simon, 2013), with other cancer genes, such as *CDH1*, requiring more focused investigations. Prior computational approaches for **synthetic lethal** discovery, in cancer, vary widely (Jerby-Arnon *et al.*, 2014; Lu *et al.*, 2015; Tiong *et al.*, 2014; Wappett *et al.*, 2016). There is no consensus as to which approach is more appropriate, and the methods are difficult to compare, as they either do not have a released code implementation or do not make predictions solely from normalised **expression** data.

However, the query-based approach demonstrated by **SLIPT** analysis is suitable for wider application on **expression** data and for augmenting experimental studies such as high-throughput screens. This approach has identified biologically plausible **synthetic lethal** pathways for *CDH1*, triaged candidates from experimental screening (Telford *et al.*, 2015), and replicates genes and pathways across breast and stomach cancer datasets. In addition, **SLIPT** avoids critical assumptions underlying the design of some approaches such as co-expression of synthetic candidates or that interacting gene pairs will have known (annotated) similarities in function.

The DAISY methodology Jerby-Arnon *et al.* (2014), which took a similar query-based approach with the **tumour suppressor** *VHL*, has been critiqued for being too stringent (Lu *et al.*, 2015) which impedes pathway analysis. Since **functional redundancy** does not require genes to be expressed at the same time, the **SLIPT** approach does not assume co-expression of **synthetic lethal** genes which may enrich for **synthetic lethal** genes in established coregulated pathways. Rather, the interpretation of **synthetic lethality** for **SLIPT** was similar to other computational methods based on

‘co-loss under-representation’, ‘compensation’, or ‘simultaneous differential expression’ (Lu *et al.*, 2015; Tiong *et al.*, 2014; Wang and Simon, 2013).

Genomics analyses are prone to false-positives and require statistical caution, particularly where working with gene-pairs scale up the number of multiple tests drastically, at the expense of statistical power. Experimental screens for synthetic lethality are also error-prone (Fece de la Cruz *et al.*, 2015; Lord *et al.*, 2015; Lu *et al.*, 2015), especially with false-positives, raising the need for understanding the expected behaviour and number of functional relationships and genetic interactions in the genomes, or in discovery of synthetic lethal partners of a particular query gene. Thus analyses throughout this thesis have focused on querying for partners of a particular gene of interest. Statistical modelling and simulations (in Section 3.3 and Chapter 6) will further support the design decisions underlying SLIPT analysis and its strengths over other approaches.

4.5.2 Synthetic Lethal Pathways for E-cadherin

Specific genes were difficult to replicate across experiments. This is consistent with gene expression profiles for synthetic lethal partners reflecting the complexity of biological pathways which are subject to higher-order interactions and do not consistently compensate for loss of gene function across all samples (Jerby-Arnon *et al.*, 2014; Kelly, 2013; Lu *et al.*, 2015). The predicted synthetic lethal partners of *CDH1* (with FDR correction) were investigated with gene expression profiles and clinical variables to find relationships in gene expression, gene function, and clinical characteristics. The large number of genes detected indicates that synthetic lethal detection is potentially error-prone, and that identifying genes relevant for clinical application will be difficult without a supporting biological pathway rationale. As such, investigations into the genes identified by SLIPT, the correlation structure between them, and those which were validated by experimental screening (Telford *et al.*, 2015) focused at the pathway level throughout this Chapter. Similarly, comparisons across analyses were largely made at the pathway level, including comparisons between expression and mutation, breast and stomach TCGA datasets.

Potential synthetic lethal partners of *CDH1* identified by SLIPT had many distinct functions, with each gene cluster highly expressed in different patient subgroups (Figure 4.1). The expression profiles of the SL partners of *CDH1* predicted from TCGA breast cancer RNA-Seq data (expected to have compensating high or stable expression) and their corresponding functional enrichment found in subgroups of genes, particularly among *CDH1* low breast tumours. Ductal breast cancers showed higher expression of

synthetic lethal partners suggesting treatment would be more effective in this tumour subtype. However, there was consistently low expression of SL partners in estrogen receptor negative tumours, although this is independent of tumour stage and consistent with poor prognosis in these patients and could inform other treatment strategies or prevent ineffective treatment further impacting quality of life in these patients. These results suggest that synthetic lethal partner expression varies between patients; that these different tumour classes would react differently to the same treatment; that treatment of different pathways and combinations in different patients is the most effective approach to target genes compensating for *CDH1* gene loss; and that the expression of synthetic partners could be a clinically important biomarker.

The pathways that synthetic lethal partners of *CDH1* identified by SLIPT were involved in a diverse range of biological functions and differed to those detected experimentally. This discrepancy may be accounted for by gene expression analyses detecting both synthetic lethal partners, as screened for experimentally by Telford *et al.* (2015), and their downstream targets (not detected by siRNA), capturing the wider pathways and mechanisms involved in synthetic lethality with *CDH1* inactivation. In particular, GPCR phosphorylation cascades (which regulate gene expression and translation in cancers (Gao and Roux, 2015)) were predicted to be synthetic lethal with *CDH1*. The predicted synthetic lethal partners occurred across functionally distinct pathways, including characterised functions of *CDH1*. The most consistently supported pathways included elastic fibres in the extracellular matrix, GPCR signalling, and translation presenting vulnerabilities for *CDH1* deficient cancer cells from extracellular stimuli to the core growth mechanisms of a cell.

This diversity in synthetic lethal functions is consistent with the wide ranging role of *CDH1* in cell-cell adhesion, cell signalling, and the cytoskeletal structure of epithelial tissues. Pathway structure may be relevant to identifying potential drug targets from gene expression signatures, indicating downstream effector genes and mechanisms leading to cell inviability. Identification of distinct synthetic lethal gene clusters may further lead to the elucidation of drug resistance mechanisms. While these pathways are indicative of the main functions of E-cadherin and synthetic lethal partners, it remains to identify the genes within these pathways that are the most actionable or supported across SLIPT analysis in patient samples and detected by experiments in preclinical models (Chen *et al.*, 2014; Telford *et al.*, 2015). The specific genes within key pathways will be discussed in Chapter 5, along with further investigations into their relation to pathway structure. While these are important clinical implications,

the **synthetic lethal** predictions lack enough confidence for direct translation into pre-clinical models or clinical applications leading to a need for statistical modelling and simulation of **synthetic lethality** in **genomics expression** data.

These **synthetic lethal** pathways have potential clinical implications, particularly those supported in pre-clinical models and in patient **expression** data. However, further validation of gene candidates will be necessary to ensure that these are able to be reproduced in further pre-clinical studies, they are applicable to tumours *in vivo*, and that effective inhibitory agents can be repurposed or designed against them.

4.5.3 Replication and Validation

4.5.3.1 Integration with **siRNA** Screening

The pathway composition across computational and experimental **synthetic lethal** candidates was informative with over-representation (Table 4.6) and supported by resampling analysis (Table 4.8), despite a modest intersection of genes between them (Figure 4.2). Either approach may be significant for a pathway in this intersection without being supported by the other: resampling analysis may support pathways that were not over-represented due to small effect sizes, thus both tests are required for a candidate pathway.

The pathways detected by both over-representation and resampling are the strongest candidates for further investigation and the **pathway** structure analyses in Chapter 5 will focus on these pathways detected by both over-representation and resampling. Particularly, those replicated across datasets or with pathway **metagenes**. In addition to GPCR pathways detected across these analyses, the **PI3K** cascade will also be investigated in Chapter 5, this signalling pathway is a well characterised mediator between GPCR receptors and regulation of translation (Gao and Roux, 2015) (both detected throughout this Chapter) and exhibited unexpected behaviour with pathway the **metagenes** (in Section 4.3). This pathway is activated by protein Phosphorylation states and thus inactivation may not be detectable with **expression**.

However, the **SLIPT** approach was shown to be predictive of which **siRNA** primary screen candidate partners of *CDH1* were validated in a secondary screen (as shown in Section 4.2.4). These results further support **SLIPT** for identifying robust **synthetic lethal** candidates which can be validated and as a triage approach for interpreting screening experiments.

4.5.3.2 Replication across Tissues

Furthermore, synthetic lethal partners identified by SLIPT were replicated across breast and stomach cancer. These were particularly concordant at the pathway level, as expected between tissues since synthetic lethal pathways have higher conservation between species (Dixon *et al.*, 2008). These findings support gene functions conserved across *CDH1* deficient cancers in breast and stomach tissues, presenting vulnerabilities that could be applied against molecular targets in both cancers. In addition, these analyses serve as a replication across independent patient cohorts from breast and stomach cancers, decreasing the likelihood of the synthetic lethal pathways detected being false positives or artifacts of either dataset.

Synthetic lethal pathways were also replicated across expression analyses of TCGA patient samples in heterogeneous tumours and homogeneous cell line isolates. This further supports that the subset of synthetic lethal functions detectable in experimental models (Chen *et al.*, 2014; Telford *et al.*, 2015) would be applicable tumours of patients with *CDH1* deficient cancers.

There are many gene functions replicated across breast cancer gene expression analyses. Many of these were also replicated with mutation analysis and with stomach cancer or cell line expression data. These pathways were more consistent across replication analyses than previous investigations with TCGA microarray data (Kelly, 2013).

4.6 Summary

We have developed a simple, interpretable, computational approach to predict synthetic lethal partners from genomics data. The analyses focus on gene expression data as it is widely available for applications in other cancers and other disease genes, particularly those with malignant loss of function.

This approach has been applied to robustly detect synthetic lethal pathways for the E-cadherin (*CDH1*) in TCGA breast cancer molecular profiles with comparisons to experimental screening (Telford *et al.*, 2015) in cell lines, and replication in TCGA stomach cancer molecular profiles and across cell types in the cancer cell line encyclopaedia. The pathway replicated across several analyses included extracellular matrix pathways (e.g., elastic fibres formation), cell signalling (including GPCRs), and core gene regulation and translation processes crucial for the growth and proliferation of cancer cells. These pathways show evidence of non-oncogene addiction for *CDH1* deficient cells and present vulnerabilities which may be exploited for specific treatment against *CDH1* mutations in HCGC and sporadic cancers. There was also support for

synthetic lethal pathways with *CDH1* in cell adhesion and cytoskeletal processes to which *CDH1* belongs, supporting the finding that *synthetic lethality* occurs within biological pathways (Boone *et al.*, 2007; Kelley and Ideker, 2005).

While translational and immune pathways detected by **SLIPT** were not supported by primary **siRNA** screening (Telford *et al.*, 2015), these were replicated across various analyses. Due to the differences between an experimental cell line model (Chen *et al.*, 2014; Fece de la Cruz *et al.*, 2015) and patient molecular profiles (Bass *et al.*, 2014; TCGA, 2012), these would not be expected to be completely concordant. Furthermore, many pathways are difficult to test in an isolated experimental system. Nevertheless, many of the genes and pathways detected by **SLIPT** are suitable to inform further investigations and triage of therapeutic targets against *CDH1* deficient tumours in combination with experimental screening.

A characteristic of gene interaction networks is a **scale-free** topology leading to highly interacting ‘hub’ genes, these represent important genes in a functional network. Cell surface interactions, the extracellular matrix, and cell signalling (particularly PI3K/AKT signalling) were also found to be *synthetic lethal* hubs with more interactions detected than other genes. This indicates that these pathways are functionally important to survival of cancer cells since they are subject to high **functional redundancy**, despite frequent disruptions in cancer. These pathways being involved in a disproportionate number of *synthetic lethal* interactions is also consistent with their detection for *CDH1*.

Thus *synthetic lethal* pathways have been identified using **TCGA** patient molecular profiles and experimental screening results. Some of these were robustly replicated across these datasets and against *CDH1* **mutation** or **expression** analysis. However, there remains the need to identify actionable genes within these pathways, relationships with experimental candidates, and how these pathways may affect viability when lost. While the genes identified between these analyses were less concordant the results of the **TCGA** breast cancer analysis will be used to test **pathway** structure relationships and further examine the *synthetic lethal* genes detected in the following Chapter.

Chapter 5

Synthetic Lethal Pathway Structure

Having identified key pathways implicated in [synthetic lethal](#) genetic interactions with *CDH1* (in Chapter 4), these were investigated for the [synthetic lethal](#) genes within them and their relationships to [pathway](#) structure in Reactome pathways. This chapter will focus on the [pathway](#) structure of biological pathways detected across analyses in Chapter 4.

The [synthetic lethal](#) genes identified were further examined within the context of biological pathways. Specifically, investigations were performed on whether [synthetic lethal](#) candidates, detected by [SLIPT](#) or [siRNA](#), exhibited differences with respect to network metrics of [pathway](#) structure of connectivity and importance in the network (as described in Sections 2.4.4 and 3.5.3). The relationships between [synthetic lethal](#) candidates, detected by either approach, were also considered to detect whether genes detected by [SLIPT](#) were upstream or downstream of genes detected by [siRNA](#). These directional relationships were tested by resampling (as described in Sections 3.4.1 and 3.4.1.1) and comparisons to the pathway hierarchical score based on biological context (as derived in Section 3.4.1.2). Together these investigations into structural relationships demonstrate how a combination of network biology and statistical techniques can be performed with genes identified by a [bioinformatics](#) analysis.

5.1 Synthetic Lethal Genes in Reactome Pathways

The [graph](#) structure for Reactome pathways was obtained from Pathway Commons via [BioPAX](#) (as described in Section 2.4.2). The pathways describe the (directional) relationships between biomolecules, including genes that encode proteins in biological pathways. These relationships include cell signalling (e.g., kinase phosphorylation cascades), gene regulation (e.g., transcription factors, chromatin modifiers, [RNA](#) bind-

ing proteins), and metabolism (e.g., the product of an enzyme being the substrate of another). Together these relationships describe the known functional pathways in a human cell with a reasonable resolution, from a curated database supported by publications documenting pathway relationships.

Pathway structures from the Reactome network (as described in Section 2.4.3) were used to derive the graph structure of each biological pathway. The synthetic lethal candidate genes for notable pathways discussed in Chapter 4, including candidate synthetic lethal pathways of *CDH1*, were examined to show the SLIPT and siRNA candidates within these pathways. The synthetic lethal genes considered here are those candidates detected by SLIPT (as described in Section 3.1) in TCGA breast cancer expression and mutation data (TCGA, 2012) in comparison to the candidate gene partners from the siRNA screening in breast cell lines (Telford *et al.*, 2015).

5.1.1 The PI3K/AKT Pathway

The phosphoinositide 3-kinase (PI3K) cascade signalling pathway exhibited unexpected results with metagene analyses (as discussed in Section 4.3). This pathway is also of interest because mediating signals between the GPCRs and regulation of protein translation have both been strongly implicated to be synthetic lethal pathways with loss of *CDH1* function (in Chapter 4). These pathways have all subject to dysregulation in cancer (Courtney *et al.*, 2010; Dorsam and Gutkind, 2007; Gao and Roux, 2015). Thus the PI3K cascade will be examined along with the most supported synthetic lethal pathways (as identified in Chapter 4).

The PI3K pathway is also an ideal pathway in which to test pathway structure because it has an established direction of signal transduction from extracellular stimuli (and membrane bound receptors) to the inner mechanisms of the cell, namely, the regulation of protein translation. The production of proteins is necessary for the growth of the cell so it is reasonable to suggest that these processes may be subject to (non-oncogene) addiction in some cancer cells which rely upon them for sustained protein production and cell growth. This is also supported by the oncogenes *PIK3CA* and *AKT1* being involved with the PI3K cascade and related PI3K/AKT pathway which may be subject to oncogene addiction when these proto-oncogenes are activated.

The PI3K cascade was not supported across SLIPT in TCGA breast expression data and the siRNA primary screen by over-representation (in Section 4.2.5) or resampling (in Section 4.2.5.1) but genes were detectable by either approach (as shown in Figure 5.1). While few genes were identified by both approaches, these include genes

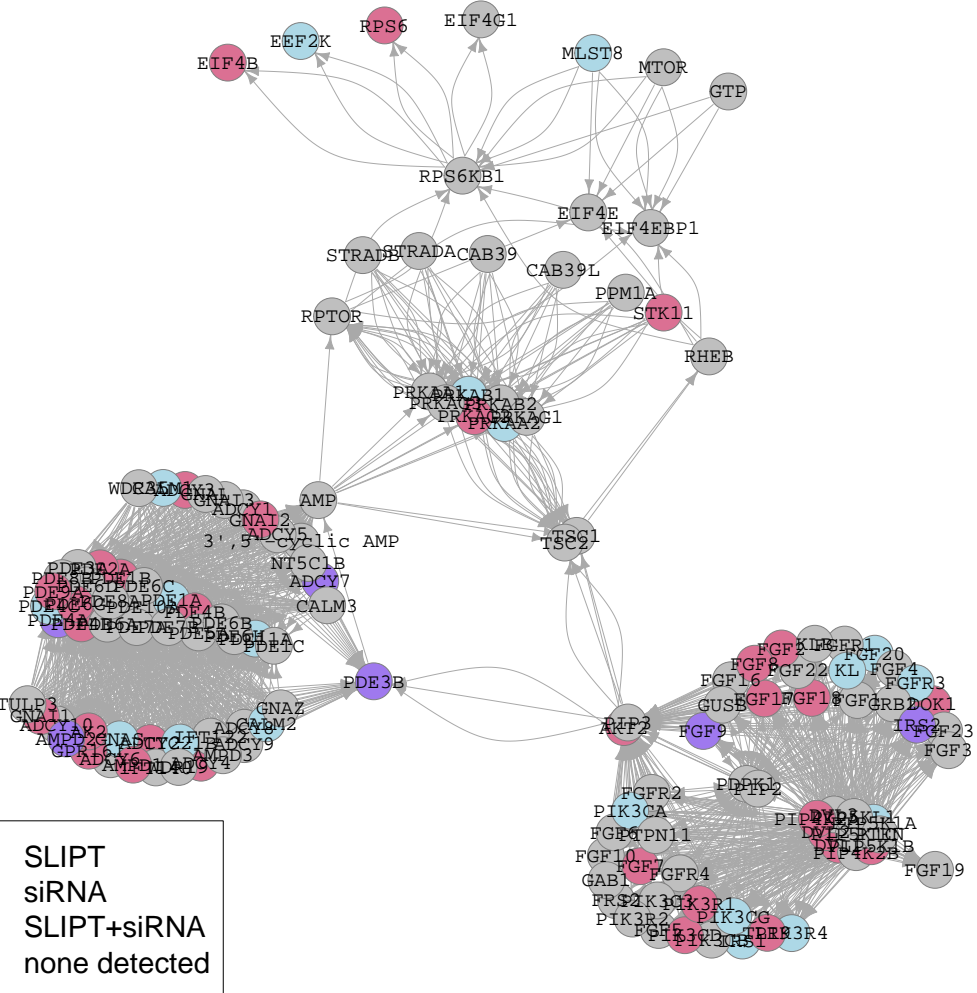


Figure 5.1: **synthetic lethality in the PI3K cascade.** The Reactome PI3K Cascade pathway with synthetic lethal candidates coloured as shown in the legend.

that are highly connected in the PI3K cascade and are hubs to information transmission such as *FGF9*, *PDE3B*, and *PDE4A*. The key upstream genes *PIK3CA* and *PIK3CG* were detected by siRNA whereas the downstream *PIK3R1* and *AKT2* genes were detected by SLIPT. Gene detected by either method were also prevalent in the PI3K, phosphodiesterase (PDE), and AMP-activated protein kinase (AMPK) modules, in addition to the downstream translation factors and ribosomal genes (*EIF4B*, *EEF2K*, and *RPS6*). Together these suggest that there may be further structure between the SLIPT and siRNA candidate partners of *CDH1* in pathways as illustrated by PI3K. As

such, **pathway** structure will be investigated to detect differences in the upstream and downstream gene candidates of those detected by either method. Pathway structure may account for the disparity between **SLIPT** and **siRNA** genes, even in pathways such as PI3K where they did not significantly intersect. For instance, **SLIPT** gene partners may be downstream of **siRNA** candidates rather than replicating them directly.

This disparity between **SLIPT** and **siRNA** gene candidate **synthetic lethal** partners of *CDH1*, that is a high number of genes detected by either approach with few detected by both, was replicated in the related PI3K/AKT pathway and the “PI3K/AKT in cancer” pathway (shown in Appendix Figures F.1 and F.2). Many **synthetic lethal** candidates were at the upstream core of these pathway networks and the downstream extremities. It is particularly notable that the many genes important in cell signalling and gene regulation were detected by either **synthetic lethal** detection approach. These include *AKT1*, *AKT2*, and *AKT3*, the Calmodulin signalling genes *CALM1* and *CAMK4*, and the forkhead family transcription factors *FOXO1* (a **tumour suppressor**) and *FOXO4* (an inhibitor of **EMT**).

5.1.2 The Extracellular Matrix

The extracellular pathways “elastic fibre formation” and “fibrin clot formation” (shown in Figures 5.2 and 5.3 respectively) were both supported across analyses (in Chapter 4). Significant over-representation and resampling the intersection between **SLIPT** (for **TCGA** breast cancer) and **siRNA** gene candidates showed that both approaches identified these pathways.

Particularly for elastic fibres (Figure 5.2), the vast majority of genes were detected by either approach in addition to a significant proportion of genes detected by both approaches (as determined in Section 4.2.5). The genes detected by both approaches also appeared to have a non-random distribution in the network with *TFGB1*, *ITGB8*, and *MFAP2* exhibiting high connectivity, and having a central role in their respective pathway modules. In addition to a structural role in the extracellular matrix and connective tissue (including the tumour microenvironment), these proteins including Furin, **transforming growth factor β (TGF β)**, and the **bone morphogenic proteins (BMPs)**, are also involved in responses to endocrine signals and interact with the cellular receptors for signalling pathways. Therefore it is plausible that *CDH1* deficient tumours will be subject to **non-oncogene addiction** to the extracellular environment and growth signals arising from this pathway. The **pathway** structure also indicative for further investigation that the genes detected by **siRNA** (or both approaches) may

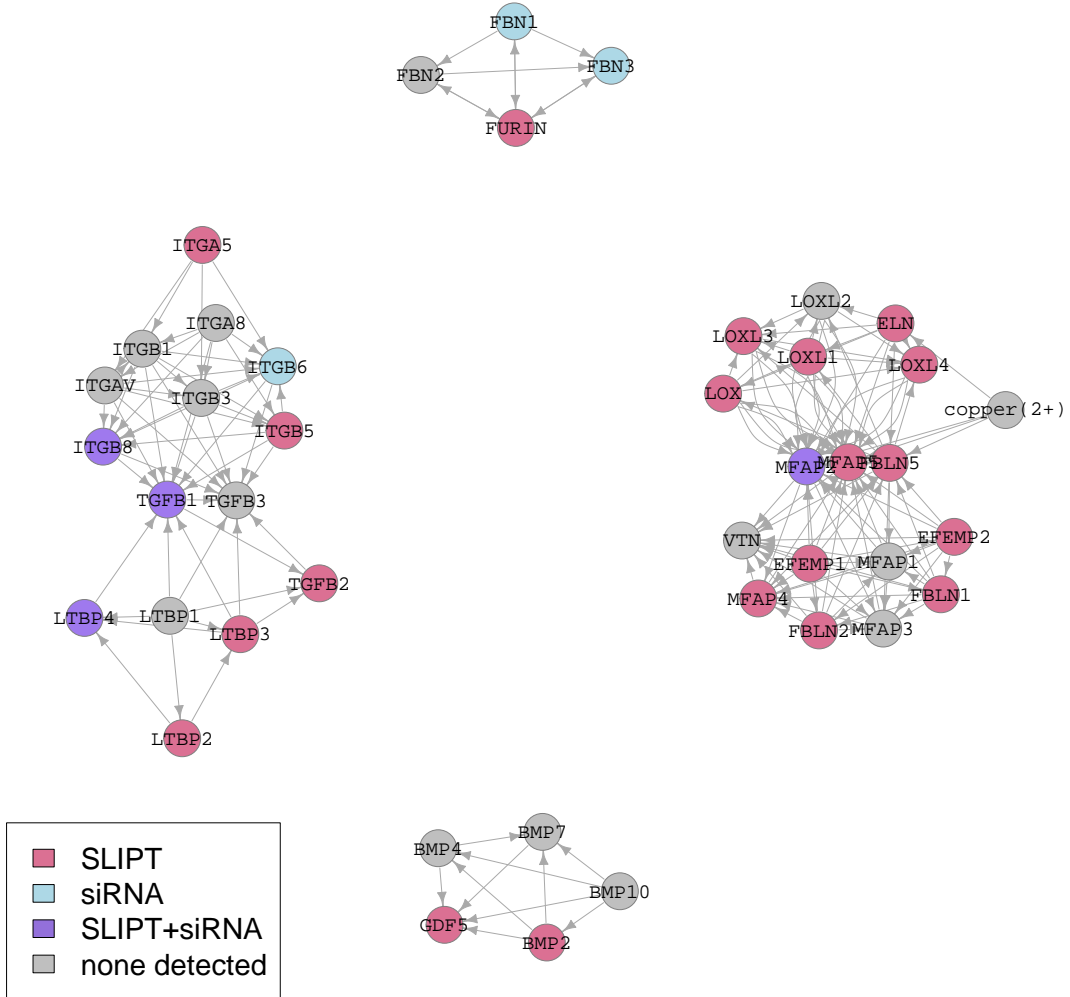


Figure 5.2: **synthetic lethality in Elastic Fibre Formation.** The Reactome Elastic Fibre Formation pathway with [synthetic lethal](#) candidates coloured as shown in the legend.

be downstream of those detected by [SLIPT](#), in addition to whether connectivity or [centrality](#) is higher for [synthetic lethal](#) candidates than other genes in the pathway.

Genes detected as [synthetic lethal](#) partners of *CDH1* by [SLIPT](#) or [siRNA](#) screening were also common in the Fibrin clot formation pathway (shown in Figure 5.3). This is consistent with the established pleiotropic role of *CDH1* in regulating fibrin clotting. It is also notable that the genes detected by either method appear to be highly connected such as *C1QBP*, *KNG1*, *F8*, *F10*, *F12*, *F13A*, and *PROC* (including many of the coagulation factors). [Synthetic lethal](#) candidates also include *SERPINE2* and *PRCP*,

which only affect downstream genes, in addition to *PROCR* and *VWF*, which are only affected by upstream genes.

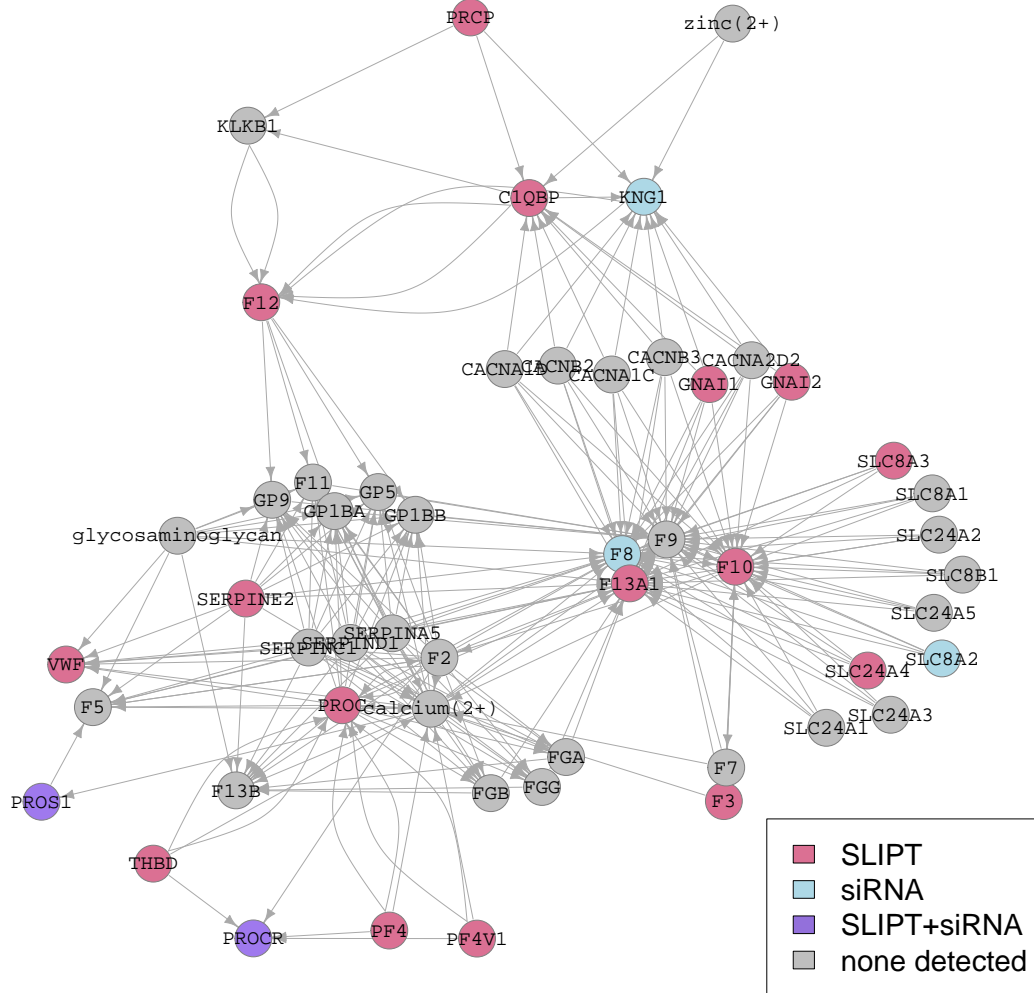


Figure 5.3: **Synthetic lethality in Fibrin Clot Formation.** The Reactome Fibrin Clot Formation pathway with [synthetic lethal](#) candidates coloured as shown in the legend.

Many of these genes are involved in the larger Extracellular Matrix pathway (shown in Appendix Figure F.3), including many of the [synthetic lethal](#) candidates discussed for elastic fibres. The number of [SLIPT](#) candidate genes outnumbers those identified by [siRNA](#), as expected from an isolated cell model. However, the endocrine response genes (e.g., *TGFB1* and *LTPB4*) which are potentially artifacts of the cell line growth process were replicated with [SLIPT](#) analysis in patient tumours (TCGA breast cancer

data). There is also additional support for **synthetic lethal** genes (e.g., *ITGB2*, *MFAP2*, and *SPARC*) being highly connected networks hubs of the pathway. The complexity of the extracellular matrix pathway lends credence to the need for formal network analysis approaches to interpret the **pathway** structure of **synthetic lethal** candidates. Furthermore statistical approaches are needed to determine whether structural relationships are unlikely to be observed between **synthetic lethal** candidates by sampling error.

5.1.3 G Protein Coupled Receptors

G protein coupled receptor (GPCR) pathways are highly complex (as shown in Appendix Figures F.4 and F.5). Many of genes in these pathways were **synthetic lethal** candidates, detected by either **SLIPT** or **siRNA** screening, including genes frequently detected with both approaches, consistent with these pathways being supported by prior analyses (in Sections 4.2.5 and 4.2.5.1). **Synthetic lethal** candidates include the **PDE** and Calmodulin genes (as discussed in Section 5.1.3) in addition to others such as the regulators of **G-protein signalling (RGS)**, **chemokine receptors (CXCR)**, **Janus kinase (JAK)**, and the **Ras homolog family (RHO)** genes. These are important regulatory signalling pathways necessary for cellular growth and cancer proliferation. Thus the **GPCR** pathways (and downstream PI3K/AKT signals) are a potentially actionable vulnerability against *CDH1* deficient cancers, particularly since many existing drug targets exist among these signalling pathways, some of which have been experimentally validated (Kelly *et al.*, unpublished; Telford *et al.*, 2015). However, the complexity of **GPCR** networks containing hundreds of genes requires the relationships between **SLIPT** and experimental candidates to be tested with a network based statistical approach, although statistically significant number of genes in GPCR pathways was detected by both approaches (in Sections 4.2.5 and 4.2.5.1).

5.1.4 Gene Regulation and Translation

While very few **synthetic lethal** genes were detected in translational pathways in an experimental screen against *CDH1* (Telford *et al.*, 2015), these were highly overrepresented in translational elongation (as shown in Appendix Figure F.6). These **SLIPT** genes include many ribosomal proteins and the regulatory “elongation factors” which may be subject to responses in the upstream signalling pathways. This observation lends support to the notion of **pathway** structure among **synthetic lethal** candidates detected by **SLIPT** in comparison with **siRNA**. The computational approach with **SLIPT** displays the ability to detect downstream genes in the core translational processes which experimental screening did not identify. The experimental screening

may similarly detect upstream regulatory genes less sensitive to inactivation, that is, genes that are less likely to be indiscriminately lethal to both genotypes at high doses of inactivation.

Many of these **SLIPT** candidate genes are also among the **nonsense-mediated decay (NMD)** pathway (shown in Appendix Figure F.7) or **3' untranslated region (UTR)** mediated translational regulation (shown in Appendix Figure F.8). While genes in these pathways were also supported by experimental screening with **siRNA**, there was differences in which genes were detected within the **pathway** structures. In particular, *UPF1* was detected in the **siRNA** screen and is the focal downstream gene for the entire **NMD** pathway showing that (in this case) **siRNA** genes are downstream effectors of those detected by **SLIPT**. **3' UTR** mediated translational regulation has a similar structure with two modules connected solely by *RPL13A*, giving an example of **SLIPT** candidate genes with high connectivity, although there were many ribosomal proteins detected by **SLIPT**. However, the detection of *EIF3K*, a regulatory elongation factor (not **essential** to ribosomal function) was replicated across **SLIPT** and **siRNA** screening, while the majority of the elongation factors were not detected by either approach. Regulatory genes, being more amenable to experimental validation, also support further investigation into **pathway** structure. The **SLIPT** candidates may support experimental candidates in biological pathways by detecting downstream genes, which may not be detectable by experimental screening with high dose inhibitors. This difference between the approaches may explain the greater number of **SLIPT** candidate partners of *CDH1* than those experimentally identified.

5.2 Network Analysis of Synthetic Lethal Genes

Genes detected as **synthetic lethal** partners of *CDH1* with the **SLIPT** computational approach and the **siRNA** screen (Telford *et al.*, 2015) were compared across network metrics in the example of the PI3K cascade pathway (where the genes differed considerably between **synthetic lethal** detection methods). These were used to test whether network metrics differed between groups of genes detected by either or both approaches. These analyses serve to test both whether **synthetic lethal** gene candidates had higher connectivity or importance in a network and whether either detection approach is biased towards genes with different network properties.

5.2.1 Gene Connectivity and Vertex Degree

Vertex degree (the number of connections) for each gene is a fundamental property of a network. The vast majority of genes had a relatively modest number of connections, each with only a few genes in the PI3K pathway (shown in Figure 5.4) having pathway relationships with a high number of genes, consistent with the [scale-free](#) property of biological networks ([Barabási and Oltvai, 2004](#)). There were few differences in the number of connections between gene groups (by [synthetic lethal](#) detection), although genes detected by [siRNA](#) included those with the fewest connections. The median connectivity of genes detected by both approaches was marginally higher.

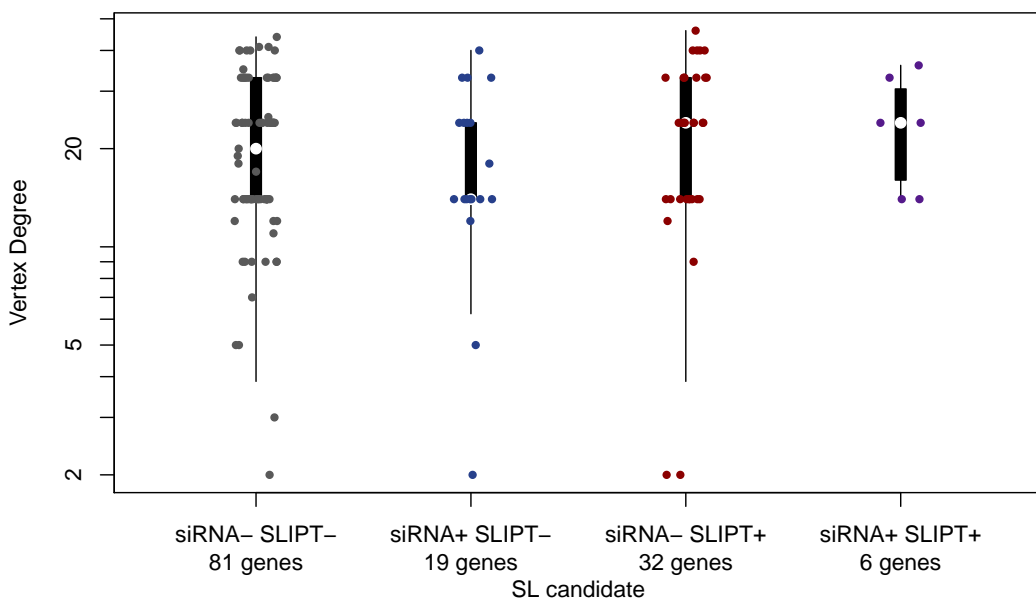


Figure 5.4: **Synthetic lethality and vertex degree.** The number of connected genes ([vertex degree](#)) was compared (on a log-scale) across genes detected by [SLIPT](#) and [siRNA](#) screening in the Reactome PI3K cascade pathway. There were very few differences in [vertex](#) degree between the groups, although genes detected by [siRNA](#) included those with the fewest connections.

Table 5.1: ANOVA for synthetic lethality and vertex degree

| | DF | Sum Squares | Mean Squares | F-value | p-value |
|---------------|----|-------------|--------------|---------|---------|
| siRNA | 1 | 15 | 15.50 | 0.0134 | 0.9082 |
| SLIPT | 1 | 506 | 506.01 | 0.4378 | 0.5105 |
| siRNA × SLIPT | 1 | 0 | 0.05 | 0.0000 | 0.9947 |

Analysis of variance for `vertex` degree against `synthetic lethal` detection approaches (with an interaction term)

The results for the PI3K pathway were very similar when testing `synthetic lethality` against `CDH1 mutation` (`mtSLIPT`). In this case, there is also indication that `mtSLIPT`-specific genes may have higher connectivity than those detected by `siRNA` screening (shown in Appendix Figure G.1).

However, these apparent differences in `vertex` degree may be due to fewer genes being detected by either approach. There was no statistically significant effect of either computational or experimental synthetic lethal detection method on `vertex` degree, as determined by analysis of variance (ANOVA) (shown by Table 5.1 and Appendix Table G.1). Thus `synthetic lethal` detection does not discriminate among genes by their connectivity in a pathway network, nor is either approach constrained to detecting highly connected genes. Both approaches have been demonstrated to detect genes with many and very few connections.

5.2.2 Gene Importance and Centrality

5.2.2.1 Information Centrality

`Information centrality` is a measure of the importance of `nodes` in a network by how vital they are to the transmission of information throughout the network. This applies well to biological pathways, particularly gene regulation and cell signalling. The `nodes` with the highest `information centrality` are not necessarily the most connected, as they may also include `nodes` that pass signals between highly connected network hubs. `Information centrality` therefore provides a distinct metric for the connectivity of a gene in a pathway, which has the added benefit of being directly related to the disruption of pathway function were it to be inactivated or removed.

`Information centrality` has also been suggested to indicate essentiality of genes or proteins (Kranthi *et al.*, 2013). The `information centrality` for each gene was computed across the entire Reactome network (as discussed in Appendix H). Reactome contains substrates and cofactors in addition to genes and proteins. In support of `centrality`

as a measure of essentiality or importance to the network, a number of **nodes** with the highest **centrality** (shown in Appendix Table H.1) were **essential** nutrients, including Mg²⁺, Ca²⁺, Zn²⁺, and Fe.

Genes important in development of epithelial tissues and breast cancer were also detected with relatively high **information centrality** (as shown by the distribution across the Reactome network in Appendix Figure H.1). Interleukin 8 (encoded by *IL8*) is a chemokine important in epithelial cells, the innate immune system, and binding GPCRs. *GATA4* is an embryonic transcription factor involved in heart development, EMT, and has been shown to be recurrently mutated in breast cancer (TCGA, 2012). β-catenin (encoded by the **proto-oncogene** *CTNNB1*) is a regulatory protein which binds to **E-cadherin**, being involved in cell-cell adhesion and **Wingless-related integration site (WNT)** signalling. Together these show that **information centrality** identifies **nodes** of importance to biological functions in pathway networks, including those relevant to *CDH1* deficient breast cancers.

Within the **PI3K** pathway, genes detected by **siRNA** did not include those with lower **centrality** (shown in Figure 5.5), although the median **information centrality** across gene groups detected by either **synthetic lethal** approach did not differ. The genes with the highest **information centrality** included the synthetic candidates *PDE3B* (detected by **SLIPT** and **siRNA**) and *AKT2* (detected by **SLIPT**) which were markedly higher than most other genes in the pathway. The higher **centrality** of these genes is consistent with their known biological role in PI3K/AKT signalling and the **pathway** structure (shown in Figure 5.1). Other biomolecules with high **centrality** included the *RPS6KB1* and *RP-TOR* genes, **adenosine monophosphate (AMP)**, **phosphatidylinositol-(4,5)-bisphosphate (PIP₂)**, and **phosphatidylinositol-(3,4,5)-trisphosphate (PIP₃)**.

These findings were replicated (shown in Appendix Figure G.2) when testing **synthetic lethality** against *CDH1* **mutation** (**mtSLIPT**). The differences in network **centrality** between gene groups detected by either method were not statistically significant as determined by **ANOVA** (shown by Table 5.2 and Appendix Table G.2). Thus neither method was unable to detect **synthetic lethal** genes with particular **centrality** constraints, although they were also not detecting genes with higher **centrality** than expected by chance.

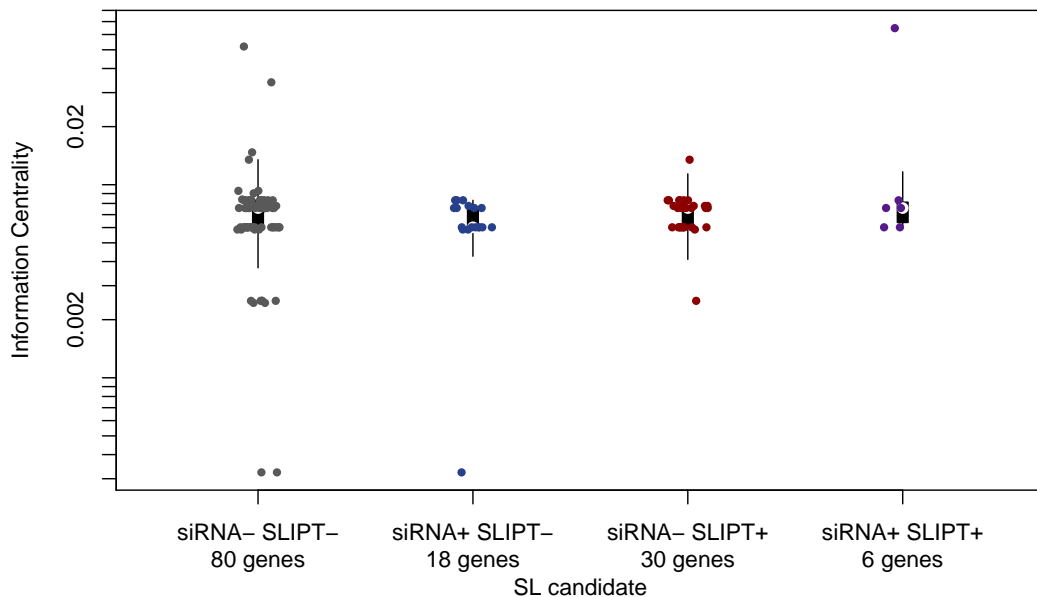


Figure 5.5: Synthetic lethality and centrality. The [information centrality](#) was compared (on a log-scale across genes detected by [SLIPT](#) and [siRNA](#) screening in the Reactome PI3K cascade pathway. Genes detected by [SLIPT](#) or [siRNA](#) did not have higher connectivity than other genes. The gene with the highest [centrality](#) was detected by both approaches.

Table 5.2: [ANOVA](#) for synthetic lethality and information centrality

| | DF | Sum Squares | Mean Squares | F-value | p-value |
|-------------|----|-------------|--------------|---------|---------|
| siRNA | 1 | 0.000256 | 0.0002561 | 0.1854 | 0.6682 |
| SLIPT | 1 | 0.003827 | 0.0038275 | 2.7717 | 0.1008 |
| siRNA×SLIPT | 1 | 0.000804 | 0.0008036 | 0.5820 | 0.4483 |

Analysis of variance for [information centrality](#) against [synthetic lethal](#) detection approaches (with an interaction term)

5.2.2.2 PageRank Centrality

[PageRank centrality](#) is another network analysis procedure to infer a hierarchy of gene importance from a network using connections and structure ([Brin and Page, 1998](#)). In contrast to the [information centrality](#) approach of removing [nodes](#), PageRank uses the eigenvalue properties of the adjacency matrix to rank genes according to the number of connections and paths they are involved in.

This distinction is immediately clear within the PI3K pathway (shown in Figure 5.6), which differs considerably from the information centrality scores. Genes detected by SLIPT span the complete range of PageRank centrality values for this pathway, which was replicated when testing synthetic lethality against *CDH1* mutation (shown in Appendix Figure G.3). However, the genes detected by both SLIPT and siRNA screening have a higher median PageRank centrality, although the differences in PageRank centrality between these methods were not statistically significant as determined by ANOVA (shown by Table 5.3 and Appendix Table G.3).

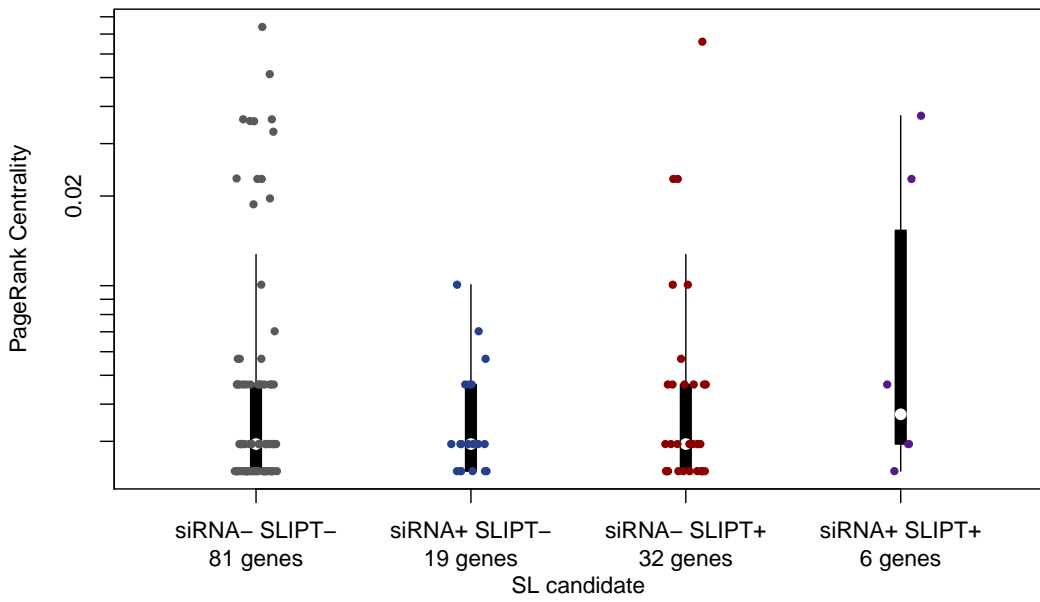


Figure 5.6: Synthetic lethality and PageRank. The PageRank centrality was compared (on a log-scale across genes detected by mtSLIPT and siRNA screening in the Reactome PI3K cascade pathway. Genes detected by siRNA had a more restricted range of centrality values (which may be constrained experimental detection in a cell line model) than other genes not detected by either approach, although these groups also had fewer genes and a higher median.

Table 5.3: ANOVA for synthetic lethality and PageRank centrality

| | DF | Sum Squares | Mean Squares | F-value | p-value |
|---------------|----|-------------|-------------------------|---------|---------|
| siRNA | 1 | 0.0002038 | 2.0385×10^{-4} | 1.1423 | 0.2892 |
| SLIPT | 1 | 0.0000208 | 2.0752×10^{-5} | 0.1163 | 0.7342 |
| siRNA × SLIPT | 1 | 0.0000137 | 1.3743×10^{-5} | 0.0770 | 0.7823 |

Analysis of variance for [PageRank centrality](#) against [synthetic lethal](#) detection approaches (with an interaction term)

5.3 Relationships between Synthetic Lethal Genes

5.3.1 Hierarchical Pathway Structure

5.3.1.1 Contextual Hierarchy of PI3K

A contextual hierarchy of genes in the [PI3K](#) pathway was performed (as described in Section 3.4.1.2) to assign scores for their relative order in the pathway. In the case of [PI3K](#) (shown in Figure 5.7), this orders genes from the upstream genes, which respond to signals from extracellular stimuli, to the downstream genes which transmit these to the [gene expression](#) (translation) responses of the cell. The directionality of this pathway is evident in transmitting signals from the [PI3K](#) complex, via [AKT](#), [PDE](#), and [mTOR](#) to the ribosomal regulatory proteins. This hierarchical procedure enables testing whether the biological context of a gene in a pathway is relevant to detection as a [synthetic lethal](#) candidate by either computational [SLIPT](#) analysis or experimental [siRNA](#) screening.

5.3.1.2 Testing Contextual Hierarchy of Synthetic Lethal Genes

This pathway hierarchy in the [PI3K](#) cascade was tested for differences between genes detected across [SLIPT](#) and [siRNA](#) screening. The [synthetic lethal](#) candidates for [CDH1](#) detected by either method (as shown by Figure 5.8a) did not differ, each being distributed throughout the pathway. When adjusted for being more numerous, there was little indication that [SLIPT](#) candidate genes are more frequently upstream or downstream of [siRNA](#) candidate genes (as shown by Figure 5.8b) and were more frequent at moderate hierarchies which contained more genes. [Synthetic lethal](#) candidates from both methods were less frequently detected in the downstream effectors of the pathway (e.g., the [mTOR](#) complex), although core pathway genes (e.g., [AKT2](#) and [PDE3B](#)) were detectable as [synthetic lethal](#) candidates (as discussed for Figures 5.1 and 5.6).

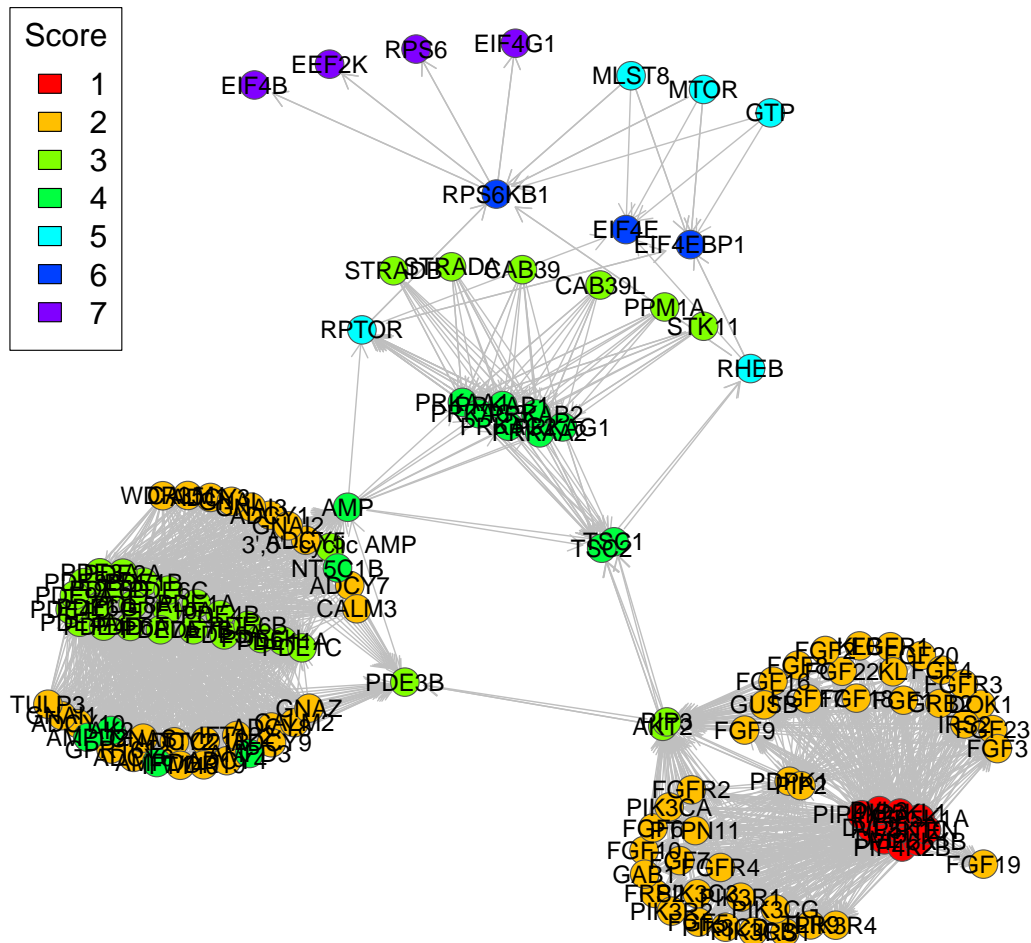
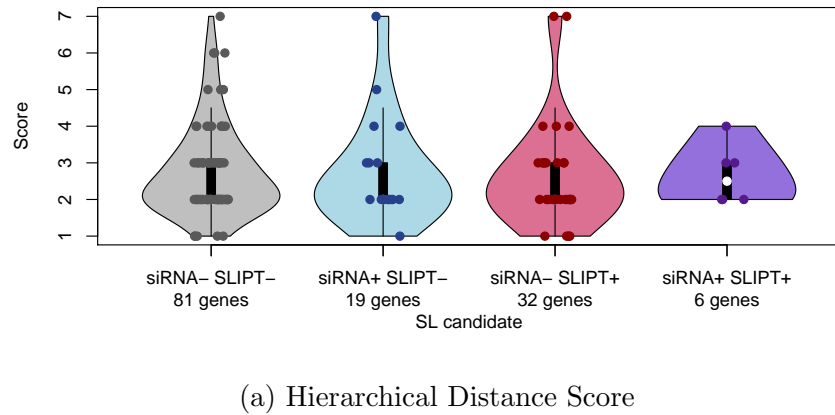


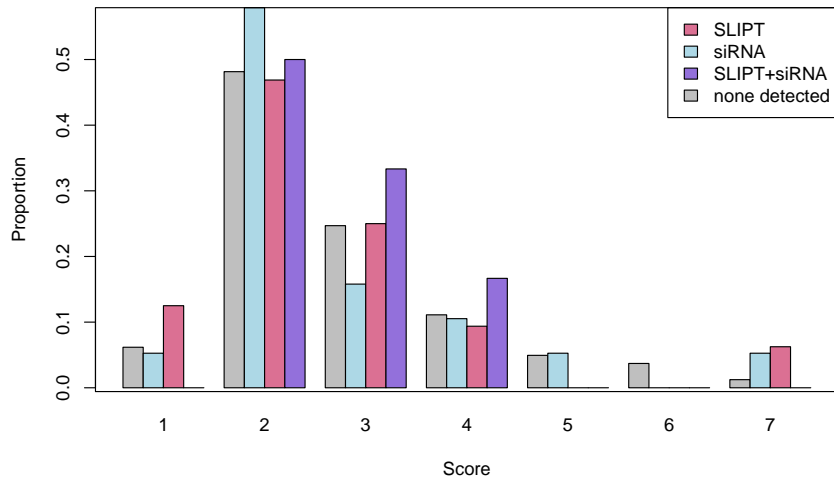
Figure 5.7: **Hierarchical structure of PI3K.** A contextual score was used for ranking genes within the PI3K Cascade to demonstrate a pathway structure analysis to examine whether genes detected by either SLIPT or siRNA were more frequently upstream or downstream in the PI3K pathway.

Similarly, when testing synthetic lethality against *CDH1* mutation (mtSLIPT), the hierarchical score for the PI3K pathway did not differ between mtSLIPT-specific and siRNA-specific gene candidates (as shown by Appendix Figure I.1). The median among genes detected by both approaches was marginally elevated such that these genes may be further downstream in the pathway than other synthetic lethal candidate partners of *CDH1*. There were fewer genes overall with higher scores (shown in Appendix

Figure 1.2). While these were more frequently detected by both **SLIPT** and **siRNA**, there was no significant effect variation in pathway hierarchy (shown by **ANOVA** in Table 5.4 and Appendix Table I.1) accounted for by **SLIPT** or **siRNA** detection in the **PI3K** pathway (as shown in Figure 5.1). Thus these hierarchical scores may be observed by sampling variation and there is no indication that **SLIPT** or **siRNA** detection differs



(a) Hierarchical Distance Score



(b) Proportion of Genes

Figure 5.8: **Hierarchy score in PI3K against synthetic lethality in PI3K.** The hierarchical distance scores were similarly distributed across **SLIPT** and **siRNA** genes. The number of **SLIPT** and **siRNA** genes against the hierarchical distance scores showing no significant tendency for either method to either of the pathway upstream or downstream extremities.

along the direction of the pathway. Genes detected by either method are no more or less common among upstream or downstream of the pathway.

Table 5.4: ANOVA for synthetic lethality and PI3K hierarchy

| | DF | Sum Squares | Mean Squares | F-value | p-value |
|-------------|----|-------------|--------------|---------|---------|
| siRNA | 1 | 0.001 | 0.00066 | 0.0004 | 0.9842 |
| SLIPT | 1 | 0.456 | 0.45605 | 0.2740 | 0.6016 |
| siRNA×SLIPT | 1 | 0.019 | 0.01878 | 0.0113 | 0.9156 |

Analysis of variance for PI3K hierarchy score against synthetic lethal detection approaches (with an interaction term)

[remove this paragraph and Figures 5.9 and I.3?]

Furthermore the pathway hierarchical scores did not exhibit different more or less SLIPT than siRNA genes above or below the given threshold. Since the ideal threshold to detect pathway structure is unclear, an exploratory analysis was performed, with χ^2 -test for the SLIPT or siRNA candidate genes upstream or downstream of each gene. It is unsurprising that these χ^2 tests were highest when the gene used as a threshold was in the middle of the pathway (as shown in Figure 5.9). However, there was no statistically significant support for pathway structure by this approach, as none of the χ^2 values were high enough to detect pathway structure between SLIPT and siRNA gene candidates. Nor was structure detectable for mtSLIPT testing synthetic lethality against CDH1 mutation (as shown in Appendix Figure I.3).

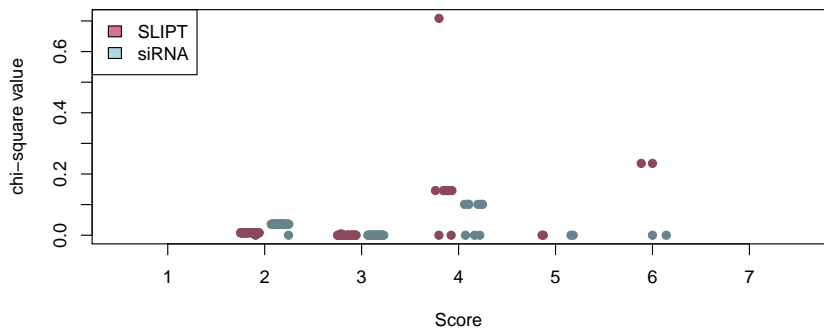


Figure 5.9: **Structure of synthetic lethality in PI3K.** The number of [SLIPT](#) and [siRNA](#) genes upstream or downstream of each gene in the Reactome PI3K pathway were tested (by the χ^2 -test). These are plotted as a split jitter stripchart against the hierarchical distance scores showing no significant tendency for either method to either of the pathway upstream or downstream extremities.

5.3.2 Upstream or Downstream Synthetic Lethality

This approach does not ascertain whether [SLIPT](#) and [siRNA](#) candidate partners of *CDH1* are upstream or downstream of one and other within a pathway such as the [PI3K](#) cascade. The hierarchical approach is designed to detect differences in pathway location between gene groups. An alternative [pathway](#) structure method has been devised to use [network](#) structures to identify directional relationships between individual [SLIPT](#) and [siRNA](#) genes. This [pathway](#) structure methodology will be applied (as described in Section 3.4.1) to detect the direction of [shortest paths](#) between [SLIPT](#) and [siRNA](#) gene candidates. This will be used to demonstrate the methodology on the [PI3K](#) pathway, to develop a statistical test for [pathway](#) structure between between [SLIPT](#) and [siRNA](#) gene candidate using resampling (as described in Section 3.4.1.1), and to apply this test for [pathway](#) structure among [synthetic lethal](#) gene candidates to the pathways identified in Chapter 4 and discussed in Section 5.1.

5.3.2.1 Measuring Structure of Candidates within PI3K

Shortest paths in a pathway network were used to devise a strategy to detect [pathway](#) structure between [SLIPT](#) and [siRNA](#) gene candidate partners of *CDH1* (as described in Section 3.4.1). Thus we can determine whether individual [SLIPT](#) genes have upstream or downstream [siRNA](#) candidates (scored as “up” or “down” events respectively). This

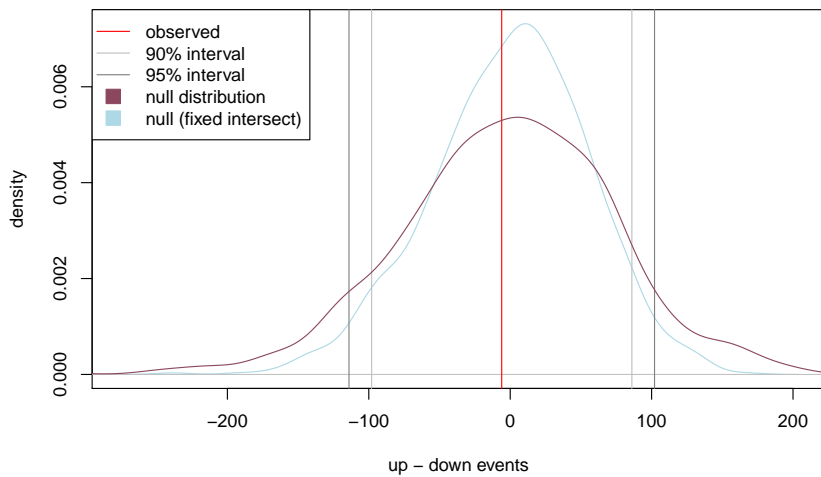


Figure 5.10: **Structure of synthetic lethality resampling in PI3K.** A null distribution with 10,000 iterations of the number of **siRNA** genes upstream or downstream of **SLIPT** genes (depicted as the difference of these) in the **PI3K** pathway. To assess significance, the observed events (with **shortest paths**) were compared to the 90% and 95% intervals for the null distribution (shown in violet). Genes detected by both methods were fixed to the same number as observed for the alternative null distribution (shown in blue), although the observed number of events (red) was not significant in either case. In both cases, these genes detected by both approaches were included in computing the number of **shortest paths** (in either direction) between **SLIPT** and **siRNA** genes.

procedure enables the detection of directional relationships between **SLIPT** and **siRNA** gene candidates (in contrast to the hierarchical approach).

The total number of gene candidate pairs in either direction can be compared within a pathway network to assess the overall directional relationships in a pathway. This directionality is detectable by the difference between the number of **SLIPT** candidate genes with upstream and downstream **siRNA** gene partners. However, this measure alone is not sufficient to determine whether there is evidence of **pathway** structure between **SLIPT** and **siRNA** gene candidate partners of *CDH1* in a pathway network. Nevertheless, it does serve to measure the magnitude (and direction) of the consensus of directional relationships (upstream and downstream) between **SLIPT** and **siRNA** gene candidate partners. This measure of **pathway** structure can be used for testing for statistical significance of **pathway** structure by resampling, using a permutation procedure to test whether these relationships are detectable among randomly selected

gene groups rather than the detected **SLIPT** and **siRNA** gene candidate partners (as described in Sections 2.3.6 and 3.4.1.1).

This resampling procedure was performed for the **PI3K** network to generate a null distribution for the difference in the number of “up events” and “down events” for this pathway (as shown in Figure 5.1). Resampling yields a distribution to detect whether genes detected by **SLIPT** had significantly more upstream or downstream **siRNA** candidates. While there was modest indication that **siRNA** genes were downstream of **SLIPT** candidate genes, resampling for the **PI3K** pathway (as shown in Figure 5.10) did not detect a significant number of **siRNA** genes upstream or downstream.

In contrast, when testing **synthetic lethality** against **CDH1** mutation (**mtSLIPT**) there was modest indication that **siRNA** genes were upstream of **SLIPT** candidate genes. However, resampling (as shown in Appendix Figure I.4) was also unable to detect a significant number of **siRNA** genes upstream or downstream of **mtSLIPT** candidates. Neither fixing the number of genes detected by both approaches (as shown by the blue line in Figure 5.10 and Appendix Figure I.4) nor excluding these jointly detected genes altered the findings of this approach. These genes were included in the analysis because they can disproportionately count towards **siRNA** genes being upstream (or downstream) of **SLIPT** genes as they may still have different proportions of gene detected by either approach upstream (or downstream) of them. Furthermore, expanding the range of **shortest paths** to consider **links** in related pathways (using the “metapathways” constructed in Section 2.4.3) also had little effect on the null distribution generated, despite increasing the computational demands of the procedure.

5.3.2.2 Resampling for Synthetic Lethal Pathway Structure

The permutation procedure (as described in Section 3.4.1.1) that was performed in Section 5.3.2.1 for the **PI3K** cascade was also applied to other pathways identified in Chapter 4 and discussed in Section 5.1. These include extracellular matrix (with constituent elastic fibre and fibrin pathways), cell signalling (by PI3K/AKT and GCPRs), and translational pathways (with **NMD** and 3'UTR regulation). The resampling results across these pathways (as shown in Table 5.5) had limited support for association between **pathway** structure and detection of **synthetic lethal** genes, with the majority of these being non-significant as shown for **PI3K** (in Appendix Figure I.4). However, the distribution for these pathways will differ depending on their structure, the number of genes they consist of, and the proportion of **synthetic lethal** candidates among them (including a higher frequency of genes detected by both methods for the pathways identified in Section 4.2.5.1). This resampling is an appropriate procedure to use to

detect structural relationships across pathways as it does not assume an underlying test statistic distribution.

Pathway structure was supported for the **NMD** pathway (which is consistent with **siRNA** being downstream in Appendix Figure F.7). However, this observation rests upon a single gene and was not replicated when testing **synthetic lethality (mtSLIPT)** against **CDH1 mutation** (as shown in Appendix Table I.2) nor was it supported by the related **3'UTR** regulation and translational elongation pathways.

Table 5.5: Resampling for **pathway** structure of **synthetic lethal detection methods**

| Pathway | Graph | | States | | Observed | | | | Permutation p-value | |
|---|-------|--------|--------|-------|----------|------|---------|---------|---------------------|----------|
| | Nodes | Edges | SLIPT | siRNA | Up | Down | Up–Down | Up/Down | Up–Down | Down–Up |
| PI3K Cascade | 138 | 1495 | 38 | 25 | 122 | 128 | -6 | 0.953 | 0.5326 | 0.4606 |
| PI3K/AKT Signalling in Cancer | 275 | 12882 | 98 | 44 | 779 | 679 | 100 | 1.147 | 0.3255 | 0.6734 |
| G_{αi} Signalling | 292 | 22003 | 95 | 58 | 836 | 1546 | -710 | 0.541 | 0.9971 | 0.0029 |
| GPCR downstream | 1270 | 142071 | 312 | 160 | 9755 | 9261 | 494 | 1.053 | 0.3692 | 0.6305 |
| Elastic fibre formation | 42 | 175 | 24 | 7 | 1 | 2 | -1 | 0.500 | 0.5461 | 0.3865 |
| Extracellular matrix | 299 | 3677 | 127 | 29 | 547 | 455 | 92 | 1.202 | 0.3351 | 0.6636 |
| Formation of Fibrin | 52 | 243 | 18 | 5 | 12 | 17 | -5 | 0.706 | 0.6198 | 0.3564 |
| Nonsense-Mediated Decay | 103 | 102 | 74 | 2 | 0 | 74 | -74 | 0 | 1.0000 | < 0.0001 |
| 3' -UTR-mediated translational regulation | 107 | 2860 | 77 | 1 | 0 | 0 | 0 | | 0.4902 | 0.5027 |
| Eukaryotic Translation Elongation | 92 | 3746 | 76 | 0 | 0 | 0 | 0 | | 0.4943 | 0.4933 |

Pathways in the Reactome network tested for structural relationships between **SLIPT** and **siRNA** genes by resampling. The raw p-value (computed without adjusting for multiple comparisons over pathways) is given for the difference in upstream and downstream paths from **SLIPT** to **siRNA** gene candidate partners of **CDH1** with significant pathways highlighted in bold. Sampling was performed only in the target pathway and **shortest paths** were computed within it. Loops or paths in either direction that could not be resolved were excluded from the analysis. The gene detected by both **SLIPT** and **siRNA** (or resampling for them) were included in the analysis and the number of these were fixed to the number observed.

There does not appear to be a consensus on the directionality of **SLIPT** and **siRNA** candidates across pathways as distinct pathways showed stronger tendency for **siRNA** genes to be either upstream or downstream. Even related pathways such as **PI3K** and **PI3K/AKT** signalling showed directional events in opposite directions. The strongest pathway (among those tested) with support for directional pathways structure is **G_{αi} signalling** which showed significant downstream **siRNA** genes for both **SLIPT** and **mt-SLIPT** from a large number of **shortest paths** (in Table 5.5 and Appendix Table I.2). This would indicate that **SLIPT** detects upstream regulators of genes experimentally validated by **siRNA**. However, these results are borderline significant (with raw permutation p-values) and are unlikely to be detected after adjusting for multiple comparisons across the 10 pathways presented here (nor in the 1652 Reactome pathways used previously in Chapter 4).

Therefore, there is insufficient evidence to determine whether there is **pathway** structure, gene detected upstream or downstream by either method, between the **SLIPT** and

siRNA candidates in many of the synthetic lethal pathways (identified in Chapter 4). In particular, directional structure among synthetic lethal candidates for *CDH1* was not strongly supported in signalling pathways upon which the rationale for pathway structure hypotheses were based on. Despite the design of a robust resampling approach to test relationships between gene groups, this did not detect many structural relationships between SLIPT and siRNA gene candidates, although it may apply more broadly to gene networks. Furthermore, the pathway relationships are unlikely to be statistically supported by resampling when testing across the search space of Reactome pathways and adjusting for multiple comparisons. While there is statistically significant over-representation of many of these pathways in genes detected by both SLIPT and siRNA (as described in Chapter 4), these did not consistently show pathway structure. Furthermore, pathway structure did not account for the discrepancy between SLIPT and siRNA gene candidates which did not significantly intersect such as the PI3K cascade.

5.4 Discussion

These investigations used a functional pathway network that encapsulates protein complexes and functional modules. The Reactome network (Croft *et al.*, 2014) uses curated, experimentally identified pathways to determine relationships between genes and does not have the limitation of relying solely on protein binding or text-mining which are prone to false positives. While it is not documented whether these relationships are activating or inhibitory, the Reactome network (Croft *et al.*, 2014) is sufficient to test pathway relationships with directional information.

Synthetic lethal genes and pathways (for *CDH1* loss in cancer) were identified across gene expression and mutation datasets in Chapter 4. These pathway structure investigations extend those investigations into synthetic lethal gene candidates including exploring the discrepancy between SLIPT and siRNA candidate genes in a pathway such as PI3K in which they did not significantly intersect. Pathways with replicated synthetic lethal genes across these detection methods, breast and stomach cancer data, and patient and cell line data were also investigated including pathways from the extra-cellular microenvironment to core translational pathways and the signalling pathways between them.

Synthetic lethal gene candidates in the context of pathway structures can also be interpreted to provide additional mechanisms and support for belonging to a synthetic lethal pathway. Gene candidates with known mechanisms are ideal for triage of targets

specific to *CDH1* deficient tumours and for further experimental validation in preclinical models. This chapter presents computational methods to use pathway structure in an attempt to detect genes with importance in a pathway and reconcile the differences between SLIPT and siRNA candidate genes with pathway relationships (e.g., one group being downstream of the other).

Many genes were detected by either method and the differences between the computational and experimental screening approaches could feasibly lead to differences in which genes within a synthetic lethal pathway are identified. Genes detected by synthetic lethal detection strategies included those of biological importance within synthetic lethal pathways, those which are actionable drug targets, and those with functional implications for the biological growth mechanisms or vulnerabilities of *CDH1* deficient tumours. It appeared that genes detected by both approaches were highly connected (or of importance) in the network structure or some pathways and that there may be some structure with SLIPT and siRNA upstream or downstream of each other. However, the complexity of biological pathways meant that relationships between gene candidates were difficult to discern without formal mathematical and computational approaches and thus these were used to analyse large biological networks.

Network analysis techniques were therefore applied to formalise and quantify the connectivity and importance (centrality) of genes within pathways (using PI3K as an example). However, these network techniques were unable to identify distinct differences in the network properties of genes detected as synthetic lethal candidates by computational or experimental methods. These network metrics support the application of synthetic detection across pathways (and the findings using pathways as gene sets in Chapter 4) as neither synthetic lethal detection approach was biased towards genes of higher importance or connectivity and neither approach was insensitive to genes of lower importance or connectivity. SLIPT is therefore not biased towards genes with more crucial role in the pathway as inferred by pathway connectivity and centrality measures and detects genes irrespective of pathway structure.

Similarly, a network hierarchy based on biological context (ordered from receiving extracellular stimuli to affecting downstream gene expression and cell growth) was devised to test whether PI3K genes of a particular upstream or downstream level were more frequently detected as synthetic lethal candidates. However, this approach was unable to ascertain whether genes detected by either method were further upstream or downstream in the pathway and there was no statistical evidence that either method differed in which levels of this structure were detected.

A measure of *pathway* structure between individual **SLIPT** and **siRNA** genes within a pathway was also devised using the direction of *shortest paths* in a directed *graph* structure. This is amenable to detecting the consensus directionality of the pathway across pairs of genes detected by either method. The *pathway* structure methodology developed here is generally applicable to comparison of *node* groups (allowing overlapping) including genes in biological pathways and their detection by different methodologies. While the *pathway* structure measure alone is not able to detect structural relationships between gene groups (e.g., **SLIPT** and **siRNA** gene candidates), it is amenable to resampling to determine whether these relationships are statistically significant.

5.5 Summary

Together these analyses of biological pathways, network metrics, and statistical procedures devised specifically for this purpose were applied to Reactome *pathway* structures to test whether structural relationships exist between *synthetic lethal* candidates. Of particular interest was whether these relationships relate to the differences between the computational (**SLIPT**) and experimental (**siRNA**) *synthetic lethal* candidate partners of *CDH1* (in the pathways discussed in Chapter 4).

While biologically relevant relationships were observed in specific pathways, there were few detectable structural relationships between **SLIPT** and **siRNA** gene candidates. These candidates did not exhibit significant differences in network connectivity or *centrality* measures. Network analyses were also unable to ascertain whether the candidates detected by either method stratified into upstream and downstream genes on the pathway and they likely do not.

A statistical resampling procedure was applied to *shortest path* analysis to test whether pairs of **SLIPT** and **siRNA** gene candidates were more likely to be upstream or downstream of each other. This approach detected very few structural relationships in the *synthetic lethal* pathways identified in Chapter 4. Overall, support for *pathway* structure between **SLIPT** and **siRNA** gene candidates is weak and the direction is inconsistent between pathways. Therefore *pathway* structure does not account for the differences between the **SLIPT** and **siRNA** gene candidates, although this does support the validity of gene set analyses in Chapter 4 and the *synthetic lethal* pathways identified.

Furthermore, the resampling procedure demonstrated in this chapter is more widely applicable to gene states in *network* structures and may be of further utility in the anal-

ysis of biological pathways or networks. This approach was able to quantify structural relationships that were otherwise difficult to interpret and to conclusively exclude many potential relationships. In this respect, the network resampling methodology may also be applicable to triage of experimental validation.

Chapter 6

Simulation and Modeling of Synthetic Lethal Pathways

Simulation and modelling of synthetic lethality in gene expression was revisited in greater detail in this chapter, building upon the results which supported the use of **SLIPT** (in Section 3.3). In Chapter 3, a simulation procedure for generating simulated data with underlying (known) synthetic lethal partners of a query gene, such as *CDH1*, was developed (as described in Section 3.2.2) by sampling from a Multivariate normal distribution based on a statistical model of synthetic lethality in expression data (as described in Section 3.2.1). This simulation framework was applied to simulated data (in Section 3.3), including simple correlation structures to assess the statistical performance of the **SLIPT** methodology and support its use as a computational approach for detecting synthetic lethal candidates from expression data throughout this thesis (Chapters 4 and 5).

While this basic framework was provided some support for the use of **SLIPT**, further investigations with simulations were conducted to assess the strengths and limitations of the **SLIPT** methodology, compare it to alternative statistical approaches to synthetic lethal detection, and assess its performance under more complex correlation structures. Together these simulation investigations assess the performance of the **SLIPT** methodology, including on pathway graph structures (e.g., those discussed in Chapter 5) and indicate whether the **SLIPT** methodology (or similar refined bioinformatics strategies) are statistically rigorous or suitable for wider genomics applications.

These simulation investigations continue to utilise the Multivariate Normal simulation procedure (as applied in Section 3.3) with further refinements. The **SLIPT** methodology (and the χ^2 test) were applied across a range of parameters (including

altering the quantiles for detecting **synthetic lethal** direction and compared to correlation). This was also applied to query correlated genes (as performed in Section 3.3).

A refined simulation procedure was developed specifically to extend the methodology described in Section 3.2 to utilise pathway **graph** structures for the correlation structures of simulated datasets (as described in Section 3.4.2). This methodology can be applied to simulated correlation structures across simple **graph** structures to test specific network modules or use **pathway** structures based on biological pathways. Thus **graph** structure and simulation approaches were combined to test whether a gene locus in a pathway affects detection by **SLIPT** and whether **SLIPT** performance is affected by **pathway** structure. The simulation procedure based on **graph** structures was applied in a computational pipeline across many parameter combinations using high-performance computing resources (as discussed in Section 2.5.3) and the core simulation functions have been released as a software package for wider use to test **bioinformatics** and statistical methods on **graph** structures (as described in Section 3.5.3).

6.1 Synthetic Lethal Detection Methods

The **SLIPT** methodology (as it has been applied throughout Chapters 4 and 5) was compared for alternative computational approaches to detecting **synthetic lethality** in simulated **gene expression** data. As discussed in Section 3.3, this procedure enabled testing ability of **SLIPT** to detect known **synthetic lethal** partner genes by sampling from a statistical model of **synthetic lethality**. While comprehensive benchmarking has not been performed, several approaches to **synthetic lethal** detection are considered (e.g., Pearson correlation, the χ^2 test, and testing for bimodality) to evaluate the strengths of the **SLIPT** methodology, including modifications to the parameters of **SLIPT**.

The following comparisons of simulations of computational detection of **synthetic lethality** with different statistical rationales suffice to discuss the strengths of **SLIPT**, evaluate whether it is appropriate for further application in **genomics** research, and identify limitations which may be addressed with further developments. Some potential avenues for further development of computational **synthetic lethal** discovery will be discussed in Section 7.3.

6.1.1 Performance of SLIPT and χ^2 across Quantiles

Simulated datasets with **synthetic lethal** partner genes were generated using the multi-variate normal simulation procedure (as described in Section 3.2.2) with performance

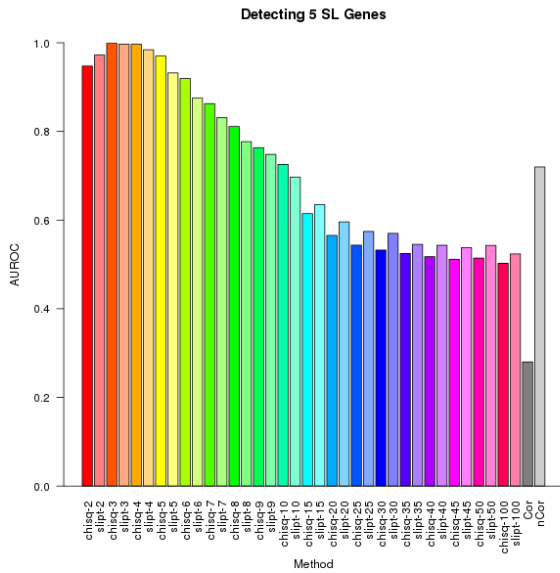
assessed using AUROC analysis (as described in Section 2.3.5). Synthetic lethal detection was compared for modifications to the SLIPT methodology (as described in Section 3.1), namely that the quantiles used to define low and high expression was varied. Rather than $1/3$ (as used throughout this thesis) the samples below the lowest $1/n$ quantile and above the highest $1/n$ quantile were used for SLIPT (and the χ^2 -test) to detect lowly and highly expressing samples respectively. The quantiles tested range from 2, splitting at the $1/2$ quantile (the median), to 100, using the lowest (1%) and highest (99%) percentiles.

This enabled testing of the threshold for lowly expressing genes which is most able to distinguish synthetic lethal genes, even with higher-order synthetic lethal interactions (as discussed in Section 3.2.1). Both SLIPT with the directional criteria for synthetic lethality and significance of the equivalent χ^2 test were performed for each quantile. Pearson correlation was also tested on simulated continuous expression data for synthetic lethal detection in simulated data, considering both positive and negative correlations separately as predictors of synthetic lethality for comparison with χ^2 based approaches, using discrete categories of gene function deriving from quantiles.

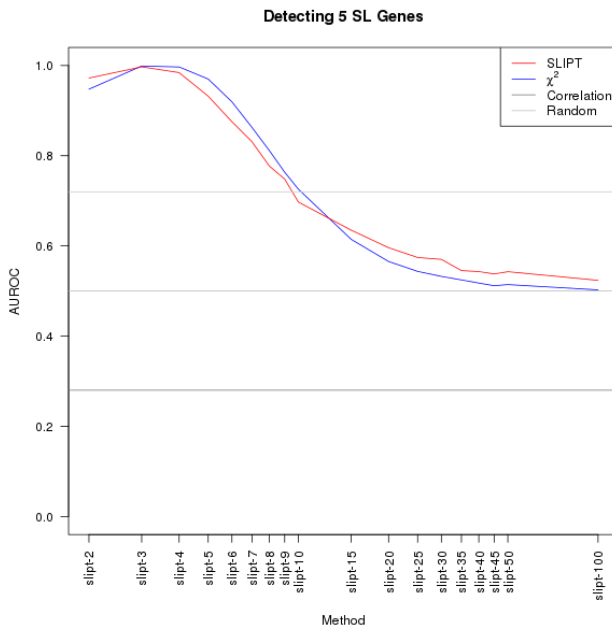
The results presented throughout this section use the example of 5 synthetic lethal partners to illustrate the differences in performance between the standard SLIPT procedure (slipt-3) to n quantiles (slipt- n), the χ^2 -test on the same quantiles, and positive or negative correlation. However, similar results across different numbers of known synthetic lethal genes are shown in Appendix J. The synthetic lethal detection procedures were compared with 10,000 simulations of a small dataset of 100 genes and 1000 samples without correlation structure between genes, as performed in Section 3.3.2). As shown in Figure 6.1, the 3-quantiles previously used have optimal performance and SLIPT has a comparable or higher performance than the χ^2 -test alone across quantiles.

Pearson correlation was also tested as a predictor of synthetic lethality (i.e., whether highly positive or negative correlations with the query gene detected synthetic lethal partners). Positive correlation performed worse than random (with an AUROC lower than 0.5) as thus coexpression of genes is not predictive of synthetic lethality in simulated data. Conversely, negative correlation is predictive of synthetic lethality, consistent with synthetic lethal gene activity being mutually exclusive. However, neither correlation approach performed as well as the optimal quantiles for the SLIPT procedure or χ^2 -test.

These results are shown in both a bar graph and lineplot to show the individual results of each parameter, and to compare SLIPT with the χ^2 -test side-by-side across



(a) Barplot of χ^2 , SLIPT, and correlation.



(b) Lineplot of χ^2 , SLIPT, and correlation.

Figure 6.1: **Performance of χ^2 and SLIPT across quantiles.** Synthetic lethal detection (of 5 genes) with quantiles as on the axes. The barplot uses the same hues for each quantile (grey for correlation) and darker for χ^2 (and positive correlation). The line plot (with log-scale quantiles) is coloured according to the legend. SLIPT and χ^2 perform similarly, peaking at $1/3$ -quantiles and converging to random (0.5). Negative correlation was higher than positive but not optimal quantiles for SLIPT or χ^2 .

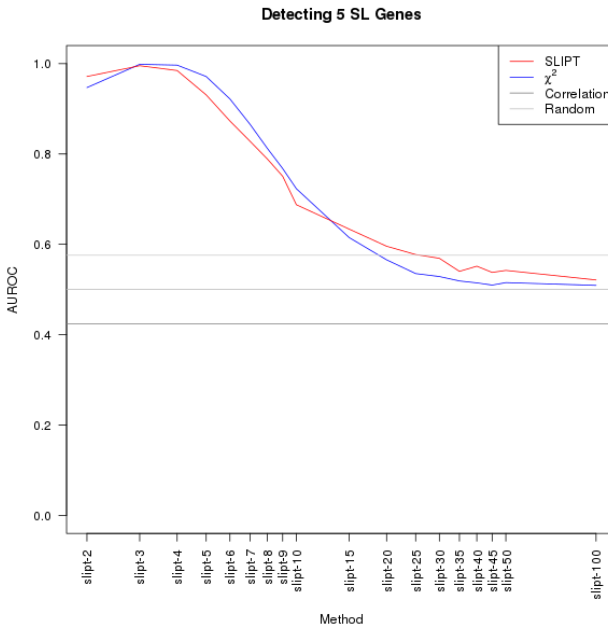


Figure 6.2: **Performance of χ^2 and SLIPT across quantiles with more genes.** Synthetic lethal detection (of 5 genes in 20,000) with quantiles as in axis labels. The line plot (with log-scale quantiles) is coloured according to the legend. As for simulations with fewer genes, SLIPT and χ^2 perform similarly, peaking at $1/3$ -quantiles and converging to random (0.5). Negative correlation was higher than positive but not optimal quantiles for SLIPT or χ^2 .

quantiles. Similarly, these plots are given for detecting a range of known synthetic lethal partners in the simulations in Figures J.1 and J.2. These demonstrate that the findings shown for 5 synthetic lethal genes are robust across different numbers of underlying synthetic lethal genes.

The synthetic lethal detection procedures were also tested with 1000 simulations of a larger dataset of 20,000 genes and 1000 samples. While fewer simulations gives a less accurate ROC result, this is sufficient to replicate the above findings with a feasible number of genes in a human gene expression dataset and assess the impact of a higher proportion of non synthetic lethal genes (potential false positives). Simulated datasets of this size were also used in Section 3.3.2 to test the specificity in a number of genes similar to that in experimental datasets for cancer genomes. As shown in Figure 6.2, the above findings were replicated in simulations of a larger dataset with 20,000 genes. These were also robustly replicated across varying numbers of underlying synthetic lethal genes (as shown in Figure J.3).

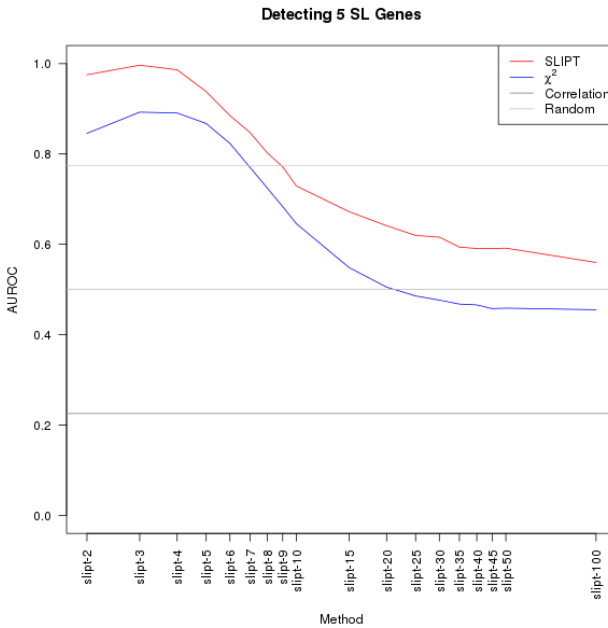


Figure 6.3: **Performance of χ^2 and SLIPT across quantiles with query correlation.** Synthetic lethal detection (of 5 genes in 100 including 5 query correlated) with quantiles as in axis labels. The line plot (with log-scale quantiles) is coloured according to the legend. SLIPT performs consistently higher than χ^2 due to higher specificity. Negative correlation performed modestly.

6.1.1.1 Correlated Query Genes affects Specificity

As discussed in Section 3.3.2.2, positively correlated genes (with the query gene) have an impact of on the performance of synthetic lethal detection. SLIPT was able to distinguish these from synthetic lethal partners and hence is likely to have a higher specificity in datasets which include positively correlated genes with the query gene (as expected in gene expression data). The synthetic lethal detection procedures were compared with 10,000 simulations of a small dataset of 100 genes (with 5 correlated with the query gene) and 1000 samples otherwise without correlation structure between genes. As shown in Figure 6.3, this specificity is reflected in the increased AUROC performance values for SLIPT (in contrast to Figure 6.1). This specificity can be attributed to the directional criteria (as described in Section 3.1) since the χ^2 -test alone performs comparatively poorly with positively correlated genes.

The synthetic lethal detection procedures were also compared with 1000 simulations of a larger dataset of 20,000 genes (with 1000 correlated with the query gene) and 1000 samples otherwise without correlation structure between genes. This simulation

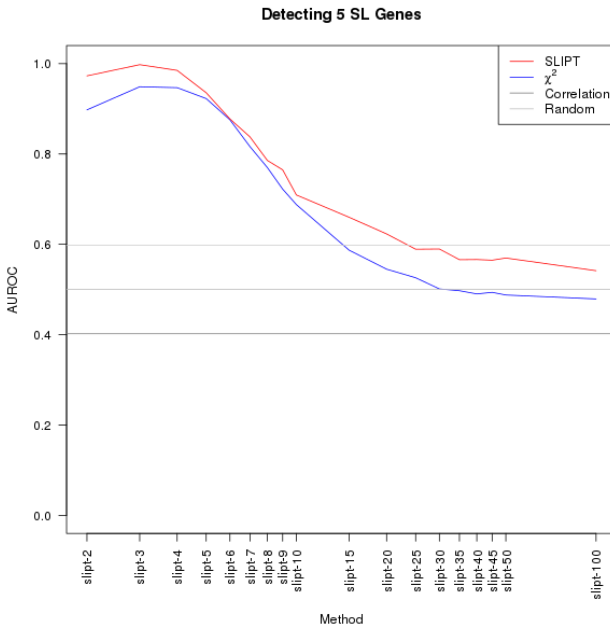


Figure 6.4: Performance of χ^2 and SLIPT across quantiles with query correlation and more genes. Synthetic lethal detection (of 5 genes in 20,000 including 1000 query correlated) with quantiles as in axis labels. The line plot (with log-scale quantiles) is coloured according to the legend. SLIPT performs consistently higher than χ^2 due to higher specificity. Negative correlation performed modestly.

increases the number of genes (and proportion of negative genes) to those comparable with a human gene expression dataset while maintaining a comparable 5% of positively correlated genes. As shown in Figure 6.4, SLIPT still outperforms χ^2 or negative correlation and is optimal at the 3-quantile. The difference between SLIPT and χ^2 was less pronounced in a larger dataset with many weakly correlated genes. The greater specificity of SLIPT than χ^2 -test to distinguish positively correlated non synthetic lethal genes is not as evident with a large number of negative genes (as potential false positives). However, specificity is an important consideration in large-scale genomics analysis where there are potentially many false positives.

Nevertheless, SLIPT with 3-quantiles (as performed throughout Chapters 4 and 5), had higher performance than when other quantile thresholds were used, particularly when positive correlations were present (replicating the Section 3.3.2.2). These findings hold across different numbers of underlying synthetic lethal genes (as shown in Figures J.5 and J.6).

Together these results support the use of **SLIPT**, particularly the use of quantiles as thresholds for gene function and specific use of 3-quantiles which perform well compared to other quantiles. A particular concern in the design of **SLIPT** for **expression** data whether the samples sizes are sufficient when the data is divided into quantiles. The **SLIPT** methodology further performed better for 3-quantiles (and other moderate values) than χ^2 or correlation as a predictor of **synthetic lethality**. These results are irrespective of sample size or p-value threshold since the results replicated across sample sizes and the **AUROC** values were independent significance thresholds. Using a moderate number of quantiles for **SLIPT** ensures that there are a sufficient number of samples expected below and above them so that deviations from these are statistically detectable. These quantiles were also optimal for the χ^2 test which uses the same expected values as the **SLIPT** directional conditions.

6.1.2 Alternative Synthetic Lethal Detection Strategies

The **SLIPT** approach (and χ^2) to detect **synthetic lethality** from binning **expression** to estimate gene function also outperforms correlations which use continuous data directly. Correlation performing poorly as a **synthetic lethal** detection strategy consistent with there not necessarily being a relationship between **synthetic lethal** partners which can be in distinct biological pathways, expressed at different times or in different cell types. Nevertheless, correlation is among the alternative detection methods considered in further detail.

The BiSEp R package (Wappett, 2014) for using bimodality to detect **synthetic lethality** (Wappett *et al.*, 2016) were also considered, along with a linear regression approach. These statistical methods span a range of computational approaches to detecting **synthetic lethality** and serve to compare alternatives to **SLIPT**, supporting its design and application. However, these comparisons are able provide supporting data from statistical modelling and simulations for the viability of the **SLIPT** methodology for **synthetic lethal** discovery in cancer (as demonstrated in Chapter 4) and further applications.

6.1.2.1 Correlation for Synthetic Lethal Detection

As shown in Section 6.1.1, negative (Pearson) correlation performed better than positive correlation, indicating the inverse relationships were more predictive of **synthetic lethality**. However, neither correlation approach performed as well as **SLIPT** or the χ^2 test as a predictor of **synthetic lethal** gene partners. It is notable that negative correlation still often performed considerably better than random chance.

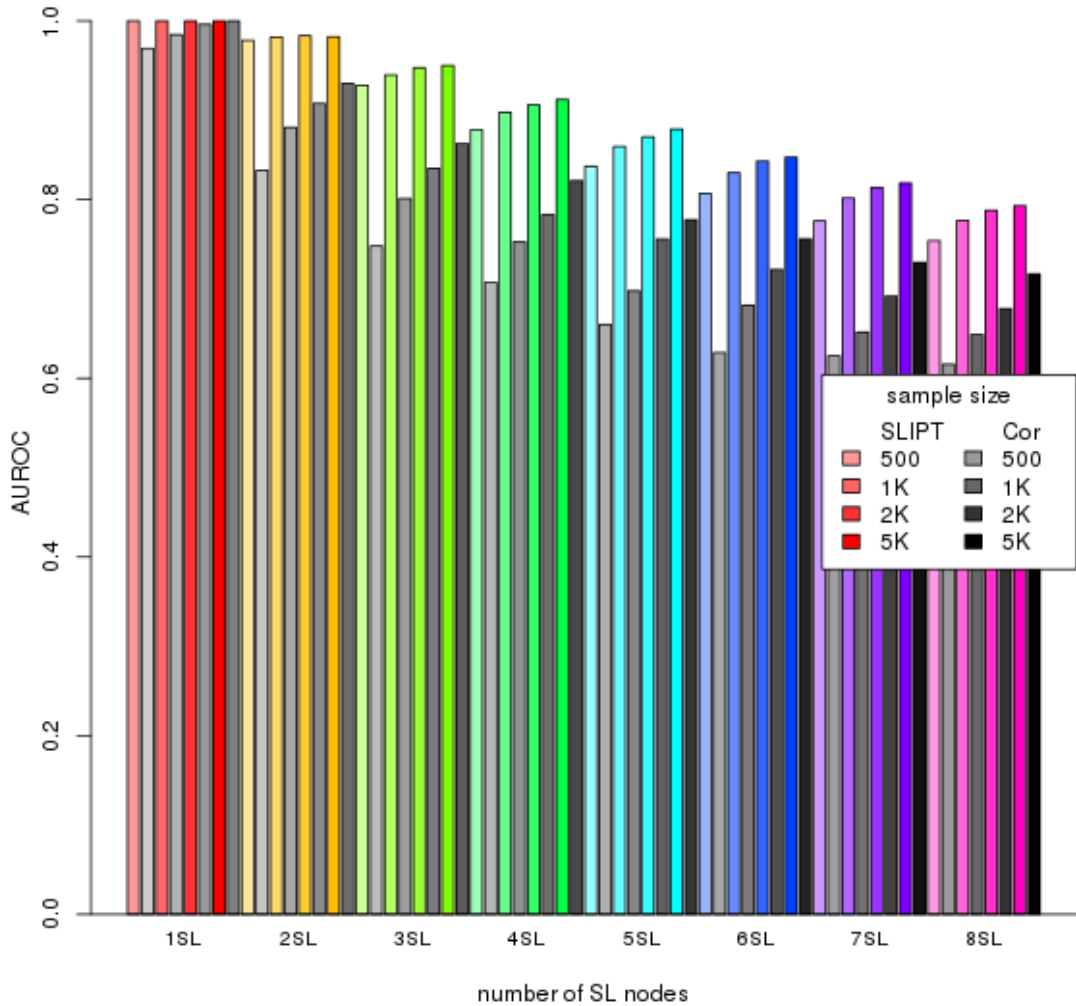


Figure 6.5: **Performance of negative correlation and SLIPT.** Synthetic lethal detection with SLIPT was compared to negative (Pearson) correlation across parameters. SLIPT consistently outperformed correlation. Both approaches had lower performance for more synthetic lethal partners and lower sample sizes. 10,000 simulations were performed with correlation structure as used in Section 6.2.1.2

Negative correlation was compared directly to the SLIPT methodology (as described in Section 3.1) across numbers of known synthetic lethal partners and sample size (ranging from 500 to 5000). This comparison used 1000 simulations of a dataset with 20,000 genes and synthetic lethal genes from within a network (sampled as in Section 3.4.2)) with a 0.8 correlation between adjacent genes. In a direct comparison of

`SLIPT` and negative correlation (shown in Figure 6.5), `SLIPT` consistently has higher performance in simulated data across parameter values and (inverse) correlation-based approaches perform modestly in comparison. Thus using thresholds to categorise `expression` data (as performed by `SLIPT` and χ^2) does not compromise the performance of these methods by losing continuous data that would be used for calculating correlations. Similarly, the slope of a linear regression did not perform as well at `synthetic lethal` detection than `SLIPT`.

Both `SLIPT` and correlation had poorer performance with increasing numbers of the `synthetic lethal` genes to detect, while they had higher performance in higher sample sizes, as expected (as previously observed for `SLIPT` in Section 3.3). Thus the issue with detection of greater numbers of `synthetic lethal` genes is not specific to `SLIPT` but occurs across computational methods of `synthetic lethal` discovery in (simulated) `expression` data and likely stems from cryptic higher-order `synthetic lethal` interactions (as conservatively assumed in Section 3.2.1).

6.1.2.2 Testing for Bimodality with BiSEp

Extensive attempts were also made to compare `SLIPT` to the `BiSEp` methodology (Wappett *et al.*, 2016), a statistical approach to identify `synthetic lethal` gene pairs from mutually exclusive relationships using bimodal distributions. This `synthetic lethal` detection methodology is also designed for `expression` analysis in cancer and is readily available as an (open-source) R package (Wappett, 2014), a practice which facilitates adoption and testing of the methodology on the same datasets and simulations procedures as previously used for `SLIPT`.

The `BiSEp` package is designed for global testing of all potential gene pairs in the genomes for `synthetic lethality` rather than focusing on the search space of potential partners of the query gene. This approach was unable to detect `synthetic lethal` gene pairs in the `TCGA` breast cancer `expression` dataset (TCGA, 2012). However, this may be due to stringent thresholds under the multiple testing of millions of potential gene pairs.

For a direct comparison with the query-based `SLIPT` approach, the source code of the `BiSEp` R functions was modified to test solely for the partners of a specific gene. This approach was still unable to detect `synthetic lethal` partners of *CDH1* in `TCGA` breast cancer `expression` data (TCGA, 2012), even with the detection thresholds for bimodality and significance greatly relaxed from those which the package defaults to.

To circumvent multiple testing issues, `BiSEp` only tests gene pairs for `synthetic lethality` between genes with a detectable bimodal distribution. However, even with

relaxed thresholds, bimodal distributions were not detectable in the normalised TCGA data (TCGA, 2012). Such normalisation Ritchie *et al.* (2015) is standard practice for expression datasets generated from microarrays or RNA-Seq and therefore BiSEp may not be appropriate to apply to this data. However, it is noted that BiSEp may also use other data types such as DNA copy number or cell line data for which it may be more applicable (Wappett *et al.*, 2016).

Nevertheless, attempts were made to test BiSEp on simulated datasets with underlying synthetic lethal genes (using the procedures described in Sections 3.2.2 and 3.4.2). However, BiSEp was also unable to detect genes with bimodal distributions of genes (and thus unable to detect synthetic lethality) in a limited number of computationally intensive simulations. Therefore investigations on a wider range of parameters were not performed.

6.2 Simulations with Graph Structures

The simulations of synthetic lethality performed in Section 3.3 included correlated blocks of genes as a rudimentary representation of pathway structure and co-regulated genes. The simulation procedure has been enhanced to account for more complex pathway structures by sampling from multivariate normal distributions with correlation structure derived from graph structures (as described in Section 3.4.2). This approach enabled the simulation of synthetic lethal pathways with known correlation structure and synthetic lethal partners (of a gene not in the pathway). Using this procedure, the performance of SLIPT was evaluated under simple controlled correlation structures and complex correlations, such as those derived from biological networks (e.g., those described in Chapter 5). The SLIPT methodology was tested in artificial constructed networks to evaluate the effect of pathway structure on synthetic lethal detection. These included large biologically feasible pathways to ensure that the SLIPT methodology is robust under complex correlation structures and applicable to such complex genomics data.

These simulations combine the approach of prior simulation analyses (in Sections 3.3 and 6.1) with the graph structures for biological pathways (as used in Chapter 5). This enabled testing whether subtle or large differences in pathway structure affect synthetic lethal detection, whether inhibiting relationships (or inverse correlations) between genes affect synthetic lethal detection, and whether synthetic lethal detection varies by which gene is synthetic lethal and which genes are closely linked within the pathway structure. In addition, large numbers of synthetic lethal genes and biologically

feasible numbers of genes (with many non-synthetic lethal genes) was tested to replicate the findings of Sections 3.3 and 6.1 in correlated structures derived from pathway graphs, including examples of biological pathways from Reactome (Croft *et al.*, 2014).

Simple and more complex constructed **graph** structures were used to demonstrate the impact of **pathway** structure of the performance of **SLIPT** for **synthetic** lethal detection in simulations. In addition, more complex constructed **graph** structures were compared to the **PI3K** and $G_{\alpha i}$ signalling pathways derived from Reactome which were used for simulation of **pathway** structures of biological complexity (as shown in Figures 5.1 and F.4).

6.2.1 Performance over Graph Structures

6.2.1.1 Simple Graph Structures

Simple pathway modules were used to test the effect of **pathway** structure on the performance of detecting **synthetic** lethal partners within **graph** structures. For an initial comparison, the **graph** structures (shown by Figure 6.6) were used where a gene has one upstream regulator and two downstream (Figure 6.6b) or a gene has two upstream regulators and one downstream gene (Figure 6.6b). **SLIPT** has a high performance in these simulations, detecting randomly selected **synthetic** lethal partners in both of these small simple networks (in Figures 6.7 and K.1).

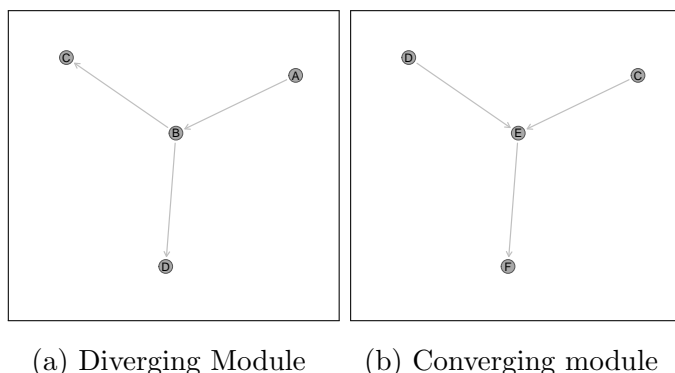


Figure 6.6: **Simple graph structures.** A simple **graph** structures used to demonstrate the simulation procedure. These are examples of a pathway diverging or converging respectively which enabled testing the importance of direction in **pathway** structures. These are used with both activating and inhibiting relationships as shown.

As previously observed (in Section 3.3), performance declined with higher numbers of **synthetic** lethal genes and lower sample sizes. However, the sensitivity of **SLIPT** is

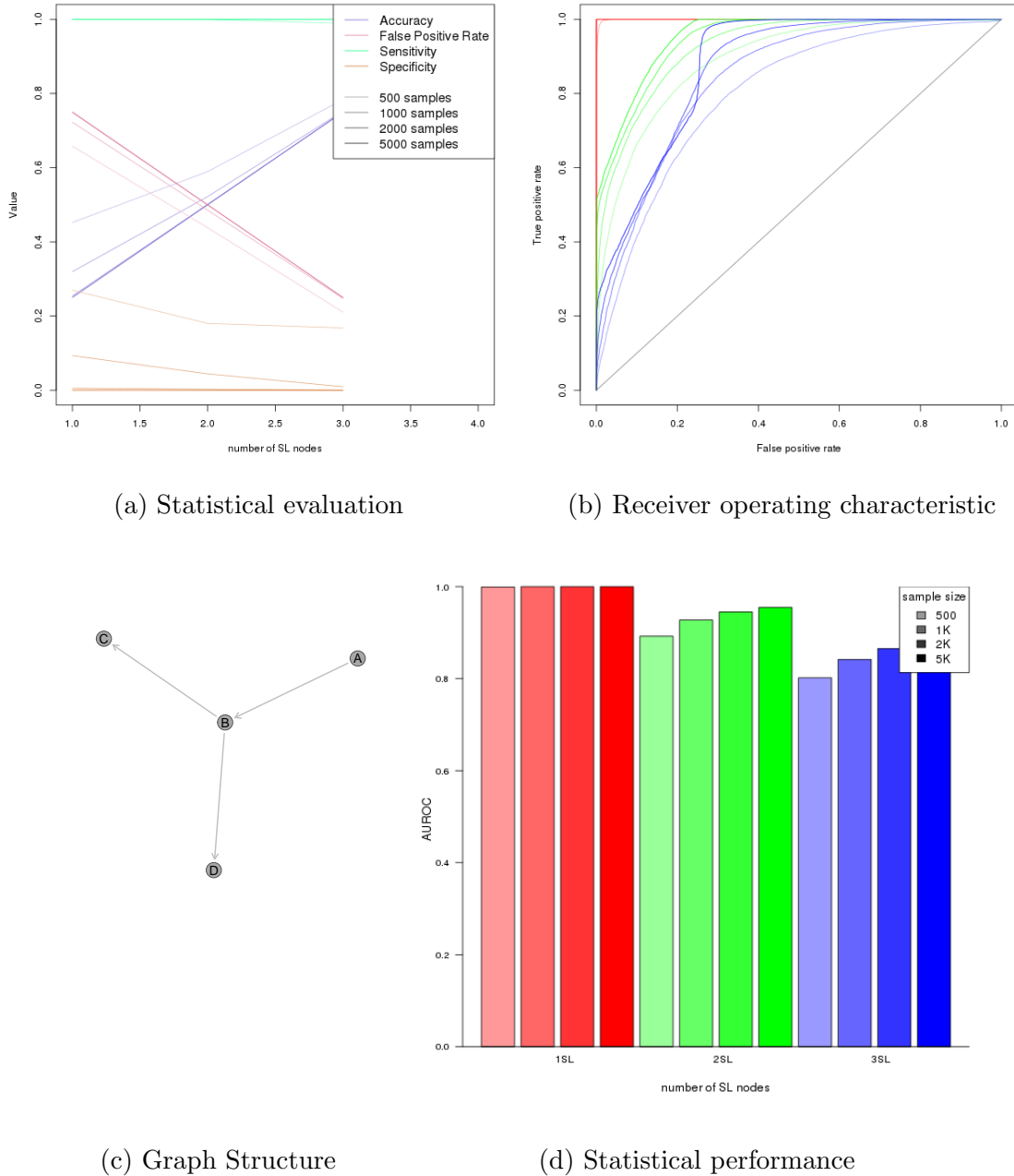


Figure 6.7: **Performance of simulations on a simple graph.** Simulation of synthetic lethality was performed sampling from a multivariate normal distribution generated from a diverging graph structure. Performance of SLIPT declines for more synthetic partners but this is mitigated by increased sample sizes (in darker colours). This manifests as a decline in specificity and the false positive rate. For each parameter value, 10,000 simulations were used. Colours of the ROC curves in Figure 6.7b correspond to the parameters in Figure 6.7d.

high with conventional p-value thresholds (adjusted by **FDR**). **Synthetic lethal** partners are often distinguishable for non synthetic lethal genes, even in simple highly correlated networks. The small number of genes and their high correlation has an impact on the **ROC** curves for higher numbers of **synthetic lethal** partners which are skewed compared to those observed previously. Specificity cannot be tested if all potential partner genes are **synthetic lethal** which limits the number of **synthetic lethal** genes that can be tested.

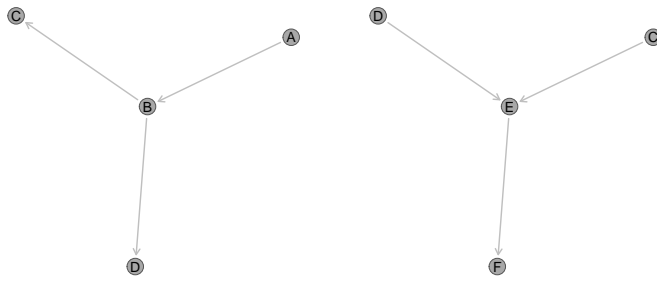
These results were consistent between the pathway modules of diverging (in Figure 6.8a) and converging signals (in Figure 6.8b). The **AUROC** performance and underlying curves were strikingly similar between these **graph** structures (as shown in Figures 6.7 and K.1). Thus the performance of **SLIPT** was not perturbed by **pathway** structure, specifically the direction of pathway relationships since these **graph** structures also demonstrate pathways in opposite direction. In a direct comparison (shown in Figure 6.8c), the performance of simulations did not differ across parameter values in these simple **graphs** and therefore **SLIPT** is robust to pathway direction.

6.2.1.2 Constructed Graph Structures

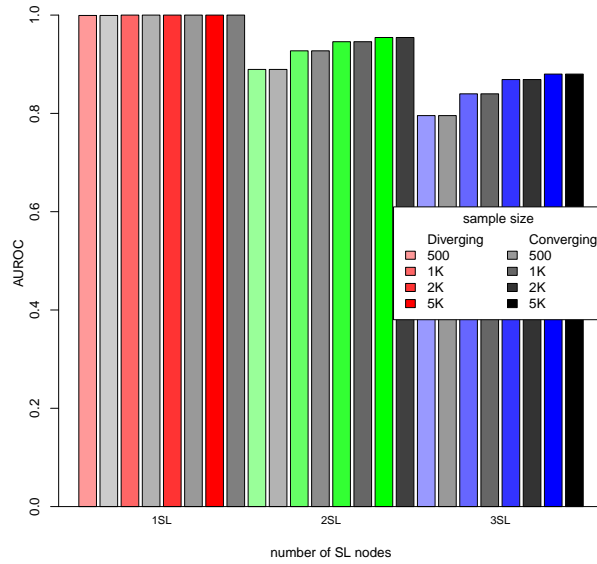
A more complex **graph** structure was used to examine the performance of detecting **synthetic lethal** partners with **SLIPT** in simulated **expression** data with pathway correlation structures. For a simple chain of gene representing a pathway (shown in Figure 6.9), the above findings were generally replicated. Performance was high across parameter values in small networks, with similar decreases in higher numbers of **synthetic lethal** genes to detect and lower sample size.

When detecting **synthetic lethal** genes with **SLIPT** using adjusted (**FDR**) p-value thresholds, the performance differences were primarily due to changes in specificity, as the small numbers of **synthetic lethal** genes still had highly significant p-values. Despite lower specificity and performance in **ROC** curves, the accuracy increases and false positive rate decreases desirably with higher numbers of **synthetic lethal** genes due to the high sensitivity and proportion of **synthetic lethal** genes detected. Therefore the thresholds imposed by adjusted p-values appear to be appropriate for detecting **synthetic lethal** partners, even in strongly correlated pathways, at least in these small-scale test cases.

An artifact of these small test cases led to the skewed **ROC** curves (as discussed in Section 6.2.1.1), which may be the result of the low number of non-synthetic lethal genes to identify as true negatives, affecting the accuracy of specificity. This issue does not occur in larger, more complex **graph** structures, even with modest total numbers of genes and high correlations (as shown in Section 6.3). This issue is unlikely to occur



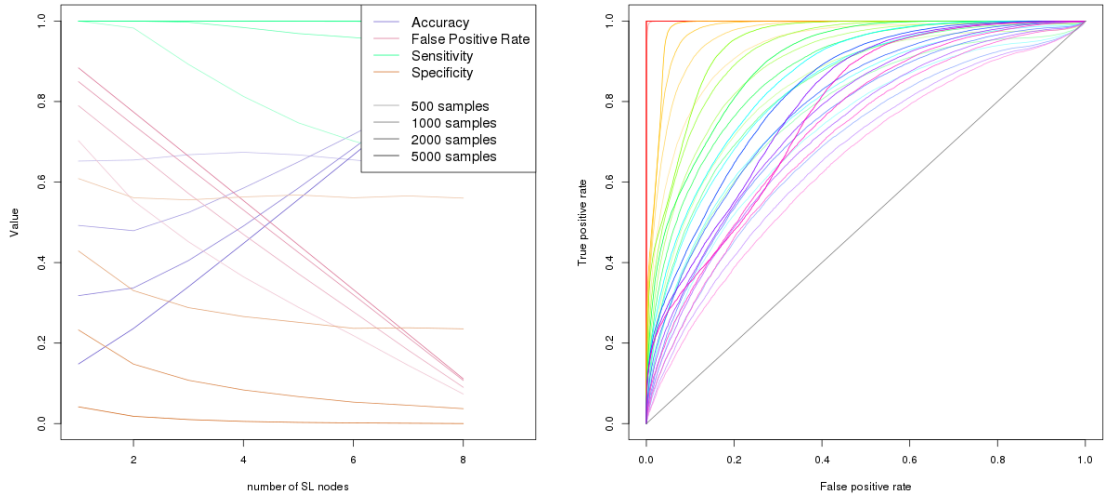
(a) Diverging Module (b) Converging module



(c) Performance between Graph Structures

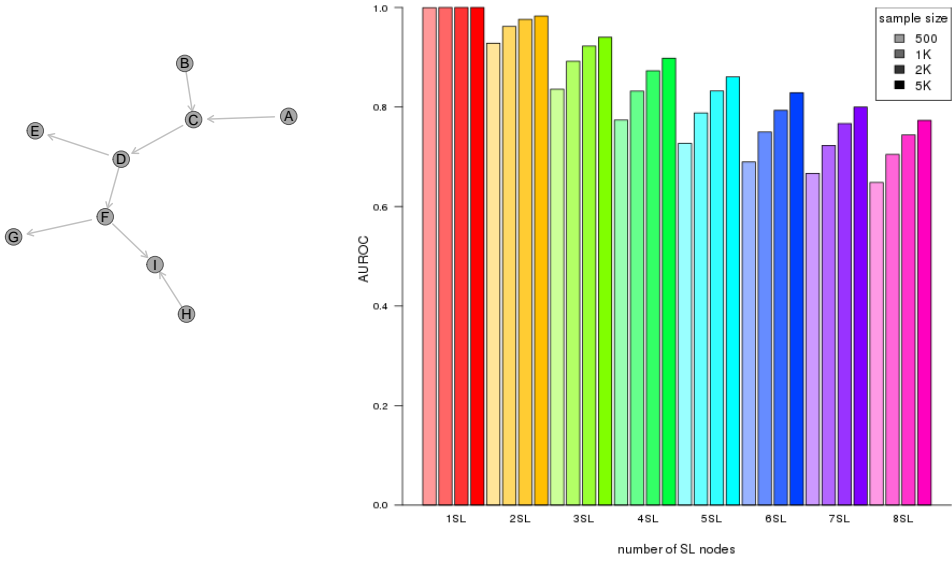
Figure 6.8: **Performance of simulations is similar in simple graphs.** The AUROC values for simulations of multivariate normal distributions based on each `graph` structure yielded indistinguishable performance across parameter values in 10,000 simulations.

in large `expression` datasets with many non synthetic lethal genes, as shown previously (in Section 3.3 and 6.2.1.1) with `graph` structures in larger datasets (in Section 6.2.4).



(a) Statistical evaluation

(b) Receiver operating characteristic



(c) Graph Structure

(d) Statistical performance

Figure 6.9: **Performance of simulations on a pathway.** Simulation of synthetic lethality was performed sampling from a multivariate normal distribution generated from a pathway structure. Performance of SLIPT declines for more synthetic partners and lower sample sizes (in darker colours). For each parameter value, 10,000 simulations were used. Colours of the ROC curves in Figure 6.9b correspond to the parameters in Figure 6.9d.

6.2.2 Performance with Inhibitions

Simulations of synthetic lethality in expression data were also performed with correlation structures derived from graphs containing inhibiting relationships (as are commonplace in biological pathways) which produce negative correlations. As shown in Figure 6.10, these are not an issue for detection by SLIPT. Rather, the SLIPT procedure performs well on simple graph modules with highly negative correlations. With synthetic lethal detection based on p-value (adjusted by FDR), there was higher specificity, higher accuracy, and lower false positive rate in an inhibitory graph than the same graph with activating relationships (as shown by Figure 6.7).

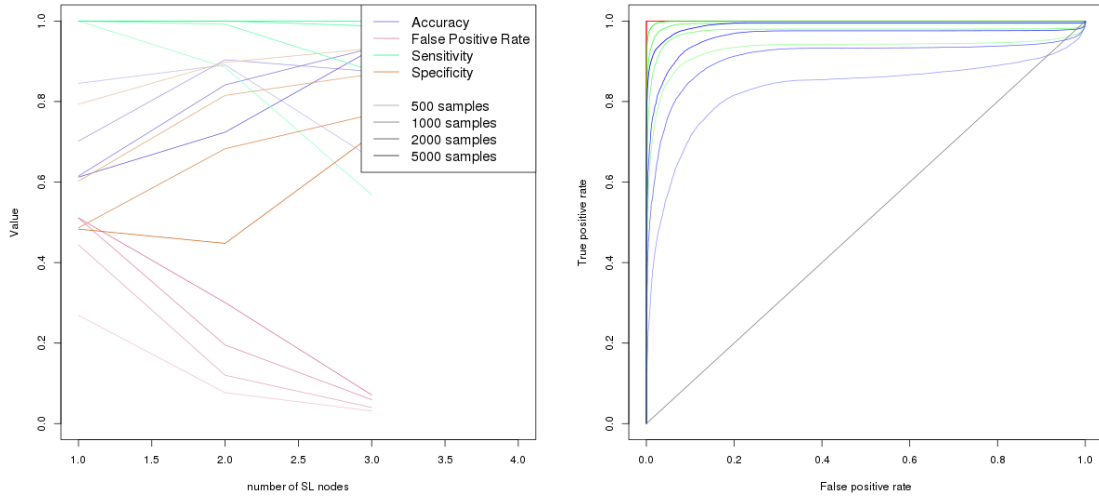
The ROC curves for an inhibiting graph also show consistently high specificity irrespective of detection threshold with only the upper extreme of the curve exhibiting a skew below random performance (in Figure 6.10). Nevertheless, the AUROC values show a high performance across parameter values, particularly avoiding issues with higher numbers of synthetic lethal partners (as observed in Section 6.2.1.1). However, performance was marginally lower for higher numbers of synthetic lethal genes to detect and lower sample sizes, consistent with previously observations.

Negatively correlated simulated datasets are also unperturbed by minor differences in graph structure, such as changing in the direction of the graph module. As observed for activating relationships in these graph modules, the performance was highly concordant between the graph modules (shown by similar results in Figures 6.10 and K.2).

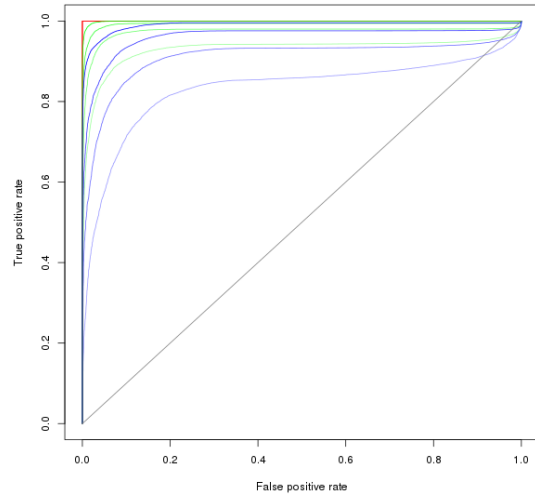
Detection of synthetic lethality by SLIPT in simulated data with inhibiting relationships outperforms simulations with activating relationships in the same graph structure (as shown in Figure 6.11). Thus SLIPT is robust in gene expression datasets with inverse correlations and performs well in them, at least in simple test cases. This is important because such relationships occur frequently in biological pathways and therefore the findings inferred from graph structures without inhibiting relationships are a conservative estimate.

The SLIPT methodology likely performs better in biological pathways (which contain negative correlations) than the graph structures discussed previously (in Section 6.2.1). This is likely since negative correlations lead to synthetic lethal partners and inversely correlated genes which are positively correlated with the query gene. As previously shown, the SLIPT methodology performs well with specificity against positively correlated query genes (in Sections 3.3.2.2 and 6.1.2.1).

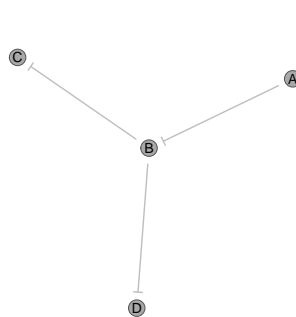
Similarly, more complex graph structures with entirely inhibiting relationships (negative correlations) also perform desirably on p-value thresholds (adjusted by FDR) and



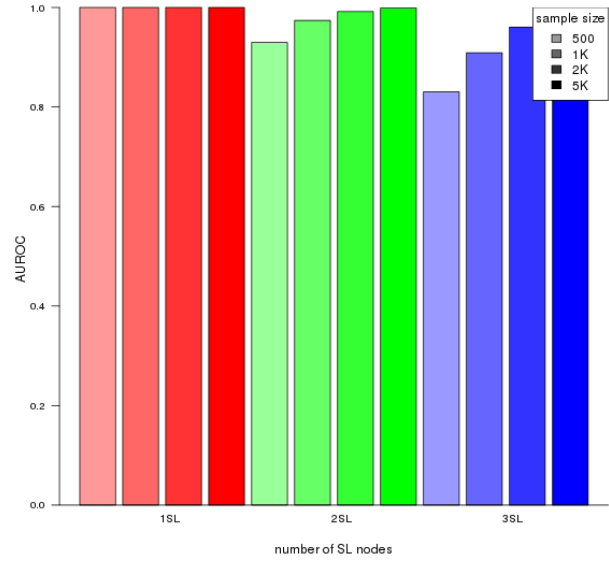
(a) Statistical evaluation



(b) Receiver operating characteristic

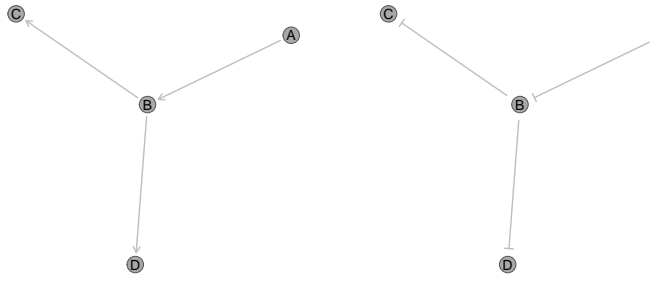


(c) Graph Structure



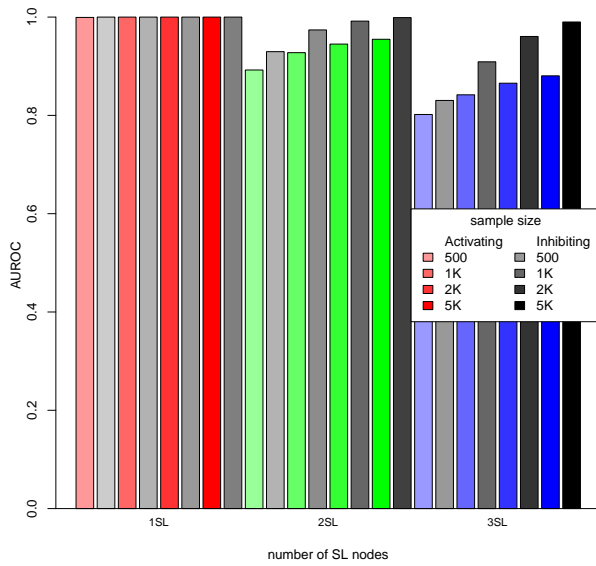
(d) Statistical performance

Figure 6.10: **Performance of simulations on a simple graph with inhibition.** Simulation of synthetic lethality was performed sampling from a multivariate normal distribution generated from an inhibiting graph. Performance of **SLIPT** declines for more synthetic partners and lower sample sizes. For each parameter value, 10,000 simulations were used. Colours of the **ROC** curves in Figure 6.10b correspond to the parameters in Figure 6.10d.



(a) Activating Graph

(b) Inhibiting Graph

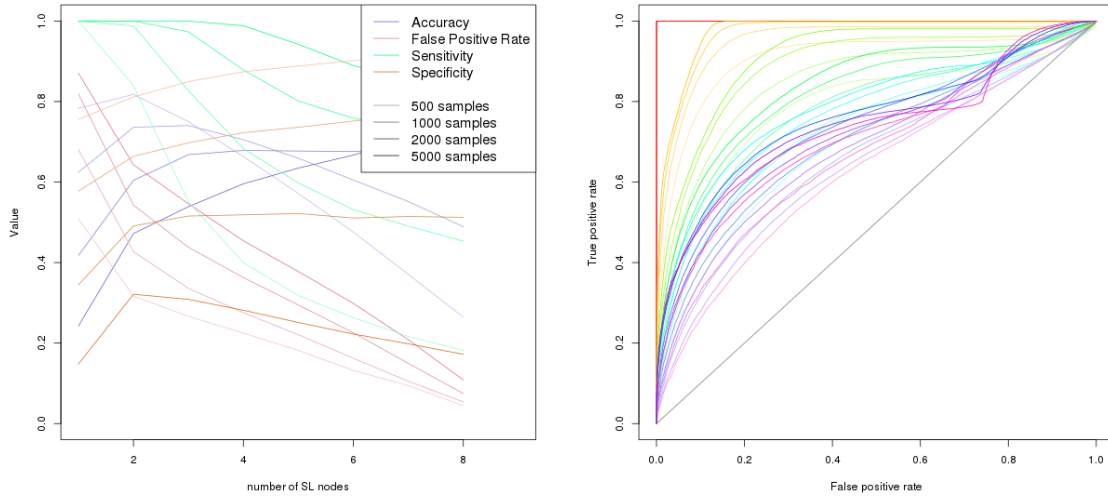


(c) Performance between Graph Structures

Figure 6.11: Performance is higher on a simple inhibiting graph. The AUROC values for simulations of multivariate normal distributions based on inhibitions in the Graph structure yielded consistently higher performance across parameter values in 10,000 simulations.

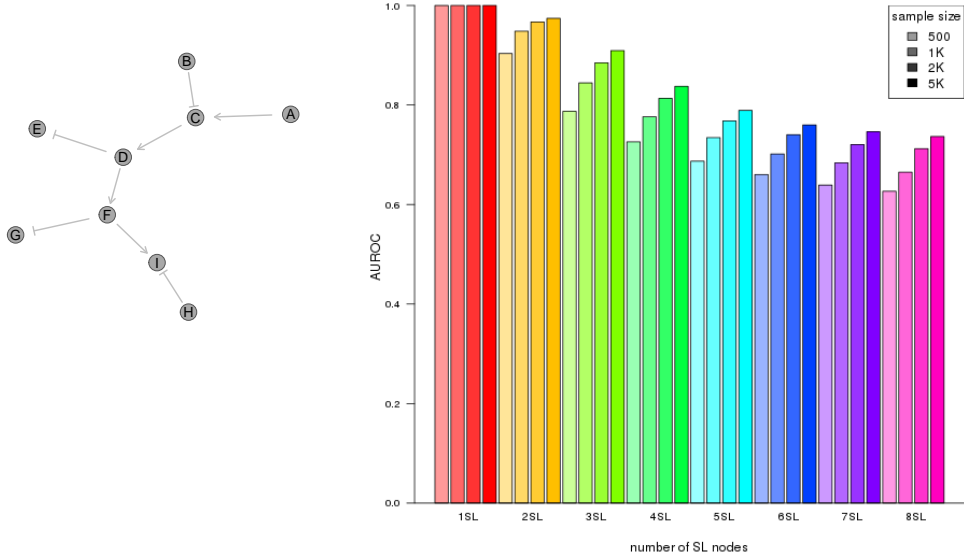
have high performance across increasing numbers of synthetic lethal genes, particularly for sufficiently high sample sizes (as shown by Figure K.3). However, this is not necessarily the case for graph structures with a combination of activating and inhibiting relationships (i.e., containing positive and negative correlations) As shown by Figure K.4, such a mixed network structure does not necessarily have high performance across parameters as observed for purely inhibiting networks.

These still appear to have desirably high sensitivity, high accuracy, and low false positive rate for detecting more synthetic lethal genes, despite poor specificity. The



(a) Statistical evaluation

(b) Receiver operating characteristic



(c) Graph Structure

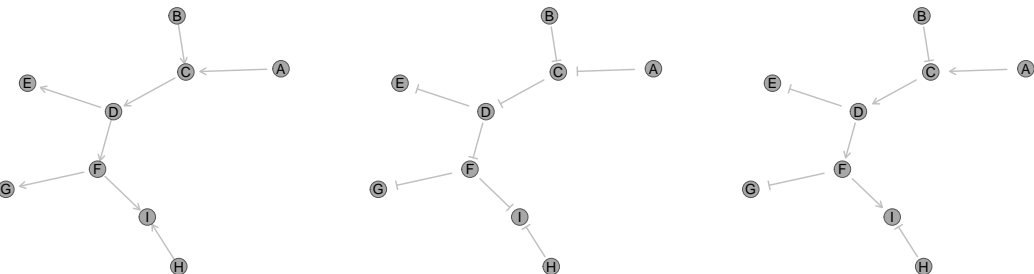
(d) Statistical performance

Figure 6.12: Performance of simulations on a constructed graph with inhibition.
 Simulation of synthetic lethality was performed sampling from a multivariate normal distribution generated from pathway structure with a combination of inhibitions. Performance of SLIPT declines for more synthetic partners and lower sample sizes. For each parameter value, 10,000 simulations were used.

ROC curves are particularly skewed for high proportions of the network being **synthetic lethal** and may stem from low numbers of true negative genes to detect (as discussed in Section 6.2.1.1). In a direct comparison of performance (shown in Figure 6.13), the purely inhibiting graph had consistently higher performance than the activating one as observed for simpler **graphs** (in Figure 6.11).

In contrast, the combination of activating and inhibiting relationships had slightly lower performance across parameters compared to the same **graph** structure with activating relationships. Therefore correlation structure can impact on the performance of **SLIPT** in a graph network, in either direction, specifically the addition of negative correlations. However, this may be an artifact of the simulation procedure as **synthetic lethal** genes from the correlation structure were randomly selected (without regard to their relationships), with the query gene added to ensure that conditions for **synthetic lethal** relationships were met.

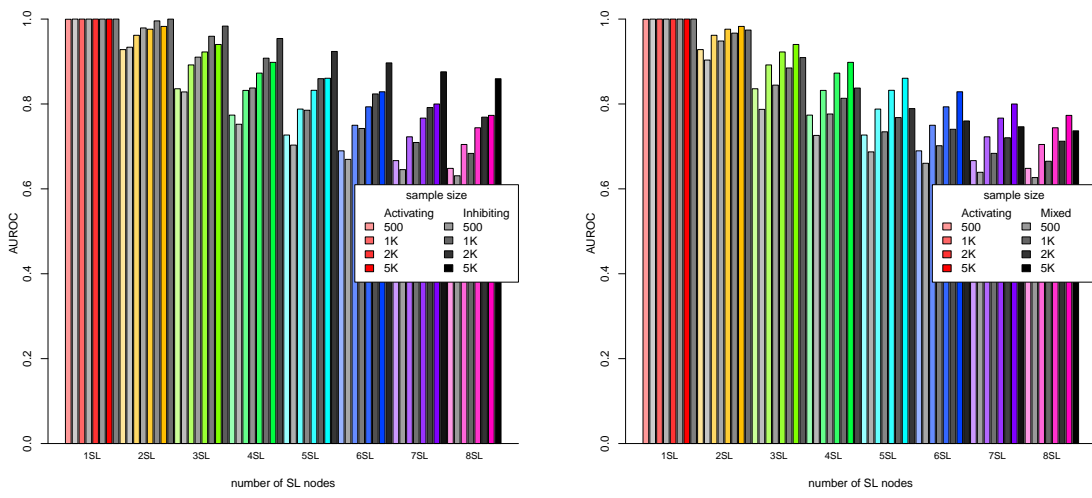
This system for simulating inhibitory pathways is not ideal since it lead to **synthetic lethal** gene combinations, by randomly selecting them, which are unlikely to occur in biological pathways. These randomly selected **synthetic lethal** genes may account for the detection results being suboptimal (i.e., difficult to detect **synthetic lethal** partners) compared to previous investigations. It is expected that inversely correlated synthetic partner genes will be highly expressed in a mutually exclusive manner such that at least one of them will be compensating for loss of the query gene in most samples, leading to a weak **synthetic lethal** signature in **expression** data in this case. Furthermore, this case may not be representative of empirical biological data with **synthetic lethal** partners of **tumour suppressor** genes which are commonly inversely correlated to the query gene (to some extent) and therefore it is unlikely that they are strongly negative correlated with each other, unless they are **synthetic lethal** partners of each other as well. It is plausible that many **synthetic lethal** partner genes will serve to separately compensate for the loss of query gene function and be positively correlated with each other. Nonetheless, these simulations are sufficient to demonstrate that correlation structure (particularly negative correlations) have an impact on the detection of **synthetic lethality**. However, **SLIPT** is still able to perform well across **graphs** with different activating and inhibiting relationships and the perturbations in performance are marginal, particularly those reducing performance compared to an activating network.



(a) Activating Graph

(b) Inhibiting Graph

(c) Mixed Graph



(d) Performance between Graphs (a) and (b) (e) Performance between Graphs (a) and (c)

Figure 6.13: **Performance is affected by inhibition in graphs.** The AUROC values for simulations of multivariate normal distributions based on graph structure containing only inhibitions in the Graph structure yielded consistently higher performance across parameter values in 10,000 simulations. A combination of activating and inhibiting relationships had lower performance but was more similar to the activating graph.

6.2.3 Synthetic Lethality across Graph Structures

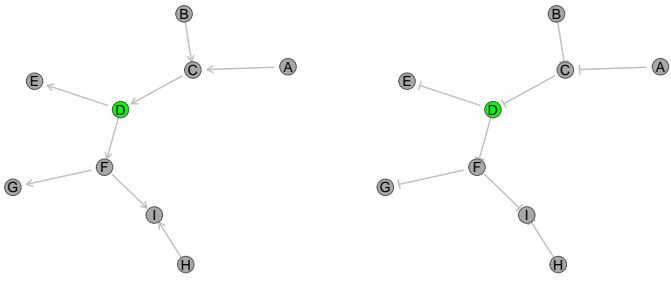
While synthetic lethal genes are distinguishable in principle from those highly positively correlated with them (as shown by ROC analysis), they are not necessarily distinguished as reflected by low specificity and high false positive rates in poorly performing simulations throughout this section. The negative correlations are not subject to the same issue, they sometimes perturb the correlation structure between synthetic lethal partner genes making it difficult to detect many of them. Thus far, synthetic

lethal genes have been selected randomly which is a limited approach. To examine the impact of pathway relationships in more detail, specific genes will be selected to be **synthetic lethal** within a network. Replicate simulations were performed for synthetic lethal detection with a fixed **synthetic lethal** gene, in contrast to previous investigations (randomly selecting **synthetic lethal** genes). This investigation was performed to demonstrate the impact of these genes being **synthetic lethal** in the detection of neighbouring genes in the pathway network, under **graph** structure activating and inhibiting relationships.

For instance, detection of a **synthetic lethal** gene in an activating **graph** structure (as shown in Figure 6.14a) is straightforward: the χ^2 values across simulations are clearly distinguishable from non synthetic lethal genes (shown in Figure 6.14c). A small number of simulations were performed for each gene being designated as **synthetic lethal**. In each case (of each gene being the **synthetic lethal** partner), the **synthetic lethal** gene was detectable with highest χ^2 value, being distinguishable amongst 20,000 genes including the highly correlated graph network (as shown in Figure K.5).

This is consistent with previous observations that **SLIPT** performed optimally for a single **synthetic lethal** partner in this network (in Figure 6.9). Despite optimal performance in a **ROC** curve irrespective of detection threshold, many of the highly correlated genes would be detected as false positives using a conventional p-value threshold (even if adjusted by **FDR**) from a χ^2 test with 4 degrees of freedom as performed by **SLIPT** (as described in Section 3.1). In particular, the genes that are adjacent to the **synthetic lethal** gene “D” within the **graph** structure exhibited high test statistics across simulations which would often be reported as false positives (as shown in Figure 6.14c). This is not specific to example of gene “D”, with the neighbouring genes exhibiting higher χ^2 test statistics for each gene in the network when it is designated as the **synthetic lethal** partner (as shown in Figure K.5).

Thus the **synthetic lethal** signal propagates from the true **synthetic lethal** gene throughout the network such genes nearer to the true **synthetic lethal** gene (more highly correlated) have higher test statistics and are more likely to be detected by **SLIPT** as false positives. This tendency for adjacent genes to be detected as **synthetic lethal** false positives is consistent with the **synthetic lethal** pathways being more concordant between **SLIPT** in **TCGA** data (TCGA, 2012) and the **siRNA** screen (Telford *et al.*, 2015) than individual gene results (in Chapter 4). False positive genes are therefore still more likely to be involved in a **synthetic lethal** pathway by being correlated with a true **synthetic lethal** gene and **synthetic lethal** pathways are likely to have



(a) Activating Graph

(b) Inhibiting Graph

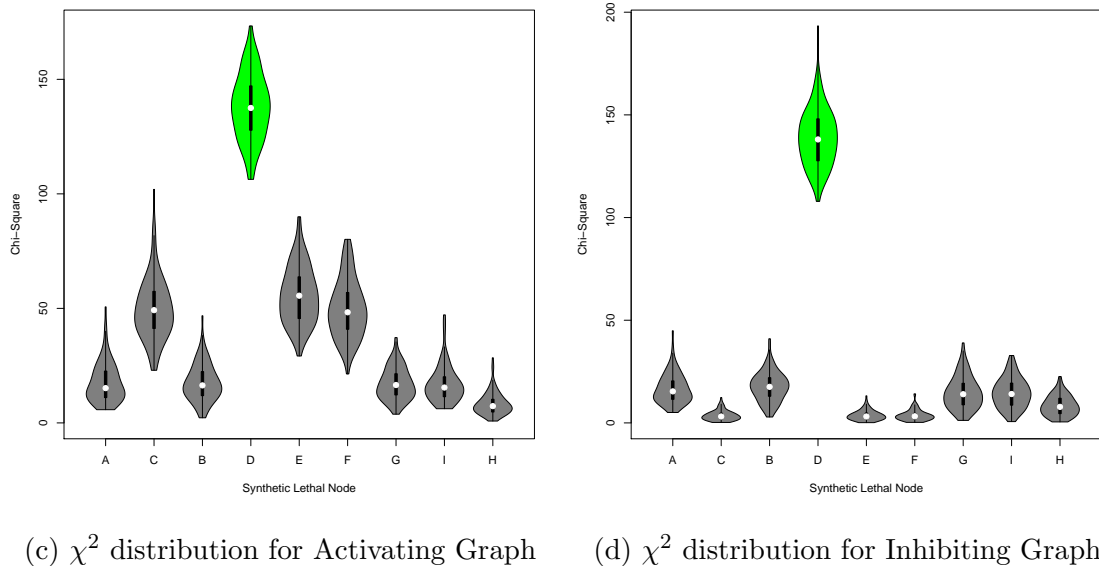


Figure 6.14: **Detection of synthetic lethality within a graph structure.** The gene “D” was designated to be synthetic lethal and the χ^2 value from [SLIPT](#) was computed for each gene across each [graph](#) structure. The χ^2 values were computed in 100 simulations of datasets of 20,000 genes including the [graph](#) structure and 1000 samples. Adjacent genes exhibited lower χ^2 values with inhibiting relationships.

many genes detected by [SLIPT](#) giving a consensus of evidence, supporting the pathway over-representation approach in particular which may account for how it differs from pathway [metagenes](#). Furthermore, [SLIPT](#) is still viable to detect true synthetic lethal partners or prioritise those most likely to be experimentally validated since those with the strongest support (i.e, higher χ^2 values and more significant p-values) are more likely to be the underlying synthetic lethal gene.

In contrast to an activating graph (Figure 6.14a), the immediately adjacent genes in an inhibiting graph (Figure 6.14b) had neither an elevated χ^2 test statistics indicating synthetic lethality nor a significant inverse effect (as shown in Figure 6.14d). Similar simulations were performed a graph structure with inhibiting relationships within a dataset of 20,000 genes. The adjacent genes to the synthetic lethal gene “D” did not have elevated χ^2 values and therefore true synthetic lethal partners were highly distinguishable from non synthetic lethal genes with inhibiting relationships. This was not specific to “D” and was shown across any gene in the graph structure if it were designated to be the synthetic lethal partner of the query gene (shown in Figure K.6). This is consistent with the detection of many genes involved in kinase signalling, gene regulation, and other known cancer pathways (in Chapter 4) which frequently have inhibitory steps. These results support SLIPT as an appropriate approach to distinguish synthetic lethal partners in biological pathways, including those relevant to cancer growth and inhibition.

However, it should be noted that the 2nd degree neighbours of the synthetic lethal gene still exhibited moderate χ^2 values (and are moderately correlated with the synthetic lethal gene). It is still possible for these to be detected as false positives as previously described for an activating graph structure although the presence of inhibitory relationships (and negative correlations) further increases the differences in test statistics for correlated genes and underlying synthetic lethal partners as shown by the extreme example (in Figure K.6).

These findings are consistent with simulations in a graph containing a combination of activating and inhibiting relationships which exhibits a either of these χ^2 profiles depending on which gene is synthetic lethal and the relationships to adjacent genes (as shown in Figure K.7). Note that in this case, the synthetic lethal gene is distinguishable and inhibitory relationships within this graph structure make it easier to detect underlying synthetic lethal genes with SLIPT by a more highly significant χ^2 test. This contrasts with randomly selecting multiple synthetic lethal genes (in Figure 6.13) where the performance of SLIPT was impeded by the inhibitory relationships between synthetic lethal partners in this graph structure. Therefore the random synthetic lethal genes selected previously with negative correlations between them which had poor performance are likely to have created an artifact in the simulation results as they are biologically implausible and constrain the synthetic lethal simulation procedure

The results with one synthetic lethal partner were sufficient to infer the impact of synthetic lethal partners within pathways on neighbouring (correlated) genes. However,

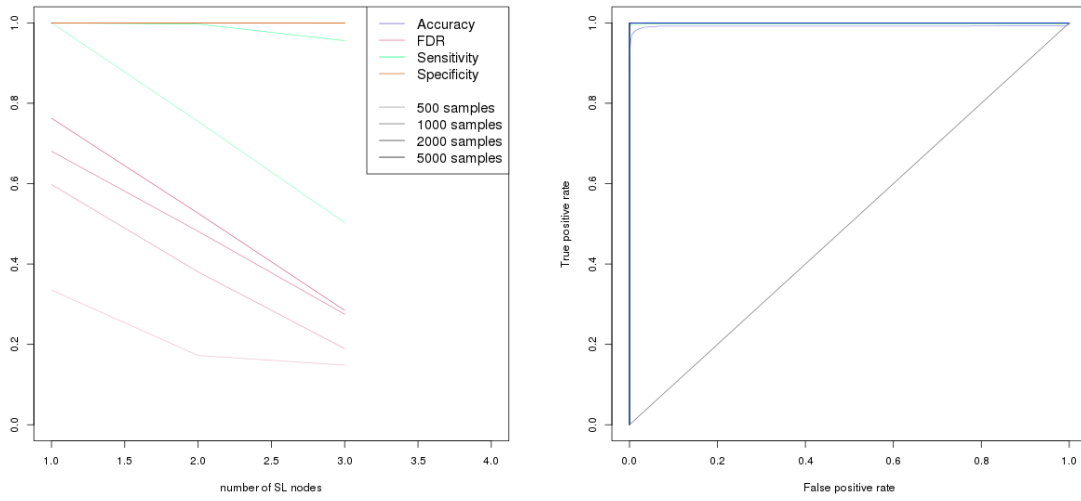
it is plausible that the synthetic lethal signatures in expression data would propagate through a network with multiple synthetic lethal partners as sources, provided that the correlations between synthetic lethal partners is biological feasible. These simulations were performed on a correlated graph structure within a larger gene expression dataset of 20,000 genes (as performed in Sections 3.3 and 6.2.4), a feasible number for a full human gene expression dataset, and as such are comparable to the findings below.

6.2.4 Performance within a Simulated Human Genome

The high proportion of synthetic lethal partners in small networks (and fewer true negatives) made it difficult to accurately assess the performance of SLIPT with higher numbers of true partners to detect (as noted in Section 6.2.1.1). The addition of more non synthetic lethal genes in previous simulations increased the performance of SLIPT, particularly the specificity to reduce the number of false positives (as shown in Sections 3.3 and 6.1). The graph structures (as used in Section 6.2.1) of genes with correlations from sampling a multivariate normal distribution were included in a larger simulated dataset of 20,000 genes. This simulation procedure enabled testing of the performance of SLIPT when detecting synthetic lethal partners within correlated graph structures (of a synthetic lethal pathway) in the context of biologically feasible numbers of genes.

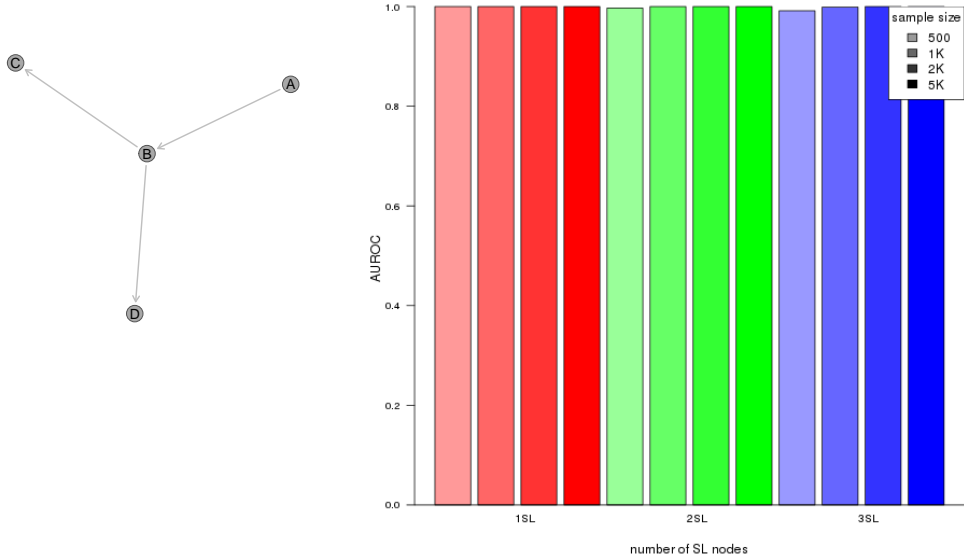
The simulations performed in Section 6.2.1.1 were replicated within a dataset of 20,000 genes with the rest being composed on non synthetic lethal genes without correlation structure. The aforementioned issue with specificity in a higher number of underlying synthetic lethal genes did not occur in a simple graph structure (as shown in Figure 6.15). For such a small graph module of highly correlated genes within a gene expression dataset, detection of synthetic lethal genes within the network by SLIPT and distinguishing these from the larger dataset had high performance across parameter values. In this case, a reduction in sensitivity resulted in poorer performance, a higher number of non synthetic lethal genes were correctly identified, with a low false positive rate and high accuracy. Thus the the use of stringent χ^2 p-value thresholds (adjusted by FDR) are suitable for testing for synthetic lethality in gene expression data across the number of genes in human and cancer data.

In a direct comparison with simulations in the graph structure alone (as performed in Section 6.2.1.1), detection of synthetic lethality with SLIPT performs consistently better in a larger dataset with many true negative genes to detect (as shown in Figure 6.16). Thhe SLIPT methodology as it has a high specificity and low false positive



(a) Statistical evaluation

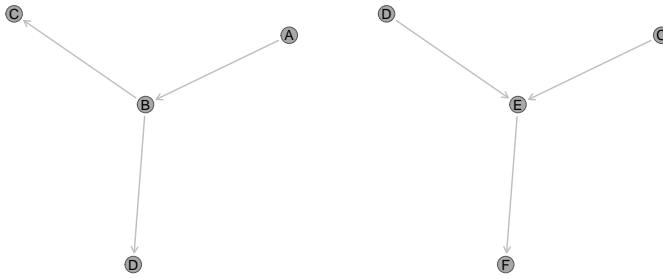
(b) Receiver operating characteristic



(c) Graph Structure

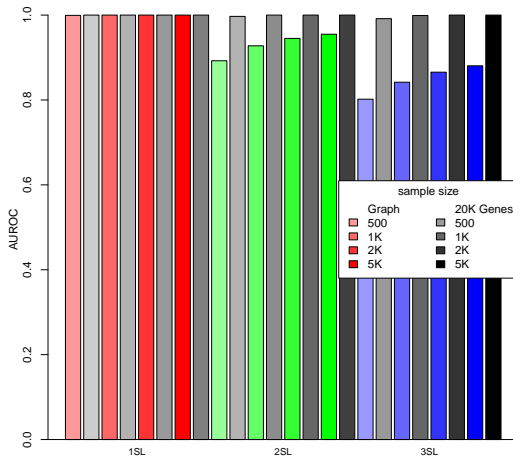
(d) Statistical performance

Figure 6.15: **Performance of simulations including a simple graph.** Simulation of synthetic lethality was performed sampling from a multivariate normal distribution (without correlation structure apart from the graph shown). Performance of **SLIPT** was high across parameters for detecting synthetic lethality in the graph structure within a larger dataset. The sensitivity decreases for a greater number of true positives to detect but the specificity remains high with a low false positive rate.

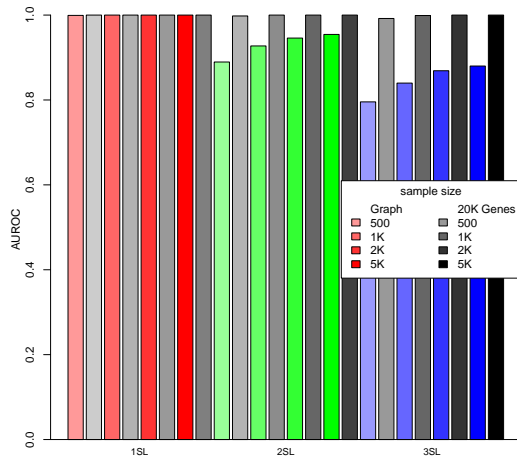


(a) Diverging Module

(b) Converging module



(c) Performance in Diverging Module



(d) Performance in Converging module

Figure 6.16: **Performance on a simple graph improves with more genes.** Simulations were performed with each of the [graph](#) structures to detect [synthetic lethal](#) partners within them. In either structure, performance of detection in a dataset containing on the [graph](#) structure (in colour) was lower than testing the [graph](#) structure within a larger dataset of non synthetic lethal genes (without correlations).

rate, which is desirable. [SLIPT](#) is therefore applicable to large [gene expression](#) datasets where these are important considerations since the number of negative genes to correctly identify often vastly outnumbers the number of positive genes to detect.

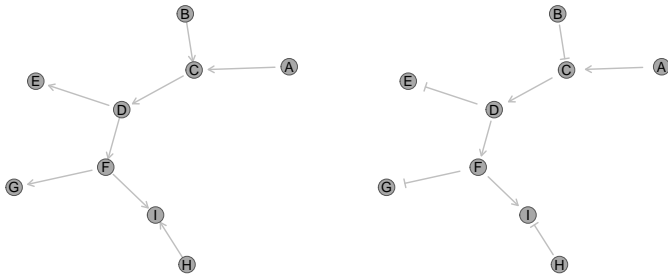
This increase in performance with more non synthetic lethal genes to detect does not necessarily apply in an inhibiting [graph](#) structure. This is an important consideration since biological pathways commonly contain inhibiting relationships (and inverse correlations), although they are unlikely to occur across an entire pathway. While an

increased performance for an activating graph was replicated, in this case, the performance of simulations of an entirely inhibiting **graph** structure did not improve within a larger dataset. Rather, the performance in the inhibiting **graph** structure was similar to simulations of the **graph** structure in isolation. It is expected that the findings based on these simulations of genes with **pathway** structures in smaller datasets (as described in Section 6.2.1) will be relevant to larger datasets. The simulation results in these inhibiting **graph** structures perform comparably or higher with more non synthetic lethal genes to distinguish from them even with inhibitory relationships within the **graph** structure

Performance of **synthetic lethal** detection of **SLIPT** in **graph** structures with inhibitions included in a larger dataset of non synthetic lethal genes did not diminish to the level of the **graph** structure simulated alone. In some cases (as shown in Figure 6.17), the performance of an inhibitory **graph** structure was consistently elevated when included within a larger data. However, these did not perform as well as the equivalent **graph** structures without inhibitory relationships within a similar dataset.

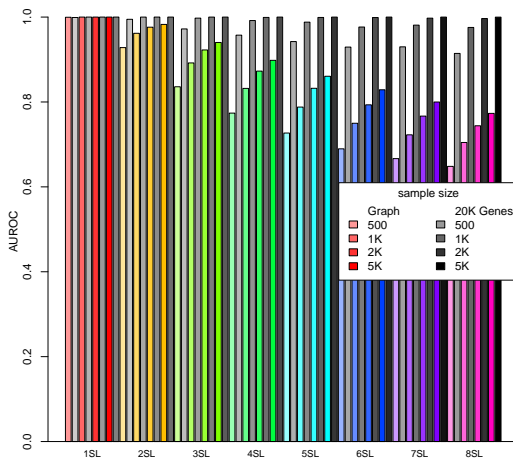
This poorer performance of inhibitory **graph** structures may be due to highly negatively correlated genes being false positives. These genes will be positively correlated with the query gene if they are negatively correlated with a **synthetic lethal** partner (i.e., within a **synthetic lethal** pathway). The **SLIPT** procedure performs well at distinguishing these positively correlated genes, as previously shown (in Sections 3.3.2.2 and 6.1.1.1). These false positives will also be a minority amongst a larger dataset of non synthetic lethal genes without correlation to the query or **synthetic lethal** genes.

It more likely that the poorer performance stems from negative correlations between **synthetic lethal** genes which makes them more difficult to individually detect (as observed in Section 6.2.2). As discussed in Section 6.2.3, this is likely an artifact of the simulation procedure selecting random **synthetic lethal** genes with strong inhibitory relationships between them. Therefore the poorer performance for inhibiting **graphs** within larger datasets is not cause for concern because the cases where **SLIPT** performs poorly are likely to be combinations of simulated **synthetic lethal** genes that are not likely to occur within biological pathways. This simulation procedure has included higher-order **synthetic lethal** to produce the weakest signal of **synthetic lethality** for individual partner genes which are still detectable by **SLIPT**.

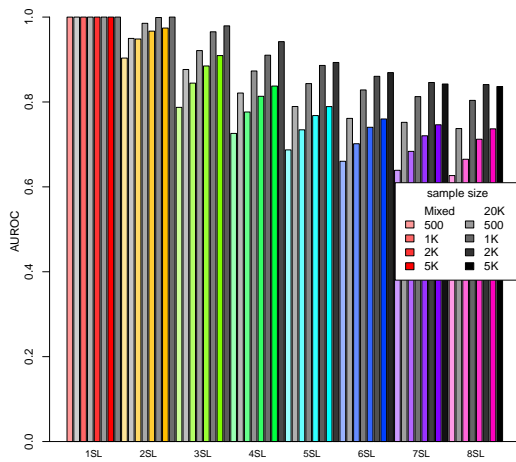


(a) Graph Structure

(b) Inhibiting Structure



(c) Performance in Graph



(d) Performance with Inhibitions

Figure 6.17: **Performance on an inhibiting graph improves with more genes.** Simulations were performed in a [graph](#) structure with activating and inhibiting relationships to detect [synthetic lethal](#) partners within them. In contrast to an activating graph, performance of detection in a dataset containing only the [graph](#) structure (in colour) was as much lower than testing the [graph](#) structure within a larger dataset of non synthetic lethal genes (without correlations) in an inhibiting [graph](#) structure with negative correlations.

6.3 Simulations in More Complex Graph Structures

Investigations with simulations based on [graph](#) structures were extended to larger [graphs](#), enabling more synthetic lethal genes within a pathway and modelling the complexity of a biological pathway. Sensitivity declines over a greater range for the number of [synthetic lethal](#) partners in a larger network with a trade-off with specificity (as shown in Figures K.8–K.10). However, the accuracy declined for greater numbers

of **synthetic lethal** partners and the false positive rate peaks at intermediate values. In this range, difference between simulations varied with greater sample size. The **AUROC** results were similar between these more complex **graph** structures, , although the larger **graph** (Figure K.10) differed in sensitivity and specificity at an adjusted (**FDR**) p-value threshold. This difference be due to different proportions of **synthetic lethal** and non-synthetic lethal genes to detect, since these **graphs** (in Figures K.8 and K.9) had fewer genes.

While the **graph** structures (of similar size) were highly distinct, they had similar performance profiles across parameters. **SLIPT** is therefore robust across **pathway** structures and is more affected by the number or proportion of genes to detect. Findings from previous simulations in similar correlation structures (in Section 3.3) should be applicable to **expression** data with more complex correlation structures, such as those occurring in biological pathways. Specifically, **synthetic lethal** partners are distinguishable from closely correlated genes in the context of a biological pathway networks, irrespective of thresholds (shown by **ROC**) and with the sensitivity and specificity of p-value thresholds (adjusted by **FDR**) as used for **SLIPT** (in Chapters 4 and 5).

The findings for inhibitory **graph** structures were replicated with larger more complex **graph** structures with inhibiting relationships and more **synthetic lethal** genes to detect (shown in Figures K.11–K.14). In each **graph** structure, simulations entirely with inhibiting relationships (Figures K.11, K.13, and K.15) had higher performance than the equivalent graph with entirely activating relationships (Figures K.8, K.9, and K.10) or a combination of activating and inhibiting relationships (Figures K.12, K.14, and K.16). While the presence of negative correlations subtly affects the performance of **SLIPT**, the methodology is robust across the exact structures of genes and is therefore applicable to detecting **synthetic lethal** genes in a range of (synthetic lethal) biological pathways with different structural relationships.

6.3.1 Simulations over Pathway-based Graphs

Simulations of **synthetic lethality** in **gene expression** with correlation structures thus far have used simple blocks of correlated genes (as used in Section 3.3) or derived from constructed **graph** structures (as used in Section 6.2). These have been used to make inferences on the impact of correlation structure, it remains to be shown whether these findings are reproducible in the complexity of the biological **network** structure. Specifically, **SLIPT** was tested on simulated data with known underlying simulated **synthetic**

lethal partners (as described in Section 3.2.2) with multivariate normal correlation structure derived from biological pathways (as described in Section 3.4.2).

The Reactome [pathway](#) structure for the [PI3K](#) cascade (as used in Chapter 5) was used to demonstrate the simulation procedure for detecting [synthetic lethality](#) in the [graph](#) structure of a biological pathway. This pathway has clear directionality and related signalling pathways were among those identified to be [synthetic lethal](#) candidates (in Chapter 4). The [PI3K](#) pathway has a relatively moderate size (138 genes) and complexity. It is therefore suitable for comparison to previous [graph](#) structures of a similar scale (50–100 genes) with the complexity of a biological pathway.

The performance of [synthetic lethal](#) detection with [SLIPT](#), in simulated [expression](#) data based on the Reactome [PI3K](#) pathway (as shown in Figure 6.18), was concordant with previous findings. [SLIPT](#) had high performance when detecting a low number of [synthetic lethal](#) genes which decreased for high numbers of [synthetic lethal](#) genes or lower sample sizes. In particular, the performance of simulations in the [PI3K](#) pathway highly resembled the simulation results for constructed [graphs](#) of similar scale and complexity (as shown in Figures K.8 and K.9). Using thresholds based on the χ^2 p-value (adjusted by [FDR](#)), simulations in the biological [PI3K](#) pathway had a higher sensitivity and lower specificity. While the performance decreased for more [synthetic lethal](#) genes to detect within the simulated [PI3K](#) pathway, this primarily involved a reduction in sensitivity to detect [synthetic lethal](#) genes rather than false positives, as the false positive rate decreased, the accuracy increased, and the specificity was relatively unperturbed (being more dependent on sample size). Thus [SLIPT](#) was stringent in an example of a biological [graph](#) structure and is appropriate for detection of [synthetic lethal](#) genes in complex correlation structures in [gene expression](#) data involving biological pathways.

These simulations were replicated in the more complex $G_{\alpha i}$ signalling pathway (of 292 genes), which was one of the most well supported [synthetic lethal](#) pathways with loss of *CDH1* in cancer (in Chapters 4 and 5). This pathway showed similar relationships between sensitivity, specificity, and false positive rate with number of [synthetic lethal](#) partners and sample size (as shown in Figure K.17). While the overall performance was lower than for smaller networks structures, many of the findings from previous networks were replicated in a larger more complex biological network. In the $G_{\alpha i}$ signalling pathway, [SLIPT](#) had high performance for detecting low numbers of [synthetic lethal](#) genes and was highly stringent against false positives for higher numbers of [synthetic lethal](#) genes.

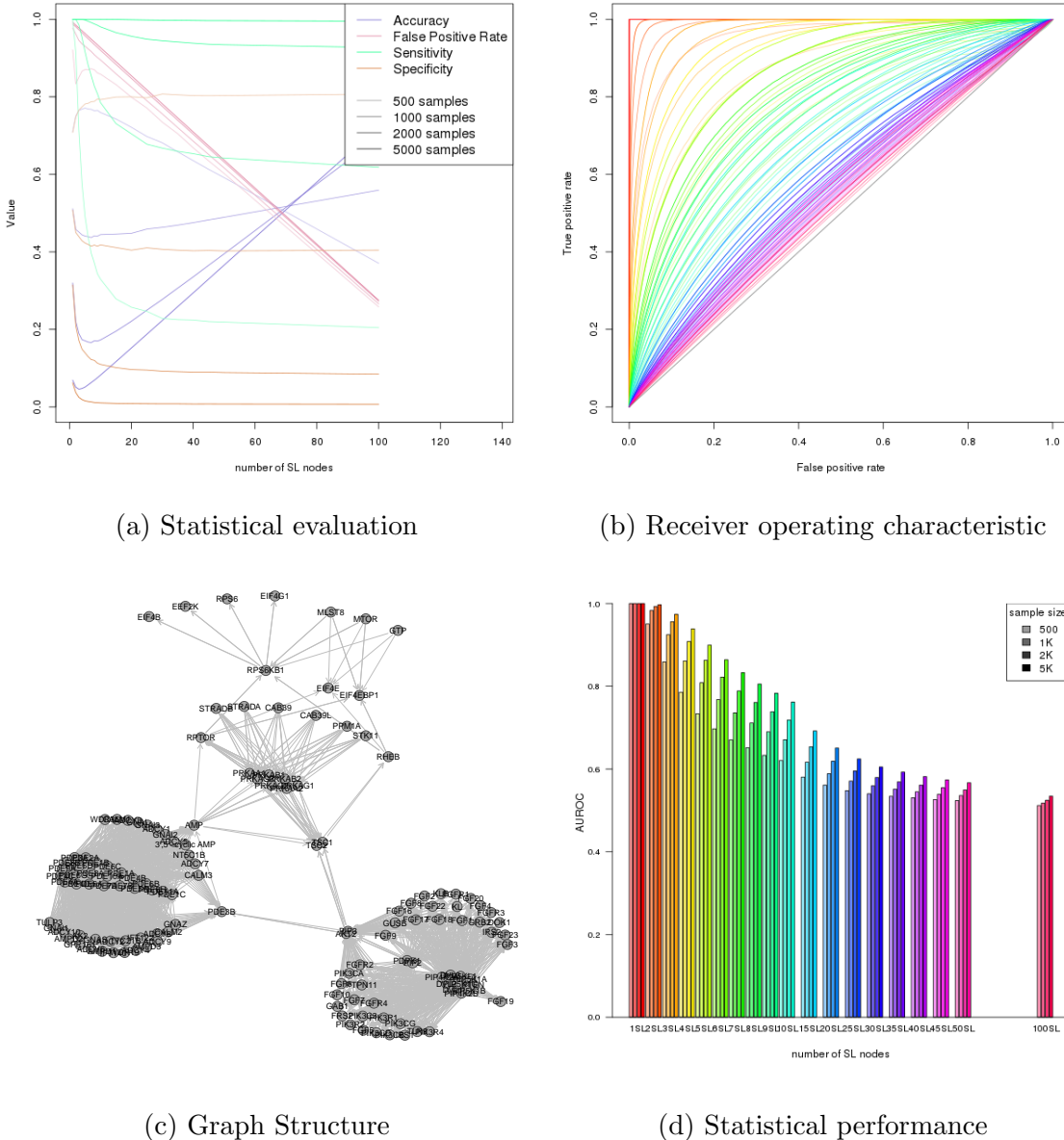


Figure 6.18: **Performance of simulations on the PI3K cascade.** Simulation of synthetic lethality was performed sampling from a multivariate normal distribution based on the Reactome PI3K cascade. Performance of SLIPT was high across parameters for detecting synthetic lethality in the graph structure within a larger dataset. The performance decreases for a greater number of true positives to detect but the accuracy increases with a low false positive rate.

6.3.2 Pathway Structures in a Simulated Human Genome

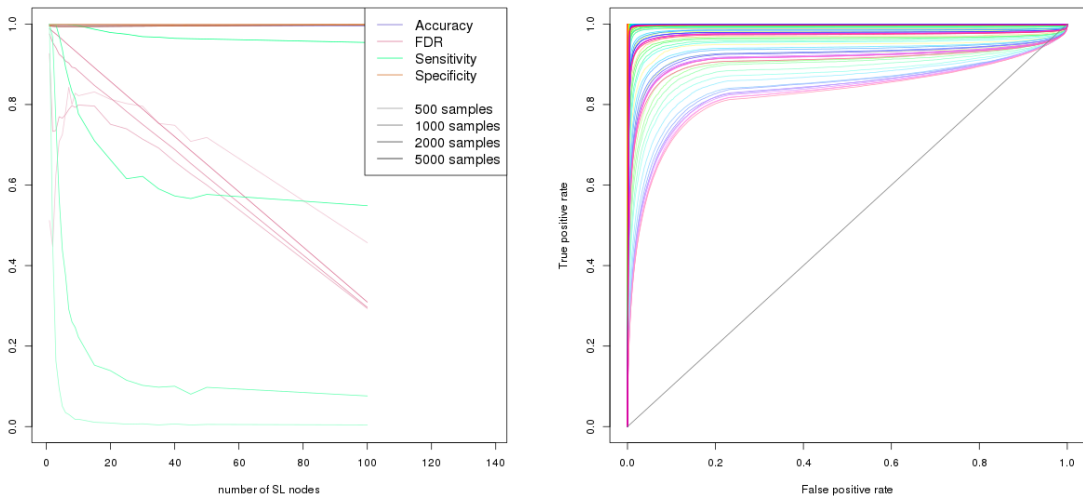
Simulations were also performed with `graph` structures from biological pathways included in a larger dataset to simulate `gene expression` data of the scale typical for human and cancer studies. These simulations (as discussed in Section 6.2.4) showed a higher specificity and therefore `SLIPT` had higher performance. The simulated `PI3K` pathway (as shown in Figure 6.19) is no exception, with high performance across parameter values, which remained high up to many genes. While the sensitivity decreases for high numbers of `synthetic lethal` genes to detect within the `PI3K` pathway, the `SLIPT` methodology remains accurate with high specificity in a large simulated `gene expression` dataset.

Therefore the `SLIPT` methodology is a highly stringent approach suitable to be applied for detecting `synthetic lethal` genes and pathways within highly complex `expression` data with biological `pathway` structure. Even the poorly performing simulations were highly stringent with low false positive rates, which are an important consideration in a `gene expression` data with many non synthetic lethal genes. The enrichment of true `synthetic lethal` partners among detect genes makes `SLIPT` valuable for triage of candidate `synthetic lethal` partners for further validation and for pathway analysis.

The performance of simulation of `synthetic lethality` within biological pathways was markedly higher in the context of a larger dataset of thousands of genes. As shown in a direct comparison with the `graph` structures alone (in Figure 6.20c), performance was consistently higher across parameters in pathways of biological complexity from the Reactome database (Croft *et al.*, 2014) such as `PI3K` cascade and the $G_{\alpha i}$ signalling pathway (shown in Figures K.18 and 6.20d).

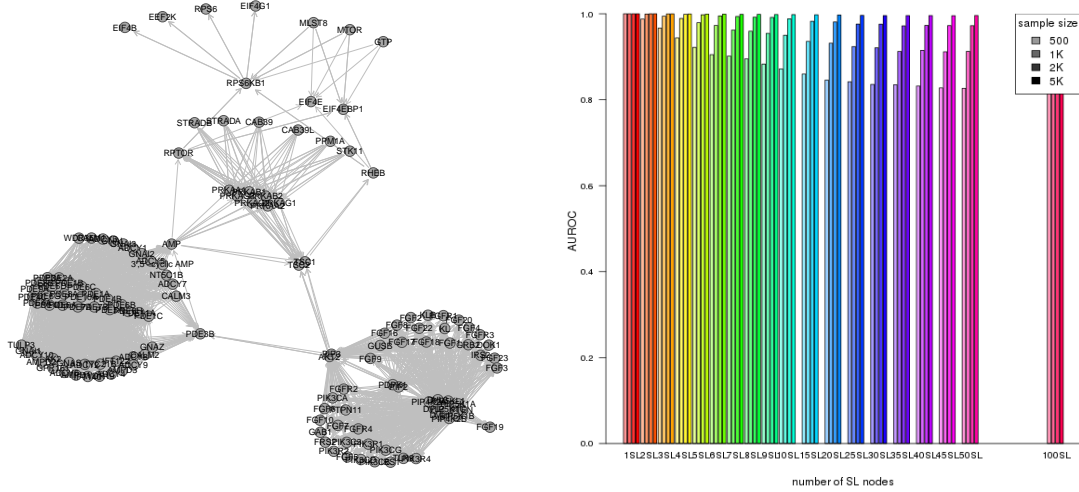
These biologically complex `graph` structures, based on the Reactome pathways, assumed activating relationships to test `synthetic lethal` detection with `SLIPT` in the context of complex correlation structures. Inhibiting relationships were not distinguished in the Reactome database (Croft *et al.*, 2014). However, these investigations with pathway based `graph` structures indicate that the findings in constructed `graphs` (as used in Section 6.2) are relevant to `gene expression` data containing real correlated pathways. Furthermore, previous comparisons between simulations with inhibiting relationships indicated that the performance of `synthetic lethal` detection in an equivalent `graph` structure with inhibitory relationships will likely be higher.

Non synthetic lethal genes, inversely correlated with the underlying `synthetic lethal` partners, were distinguishable by `SLIPT` with high specificity. `Synthetic lethal` genes were detectable with reasonable performance in large scale simulated `gene expression`



(a) Statistical evaluation

(b) Receiver operating characteristic

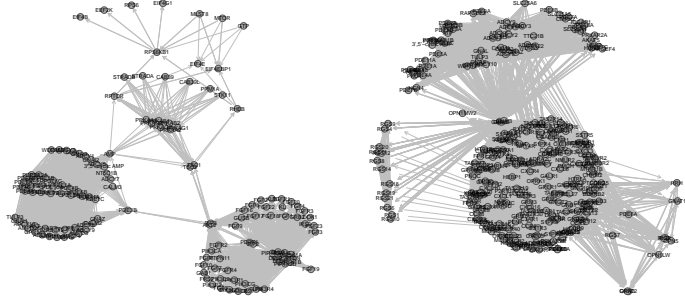


(c) Graph Structure

(d) Statistical performance

Figure 6.19: Performance of simulations including the PI3K cascade. Simulation of synthetic lethality was performed sampling from a multivariate normal distribution (without correlation structure apart from the Reactome PI3K cascade). Performance of SLIPT was high across parameters for detecting synthetic lethality in the graph structure within a larger dataset. The sensitivity decreases for a greater number of true positives to detect but the specificity remains high with a low false positive rate.

data and highly (positively) correlated genes in *pathway* structures. These findings serve as a conservative estimate for the performance of **SLIPT** to detect synthetic lethal



(a) The PI3K cascade

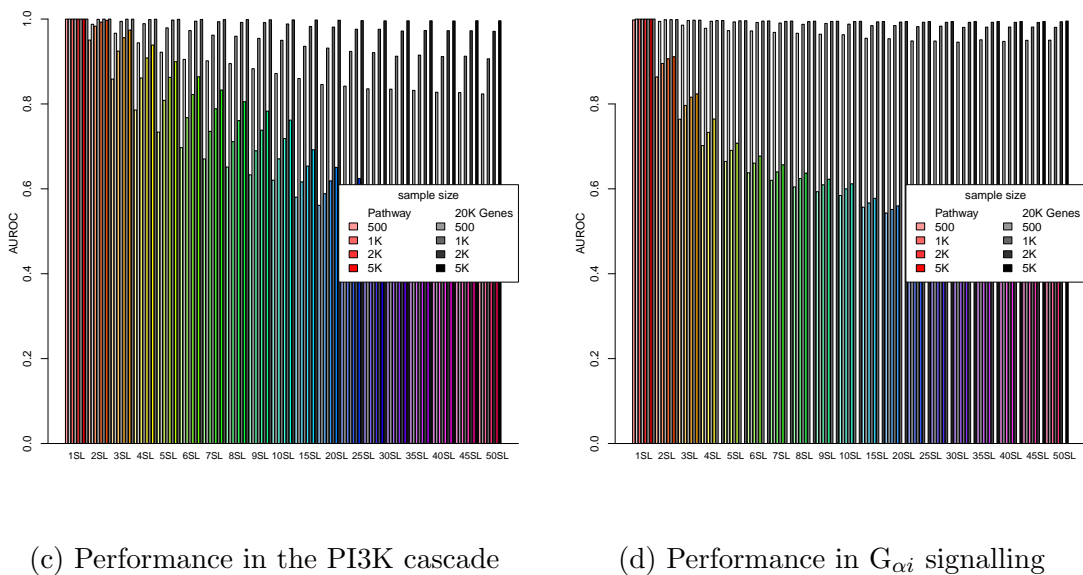
(b) $G_{\alpha i}$ signalling

Figure 6.20: **Performance on pathways improves with more genes.** Simulations were performed in a graph structures for the PI3K cascade and $G_{\alpha i}$ signalling pathways structures to detect synthetic lethal partners within them. As for constructed graphs, performance of detection in a dataset containing only the graph structure (in colour) was as much lower than testing the graph structure within a larger dataset of non synthetic lethal genes (without correlations) for both graphs of biological complexity.

genes within a synthetic lethal biological pathway in empirical data. Synthetic lethal genes are distinguishable from correlated genes, to varying extents, in simulations. False positives are also more likely to occur within the same (synthetic lethal) pathways. Therefore SLIPT is both effective at triage of synthetic lethal candidates within a biological pathway and at identifying synthetic lethal pathways in high dimensional gene expression data.

6.4 Discussion

6.4.1 Simulation Procedure

Simulations have been performed to assess the performance of the **SLIPT** methodology (as described in Section 3.1 and with modifications) for detecting known underlying synthetic lethal partners of a query gene. These simulations support the the findings in empirical data (in Chapters 4 and 5) by addressing whether the methodology used to generate them is accurate or has desirable statistical performance in controlled simulated conditions. These investigations include adjusting parameters such as the numbers of synthetic lethal genes which were known in empirical data to assess the performance of the **SLIPT** methodology across simulation parameters and characterise the datasets for which **SLIPT** performs well. Simulation and statistically modelling also enabled comparison of the **SLIPT** methodology to other statistical approaches to synthetic lethal detection in expression data.

These simulations are based on a statistical model of synthetic lethality (as described in Section 3.2.1) which was designed stringently to ensure that if synthetic lethality is detectable in the simulated datasets it would also be detectable by the same methodology in empirical expression data. The model of synthetic lethality made conservative assumptions such as the low threshold of expression for gene function or the inclusion of cryptic higher-order synthetic lethality (when testing pairwise). These assumptions decrease the likelihood that synthetic lethal signatures would be detectable in expression data. Thus it is reassuring that synthetic lethality is still detectable in under many simulation parameters as the performance of **SLIPT** would be expected to be higher were these assumptions to be violated in empirical data.

The simulation procedure (as described in Section 3.2.2) is designed as a computational pipeline with arguments passes to scripts. The **SLIPT** methodology and simulation of expression from graph structures were both used as R (R Core Team, 2016) software packages developed and released for this project (as described in Section 3.5). This design ensures that the simulations can be robustly applied across parameters with consistency between simulations apart from the differences discussed. The simulation procedure is also flexible to simulating other datasets, including synthetic lethal relationships and pathway correlation structures, should these be relevant to future investigations or bioinformatics tool development. The computational pipeline is also compatible with parallel computing and made use of High Performance Computing (HPC) infrastructure provided by the New Zealand eScience Infrastructure (NeSI) us-

ing the Simple Linux Utility for Resource Management (Slurm) submission system (as described in Section 2.5.3). This parallel computing pipeline enabled extensive investigations into synthetic lethality in simulated data, including approximately 2 million cpu-hours on NeSI.

6.4.2 Comparing Methods with Simulated Data

Attempts were made to implement alternative synthetic lethal detection approaches such as linear regression and the BiSEp R package (discussed in Section 6.1). However, those tested were ineffective at detecting synthetic lethality in multivariate normal simulated data in comparison to SLIPT. While some of the published synthetic lethal detection methods (Jerby-Arnon *et al.*, 2014; Lu *et al.*, 2015) did not provide reproducible software releases for direct comparison, some of the central assumptions used in their design were tested by the statistical methods considered for synthetic lethal detection in expression data.

Another consideration is that BiSEp takes considerably more time to compute predictions than SLIPT or χ^2 which limited the number of simulations that were feasible and made it difficult to apply across parameters in the simulation pipeline (even when using supercomputing infrastructure as discussed in Section 2.5.3). The computationally intensive nature of the BiSEp procedure does not appear to be the issue for detecting synthetic lethal genes in TCGA data or simulations, although it has made more extensive simulations challenging. Rather, BiSEp is not suitable in either case since the TCGA data is normalised with voom (Ritchie *et al.*, 2015) and simulated data is generated by sampling from a multivariate normal distribution. In either case, even subtle bimodal signatures in expression data were not consistently detectable or sufficient to detect synthetic lethality.

The BiSEp methodology may perform better on other data types but it cannot be directly compared with the results for SLIPT throughout this thesis which have used normalised or (multivariate) normally distributed data. Since it requires bimodal distributions, BiSEp is not suitable for stringently normalised expression data nor would it be expected to perform on (ranked) pathway metagenes. Thus SLIPT represents a distinct approach more suitable for these data types whereas BiSEp may be applicable to other applications in which bimodal distributions are more frequent.

This investigation also demonstrates that implementing scientific software from other research groups is not a trivial exercise, even when released as an open-source R package. Therefore, the above results were used to evaluate SLIPT and compare it to

other statistical rationales. An comprehensive comparison to contemporary **synthetic lethal** detection approaches (and those released in the future) or further benchmarking is left to an impartial researcher to evaluate. The above findings show that the **SLIPT** approach is able to detect **synthetic lethal** genes in simulated data with comparable or better performance than a range of distinct statistical techniques and was appropriate for use throughout this thesis.

6.4.3 Design and Performance of SLIPT

The simulation procedure using sampling from a multivariate normal distribution was used throughout the majority of the simulation investigations in this thesis. This approach has the advantages of emulating the continuous normalised **expression** data used for **gene expression** analysis and enabled the simulation of correlation structures (as discussed in Section 3.3). These simulations scaled to datasets of comparable scale to those used in **gene expression** analysis with thousands of genes. The **SLIPT** methodology was shown to perform robustly across large numbers of genes and simple correlation structures. This includes high specificity against genes positively correlated with the query gene for which the directional **SLIPT** methodology more suited to distinguishing **synthetic lethal** genes from than the χ^2 test without directional criteria on the number of samples observed.

These findings were expanded upon in this chapter. Specifically, different quantiles were compared for **SLIPT** and the χ^2 test. These approaches using threshold based discrete gene function were compared to the Pearson correlation without loss of the continuous **expression** data. The 3-quantiles for **SLIPT** (as described in Section 3.1) were optimal for both **SLIPT** and the χ^2 alone. In addition to being optimal for estimating the significance of **synthetic lethal** interactions, these quantiles were also optimal for the directional criteria of **SLIPT** since this method outperformed the χ^2 test and was the most different at the 3-quantile. As previously, noted this difference was more pronounced with positively correlated genes (with the query gene) for which the specificity of **SLIPT** improves and was replicated in large datasets with thousands of genes as occur in human **expression** data. These results were not simply due to sufficient samples for significant p-values since the performance as determined by **AUROC** analysis is independent from significance thresholds. This indicates that the **SLIPT** methodology (as it has been used in Chapters 4 and 5) is optimal and the parameters used to design it were appropriate.

Both discrete functional approaches (**SLIPT** and χ^2) were able to outperform negative correlation which supports their use. In particular, this result addresses the concern that arbitrary thresholds of low and high gene function (as used by **SLIPT**) lose useful data by compressing the spectrum of gene expression into categorical data. However, this does not impede the performance of **SLIPT** and can reduce statistical if the quantiles used are optimal. The poorer performance of correlation-based detection of synthetic lethality also indicates affirms the concept of gene function for synthetic lethality being qualitative, that is expression must be sufficient for cell viability and higher expression is not necessarily higher function (as this is not the case for all genes). Furthermore, the finding that negative correlation outperforms positive correlation is also consistent with co-expression being a poor predictor of synthetic lethality compared to other approaches (Jerby-Arnon *et al.*, 2014), supporting the claims of Lu *et al.* (2015).

Compared with **SLIPT**, neither correlation approaches nor bimodality signatures were suitable for detecting synthetic lethality in expression data. The correlation-based approaches make assumptions about the relationship between gene expression and function which do not necessarily hold for all genes. Similarly, the bimodal approach is not appropriate for normalised data since deviations from a normal distribution have already been used for ensuring data quality, as is common practice for RNA-Seq data. Other approaches were continuous data such as fitting linear models are likely to be prone to similar issues and not perform as well as **SLIPT**. However, it is possible that these may be improved with conditioning on known synthetic lethal partners with multivariate regression or Bayesian priors. Similarly, synthetic lethal detection could be performed by iteratively conditioning upon the strong candidate from previous analysis. These approaches may be able to better circumvent the issues of high-order synthetic lethality and multiple testing.

Nevertheless, the above findings are sufficient to assess the performance of **SLIPT** and present an effective straightforward approach to synthetic lethal detection in gene expression data. Further development of linear models, Bayesian inference approaches, or comparison to existing synthetic lethal approaches (e.g., machine learning) remain as future directions. Developing and testing more sophisticated statistical approach to synthetic lethal detection may benefit from the concepts discussed with regard to the relatively simple **SLIPT** methodology. Similarly, further comparisons and benchmarking of **SLIPT** against other computational approaches to synthetic lethal detection in gene expression data is more suitable for an independent researcher and the **slipt** R

package has been released (as described in Section 3.5) for this purpose, in addition to further application in research.

6.4.4 Simulations from Graph Structures

The simple correlation structures (as used in Section 3.3) were expanded upon to simulate correlated genes based on `graph` structures using the multivariate normal simulation procedure on correlation structures generated from graph structures (as described in Section 6.2). These simulations enable further investigations into the performance of `SLIPT` in the context of more complex correlation structures. The simulation of `expression` from `network` structures is widely applicable to simulating pathway `expression` data and as such the `graphsim` R package has been released (as described in Section 3.5).

These investigations show that `SLIPT` performs robustly across datasets with different correlation structures, including those derived from `graphs` with the complexity of biological pathways. The `SLIPT` methodology was able to detect `synthetic lethal` genes within `synthetic lethal` pathways across many `graph` structures. This methodology performed particularly well with `synthetic lethal` pathways in the context of a larger dataset with a high specificity which supports `SLIPT` as a stringent approach to `synthetic lethal` detection in highly dimensional `gene expression` data. Together these results support the use of `SLIPT` in biological gene expression data since it is able to detect `synthetic lethal` genes in highly complex correlation structures.

Similarly, the inclusion of inhibitory relationships in `graph` structures was shown to increase the performance in simple networks supporting `SLIPT` being applicable to biological data in which these relationships are common. While these results were not replicated in more complex inhibitory `graph` structures, this is likely an artifact of the simulation procedure (which randomly selects `synthetic lethal` genes) generating biologically implausible combinations of `synthetic lethal` genes which are difficult to detect. When the test statistics in simulations with a `synthetic lethal` gene were examined in more detail, the test statistics of the `synthetic lethal` gene were consistently higher and distinguishable from nearby genes in the `graph` structure. In contrast to previous concerns with inhibiting relationships, these differences were more pronounced with genes which had inhibitory relationships with `synthetic lethal` genes. While distinguishable from nearby genes in a `pathway` structure, the genes correlated with `synthetic lethal` still had higher test statistics than more distant genes (similar to observations with correlated genes in Section 3.3).

In addition to being able to detect **synthetic lethal** genes in a pathway, the proximal genes in a pathway are most likely to be false positives and therefore **SLIPT** is also able to detect **synthetic lethal** pathways. Therefore **SLIPT** identifies genes which are likely to be constituent of a **synthetic lethal** pathway and is more likely to rank underlying **synthetic lethal** genes with greater significance. Together these findings support the use of **SLIPT** throughout this thesis, further application of **SLIPT**, and further development of such strategies for **synthetic lethal** detection. Similarly, the simulation procedures developed and demonstrated for examining **synthetic lethal** detection in **expression** data using **graph** structures is amenable to further development and investigations into **pathway** structure in **expression** data such as predicting biological pathways from **expression** data or the impact of pathways on differential **expression** analyses.

6.5 Summary

A statistical model and simulation procedure has been developed to test the performance of the **SLIPT** methodology in controlled conditions, using multivariate normal distributions. This simulation procedure has been developed into a computational pipeline which was able to test the statistical performance (using stringent assumptions) of **SLIPT** across many parameters and compare it to alternative **synthetic lethal** detection strategies. The **SLIPT** methodology performs well at detecting small numbers of **synthetic lethal** genes in simple systems. It does not perform as well in more complex systems but neither do alternative strategies. The **SLIPT** methodology performs well compared to Pearson correlation and similar methods based on the χ^2 test. Thus **SLIPT** is an effective detection method for **synthetic lethal** relationships in **expression** data despite its relatively simple design.

Simulations of more complex datasets, including large numbers of genes, complex correlation structure derived from **graph** structures, and correlations with the query gene. **SLIPT** performs robustly across these, including correlation structures based on complex biological pathways. The performance of **SLIPT** improves in larger datasets, datasets with positive correlations with the query genes, and some **graph** structures which include inhibiting relationships, namely those datasets more representative of **gene expression** in biological data. **SLIPT** was both capable of recurrently detecting genes within a **synthetic lethal** pathway and distinguishing **synthetic lethal** genes from correlated with them, even in highly complex correlation structures. Therefore **SLIPT** is a stringent **synthetic lethal** detection strategy and is applicable to **gene expression**

as previously demonstrated for the partners of *CDH1* in breast and stomach cancer in this thesis.

Chapter 7

Discussion

This thesis combines analysis of gene expression data from TCGA with experimental screening results (Telford *et al.*, 2015) to demonstrate synthetic lethal discovery for partners of *CDH1*. Together these findings further elucidate the functions of *CDH1* in the cell, functional redundancy in cancer, and represent potential targets against loss of *CDH1* function. These candidate synthetic lethal genes were further investigated for relationships within synthetic lethal pathways, developing a network-based approach to comparing genes identified in genomics experiments and analyses in the process.

The synthetic lethal detection methodology, SLIPT, was applied to gene expression data throughout this thesis was evaluated with simulated data. A simulation procedure was developed to stringently generate gene expression data from known synthetic lethal partners in simulated data. These simulations included simple and complex correlation structures and modelling synthetic lethal genes within pathways. Together, these results demonstrate SLIPT as a robust widely applicable gene expression analysis procedure (for which an R package has been released) for discovery of synthetic lethal partner genes. Performance of SLIPT on simulated data also highlights the strengths of the procedure and future directions to improve upon it.

7.1 Synthetic Lethality and *CDH1* Biology

The *CDH1* tumour suppressor gene was the focus of identifying synthetic lethal partners to demonstrate the novel SLIPT methodology. This gene is important in sporadic breast and stomach cancers, in addition to familial syndromes, such as HDGC. The analysis of synthetic lethal partners of *CDH1* in breast and stomach cancers was enabled by the availability of molecular data (Bass *et al.*, 2014; TCGA, 2012) and a

synthetic lethal screen conducted in MCF10A cell line breast cells (Chen *et al.*, 2014; Telford *et al.*, 2015).

Synthetic lethal interactions arise due to functional redundancy (Boone *et al.*, 2007; Fece de la Cruz *et al.*, 2015; Kaelin, Jr, 2005) and as such the synthetic lethal partners of *CDH1* indicates the wide-ranging biological functions that E-cadherin is involved in. The diverse synthetic lethal pathways identified supports the known pleiotropic nature of the *CDH1* gene by detecting established functions of *CDH1*, replicating candidates from an experimental screen (Telford *et al.*, 2015), and identifying novel interactions with candidate genes and pathways for further investigation. The highly pleiotropic functions of E-cadherin was also consistent with *CDH1* being a tumour suppressor gene.

7.1.1 Established Functions of *CDH1*

The *CDH1* has established functions in cell-cell communication and maintaining the cytoskeleton, specifically with cell-cell adhesion by forming tight junctions and the adherens complex. More recently, additional functions of *CDH1* in the extracellular matrix and fibrin clotting have also been identified. Synthetic lethal interactions within biological pathways (i.e., partners in the same pathway as the query gene) are expected according to previous synthetic lethal experiments (Boone *et al.*, 2007; Kelley and Ideker, 2005). Synthetic lethal interactions identified in these pathways are consistent with these being functions of *CDH1*, in addition to potentially actionable targets against cancers.

7.1.2 The Molecular Role of *CDH1* in Cancer

The involvement of *CDH1* in the extracellular matrix is important in cancers as it indicates a mechanism by which *CDH1* loss may affect the tumour microenvironment, contributing to its role as a tumour and invasion suppressor. Furthermore, perturbations in the extracellular matrix and tumour microenvironment present a means by which to specifically inhibit (cancerous) *CDH1*-deficient cells, in addition to those currently being considered. These may be further supported in further investigations with 3D cell culture, “organoid”, or mouse xenograft cancer models.

In contrast, many of the pathways involved in cell signalling, including GPCRs, were identified by SLIPT in addition to the experimental screen (Telford *et al.*, 2015). These support the previous results in cell line models, that these pathways are essential to growth of *CDH1*-deficient cancers and present a potential vulnerability specific to these (cancerous) cells. Furthermore, the replication of synthetic lethality of *CDH1*

with cell signalling pathways in TCGA data across cancer types and genetic backgrounds robustly supports these pathways being clinically applicable beyond the genetic background of the model system of *CDH1*^{-/-} MCF10A cell line cells (Chen *et al.*, 2014). While the specific synthetic lethal genes were not as consistently detected between the SLIPT analyses and siRNA screen (Telford *et al.*, 2015), they were sufficient to identify synthetic lethal pathways for further experimental investigation, which are more likely to be replicated between genetic backgrounds (Dixon *et al.*, 2008). Together these results demonstrate how SLIPT can be integrated with an experimental screen to triage potential therapeutic targets for further pre-clinical investigation.

The analysis of expression data with SLIPT is also indicative of additional biological mechanisms of synthetic lethality in pathways beyond those identified in screening experiments (Telford *et al.*, 2015). In particular, translation and regulatory pathways, involving 3' UTRs and NMD, were identified as candidate synthetic lethal pathways with *CDH1* by SLIPT. These pathways represent downstream targets regulated by the putative synthetic lethal signalling pathways which cancer cells are dependent on for sustained protein expression to proliferate and evade host defense processes such as apoptosis and immune responses (Gao and Roux, 2015) .

7.2 Significance

7.2.1 Synthetic Lethality in the Genomic Era

Development of an effective synthetic lethal discovery tool for bioinformatic analysis has a wide range of applications in genetics research including functional genomics, medical and agricultural applications. The SLIPT approach demonstrated in this thesis is widely applicable to other genes and biological questions. In addition to further query of cancer genes, including other tissues, synthetic lethal gene functions are also of wider interest for their implications for genetic redundancy. Highly redundant genes, and the genetically robust systems they give rise to, are of further relevance to evolutionary, developmental, and systems biology to understand how these change over time and play a role in fundamental development of cell types, in addition to cancers (Boone *et al.*, 2007; Nowak *et al.*, 1997; Tischler *et al.*, 2008).

Developmental genes in particular, are highly evolutionary conserved and subject to high rates of redundancy (Fromental-Ramain *et al.*, 1996; Kockel *et al.*, 1997; Nowak *et al.*, 1997). These are often difficult to study with conventional functional genetics since individual knockouts of redundant genes do not necessarily have a mutant pheno-

type. Identifying genes with a common function is therefore also important to the study of developmental genes with unknown functions. Synthetic lethal discovery methods such as **SLIPT** provide a genomic approach to further systematic characterisation of gene function including such highly redundant developmental genes.

Similarly, variants of unknown significance and modifier loci are a major concern in human genetics, including “monogenic” and “rare” diseases. Many of these could potentially be difficult to characterise individually due to synthetic lethal interactions where additional loci contribute to the disease (or only compensate for some variants). As such systematic identification of synthetic lethal interactions also has applications in the study of such “oligogenic” diseases along with similar applications in the study of heritability for traits including agricultural genomic selection.

Genetic redundancy is also a concern in pharmacology. Polypharmacology and network medicine are rationales to account for this by using drugs with multiple (known and specific) targets (Barabási *et al.*, 2011; Hopkins, 2008). Further characterisation of synthetic lethal genes will be valuable to the design of effective multi-target drugs or combination therapies in a range of therapeutic applications including molecular targeted therapies against cancer for which combination therapies are a popular solution for acquired resistance against individual targeted therapies. Characterisation of genetic interactions and combination therapies also has the potential to expand pharmacogenomic investigations. These may elucidate the impact of genotypes at multiple loci, which lead to adverse effects in a subset of the population due to variants in synthetic lethal genes.

Furthermore, redundant functions and synthetic lethal interactions also present a means to expand upon the concept of the “minimal” genome (Hutchison *et al.*, 2016). It is important to account for essential gene functions that are performed by redundant genes (or in combination with pleiotropic genes), rather than simply those that are perturbed by individual genes. An essential gene approach is likely to produce an underestimate that does not account for synthetic lethal interactions.

Synthetic lethal interactions are fundamentally important throughout genetics. Further understanding of them in a genomic context, facilitated by methods such as **SLIPT**, would contribute towards deeper understanding of gene functions and their role in traits or diseases in the post-genomic era. Genes do not function in isolation and understanding them in the context of the complexity of a cell and across genetic backgrounds is essential to further characterise their functions and ensure that findings can be validated or applied beyond experimental systems.

7.2.2 Clinical Interventions based on Synthetic Lethality

Synthetic lethal discovery with **SLIPT** is of particular interest in cancer research as a complementary approach to discovery of **synthetic lethal** drug targets. The cancer research community relies on cell line and mouse models for screening and validation experiments (Fece de la Cruz *et al.*, 2015) which would benefit from integration with **gene expression** analysis as demonstrated for *CDH1* and the screen conducted by Telford *et al.* (2015). **Synthetic lethal** drug design against cancer **mutations**, including gene loss or over-expression, could lead to a revolution in cancer **therapy** and **chemoprevention**. Such therapeutics would enable personalised **treatment** for cancer patients and high risk individuals. Examples of the **synthetic lethal** strategy (Bryant *et al.*, 2005; Farmer *et al.*, 2005) for cancer **treatment** have been shown to be clinically effective McLachlan *et al.* (2016). Many large-scale **RNAi** screens have been conducted recently, aiming to discover gene function and drug targets for similar application with other cancer genes, including cancers in other tissues (Fece de la Cruz *et al.*, 2015).

While **SLIPT** analysis and **RNAi** screens represent a significant step towards anti-cancer medicines, further validation is required to ensure that the **synthetic lethal** candidate genes and pathways identified for *CDH1* in breast and stomach cancer are applicable against *CDH1*-deficient cancers in the clinic. Validation with **RNAi** or pharmacological inhibitors is needed since false positives may occur in **SLIPT** analysis or **siRNA** screens. These candidates will need to be tested in pre-clinical models (cell lines and mouse xenografts) before proceeding to clinical trials. A therapeutic intervention will also require a **targeted therapeutic** to develop developed or repurposed against the **synthetic lethal** partner. Drug targets could be triaged from **synthetic lethal** genes by functions known to be amenable to drugs or structure with conserved specific sites that are not homologous to other genes, or those with existing drugs approved in trial for other applications. Both structure-aided drug design and compound screening are viable ways to target **synthetic lethal** partners.

Targeted therapeutics designed based on **synthetic lethal** interactions could expand the applications of “precision medicine” against molecular targets. **Synthetic lethality** expands the range of cancer genes which can be (indirectly) targeted to include **tumour suppressor** genes with loss of function, such as *CDH1*. **Oncogenes** with disrupted functions that are over-expressed or highly homologous to non-cancerous **proto-oncogenes**, such as *MYC*, *EGFR* or *KRAS*, may also be targeted by **synthetic lethality**. Applications against **tumour suppressor** genes is particularly important, as these cannot be approached by careful dosing. **Synthetic lethal** drug design has the benefit of being

highly specific against a particular genotype (such as *CDH1*^{-/-}) with the potential for **targeted therapies** with a wide therapeutic index and few adverse effects, in contrast to many current anti-cancer drug regimens (Hopkins, 2008; Kaelin, Jr, 2009). These properties are highly desirable for **chemoprevention** applications, such as **treatment** against *CDH1*-deficient in **HDGC** patients (Guilford *et al.*, 2010), as an alternative to monitoring or surgery.

7.3 Future Directions

While further validation and pre-clinical tested is required to translate the findings for *CDH1* to cancer therapy or prevention, there are also further avenues for research into the detection of **synthetic lethality** in **gene expression** and other **genomics** data. The **SLIPT** methodology is amenable to wider application against a range of genes for which loss of function is deleterious, including other cancer genes in breast cancer or other tissues. **Synthetic lethal** interactions are functionally informative, particularly for mode-of-action of known drug targets, and are also relevant for identifying functions of newly characterised genes in **genomics** studies and designing specific interventions against cells with loss of function in cancer and other diseases. Thus **synthetic lethal** detection using **SLIPT** in **expression** data could be further used for many other genes, including others relevant to human health and disease.

These investigations do not need to limited to **expression** data. While **expression** as a measure of gene function has been the focus of this thesis, other **genomics** data could be used for a similar purpose for **SLIPT** analysis. These include **DNA copy number**, **DNA** methylation, histone activation, **mutation** status, protein abundance, and protein activation state. For some applications or genes these molecular profiles may be more informative of gene function and **synthetic lethal** relationships. However, **expression** was the focus of the investigations thus far as a widely accepted measure of gene function which has widely available **genomics** data. **SLIPT** is compatible with each of these data types (if the thresholds are selected appropriately) and may perform better for some applications with these molecular profiles or a weighted combination of these. As demonstrated, **SLIPT** is also suitable for future investigations with pathway **metagenes** and other summary data as well.

It may also be possible to improve the performance of **SLIPT** with refinements to the statistical or computational approach. This thesis has focused on rational query-based approach which computes relatively quickly, even in R (**R Core Team**, 2016), and is relatively intuitive to interpret. These computations are compatible with parallel

computing and the computational resources may be further reduced by using a different computing language. The `slipt` R package has been documented and released open-source (as described in Section 3.5) to facilitate further development, wider adoption, or comparison with other scientific software for similar purposes.

Alternative methods may be also be able to improve on the statistical performance of **SLIPT**. In particular, the sensitivity was generally an issue with higher numbers of synthetic lethal partners in simulated data. While approaches using continuous data such as Pearson correlation and linear regression did not perform as well as **SLIPT**, they could be improved. A least squares regression approach in particular, enables multiple measures of relationships such as the coefficients of the fitted curve and significance of the fit (computed from the residuals). A linear modelling approach using regression is also amenable to refinement such as extending from fitting a linear relationships to a polynomial or logistic regression. Another benefit to fitting linear models is that these would enable the conditioning of known synthetic lethal partners to identify subtle signatures of further interacting partners.

This approach could also be applied iteratively on the strongest candidates from previous synthetic lethal analyses in further rounds of prediction conditioned upon them. Similarly, synthetic lethal prediction could also be approached with a Bayesian framework which is also amenable to Bayesian priors on known or previously predicted synthetic lethal partners. Either of these approaches has the potential to improve upon the synthetic lethal predictions which have been demonstrated as possible and biologically relevant by **SLIPT**.

7.4 Conclusions

Synthetic lethal interactions are important for understanding gene function and development of highly specific targeted anti-cancer treatments. Synthetic lethality could expand the repertoire of applications for precision cancer medicine to indirectly targeting loss of function in [tumour suppressor](#) genes. Synthetic lethal discovery with experimental screening is error prone and limited by the model systems in which it is performed. There is a need for [bioinformatics](#) tool to predict synthetic lethal interactions from [gene expression](#) data facilitates rapid identification of synthetic lethal candidates to augment functional genetic screens and cancer drug target triage. I present the original [Synthetic Lethal Interaction Prediction Tool \(SLIPT\)](#) methodology as a statically robust procedure which performs this analysis.

The [SLIPT](#) methodology has been demonstrated to identify biologically relevant genes and pathways. An comprehensive analysis of synthetic lethal partners of the *CDH1* was performed in [TCGA](#) breast cancer data ([TCGA](#), 2012) with many of these findings replicated in stomach cancer data ([Bass et al.](#), 2014). These genes clustered into several distinct groups, with distinct biological functions and elevated [expression](#) in different clinical subtypes. These analyses identified of synthetic lethal candidates in the *G_{αi}* signalling, cytoplasmic microfibres, and extracellular fibrin clotting pathways which were validated in an [siRNA](#) screen performed by [Telford et al.](#) (2015) and consistent with the known cytoskeletal and cell signalling roles of [E-cadherin](#). These findings support interventions against these pathways being applicable to specific cancer therapeutics beyond the pre-clinical cell line models in which they were validated. [SLIPT](#) has also identified synthetic lethal partners in novel pathways for *CDH1* including the regulation of immune signalling and translational elongation which extend the range of pleiotropic functions of *CDH1* and present further biological mechanisms to investigate the malignancy and vulnerabilities of *CDH1*-deficient cancers.

While some of these pathways are not expected to be detected in an isolated experimental cell line model, [pathway](#) structure may have accounted for this disparity. Thus synthetic lethal candidates detected by [SLIPT](#) and [siRNA](#) were compared within graph structures of the candidate synthetic lethal pathways. However, this did not generally account for differences between detection by these approaches. Neither synthetic lethal detection methodology preferentially detected genes of more importance or connectivity in [pathway](#) structures using established network metrics. Nor could it

be generally established that **SLIPT** gene candidates were upstream or downstream of **siRNA** gene candidates in **pathway** structures across biological pathways.

Pathway **graph** structures were also included in investigations with simulated data to ascertain whether the **SLIPT** procedure performed desirably in data with complex correlation structures derived based on biological pathways. A simulation procedure was developed based on a statistical model of **synthetic lethality** which generates multivariate normal data with known **synthetic lethal** partners and correlation structures. The **SLIPT** methodology had high statistical performance, particularly when detecting few **synthetic lethal** genes, with large sample sizes, and a background of many non **synthetic lethal** genes to distinguish true partners from. This method had high specificity, performed better than Pearson's correlation or the χ^2 -test, and had had optimal performance across simulation parameter combinations for the thresholds used throughout this thesis. These findings were robust across correlation structures, including those derived from complex **pathway** structures containing strong positive and negative correlations between genes. Together these findings support the release of the **SLIPT** software R packages and the application of the method to identify **synthetic lethal** genes within pathways and use candidate **synthetic lethal** genes to identify **synthetic lethal** pathways as demonstrated in this thesis.

Therefore, I present a widely applicable **synthetic lethal** procedure using **gene expression** data for wider use in **genomics** research, including the development of precision cancer medicine. This methodology is supported by the release of a software package in R, simulation results based on a statistical model of **synthetic lethality**, the demonstration of **bioinformatics** and network biology investigations into interactions with the *CDH1* gene in breast and stomach cancers.

Bibliography

- Aarts, M., Bajrami, I., Herrera-Abreu, M.T., Elliott, R., Brough, R., Ashworth, A., Lord, C.J., and Turner, N.C. (2015) Functional genetic screen identifies increased sensitivity to wee1 inhibition in cells with defects in fanconi anemia and hr pathways. *Mol Cancer Ther*, **14**(4): 865–76.
- Abeshouse, A., Ahn, J., Akbani, R., Ally, A., Amin, S., Andry, C.D., Annala, M., Aprikian, A., Armenia, J., Arora, A., *et al.* (2015) The Molecular Taxonomy of Primary Prostate Cancer. *Cell*, **163**(4): 1011–1025.
- Adler, D. (2005) *vioplot: Violin plot*. R package version 0.2.
- Akbani, R., Akdemir, K.C., Aksoy, B.A., Albert, M., Ally, A., Amin, S.B., Arachchi, H., Arora, A., Auman, J.T., Ayala, B., *et al.* (2015) Genomic Classification of Cutaneous Melanoma. *Cell*, **161**(7): 1681–1696.
- Akobeng, A.K. (2007) Understanding diagnostic tests 3: receiver operating characteristic curves. *Acta Paediatrica*, **96**(5): 644–647.
- American Cancer Society (2017) Genetics and cancer. <https://www.cancer.org/cancer/cancer-causes/genetics.html>. Accessed: 22/03/2017.
- Anjomshoaa, A., Lin, Y.H., Black, M.A., McCall, J.L., Humar, B., Song, S., Fukuzawa, R., Yoon, H.S., Holzmann, B., Friederichs, J., *et al.* (2008) Reduced expression of a gene proliferation signature is associated with enhanced malignancy in colon cancer. *Br J Cancer*, **99**(6): 966–973.
- Araki, H., Knapp, C., Tsai, P., and Print, C. (2012) GeneSetDB: A comprehensive meta-database, statistical and visualisation framework for gene set analysis. *FEBS Open Bio*, **2**: 76–82.

- Ashburner, M., Ball, C.A., Blake, J.A., Botstein, D., Butler, H., Cherry, J.M., Davis, A.P., Dolinski, K., Dwight, S.S., Eppig, J.T., *et al.* (2000) Gene ontology: tool for the unification of biology. The Gene Ontology Consortium. *Nat Genet*, **25**(1): 25–29.
- Ashworth, A. (2008) A synthetic lethal therapeutic approach: poly(adp) ribose polymerase inhibitors for the treatment of cancers deficient in dna double-strand break repair. *J Clin Oncol*, **26**(22): 3785–90.
- Audeh, M.W., Carmichael, J., Penson, R.T., Friedlander, M., Powell, B., Bell-McGuinn, K.M., Scott, C., Weitzel, J.N., Oaknin, A., Loman, N., *et al.* (2010) Oral poly(adp-ribose) polymerase inhibitor olaparib in patients with *BRCA1* or *BRCA2* mutations and recurrent ovarian cancer: a proof-of-concept trial. *Lancet*, **376**(9737): 245–51.
- Babyak, M.A. (2004) What you see may not be what you get: a brief, nontechnical introduction to overfitting in regression-type models. *Psychosom Med*, **66**(3): 411–21.
- Bamford, S., Dawson, E., Forbes, S., Clements, J., Pettett, R., Dogan, A., Flanagan, A., Teague, J., Futreal, P.A., Stratton, M.R., *et al.* (2004) The COSMIC (Catalogue of Somatic Mutations in Cancer) database and website. *Br J Cancer*, **91**(2): 355–358.
- Barabási, A.L. and Albert, R. (1999) Emergence of scaling in random networks. *Science*, **286**(5439): 509–12.
- Barabási, A.L., Gulbahce, N., and Loscalzo, J. (2011) Network medicine: a network-based approach to human disease. *Nat Rev Genet*, **12**(1): 56–68.
- Barabási, A.L. and Oltvai, Z.N. (2004) Network biology: understanding the cell's functional organization. *Nat Rev Genet*, **5**(2): 101–13.
- Barrat, A. and Weigt, M. (2000) On the properties of small-world network models. *The European Physical Journal B - Condensed Matter and Complex Systems*, **13**(3): 547–560.
- Barretina, J., Caponigro, G., Stransky, N., Venkatesan, K., Margolin, A.A., Kim, S., Wilson, C.J., Lehar, J., Kryukov, G.V., Sonkin, D., *et al.* (2012) The Cancer Cell Line Encyclopedia enables predictive modelling of anticancer drug sensitivity. *Nature*, **483**(7391): 603–607.

Barry, W.T. (2016) *safe: Significance Analysis of Function and Expression*. R package version 3.14.0.

Baryshnikova, A., Costanzo, M., Dixon, S., Vizeacoumar, F.J., Myers, C.L., Andrews, B., and Boone, C. (2010a) Synthetic genetic array (sga) analysis in *saccharomyces cerevisiae* and *schizosaccharomyces pombe*. *Methods Enzymol*, **470**: 145–79.

Baryshnikova, A., Costanzo, M., Kim, Y., Ding, H., Koh, J., Toufighi, K., Youn, J.Y., Ou, J., San Luis, B.J., Bandyopadhyay, S., *et al.* (2010b) Quantitative analysis of fitness and genetic interactions in yeast on a genome scale. *Nat Meth*, **7**(12): 1017–1024.

Bass, A.J., Thorsson, V., Shmulevich, I., Reynolds, S.M., Miller, M., Bernard, B., Hinoue, T., Laird, P.W., Curtis, C., Shen, H., *et al.* (2014) Comprehensive molecular characterization of gastric adenocarcinoma. *Nature*, **513**(7517): 202–209.

Bates, D. and Maechler, M. (2016) *Matrix: Sparse and Dense Matrix Classes and Methods*. R package version 1.2-7.1.

Bateson, W. and Mendel, G. (1909) *Mendel's principles of heredity, by W. Bateson*. University Press, Cambridge [Eng.].

Becker, K.F., Atkinson, M.J., Reich, U., Becker, I., Nekarda, H., Siewert, J.R., and Höfler, H. (1994) E-cadherin gene mutations provide clues to diffuse type gastric carcinomas. *Cancer Research*, **54**(14): 3845–3852.

Bell, D., Berchuck, A., Birrer, M., Chien, J., Cramer, D., Dao, F., Dhir, R., DiSaia, P., Gabra, H., Glenn, P., *et al.* (2011) Integrated genomic analyses of ovarian carcinoma. *Nature*, **474**(7353): 609–615.

Benjamini, Y. and Hochberg, Y. (1995) Controlling the false discovery rate: A practical and powerful approach to multiple testing. *Journal of the Royal Statistical Society Series B (Methodological)*, **57**(1): 289–300.

Berx, G., Cleton-Jansen, A.M., Nollet, F., de Leeuw, W.J., van de Vijver, M., Cornelisse, C., and van Roy, F. (1995) E-cadherin is a tumour/invasion suppressor gene mutated in human lobular breast cancers. *EMBO J*, **14**(24): 6107–15.

Berx, G., Cleton-Jansen, A.M., Strumane, K., de Leeuw, W.J., Nollet, F., van Roy, F., and Cornelisse, C. (1996) E-cadherin is inactivated in a majority of invasive human

- lobular breast cancers by truncation mutations throughout its extracellular domain. *Oncogene*, **13**(9): 1919–25.
- Berx, G. and van Roy, F. (2009) Involvement of members of the cadherin superfamily in cancer. *Cold Spring Harb Perspect Biol*, **1**: a003129.
- Bitler, B.G., Aird, K.M., Garipov, A., Li, H., Amatangelo, M., Kossenkov, A.V., Schultz, D.C., Liu, Q., Shih Ie, M., Conejo-Garcia, J.R., *et al.* (2015) Synthetic lethality by targeting ezh2 methyltransferase activity in arid1a-mutated cancers. *Nat Med*, **21**(3): 231–8.
- Blake, J.A., Christie, K.R., Dolan, M.E., Drabkin, H.J., Hill, D.P., Ni, L., Sitnikov, D., Burgess, S., Buza, T., Gresham, C., *et al.* (2015) Gene Ontology Consortium: going forward. *Nucleic Acids Res*, **43**(Database issue): D1049–1056.
- Boettcher, M., Lawson, A., Ladenburger, V., Fredebohm, J., Wolf, J., Hoheisel, J.D., Frezza, C., and Shlomi, T. (2014) High throughput synthetic lethality screen reveals a tumorigenic role of adenylate cyclase in fumarate hydratase-deficient cancer cells. *BMC Genomics*, **15**: 158.
- Boone, C., Bussey, H., and Andrews, B.J. (2007) Exploring genetic interactions and networks with yeast. *Nat Rev Genet*, **8**(6): 437–49.
- Borgatti, S.P. (2005) Centrality and network flow. *Social Networks*, **27**(1): 55 – 71.
- Boucher, B. and Jenna, S. (2013) Genetic interaction networks: better understand to better predict. *Front Genet*, **4**: 290.
- Bozovic-Spasojevic, I., Azambuja, E., McCaskill-Stevens, W., Dinh, P., and Cardoso, F. (2012) Chemoprevention for breast cancer. *Cancer treatment reviews*, **38**(5): 329–339.
- Breiman, L. (2001) Random forests. *Machine Learning*, **45**(1): 5–32.
- Brin, S. and Page, L. (1998) The anatomy of a large-scale hypertextual web search engine. *Computer Networks and ISDN Systems*, **30**(1): 107 – 117.
- Broulxhon, S.M., Kyrkanides, S., Teng, X., Athar, M., Ghazizadeh, S., Simon, M., O'Banion, M.K., and Ma, L. (2014) Soluble E-cadherin: a critical oncogene modulating receptor tyrosine kinases, MAPK and PI3K/Akt/mTOR signaling. *Oncogene*, **33**(2): 225–235.

- Bryant, H.E., Schultz, N., Thomas, H.D., Parker, K.M., Flower, D., Lopez, E., Kyle, S., Meuth, M., Curtin, N.J., and Helleday, T. (2005) Specific killing of *BRCA2*-deficient tumours with inhibitors of polyadribose polymerase. *Nature*, **434**(7035): 913–7.
- Bussey, H., Andrews, B., and Boone, C. (2006) From worm genetic networks to complex human diseases. *Nat Genet*, **38**(8): 862–3.
- Butland, G., Babu, M., Diaz-Mejia, J.J., Bohdana, F., Phanse, S., Gold, B., Yang, W., Li, J., Gagarinova, A.G., Pogoutse, O., *et al.* (2008) esga: *E. coli* synthetic genetic array analysis. *Nat Methods*, **5**(9): 789–95.
- cBioPortal for Cancer Genomics (cBioPortal) (2017) cBioPortal for Cancer Genomics. <http://www.cbioportal.org/>. Accessed: 26/03/2017.
- Cerami, E.G., Gross, B.E., Demir, E., Rodchenkov, I., Babur, O., Anwar, N., Schultz, N., Bader, G.D., and Sander, C. (2011) Pathway Commons, a web resource for biological pathway data. *Nucleic Acids Res*, **39**(Database issue): D685–690.
- Chen, A., Beetham, H., Black, M.A., Priya, R., Telford, B.J., Guest, J., Wiggins, G.A.R., Godwin, T.D., Yap, A.S., and Guilford, P.J. (2014) E-cadherin loss alters cytoskeletal organization and adhesion in non-malignant breast cells but is insufficient to induce an epithelial-mesenchymal transition. *BMC Cancer*, **14**(1): 552.
- Chen, S. and Parmigiani, G. (2007) Meta-analysis of BRCA1 and BRCA2 penetrance. *J Clin Oncol*, **25**(11): 1329–1333.
- Chen, X. and Tompa, M. (2010) Comparative assessment of methods for aligning multiple genome sequences. *Nat Biotechnol*, **28**(6): 567–572.
- Chipman, K. and Singh, A. (2009) Predicting genetic interactions with random walks on biological networks. *BMC Bioinformatics*, **10**(1): 17.
- Christofori, G. and Semb, H. (1999) The role of the cell-adhesion molecule E-cadherin as a tumour-suppressor gene. *Trends in Biochemical Sciences*, **24**(2): 73 – 76.
- Ciriello, G., Gatza, M.L., Beck, A.H., Wilkerson, M.D., Rhie, S.K., Pastore, A., Zhang, H., McLellan, M., Yau, C., Kandoth, C., *et al.* (2015) Comprehensive Molecular Portraits of Invasive Lobular Breast Cancer. *Cell*, **163**(2): 506–519.

- Clark, M.J. (2004) Endogenous Regulator of G Protein Signaling Proteins Suppress G_o-Dependent -Opioid Agonist-Mediated Adenylyl Cyclase Supersensitization. *Journal of Pharmacology and Experimental Therapeutics*, **310**(1): 215–222.
- Clough, E. and Barrett, T. (2016) The Gene Expression Omnibus Database. *Methods Mol Biol*, **1418**: 93–110.
- Collingridge, D.S. (2013) A primer on quantitized data analysis and permutation testing. *Journal of Mixed Methods Research*, **7**(1): 81–97.
- Collins, F.S. and Barker, A.D. (2007) Mapping the cancer genome. Pinpointing the genes involved in cancer will help chart a new course across the complex landscape of human malignancies. *Sci Am*, **296**(3): 50–57.
- Collisson, E., Campbell, J., Brooks, A., Berger, A., Lee, W., Chmielecki, J., Beer, D., Cope, L., Creighton, C., Danilova, L., et al. (2014) Comprehensive molecular profiling of lung adenocarcinoma. *Nature*, **511**(7511): 543–550.
- Corcoran, R.B., Ebi, H., Turke, A.B., Coffee, E.M., Nishino, M., Cogdill, A.P., Brown, R.D., Della Pelle, P., Dias-Santagata, D., Hung, K.E., et al. (2012) Egfr-mediated reactivation of mapk signaling contributes to insensitivity of BRAF-mutant colorectal cancers to raf inhibition with vemurafenib. *Cancer Discovery*, **2**(3): 227–235.
- Costanzo, M., Baryshnikova, A., Bellay, J., Kim, Y., Spear, E.D., Sevier, C.S., Ding, H., Koh, J.L., Toufighi, K., Mostafavi, S., et al. (2010) The genetic landscape of a cell. *Science*, **327**(5964): 425–31.
- Costanzo, M., Baryshnikova, A., Myers, C.L., Andrews, B., and Boone, C. (2011) Charting the genetic interaction map of a cell. *Curr Opin Biotechnol*, **22**(1): 66–74.
- Courtney, K.D., Corcoran, R.B., and Engelman, J.A. (2010) The PI3K pathway as drug target in human cancer. *J Clin Oncol*, **28**(6): 1075–1083.
- Creighton, C.J., Morgan, M., Gunaratne, P.H., Wheeler, D.A., Gibbs, R.A., Robertson, A., Chu, A., Beroukhim, R., Cibulskis, K., Signoretti, S., et al. (2013) Comprehensive molecular characterization of clear cell renal cell carcinoma. *Nature*, **499**(7456): 43–49.
- Croft, D., Mundo, A.F., Haw, R., Milacic, M., Weiser, J., Wu, G., Caudy, M., Garapati, P., Gillespie, M., Kamdar, M.R., et al. (2014) The Reactome pathway knowledgebase. *Nucleic Acids Res*, **42**(database issue): D472–D477.

- Crunkhorn, S. (2014) Cancer: Predicting synthetic lethal interactions. *Nat Rev Drug Discov*, **13**(11): 812.
- Csardi, G. and Nepusz, T. (2006) The igraph software package for complex network research. *InterJournal, Complex Systems*: 1695.
- Dai, X., Li, T., Bai, Z., Yang, Y., Liu, X., Zhan, J., and Shi, B. (2015) Breast cancer intrinsic subtype classification, clinical use and future trends. *Am J Cancer Res*, **5**(10): 2929–2943.
- Davierwala, A.P., Haynes, J., Li, Z., Brost, R.L., Robinson, M.D., Yu, L., Mnaimneh, S., Ding, H., Zhu, H., Chen, Y., *et al.* (2005) The synthetic genetic interaction spectrum of essential genes. *Nat Genet*, **37**(10): 1147–1152.
- De Leeuw, W.J., Berx, G., Vos, C.B., Peterse, J.L., Van de Vijver, M.J., Litvinov, S., Van Roy, F., Cornelisse, C.J., and Cleton-Jansen, A.M. (1997) Simultaneous loss of E-cadherin and catenins in invasive lobular breast cancer and lobular carcinoma in situ. *J Pathol*, **183**(4): 404–11.
- De Santis, G., Miotti, S., Mazzi, M., Canevari, S., and Tomassetti, A. (2009) E-cadherin directly contributes to PI3K/AKT activation by engaging the PI3K-p85 regulatory subunit to adherens junctions of ovarian carcinoma cells. *Oncogene*, **28**(9): 1206–1217.
- Demir, E., Babur, O., Rodchenkov, I., Aksoy, B.A., Fukuda, K.I., Gross, B., Sumer, O.S., Bader, G.D., and Sander, C. (2013) Using biological pathway data with Paxtools. *PLoS Comput Biol*, **9**(9): e1003194.
- Deshpande, R., Asiedu, M.K., Klebig, M., Sutor, S., Kuzmin, E., Nelson, J., Piotrowski, J., Shin, S.H., Yoshida, M., Costanzo, M., *et al.* (2013) A comparative genomic approach for identifying synthetic lethal interactions in human cancer. *Cancer Res*, **73**(20): 6128–36.
- Dickson, D. (1999) Wellcome funds cancer database. *Nature*, **401**(6755): 729.
- Dienstmann, R. and Tabernero, J. (2011) BRAF as a target for cancer therapy. *Anti-cancer Agents Med Chem*, **11**(3): 285–95.
- Dijkstra, E.W. (1959) A note on two problems in connexion with graphs. *Numerische Mathematik*, **1**(1): 269–271.

- Dixon, S.J., Andrews, B.J., and Boone, C. (2009) Exploring the conservation of synthetic lethal genetic interaction networks. *Commun Integr Biol*, **2**(2): 78–81.
- Dixon, S.J., Fedyshyn, Y., Koh, J.L., Prasad, T.S., Chahwan, C., Chua, G., Toufighi, K., Baryshnikova, A., Hayles, J., Hoe, K.L., et al. (2008) Significant conservation of synthetic lethal genetic interaction networks between distantly related eukaryotes. *Proc Natl Acad Sci U S A*, **105**(43): 16653–8.
- Dong, L.L., Liu, L., Ma, C.H., Li, J.S., Du, C., Xu, S., Han, L.H., Li, L., and Wang, X.W. (2012) E-cadherin promotes proliferation of human ovarian cancer cells in vitro via activating MEK/ERK pathway. *Acta Pharmacol Sin*, **33**(6): 817–822.
- Dorogovtsev, S.N. and Mendes, J.F. (2003) *Evolution of networks: From biological nets to the Internet and WWW*. Oxford University Press, USA.
- Dorsam, R.T. and Gutkind, J.S. (2007) G-protein-coupled receptors and cancer. *Nat Rev Cancer*, **7**(2): 79–94.
- Erdős, P. and Rényi, A. (1959) On random graphs I. *Publ Math Debrecen*, **6**: 290–297.
- Erdős, P. and Rényi, A. (1960) On the evolution of random graphs. In *Publ. Math. Inst. Hung. Acad. Sci*, volume 5, 17–61.
- Eroles, P., Bosch, A., Perez-Fidalgo, J.A., and Lluch, A. (2012) Molecular biology in breast cancer: intrinsic subtypes and signaling pathways. *Cancer Treat Rev*, **38**(6): 698–707.
- Farmer, H., McCabe, N., Lord, C.J., Tutt, A.N., Johnson, D.A., Richardson, T.B., Santarosa, M., Dillon, K.J., Hickson, I., Knights, C., et al. (2005) Targeting the dna repair defect in BRCA mutant cells as a therapeutic strategy. *Nature*, **434**(7035): 917–21.
- Fawcett, T. (2006) An introduction to ROC analysis. *Pattern Recognition Letters*, **27**(8): 861 – 874. {ROC} Analysis in Pattern Recognition.
- Fece de la Cruz, F., Gapp, B.V., and Nijman, S.M. (2015) Synthetic lethal vulnerabilities of cancer. *Annu Rev Pharmacol Toxicol*, **55**: 513–531.
- Ferlay, J., Soerjomataram, I., Dikshit, R., Eser, S., Mathers, C., Rebelo, M., Parkin, D.M., Forman, D., and Bray, F. (2015) Cancer incidence and mortality worldwide:

sources, methods and major patterns in GLOBOCAN 2012. *Int J Cancer*, **136**(5): E359–386.

Fisher, R.A. (1919) Xv.—the correlation between relatives on the supposition of mendelian inheritance. *Earth and Environmental Science Transactions of the Royal Society of Edinburgh*, **52**(02): 399–433.

Fong, P.C., Boss, D.S., Yap, T.A., Tutt, A., Wu, P., Mergui-Roelvink, M., Mortimer, P., Swaisland, H., Lau, A., O'Connor, M.J., *et al.* (2009) Inhibition of poly(adp-ribose) polymerase in tumors from BRCA mutation carriers. *N Engl J Med*, **361**(2): 123–34.

Fong, P.C., Yap, T.A., Boss, D.S., Carden, C.P., Mergui-Roelvink, M., Gourley, C., De Greve, J., Lubinski, J., Shanley, S., Messiou, C., *et al.* (2010) Poly(adp)-ribose polymerase inhibition: frequent durable responses in BRCA carrier ovarian cancer correlating with platinum-free interval. *J Clin Oncol*, **28**(15): 2512–9.

Forbes, S.A., Beare, D., Gunasekaran, P., Leung, K., Bindal, N., Boutselakis, H., Ding, M., Bamford, S., Cole, C., Ward, S., *et al.* (2015) COSMIC: exploring the world's knowledge of somatic mutations in human cancer. *Nucleic Acids Res*, **43**(Database issue): D805–811.

Fraser, A. (2004) Towards full employment: using RNAi to find roles for the redundant. *Oncogene*, **23**(51): 8346–52.

Fromental-Ramain, C., Warot, X., Lakkaraju, S., Favier, B., Haack, H., Birling, C., Dierich, A., Doll e, P., and Chambon, P. (1996) Specific and redundant functions of the paralogous Hoxa-9 and Hoxd-9 genes in forelimb and axial skeleton patterning. *Development*, **122**(2): 461–472.

Futreal, P.A., Coin, L., Marshall, M., Down, T., Hubbard, T., Wooster, R., Rahman, N., and Stratton, M.R. (2004) A census of human cancer genes. *Nat Rev Cancer*, **4**(3): 177–183.

Futreal, P.A., Kasprzyk, A., Birney, E., Mullikin, J.C., Wooster, R., and Stratton, M.R. (2001) Cancer and genomics. *Nature*, **409**(6822): 850–852.

Gao, B. and Roux, P.P. (2015) Translational control by oncogenic signaling pathways. *Biochimica et Biophysica Acta*, **1849**(7): 753–65.

- Gatza, M.L., Kung, H.N., Blackwell, K.L., Dewhirst, M.W., Marks, J.R., and Chi, J.T. (2011) Analysis of tumor environmental response and oncogenic pathway activation identifies distinct basal and luminal features in HER2-related breast tumor subtypes. *Breast Cancer Res*, **13**(3): R62.
- Gatza, M.L., Lucas, J.E., Barry, W.T., Kim, J.W., Wang, Q., Crawford, M.D., Datto, M.B., Kelley, M., Mathey-Prevot, B., Potti, A., *et al.* (2010) A pathway-based classification of human breast cancer. *Proc Natl Acad Sci USA*, **107**(15): 6994–6999.
- Gatza, M.L., Silva, G.O., Parker, J.S., Fan, C., and Perou, C.M. (2014) An integrated genomics approach identifies drivers of proliferation in luminal-subtype human breast cancer. *Nat Genet*, **46**(10): 1051–1059.
- Gentleman, R.C., Carey, V.J., Bates, D.M., Bolstad, B., Dettling, M., Dudoit, S., Ellis, B., Gautier, L., Ge, Y., Gentry, J., *et al.* (2004) Bioconductor: open software development for computational biology and bioinformatics. *Genome Biol*, **5**(10): R80.
- Genz, A. and Bretz, F. (2009) Computation of multivariate normal and t probabilities. In *Lecture Notes in Statistics*, volume 195. Springer-Verlag, Heidelberg.
- Genz, A., Bretz, F., Miwa, T., Mi, X., Leisch, F., Scheipl, F., and Hothorn, T. (2016) *mvtnorm: Multivariate Normal and t Distributions*. R package version 1.0-5. URL.
- Glaire, M.A., Brown, M., Church, D.N., and Tomlinson, I. (2017) Cancer predisposition syndromes: lessons for truly precision medicine. *J Pathol*, **241**(2): 226–235.
- Globus (Globus) (2017) Research data management simplified. <https://www.globus.org/>. Accessed: 25/03/2017.
- Goodwin, S., McPherson, J.D., and McCombie, W.R. (2016) Coming of age: ten years of next-generation sequencing technologies. *Nat Rev Genet*, **17**(6): 333–351.
- Grady, W.M., Willis, J., Guilford, P.J., Dunbier, A.K., Toro, T.T., Lynch, H., Wiesner, G., Ferguson, K., Eng, C., Park, J.G., *et al.* (2000) Methylation of the CDH1 promoter as the second genetic hit in hereditary diffuse gastric cancer. *Nat Genet*, **26**(1): 16–17.
- Graziano, F., Humar, B., and Guilford, P. (2003) The role of the E-cadherin gene (*CDH1*) in diffuse gastric cancer susceptibility: from the laboratory to clinical practice. *Annals of Oncology*, **14**(12): 1705–1713.

- Güell, O., Sagués, F., and Serrano, M. (2014) Essential plasticity and redundancy of metabolism unveiled by synthetic lethality analysis. *PLoS Comput Biol*, **10**(5): e1003637.
- Guilford, P. (1999) E-cadherin downregulation in cancer: fuel on the fire? *Molecular Medicine Today*, **5**(4): 172 – 177.
- Guilford, P., Hopkins, J., Harraway, J., McLeod, M., McLeod, N., Harawira, P., Taite, H., Scouler, R., Miller, A., and Reeve, A.E. (1998) E-cadherin germline mutations in familial gastric cancer. *Nature*, **392**(6674): 402–5.
- Guilford, P., Humar, B., and Blair, V. (2010) Hereditary diffuse gastric cancer: translation of *CDH1* germline mutations into clinical practice. *Gastric Cancer*, **13**(1): 1–10.
- Guilford, P.J., Hopkins, J.B., Grady, W.M., Markowitz, S.D., Willis, J., Lynch, H., Rajput, A., Wiesner, G.L., Lindor, N.M., Burgart, L.J., *et al.* (1999) E-cadherin germline mutations define an inherited cancer syndrome dominated by diffuse gastric cancer. *Hum Mutat*, **14**(3): 249–55.
- Guo, J., Liu, H., and Zheng, J. (2016) SynLethDB: synthetic lethality database toward discovery of selective and sensitive anticancer drug targets. *Nucleic Acids Res*, **44**(D1): D1011–1017.
- Hajian-Tilaki, K. (2013) Receiver Operating Characteristic (ROC) Curve Analysis for Medical Diagnostic Test Evaluation. *Caspian J Intern Med*, **4**(2): 627–635.
- Hall, M., Frank, E., Holmes, G., Pfahringer, B., Reutemann, P., and Witten, I.H. (2009) The weka data mining software: an update. *SIGKDD Explor Newsl*, **11**(1): 10–18.
- Hamerman, P.S., Lawrence, M.S., Voet, D., Jing, R., Cibulskis, K., Sivachenko, A., Stojanov, P., McKenna, A., Lander, E.S., Gabriel, S., *et al.* (2012) Comprehensive genomic characterization of squamous cell lung cancers. *Nature*, **489**(7417): 519–525.
- Hanahan, D. and Weinberg, R.A. (2000) The hallmarks of cancer. *Cell*, **100**(1): 57–70.
- Hanahan, D. and Weinberg, R.A. (2011) Hallmarks of cancer: the next generation. *Cell*, **144**(5): 646–674.

- Hanna, S. (2003) Cancer incidence in new zealand (2003-2007). In D. Forman, D. Bray F Brewster, C. Gombe Mbalawa, B. Kohler, M. Piñeros, E. Steliarova-Foucher, R. Swaminathan, and J. Ferlay (editors), *Cancer Incidence in Five Continents*, volume X, 902–907. International Agency for Research on Cancer, Lyon, France. Electronic version <http://ci5.iarc.fr> Accessed 22/03/2017.
- Hansford, S., Kaurah, P., Li-Chang, H., Woo, M., Senz, J., Pinheiro, H., Schrader, K.A., Schaeffer, D.F., Shumansky, K., Zogopoulos, G., *et al.* (2015) Hereditary Diffuse Gastric Cancer Syndrome: CDH1 Mutations and Beyond. *JAMA Oncol*, **1**(1): 23–32.
- Heiskanen, M., Bian, X., Swan, D., and Basu, A. (2014) caArray microarray database in the cancer biomedical informatics gridTM (caBIGTM). *Cancer Research*, **67**(9 Supplement): 3712–3712.
- Heiskanen, M.A. and Aittokallio, T. (2012) Mining high-throughput screens for cancer drug targets—lessons from yeast chemical-genomic profiling and synthetic lethality. *Wiley Interdisciplinary Reviews: Data Mining and Knowledge Discovery*, **2**(3): 263–272.
- Hell, P. (1976) Graphs with given neighbourhoods i. problèmes combinatoires at theorie des graphes. *Proc Coll Int CNRS, Orsay*, **260**: 219–223.
- Hillenmeyer, M.E. (2008) The chemical genomic portrait of yeast: uncovering a phenotype for all genes. *Science*, **320**: 362–365.
- Hoadley, K.A., Yau, C., Wolf, D.M., Cherniack, A.D., Tamborero, D., Ng, S., Leiserson, M.D., Niu, B., McLellan, M.D., Uzunangelov, V., *et al.* (2014) Multiplatform analysis of 12 cancer types reveals molecular classification within and across tissues of origin. *Cell*, **158**(4): 929–944.
- Hoehndorf, R., Hardy, N.W., Osumi-Sutherland, D., Tweedie, S., Schofield, P.N., and Gkoutos, G.V. (2013) Systematic analysis of experimental phenotype data reveals gene functions. *PLoS ONE*, **8**(4): e60847.
- Holm, S. (1979) A simple sequentially rejective multiple test procedure. *Scandinavian Journal of Statistics*, **6**(2): 65–70.
- Holme, P. and Kim, B.J. (2002) Growing scale-free networks with tunable clustering. *Physical Review E*, **65**(2): 026107.

- Hopkins, A.L. (2008) Network pharmacology: the next paradigm in drug discovery. *Nat Chem Biol*, **4**(11): 682–690.
- Hu, Z., Fan, C., Oh, D.S., Marron, J.S., He, X., Qaqish, B.F., Livasy, C., Carey, L.A., Reynolds, E., Dressler, L., et al. (2006) The molecular portraits of breast tumors are conserved across microarray platforms. *BMC Genomics*, **7**: 96.
- Huang, E., Cheng, S., Dressman, H., Pittman, J., Tsou, M., Horng, C., Bild, A., Iversen, E., Liao, M., Chen, C., et al. (2003) Gene expression predictors of breast cancer outcomes. *Lancet*, **361**: 1590–1596.
- Hutchison, C.A., Chuang, R.Y., Noskov, V.N., Assad-Garcia, N., Deering, T.J., Ellsman, M.H., Gill, J., Kannan, K., Karas, B.J., Ma, L., et al. (2016) Design and synthesis of a minimal bacterial genome. *Science*, **351**(6280): aad6253.
- International HapMap 3 Consortium (HapMap) (2003) The International HapMap Project. *Nature*, **426**(6968): 789–796.
- Jeanes, A., Gottardi, C.J., and Yap, A.S. (2008) Cadherins and cancer: how does cadherin dysfunction promote tumor progression? *Oncogene*, **27**(55): 6920–6929.
- Jerby-Arnon, L., Pfeffer, N., Waldman, Y., McGarry, L., James, D., Shanks, E., Seashore-Ludlow, B., Weinstock, A., Geiger, T., Clemons, P., et al. (2014) Predicting cancer-specific vulnerability via data-driven detection of synthetic lethality. *Cell*, **158**(5): 1199–1209.
- Joachims, T. (1999) Making large-scale support vector machine learning practical. In S. Bernhard, lkopf, J.C.B. Christopher, and J.S. Alexander (editors), *Advances in kernel methods*, 169–184. MIT Press.
- Ju, Z., Liu, W., Roebuck, P.L., Siwak, D.R., Zhang, N., Lu, Y., Davies, M.A., Akbani, R., Weinstein, J.N., Mills, G.B., et al. (2015) Development of a robust classifier for quality control of reverse-phase protein arrays. *Bioinformatics*, **31**(6): 912.
- Kaelin, Jr, W. (2005) The concept of synthetic lethality in the context of anticancer therapy. *Nat Rev Cancer*, **5**(9): 689–98.
- Kaelin, Jr, W. (2009) Synthetic lethality: a framework for the development of wiser cancer therapeutics. *Genome Med*, **1**: 99.

- Kamada, T. and Kawai, S. (1989) An algorithm for drawing general undirected graphs. *Information Processing Letters*, **31**(1): 7–15.
- Kawai, J., Shinagawa, A., Shibata, K., Yoshino, M., Itoh, M., Ishii, Y., Arakawa, T., Hara, A., Fukunishi, Y., Konno, H., et al. (2001) Functional annotation of a full-length mouse cDNA collection. *Nature*, **409**(6821): 685–690.
- Kelley, R. and Ideker, T. (2005) Systematic interpretation of genetic interactions using protein networks. *Nat Biotech*, **23**(5): 561–566.
- Kelly, S.T. (2013) *Statistical Predictions of Synthetic Lethal Interactions in Cancer*. Dissertation, University of Otago.
- Kelly, S.T., Single, A.B., Telford, B.J., Beetham, H.G., Godwin, T.D., Chen, A., Black, M.A., and Guilford, P.J. (unpublished) Towards HDGC chemoprevention: vulnerabilities in E-cadherin-negative cells identified by genome-wide interrogation of isogenic cell lines and whole tumors. Submitted to *Cancer Prev Res*.
- Kim, N.G., Koh, E., Chen, X., and Gumbiner, B.M. (2011) E-cadherin mediates contact inhibition of proliferation through Hippo signaling-pathway components. *Proc Natl Acad Sci USA*, **108**(29): 11930–11935.
- Kockel, L., Zeitlinger, J., Staszewski, L.M., Mlodzik, M., and Bohmann, D. (1997) Jun in drosophila development: redundant and nonredundant functions and regulation by two mapk signal transduction pathways. *Genes Development*, **11**(13): 1748–1758.
- Kozlov, K.N., Gursky, V.V., Kulakovskiy, I.V., and Samsonova, M.G. (2015) Sequence-based model of gap gene regulation network. *BMC Genomics*, **15**(Suppl 12): S6.
- Kranthi, S., Rao, S., and Manimaran, P. (2013) Identification of synthetic lethal pairs in biological systems through network information centrality. *Mol BioSyst*, **9**(8): 2163–2167.
- Kroepil, F., Fluegen, G., Totikov, Z., Baldus, S.E., Vay, C., Schauer, M., Topp, S.A., Esch, J.S., Knoefel, W.T., and Stoecklein, N.H. (2012) Down-regulation of CDH1 is associated with expression of SNAI1 in colorectal adenomas. *PLoS ONE*, **7**(9): e46665.
- Lander, E.S. (2011) Initial impact of the sequencing of the human genome. *Nature*, **470**(7333): 187–197.

- Lander, E.S., Linton, L.M., Birren, B., Nusbaum, C., Zody, M.C., Baldwin, J., Devon, K., Dewar, K., Doyle, M., FitzHugh, W., *et al.* (2001) Initial sequencing and analysis of the human genome. *Nature*, **409**(6822): 860–921.
- Langmead, B., Trapnell, C., Pop, M., and Salzberg, S.L. (2009) Ultrafast and memory-efficient alignment of short DNA sequences to the human genome. *Genome Biol*, **10**(3): R25.
- Latora, V. and Marchiori, M. (2001) Efficient behavior of small-world networks. *Phys Rev Lett*, **87**: 198701.
- Laufer, C., Fischer, B., Billmann, M., Huber, W., and Boutros, M. (2013) Mapping genetic interactions in human cancer cells with RNAi and multiparametric phenotyping. *Nat Methods*, **10**(5): 427–31.
- Law, C.W., Chen, Y., Shi, W., and Smyth, G.K. (2014) voom: precision weights unlock linear model analysis tools for RNA-seq read counts. *Genome Biol*, **15**(2): R29.
- Le Meur, N. and Gentleman, R. (2008) Modeling synthetic lethality. *Genome Biol*, **9**(9): R135.
- Le Meur, N., Jiang, Z., Liu, T., Mar, J., and Gentleman, R.C. (2014) Slgi: Synthetic lethal genetic interaction. r package version 1.26.0.
- Lee, A.Y., Perreault, R., Harel, S., Boulier, E.L., Suderman, M., Hallett, M., and Jenna, S. (2010a) Searching for signaling balance through the identification of genetic interactors of the rab guanine-nucleotide dissociation inhibitor gdi-1. *PLoS ONE*, **5**(5): e10624.
- Lee, I., Lehner, B., Vavouri, T., Shin, J., Fraser, A.G., and Marcotte, E.M. (2010b) Predicting genetic modifier loci using functional gene networks. *Genome Research*, **20**(8): 1143–1153.
- Lee, I. and Marcotte, E.M. (2009) Effects of functional bias on supervised learning of a gene network model. *Methods Mol Biol*, **541**: 463–75.
- Lee, M.J., Ye, A.S., Gardino, A.K., Heijink, A.M., Sorger, P.K., MacBeath, G., and Yaffe, M.B. (2012) Sequential application of anticancer drugs enhances cell death by rewiring apoptotic signaling networks. *Cell*, **149**(4): 780–94.

- Lehner, B., Crombie, C., Tischler, J., Fortunato, A., and Fraser, A.G. (2006) Systematic mapping of genetic interactions in *caenorhabditis elegans* identifies common modifiers of diverse signaling pathways. *Nat Genet*, **38**(8): 896–903.
- Li, X.J., Mishra, S.K., Wu, M., Zhang, F., and Zheng, J. (2014) Syn-lethality: An integrative knowledge base of synthetic lethality towards discovery of selective anticancer therapies. *Biomed Res Int*, **2014**: 196034.
- Linehan, W.M., Spellman, P.T., Ricketts, C.J., Creighton, C.J., Fei, S.S., Davis, C., Wheeler, D.A., Murray, B.A., Schmidt, L., Vocke, C.D., *et al.* (2016) Comprehensive Molecular Characterization of Papillary Renal-Cell Carcinoma. *N Engl J Med*, **374**(2): 135–145.
- Lokody, I. (2014) Computational modelling: A computational crystal ball. *Nature Reviews Cancer*, **14**(10): 649–649.
- Lord, C.J., Tutt, A.N., and Ashworth, A. (2015) Synthetic lethality and cancer therapy: lessons learned from the development of PARP inhibitors. *Annu Rev Med*, **66**: 455–470.
- Lu, X., Kensche, P.R., Huynen, M.A., and Notebaart, R.A. (2013) Genome evolution predicts genetic interactions in protein complexes and reveals cancer drug targets. *Nat Commun*, **4**: 2124.
- Lu, X., Megchelenbrink, W., Notebaart, R.A., and Huynen, M.A. (2015) Predicting human genetic interactions from cancer genome evolution. *PLoS One*, **10**(5): e0125795.
- Lum, P.Y., Armour, C.D., Stepaniants, S.B., Cavet, G., Wolf, M.K., Butler, J.S., Hinchshaw, J.C., Garnier, P., Prestwich, G.D., Leonardson, A., *et al.* (2004) Discovering modes of action for therapeutic compounds using a genome-wide screen of yeast heterozygotes. *Cell*, **116**(1): 121–137.
- Luo, J., Solimini, N.L., and Elledge, S.J. (2009) Principles of Cancer Therapy: Oncogene and Non-oncogene Addiction. *Cell*, **136**(5): 823–837.
- Machado, J., Olivera, C., Carvalh, R., Soares, P., Berx, G., Caldas, C., Sercuca, R., Carneiro, F., and Sorbrinho-Simoes, M. (2001) E-cadherin gene (*CDH1*) promoter methylation as the second hit in sporadic diffuse gastric carcinoma. *Oncogene*, **20**: 1525–1528.

- Markowetz, F. (2017) All biology is computational biology. *PLoS Biol*, **15**(3): e2002050.
- Masciari, S., Larsson, N., Senz, J., Boyd, N., Kaurah, P., Kandel, M.J., Harris, L.N., Pinheiro, H.C., Troussard, A., Miron, P., *et al.* (2007) Germline E-cadherin mutations in familial lobular breast cancer. *J Med Genet*, **44**(11): 726–31.
- Mattison, J., van der Weyden, L., Hubbard, T., and Adams, D.J. (2009) Cancer gene discovery in mouse and man. *Biochim Biophys Acta*, **1796**(2): 140–161.
- McLachlan, J., George, A., and Banerjee, S. (2016) The current status of parp inhibitors in ovarian cancer. *Tumori*, **102**(5): 433–440.
- McLendon, R., Friedman, A., Bigner, D., Van Meir, E.G., Brat, D.J., Mastrogianakis, G.M., Olson, J.J., Mikkelsen, T., Lehman, N., Aldape, K., *et al.* (2008) Comprehensive genomic characterization defines human glioblastoma genes and core pathways. *Nature*, **455**(7216): 1061–1068.
- Miles, D.W. (2001) Update on HER-2 as a target for cancer therapy: herceptin in the clinical setting. *Breast Cancer Res*, **3**(6): 380–384.
- Mortazavi, A., Williams, B.A., McCue, K., Schaeffer, L., and Wold, B. (2008) Mapping and quantifying mammalian transcriptomes by RNA-Seq. *Nat Methods*, **5**(7): 621–628.
- Muzny, D.M., Bainbridge, M.N., Chang, K., Dinh, H.H., Drummond, J.A., Fowler, G., Kovar, C.L., Lewis, L.R., Morgan, M.B., Newsham, I.F., *et al.* (2012) Comprehensive molecular characterization of human colon and rectal cancer. *Nature*, **487**(7407): 330–337.
- Nagalla, S., Chou, J.W., Willingham, M.C., Ruiz, J., Vaughn, J.P., Dubey, P., Lash, T.L., Hamilton-Dutoit, S.J., Bergh, J., Sotiriou, C., *et al.* (2013) Interactions between immunity, proliferation and molecular subtype in breast cancer prognosis. *Genome Biol*, **14**(4): R34.
- Neeley, E.S., Kornblau, S.M., Coombes, K.R., and Baggerly, K.A. (2009) Variable slope normalization of reverse phase protein arrays. *Bioinformatics*, **25**(11): 1384.
- Novomestky, F. (2012) *matrixcalc: Collection of functions for matrix calculations*. R package version 1.0-3.

- Nowak, M.A., Boerlijst, M.C., Cooke, J., and Smith, J.M. (1997) Evolution of genetic redundancy. *Nature*, **388**(6638): 167–171.
- Oliveira, C., Senz, J., Kaurah, P., Pinheiro, H., Sanges, R., Haegert, A., Corso, G., Schouten, J., Fitzgerald, R., Vogelsang, H., et al. (2009) Germline *CDH1* deletions in hereditary diffuse gastric cancer families. *Human Molecular Genetics*, **18**(9): 1545–1555.
- Oliveira, C., Seruca, R., Hoogerbrugge, N., Ligtenberg, M., and Carneiro, F. (2013) Clinical utility gene card for: Hereditary diffuse gastric cancer (HDGC). *Eur J Hum Genet*, **21**(8).
- Pandey, G., Zhang, B., Chang, A.N., Myers, C.L., Zhu, J., Kumar, V., and Schadt, E.E. (2010) An integrative multi-network and multi-classifier approach to predict genetic interactions. *PLoS Comput Biol*, **6**(9).
- Parker, J., Mullins, M., Cheung, M., Leung, S., Voduc, D., Vickery, T., Davies, S., Fauron, C., He, X., Hu, Z., et al. (2009) Supervised risk predictor of breast cancer based on intrinsic subtypes. *Journal of Clinical Oncology*, **27**(8): 1160–1167.
- Pereira, B., Chin, S.F., Rueda, O.M., Vollan, H.K., Provenzano, E., Bardwell, H.A., Pugh, M., Jones, L., Russell, R., Sammut, S.J., et al. (2016) Erratum: The somatic mutation profiles of 2,433 breast cancers refine their genomic and transcriptomic landscapes. *Nat Commun*, **7**: 11908.
- Perou, C.M., Sørlie, T., Eisen, M.B., van de Rijn, M., Jeffrey, S.S., Rees, C.A., Pollack, J.R., Ross, D.T., Johnsen, H., Akslen, L.A., et al. (2000) Molecular portraits of human breast tumours. *Nature*, **406**(6797): 747–752.
- Polyak, K. and Weinberg, R.A. (2009) Transitions between epithelial and mesenchymal states: acquisition of malignant and stem cell traits. *Nat Rev Cancer*, **9**(4): 265–73.
- Prahallas, A., Sun, C., Huang, S., Di Nicolantonio, F., Salazar, R., Zecchin, D., Beijersbergen, R.L., Bardelli, A., and Bernards, R. (2012) Unresponsiveness of colon cancer to *BRAF*(v600e) inhibition through feedback activation of egfr. *Nature*, **483**(7387): 100–3.
- R Core Team (2016) *R: A Language and Environment for Statistical Computing*. R Foundation for Statistical Computing, Vienna, Austria. R version 3.3.2.

- Ravnan, M.C. and Matalka, M.S. (2012) Vemurafenib in patients with *BRAF* v600e mutation-positive advanced melanoma. *Clin Ther*, **34**(7): 1474–86.
- Ritchie, M.E., Phipson, B., Wu, D., Hu, Y., Law, C.W., Shi, W., and Smyth, G.K. (2015) limma powers differential expression analyses for RNA-sequencing and microarray studies. *Nucleic Acids Research*, **43**(7): e47.
- Robinson, M.D. and Oshlack, A. (2010) A scaling normalization method for differential expression analysis of RNA-seq data. *Genome Biol*, **11**(3): R25.
- Roguev, A., Bandyopadhyay, S., Zofall, M., Zhang, K., Fischer, T., Collins, S.R., Qu, H., Shales, M., Park, H.O., Hayles, J., et al. (2008) Conservation and rewiring of functional modules revealed by an epistasis map in fission yeast. *Science*, **322**(5900): 405–10.
- Roychowdhury, S. and Chinnaiyan, A.M. (2016) Translating cancer genomes and transcriptomes for precision oncology. *CA Cancer J Clin*, **66**(1): 75–88.
- Rung, J. and Brazma, A. (2013) Reuse of public genome-wide gene expression data. *Nat Rev Genet*, **14**(2): 89–99.
- Rustici, G., Kolesnikov, N., Brandizi, M., Burdett, T., Dylag, M., Emam, I., Farne, A., Hastings, E., Ison, J., Keays, M., et al. (2013) ArrayExpress update—trends in database growth and links to data analysis tools. *Nucleic Acids Res*, **41**(Database issue): D987–990.
- Ryan, C., Lord, C., and Ashworth, A. (2014) Daisy: Picking synthetic lethals from cancer genomes. *Cancer Cell*, **26**(3): 306–308.
- Schena, M. (1996) Genome analysis with gene expression microarrays. *Bioessays*, **18**(5): 427–431.
- Scheuer, L., Kauff, N., Robson, M., Kelly, B., Barakat, R., Satagopan, J., Ellis, N., Hensley, M., Boyd, J., Borgen, P., et al. (2002) Outcome of preventive surgery and screening for breast and ovarian cancer in BRCA mutation carriers. *J Clin Oncol*, **20**(5): 1260–1268.
- Semb, H. and Christofori, G. (1998) The tumor-suppressor function of E-cadherin. *Am J Hum Genet*, **63**(6): 1588–93.

Sing, T., Sander, O., Beerenwinkel, N., and Lengauer, T. (2005) Rocr: visualizing classifier performance in r. *Bioinformatics*, **21**(20): 7881.

Slurm development team (Slurm) (2017) Slurm workload manager. <https://slurm.schedmd.com/>. Accessed: 25/03/2017.

Sørlie, T., Perou, C.M., Tibshirani, R., Aas, T., Geisler, S., Johnsen, H., Hastie, T., Eisen, M.B., van de Rijn, M., Jeffrey, S.S., *et al.* (2001) Gene expression patterns of breast carcinomas distinguish tumor subclasses with clinical implications. *Proc Natl Acad Sci USA*, **98**(19): 10869–10874.

Stajich, J.E. and Lapp, H. (2006) Open source tools and toolkits for bioinformatics: significance, and where are we? *Brief Bioinformatics*, **7**(3): 287–296.

Stratton, M.R., Campbell, P.J., and Futreal, P.A. (2009) The cancer genome. *Nature*, **458**(7239): 719–724.

Ström, C. and Helleday, T. (2012) Strategies for the use of poly(adenosine diphosphate ribose) polymerase (parp) inhibitors in cancer therapy. *Biomolecules*, **2**(4): 635–649.

Sun, C., Wang, L., Huang, S., Heynen, G.J.J.E., Prahallad, A., Robert, C., Haanen, J., Blank, C., Wesseling, J., Willems, S.M., *et al.* (2014) Reversible and adaptive resistance to *BRAF*(v600e) inhibition in melanoma. *Nature*, **508**(7494): 118–122.

Telford, B.J., Chen, A., Beetham, H., Frick, J., Brew, T.P., Gould, C.M., Single, A., Godwin, T., Simpson, K.J., and Guilford, P. (2015) Synthetic lethal screens identify vulnerabilities in gpcr signalling and cytoskeletal organization in E-cadherin-deficient cells. *Mol Cancer Ther*, **14**(5): 1213–1223.

The 1000 Genomes Project Consortium (1000 Genomes) (2010) A map of human genome variation from population-scale sequencing. *Nature*, **467**(7319): 1061–1073.

The Cancer Genome Atlas Research Network (TCGA) (2012) Comprehensive molecular portraits of human breast tumours. *Nature*, **490**(7418): 61–70.

The Cancer Genome Atlas Research Network (TCGA) (2017) The Cancer Genome Atlas Project. <https://cancergenome.nih.gov/>. Accessed: 26/03/2017.

The Catalogue Of Somatic Mutations In Cancer (COSMIC) (2016) Cosmic: The catalogue of somatic mutations in cancer. <http://cancer.sanger.ac.uk/cosmic>. Release 79 (23/08/2016), Accessed: 05/02/2017.

The Comprehensive R Archive Network (CRAN) (2017) Cran. <https://cran.r-project.org/>. Accessed: 24/03/2017.

The ENCODE Project Consortium (ENCODE) (2004) The ENCODE (ENCyclopedia Of DNA Elements) Project. *Science*, **306**(5696): 636–640.

The National Cancer Institute (NCI) (2015) The genetics of cancer. <https://www.cancer.gov/about-cancer/causes-prevention/genetics>. Published: 22/04/2015, Accessed: 22/03/2017.

The New Zealand eScience Infrastructure (NeSI) (2017) NeSI. <https://www.nesi.org.nz/>. Accessed: 25/03/2017.

Tierney, L., Rossini, A.J., Li, N., and Sevcikova, H. (2015) *snow: Simple Network of Workstations*. R package version 0.4-2.

Tiong, K.L., Chang, K.C., Yeh, K.T., Liu, T.Y., Wu, J.H., Hsieh, P.H., Lin, S.H., Lai, W.Y., Hsu, Y.C., Chen, J.Y., *et al.* (2014) Csnk1e/ctnnb1 are synthetic lethal to tp53 in colorectal cancer and are markers for prognosis. *Neoplasia*, **16**(5): 441–50.

Tischler, J., Lehner, B., and Fraser, A.G. (2008) Evolutionary plasticity of genetic interaction networks. *Nat Genet*, **40**(4): 390–391.

Tomasetti, C. and Vogelstein, B. (2015) Cancer etiology. Variation in cancer risk among tissues can be explained by the number of stem cell divisions. *Science*, **347**(6217): 78–81.

Tong, A.H., Evangelista, M., Parsons, A.B., Xu, H., Bader, G.D., Page, N., Robinson, M., Raghibizadeh, S., Hogue, C.W., Bussey, H., *et al.* (2001) Systematic genetic analysis with ordered arrays of yeast deletion mutants. *Science*, **294**(5550): 2364–8.

Tong, A.H., Lesage, G., Bader, G.D., Ding, H., Xu, H., Xin, X., Young, J., Berriz, G.F., Brost, R.L., Chang, M., *et al.* (2004) Global mapping of the yeast genetic interaction network. *Science*, **303**(5659): 808–13.

Tran, B., Dancey, J.E., Kamel-Reid, S., McPherson, J.D., Bedard, P.L., Brown, A.M., Zhang, T., Shaw, P., Onetto, N., Stein, L., *et al.* (2012) Cancer genomics: technology, discovery, and translation. *J Clin Oncol*, **30**(6): 647–660.

Travers, J. and Milgram, S. (1969) An experimental study of the small world problem. *Sociometry*, **32**(4): 425–443.

- Tsai, H.C., Li, H., Van Neste, L., Cai, Y., Robert, C., Rassool, F.V., Shin, J.J., Harbom, K.M., Beaty, R., Pappou, E., *et al.* (2012) Transient low doses of dna-demethylating agents exert durable antitumor effects on hematological and epithelial tumor cells. *Cancer Cell*, **21**(3): 430–46.
- Tunggal, J.A., Helfrich, I., Schmitz, A., Schwarz, H., Gunzel, D., Fromm, M., Kemler, R., Krieg, T., and Niessen, C.M. (2005) E-cadherin is essential for in vivo epidermal barrier function by regulating tight junctions. *EMBO J*, **24**(6): 1146–1156.
- Tutt, A., Robson, M., Garber, J.E., Domchek, S.M., Audeh, M.W., Weitzel, J.N., Friedlander, M., Arun, B., Loman, N., Schmutzler, R.K., *et al.* (2010) Oral poly(adt-ribose) polymerase inhibitor olaparib in patients with *BRCA1* or *BRCA2* mutations and advanced breast cancer: a proof-of-concept trial. *Lancet*, **376**(9737): 235–44.
- University of California, Santa Cruz (UCSC) (2012) Ucsc cancer browser. Accessed 29/03/2012.
- van der Meer, R., Song, H.Y., Park, S.H., Abdulkadir, S.A., and Roh, M. (2014) RNAi screen identifies a synthetic lethal interaction between PIM1 overexpression and PLK1 inhibition. *Clinical Cancer Research*, **20**(12): 3211–3221.
- van der Post, R.S., Vogelaar, I.P., Carneiro, F., Guilford, P., Huntsman, D., Hoogerbrugge, N., Caldas, C., Schreiber, K.E., Hardwick, R.H., Ausems, M.G., *et al.* (2015) Hereditary diffuse gastric cancer: updated clinical guidelines with an emphasis on germline CDH1 mutation carriers. *J Med Genet*, **52**(6): 361–374.
- van Steen, K. (2012) Travelling the world of gene–gene interactions. *Briefings in Bioinformatics*, **13**(1): 1–19.
- van Steen, M. (2010) *Graph Theory and Complex Networks: An Introduction*. Maarten van Steen, VU Amsterdam.
- Vapnik, V.N. (1995) *The nature of statistical learning theory*. Springer-Verlag New York, Inc.
- Vizeacoumar, F.J., Arnold, R., Vizeacoumar, F.S., Chandrashekhar, M., Buzina, A., Young, J.T., Kwan, J.H., Sayad, A., Mero, P., Lawo, S., *et al.* (2013) A negative genetic interaction map in isogenic cancer cell lines reveals cancer cell vulnerabilities. *Mol Syst Biol*, **9**: 696.

- Vogelstein, B., Papadopoulos, N., Velculescu, V.E., Zhou, S., Diaz, L.A., and Kinzler, K.W. (2013) Cancer genome landscapes. *Science*, **339**(6127): 1546–1558.
- Vos, C.B., Cleton-Jansen, A.M., Berx, G., de Leeuw, W.J., ter Haar, N.T., van Roy, F., Cornelisse, C.J., Peterse, J.L., and van de Vijver, M.J. (1997) E-cadherin inactivation in lobular carcinoma in situ of the breast: an early event in tumorigenesis. *Br J Cancer*, **76**(9): 1131–3.
- Waldron, D. (2016) Cancer genomics: A multi-layer omics approach to cancer. *Nat Rev Genet*, **17**(8): 436–437.
- Wang, K., Singh, D., Zeng, Z., Coleman, S.J., Huang, Y., Savich, G.L., He, X., Mieczkowski, P., Grimm, S.A., Perou, C.M., *et al.* (2010) MapSplice: accurate mapping of RNA-seq reads for splice junction discovery. *Nucleic Acids Res*, **38**(18): e178.
- Wang, X. and Simon, R. (2013) Identification of potential synthetic lethal genes to p53 using a computational biology approach. *BMC Medical Genomics*, **6**(1): 30.
- Wappett, M. (2014) Bisep: Toolkit to identify candidate synthetic lethality. r package version 2.0.
- Wappett, M., Dulak, A., Yang, Z.R., Al-Watban, A., Bradford, J.R., and Dry, J.R. (2016) Multi-omic measurement of mutually exclusive loss-of-function enriches for candidate synthetic lethal gene pairs. *BMC Genomics*, **17**: 65.
- Warnes, G.R., Bolker, B., Bonebakker, L., Gentleman, R., Liaw, W.H.A., Lumley, T., Maechler, M., Magnusson, A., Moeller, S., Schwartz, M., *et al.* (2015) *gplots: Various R Programming Tools for Plotting Data*. R package version 2.17.0.
- Watts, D.J. and Strogatz, S.H. (1998) Collective dynamics of 'small-world' networks. *Nature*, **393**(6684): 440–2.
- Weinstein, I.B. (2000) Disorders in cell circuitry during multistage carcinogenesis: the role of homeostasis. *Carcinogenesis*, **21**(5): 857–864.
- Weinstein, J.N., Akbani, R., Broom, B.M., Wang, W., Verhaak, R.G., McConkey, D., Lerner, S., Morgan, M., Creighton, C.J., Smith, C., *et al.* (2014) Comprehensive molecular characterization of urothelial bladder carcinoma. *Nature*, **507**(7492): 315–322.

- Weinstein, J.N., Collisson, E.A., Mills, G.B., Shaw, K.R., Ozenberger, B.A., Ellrott, K., Shmulevich, I., Sander, C., Stuart, J.M., Chang, K., *et al.* (2013) The Cancer Genome Atlas Pan-Cancer analysis project. *Nat Genet*, **45**(10): 1113–1120.
- Wickham, H. and Chang, W. (2016) *devtools: Tools to Make Developing R Packages Easier*. R package version 1.12.0.
- Wickham, H., Danenberg, P., and Eugster, M. (2017) *roxygen2: In-Line Documentation for R*. R package version 6.0.1.
- Wong, S.L., Zhang, L.V., Tong, A.H.Y., Li, Z., Goldberg, D.S., King, O.D., Lesage, G., Vidal, M., Andrews, B., Bussey, H., *et al.* (2004) Combining biological networks to predict genetic interactions. *Proceedings of the National Academy of Sciences of the United States of America*, **101**(44): 15682–15687.
- World Health Organization (WHO) (2017) Fact sheet: Cancer. <http://www.who.int/mediacentre/factsheets/fs297/en/>. Updated February 2017, Accessed: 22/03/2017.
- Wu, M., Li, X., Zhang, F., Li, X., Kwoh, C.K., and Zheng, J. (2014) In silico prediction of synthetic lethality by meta-analysis of genetic interactions, functions, and pathways in yeast and human cancer. *Cancer Inform*, **13**(Suppl 3): 71–80.
- Yu, H. (2002) Rmpi: Parallel statistical computing in r. *R News*, **2**(2): 10–14.
- Zhang, F., Wu, M., Li, X.J., Li, X.L., Kwoh, C.K., and Zheng, J. (2015) Predicting essential genes and synthetic lethality via influence propagation in signaling pathways of cancer cell fates. *J Bioinform Comput Biol*, **13**(3): 1541002.
- Zhang, J., Baran, J., Cros, A., Guberman, J.M., Haider, S., Hsu, J., Liang, Y., Rivkin, E., Wang, J., Whitty, B., *et al.* (2011) International cancer genome consortium data portal—a one-stop shop for cancer genomics data. *Database: The Journal of Biological Databases and Curation*, **2011**: bar026.
- Zhong, W. and Sternberg, P.W. (2006) Genome-wide prediction of c. elegans genetic interactions. *Science*, **311**(5766): 1481–1484.
- Zweig, M.H. and Campbell, G. (1993) Receiver-operating characteristic (roc) plots: a fundamental evaluation tool in clinical medicine. *Clinical Chemistry*, **39**(4): 561–577.

Appendix A

Sample Quality

A.1 Sample Correlation

Samples were excluded from expression analysis based on sample correlations and the clustering analysis presented below, as described in Section 2.2.2.

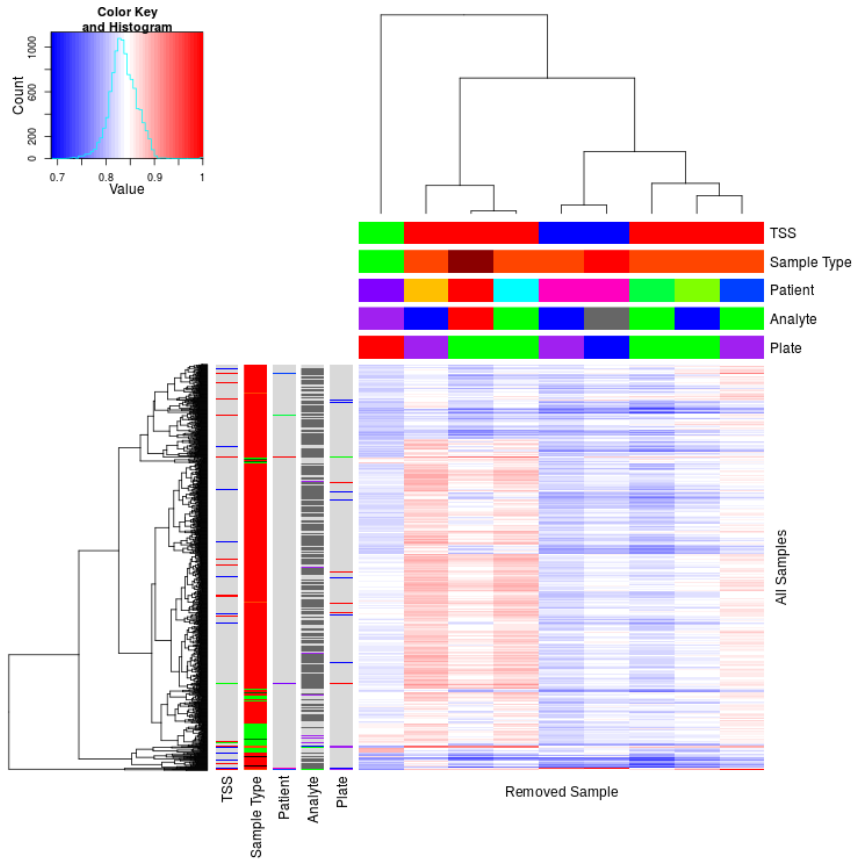


Figure A.1: Correlation profiles of removed samples. Correlation matrix heatmap (Euclidean distance) of all samples in [TCGA](#) breast cancer dataset (left) clustered for all samples against removed samples (top): tissue source site (TSS), sample type with reds for tumour and greens for normal, patient (A2QH in pink), with varied analyte and plate (corresponding to batch in Table 2.1). Excluded samples cluster at the bottom and annotation (left) show shared properties between samples in the dataset.

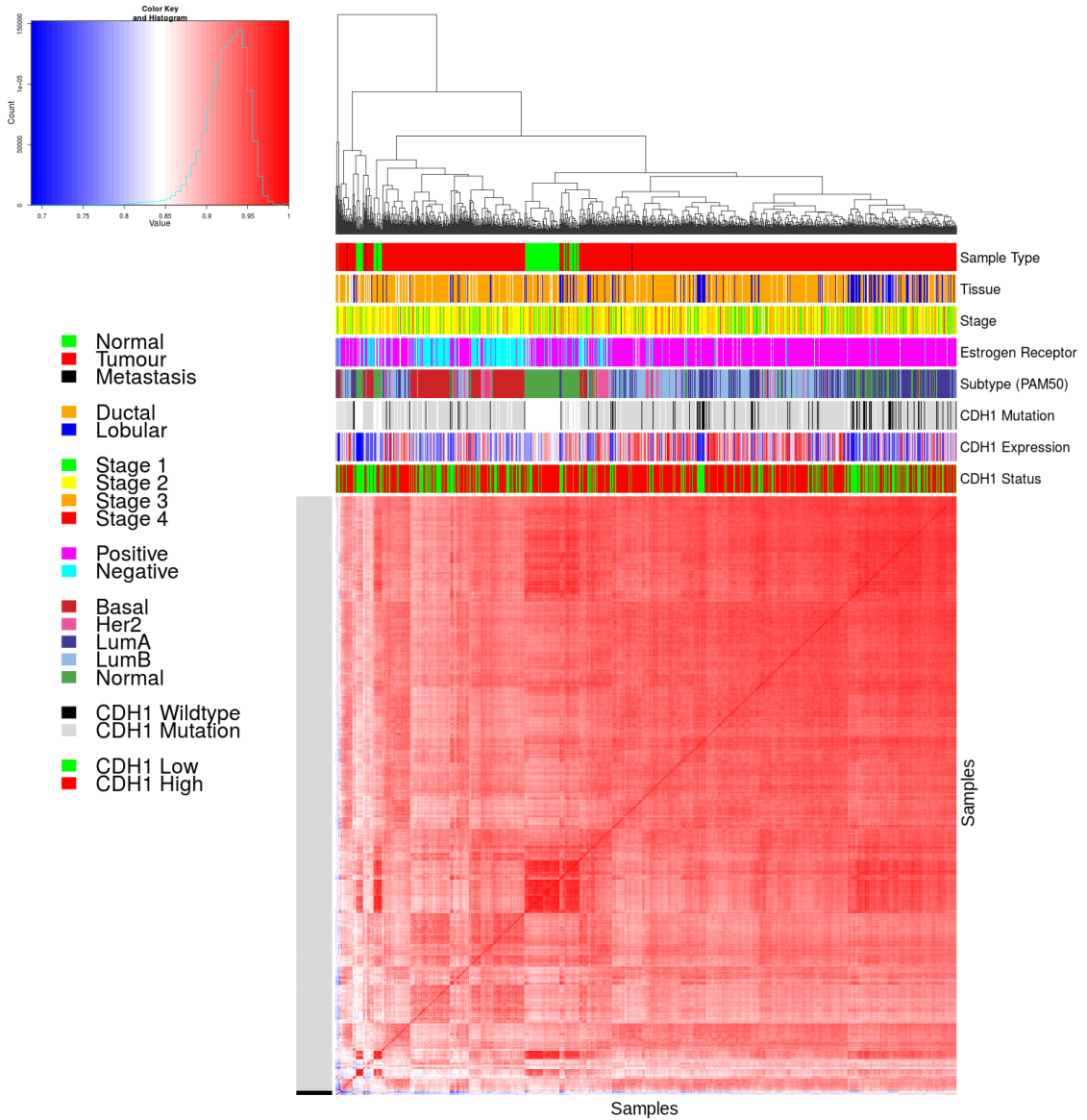


Figure A.2: Correlation analysis and sample removal. Correlation matrix heatmap (Euclidean distance) of all samples in [TCGA](#) breast cancer dataset against each other annotated for sample clinical data: sample type, tissue type, tumour stage, Estrogen receptor (IHC) and intrinsic subtype (from the [PAM50](#) method). CDH1 somatic mutation, gene expression, and status for [SLIPT](#) prediction are also annotated. Discrete variables are coloured as displayed in the legend and continuous variables on a blue-red scale as shown in the colour key. Trimmed samples cluster at the bottom of the heatmap and the colour bars of the left show which were removed for quality concerns.

A.2 Replicate Samples in TCGA Breast

Replicate samples were picked where possible from the TCGA breast cancer gene expression data to examine for sample quality. Independent samples of the same tumour are expected to have very high Pearson's correlation between their expression profiles unless there were issues with sample collection or preparation and are thus an indicator of sample quality. The log-transformed raw read counts for replicate samples were examined in Figures A.3–A.5. These were examined before normalisation which would be expected to increase sample concordance.

Another consideration are the samples which were removed for quality concerns (in Section 2.2.2). While these were selected by unbiased hierarchical clustering (See Figure A.2), it is notable that many of the excluded (tumour) samples were performed in replicate despite relatively few replicate samples in the overall dataset. These samples correlate poorly with the rest of the dataset, in addition to with replicate samples.

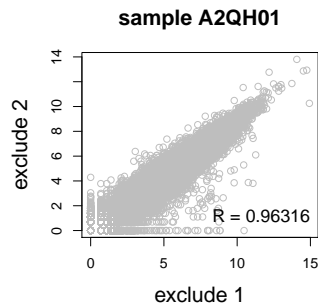


Figure A.3: **Replicate excluded samples.** Both tumour samples of patient A2QH were excluded as they were poorly correlated with other samples, although they are highly similar to each other as shown by Pearson's correlation of log-raw counts.

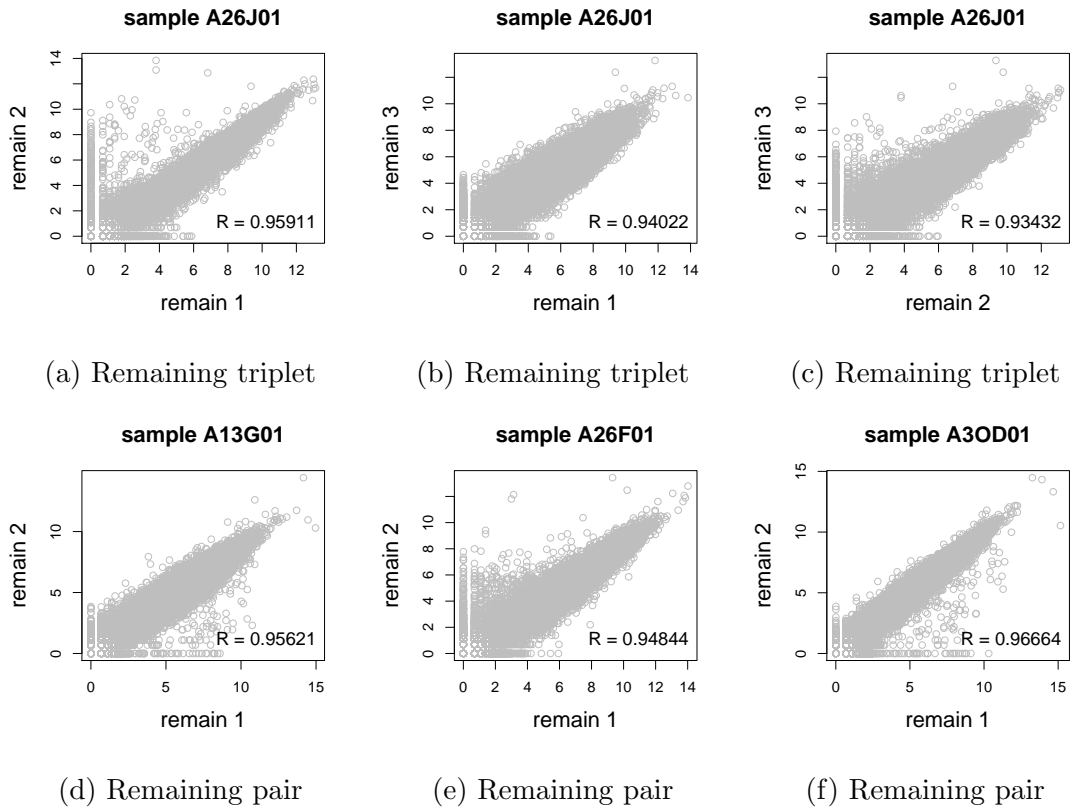


Figure A.4: **Replicate samples with all remaining.** Patient A26J was sampled 3 times and compared pairwise. Pairs of samples were also compared for other patients with replicate samples. In all cases, replicate samples remaining in the dataset were highly concordant as shown by Pearson's correlation of log-raw counts.

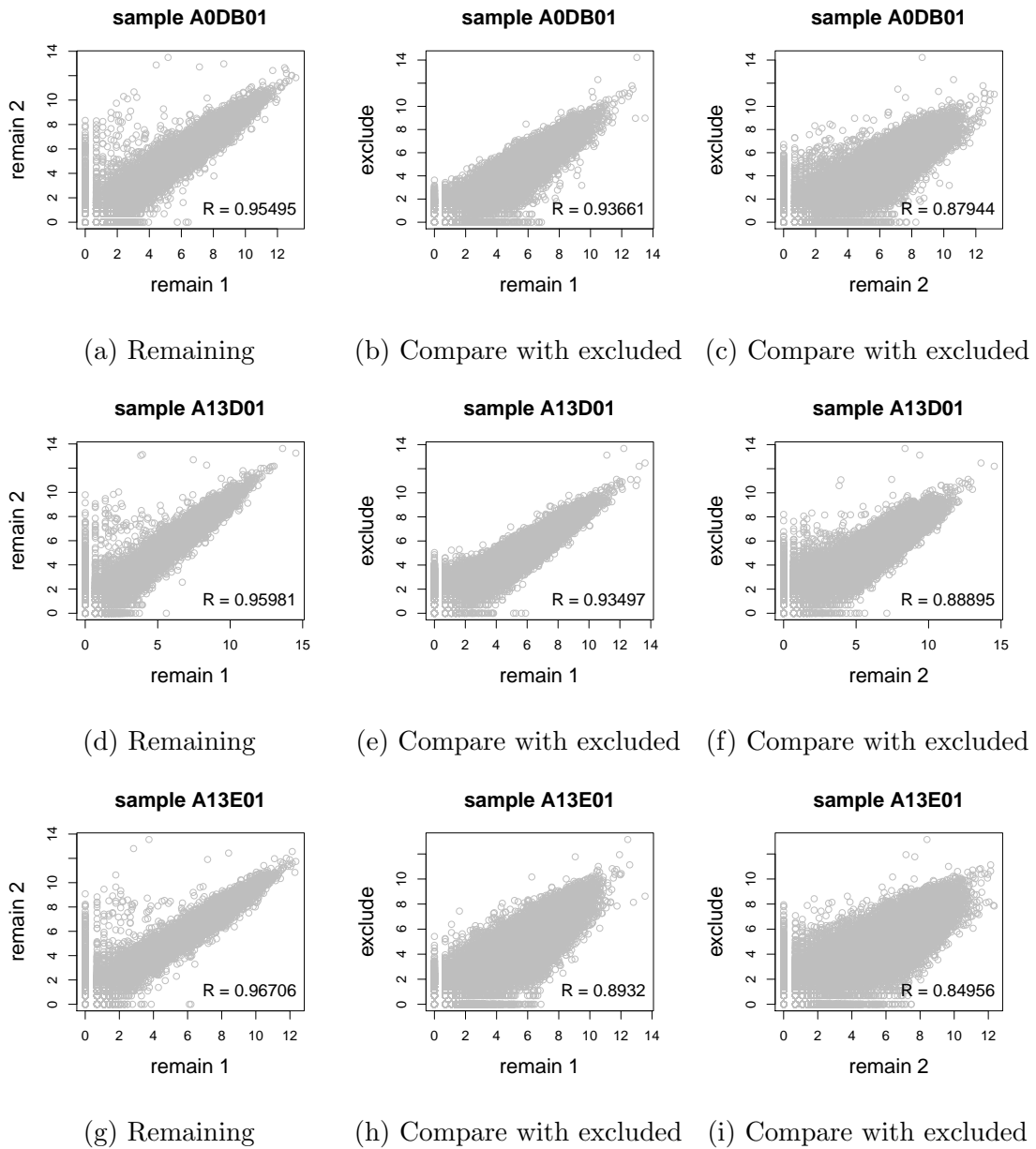


Figure A.5: **Replicate samples with some excluded.** (continued on next page)

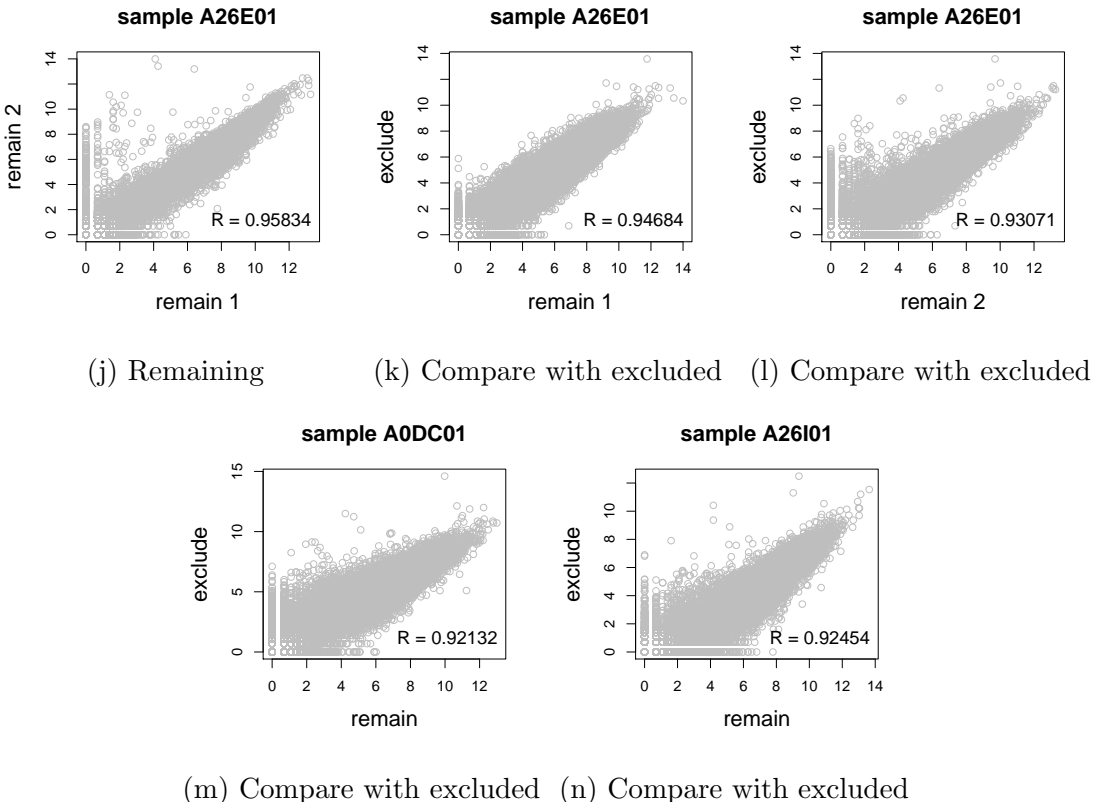


Figure A.5: Replicate samples with some excluded. Patients A0DB, A13D, A13E, and A26E were each sampled 3 times and compared pairwise. Pairs of samples were also compared for other patients with replicate samples. In all cases, the replicate samples remaining in the dataset more were highly concordant (as shown by Pearson's correlation of log-raw counts) than those excluded from the analysis.

Appendix B

Software Used for Thesis

Table B.1: R packages used during thesis

| Package | Repository | Laptop | Lab | Server | NeSI |
|---------------|--------------|----------|----------|----------|----------|
| base | base | 3.3.2 | 3.3.2 | 3.3.1 | 3.3.0 |
| abind | CRAN | | 1.4-5 | | 1.4-3 |
| acepack | CRAN | | 1.4.1 | | 1.3-3.3 |
| ade4 | CRAN | | 1.7-5 | | |
| annaffy | Bioconductor | | 1.46.0 | | |
| AnnotationDbi | Bioconductor | | 1.36.0 | 1.36.0 | 1.34.4 |
| apComplex | CRAN | | 2.40.0 | | |
| ape | CRAN | | 4 | | 3.4 |
| arm | CRAN | | 1.9-3 | | |
| assertthat | CRAN | 0.1 | 0.1 | 0.1 | 0.1 |
| backports | CRAN | 1.0.5 | 1.0.4 | 1.0.5 | 1.0.2 |
| base64 | CRAN | | | 2 | 2 |
| base64enc | CRAN | | 0.1-3 | | 0.1-3 |
| beanplot | CRAN | | 1.2 | 1.2 | 1.2 |
| BH | CRAN | 1.60.0-2 | 1.62.0-1 | 1.62.0-1 | 1.60.0-2 |
| Biobase | Bioconductor | | 2.34.0 | 2.34.0 | 2.32.0 |
| BiocGenerics | Bioconductor | | 0.20.0 | 0.20.0 | 0.18.0 |
| BiocInstaller | Bioconductor | | 1.24.0 | 1.20.3 | 1.22.3 |
| BiocParallel | Bioconductor | | 1.8.1 | 1.8.1 | |
| Biostrings | Bioconductor | | 2.42.1 | 2.42.0 | |
| BiSEp | Bioconductor | | 2.0.1 | 2.0.1 | 2.0.1 |

| | | | | | |
|------------|------|--------|---------|--------|--------|
| bitops | CRAN | 1.0-6 | 1.0-6 | 1.0-6 | 1.0-6 |
| boot | base | 1.3-18 | 1.3-18 | 1.3-18 | 1.3-18 |
| brew | CRAN | 1.0-6 | 1.0-6 | 1.0-6 | 1.0-6 |
| broom | CRAN | 0.4.1 | | | |
| caTools | CRAN | 1.17.1 | 1.17.1 | 1.17.1 | 1.17.1 |
| cgdssr | CRAN | | 1.2.5 | | |
| checkmate | CRAN | | 1.8.2 | | 1.7.4 |
| chron | CRAN | 2.3-47 | 2.3-48 | 2.3-50 | 2.3-47 |
| class | base | 7.3-14 | 7.3-14 | 7.3-14 | 7.3-14 |
| cluster | base | 2.0.5 | 2.0.5 | 2.0.5 | 2.0.4 |
| coda | CRAN | | 0.19-1 | | 0.18-1 |
| codetools | base | 0.2-15 | 0.2-15 | 0.2-15 | 0.2-14 |
| colorRamps | CRAN | | 2.3 | | |
| colorspace | CRAN | 1.2-6 | 1.3-2 | 1.3-2 | 1.2-6 |
| commonmark | CRAN | 1.1 | | 1.2 | |
| compiler | base | 3.3.2 | 3.3.2 | 3.3.1 | 3.3.0 |
| corpcor | CRAN | | 1.6.8 | 1.6.8 | 1.6.8 |
| Cprob | CRAN | | 1.2.4 | | |
| crayon | CRAN | 1.3.2 | 1.3.2 | 1.3.2 | 1.3.2 |
| crop | CRAN | | 0.0-2 | 0.0-2 | |
| curl | CRAN | 1.2 | 2.3 | 2.3 | 0.9.7 |
| d3Network | CRAN | | 0.5.2.1 | | |
| data.table | CRAN | 1.9.6 | 1.10.0 | 1.10.1 | 1.9.6 |
| data.tree | CRAN | | 0.7.0 | 0.7.0 | |
| datasets | base | 3.3.2 | 3.3.2 | 3.3.1 | 3.3.0 |
| DBI | CRAN | 0.5-1 | 0.5-1 | 0.5-1 | 0.5-1 |
| dendextend | CRAN | 1.4.0 | 1.4.0 | 1.4.0 | |
| DEoptimR | CRAN | 1.0-8 | 1.0-8 | 1.0-8 | 1.0-4 |
| desc | CRAN | 1.1.0 | | 1.1.0 | |
| devtools | CRAN | 1.12.0 | 1.12.0 | 1.12.0 | 1.12.0 |
| DiagrammeR | CRAN | | 0.9.0 | 0.9.0 | |
| dichromat | CRAN | 2.0-0 | 2.0-0 | 2.0-0 | 2.0-0 |
| digest | CRAN | 0.6.10 | 0.6.11 | 0.6.12 | 0.6.9 |
| diptest | CRAN | 0.75-7 | 0.75-7 | 0.75-7 | |
| doParallel | CRAN | 1.0.10 | 1.0.10 | 1.0.10 | 1.0.10 |

| | | | | | |
|-------------------|----------------------------|--------|--------|--------|--------|
| dplyr | CRAN | 0.5.0 | 0.5.0 | 0.5.0 | 0.5.0 |
| ellipse | CRAN | | 0.3-8 | 0.3-8 | 0.3-8 |
| evaluate | CRAN | | 0.1 | 0.1 | 0.9 |
| fdrtool | CRAN | | 1.2.15 | | |
| fields | CRAN | | 8.1 | | |
| flexmix | CRAN | 2.3-13 | 2.3-13 | 2.3-13 | |
| forcats | CRAN | 0.2.0 | | | |
| foreach | CRAN | 1.4.3 | 1.4.3 | 1.4.3 | 1.4.3 |
| foreign | base | 0.8-67 | 0.8-67 | 0.8-67 | 0.8-66 |
| formatR | CRAN | | 1.4 | 1.4 | 1.4 |
| Formula | CRAN | | 1.2-1 | | 1.2-1 |
| fpc | CRAN | 2.1-10 | 2.1-10 | 2.1-10 | |
| futile.logger | CRAN | | 1.4.3 | 1.4.3 | 1.4.1 |
| futile.options | CRAN | | 1.0.0 | 1.0.0 | 1.0.0 |
| gdata | CRAN | 2.17.0 | 2.17.0 | 2.17.0 | 2.17.0 |
| geepack | CRAN | | 1.2-1 | | |
| GenomeInfoDb | Bioconductor | | 1.10.2 | 1.10.1 | |
| GenomicAlignments | Bioconductor | | 1.10.0 | 1.10.0 | |
| GenomicRanges | Bioconductor | | 1.26.2 | 1.26.1 | |
| ggm | CRAN | | 2.3 | | |
| ggplot2 | CRAN | 2.1.0 | 2.2.1 | 2.2.1 | 2.1.0 |
| git2r | CRAN | 0.15.0 | 0.18.0 | 0.16.0 | 0.15.0 |
| glasso | CRAN | | 1.8 | | |
| GO.db | Bioconductor | | 3.4.0 | 3.2.2 | 3.3.0 |
| GOSemSim | Bioconductor | | 2.0.3 | 1.28.2 | 1.30.3 |
| gplots | CRAN | 3.0.1 | 3.0.1 | 3.0.1 | 3.0.1 |
| graph | Bioconductor | | 1.52.0 | | |
| graphics | base | 3.3.2 | 3.3.2 | 3.3.1 | 3.3.0 |
| graphsim | GitHub TomKellyGenetics | 0.1.0 | 0.1.0 | 0.1.0 | 0.1.0 |
| grDevices | base | 3.3.2 | 3.3.2 | 3.3.1 | 3.3.0 |
| grid | base | 3.3.2 | 3.3.2 | 3.3.1 | 3.3.0 |
| gridBase | CRAN | 0.4-7 | 0.4-7 | 0.4-7 | 0.4-7 |
| gridExtra | CRAN | 2.2.1 | 2.2.1 | 2.2.1 | 2.2.1 |
| gridGraphics | CRAN | | 0.1-5 | | |

| | | | | | |
|-------------------|----------------------------|------------|------------|------------|------------|
| gtable | CRAN | 0.2.0 | 0.2.0 | 0.2.0 | 0.2.0 |
| gtools | CRAN | 3.5.0 | 3.5.0 | 3.5.0 | 3.5.0 |
| haven | CRAN | 1.0.0 | | | |
| heatmap.2x | GitHub TomKellyGenetics | 0.0.0.9000 | 0.0.0.9000 | 0.0.0.9000 | 0.0.0.9000 |
| hgu133plus2.db | Bioconductor | | 3.2.3 | | |
| highr | CRAN | | 0.6 | 0.6 | 0.6 |
| Hmisc | CRAN | | 4.0-2 | 4.0-2 | 3.17-4 |
| hms | CRAN | 0.2 | 0.3 | | |
| htmlTable | CRAN | | 1.8 | 1.9 | |
| htmltools | CRAN | 0.3.5 | 0.3.5 | 0.3.5 | 0.3.5 |
| htmlwidgets | CRAN | | 0.8 | 0.8 | |
| httpuv | CRAN | 1.3.3 | | 1.3.3 | |
| httr | CRAN | 1.2.1 | 1.2.1 | 1.2.1 | 1.1.0 |
| huge | CRAN | | 1.2.7 | | |
| hunspell | CRAN | | 2.3 | | 2 |
| hypergraph | CRAN | | 1.46.0 | | |
| igraph | CRAN | 1.0.1 | 1.0.1 | 1.0.1 | 1.0.1 |
| igraph.extensions | GitHub TomKellyGenetics | 0.1.0.9001 | 0.1.0.9001 | 0.1.0.9001 | 0.1.0.9001 |
| influenceR | CRAN | | 0.1.0 | 0.1.0 | |
| info.centrality | GitHub TomKellyGenetics | 0.1.0 | 0.1.0 | 0.1.0 | 0.1.0 |
| IRanges | Bioconductor | | 2.8.1 | 2.8.1 | 2.6.1 |
| irlba | CRAN | 2.1.1 | 2.1.2 | 2.1.2 | 2.0.0 |
| iterators | CRAN | 1.0.8 | 1.0.8 | 1.0.8 | 1.0.8 |
| jpeg | CRAN | | 0.1-8 | | |
| jsonlite | CRAN | 1.1 | 1.2 | 1.3 | 0.9.20 |
| KEGG.db | Bioconductor | | 3.2.3 | | |
| kernlab | CRAN | 0.9-25 | 0.9-25 | 0.9-25 | |
| KernSmooth | base | 2.23-15 | 2.23-15 | 2.23-15 | 2.23-15 |
| knitr | CRAN | | 1.15.1 | 1.15.1 | 1.14 |
| labeling | CRAN | 0.3 | 0.3 | 0.3 | 0.3 |
| lambda.r | CRAN | | 1.1.9 | 1.1.9 | 1.1.7 |
| lattice | base | 0.20-34 | 0.20-34 | 0.20-34 | 0.20-33 |

| | | | | | |
|--------------|--------------|---------|----------|---------|----------|
| latticeExtra | CRAN | | 0.6-28 | | 0.6-28 |
| lava | CRAN | | 1.4.6 | | |
| lavaan | CRAN | | 0.5-22 | | |
| lazyeval | CRAN | 0.2.0 | 0.2.0 | 0.2.0 | 0.2.0 |
| les | CRAN | | 1.24.0 | | |
| lgtdl | CRAN | | 1.1.3 | | |
| limma | Bioconductor | | 3.30.7 | 3.30.3 | |
| lme4 | CRAN | | 1.1-12 | | 1.1-12 |
| lubridate | CRAN | 1.6.0 | | | |
| magrittr | CRAN | 1.5 | 1.5 | 1.5 | 1.5 |
| maps | CRAN | | 3.1.1 | | |
| markdown | CRAN | | 0.7.7 | 0.7.7 | 0.7.7 |
| MASS | base | 7.3-45 | 7.3-45 | 7.3-45 | 7.3-45 |
| Matrix | base | 1.2-7.1 | 1.2-7.1 | 1.2-8 | 1.2-6 |
| matrixcalc | CRAN | 1.0-3 | 1.0-3 | 1.0-3 | 1.0-3 |
| mclust | CRAN | 5.2 | 5.2.1 | 5.2.2 | 5.2 |
| memoise | CRAN | 1.0.0 | 1.0.0 | 1.0.0 | 1.0.0 |
| methods | base | 3.3.2 | 3.3.2 | 3.3.1 | 3.3.0 |
| mgcv | base | 1.8-16 | 1.8-16 | 1.8-17 | 1.8-12 |
| mi | CRAN | | 1 | | |
| mime | CRAN | 0.5 | 0.5 | 0.5 | 0.4 |
| minqa | CRAN | | 1.2.4 | | 1.2.4 |
| mnormt | CRAN | 1.5-5 | 1.5-5 | | 1.5-4 |
| modelr | CRAN | 0.1.0 | | | |
| modeltools | CRAN | 0.2-21 | 0.2-21 | 0.2-21 | |
| multtest | Bioconductor | | 2.30.0 | 2.30.0 | |
| munsell | CRAN | 0.4.3 | 0.4.3 | 0.4.3 | 0.4.3 |
| mvtnorm | CRAN | 1.0-5 | 1.0-5 | 1.0-6 | 1.0-5 |
| network | CRAN | | 1.13.0 | | |
| nlme | base | 3.1-128 | 3.1-128 | 3.1-131 | 3.1-128 |
| nloptr | CRAN | | 1.0.4 | | 1.0.4 |
| NMF | CRAN | 0.20.6 | 0.20.6 | 0.20.6 | 0.20.6 |
| nnet | base | 7.3-12 | 7.3-12 | 7.3-12 | 7.3-12 |
| numDeriv | CRAN | | 2016.8-1 | | 2014.2-1 |
| openssl | CRAN | 0.9.4 | 0.9.6 | 0.9.6 | 0.9.4 |

| | | | | | |
|-------------------|------------------|------------|------------|-------------|-------------|
| org.Hs.eg.db | Bioconductor | | 3.1.2 | | 3.3.0 |
| org.Sc.sgd.db | Bioconductor | | 3.4.0 | | |
| parallel | base | 3.3.2 | 3.3.2 | 3.3.1 | 3.3.0 |
| pathway.structure | GitHub | 0.1.0 | 0.1.0 | 0.1.0 | 0.1.0 |
| .permutation | TomKellyGenetics | | | | |
| pbivnorm | CRAN | | 0.6.0 | | |
| PGSEA | Bioconductor | | 1.48.0 | | |
| pkgmaker | CRAN | 0.22 | 0.22 | 0.22 | 0.22 |
| PKI | CRAN | | 0.1-3 | | |
| plogr | CRAN | | 0.1-1 | 0.1-1 | |
| plot.igraph | GitHub | 0.0.0.9001 | 0.0.0.9001 | 0.0.0.9001 | 0.0.0.9001 |
| | TomKellyGenetics | | | | |
| plotrix | CRAN | | 3.6-4 | | |
| plyr | CRAN | 1.8.4 | 1.8.4 | 1.8.4 | 1.8.3 |
| png | CRAN | | 0.1-7 | | 0.1-7 |
| prabclus | CRAN | 2.2-6 | 2.2-6 | 2.2-6 | |
| praise | CRAN | 1.0.0 | 1.0.0 | | 1.0.0 |
| pROC | CRAN | | 1.8 | 1.9.1 | |
| prodlim | CRAN | | 1.5.7 | | |
| prof.tree | CRAN | | 0.1.0 | | |
| proftools | CRAN | | 0.99-2 | | |
| progress | CRAN | | | 1.1.2 | |
| psych | CRAN | 1.6.12 | 1.6.12 | | |
| purrr | CRAN | 0.2.2 | 0.2.2 | 0.2.2 | 0.2.2 |
| qgraph | CRAN | | 1.4.1 | | |
| quadprog | CRAN | | 1.5-5 | 1.5-5 | 1.5-5 |
| R.methodsS3 | CRAN | | 1.7.1 | | 1.7.1 |
| R.oo | CRAN | | 1.21.0 | | 1.20.0 |
| R.utils | CRAN | | 2.5.0 | | |
| R6 | CRAN | 2.1.3 | 2.2.0 | 2.2.0 | 2.1.3 |
| RBGL | CRAN | | 1.50.0 | | |
| RColorBrewer | CRAN | 1.1-2 | 1.1-2 | 1.1-2 | 1.1-2 |
| Rcpp | CRAN | 0.12.7 | 0.12.9 | 0.12.9 | 0.12.7 |
| RcppArmadillo | CRAN | | | 0.7.700.0.0 | 0.6.700.6.0 |
| RcppEigen | CRAN | | 0.3.2.9.0 | | 0.3.2.8.1 |

| | | | | | |
|--------------|----------------------|--------|----------|----------|-----------|
| RCurl | CRAN | | 1.95-4.8 | 1.95-4.8 | 1.95-4.8 |
| reactome.db | Bioconductor | | 1.52.1 | 1.52.1 | |
| reactometree | GitHub | | 0.1 | | |
| | TomKellyGenetics | | | | |
| readr | CRAN | 1.0.0 | 1.0.0 | | |
| readxl | CRAN | 0.1.1 | | | |
| registry | CRAN | 0.3 | 0.3 | 0.3 | 0.3 |
| reshape2 | CRAN | 1.4.1 | 1.4.2 | 1.4.2 | 1.4.1 |
| rgeff | CRAN | | 0.15.3 | 0.15.3 | |
| rgl | CRAN | | | 0.97.0 | 0.95.1441 |
| Rgraphviz | CRAN | | 2.18.0 | | |
| rjson | CRAN | | 0.2.15 | | |
| RJSONIO | CRAN | | 1.3-0 | | |
| rmarkdown | CRAN | | 1.3 | 1.3 | 1 |
| Rmpi | CRAN | | 0.6-6 | | 0.6-5 |
| rngtools | CRAN | 1.2.4 | 1.2.4 | 1.2.4 | 1.2.4 |
| robustbase | CRAN | 0.92-7 | 0.92-7 | 0.92-7 | 0.92-5 |
| ROCR | CRAN | 1.0-7 | 1.0-7 | 1.0-7 | 1.0-7 |
| Rook | CRAN | | 1.1-1 | 1.1-1 | |
| roxygen2 | CRAN | 6.0.1 | 5.0.1 | 6.0.1 | 5.0.1 |
| rpart | base | 4.1-10 | 4.1-10 | 4.1-10 | 4.1-10 |
| rprojroot | CRAN | 1.2 | 1.1 | 1.2 | |
| Rsamtools | Bioconductor | | 1.26.1 | 1.26.1 | |
| rsconnect | CRAN | | 0.7 | | |
| RSQLite | CRAN | | 1.1-2 | 1.1-2 | 1.0.0 |
| rstudioapi | CRAN | 0.6 | 0.6 | 0.6 | 0.6 |
| rvest | CRAN | 0.3.2 | | | |
| S4Vectors | Bioconductor | | 0.12.1 | 0.12.0 | 0.10.3 |
| safe | Bioconductor | | 3.14.0 | 3.10.0 | |
| scales | CRAN | 0.4.0 | 0.4.1 | 0.4.1 | 0.4.0 |
| selectr | CRAN | 0.3-1 | | | |
| sem | CRAN | | 3.1-8 | | |
| shiny | CRAN | 0.14 | | 1.0.0 | |
| slipt | GitHub | 0.1.0 | 0.1.0 | 0.1.0 | 0.1.0 |
| | TomKellyGenetics | | | | |

| | | | | | |
|----------------------|----------------------------|------------|------------|----------|----------|
| sm | CRAN | 2.2-5.4 | 2.2-5.4 | | |
| sna | CRAN | | 2.4 | | |
| snow | CRAN | 0.4-1 | 0.4-2 | 0.4-2 | 0.3-13 |
| sourcetools | CRAN | 0.1.5 | | 0.1.5 | |
| SparseM | CRAN | | 1.74 | | 1.7 |
| spatial | base | 7.3-11 | 7.3-11 | 7.3-11 | 7.3-11 |
| splines | base | 3.3.2 | 3.3.2 | 3.3.1 | 3.3.0 |
| statnet.common | CRAN | | 3.3.0 | | |
| stats | base | 3.3.2 | 3.3.2 | 3.3.1 | 3.3.0 |
| stats4 | base | 3.3.2 | 3.3.2 | 3.3.1 | 3.3.0 |
| stringi | CRAN | 1.1.1 | 1.1.2 | 1.1.2 | 1.0-1 |
| stringr | CRAN | 1.1.0 | 1.1.0 | 1.2.0 | 1.0.0 |
| SummarizedExperiment | Bioconductor | | 1.4.0 | 1.4.0 | |
| survival | base | 2.39-4 | 2.40-1 | 2.40-1 | 2.39-4 |
| tcltk | base | 3.3.2 | 3.3.2 | 3.3.1 | 3.3.0 |
| testthat | CRAN | 1.0.2 | 1.0.2 | | 1.0.2 |
| tibble | CRAN | 1.2 | 1.2 | 1.2 | 1.2 |
| tidyverse | GitHub hadley | 1.1.1 | | | |
| timeline | CRAN | | 0.9 | | |
| tools | base | 3.3.2 | 3.3.2 | 3.3.1 | 3.3.0 |
| tpr | CRAN | | 0.3-1 | | |
| trimcluster | CRAN | 0.1-2 | 0.1-2 | 0.1-2 | |
| Unicode | CRAN | 9.0.0-1 | 9.0.0-1 | 9.0.0-1 | |
| utils | base | 3.3.2 | 3.3.2 | 3.3.1 | 3.3.0 |
| vioplot | CRAN | | 0.2 | | |
| vioplotx | GitHub TomKellyGenetics | 0.0.0.9000 | 0.0.0.9000 | | |
| viridis | CRAN | 0.3.4 | 0.3.4 | 0.3.4 | |
| visNetwork | CRAN | | 1.0.3 | 1.0.3 | |
| whisker | CRAN | 0.3-2 | 0.3-2 | 0.3-2 | 0.3-2 |
| withr | CRAN | 1.0.2 | 1.0.2 | 1.0.2 | 1.0.2 |
| XML | base | 3.98-1.3 | 3.98-1.1 | 3.98-1.5 | 3.98-1.4 |

| | | | | |
|----------|----------------------|--------|--------|--------|
| xml2 | CRAN | 1.1.1 | 1.1.1 | 1.0.0 |
| xtable | CRAN | 1.8-2 | 1.8-2 | 1.8-2 |
| XVector | Bioconductor | | 0.14.0 | 0.14.0 |
| yaml | CRAN | | 2.1.14 | 2.1.14 |
| zlibbioc | CRAN | | 1.20.0 | 1.20.0 |
| zoo | CRAN | 1.7-13 | 1.7-14 | 1.7-13 |

Appendix C

Mutation Analysis in Breast Cancer

C.1 Synthetic Lethal Genes and Pathways

SLIPT expression analysis (described in Section 3.1) on TCGA breast cancer data ($n = 969$) found the following genes and pathways, described in sections 4.1 and 4.1.1.

Table C.1: Candidate synthetic lethal gene partners of *CDH1* from mtSLIPT

| Gene | Observed | Expected | χ^2 value | p-value | p-value (FDR) |
|-----------------|----------|----------|----------------|------------------------|------------------------|
| <i>TFAP2B</i> | 8 | 36.7 | 89.5 | 3.60×10^{-20} | 8.37×10^{-17} |
| <i>ZNF423</i> | 15 | 36.7 | 78.8 | 7.89×10^{-18} | 1.22×10^{-14} |
| <i>CALCOCO1</i> | 11 | 36.7 | 76.8 | 2.09×10^{-17} | 2.59×10^{-14} |
| <i>RBM5</i> | 13 | 36.7 | 75.7 | 3.65×10^{-17} | 4.00×10^{-14} |
| <i>BTG2</i> | 7 | 36.7 | 71.7 | 2.72×10^{-16} | 1.81×10^{-13} |
| <i>RXRA</i> | 6 | 36.7 | 70.5 | 5.00×10^{-16} | 2.97×10^{-13} |
| <i>SLC27A1</i> | 11 | 36.7 | 70.3 | 5.42×10^{-16} | 2.97×10^{-13} |
| <i>MEF2D</i> | 12 | 36.7 | 69.6 | 7.86×10^{-16} | 3.95×10^{-13} |
| <i>NISCH</i> | 12 | 36.7 | 69.6 | 7.86×10^{-16} | 3.95×10^{-13} |
| <i>AVPR2</i> | 9 | 36.7 | 69.2 | 9.36×10^{-16} | 4.58×10^{-13} |
| <i>CRY2</i> | 13 | 36.7 | 68.9 | 1.07×10^{-15} | 4.98×10^{-13} |
| <i>RAPGEF3</i> | 13 | 36.7 | 68.9 | 1.07×10^{-15} | 4.98×10^{-13} |
| <i>NRIP2</i> | 10 | 36.7 | 68.2 | 1.58×10^{-15} | 7.18×10^{-13} |
| <i>DARC</i> | 12 | 36.7 | 66.4 | 3.76×10^{-15} | 1.54×10^{-12} |
| <i>SFRS5</i> | 12 | 36.7 | 66.4 | 3.76×10^{-15} | 1.54×10^{-12} |
| <i>NOSTRIN</i> | 5 | 36.7 | 65.1 | 7.40×10^{-15} | 2.70×10^{-12} |
| <i>KIF13B</i> | 12 | 36.7 | 63.4 | 1.69×10^{-14} | 5.16×10^{-12} |
| <i>TENC1</i> | 10 | 36.7 | 62.5 | 2.67×10^{-14} | 7.40×10^{-12} |
| <i>MFAP4</i> | 12 | 36.7 | 60.5 | 7.17×10^{-14} | 1.67×10^{-11} |
| <i>ELN</i> | 13 | 36.7 | 59.7 | 1.07×10^{-13} | 2.32×10^{-11} |
| <i>SGK223</i> | 14 | 36.7 | 59 | 1.51×10^{-13} | 3.05×10^{-11} |
| <i>KIF12</i> | 11 | 36.7 | 58.8 | 1.74×10^{-13} | 3.34×10^{-11} |
| <i>SELP</i> | 11 | 36.7 | 58.8 | 1.74×10^{-13} | 3.34×10^{-11} |
| <i>CIRBP</i> | 9 | 36.7 | 58.7 | 1.83×10^{-13} | 3.41×10^{-11} |
| <i>CTDSP1</i> | 9 | 36.7 | 58.7 | 1.83×10^{-13} | 3.41×10^{-11} |

Strongest candidate SL partners for *CDH1* by mtSLIPT with observed and expected numbers of *CDH1* mutant TCGA breast tumours with low expression of partner genes.

Table C.2: Pathways for *CDH1* partners from mtSLIPT

| Pathways Over-represented | Pathway Size | SL Genes | p-value (FDR) |
|---|--------------|----------|------------------------|
| Eukaryotic Translation Elongation | 86 | 60 | 2.0×10^{-128} |
| Peptide chain elongation | 83 | 59 | 2.0×10^{-128} |
| Eukaryotic Translation Termination | 83 | 58 | 2.3×10^{-125} |
| Viral mRNA Translation | 81 | 57 | 2.5×10^{-124} |
| Nonsense Mediated Decay independent of the Exon Junction Complex | 88 | 59 | 8.6×10^{-124} |
| Nonsense-Mediated Decay | 103 | 61 | 5.2×10^{-117} |
| Nonsense Mediated Decay enhanced by the Exon Junction Complex | 103 | 61 | 5.2×10^{-117} |
| Formation of a pool of free 40S subunits | 93 | 58 | 1.6×10^{-116} |
| L13a-mediated translational silencing of Ceruloplasmin expression | 103 | 59 | 1.3×10^{-111} |
| 3' -UTR-mediated translational regulation | 103 | 59 | 1.3×10^{-111} |
| GTP hydrolysis and joining of the 60S ribosomal subunit | 104 | 59 | 6.2×10^{-111} |
| SRP-dependent cotranslational protein targeting to membrane | 104 | 58 | 2.9×10^{-108} |
| Eukaryotic Translation Initiation | 111 | 59 | 3.0×10^{-106} |
| Cap-dependent Translation Initiation | 111 | 59 | 3.0×10^{-106} |
| Influenza Viral RNA Transcription and Replication | 108 | 57 | 5.1×10^{-103} |
| Influenza Infection | 117 | 59 | 1.5×10^{-102} |
| Translation | 141 | 64 | 3.7×10^{-101} |
| Influenza Life Cycle | 112 | 57 | 1.4×10^{-100} |
| GPCR downstream signalling | 472 | 116 | 1.0×10^{-80} |
| Hemostasis | 422 | 105 | 1.4×10^{-78} |

Gene set over-representation analysis (hypergeometric test) for Reactome pathways in mtSLIPT partners for *CDH1*.

The genes and pathways identified in Tables C.1 and C.2 were derived from comparing the expression profiles of potential partners to the mutation status of *CDH1* (as shown in Figure 3.2). Thus the following analysis is only limited the samples for which TCGA provides both expression and somatic mutation data.

C.2 Synthetic Lethal Expression Profiles

Similar to the analysis of synthetic lethal partners against low *CDH1* expression in 4.1.2, the partners detected from *CDH1* mutation were also examined for their expression profiles and the pathway composition of gene clusters. Hierarchical clustering was performed on mtSLIPT partners for *CDH1* as showing in Figure C.1. Overrepresentation for Reactome pathways for each of the gene clusters identified is given in Table C.3.

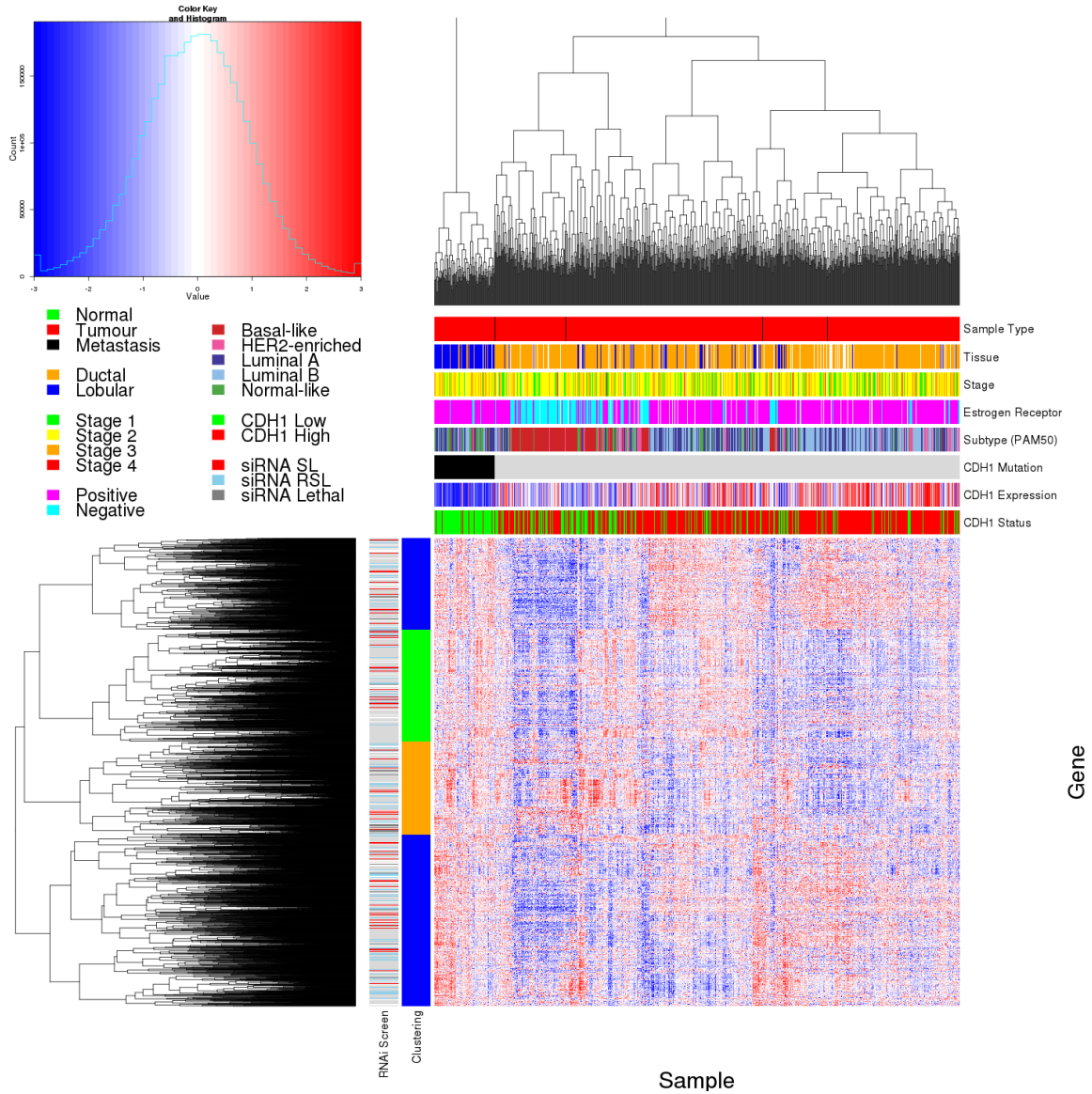


Figure C.1: Synthetic lethal expression profiles of analysed samples. Gene expression profile heatmap (correlation distance) of all samples (separated by *CDH1* somatic mutation status) analysed in **TCGA** breast cancer dataset for gene expression of 3743 candidate partners of **E-cadherin** (*CDH1*) from **mtSLIPT** prediction (with significant **FDR** adjusted $p < 0.05$). Deeply clustered, inter-correlated genes form several main groups, each containing genes that were SL candidates or toxic in an **siRNA** screen [Telford et al. \(2015\)](#). Clusters had different sample groups highly expressing the synthetic lethal candidates in *CDH1* mutant samples and often lowly expressing *CDH1* wildtype samples (which were not tested for), although many of the *CDH1* mutant samples had among the lowest *CDH1* expression. In contrast to the expression analysis the (predominantly *CDH1* wildtype) basal subtype and estrogen receptor negative samples have depleted expression among most candidate synthetic lethal partners.

Table C.3: Pathways for clusters of *CDH1* partners from mtSLIPT

| Pathways Over-represented in Cluster 1 | Pathway | Size | Cluster Genes | p-value (FDR) |
|---|---------|------|---------------|------------------------|
| Olfactory Signalling Pathway | | 57 | 8 | 7.1×10^{-9} |
| Assembly of the primary cilium | | 149 | 14 | 8.0×10^{-9} |
| Sphingolipid metabolism | | 62 | 8 | 9.6×10^{-9} |
| Signalling by ERBB4 | | 133 | 12 | 5.1×10^{-8} |
| PI3K Cascade | | 65 | 7 | 4.9×10^{-7} |
| Circadian Clock | | 33 | 5 | 4.9×10^{-7} |
| Nuclear signalling by ERBB4 | | 34 | 5 | 4.9×10^{-7} |
| Intraflagellar transport | | 35 | 5 | 4.9×10^{-7} |
| PI3K events in ERBB4 signalling | | 87 | 8 | 4.9×10^{-7} |
| PIP3 activates AKT signalling | | 87 | 8 | 4.9×10^{-7} |
| PI3K events in ERBB2 signalling | | 87 | 8 | 4.9×10^{-7} |
| PI-3K cascade:FGFR1 | | 87 | 8 | 4.9×10^{-7} |
| PI-3K cascade:FGFR2 | | 87 | 8 | 4.9×10^{-7} |
| PI-3K cascade:FGFR3 | | 87 | 8 | 4.9×10^{-7} |
| PI-3K cascade:FGFR4 | | 87 | 8 | 4.9×10^{-7} |
| Deadenylation of mRNA | | 22 | 4 | 5.6×10^{-7} |
| PI3K/AKT activation | | 90 | 8 | 5.6×10^{-7} |
| Cargo trafficking to the periciliary membrane | | 38 | 5 | 5.6×10^{-7} |
| Pathways Over-represented in Cluster 2 | Pathway | Size | Cluster Genes | p-value (FDR) |
| G _{αs} signalling events | | 83 | 19 | 5.1×10^{-25} |
| Extracellular matrix organization | | 238 | 30 | 1.4×10^{-18} |
| Hemostasis | | 422 | 46 | 2.7×10^{-16} |
| Aquaporin-mediated transport | | 32 | 9 | 2.7×10^{-16} |
| Transcriptional regulation of white adipocyte differentiation | | 56 | 11 | 1.7×10^{-15} |
| Degradation of the extracellular matrix | | 102 | 15 | 1.7×10^{-15} |
| Integration of energy metabolism | | 84 | 13 | 8.8×10^{-15} |
| GPCR downstream signalling | | 472 | 48 | 2.8×10^{-14} |
| G _{αz} signalling events | | 15 | 6 | 5.0×10^{-14} |
| Molecules associated with elastic fibres | | 33 | 8 | 5.4×10^{-14} |
| Phase 1 - Functionalization of compounds | | 67 | 11 | 5.6×10^{-14} |
| Platelet activation, signalling and aggregation | | 179 | 20 | 5.6×10^{-14} |
| Vasopressin regulates renal water homeostasis via Aquaporins | | 24 | 7 | 6.1×10^{-14} |
| Elastic fibre formation | | 37 | 8 | $.03 \times 10^{-13}$ |
| Calmodulin induced events | | 27 | 7 | 3.3×10^{-13} |
| CaM pathway | | 27 | 7 | 3.3×10^{-13} |
| cGMP effects | | 18 | 6 | 3.6×10^{-13} |
| G _{αi} signalling events | | 167 | 18 | 6.3×10^{-13} |
| Pathways Over-represented in Cluster 3 | Pathway | Size | Cluster Genes | p-value (FDR) |
| Eukaryotic Translation Elongation | | 86 | 55 | 1.1×10^{-112} |
| Peptide chain elongation | | 83 | 54 | 1.3×10^{-112} |
| Viral mRNA Translation | | 81 | 53 | 1.6×10^{-111} |
| Eukaryotic Translation Termination | | 83 | 53 | 7.1×10^{-110} |
| Nonsense Mediated Decay independent of the Exon Junction Complex | | 88 | 54 | 1.0×10^{-108} |
| Formation of a pool of free 40S subunits | | 93 | 53 | 4.1×10^{-102} |
| Nonsense-Mediated Decay | | 103 | 54 | 3.9×10^{-98} |
| Nonsense Mediated Decay enhanced by the Exon Junction Complex | | 103 | 54 | 3.9×10^{-98} |
| L13a-mediated translational silencing of Ceruloplasmin expression | | 103 | 53 | 1.2×10^{-95} |
| 3' -UTR-mediated translational regulation | | 103 | 53 | 1.2×10^{-95} |
| SRP-dependent cotranslational protein targeting to membrane | | 104 | 53 | 4.3×10^{-95} |
| GTP hydrolysis and joining of the 60S ribosomal subunit | | 104 | 53 | 4.3×10^{-95} |
| Influenza Viral RNA Transcription and Replication | | 108 | 53 | 9.6×10^{-93} |
| Eukaryotic Translation Initiation | | 111 | 53 | 4.2×10^{-91} |
| Cap-dependent Translation Initiation | | 111 | 53 | 4.2×10^{-91} |
| Influenza Life Cycle | | 112 | 53 | 1.4×10^{-90} |
| Influenza Infection | | 117 | 53 | 6.2×10^{-88} |
| Translation | | 141 | 55 | 3×10^{-81} |
| Pathways Over-represented in Cluster 4 | Pathway | Size | Cluster Genes | p-value (FDR) |
| ECM proteoglycans | | 66 | 10 | 2.9×10^{-11} |
| deactivation of the beta-catenin transactivating complex | | 38 | 7 | 5.1×10^{-10} |
| Arachidonic acid metabolism | | 41 | 7 | 1.1×10^{-9} |
| G _{αq} signalling events | | 149 | 14 | 4.0×10^{-9} |
| HS-GAG degradation | | 21 | 5 | 4.5×10^{-9} |
| Uptake and actions of bacterial toxins | | 22 | 5 | 6.1×10^{-9} |
| Gastrin-CREB signalling pathway via PKC and MAPK | | 170 | 15 | 6.1×10^{-9} |
| RNA Polymerase I, RNA Polymerase III, and Mitochondrial Transcription | | 64 | 8 | 6.1×10^{-9} |
| Non-integrin membrane-ECM interactions | | 53 | 7 | 1.5×10^{-8} |
| Syndecan interactions | | 25 | 5 | 1.5×10^{-8} |
| NOTCH1 Intracellular Domain Regulates Transcription | | 40 | 6 | 2.3×10^{-8} |
| Synthesis of Leukotrienes and Exoxins | | 15 | 4 | 3.2×10^{-8} |
| Signalling by NOTCH1 | | 59 | 7 | 5.3×10^{-8} |
| Regulation of insulin secretion | | 44 | 6 | 6.0×10^{-8} |
| Metabolism of lipids and lipoproteins | | 471 | 37 | 8.2×10^{-8} |
| Signalling by NOTCH1 | | 80 | 8 | 1.2×10^{-7} |
| Platelet activation, signalling and aggregation | | 179 | 14 | 1.2×10^{-7} |
| Recruitment of mitotic centrosome proteins and complexes | | 64 | 7 | 1.2×10^{-7} |

Pathway over-representation analysis for Reactome pathways with the number of genes in each pathway (Pathway Size), number of genes within the pathway identified (Cluster Genes), and the pathway over-representation p-value (adjusted by FDR) from the hypergeometric test.

C.3 Comparison to Primary Screen

The mutation synthetic lethal partners with *CDH1* were also compared to [siRNA](#) primary screen data ([Telford et al., 2015](#)), as performed in Section 4.2.1. These are expected to be more concordant with the experimental results performed on a null mutant, however this is not the case at the gene level: less genes overlapped with experimental candidates in Figure C.2. This may be affected by lower sample size for mutations in [TCGA](#) data or lower frequency (expected value) of *CDH1* mutations compared to low expression.

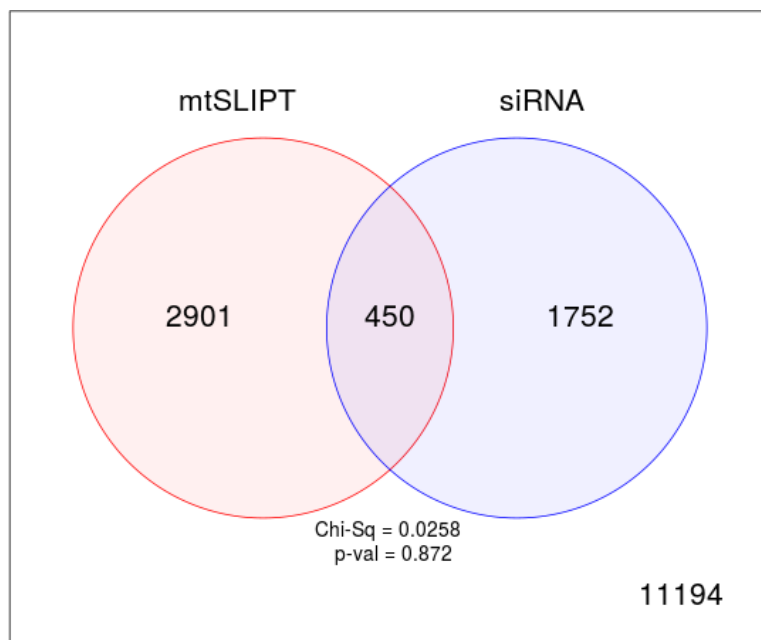


Figure C.2: **Comparison of mtSLIPT to siRNA.** Testing the overlap of gene candidates for [E-cadherin](#) synthetic lethal partners between computational (SLIPT) and experimental screening (siRNA) approaches. The χ^2 test suggests that the overlap is no more than would be expected by chance ($p = 0.281$).

Despite a lower sample size (and low number of predicted partners) for mutation analysis, the pathway composition (Tables C.2 and C.4) is similar to expression analysis, as described in Section 4.2.5. In particular, the resampling analysis (Section C.3.1) supported many of the results of expression analysis (Section 4.2.5.1) with Tables C.5 and C.6 detecting many of the same or functionally-related pathways.

Table C.4: Pathways for *CDH1* partners from mtSLIPT and siRNA

| Predicted only by SLIPT (2901 genes) | Pathway | Size | Genes Identified | p-value (FDR) |
|---|---------|------|------------------|------------------------|
| Eukaryotic Translation Elongation | | 87 | 57 | 2.8×10^{-120} |
| Peptide chain elongation | | 84 | 56 | 3.1×10^{-120} |
| Eukaryotic Translation Termination | | 84 | 55 | 2.8×10^{-117} |
| Viral mRNA Translation | | 82 | 54 | 4.1×10^{-116} |
| Nonsense Mediated Decay independent of the Exon Junction Complex | | 89 | 55 | 3.7×10^{-113} |
| Formation of a pool of free 40S subunits | | 94 | 55 | 2.8×10^{-109} |
| Nonsense-Mediated Decay | | 104 | 57 | 8.4×10^{-108} |
| Nonsense Mediated Decay enhanced by the Exon Junction Complex | | 104 | 57 | 8.4×10^{-108} |
| L13a-mediated translational silencing of Ceruloplasmin expression | | 104 | 56 | 3.4×10^{-105} |
| 3' -UTR-mediated translational regulation | | 104 | 56 | 3.4×10^{-105} |
| GTP hydrolysis and joining of the 60S ribosomal subunit | | 105 | 56 | 1.4×10^{-104} |
| Eukaryotic Translation Initiation | | 112 | 56 | 2.8×10^{-100} |
| Cap-dependent Translation Initiation | | 112 | 56 | 2.8×10^{-100} |
| SRP-dependent cotranslational protein targeting to membrane | | 105 | 54 | 2.2×10^{-99} |
| Influenza Viral RNA Transcription and Replication | | 109 | 54 | 5.3×10^{-97} |
| Influenza Life Cycle | | 113 | 54 | 9.6×10^{-95} |
| Influenza Infection | | 118 | 55 | 1.7×10^{-94} |
| Translation | | 142 | 60 | 3.5×10^{-94} |
| Infectious disease | | 349 | 77 | 5.9×10^{-62} |
| Extracellular matrix organization | | 241 | 54 | 3.0×10^{-52} |

| Detected only by siRNA screen (1752 genes) | Pathway | Size | Genes Identified | p-value (FDR) |
|--|---------|------|------------------|-----------------------|
| Class A/1 (Rhodopsin-like receptors) | | 282 | 69 | 1.9×10^{-59} |
| GPCR ligand binding | | 363 | 78 | 2.7×10^{-54} |
| Peptide ligand-binding receptors | | 175 | 41 | 1.5×10^{-42} |
| $G_{\alpha i}$ signalling events | | 184 | 41 | 1.1×10^{-40} |
| Gastrin-CREB signalling pathway via PKC and MAPK | | 180 | 37 | 1.5×10^{-35} |
| $G_{\alpha q}$ signalling events | | 159 | 34 | 3.7×10^{-35} |
| DAP12 interactions | | 159 | 27 | 1.1×10^{-24} |
| VEGFA-VEGFR2 Pathway | | 91 | 19 | 1.0×10^{-23} |
| Downstream signal transduction | | 146 | 24 | 1.9×10^{-22} |
| Signalling by VEGF | | 99 | 19 | 2.6×10^{-22} |
| DAP12 signalling | | 149 | 24 | 4.2×10^{-22} |
| Organelle biogenesis and maintenance | | 264 | 34 | 4.3×10^{-20} |
| Downstream signalling of activated FGFR1 | | 134 | 21 | 4.3×10^{-20} |
| Downstream signalling of activated FGFR2 | | 134 | 21 | 4.3×10^{-20} |
| Downstream signalling of activated FGFR3 | | 134 | 21 | 4.3×10^{-20} |
| Downstream signalling of activated FGFR4 | | 134 | 21 | 4.3×10^{-20} |
| Signalling by ERBB2 | | 146 | 22 | 5.3×10^{-20} |
| Signalling by FGFR | | 146 | 22 | 5.3×10^{-20} |
| Signalling by FGFR1 | | 146 | 22 | 5.3×10^{-20} |
| Signalling by FGFR2 | | 146 | 22 | 5.3×10^{-20} |

| Intersection of SLIPT and siRNA screen (450 genes) | Pathway | Size | Genes Identified | p-value (FDR) |
|--|---------|------|------------------|----------------------|
| HS-GAG degradation | | 21 | 4 | 4.9×10^{-6} |
| Retinoid metabolism and transport | | 39 | 5 | 4.9×10^{-6} |
| Platelet activation, signalling and aggregation | | 186 | 13 | 4.9×10^{-6} |
| Signalling by NOTCH4 | | 11 | 3 | 4.9×10^{-6} |
| $G_{\alpha s}$ signalling events | | 100 | 8 | 5.0×10^{-6} |
| Defective EXT2 causes exostoses 2 | | 12 | 3 | 5.0×10^{-6} |
| Defective EXT1 causes exostoses 1, TRPS2 and CHDS | | 12 | 3 | 5.0×10^{-6} |
| Class A/1 (Rhodopsin-like receptors) | | 289 | 18 | 2.2×10^{-5} |
| Signalling by PDGF | | 173 | 11 | 2.9×10^{-5} |
| Circadian Clock | | 34 | 4 | 2.9×10^{-5} |
| Signalling by ERBB4 | | 139 | 9 | 4.3×10^{-5} |
| Role of LAT2/NTAL/LAB on calcium mobilization | | 99 | 7 | 4.4×10^{-5} |
| Peptide ligand-binding receptors | | 181 | 11 | 4.5×10^{-5} |
| Defective B4GALT7 causes EDS, progeroid type | | 19 | 3 | 4.5×10^{-5} |
| Defective B3GAT3 causes JDSSDHD | | 19 | 3 | 4.5×10^{-5} |
| Signalling by NOTCH | | 80 | 6 | 4.5×10^{-5} |
| $G_{\alpha q}$ signalling events | | 164 | 10 | 5.1×10^{-5} |
| Response to elevated platelet cytosolic Ca^{2+} | | 84 | 6 | 7.1×10^{-5} |
| Signalling by ERBB2 | | 148 | 9 | 7.1×10^{-5} |
| Signalling by SCF-KIT | | 129 | 8 | 8.3×10^{-5} |

C.3.1 Resampling Analysis

Table C.5: Pathways for *CDH1* partners from mtSLIPT

| Reactome Pathway | Over-representation | Permutation |
|---|------------------------|--------------------------|
| Eukaryotic Translation Elongation | 3.2×10^{-128} | $< 7.035 \times 10^{-4}$ |
| Peptide chain elongation | 3.2×10^{-128} | $< 7.035 \times 10^{-4}$ |
| Eukaryotic Translation Termination | 3.7×10^{-125} | $< 7.035 \times 10^{-4}$ |
| Viral mRNA Translation | 4.1×10^{-124} | $< 7.035 \times 10^{-4}$ |
| Nonsense Mediated Decay independent of the Exon Junction Complex | 1.4×10^{-123} | $< 7.035 \times 10^{-4}$ |
| Nonsense-Mediated Decay | 8.4×10^{-117} | $< 7.035 \times 10^{-4}$ |
| Nonsense Mediated Decay enhanced by the Exon Junction Complex | 8.4×10^{-117} | $< 7.035 \times 10^{-4}$ |
| Formation of a pool of free 40S subunits | 2.6×10^{-116} | $< 7.035 \times 10^{-4}$ |
| L13a-mediated translational silencing of Ceruloplasmin expression | 2.0×10^{-111} | $< 7.035 \times 10^{-4}$ |
| 3' -UTR-mediated translational regulation | 2.0×10^{-111} | $< 7.035 \times 10^{-4}$ |
| GTP hydrolysis and joining of the 60S ribosomal subunit | 9.9×10^{-111} | $< 7.035 \times 10^{-4}$ |
| SRP-dependent cotranslational protein targeting to membrane | 4.7×10^{-108} | $< 7.035 \times 10^{-4}$ |
| Eukaryotic Translation Initiation | 4.8×10^{-106} | $< 7.035 \times 10^{-4}$ |
| Cap-dependent Translation Initiation | 4.8×10^{-106} | $< 7.035 \times 10^{-4}$ |
| Influenza Viral RNA Transcription and Replication | 8.1×10^{-103} | $< 7.035 \times 10^{-4}$ |
| Influenza Infection | 2.4×10^{-102} | $< 7.035 \times 10^{-4}$ |
| Translation | 6.0×10^{-101} | $< 7.035 \times 10^{-4}$ |
| Influenza Life Cycle | 2.2×10^{-100} | $< 7.035 \times 10^{-4}$ |
| Disease | 2.1×10^{-90} | 0.013347 |
| GPCR downstream signalling | 1.6×10^{-80} | 0.095478 |
| Hemostasis | 2.1×10^{-78} | 0.2671 |
| Signalling by GPCR | 1.2×10^{-73} | 0.44939 |
| <i>Extracellular matrix organization</i> | 2.2×10^{-67} | 0.054008 |
| Metabolism of proteins | 1.4×10^{-66} | 0.9607 |
| Signal Transduction | 2.1×10^{-66} | 0.48184 |
| Developmental Biology | 2.5×10^{-66} | 0.54075 |
| Innate Immune System | 5.3×10^{-66} | 0.9589 |
| Infectious disease | 9.6×10^{-66} | 0.21075 |
| Signalling by NGF | 1.1×10^{-62} | 0.43356 |
| Immune System | 2.8×10^{-62} | 0.23052 |

Over-representation (hypergeometric test) and Permutation p-values adjusted for multiple tests across pathways (**FDR**). Significant pathways are marked in bold (**FDR** < 0.05) and italics (**FDR** < 0.1).

Table C.6: Pathways for *CDH1* partners from mtSLIPT and siRNA primary screen

| Reactome Pathway | Over-representation | Permutation |
|---|----------------------|-------------|
| Visual phototransduction | 1.2×10^{-9} | 0.86279 |
| G_{as} signalling events | 2.9×10^{-7} | 0.023066 |
| Retinoid metabolism and transport | 2.9×10^{-7} | 0.299 |
| Acylic chain remodelling of PS | 1.1×10^{-5} | 0.42584 |
| Transcriptional regulation of white adipocyte differentiation | 1.1×10^{-5} | 0.53928 |
| Chemokine receptors bind chemokines | 1.1×10^{-5} | 0.95259 |
| <i>Signalling by NOTCH4</i> | 1.2×10^{-5} | 0.079229 |
| Defective EXT2 causes exostoses 2 | 1.2×10^{-5} | 0.22292 |
| Defective EXT1 causes exostoses 1, TRPS2 and CHDS | 1.2×10^{-5} | 0.22292 |
| Platelet activation, signalling and aggregation | 1.2×10^{-5} | 0.48853 |
| Serotonin receptors | 1.4×10^{-5} | 0.34596 |
| Nicotinamide salvaging | 1.4×10^{-5} | 0.70881 |
| Phase 1 - Functionalization of compounds | 2×10^{-5} | 0.31142 |
| Amine ligand-binding receptors | 2.5×10^{-5} | 0.34934 |
| Acylic chain remodelling of PE | 3.8×10^{-5} | 0.42615 |
| Signalling by GPCR | 3.8×10^{-5} | 0.93888 |
| Molecules associated with elastic fibres | 3.9×10^{-5} | 0.017982 |
| DAP12 interactions | 3.9×10^{-5} | 0.71983 |
| Beta defensins | 3.9×10^{-5} | 0.91458 |
| Cytochrome P ₄₅₀ - arranged by substrate type | 4.7×10^{-5} | 0.83493 |
| GPCR ligand binding | 5.7×10^{-5} | 0.95258 |
| Acylic chain remodelling of PC | 6.1×10^{-5} | 0.42584 |
| Response to elevated platelet cytosolic Ca ²⁺ | 6.4×10^{-5} | 0.54046 |
| Arachidonic acid metabolism | 6.7×10^{-5} | 0.026696 |
| Defective B4GALT7 causes EDS, progeroid type | 7.3×10^{-5} | 0.24921 |
| Defective B3GAT3 causes JDSSDHD | 7.3×10^{-5} | 0.24921 |
| Hydrolysis of LPC | 7.3×10^{-5} | 0.80663 |
| Elastic fibre formation | 7.4×10^{-5} | 0.0058768 |
| HS-GAG degradation | 9.4×10^{-5} | 0.0083179 |
| <i>Bile acid and bile salt metabolism</i> | 9.4×10^{-5} | 0.079905 |
| Netrin-1 signalling | 0.00011 | 0.92216 |
| Integration of energy metabolism | 0.00011 | 0.011152 |
| Dectin-2 family | 0.00012 | 0.10385 |
| Platelet sensitization by LDL | 0.00012 | 0.34596 |
| DAP12 signalling | 0.00012 | 0.62787 |
| Defensins | 0.00012 | 0.77542 |
| GPCR downstream signalling | 0.00012 | 0.79454 |
| <i>Diseases associated with glycosaminoglycan metabolism</i> | 0.00013 | 0.065927 |
| <i>Diseases of glycosylation</i> | 0.00013 | 0.065927 |
| Signalling by Retinoic Acid | 0.00013 | 0.22292 |
| Signalling by Leptin | 0.00013 | 0.34596 |
| Signalling by SCF-KIT | 0.00013 | 0.70881 |
| Opioid Signalling | 0.00013 | 0.96053 |
| Signalling by NOTCH | 0.00015 | 0.26884 |
| Platelet homeostasis | 0.00015 | 0.4878 |
| Signalling by NOTCH1 | 0.00016 | 0.13043 |
| Class B/2 (Secretin family receptors) | 0.00016 | 0.13994 |
| <i>Diseases of Immune System</i> | 0.0002 | 0.0795 |
| <i>Diseases associated with the TLR signalling cascade</i> | 0.0002 | 0.0795 |
| A tetrasaccharide linker sequence is required for GAG synthesis | 0.0002 | 0.42615 |

Over-representation (hypergeometric test) and Permutation p-values adjusted for multiple tests across pathways (**FDR**). Significant pathways are marked in bold (**FDR** < 0.05) and italics (**FDR** < 0.1).

C.4 Compare SLIPT genes

The mutation synthetic lethal partners with *CDH1* were also compared to siRNA primary screen data (Telford *et al.*, 2015), by correlation and siRNA viability as described in sections 4.2.2 and 4.2.3.

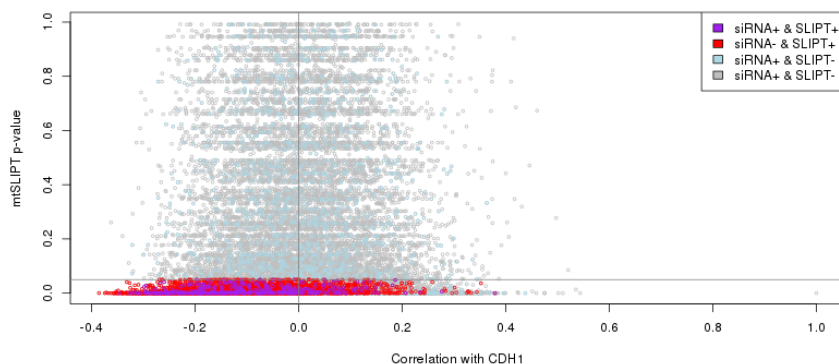


Figure C.3: **Compare mtSLIPT and siRNA genes with correlation.** The mtSLIPT p-values were compared against Pearson’s correlation of expression with *CDH1*. Genes detected by SLIPT or siRNA are coloured according to the legend.

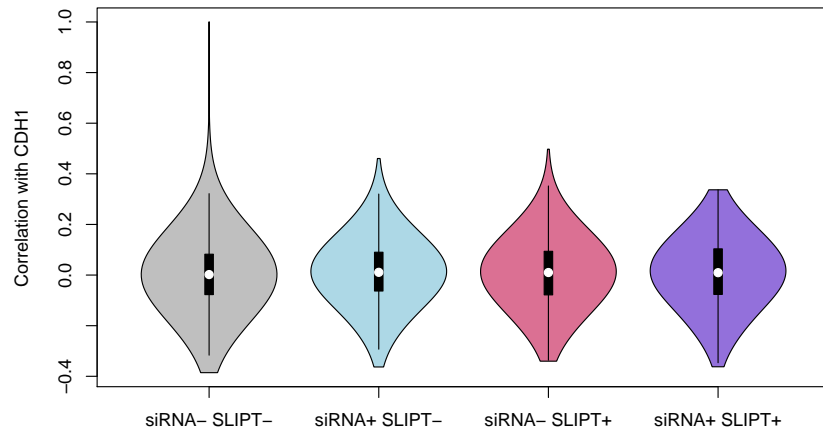


Figure C.4: **Compare mtSLIPT and siRNA genes with correlation.** Genes detected by mtSLIPT against *CDH1* mutation and siRNA screening were compared against Pearson’s correlation of expression with *CDH1*. There were no differences in correlation between the gene groups.

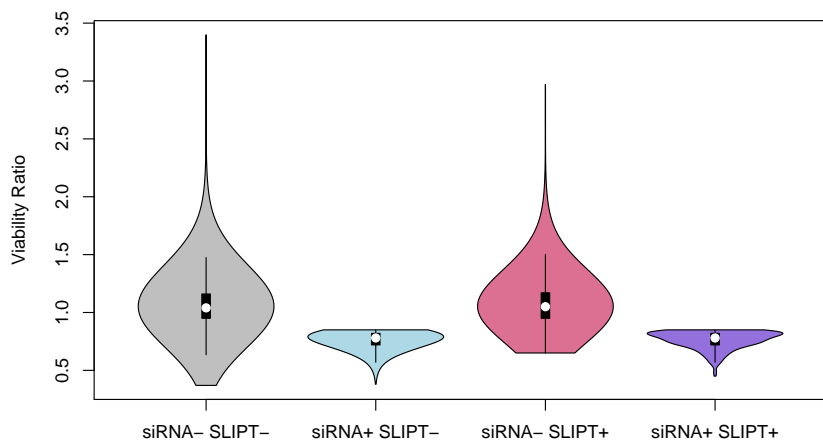


Figure C.5: Compare mtSLIPT and siRNA genes with siRNA viability. Genes detected as candidate synthetic lethal partners by mtSLIPT (in TCGA breast cancer) expression analysis against *CDH1* mutation and experimental screening (with siRNA) were compared against the viability ratio of *CDH1* mutant and wildtype cells in the primary siRNA screen. There were clear no differences in viability between genes detected by mtSLIPT and those not with the differences being primarily due to viability thresholds being used to detect synthetic lethality by Telford *et al.* (2015).

C.5 Metagene Analysis

Metagene analysis was also performed for synthetic lethal candidates for *CDH1* mutation. These are described and compared to expression analysis in Section 4.3.3.

Table C.7: Candidate synthetic lethal metagenes against *CDH1* from mtSLIPT

| Pathway | ID | Observed | Expected | χ^2 value | p-value | p-value (FDR) |
|--|---------|----------|----------|----------------|------------------------|------------------------|
| Neurotoxicity of clostridium toxins | 168799 | 8 | 36.7 | 79.4 | 5.71×10^{-18} | 3.14×10^{-15} |
| Aquaporin-mediated transport | 445717 | 8 | 36.7 | 76.3 | 2.73×10^{-17} | 9.01×10^{-15} |
| Toxicity of botulinum toxin type G (BoNT/G) | 5250989 | 8 | 36.7 | 76.3 | 2.73×10^{-17} | 9.01×10^{-15} |
| ABC-family proteins mediated transport | 382556 | 10 | 36.7 | 68.2 | 1.58×10^{-15} | 1.86×10^{-13} |
| G _{αz} signalling events | 418597 | 10 | 36.7 | 59.9 | 9.97×10^{-14} | 5.48×10^{-12} |
| Regulation of IGF transport and uptake by IGFBPs | 381426 | 9 | 36.7 | 56.3 | 5.88×10^{-13} | 2.11×10^{-11} |
| GP1b-IX-V activation signalling | 430116 | 8 | 36.7 | 55.7 | 8.20×10^{-13} | 2.76×10^{-11} |
| GABA receptor activation | 977443 | 12 | 36.7 | 55.1 | 1.07×10^{-12} | 3.26×10^{-11} |
| Vasopressin regulates renal water homeostasis via Aquaporins | 432040 | 9 | 36.7 | 54.1 | 1.77×10^{-12} | 4.88×10^{-11} |
| Toxicity of botulinum toxin type D (BoNT/D) | 5250955 | 14 | 36.7 | 53.4 | 2.54×10^{-12} | 6.64×10^{-11} |
| Toxicity of botulinum toxin type F (BoNT/F) | 5250981 | 14 | 36.7 | 53.4 | 2.54×10^{-12} | 6.64×10^{-11} |
| STAT6-mediated induction of chemokines | 3249367 | 16 | 36.7 | 52.2 | 4.72×10^{-12} | 1.13×10^{-10} |
| Toxicity of botulinum toxin type B (BoNT/B) | 5250958 | 14 | 36.7 | 50.8 | 9.5×10^{-12} | 1.98×10^{-10} |
| S6K1 signalling | 165720 | 12 | 36.7 | 50.2 | 1.24×10^{-11} | 2.5×10^{-10} |
| G _{αs} signalling events | 418555 | 11 | 36.7 | 49.2 | 2.08×10^{-11} | 3.85×10^{-10} |
| RHO GTPases activate CIT | 5625900 | 14 | 36.7 | 48.2 | 3.34×10^{-11} | 5.9×10^{-10} |
| NADE modulates death signalling | 205025 | 15 | 36.7 | 47.4 | 5.00×10^{-11} | 8.32×10^{-10} |
| Keratan sulfate degradation | 2022857 | 10 | 36.7 | 46.6 | 7.5×10^{-11} | 1.15×10^{-9} |
| Signalling by Retinoic Acid | 5362517 | 10 | 36.7 | 46.6 | 7.5×10^{-11} | 1.15×10^{-9} |
| Adenylate cyclase inhibitory pathway | 170670 | 14 | 36.7 | 45.9 | 1.11×10^{-10} | 1.59×10^{-9} |
| Inhibition of adenylate cyclase pathway | 997269 | 14 | 36.7 | 45.9 | 1.11×10^{-10} | 1.59×10^{-9} |
| Fatty acids | 211935 | 6 | 36.7 | 45.7 | 1.21×10^{-10} | 1.72×10^{-9} |
| Ionotropic activity of Kainate Receptors | 451306 | 13 | 36.7 | 44.6 | 2.03×10^{-10} | 2.58×10^{-9} |
| Activation of Ca-permeable Kainate Receptor | 451308 | 13 | 36.7 | 44.6 | 2.03×10^{-10} | 2.58×10^{-9} |
| RA biosynthesis pathway | 5365859 | 13 | 36.7 | 44.6 | 2.03×10^{-10} | 2.58×10^{-9} |

Strongest candidate SL partners for *CDH1* by mtSLIPT with observed and expected numbers of mutant *CDH1* TCGA breast cancer tumours with low expression of partner metagenes.

C.6 Expression of Somatic Mutations

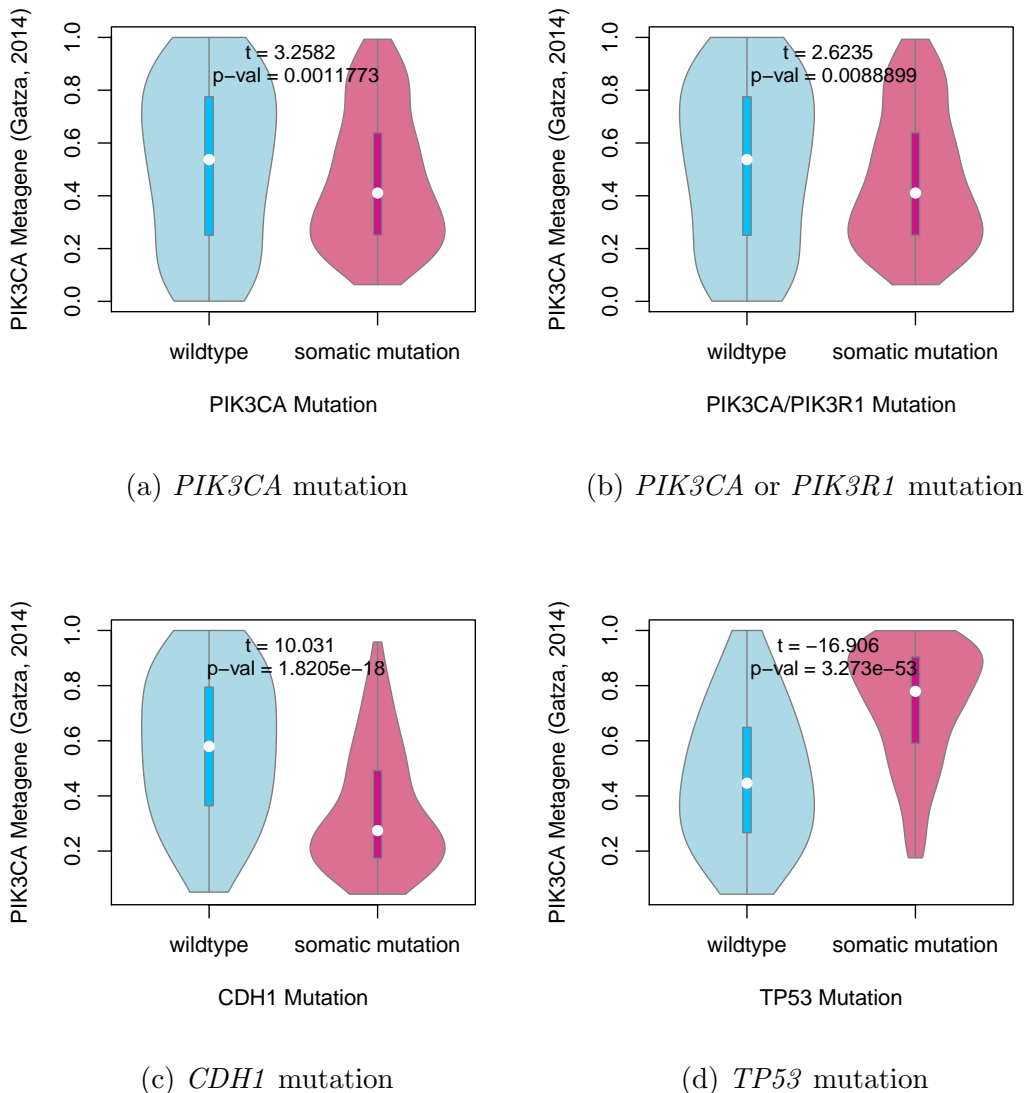


Figure C.6: **Somatic mutation against PIK3CA metagene.** Mutations in *PIK3CA*, *PIK3R1*, *CDH1*, and *TP53* were examined in [TCGA](#) breast cancer for their effect on the PIK3CA (Gatza *et al.*, 2014) pathway metagene. The tumour suppressors *CDH1* and *TP53* showed an increase and decrease in the metagene respectively, whereas *PIK3CA* and *PIK3R1* mutations weaker evidence of decrease in metagene levels.

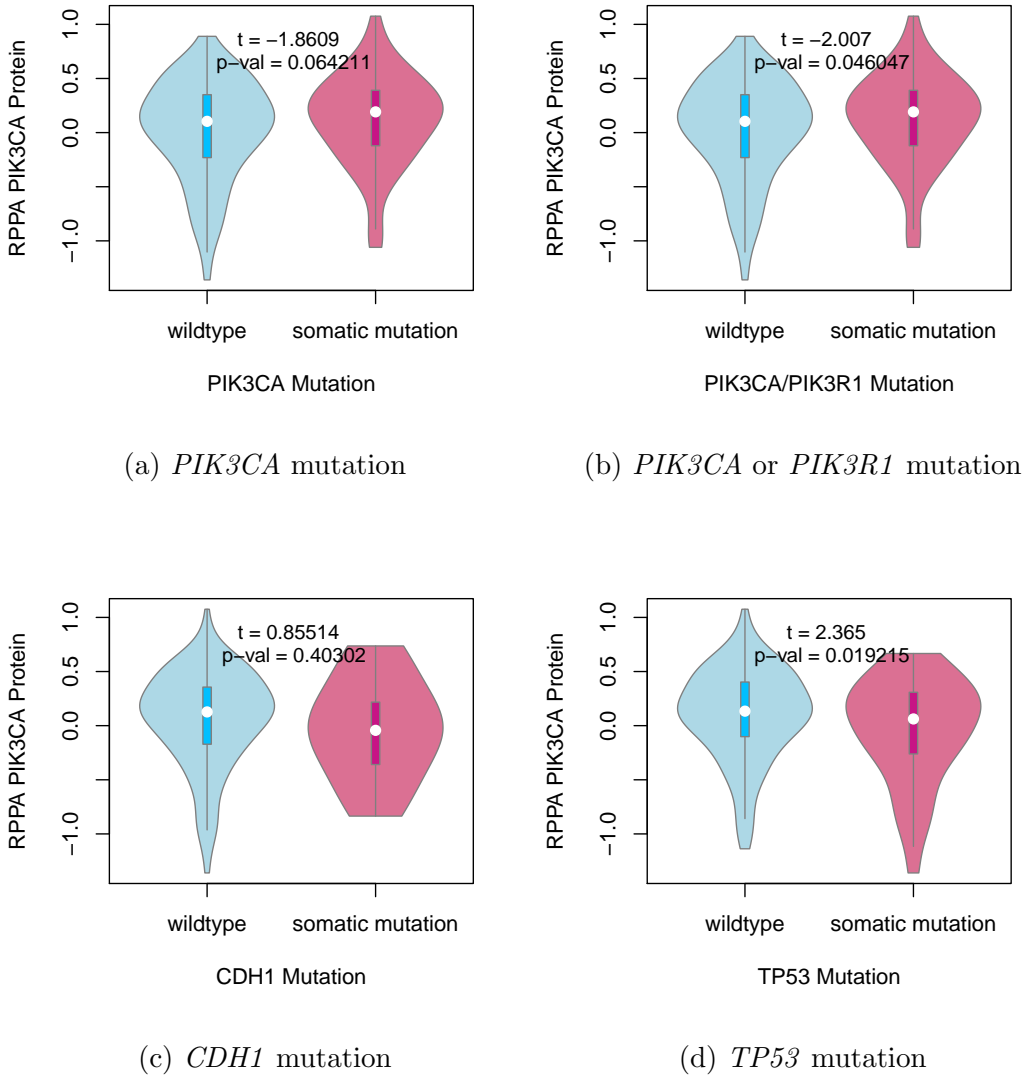


Figure C.7: Somatic mutation against PI3K protein. Mutations in *PIK3CA*, *PIK3R1*, *CDH1*, and *TP53* were examined in TCGA breast cancer for their effect on the expression of the p110 α protein (encoded by *PIK3CA*). Protein levels were significantly elevated in samples with *PIK3CA* or *PIK3R1* mutations and lower in samples with *TP53* mutations.

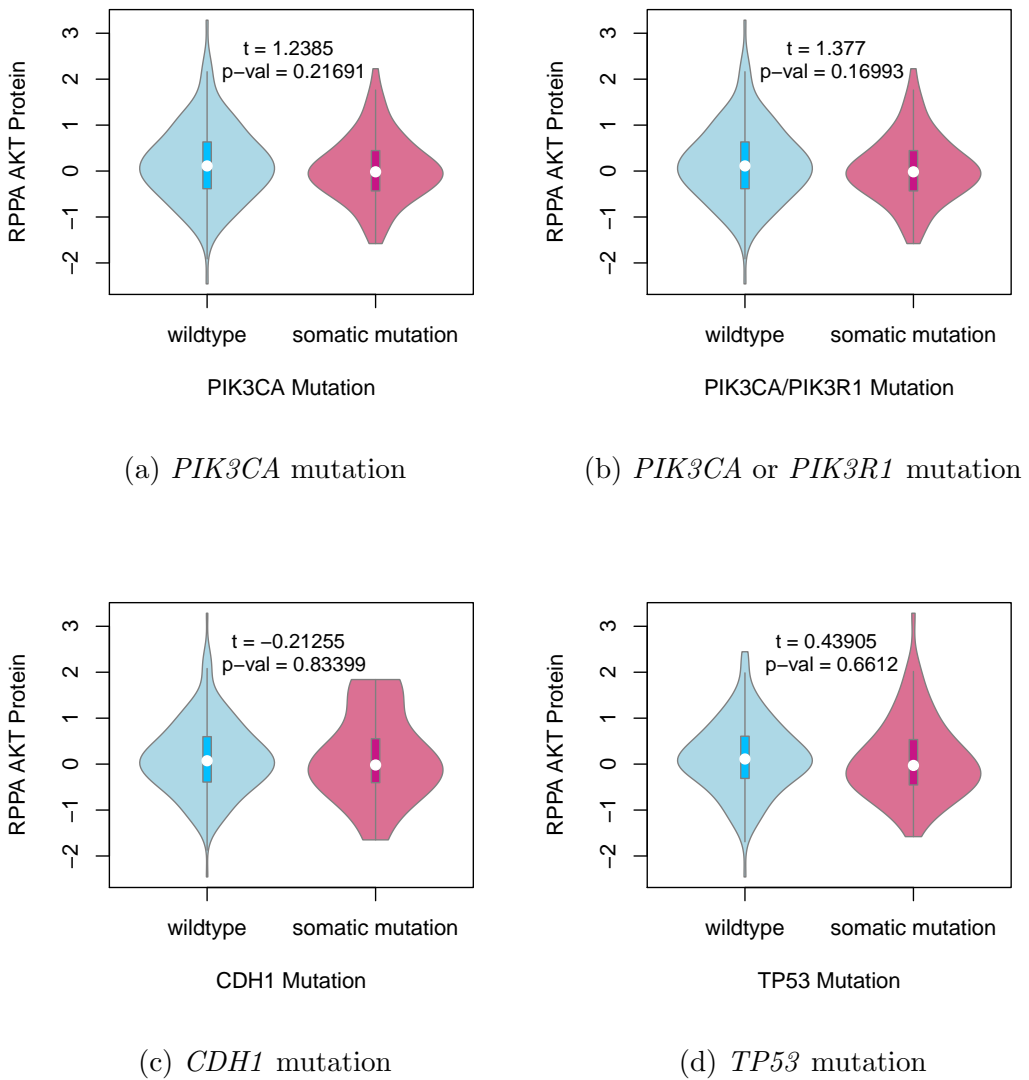


Figure C.8: Somatic mutation against AKT protein. Mutations in *PIK3CA*, *PIK3R1*, *CDH1*, and *TP53* were examined in TCGA breast cancer for their effect on the expression of the AKT protein (a downstream target of *PIK3CA*). Protein levels were not significantly different in samples with mutations in any of these cancer genes.

C.7 Metagene Expression Profiles

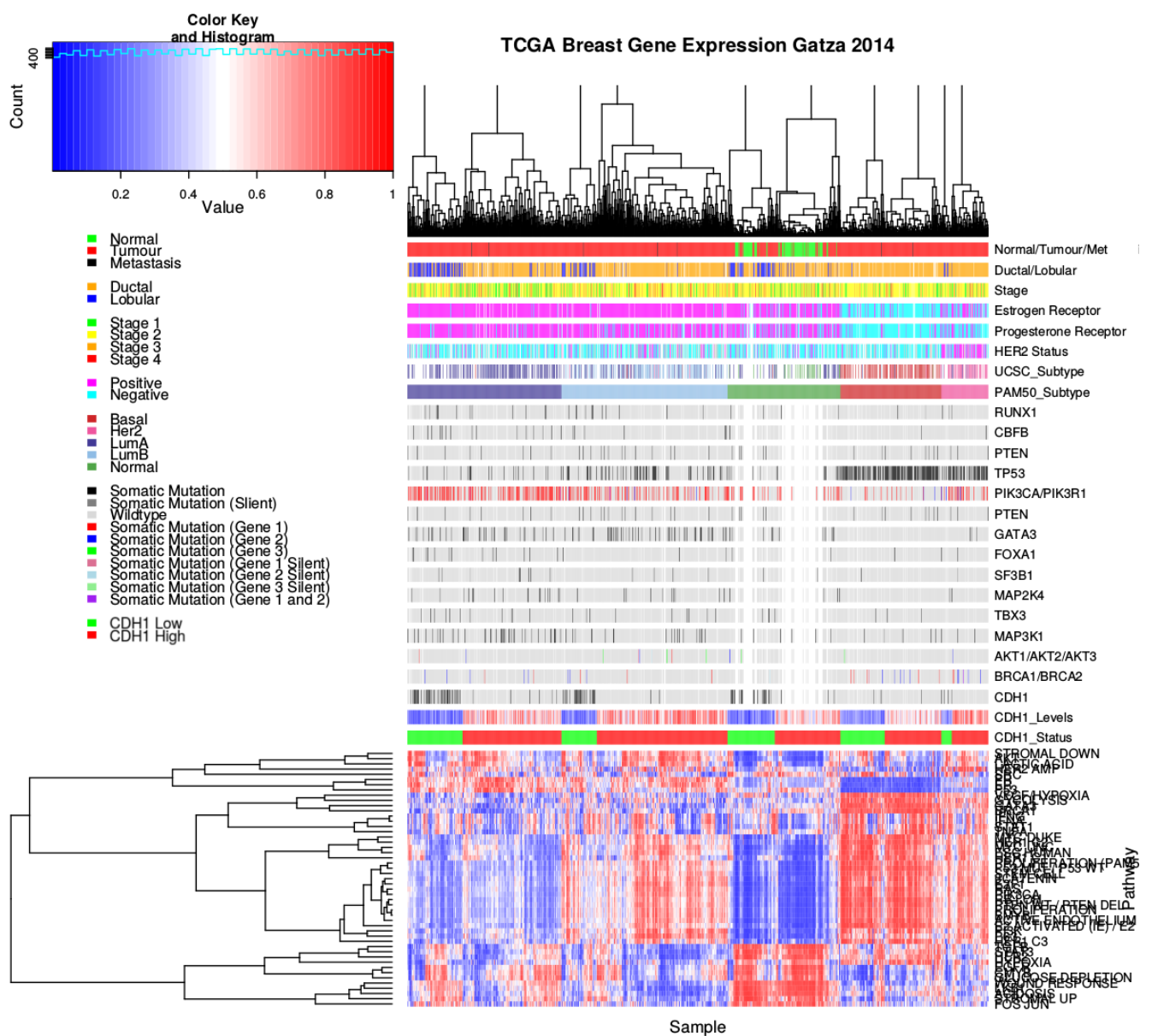


Figure C.9: **Pathway metagene expression profiles.** Expression profiles for metagene signatures from Gatza *et al.* (2014) in TCGA breast data, annotated for clinical factors and cancer gene mutations.

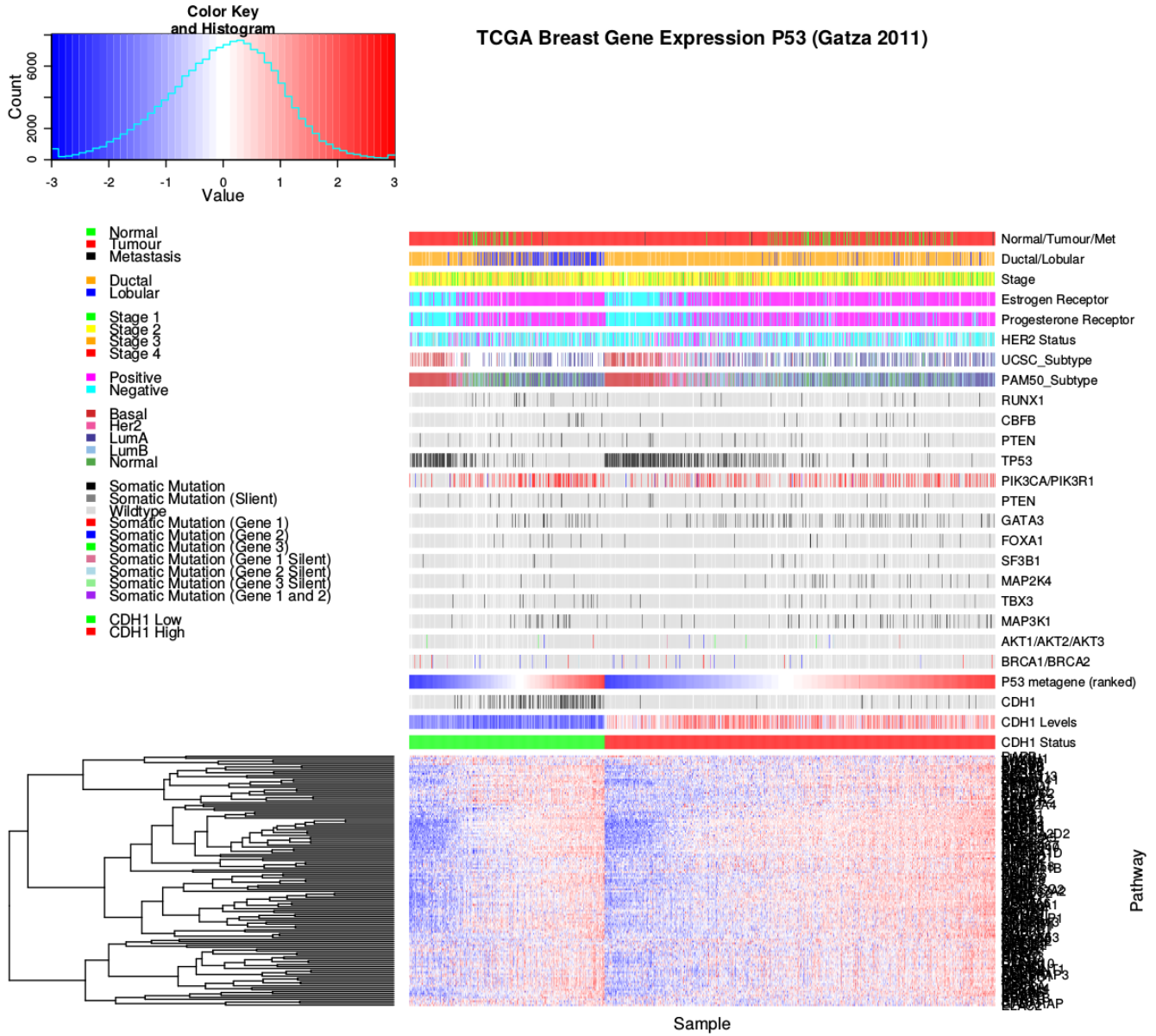


Figure C.10: **Expression profiles for p53 related genes.** Expression profiles the genes contained in the *TP53* gene signature from [Gatza et al. \(2011\)](#) in TCGA breast data, annotated for clinical factors and cancer gene mutations. Samples are separated by *CDH1* expression status and sorted by the metagene. In both cases, the majority of genes were consistent with the direction of the metagene, with few very exceptions. *TP53* mutant samples had low metagene expression, consistent with loss of tumour suppressor functions, and were less likely to have *CDH1* or *PIK3CA* mutations.

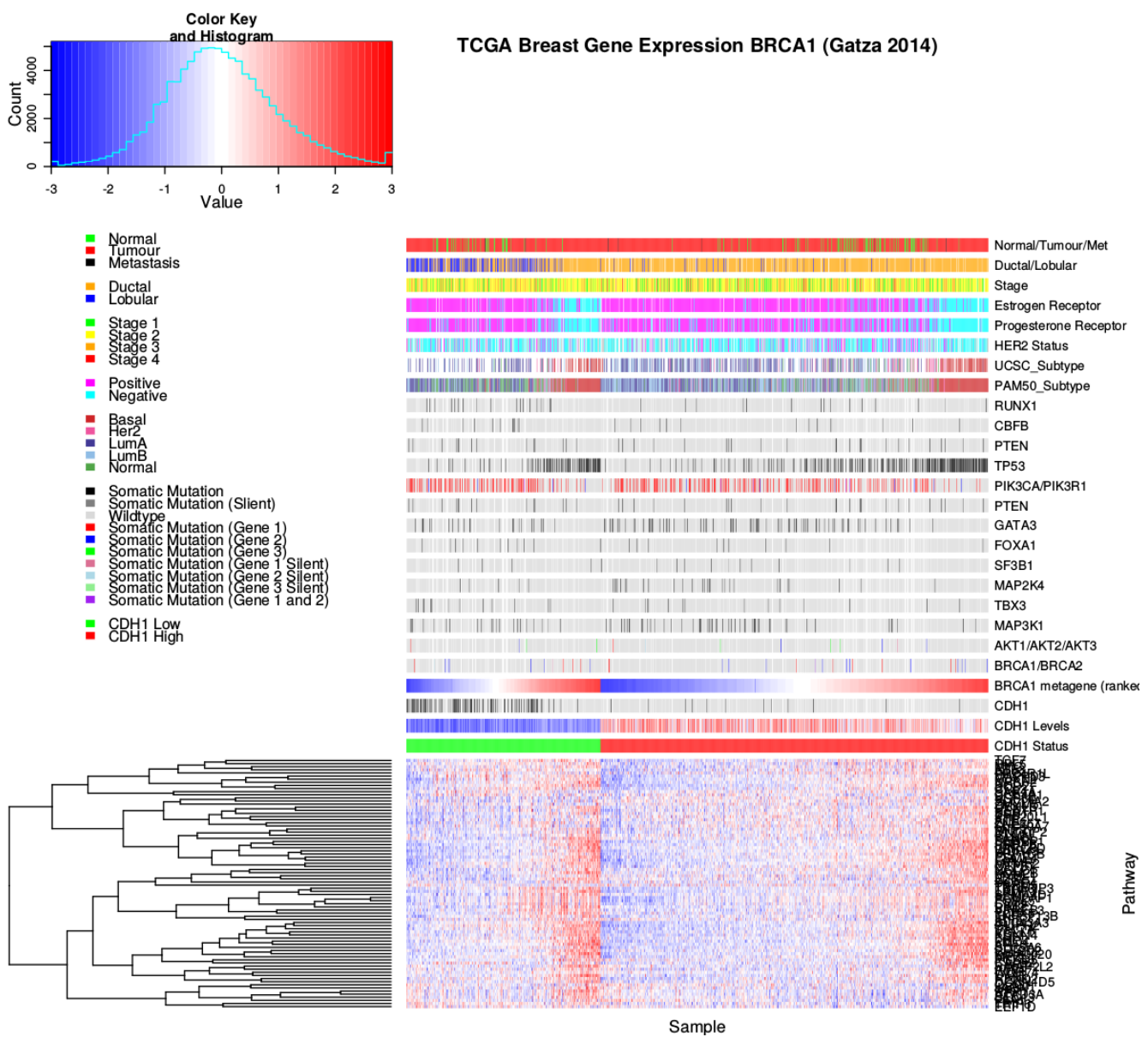


Figure C.11: **Expression profiles for BRCA related genes.** Expression profiles the genes contained in the gene signature related to *BRCA1* and *BRCA2* functions from [Gatza et al. \(2014\)](#) in TCGA breast data, annotated for clinical factors and cancer gene mutations. Samples are separated by *CDH1* expression status and sorted by the metagene. In both cases, the majority of genes were consistent with the direction of the metagene, with few very exceptions. *BRCA1* and *BRCA2* mutant samples had higher metagene expression than most samples for the ductal subtype, although this was not the case (for the lobular samples for which the metagene was lower). However, the metagene was higher for basal subtype and estrogen receptor negative samples.

Appendix D

Intrinsic Subtyping

The intrinsic subtypes for [TCGA](#) breast cancer samples provided by [UCSC](#) ([TCGA, 2012](#)) that were derived from microarray analysis have been compared to the [PAM50](#) results for performing subtyping from [RNA-Seq](#) data ([Parker *et al.*, 2009](#)). As shown in Table D.1, these subtypes were highly concordant for samples which had both procedures performed upon them ($\chi^2 = 1305.9, p = 2.73 \times 10^{-268}$). The main exception were the luminal A samples some of which were reclassified as luminal B or “normal-like”.

Table D.1: Comparison of intrinsic subtypes

| UCSC Subtype | | | | | |
|---------------|------------|---------------|-----------|-----------|-------------|
| | Basal-like | HER2-enriched | Luminal A | Luminal B | Normal-like |
| | 100 | 58 | 232 | 128 | 30 |
| PAM50 Subtype | | | | | |
| | Basal-like | HER2-enriched | Luminal A | Luminal B | Normal-like |
| | 208 | 94 | 314 | 334 | 227 |
| UCSC Subtype | | | | | |
| PAM50 Subtype | Basal-like | HER2-enriched | Luminal A | Luminal B | Normal-like |
| Basal-like | 96 | 4 | 2 | 2 | 1 |
| HER2-enriched | 0 | 47 | 5 | 3 | 0 |
| Luminal A | 1 | 0 | 141 | 1 | 0 |
| Luminal B | 2 | 7 | 49 | 121 | 0 |
| Normal-like | 1 | 0 | 35 | 1 | 29 |

The intrinsic subtypes of [TCGA](#) breast samples were compared between those provided by [UCSC](#) ([TCGA, 2012](#)) from microarray expression to those derived from [RNA-Seq](#) data ([Parker *et al.*, 2009](#)). Comparisons between these were limited to samples for which both data types were available.

The [PAM50](#) subtypes are potentially more accurate given similarity of these subtypes and that the remainder of the subtypes were accurately recapitulated with [RNA-](#)

Seq data. Furthermore, **UCSC** subtypes correctly identified 22/22 normal samples as “normal-like” and **PAM50** subtyping in **RNA-Seq** data had a success rate of 112/113 (including all of those identified from microarrays). Therefore the **PAM50** subtypes (performed on a larger cohort of samples) are appropriate to use for further interpretation, superceeding the **UCSC** subtypes available for a limited set of samples.

Appendix E

Expression Analysis in Stomach Cancer

The following results are a replication of the [TCGA](#) results (in Chapter 4) with stomach cancer data, using synthetic lethality (SLIPT) against *CDH1*.

E.1 Synthetic Lethal Genes and Pathways

Table E.1: Synthetic lethal gene partners of *CDH1* from SLIPT in stomach cancer

| Gene | Observed | Expected | χ^2 value | p-value | p-value (FDR) |
|------------------|----------|----------|----------------|------------------------|------------------------|
| <i>PRAF2</i> | 17 | 50.4 | 121 | 3.54×10^{-25} | 1.45×10^{-21} |
| <i>EMP3</i> | 17 | 50.4 | 115 | 5.06×10^{-24} | 1.48×10^{-20} |
| <i>PLEKHO1</i> | 22 | 50.4 | 112 | 2.14×10^{-23} | 4.75×10^{-20} |
| <i>SELM</i> | 20 | 50.4 | 111 | 5.13×10^{-23} | 8.09×10^{-20} |
| <i>GYPC</i> | 20 | 50.4 | 110 | 5.77×10^{-23} | 8.45×10^{-20} |
| <i>COX7A1</i> | 18 | 50.4 | 109 | 1.15×10^{-22} | 1.39×10^{-19} |
| <i>TNFSF12</i> | 20 | 50.4 | 106 | 4.06×10^{-22} | 4.38×10^{-19} |
| <i>SEPT4</i> | 17 | 50.4 | 106 | 6.58×10^{-22} | 5.91×10^{-19} |
| <i>LGALS1</i> | 19 | 50.4 | 105 | 6.64×10^{-22} | 5.91×10^{-19} |
| <i>RARRES2</i> | 27 | 50.4 | 105 | 8.02×10^{-22} | 6.85×10^{-19} |
| <i>VEGFB</i> | 16 | 50.4 | 104 | 1.19×10^{-21} | 9.74×10^{-19} |
| <i>PRR24</i> | 22 | 50.4 | 102 | 2.96×10^{-21} | 2.02×10^{-18} |
| <i>SYNC</i> | 19 | 50.4 | 102 | 3.73×10^{-21} | 2.39×10^{-18} |
| <i>MAGEH1</i> | 17 | 50.4 | 100 | 9.52×10^{-21} | 5.01×10^{-18} |
| <i>HSPB2</i> | 23 | 50.4 | 99.6 | 1.19×10^{-20} | 5.82×10^{-18} |
| <i>SMARCD3</i> | 19 | 50.4 | 99 | 1.59×10^{-20} | 7.57×10^{-18} |
| <i>CREM</i> | 13 | 50.4 | 98.1 | 2.48×10^{-20} | 1.13×10^{-17} |
| <i>GNG11</i> | 20 | 50.4 | 97.3 | 3.68×10^{-20} | 1.59×10^{-17} |
| <i>GNAI2</i> | 17 | 50.4 | 96.4 | 5.75×10^{-20} | 2.36×10^{-17} |
| <i>FUNDC2</i> | 22 | 50.4 | 95.9 | 7.39×10^{-20} | 2.91×10^{-17} |
| <i>CNRIP1</i> | 21 | 50.4 | 95.3 | 1.0×10^{-19} | 3.66×10^{-17} |
| <i>CALHM2</i> | 22 | 50.4 | 93.1 | 2.94×10^{-19} | 1.06×10^{-16} |
| <i>ARID5A</i> | 18 | 50.4 | 92.7 | 3.47×10^{-19} | 1.22×10^{-16} |
| <i>ST3GAL3</i> | 27 | 50.4 | 92.2 | 4.49×10^{-19} | 1.56×10^{-16} |
| <i>LOC339524</i> | 21 | 50.4 | 92.1 | 4.8×10^{-19} | 1.59×10^{-16} |

SLIPT partners of *CDH1* with observed and expected numbers of [TCGA](#) stomach cancer samples with low expression of both genes.

Table E.2: Pathways for *CDH1* partners from SLIPT in stomach cancer

| Pathways Over-represented | Pathway Size | SL Genes | p-value (FDR) |
|---|--------------|----------|------------------------|
| Extracellular matrix organization | 241 | 104 | 7.5×10^{-140} |
| Hemostasis | 445 | 138 | 1.8×10^{-121} |
| Developmental Biology | 432 | 125 | 9.2×10^{-107} |
| Axon guidance | 289 | 94 | 1.5×10^{-102} |
| Eukaryotic Translation Termination | 84 | 49 | 1.9×10^{-99} |
| GPCR ligand binding | 373 | 108 | 3.8×10^{-99} |
| Viral mRNA Translation | 82 | 48 | 3.3×10^{-98} |
| Formation of a pool of free 40S subunits | 94 | 51 | 3.3×10^{-98} |
| Eukaryotic Translation Elongation | 87 | 49 | 1.6×10^{-97} |
| Peptide chain elongation | 84 | 48 | 7.2×10^{-97} |
| Class A/1 (Rhodopsin-like receptors) | 289 | 90 | 2.7×10^{-96} |
| Nonsense Mediated Decay independent of the Exon Junction Complex | 89 | 49 | 3.0×10^{-96} |
| Infectious disease | 349 | 100 | 2.6×10^{-94} |
| GTP hydrolysis and joining of the 60S ribosomal subunit | 105 | 52 | 3.4×10^{-94} |
| L13a-mediated translational silencing of Ceruloplasmin expression | 104 | 51 | 2.8×10^{-92} |
| 3' -UTR-mediated translational regulation | 104 | 51 | 2.8×10^{-92} |
| Neuronal System | 272 | 84 | 8.4×10^{-92} |
| SRP-dependent cotranslational protein targeting to membrane | 105 | 51 | 9.5×10^{-92} |
| Eukaryotic Translation Initiation | 112 | 52 | 2.0×10^{-90} |
| Cap-dependent Translation Initiation | 112 | 52 | 2.0×10^{-90} |

Gene set over-representation analysis (hypergeometric test) for Reactome pathways in [SLIPT](#) partners for *CDH1*.

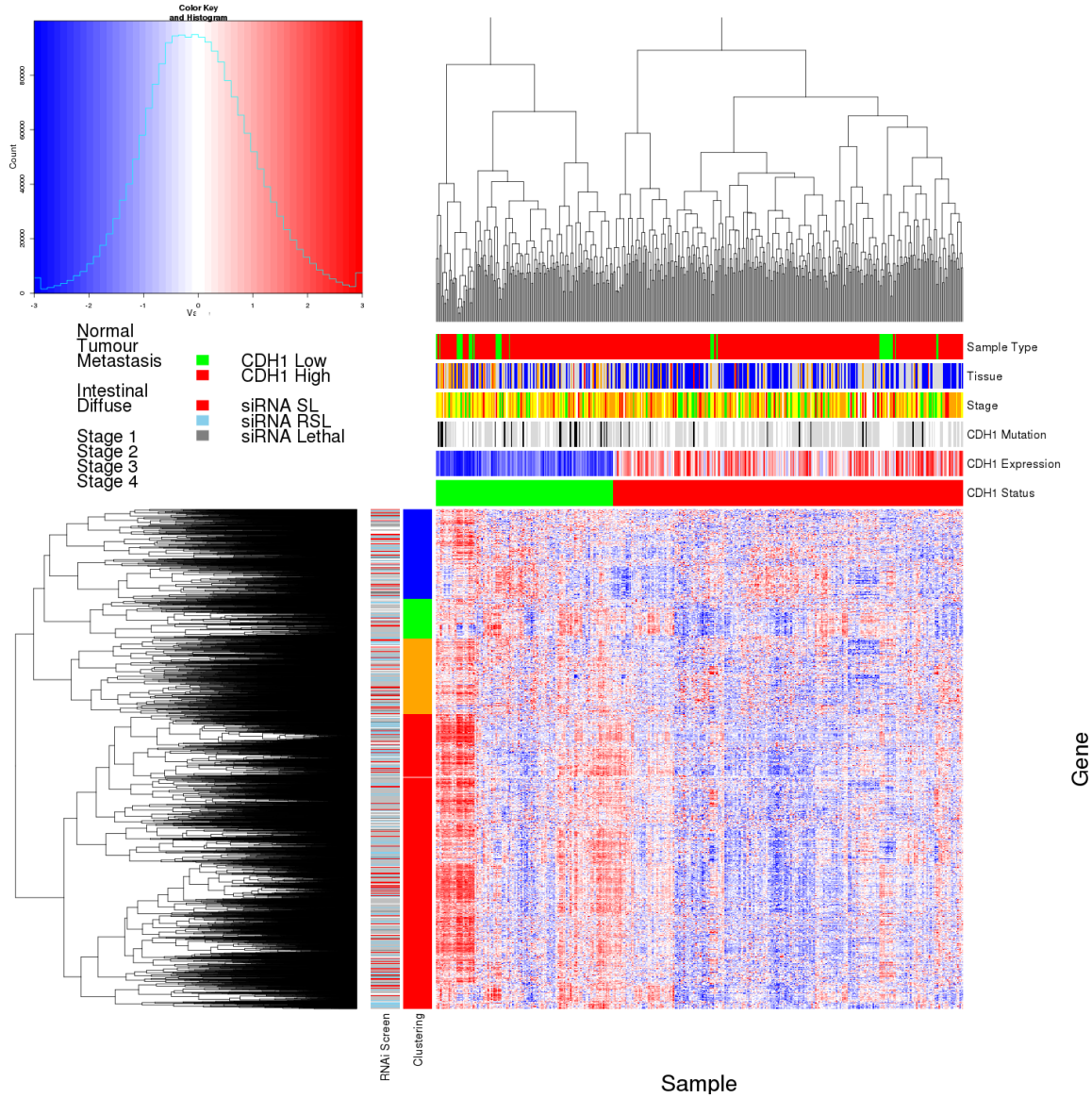


Figure E.1: Synthetic lethal expression profiles of analysed samples. Gene expression profile heatmap (correlation distance) of all samples (separated by the 1/3 quantile of *CDH1* expression) analysed in [TCGA](#) stomach cancer dataset for gene expression of 4365 candidate partners of **E-cadherin** (*CDH1*) from [SLIPT](#) prediction (with significant **FDR** adjusted $p < 0.05$). Deeply clustered, inter-correlated genes form several main groups, each containing genes that were **SL** candidates or toxic in an [siRNA](#) screen [Telford et al. \(2015\)](#). Clusters had different sample groups highly expressing the synthetic lethal candidates in *CDH1* low samples, notably diffuse and *CDH1* mutant samples have elevated expression in one or more distinct clusters, although there was less complexity and variation among candidate synthetic lethal partners than in breast data. *CDH1* low samples also contained most of samples with *CDH1* mutations.

Table E.3: Pathways for clusters of *CDH1* partners in stomach SLIPT

| Pathways Over-represented in Cluster 1 | Pathway Size | Cluster Genes | p-value (FDR) |
|--|--------------|---------------|------------------------|
| Viral mRNA Translation | 82 | 48 | 1.3×10^{-97} |
| Formation of a pool of free 40S subunits | 94 | 51 | 1.3×10^{-97} |
| Eukaryotic Translation Elongation | 87 | 49 | 4.8×10^{-97} |
| Peptide chain elongation | 84 | 48 | 1.4×10^{-96} |
| Eukaryotic Translation Termination | 84 | 48 | 1.4×10^{-96} |
| GTP hydrolysis and joining of the 60S ribosomal subunit | 105 | 52 | 7.9×10^{-94} |
| Nonsense Mediated Decay independent of the Exon Junction Complex | 89 | 48 | 3.1×10^{-93} |
| L13a-mediated translational silencing of Ceruloplasmin expression | 104 | 51 | 5.1×10^{-92} |
| 3' -UTR-mediated translational regulation | 104 | 51 | 5.1×10^{-92} |
| SRP-dependent cotranslational protein targeting to membrane | 105 | 51 | 1.7×10^{-91} |
| Eukaryotic Translation Initiation | 112 | 52 | 3.3×10^{-90} |
| Cap-dependent Translation Initiation | 112 | 52 | 3.3×10^{-90} |
| Translation | 142 | 56 | 3.6×10^{-85} |
| Nonsense-Mediated Decay | 104 | 48 | 1.2×10^{-84} |
| Nonsense Mediated Decay enhanced by the Exon Junction Complex | 104 | 48 | 1.2×10^{-84} |
| Influenza Viral RNA Transcription and Replication | 109 | 48 | 4.1×10^{-82} |
| Influenza Life Cycle | 113 | 48 | 3.4×10^{-80} |
| Influenza Infection | 118 | 48 | 6.4×10^{-78} |
| Pathways Over-represented in Cluster 2 | Pathway Size | Cluster Genes | p-value (FDR) |
| Immunoregulatory interactions between a Lymphoid and a non-Lymphoid cell | 65 | 12 | 1.3×10^{-15} |
| Phosphorylation of CD3 and TCR zeta chains | 18 | 6 | 1.7×10^{-12} |
| Generation of second messenger molecules | 29 | 7 | 2.7×10^{-12} |
| PD-1 signalling | 21 | 6 | 7.4×10^{-12} |
| TCR signalling | 62 | 9 | 4.3×10^{-11} |
| Translocation of ZAP-70 to Immunological synapse | 16 | 5 | 1.1×10^{-10} |
| Interferon alpha/beta signalling | 68 | 9 | 1.6×10^{-10} |
| Initial triggering of complement | 17 | 5 | 1.6×10^{-10} |
| IKK complex recruitment mediated by RIP1 | 19 | 5 | 5.1×10^{-10} |
| TRIF-mediated programmed cell death | 10 | 4 | 6.2×10^{-10} |
| Creation of C4 and C2 activators | 11 | 4 | 1.3×10^{-9} |
| RHO GTPases Activate NADPH Oxidases | 11 | 4 | 1.3×10^{-9} |
| Interferon Signalling | 175 | 15 | 2.3×10^{-9} |
| Chemokine receptors bind chemokines | 52 | 7 | 4.0×10^{-9} |
| Interferon gamma signalling | 74 | 8 | 1.6×10^{-8} |
| TRAF6 mediated induction of TAK1 complex | 15 | 4 | 1.6×10^{-8} |
| Activation of IRF3/IRF7 mediated by TBK1/IKK epsilon | 16 | 4 | 2.7×10^{-8} |
| Downstream TCR signalling | 45 | 6 | 3.5×10^{-8} |
| Pathways Over-represented in Cluster 3 | Pathway Size | Cluster Genes | p-value (FDR) |
| Uptake and actions of bacterial toxins | 22 | 4 | 3.5×10^{-6} |
| Neurotoxicity of clostridium toxins | 10 | 3 | 3.5×10^{-6} |
| Activation of PPARGC1A (PGC-1alpha) by phosphorylation | 10 | 3 | 3.5×10^{-6} |
| SMAD2/SMAD3:SMAD4 heterotrimer regulates transcription | 28 | 4 | 1.4×10^{-5} |
| Assembly of the primary cilium | 149 | 10 | 2.5×10^{-5} |
| Serotonin Neurotransmitter Release Cycle | 15 | 3 | 2.5×10^{-5} |
| Glycosaminoglycan metabolism | 114 | 8 | 3.3×10^{-5} |
| Platelet homeostasis | 54 | 5 | 3.3×10^{-5} |
| Norepinephrine Neurotransmitter Release Cycle | 17 | 3 | 3.3×10^{-5} |
| Acetylcholine Neurotransmitter Release Cycle | 17 | 3 | 3.3×10^{-5} |
| G _{αs} signalling events | 100 | 7 | 5.5×10^{-5} |
| GABA synthesis, release, reuptake and degradation | 19 | 3 | 5.6×10^{-5} |
| deactivation of the beta-catenin transactivating complex | 39 | 4 | 6.7×10^{-5} |
| Dopamine Neurotransmitter Release Cycle | 20 | 3 | 6.7×10^{-5} |
| IRS-related events triggered by IGF1R | 83 | 6 | 7.1×10^{-5} |
| Generic Transcription Pathway | 186 | 11 | 7.1×10^{-5} |
| Termination of O-glycan biosynthesis | 21 | 3 | 7.4×10^{-5} |
| Kinesins | 22 | 3 | 8.5×10^{-5} |
| Pathways Over-represented in Cluster 4 | Pathway Size | Cluster Genes | p-value (FDR) |
| Extracellular matrix organization | 241 | 97 | 8.8×10^{-126} |
| Axon guidance | 289 | 75 | 8.3×10^{-72} |
| Hemostasis | 445 | 101 | 8.3×10^{-72} |
| Developmental Biology | 432 | 95 | 3.0×10^{-67} |
| Response to elevated platelet cytosolic Ca ²⁺ | 84 | 37 | 5.8×10^{-67} |
| Platelet degranulation | 79 | 36 | 5.8×10^{-67} |
| Degradation of the extracellular matrix | 104 | 39 | 6.7×10^{-63} |
| Platelet activation, signalling and aggregation | 186 | 52 | 6.6×10^{-62} |
| ECM proteoglycans | 66 | 31 | 8.1×10^{-61} |
| Neuronal System | 272 | 64 | 5.1×10^{-60} |
| Signalling by PDGF | 173 | 47 | 9.7×10^{-57} |
| Integrin cell surface interactions | 82 | 31 | 1.9×10^{-53} |
| Collagen biosynthesis and modifying enzymes | 56 | 26 | 1.1×10^{-52} |
| Collagen formation | 67 | 28 | 1.4×10^{-52} |
| Class A/1 (Rhodopsin-like receptors) | 289 | 61 | 2.3×10^{-52} |
| GPCR ligand binding | 373 | 73 | 2.8×10^{-52} |
| Elastic fibre formation | 38 | 22 | 4.7×10^{-52} |
| Non-integrin membrane-ECM interactions | 53 | 24 | 7.0×10^{-49} |

Pathway over-representation analysis for Reactome pathways with the number of genes in each pathway (Pathway Size), number of genes within the pathway identified (Cluster Genes), and the pathway over-representation p-value (adjusted by FDR) from the hypergeometric test.

E.2 Comparison to Primary Screen

The synthetic lethal partners with *CDH1* expression in stomach cancers were also compared to [siRNA](#) primary screen data (Telford *et al.*, 2015), as performed in Section 4.2.1. These are expected to be more concordant with the experimental results performed on a null mutant, however this is not the case at the gene level: less genes overlapped with experimental candidates in Figure E.2. This may be affected by lower sample size for mutations in [TCGA](#) data or lower frequency (expected value) of *CDH1* mutations compared to low expression.

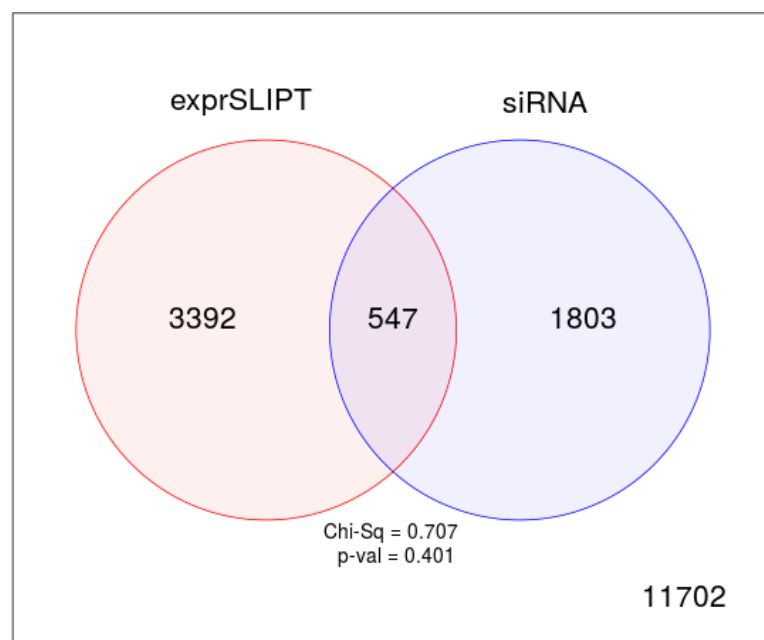


Figure E.2: **Comparison of SLIPT in stomach to siRNA.** Testing the overlap of gene candidates for [E-cadherin](#) synthetic lethal partners between computational (SLIPT) and experimental screening (siRNA) approaches. The χ^2 test suggests that the overlap is no more than would be expected by chance ($p = 0.281$).

Table E.4: Pathways for *CDH1* partners from SLIPT and siRNA

| Predicted only by SLIPT (3392 genes) | Pathway Size | Genes Identified | p-value (FDR) |
|---|--------------|------------------|------------------------|
| Extracellular matrix organization | 238 | 90 | 3.4×10^{-107} |
| Eukaryotic Translation Termination | 79 | 46 | 7.6×10^{-91} |
| Viral mRNA Translation | 77 | 45 | 1.2×10^{-89} |
| Eukaryotic Translation Elongation | 82 | 46 | 5.8×10^{-89} |
| Peptide chain elongation | 79 | 45 | 2.1×10^{-88} |
| Nonsense Mediated Decay independent of the Exon Junction Complex | 84 | 46 | 9.4×10^{-88} |
| Formation of a pool of free 40S subunits | 89 | 47 | 3.3×10^{-87} |
| GTP hydrolysis and joining of the 60S ribosomal subunit | 100 | 48 | 3.2×10^{-83} |
| Axon guidance | 284 | 84 | 3.9×10^{-82} |
| Developmental Biology | 426 | 111 | 4.2×10^{-82} |
| L13a-mediated translational silencing of Ceruloplasmin expression | 99 | 47 | 1.4×10^{-81} |
| 3' -UTR-mediated translational regulation | 99 | 47 | 1.4×10^{-81} |
| SRP-dependent cotranslational protein targeting to membrane | 99 | 47 | 1.4×10^{-81} |
| Nonsense-Mediated Decay | 99 | 47 | 1.4×10^{-81} |
| Nonsense Mediated Decay enhanced by the Exon Junction Complex | 99 | 47 | 1.4×10^{-81} |
| Hemostasis | 438 | 112 | 1.2×10^{-80} |
| Eukaryotic Translation Initiation | 107 | 48 | 8.0×10^{-80} |
| Cap-dependent Translation Initiation | 107 | 48 | 8.0×10^{-80} |
| Infectious disease | 338 | 90 | 1.6×10^{-76} |
| Neuronal System | 267 | 77 | 1.6×10^{-76} |

| Detected only by siRNA screen (1803 genes) | Pathway Size | Genes Identified | p-value (FDR) |
|--|--------------|------------------|-----------------------|
| Class A/1 (Rhodopsin-like receptors) | 282 | 62 | 8.1×10^{-50} |
| GPCR ligand binding | 363 | 71 | 4.9×10^{-46} |
| Peptide ligand-binding receptors | 175 | 38 | 7.9×10^{-38} |
| G _{αi} signalling events | 184 | 37 | 1.1×10^{-34} |
| Gastrin-CREB signalling pathway via PKC and MAPK | 180 | 35 | 1.4×10^{-32} |
| G _{αq} signalling events | 159 | 32 | 4.8×10^{-32} |
| DAP12 interactions | 159 | 29 | 1.4×10^{-27} |
| Downstream signal transduction | 146 | 26 | 2.4×10^{-25} |
| DAP12 signalling | 149 | 26 | 6.4×10^{-25} |
| VEGFA-VEGFR2 Pathway | 91 | 19 | 8.1×10^{-24} |
| Signalling by PDGF | 172 | 27 | 5.7×10^{-23} |
| Signalling by ERBB2 | 146 | 24 | 1.4×10^{-22} |
| Signalling by VEGF | 99 | 19 | 2.0×10^{-22} |
| Visual phototransduction | 85 | 17 | 1.3×10^{-21} |
| Downstream signalling of activated FGFR1 | 134 | 22 | 1.3×10^{-21} |
| Downstream signalling of activated FGFR2 | 134 | 22 | 1.3×10^{-21} |
| Downstream signalling of activated FGFR3 | 134 | 22 | 1.3×10^{-21} |
| Downstream signalling of activated FGFR4 | 134 | 22 | 1.3×10^{-21} |
| Signalling by FGFR | 146 | 23 | 2.0×10^{-21} |
| Signalling by FGFR1 | 146 | 23 | 2.0×10^{-21} |

| Intersection of SLIPT and siRNA screen (547 genes) | Pathway Size | Genes Identified | p-value (FDR) |
|--|--------------|------------------|----------------------|
| Class A/1 (Rhodopsin-like receptors) | 282 | 25 | 3.9×10^{-9} |
| Platelet activation, signalling and aggregation | 182 | 17 | 3.9×10^{-9} |
| Response to elevated platelet cytosolic Ca ²⁺ | 82 | 9 | 5.5×10^{-8} |
| Platelet homeostasis | 53 | 7 | 5.7×10^{-8} |
| Nucleotide-like (purinergic) receptors | 16 | 4 | 1.8×10^{-7} |
| Platelet degranulation | 77 | 8 | 2.8×10^{-7} |
| Peptide ligand-binding receptors | 175 | 14 | 3.8×10^{-7} |
| Molecules associated with elastic fibres | 34 | 5 | 7.1×10^{-7} |
| Amine ligand-binding receptors | 35 | 5 | 8.6×10^{-7} |
| G _{αi} signalling events | 184 | 14 | 9.8×10^{-7} |
| GPCR ligand binding | 363 | 27 | 1.1×10^{-6} |
| Elastic fibre formation | 38 | 5 | 1.5×10^{-6} |
| G _{αq} signalling events | 159 | 12 | 1.9×10^{-6} |
| Serotonin receptors | 12 | 3 | 3.8×10^{-6} |
| P2Y receptors | 12 | 3 | 3.8×10^{-6} |
| Signal amplification | 16 | 3 | 2.3×10^{-5} |
| Gastrin-CREB signalling pathway via PKC and MAPK | 180 | 12 | 2.3×10^{-5} |
| Complement cascade | 33 | 4 | 2.4×10^{-5} |
| Glycosaminoglycan metabolism | 110 | 8 | 2.5×10^{-5} |
| Glycogen breakdown (glycogenolysis) | 17 | 3 | 2.7×10^{-5} |

E.2.1 Resampling Analysis

Table E.5: Pathways for *CDH1* partners from SLIPT in stomach cancer

| Reactome Pathway | Over-representation | Permutation |
|---|------------------------|--------------------------|
| <i>Extracellular matrix organization</i> | 7.5×10^{-140} | 0.070215 |
| Hemostasis | 1.8×10^{-121} | 0.25804 |
| Developmental Biology | 9.2×10^{-107} | 0.53032 |
| Axon guidance | 1.5×10^{-102} | 0.6704 |
| Eukaryotic Translation Termination | 1.9×10^{-99} | $> 1.031 \times 10^{-5}$ |
| GPCR ligand binding | 3.8×10^{-99} | 0.54914 |
| Viral mRNA Translation | 3.3×10^{-98} | $> 1.031 \times 10^{-5}$ |
| Formation of a pool of free 40S subunits | 3.3×10^{-98} | $> 1.031 \times 10^{-5}$ |
| Eukaryotic Translation Elongation | 1.6×10^{-97} | $> 1.031 \times 10^{-5}$ |
| Peptide chain elongation | 7.2×10^{-97} | $> 1.031 \times 10^{-5}$ |
| Class A/1 (Rhodopsin-like receptors) | 2.7×10^{-96} | 0.58174 |
| Nonsense Mediated Decay independent of the Exon Junction Complex | 3×10^{-96} | $> 1.031 \times 10^{-5}$ |
| Infectious disease | 2.6×10^{-94} | 0.25484 |
| GTP hydrolysis and joining of the 60S ribosomal subunit | 3.4×10^{-94} | $> 1.031 \times 10^{-5}$ |
| L13a-mediated translational silencing of Ceruloplasmin expression | 2.8×10^{-92} | $> 1.031 \times 10^{-5}$ |
| 3' -UTR-mediated translational regulation | 2.8×10^{-92} | $> 1.031 \times 10^{-5}$ |
| Neuronal System | 8.4×10^{-92} | 0.53433 |
| SRP-dependent cotranslational protein targeting to membrane | 9.5×10^{-92} | $> 1.031 \times 10^{-5}$ |
| Eukaryotic Translation Initiation | 2.0×10^{-90} | $> 1.031 \times 10^{-5}$ |
| Cap-dependent Translation Initiation | 2.0×10^{-90} | $> 1.031 \times 10^{-5}$ |
| Nonsense-Mediated Decay | 7.4×10^{-90} | $> 1.031 \times 10^{-5}$ |
| Nonsense Mediated Decay enhanced by the Exon Junction Complex | 7.4×10^{-90} | $> 1.031 \times 10^{-5}$ |
| Adaptive Immune System | 8.1×10^{-88} | 0.14116 |
| Translation | 1.3×10^{-87} | $> 1.031 \times 10^{-5}$ |
| Platelet activation, signalling and aggregation | 1.3×10^{-86} | 0.28959 |
| Influenza Infection | 1×10^{-82} | $> 1.031 \times 10^{-5}$ |
| Influenza Viral RNA Transcription and Replication | 2.4×10^{-82} | $> 1.031 \times 10^{-5}$ |
| Influenza Life Cycle | 2×10^{-80} | $> 1.031 \times 10^{-5}$ |
| Response to elevated platelet cytosolic Ca2+ | 4.9×10^{-78} | 0.50817 |
| Signalling by NGF | 1.6×10^{-75} | 0.38518 |
| Rho GTPase cycle | 5.1×10^{-75} | 0.14864 |
| Signalling by PDGF | 7.4×10^{-74} | 0.40493 |
| <i>Signalling by Rho GTPases</i> | 5.1×10^{-73} | 0.077217 |
| Glycosaminoglycan metabolism | 1.4×10^{-68} | 0.52984 |
| <i>G_{ai} signalling events</i> | 1.8×10^{-66} | 0.9254 |
| Metabolism of carbohydrates | 1.1×10^{-65} | 0.39501 |
| G_{as} signalling events | 2.7×10^{-65} | 0.0050293 |
| Potassium Channels | 2.7×10^{-65} | 0.53359 |
| Transmission across Chemical Synapses | 1.8×10^{-64} | 0.81833 |
| ECM proteoglycans | 3.4×10^{-64} | 0.083482 |
| Peptide ligand-binding receptors | 4.8×10^{-64} | 0.62817 |
| Degradation of the extracellular matrix | 1.1×10^{-63} | 0.80879 |
| Platelet homeostasis | 5.3×10^{-63} | 0.53134 |
| NGF signalling via TRKA from the plasma membrane | 6.1×10^{-63} | 0.57117 |
| Integration of energy metabolism | 4.5×10^{-61} | 0.10889 |
| Collagen formation | 5.4×10^{-61} | 0.29896 |
| Integrin cell surface interactions | 7×10^{-59} | 0.18167 |
| Collagen biosynthesis and modifying enzymes | 7×10^{-59} | 0.30208 |
| Neurotransmitter Receptor Binding And Downstream Transmission | 8.7×10^{-57} | 0.82522 |
| In The Postsynaptic Cell | | |
| Signalling by Wnt | 8.7×10^{-57} | 0.25468 |

Over-representation (hypergeometric test) and Permutation p-values adjusted for multiple tests across pathways (**FDR**). Significant pathways are marked in bold (**FDR** < 0.05) and italics (**FDR** < 0.1).

Table E.6: Pathways for *CDH1* partners from SLIPT in stomach and siRNA

| Reactome Pathway | Over-representation | Permutation |
|---|----------------------|---------------------------|
| Platelet activation, signalling and aggregation | 3.9×10^{-9} | 0.49557 |
| Class A/1 (Rhodopsin-like receptors) | 3.9×10^{-9} | 0.98432 |
| Response to elevated platelet cytosolic Ca ²⁺ | 5.5×10^{-8} | 0.54349 |
| Platelet homeostasis | 5.7×10^{-8} | 0.45017 |
| Nucleotide-like (purinergic) receptors | 1.8×10^{-7} | 0.36966 |
| Peptide ligand-binding receptors | 3.8×10^{-7} | 0.91294 |
| Molecules associated with elastic fibres | 7.1×10^{-7} | 0.0025868 |
| Amine ligand-binding receptors | 8.6×10^{-7} | 0.43303 |
| G _{ai} signalling events | 9.8×10^{-7} | 0.99626 |
| GPCR ligand binding | 1.1×10^{-6} | 0.97733 |
| Elastic fibre formation | 1.5×10^{-6} | 0.0025868 |
| G _{aq} signalling events | 1.9×10^{-6} | 0.86089 |
| P2Y receptors | 3.8×10^{-6} | 0.18795 |
| Serotonin receptors | 3.8×10^{-6} | 0.37853 |
| Signal amplification | 2.3×10^{-5} | 0.47856 |
| Gastrin-CREB signalling pathway via PKC and MAPK | 2.3×10^{-5} | 0.98567 |
| Complement cascade | 2.4×10^{-5} | $> 3.4628 \times 10^{-6}$ |
| Glycosaminoglycan metabolism | 2.5×10^{-5} | 0.38953 |
| Glycogen breakdown (glycogenolysis) | 2.7×10^{-5} | 0.83772 |
| Defective B4GALT7 causes EDS, progeroid type | 4.9×10^{-5} | 0.10792 |
| Defective B3GAT3 causes JDSSDHD | 4.9×10^{-5} | 0.10792 |
| Role of LAT2/NTAL/LAB on calcium mobilization | 5.6×10^{-5} | 0.35373 |
| Cell surface interactions at the vascular wall | 5.6×10^{-5} | 0.47642 |
| G_{as} signalling events | 6×10^{-5} | 0.019858 |
| Signalling by NOTCH | 6×10^{-5} | 0.19008 |
| A tetrasaccharide linker sequence is required for GAG synthesis | 0.00017 | 0.47642 |
| Extracellular matrix organization | 0.00018 | 0.0047308 |
| Collagen formation | 0.00018 | 0.19245 |
| Effects of PIP2 hydrolysis | 0.0002 | 0.37779 |
| Syndecan interactions | 0.0002 | 0.37779 |
| Diseases associated with glycosaminoglycan metabolism | 0.00023 | 0.01028 |
| Diseases of glycosylation | 0.00023 | 0.01028 |
| <i>Chondroitin sulfate/dermatan sulfate metabolism</i> | 0.00023 | 0.085541 |
| Integrin alphaIIb beta3 signalling | 0.00028 | 0.76936 |
| Keratan sulfate biosynthesis | 0.00034 | 0.68744 |
| Rho GTPase cycle | 0.00034 | 0.15675 |
| Creation of C4 and C2 activators | 0.00035 | 0.12275 |
| Abacavir transport and metabolism | 0.00035 | 0.12443 |
| Amine compound SLC transporters | 0.00037 | 0.69773 |
| FCER1 mediated NF-κB activation | 0.00037 | 0.69846 |
| Fc epsilon receptor (FCER1) signalling | 0.00056 | 0.43303 |
| Defective EXT2 causes exostoses 2 | 0.00067 | 0.16053 |
| Defective EXT1 causes exostoses 1, TRPS2 and CHDS | 0.00067 | 0.16053 |
| <i>Collagen biosynthesis and modifying enzymes</i> | 0.00071 | 0.052911 |
| Keratan sulfate/keratin metabolism | 0.00073 | 0.46533 |
| G alpha (12/13) signalling events | 0.00078 | 0.59164 |
| SEMA3A-Plexin repulsion signalling by inhibiting Integrin adhesion | 0.00084 | 0.038504 |
| Signal attenuation | 0.00084 | 0.37779 |
| Eicosanoid ligand-binding receptors | 0.0011 | 0.11117 |
| SOS-mediated signalling | 0.0011 | 0.25387 |

Over-representation (hypergeometric test) and Permutation p-values adjusted for multiple tests across pathways (**FDR**). Significant pathways are marked in bold (**FDR** < 0.05) and italicics (**FDR** < 0.1).

E.3 Metagene Analysis

Metagene analysis was also performed for synthetic lethal candidates for *CDH1* expression in stomach cancer.

Table E.7: Synthetic lethal metagenes against *CDH1* in stomach cancer

| Pathway | ID | Observed | Expected | χ^2 value | p-value | p-value (FDR) |
|---|---------|----------|----------|----------------|------------------------|------------------------|
| Cell-Cell communication | 1500931 | 18 | 50.4 | 110 | 7.43×10^{-23} | 1.53×10^{-20} |
| VEGFR2 mediated vascular permeability | 5218920 | 19 | 50.4 | 109 | 1.36×10^{-22} | 2.49×10^{-20} |
| Sema4D in semaphorin signalling | 400685 | 20 | 50.4 | 104 | 1.62×10^{-21} | 2.12×10^{-19} |
| Ion transport by P-type ATPases | 936837 | 17 | 50.4 | 100 | 8.29×10^{-21} | 8.06×10^{-19} |
| Sialic acid metabolism | 4085001 | 19 | 50.4 | 95.3 | 9.95×10^{-20} | 7.82×10^{-18} |
| Synthesis of pyrophosphates in the cytosol | 1855167 | 26 | 50.4 | 94 | 1.86×10^{-19} | 1.23×10^{-17} |
| Keratan sulfate/keratin metabolism | 1638074 | 25 | 50.4 | 93.5 | 2.36×10^{-19} | 1.44×10^{-17} |
| Ion channel transport | 983712 | 19 | 50.4 | 92.8 | 3.37×10^{-19} | 1.99×10^{-17} |
| Keratan sulfate biosynthesis | 2022854 | 26 | 50.4 | 91.4 | 6.79×10^{-19} | 3.62×10^{-17} |
| Arachidonic acid metabolism | 2142753 | 22 | 50.4 | 90.6 | 9.81×10^{-19} | 5.07×10^{-17} |
| RHO GTPases activate CIT | 5625900 | 22 | 50.4 | 87 | 5.80×10^{-18} | 2.66×10^{-16} |
| Stimuli-sensing channels | 2672351 | 25 | 50.4 | 85.8 | 1.03×10^{-17} | 4.58×10^{-16} |
| Synthesis of PI | 1483226 | 19 | 50.4 | 85.6 | 1.15×10^{-17} | 4.89×10^{-16} |
| G-protein activation | 202040 | 19 | 50.4 | 85.3 | 1.34×10^{-17} | 5.53×10^{-16} |
| NrCAM interactions | 447038 | 22 | 50.4 | 84.3 | 2.1×10^{-17} | 8.27×10^{-16} |
| Inwardly rectifying K^+ channels | 1296065 | 24 | 50.4 | 83.5 | 3.19×10^{-17} | 1.22×10^{-15} |
| Calcitonin-like ligand receptors | 419812 | 20 | 50.4 | 82.2 | 6.07×10^{-17} | 2.13×10^{-15} |
| Prostacyclin signalling through prostacyclin receptor | 392851 | 24 | 50.4 | 81.8 | 7.27×10^{-17} | 2.5×10^{-15} |
| Presynaptic function of Kainate receptors | 500657 | 26 | 50.4 | 79.7 | 2.00×10^{-16} | 6.34×10^{-15} |
| ADP signalling through P2Y purinoceptor 12 | 392170 | 23 | 50.4 | 79.2 | 2.57×10^{-16} | 7.71×10^{-15} |
| regulation of FZD by ubiquitination | 4641263 | 22 | 50.4 | 78.8 | 3.15×10^{-16} | 9.3×10^{-15} |
| Toxicity of tetanus toxin (TeNT) | 5250982 | 27 | 50.4 | 78.7 | 3.36×10^{-16} | 9.75×10^{-15} |
| Gap junction degradation | 190873 | 21 | 50.4 | 78.5 | 3.66×10^{-16} | 1.04×10^{-14} |
| Nephrin interactions | 373753 | 25 | 50.4 | 78.2 | 4.21×10^{-16} | 1.14×10^{-14} |
| GABA synthesis, release, reuptake and degradation | 888590 | 26 | 50.4 | 77 | 7.69×10^{-16} | 1.95×10^{-14} |

Strongest candidate SL partners for *CDH1* by SLIPT with observed and expected numbers of TCGA stomach cancer samples with low expression of both genes.

Appendix F

Synthetic Lethal Genes in Pathways

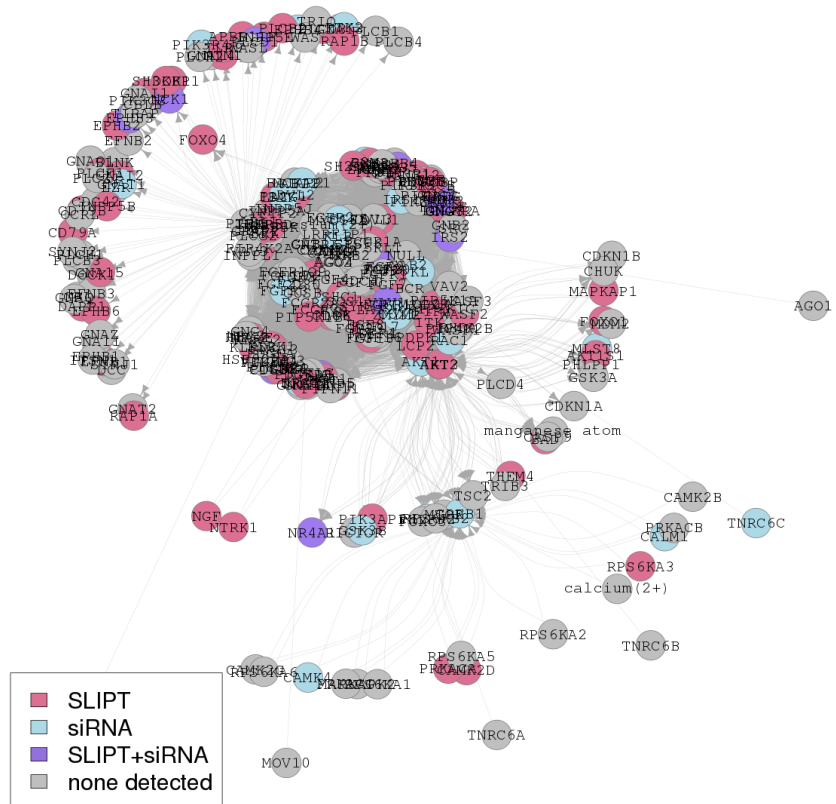


Figure F.1: **Synthetic lethality in the PI3K/AKT pathway.** The Reactome PI3K/AKT pathway with synthetic lethal candidates coloured as shown in the legend.

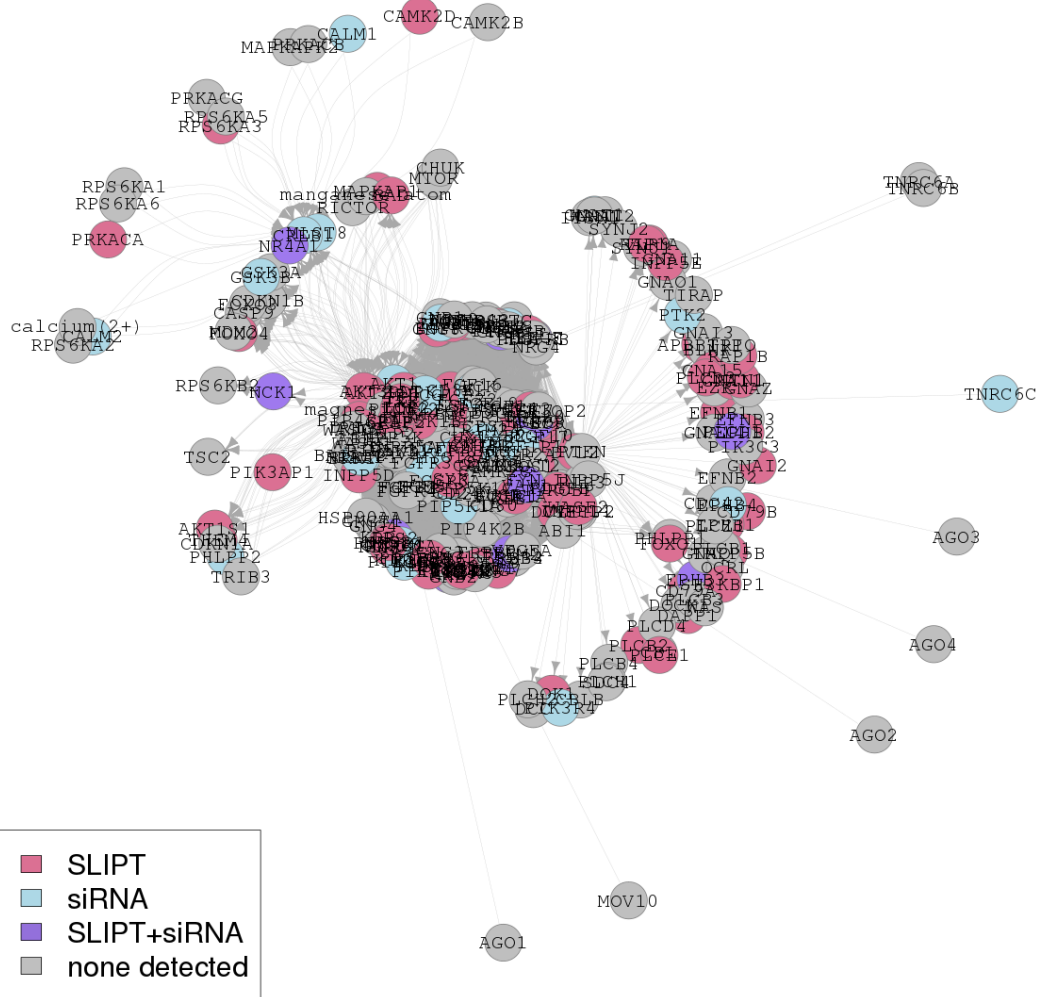


Figure F.2: Synthetic lethality in the PI3K/AKT pathway in cancer. The Reactome PI3K/AKT Pathway in Cancer pathway with synthetic lethal candidates coloured as shown in the legend.

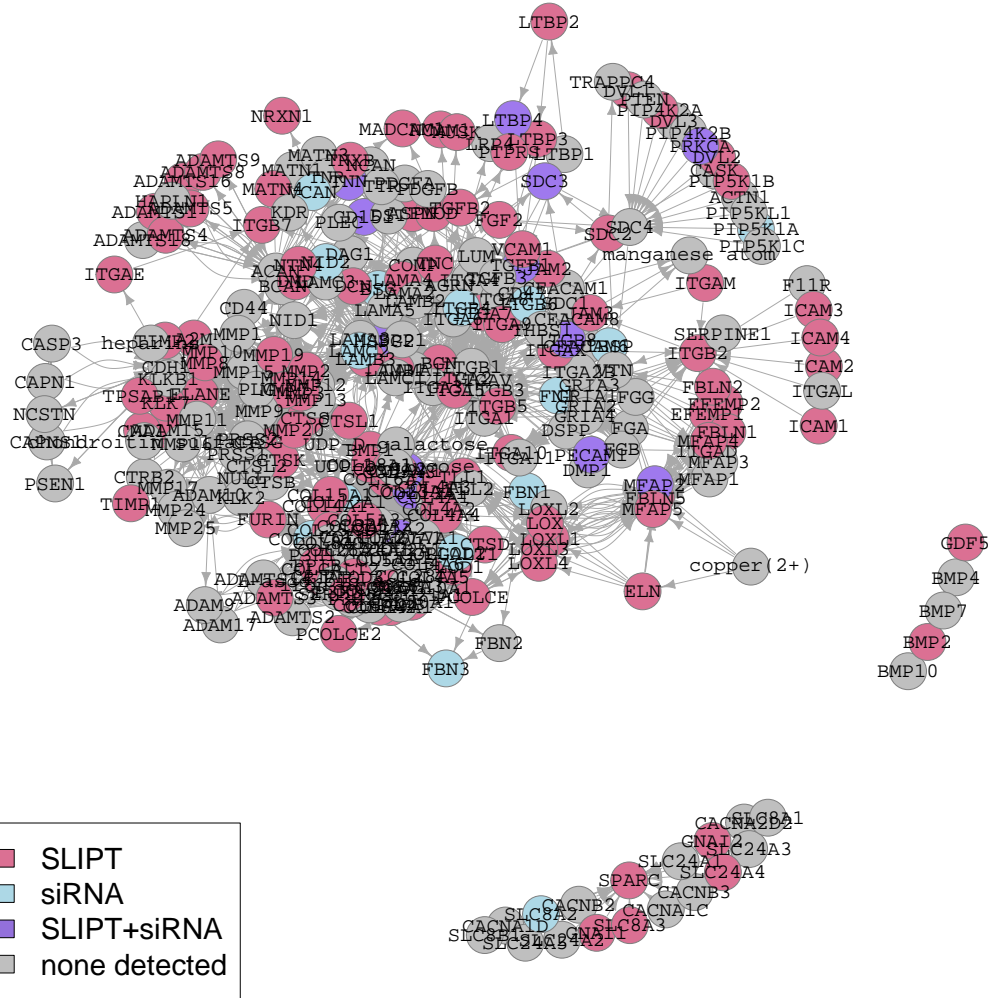


Figure F.3: Synthetic lethality in the Extracellular Matrix. The Reactome Extracellular Matrix pathway with synthetic lethal candidates coloured as shown in the legend.

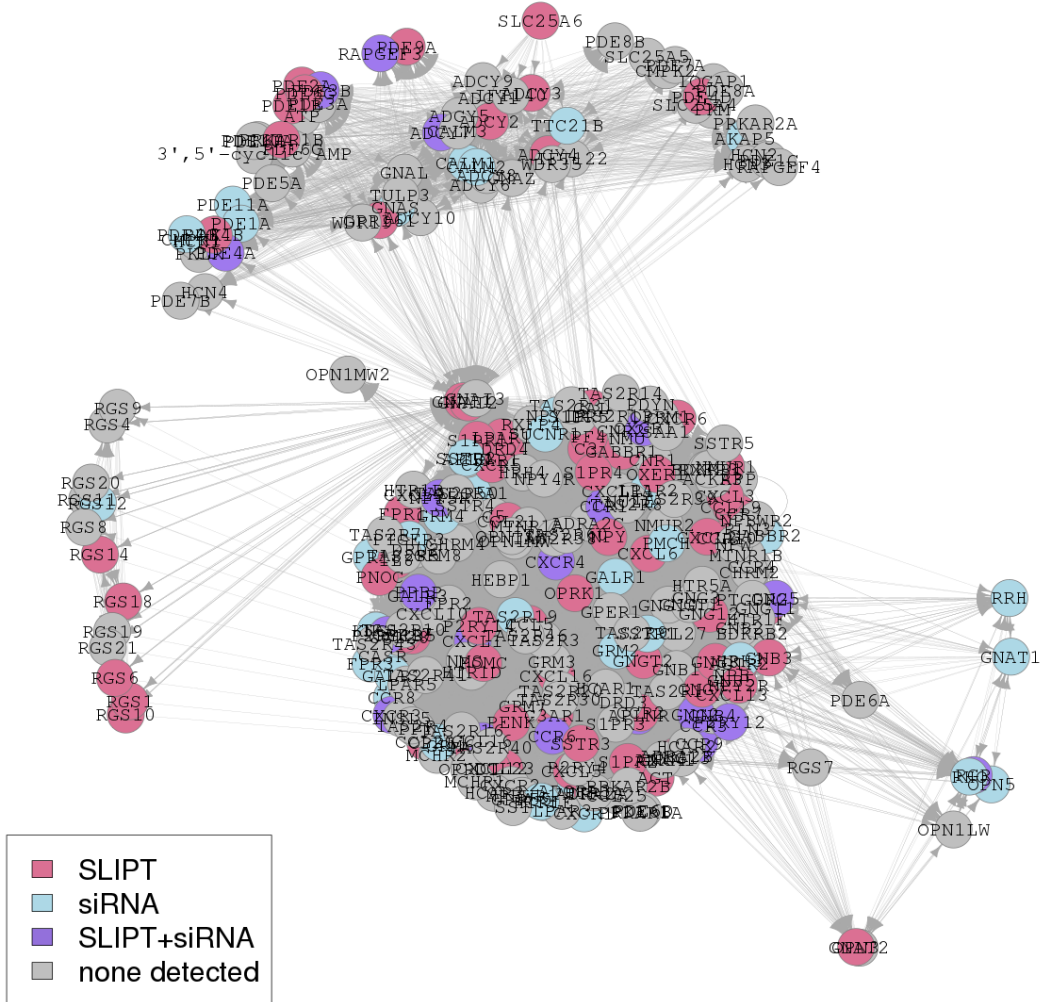


Figure F.4: Synthetic lethality in the GPCRs. The Reactome $G_{\alpha i}$ pathway with synthetic lethal candidates coloured as shown in the legend.

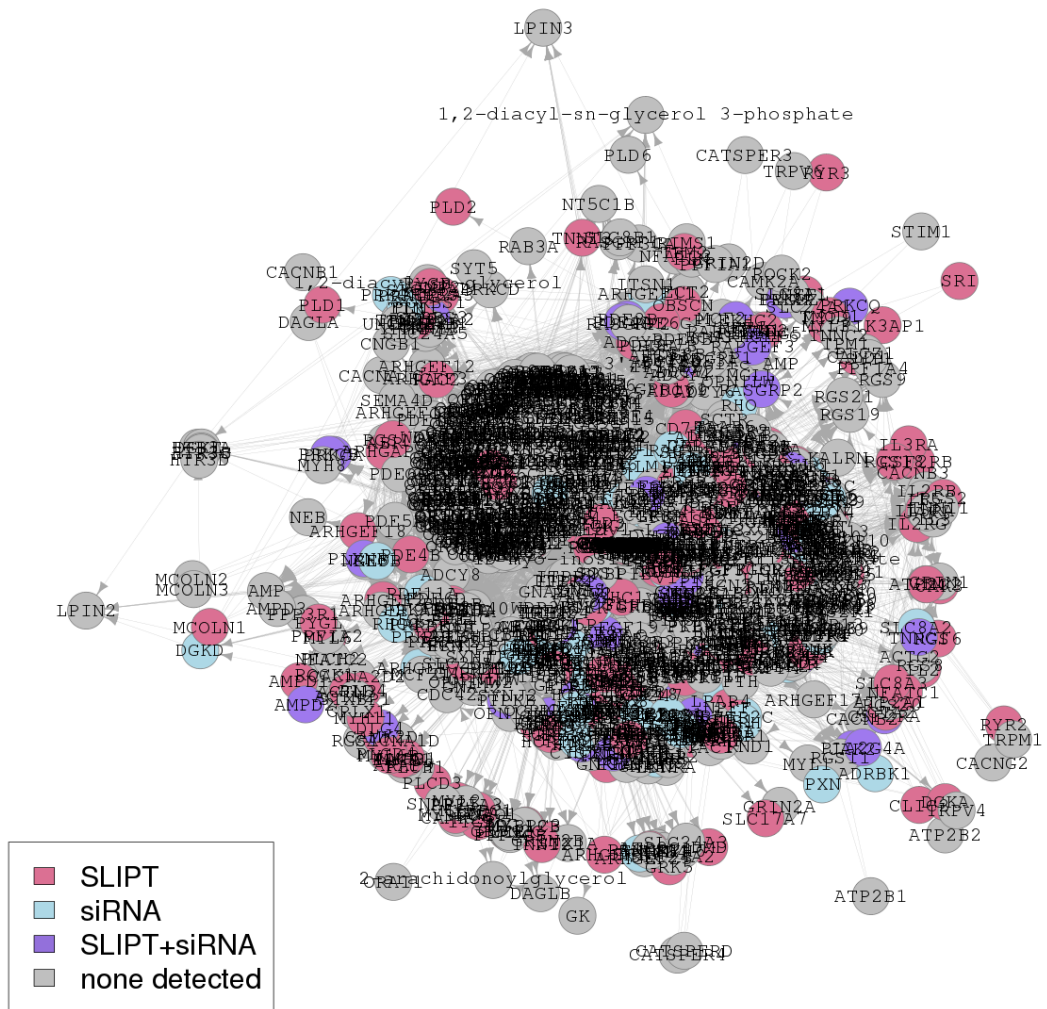


Figure F.5: Synthetic lethality in the GPCR Downstream. The Reactome GPCR Downstream pathway with synthetic lethal candidates coloured as shown in the legend.

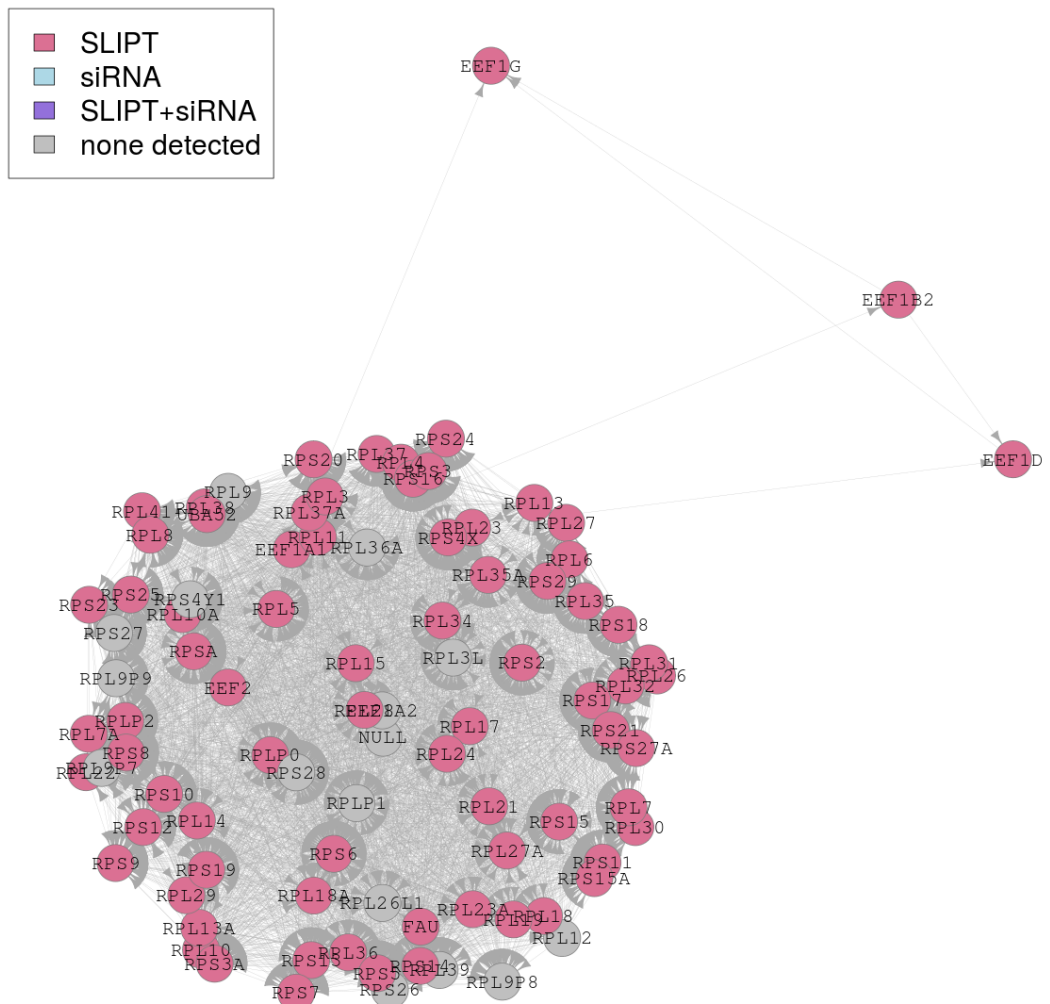


Figure F.6: **Synthetic lethality in the Translation Elongation**. The Reactome Translation Elongation pathway with synthetic lethal candidates coloured as shown in the legend.

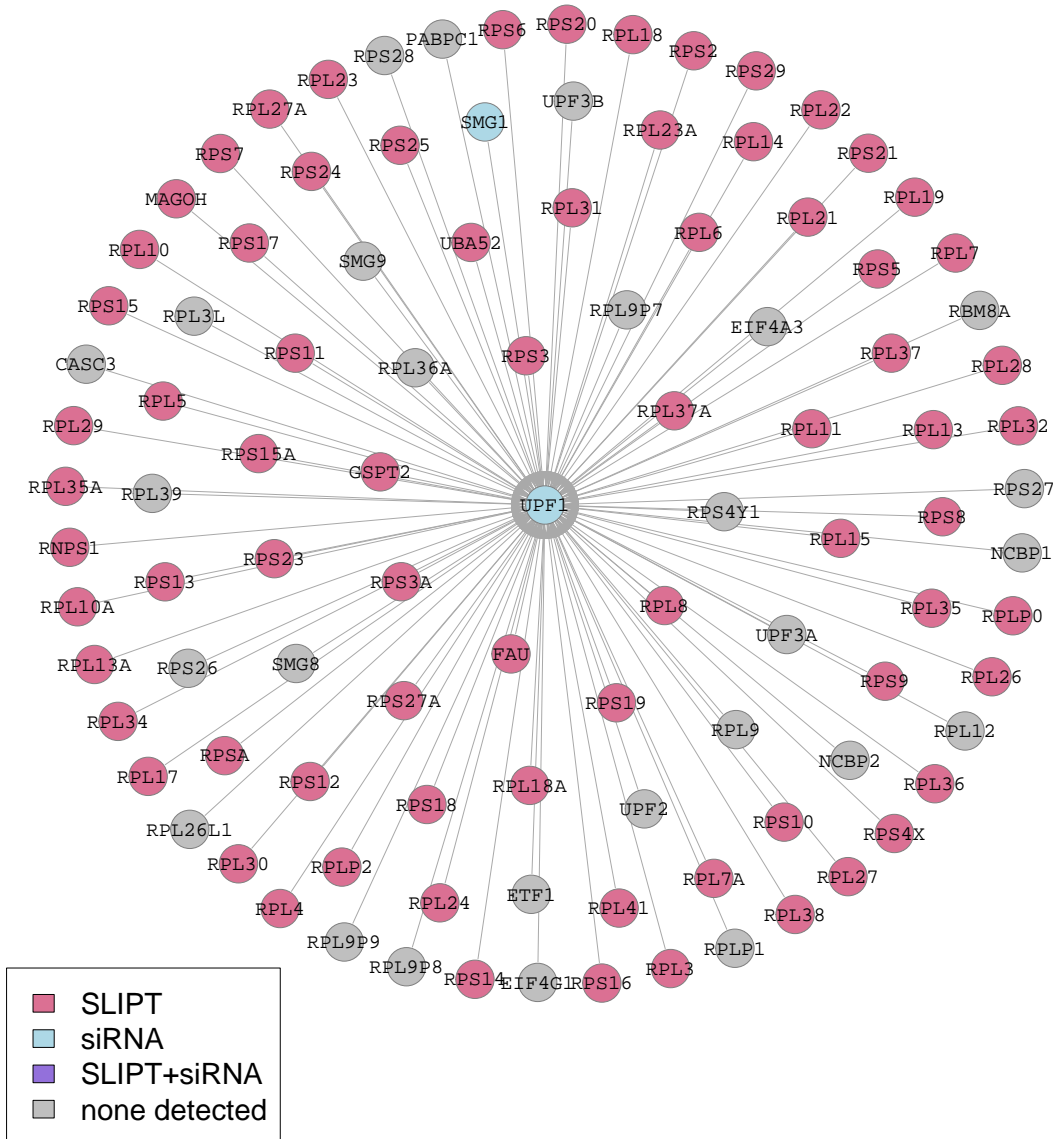


Figure F.7: Synthetic lethality in the Nonsense-mediated Decay. The Reactome Nonsense-mediated Decay pathway with synthetic lethal candidates coloured as shown in the legend.

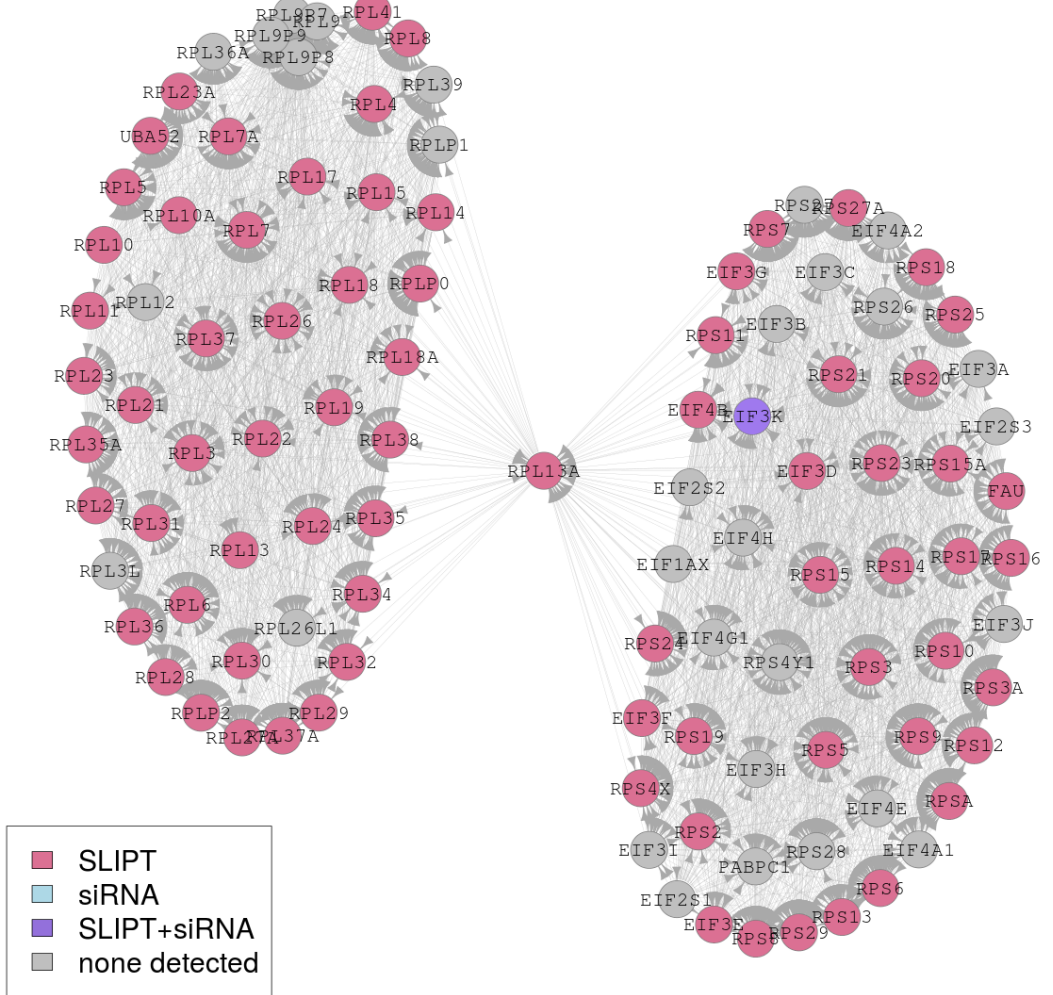


Figure F.8: **Synthetic lethality in the 3' UTR.** The Reactome 3' UTR pathway with synthetic lethal candidates coloured as shown in the legend.

Appendix G

Pathway Connectivity for Mutation SLIPT

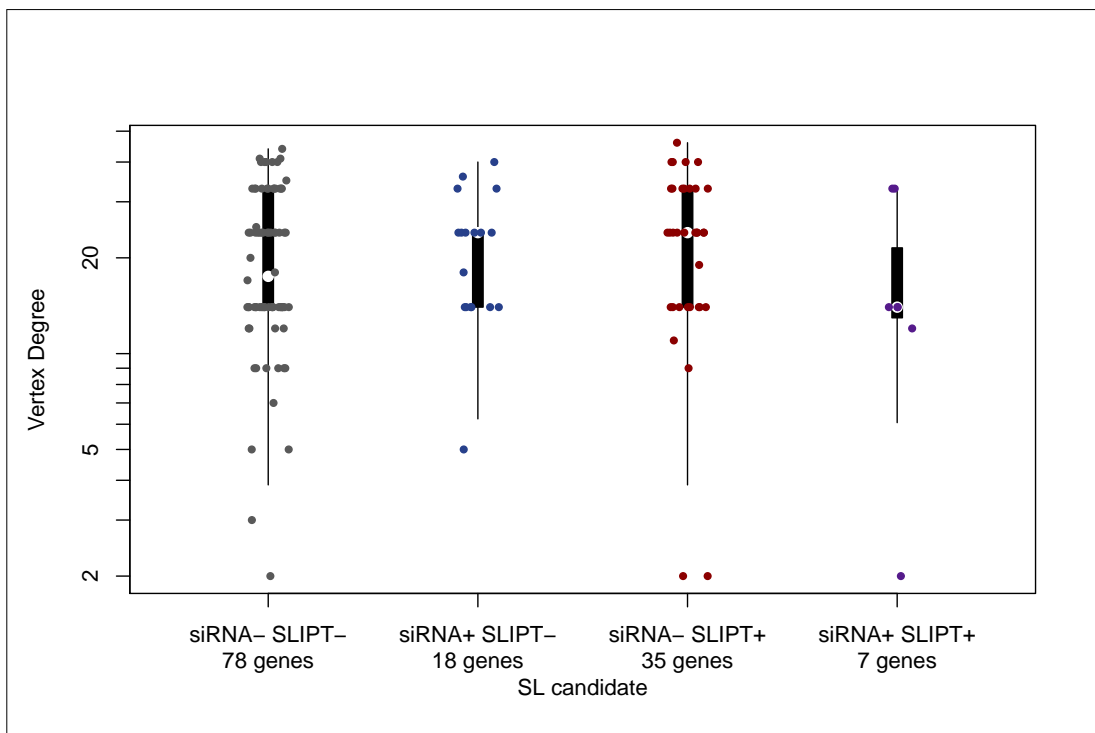


Figure G.1: **Synthetic lethality and vertex degree.** The number of connected genes (vertex degree) was compared (on a log-scale across genes detected by [mtSLIPT](#) and [siRNA](#) screening in the Reactome PI3K cascade pathway. There were very few differences in vertex degree between the groups, although genes detected by [siRNA](#) included those with the fewest connections.

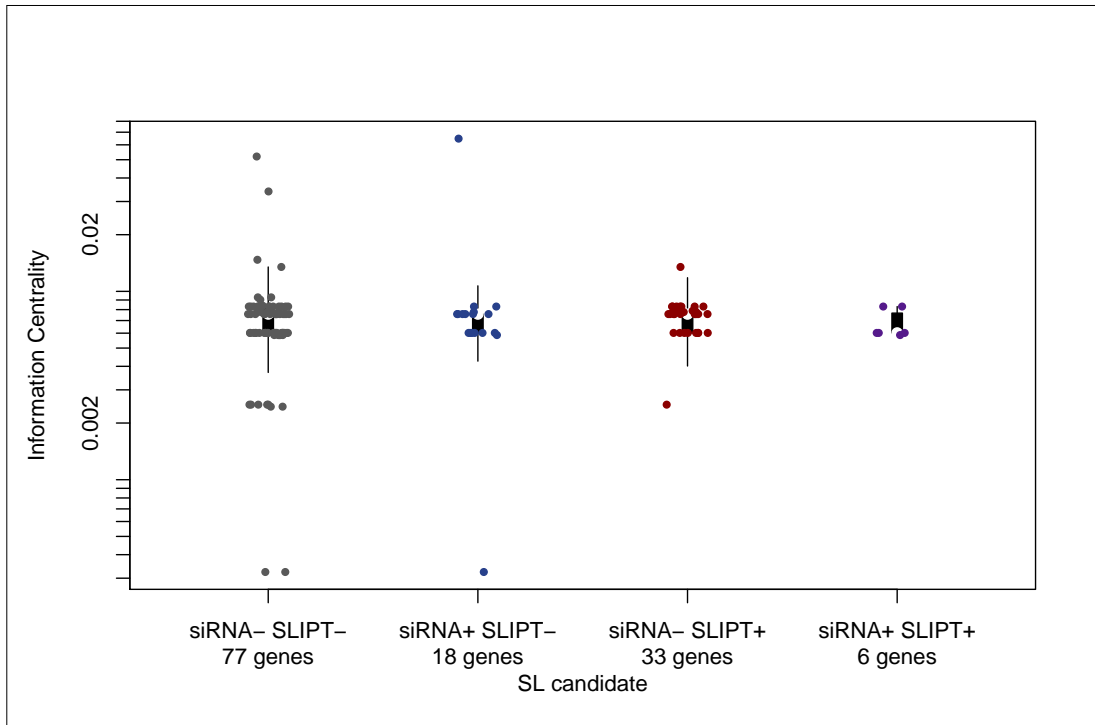


Figure G.2: **Synthetic lethality and centrality.** The information centrality was compared (on a log-scale across genes detected by [mtSLIPT](#) and [siRNA](#) screening in the Reactome PI3K cascade pathway. Genes detected by [mtSLIPT](#) or [siRNA](#) did not have higher connectivity than genes not detected by either approach. The gene with the highest centrality was detected by [siRNA](#).

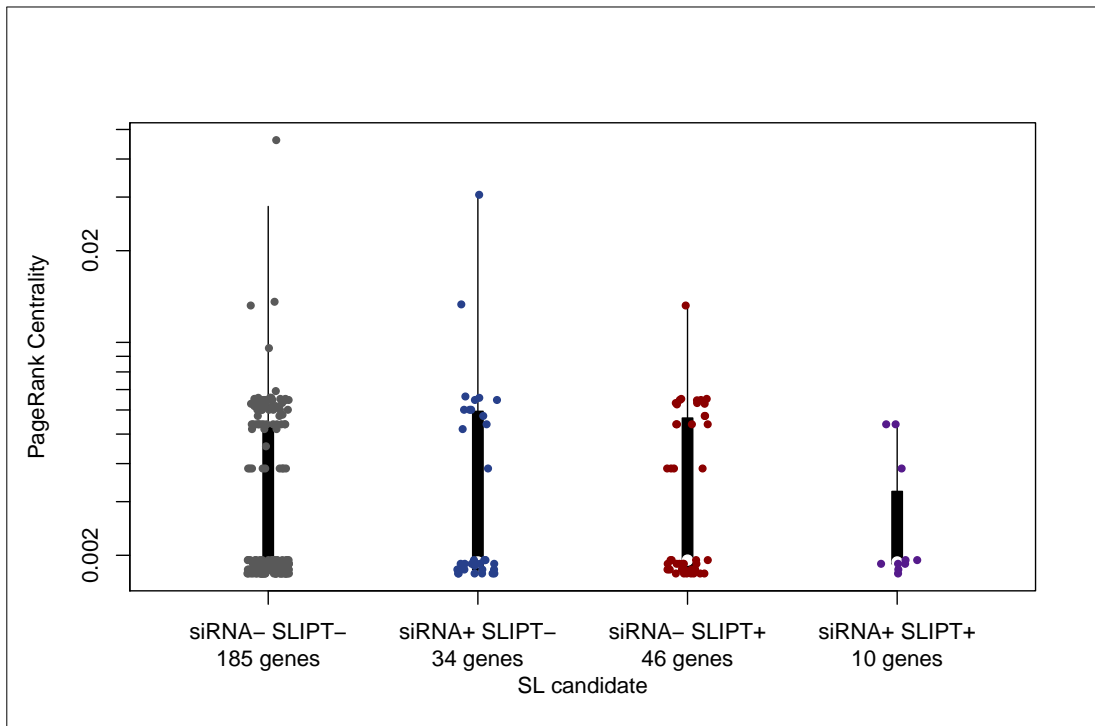


Figure G.3: Synthetic lethality and PageRank. The PageRank centrality was compared (on a log-scale across genes detected by [mtSLIPT](#) and [siRNA](#) screening in the Reactome PI3K cascade pathway. Genes detected by [siRNA](#) had a more restricted range of centrality values than other genes not detected by either approach, although these groups also had fewer genes.

Table G.1: ANOVA for synthetic lethality and vertex degree

| | DF | Sum Squares | Mean Squares | F-value | p-value |
|---------------|----|-------------|--------------|---------|---------|
| siRNA | 1 | 15 | 15.50 | 0.0134 | 0.9084 |
| mtSLIPT | 1 | 196 | 195.94 | 0.1689 | 0.6825 |
| siRNA×mtSLIPT | 1 | 9 | 9.17 | 0.0079 | 0.9294 |

Analysis of variance for vertex degree against synthetic lethal detection approaches (with an interaction term)

Table G.2: ANOVA for synthetic lethality and information centrality

| | DF | Sum Squares | Mean Squares | F-value | p-value |
|---------------|----|-------------|--------------|---------|---------|
| siRNA | 1 | 0.000256 | 0.0002561 | 0.1851 | 0.6685 |
| mtSLIPT | 1 | 0.003225 | 0.0032247 | 2.3308 | 0.1318 |
| siRNA×mtSLIPT | 1 | 0.001238 | 0.0012385 | 0.8952 | 0.3476 |

Analysis of variance for information centrality against synthetic lethal detection approaches (with an interaction term)

Table G.3: ANOVA for synthetic lethality and PageRank centrality

| | DF | Sum Squares | Mean Squares | F-value | p-value |
|---------------|----|-------------|-------------------------|---------|---------|
| siRNA | 1 | 0.0002038 | 2.0385×10^{-4} | 1.1423 | 0.2892 |
| mtSLIPT | 1 | 0.0000208 | 2.0752×10^{-5} | 0.1163 | 0.7342 |
| siRNA×mtSLIPT | 1 | 0.0000137 | 1.3743×10^{-5} | 0.0770 | 0.7823 |

Analysis of variance for PageRank centrality against synthetic lethal detection approaches (with an interaction term)

Appendix H

Information Centrality for Gene Essentiality

Network structure is another useful strategy to analyse gene function and this has been used to investigate network properties of a network constructed from of Reactome pathways imported via Pathway Commons with Paxtools (Cerami *et al.*, 2011; Demir *et al.*, 2013). Most notably, information centrality which has been proposed as a measure of gene essentiality was calculated as performed by Kranthi *et al.* (2013) using the efficiency and shortest path between each pair of nodes in the network before and after a node of interest is removed to test the importance of a node to network connectivity. Reactome contains substrates and cofactors in addition to genes or proteins. In support of centrality as a measure of essentiality, a number nodes with the highest centrality (shown in Table H.1) were essential nutrients including Mg^{2+} , Ca^{2+} , Zn^{2+} , and Fe. In addition, there were genes important in development of epithelial tissues and breast cancer such as *IL8*, *GATA3*, and *CTNNB1* detected with relatively high information centrality.

Table H.1: Information centrality for genes and molecules in the Reactome network

| Node | Centrality |
|-----------------------|------------|
| <i>ZNF473</i> | 0.0510 |
| magnesium(2+) | 0.0082 |
| <i>XBP1</i> | 0.0053 |
| calcium(2+) | 0.0050 |
| zinc(2+) | 0.0048 |
| iron atom | 0.0041 |
| <i>FMN</i> | 0.0040 |
| <i>AGT</i> | 0.0037 |
| <i>HSP90AA1</i> | 0.0029 |
| phosphatidyl-L-serine | 0.0029 |
| <i>P2RX7</i> | 0.0026 |
| <i>PANX1</i> | 0.0024 |
| <i>NCAM1</i> | 0.0022 |
| <i>NUDT1</i> | 0.0021 |
| <i>PLAUR</i> | 0.0020 |
| <i>IL8</i> | 0.0020 |
| <i>HSPA8</i> | 0.0019 |
| <i>TYROBP</i> | 0.0019 |
| <i>CASP3</i> | 0.0017 |
| <i>GNAL</i> | 0.0015 |
| <i>CBLB</i> | 0.0015 |
| <i>HBB</i> | 0.0014 |
| <i>GATA4</i> | 0.0013 |
| <i>TGS1</i> | 0.0013 |
| <i>CTNNB1</i> | 0.0012 |

Highest information centrality for genes (proteins), cofactors, and minerals in the Reactome network

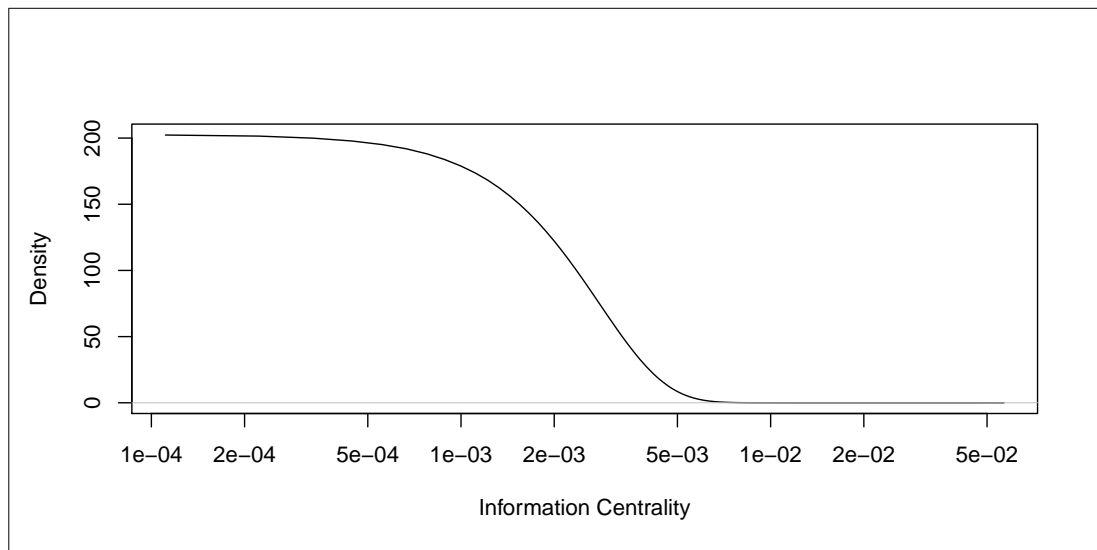


Figure H.1: **Information centrality distribution.** Information centrality in the Reactome network for nodes, including genes/proteins and other biomolecules.

Appendix I

Pathway Structure for Mutation SLIPT

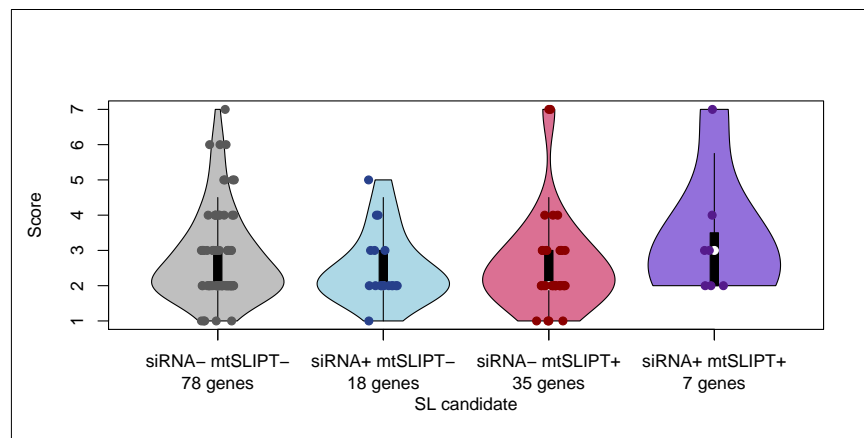


Figure I.1: **Synthetic lethality and hierarchy score in PI3K.** The hierarchical distance scores were similarly distributed across **mtSLIPT** and **siRNA** genes. Genes detected by both methods had a higher (downstream) median than either group.

Table I.1: ANOVA for synthetic lethality and PI3K hierarchy

| | DF | Sum Squares | Mean Squares | F-value | p-value |
|---------------|----|-------------|--------------|---------|---------|
| siRNA | 1 | 0.001 | 0.00070 | 0.0004 | 0.9841 |
| mtSLIPT | 1 | 0.007 | 0.0066 | 0.0040 | 0.9496 |
| siRNA×mtSLIPT | 1 | 3.906 | 3.9056 | 2.3829 | 0.1250 |

Analysis of variance for PI3K hierarchy score against synthetic lethal detection approaches (with an interaction term)

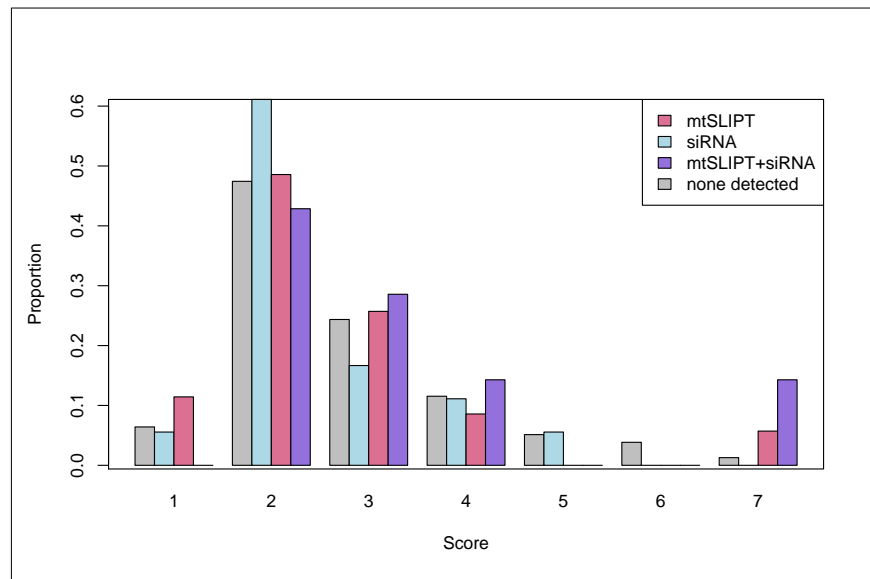


Figure I.2: Hierarchy score in PI3K against synthetic lethality in PI3K. The number of [mtSLIPT](#) and [siRNA](#) genes against the hierarchical distance scores showing no significant tendency for either method to either of the pathway upstream or downstream extremities.

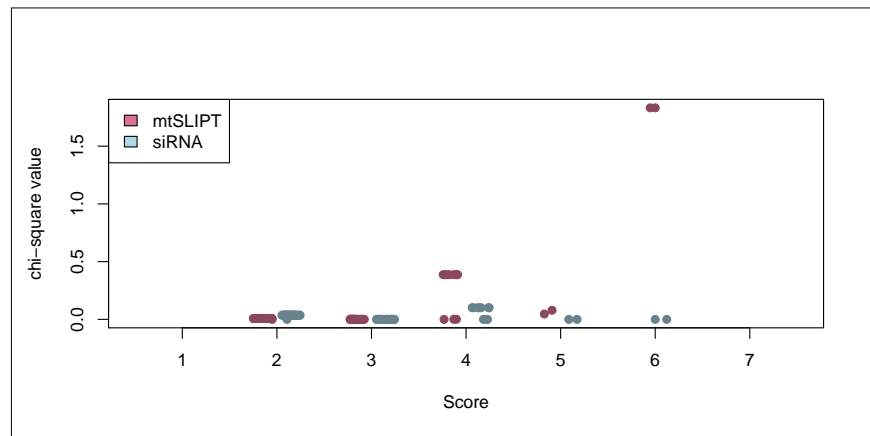


Figure I.3: Structure of synthetic lethality in PI3K. The number of [mtSLIPT](#) and [siRNA](#) genes against the hierarchical distance scores showing no significant tendency for either method to either of the pathway upstream or downstream extremities. The number of [mtSLIPT](#) and [siRNA](#) genes upstream or downstream of each gene in the Reactome PI3K pathway were tested (by the χ^2 -test). These are plotted as a split jitter stripchart against the hierarchical distance scores showing no significant tendency for either method to either of the pathway upstream or downstream extremities.

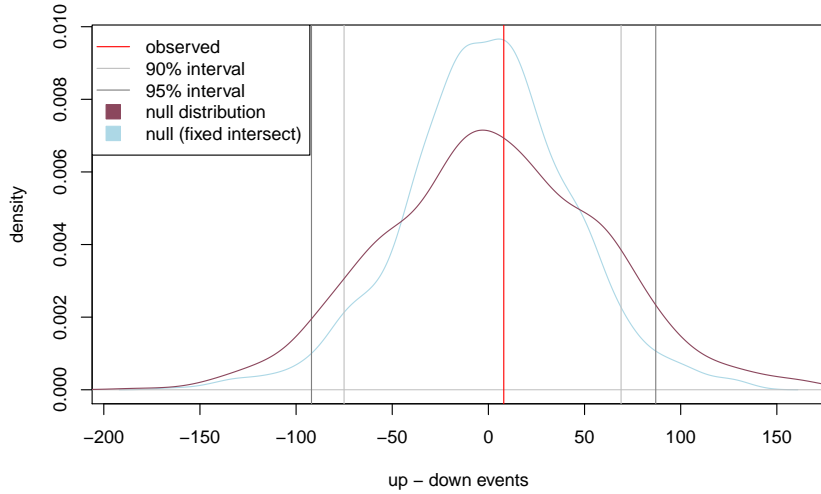


Figure I.4: Structure of synthetic lethality resampling. A null distribution (10,000 iterations) of the siRNA genes upstream or downstream of mtSLIPT genes (shown by the difference) in the PI3K pathway. The observed events (red) were compared to the the distribution (violet) and were not significant. Genes detected by both methods were fixed for the distribution (blue). The genes detected by both approaches were used.

Table I.2: Resampling for pathway structure of synthetic lethal detection methods

| Pathway | Graph | | States | | Observed | | | | Permutation p-value | |
|--|-------|--------|--------|-------|----------|------|---------|---------|---------------------|---------|
| | Nodes | Edges | mtSL | siRNA | Up | Down | Up-Down | Up/Down | Up-Down | Down-Up |
| PI3K Cascade | 138 | 1495 | 42 | 25 | 131 | 123 | 8 | 1.065 | 0.4473 | 0.5466 |
| PI3K/AKT Signalling in Cancer | 275 | 12882 | 56 | 44 | 478 | 440 | 38 | 1.086 | 0.4163 | 0.5810 |
| G_{αi} Signalling | 292 | 22003 | 57 | 58 | 543 | 866 | -323 | 0.627 | 0.9507 | 0.0488 |
| GPCR downstream | 1270 | 142071 | 218 | 160 | 7632 | 6500 | 1132 | 1.174 | 0.1707 | 0.8291 |
| Elastic fibre formation | 42 | 175 | 16 | 7 | 6 | 7 | -1 | 0.857 | 0.5512 | 0.3681 |
| Extracellular matrix | 299 | 3677 | 81 | 29 | 313 | 347 | -34 | 0.902 | 0.5762 | 0.4215 |
| Formation of Fibrin | 52 | 243 | 11 | 5 | 8 | 19 | -11 | 0.421 | 0.7993 | 0.1800 |
| Nonsense-Mediated Decay | 103 | 102 | 56 | 2 | 0 | 0 | 0 | | 0.197 | 0.1373 |
| 3'-UTR-mediated translational regulation | 107 | 2860 | 56 | 1 | 52 | 1 | 51 | 52 | 0.1210 | 0.8751 |
| Eukaryotic Translation Elongation | 92 | 3746 | 57 | 0 | 0 | 0 | 0 | | 0.4952 | 0.4892 |

Pathways in the Reactome network tested for structural relationships between mtSLIPT and siRNA genes by resampling. The raw p-value (computed without adjusting for multiple comparisons over pathways) is given for the difference in upstream and downstream paths from mtSLIPT to siRNA gene candidate partners of CDH1 with significant pathways highlighted in bold. Sampling was performed only in the target pathway and shortest paths were computed within it. Loops or paths in either direction that could not be resolved were excluded from the analysis. The gene detected by both mtSLIPT and siRNA (or resampling for them) were included in the analysis and the number of these were fixed to the number observed.

Appendix J

Performance of SLIPT and χ^2

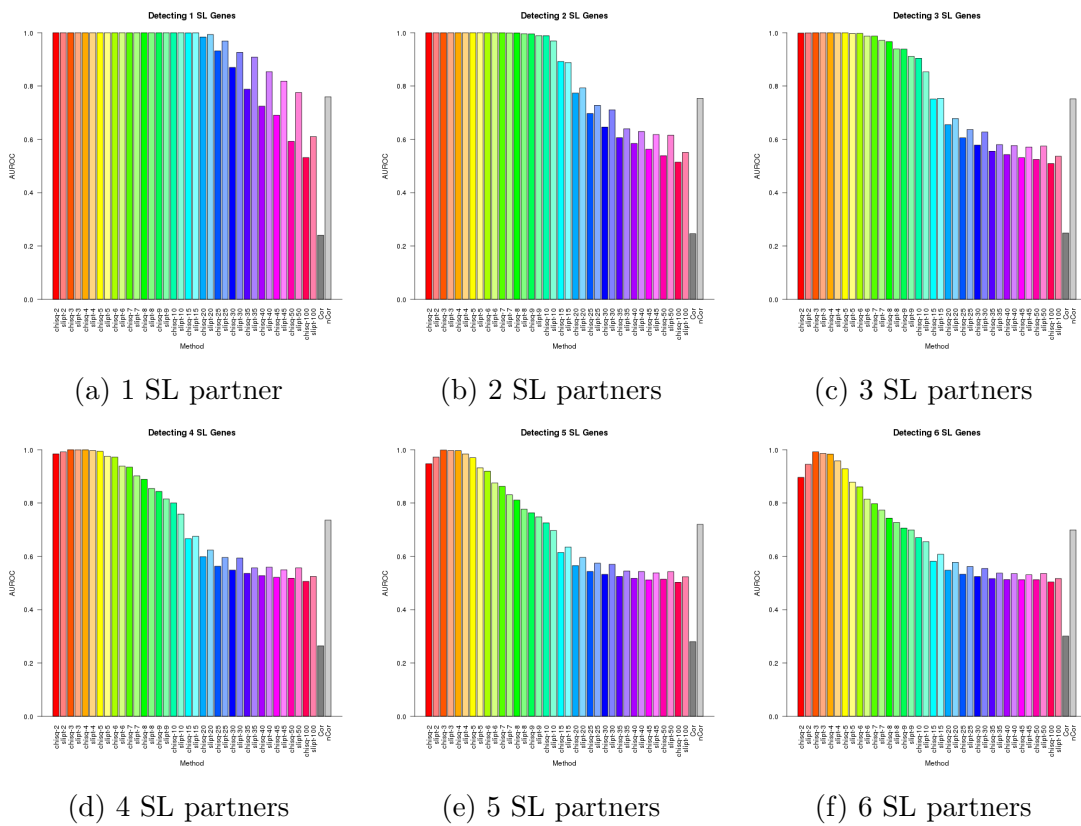


Figure J.1: Performance of χ^2 and SLIPT across quantiles. (continued on next page)

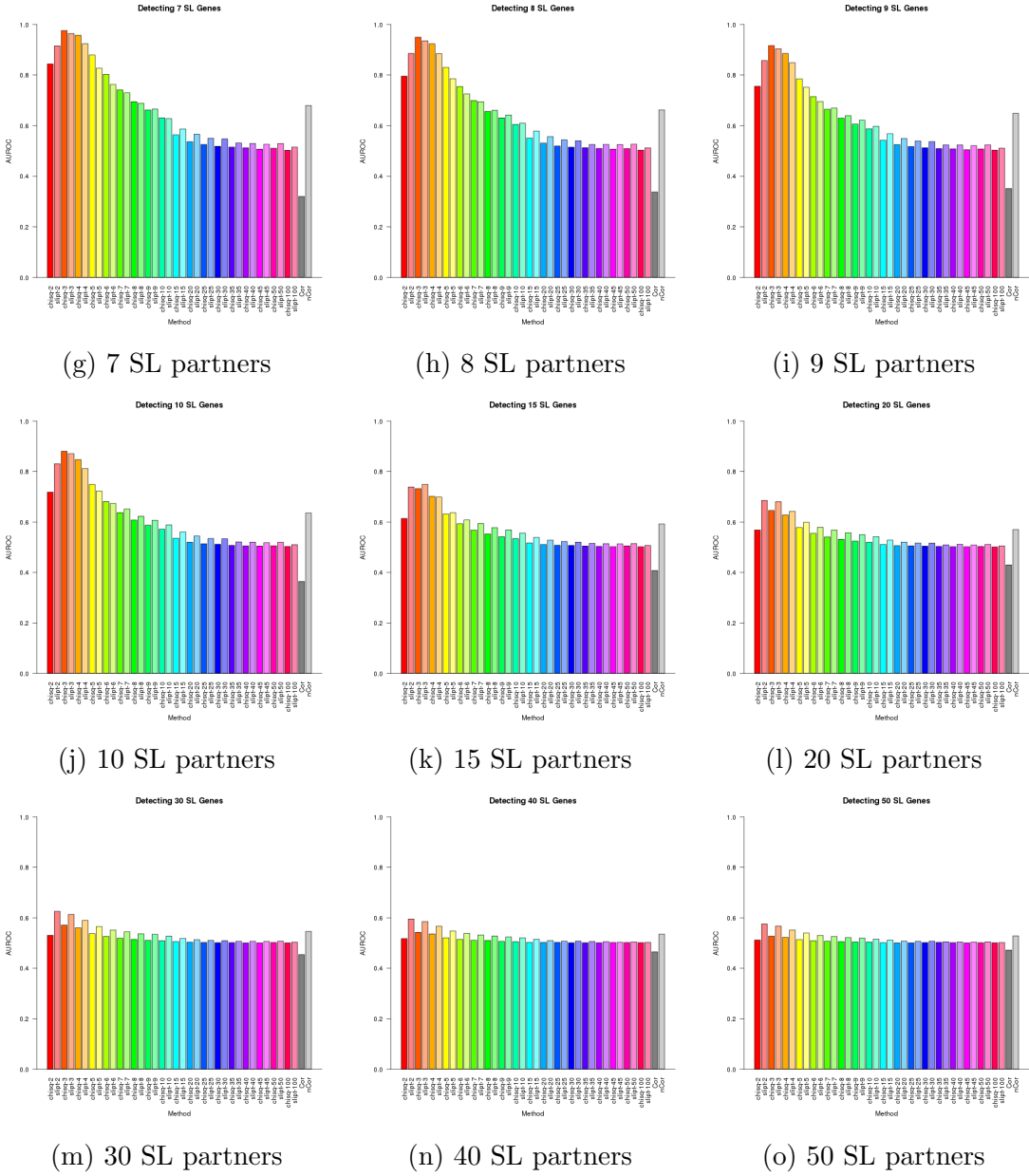


Figure J.1: Performance of χ^2 and SLIPT across quantiles. Synthetic lethal detection with quantiles as in axis labels. The barplot uses the same hues for each quantile (grey for correlation) and darker for χ^2 (and positive correlation). SLIPT and χ^2 perform similarly, peaking at $\frac{1}{3}$ -quantiles and converging to random (0.5). Negative correlation was higher than positive but not optimal quantiles for SLIPT or χ^2 . These findings are robust across different numbers of underlying synthetic lethal genes in 10,000 simulations of 100 genes and 1000 samples. SLIPT performs better than χ^2 for higher numbers of synthetic lethal genes and finer quantiles.

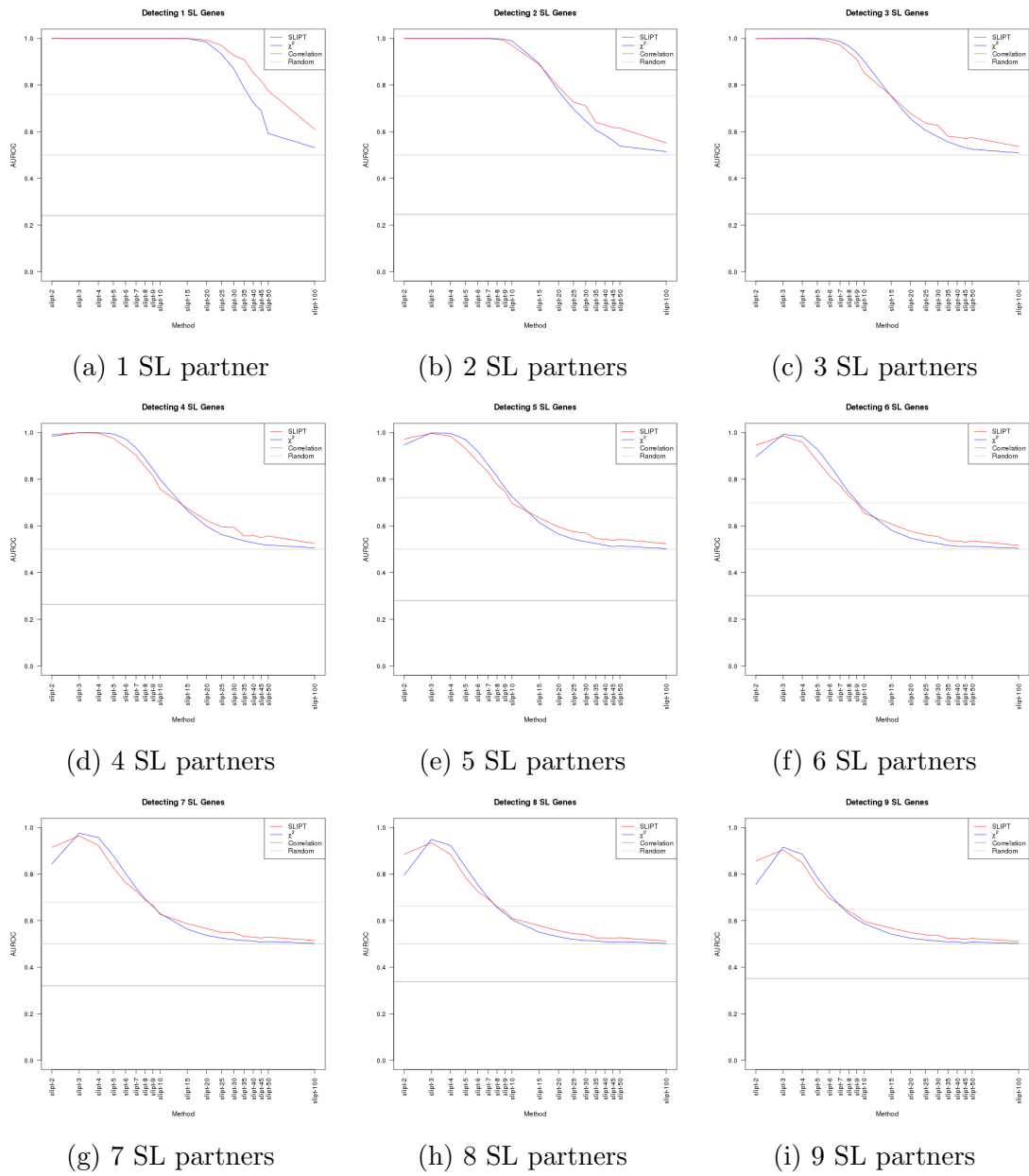


Figure J.2: **Performance of χ^2 and SLIPT across quantiles.** (continued on next page)

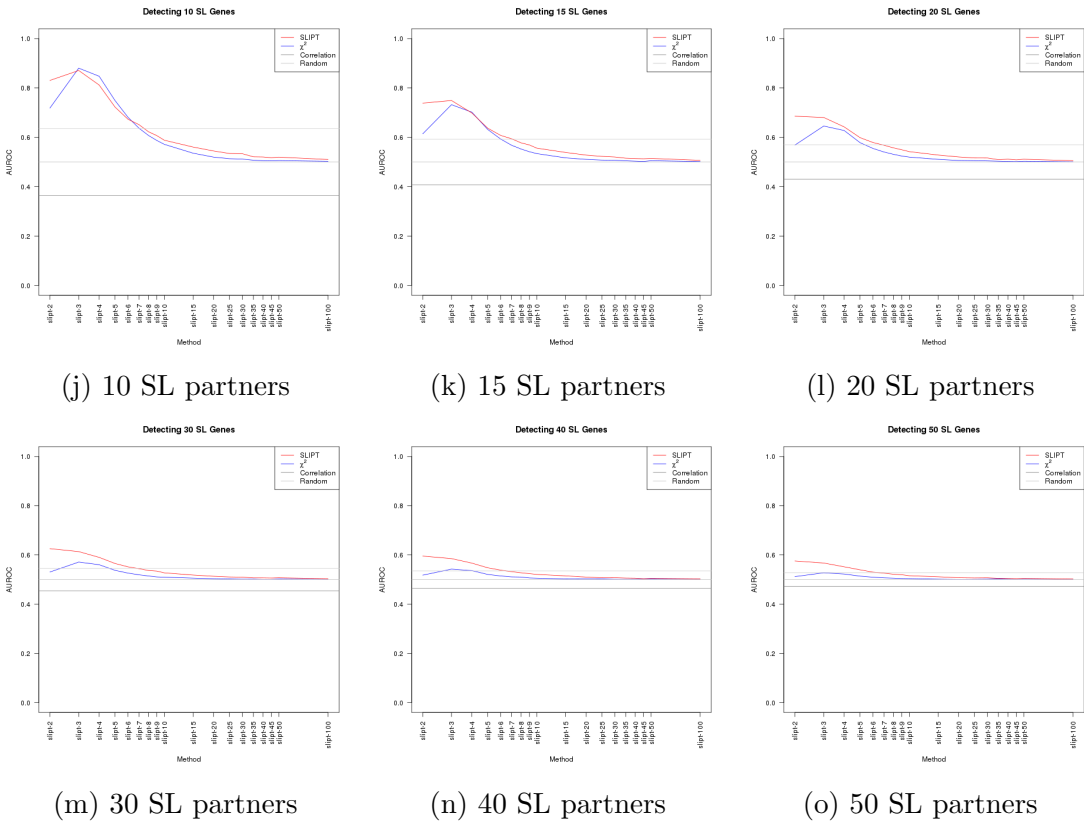


Figure J.2: Performance of χ^2 and SLIPT across quantiles. Synthetic lethal detection with quantiles as in axis labels. The line plots are coloured for SLIPT (red), χ^2 (blue) and correlation (grey) according to the legend. SLIPT and χ^2 perform similarly, peaking at $\frac{1}{3}$ -quantiles and converging to random (0.5). Negative correlation was higher than positive but not optimal quantiles for SLIPT or χ^2 . These findings are robust across different numbers of underlying synthetic lethal genes in 10,000 simulations of 100 genes and 1000 samples. SLIPT performs better than χ^2 for higher numbers of synthetic lethal genes and finer quantiles.

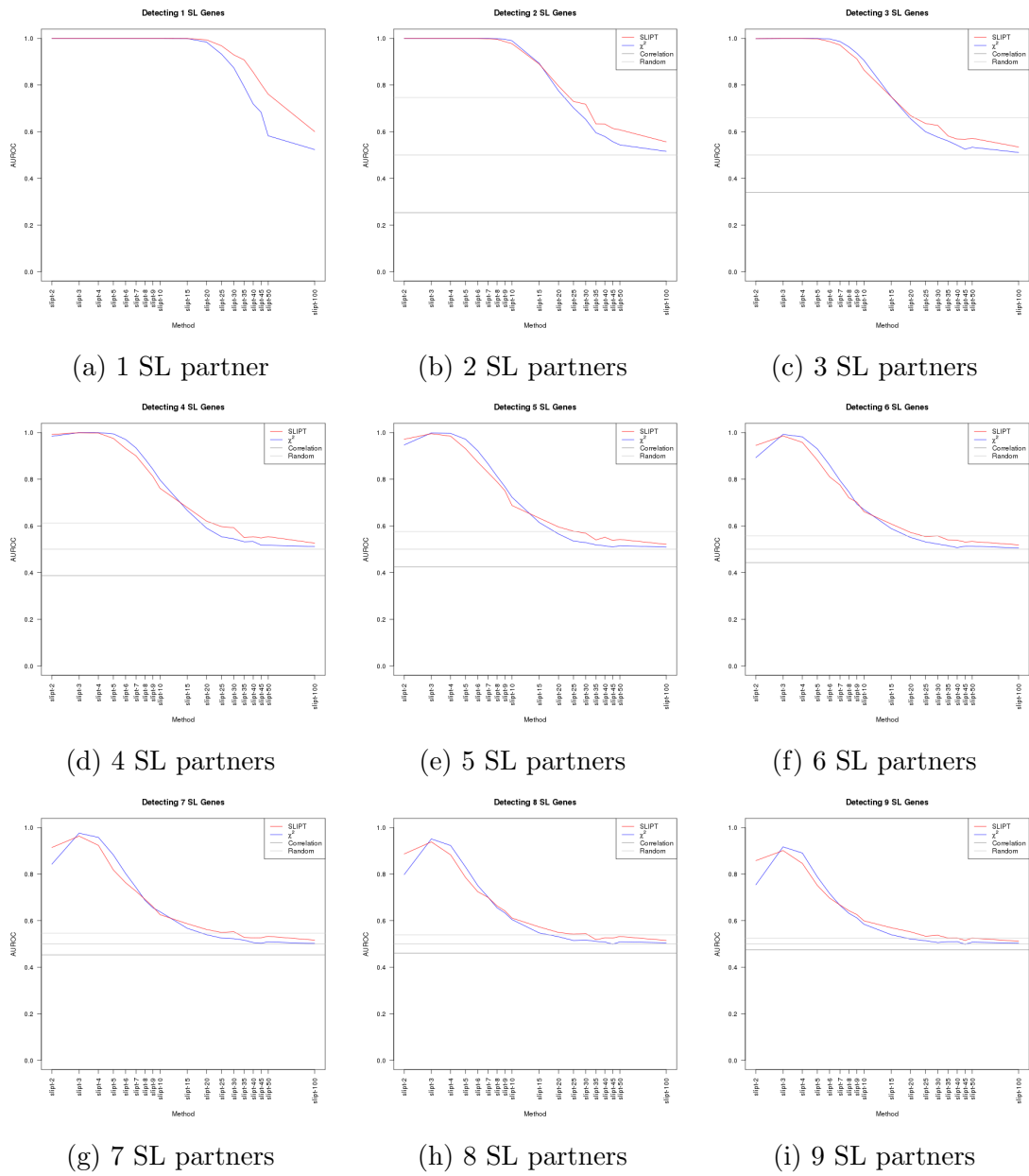


Figure J.3: **Performance of χ^2 and SLIPT across quantiles with more genes.**
 (continued on next page)

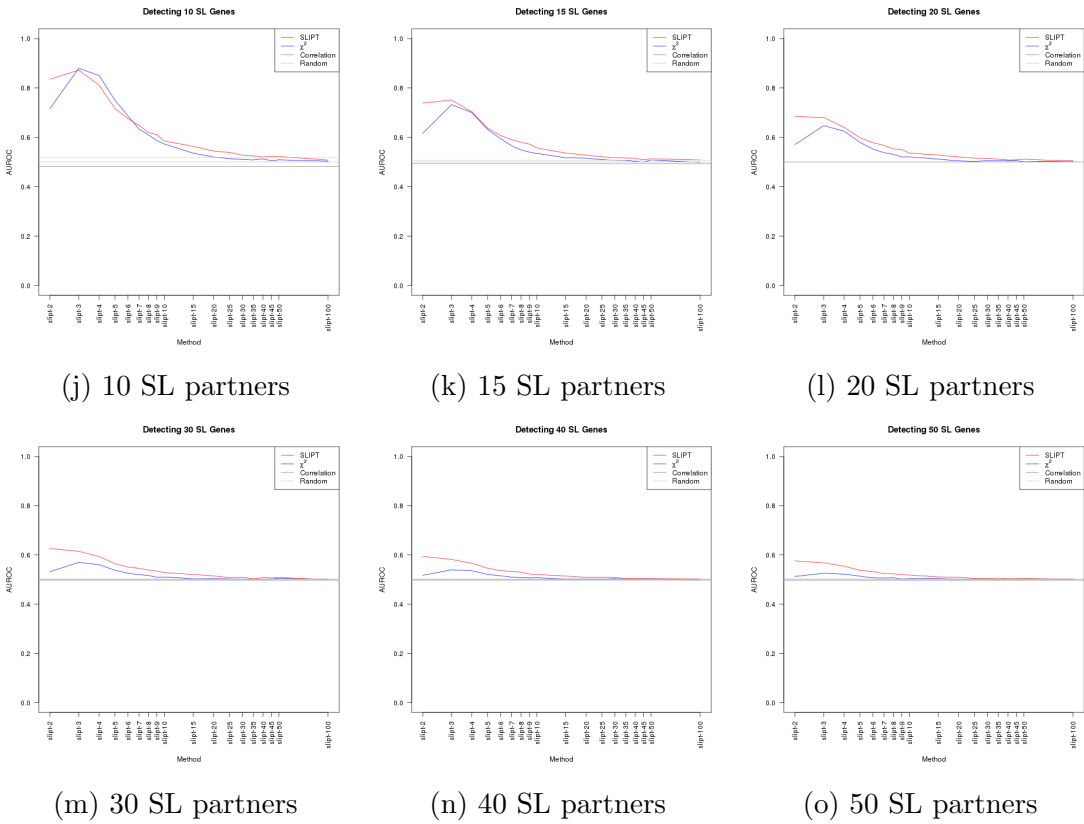


Figure J.3: Performance of χ^2 and SLIPT across quantiles with more genes. Synthetic lethal detection with quantiles as in axis labels. The line plots are coloured for SLIPT (red), χ^2 (blue) and correlation (grey) according to the legend. SLIPT and χ^2 perform similarly, peaking at $\frac{1}{3}$ -quantiles and converging to random (0.5). Negative correlation was higher than positive but not optimal quantiles for SLIPT or χ^2 . These findings are robust across different numbers of underlying synthetic lethal genes in 1000 simulations of 20,000 genes and 1000 samples. SLIPT performs better than χ^2 for higher numbers of synthetic lethal genes and finer quantiles.

J.1 Correlated Query Genes affects Specificity

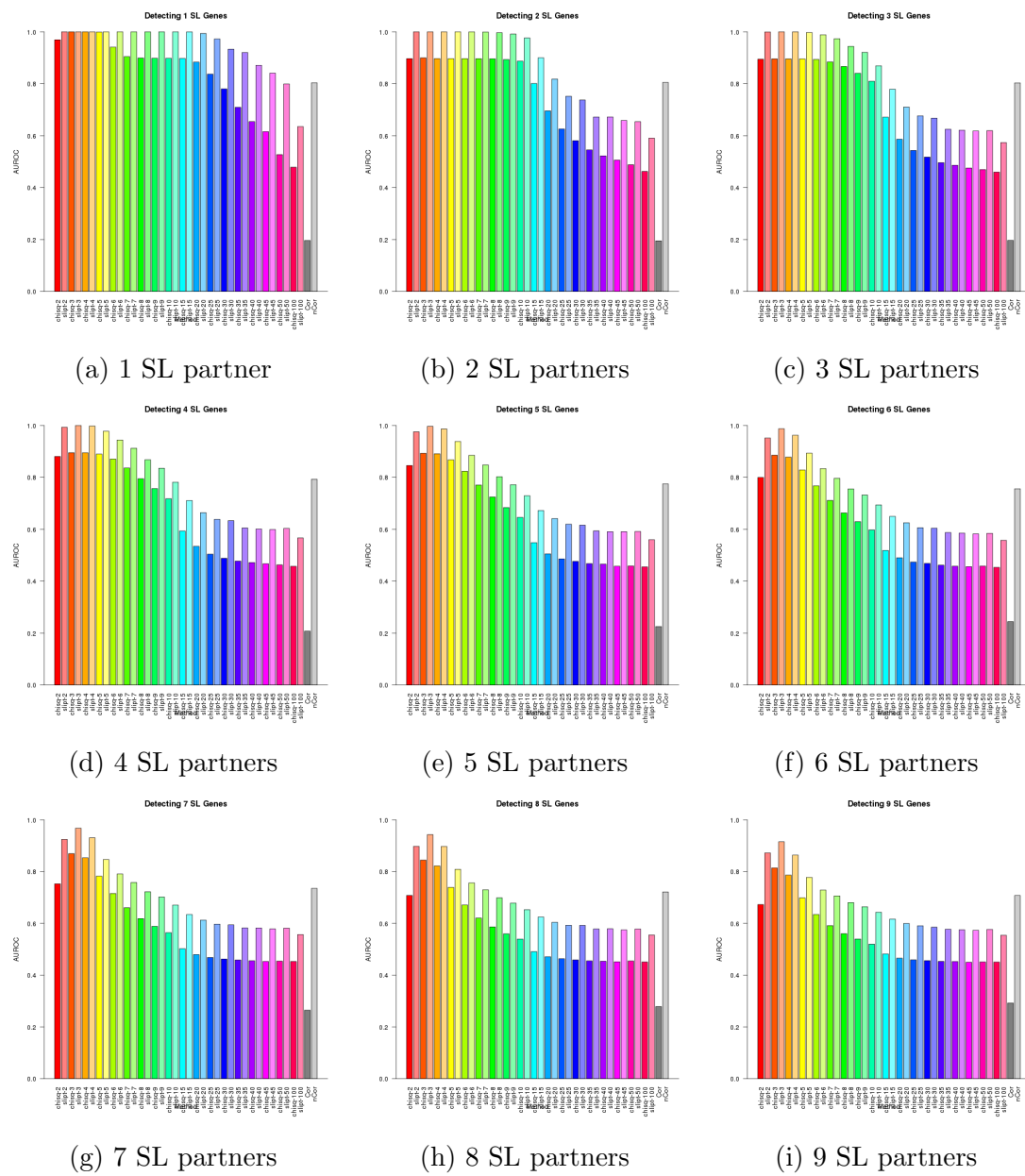


Figure J.4: Performance of χ^2 and SLIPT across quantiles with query correlation. (continued on next page)

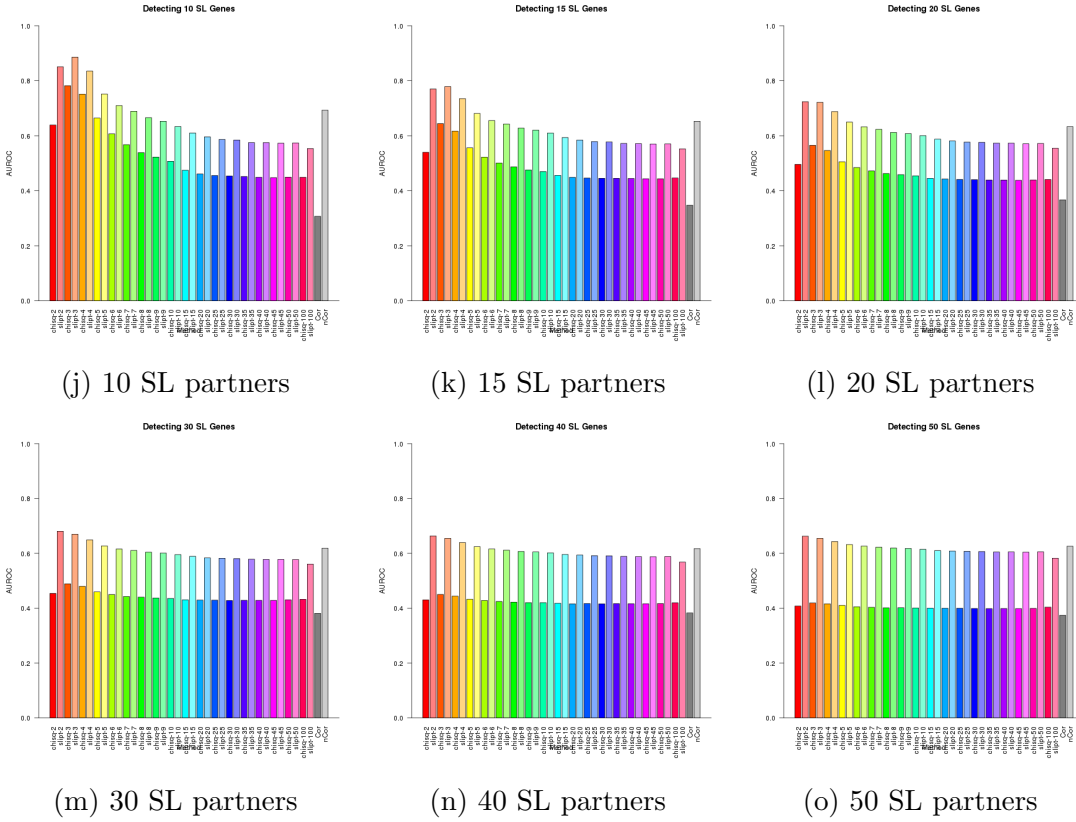


Figure J.4: Performance of χ^2 and SLIPT across quantiles with query correlation. Synthetic lethal detection with quantiles as in axis labels. The barplot uses the same hues for each quantile (grey for correlation) and darker for χ^2 (and positive correlation). SLIPT and χ^2 perform similarly, peaking at $\frac{1}{3}$ -quantiles and converging to random (0.5). Negative correlation was higher than positive but not optimal quantiles for SLIPT or χ^2 . These findings are robust across different numbers of underlying synthetic lethal genes in 10,000 simulations of 100 genes (including 10 correlated with the query) and 1000 samples. SLIPT performs consistently better than χ^2 with positively correlated genes.

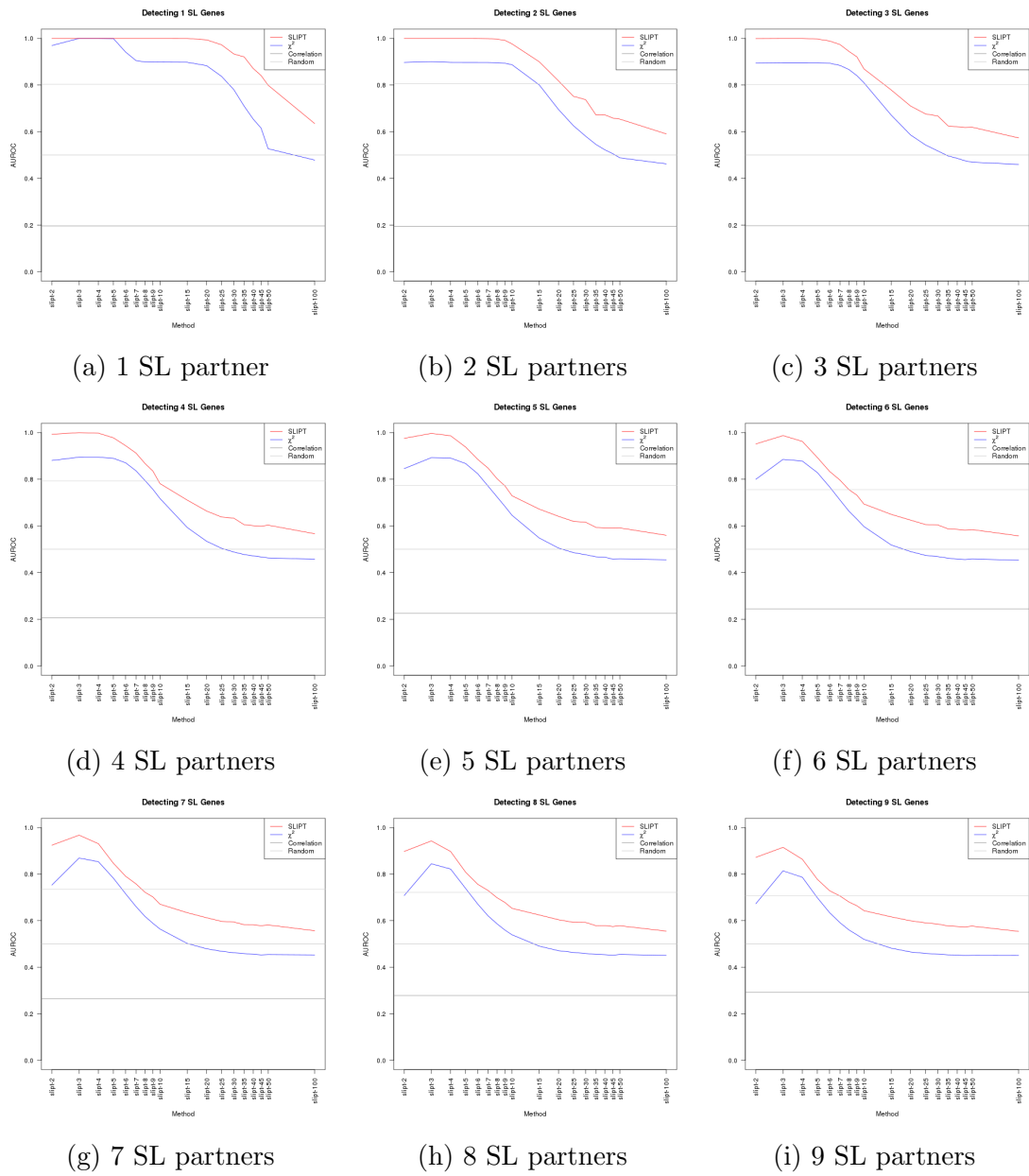


Figure J.5: **Performance of χ^2 and SLIPT across quantiles with query correlation.** (continued on next page)

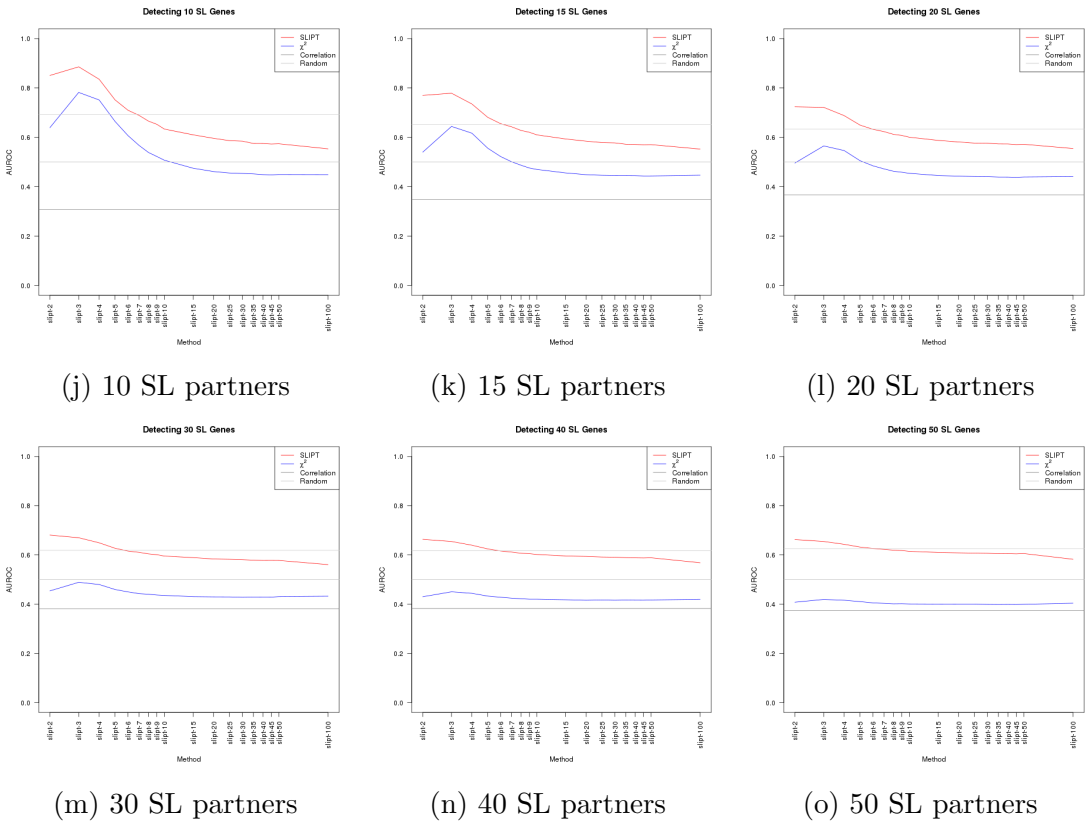


Figure J.5: Performance of χ^2 and SLIPT across quantiles with query correlation. Synthetic lethal detection with quantiles as in axis labels. The line plots are coloured for SLIPT (red), χ^2 (blue) and correlation (grey) according to the legend. SLIPT and χ^2 perform similarly, peaking at $\frac{1}{3}$ -quantiles and converging to random (0.5). Negative correlation was higher than positive but not optimal quantiles for SLIPT or χ^2 . These findings are robust across different numbers of underlying synthetic lethal genes in 10,000 simulations of 100 genes (including 10 correlated with the query) and 1000 samples. SLIPT performs consistently better than χ^2 with positively correlated genes.

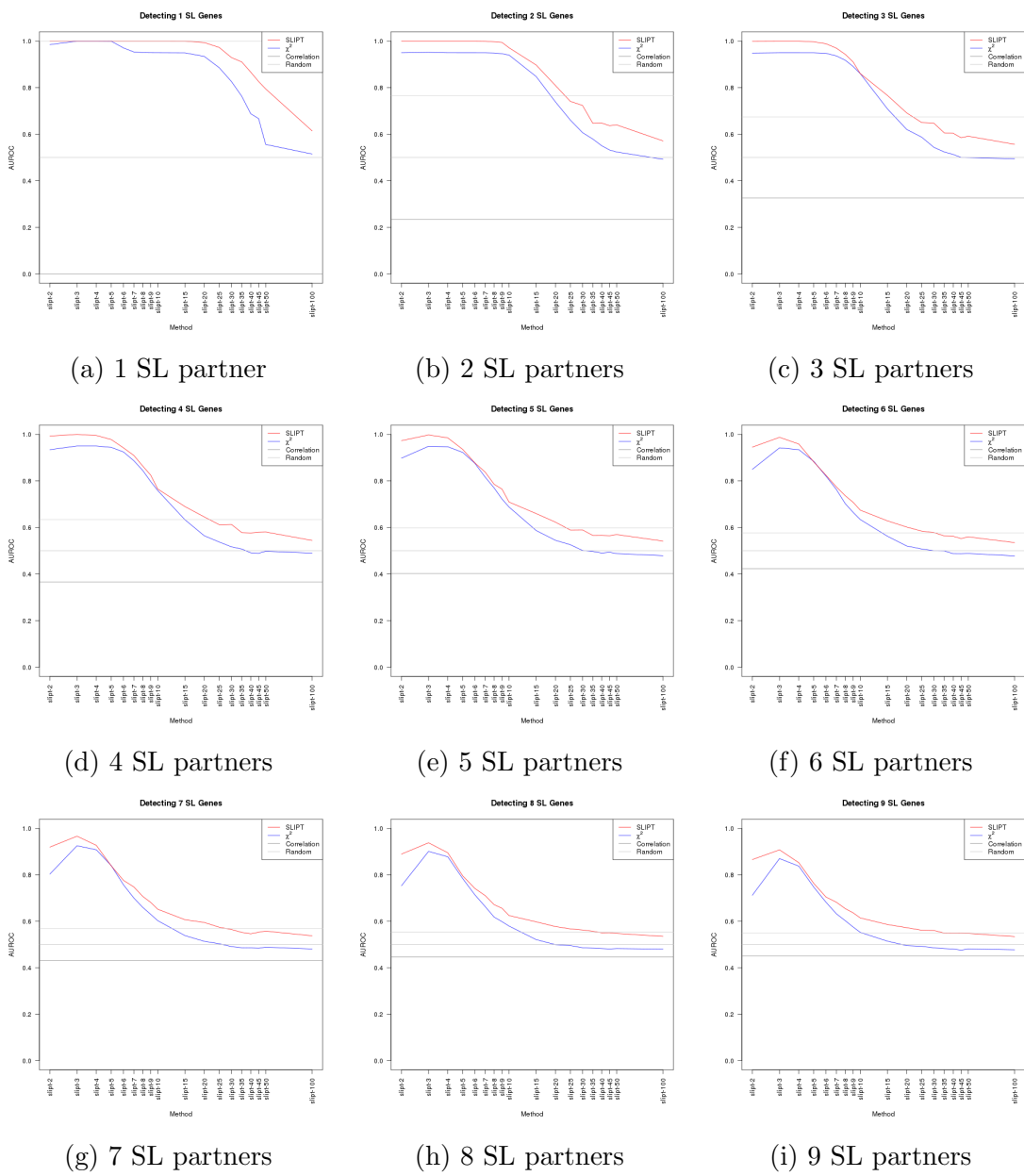


Figure J.6: Performance of χ^2 and SLIPT across quantiles with query correlation and more genes. (continued on next page)

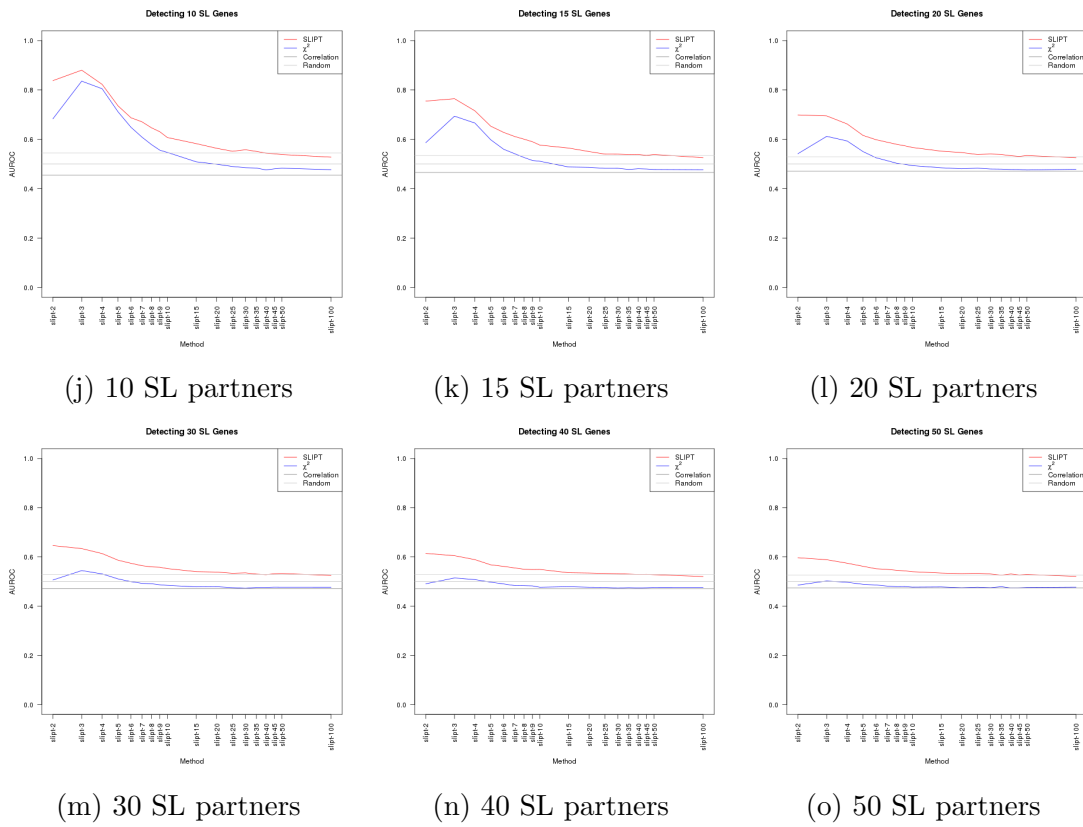


Figure J.6: Performance of χ^2 and SLIPT across quantiles with query correlation and more genes. Synthetic lethal detection with quantiles as in axis labels. The line plots are coloured for SLIPT (red), χ^2 (blue) and correlation (grey) according to the legend. SLIPT and χ^2 perform similarly, peaking at $\frac{1}{3}$ -quantiles and converging to random (0.5). Negative correlation was higher than positive but not optimal quantiles for SLIPT or χ^2 . These findings are robust across different numbers of underlying synthetic lethal genes in 1000 simulations of 20,000 genes (including 1000 correlated with the query) and 1000 samples. SLIPT performs consistently better than χ^2 with positively correlated genes.

Appendix K

Graph Structures

K.1 Simulations from Simple Graph Structures

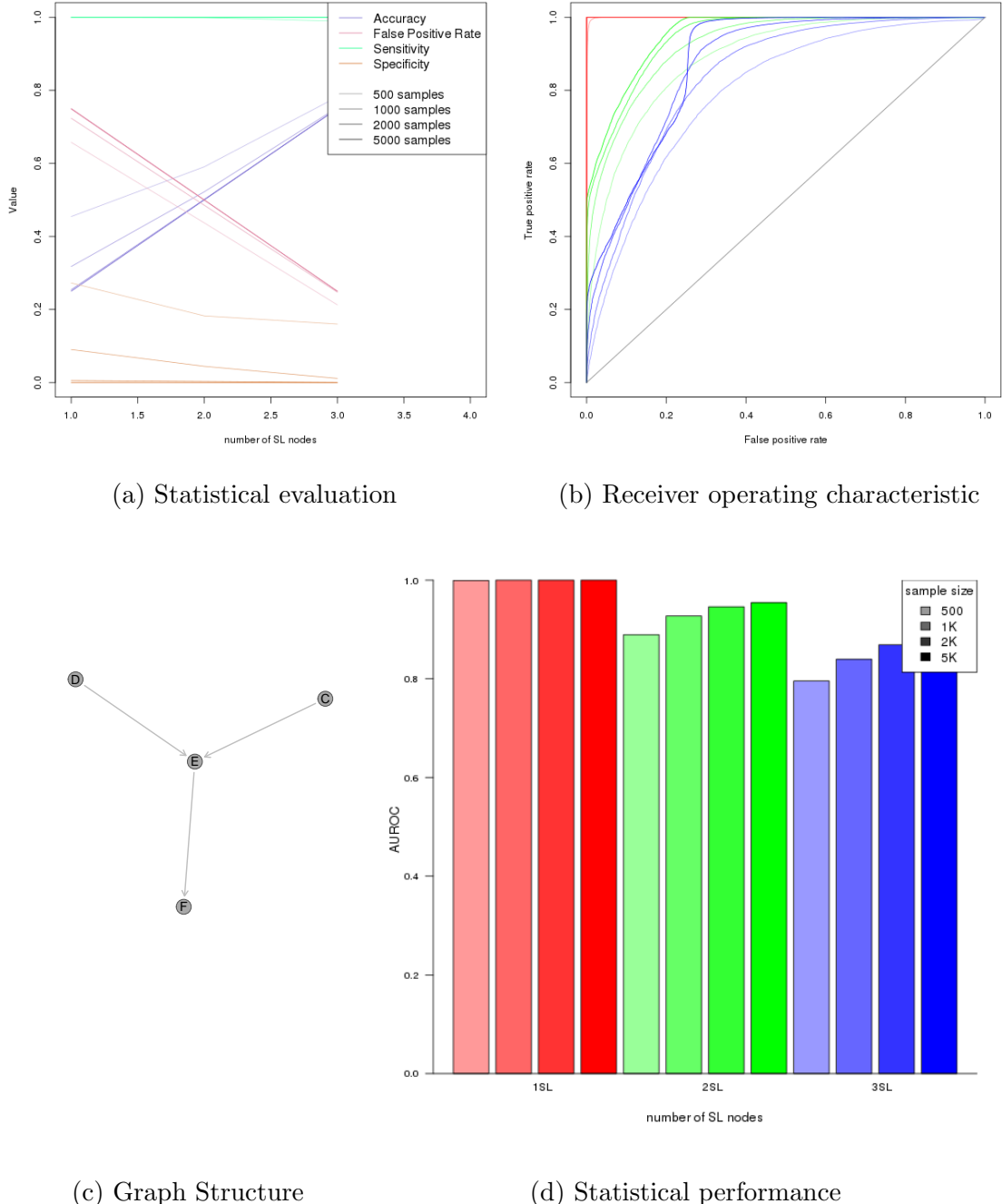


Figure K.1: Performance of simulations on a simple graph. Simulation of synthetic lethality was performed using a multivariate normal distribution from a converging graph. For each parameter, 10,000 simulations were used. Colours in Figure K.1b match Figure K.1d.

K.1.1 Simulations from Inhibiting Graph Structures

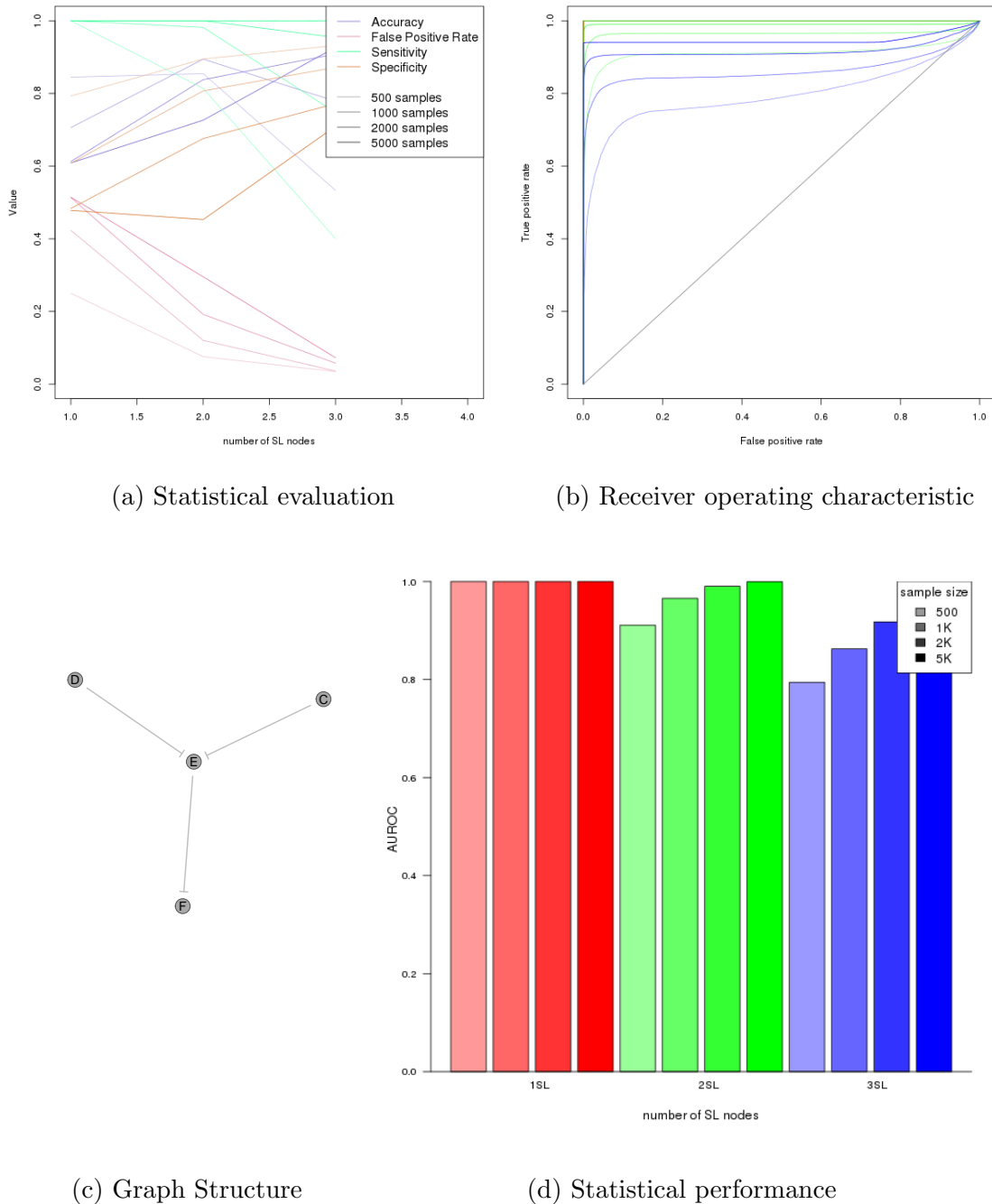
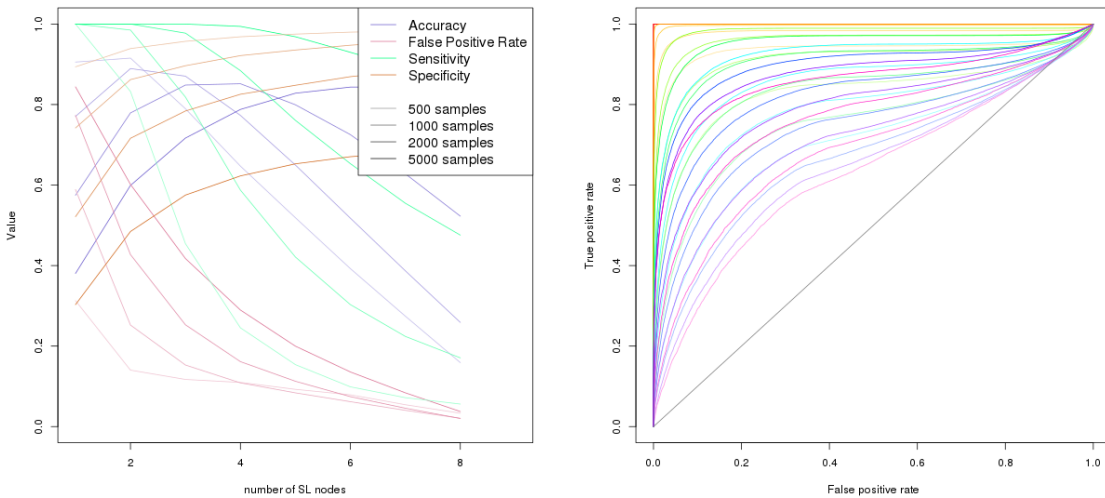
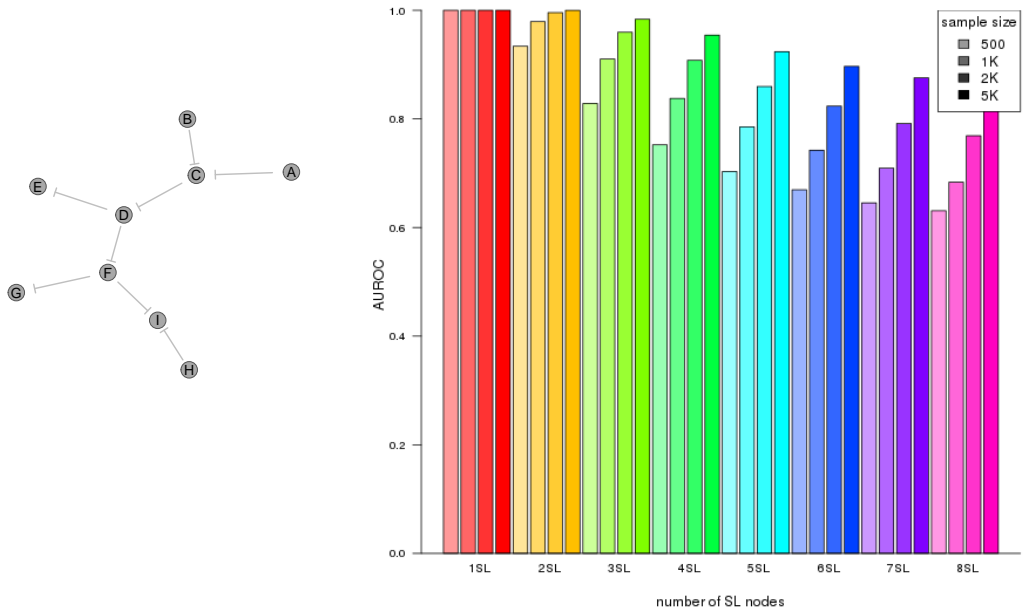


Figure K.2: Performance of simulations on an inhibiting graph. Simulation of synthetic lethality used a multivariate normal distribution from a converging graph. For each parameter, 10,000 simulations were used. Colours in Figure K.2b match Figure K.2d.



(a) Statistical evaluation

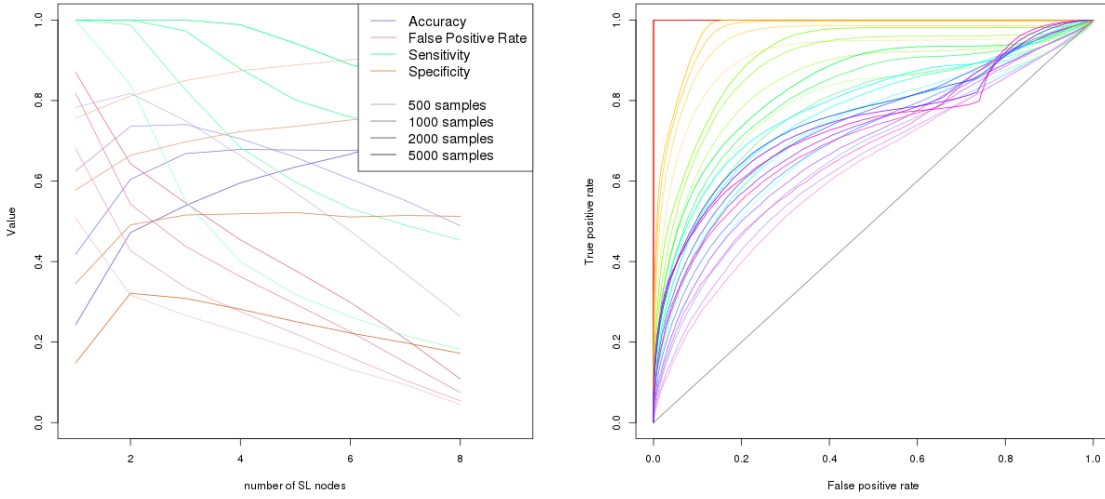
(b) Receiver operating characteristic



(c) Graph Structure

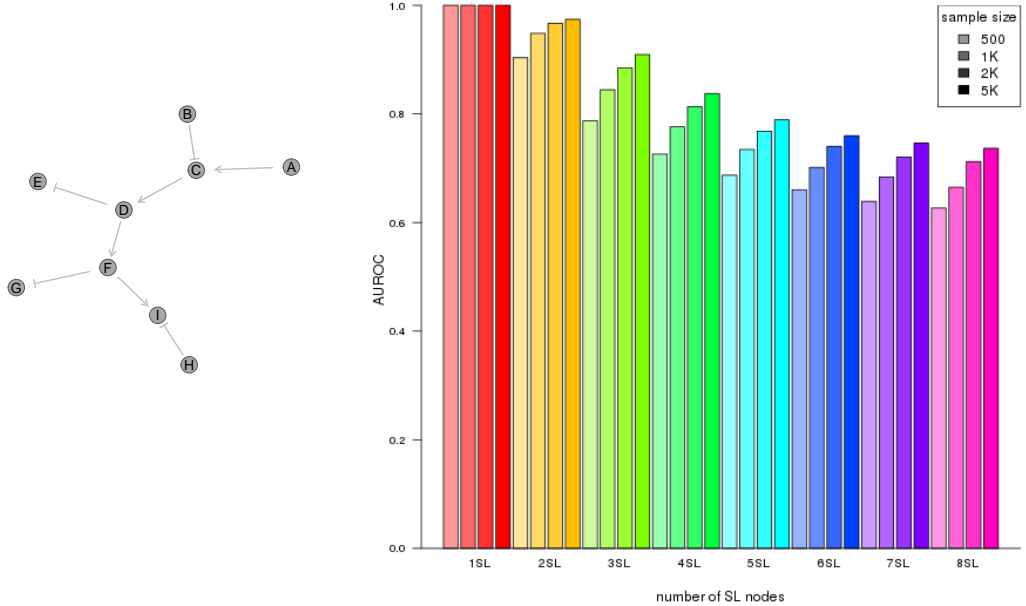
(d) Statistical performance

Figure K.3: Performance of simulations on a constructed graph with inhibition.
 Simulation of synthetic lethality used a multivariate normal distribution from Graph4 with only inhibitions. Performance of [SLIPT](#) declines for more synthetic partners and lower sample sizes. For each parameter, 10,000 simulations were used.



(a) Statistical evaluation

(b) Receiver operating characteristic

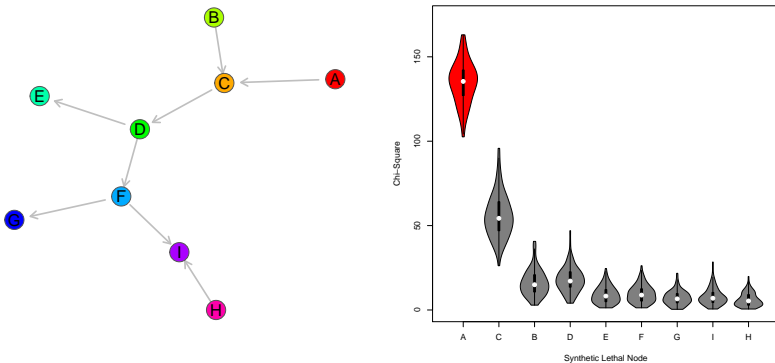


(c) Graph Structure

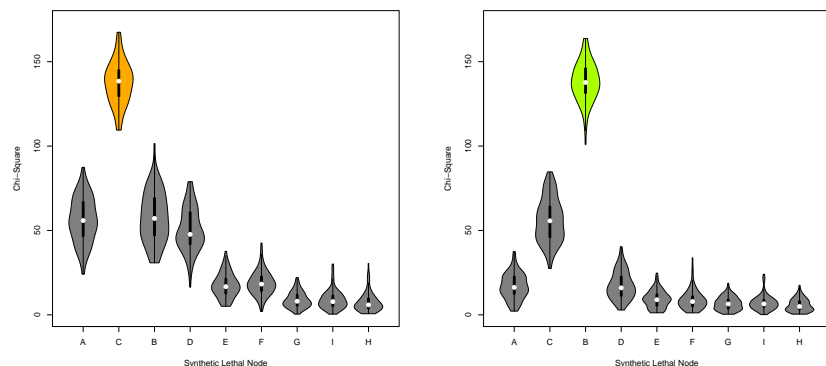
(d) Statistical performance

Figure K.4: Performance of simulations on a constructed graph with inhibition.
 Simulation of synthetic lethality used a multivariate normal distribution from Graph4 with a combination of inhibitions. Performance of **SLIPT** declines for more synthetic partners and lower sample sizes. For each parameter, 10,000 simulations were used.

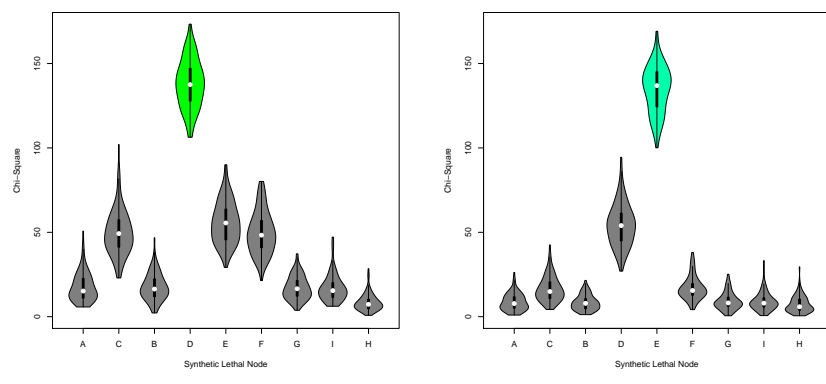
K.2 Simulation across Graph Structures



(a) Activating Graph Structure (b) χ^2 distribution for “A” SL



(c) Gene “B” SL (d) Gene “C” SL



(e) Gene “D” SL (f) Gene “E” SL

Figure K.5: **Detection of synthetic lethality within a graph Structure.** (continued on next page)

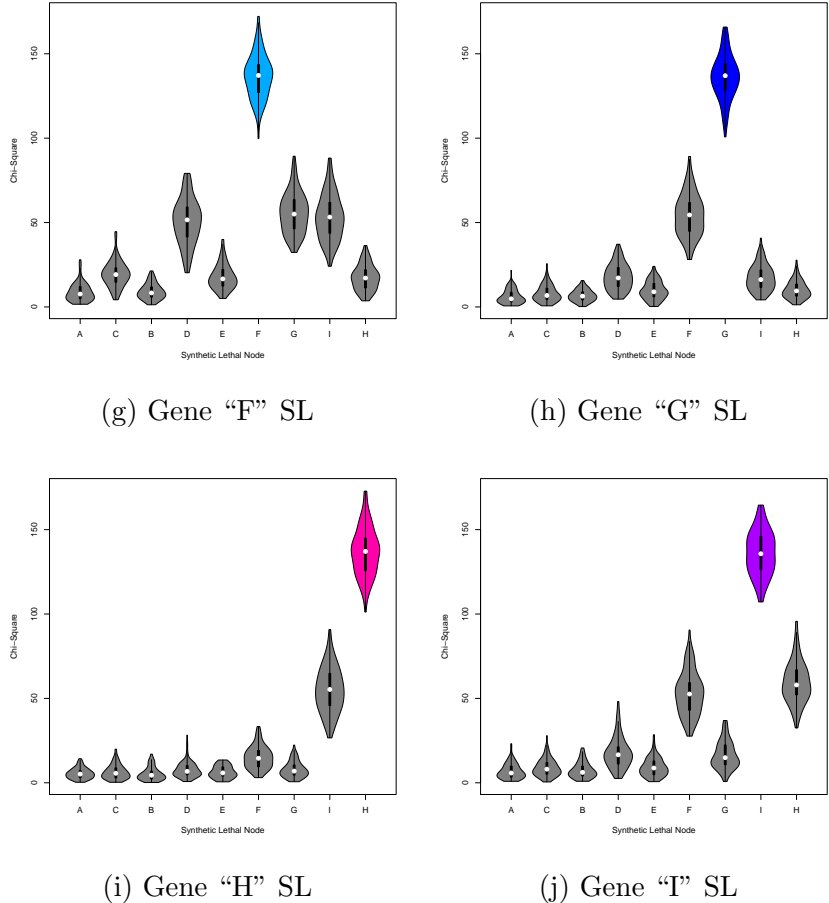
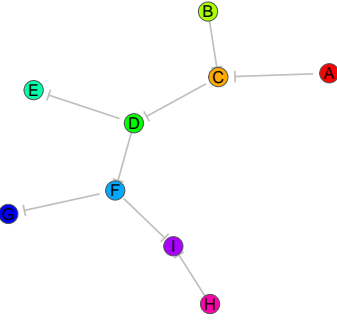
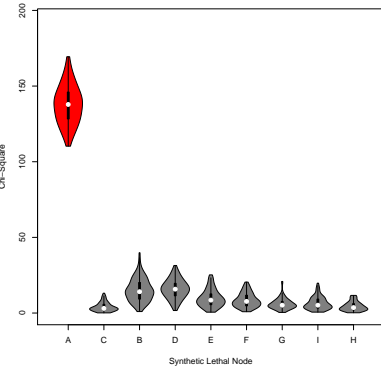


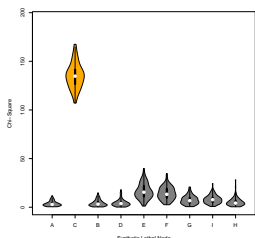
Figure K.5: Detection of synthetic lethality within a graph structure. Each gene was designated to be synthetic lethal separately and the χ^2 value from [SLIPT](#) was computed for each gene across the graph. For each synthetic lethal gene (highlighted in the respective colours), the χ^2 values were computed in 100 simulations of datasets of 20,000 genes including the graph structure and 1000 samples. For each synthetic lethal gene, the adjacent genes in the network also had elevated test statistics.



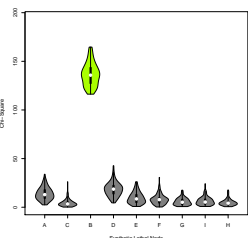
(a) Inhibiting Graph Structure



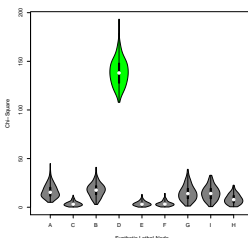
(b) χ^2 distribution for "A" SL



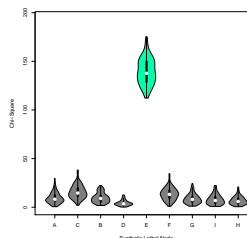
(c) Gene "B" SL



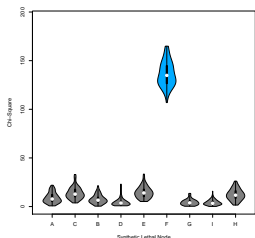
(d) Gene "C" SL



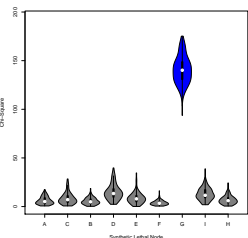
(e) Gene "D" SL



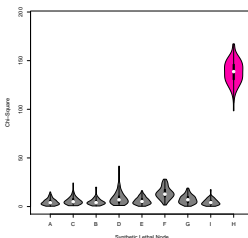
(f) Gene "E" SL



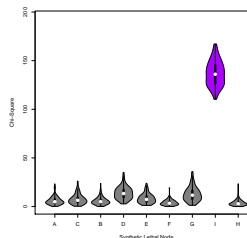
(g) Gene "F" SL



(h) Gene "G" SL

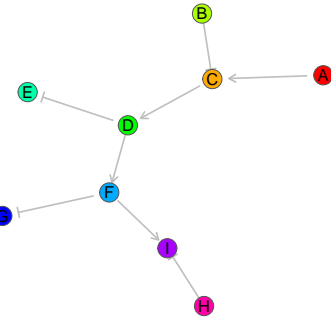


(i) Gene "H" SL

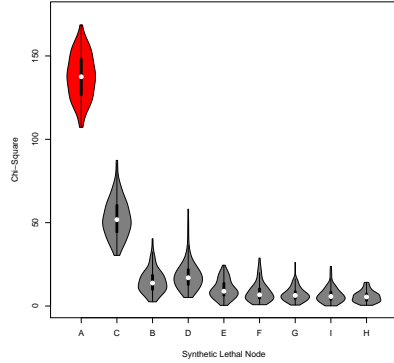


(j) Gene "I" SL

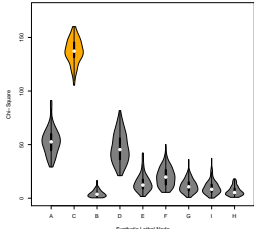
Figure K.6: Detection of synthetic lethality within an inhibiting graph. Each gene was designated to be synthetic lethal separately and the χ^2 value from [SLIPT](#) was computed for each gene across the graph structure with inhibiting relationships. For each synthetic lethal gene (highlighted in the respective colours), the χ^2 values were computed in 100 simulations of datasets of 20,000 genes including the graph structure and 1000 samples. For each synthetic lethal gene, the adjacent genes exhibited lower χ^2 values with inhibiting relationships.



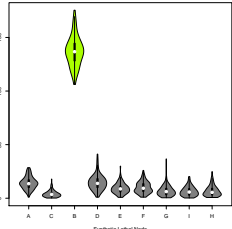
(a) Inhibiting Graph Structure



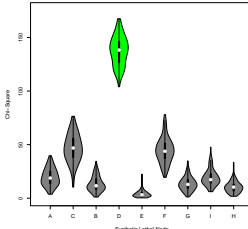
(b) χ^2 distribution for "A" SL



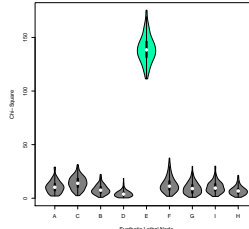
(c) Gene "B" SL



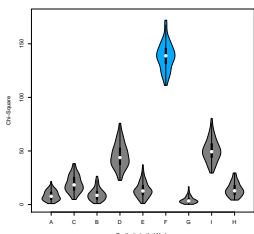
(d) Gene "C" SL



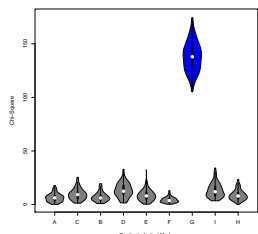
(e) Gene "D" SL



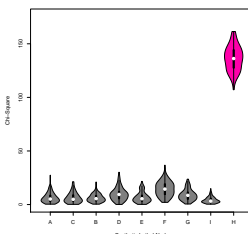
(f) Gene "E" SL



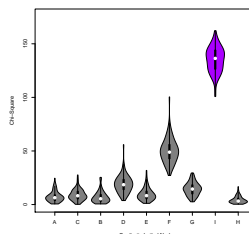
(g) Gene "F" SL



(h) Gene "G" SL



(i) Gene "H" SL



(j) Gene "I" SL

Figure K.7: Detection of synthetic lethality within an inhibiting graph. Each gene was designated to be synthetic lethal separately and the χ^2 value from **SLIPT** was computed for each gene across the graph structure with inhibiting and relationships. For each synthetic lethal gene (highlighted in the respective colours), the χ^2 values were computed in 100 simulations of datasets of 20,000 genes including the graph structure and 1000 samples.

K.3 Simulations from Complex Graph Structures

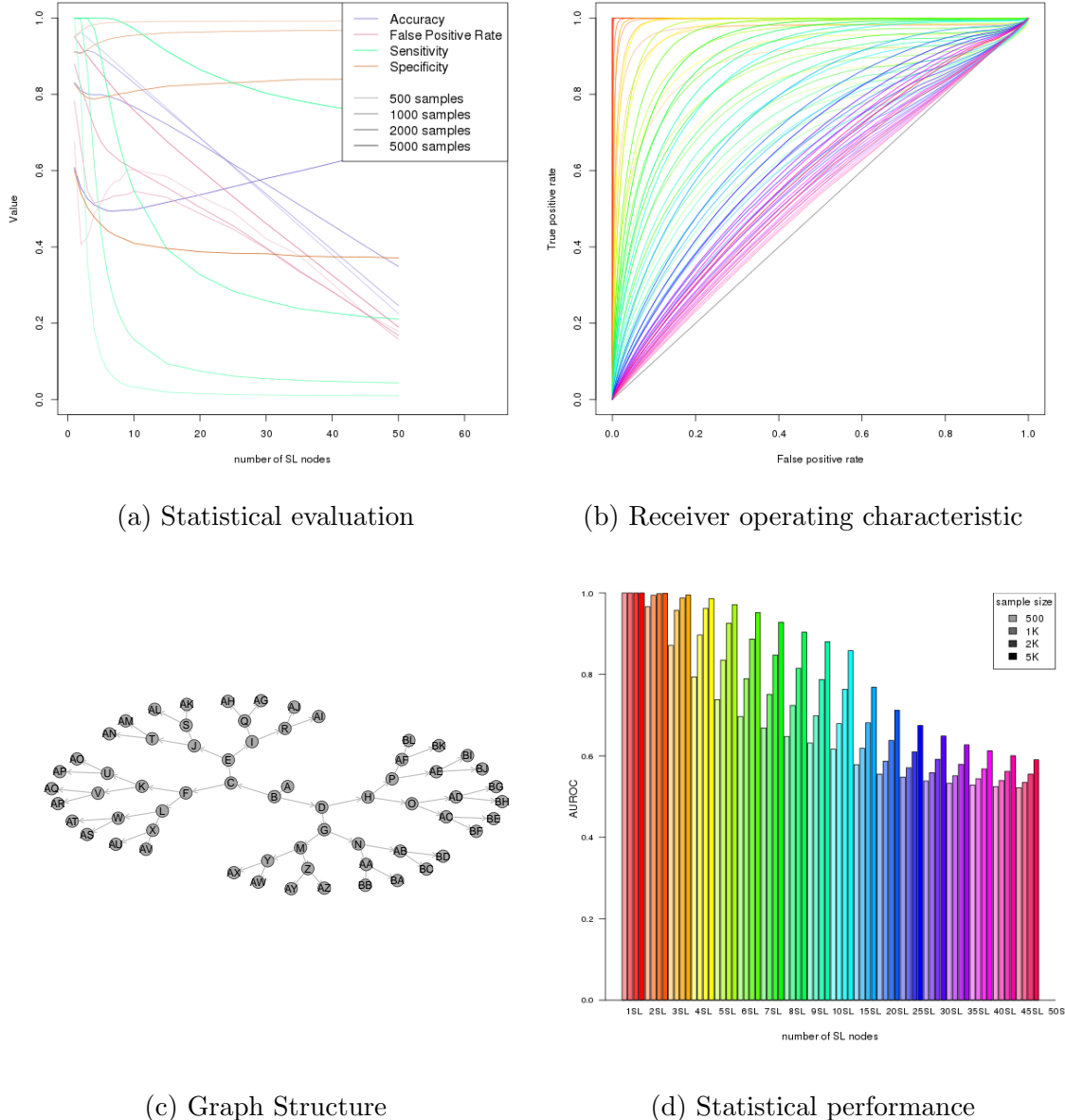
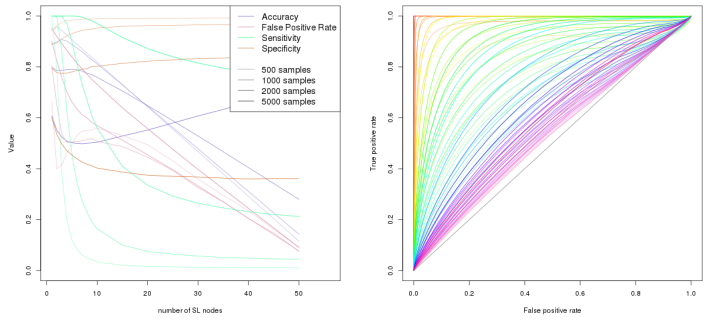
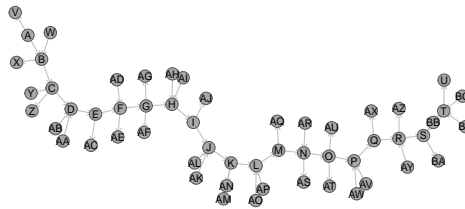


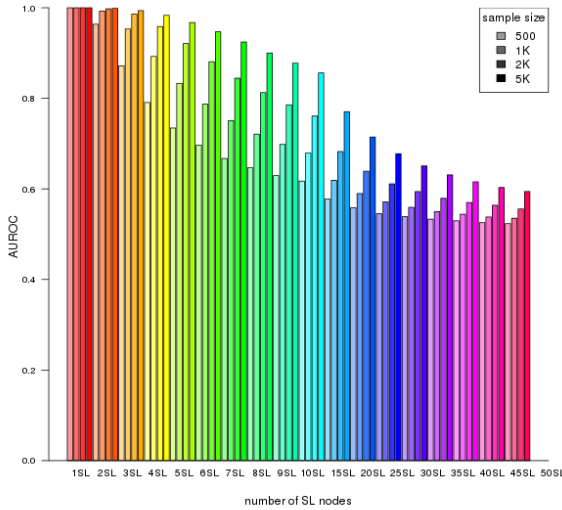
Figure K.8: **Performance of simulations on a branching graph.** Simulation of synthetic lethality used a multivariate normal distribution from a branching graph. For each parameter, 10,000 simulations were used. Colours in Figure K.8b match Figure K.8d.



(a) Statistical evaluation (b) Receiver operating characteristic

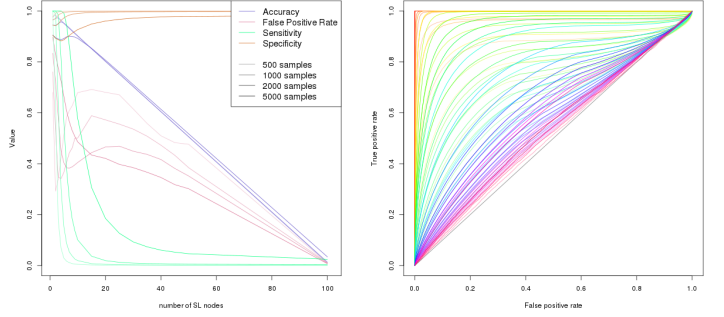


(c) Graph Structure

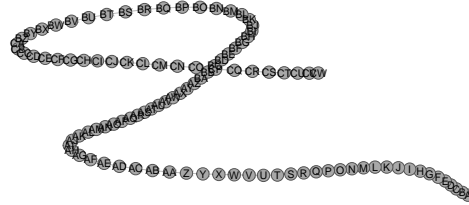


(d) Statistical performance

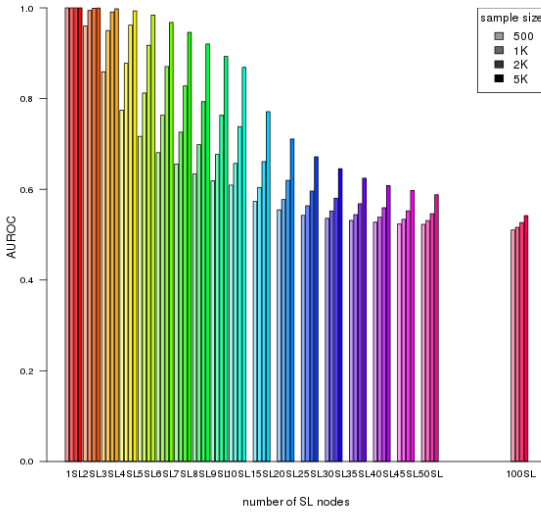
Figure K.9: Performance of simulations on a complex graph. Simulation of synthetic lethality used a multivariate normal distribution from a complex graph. Performance of **SLIPT** declines for more synthetic partners and lower sample sizes. For each parameter, 10,000 simulations were used. Colours in Figure K.9b match Figure K.9d.



(a) Statistical evaluation (b) Receiver operating characteristic



(c) Graph Structure



(d) Statistical performance

Figure K.10: **Performance of simulations on a large graph.** Simulation of synthetic lethality used a multivariate normal distribution from a large graph. For each parameter, 10,000 simulations were used. Colours in Figure K.10b match Figure K.10d.

K.3.1 Simulations from Complex Inhibiting Graphs

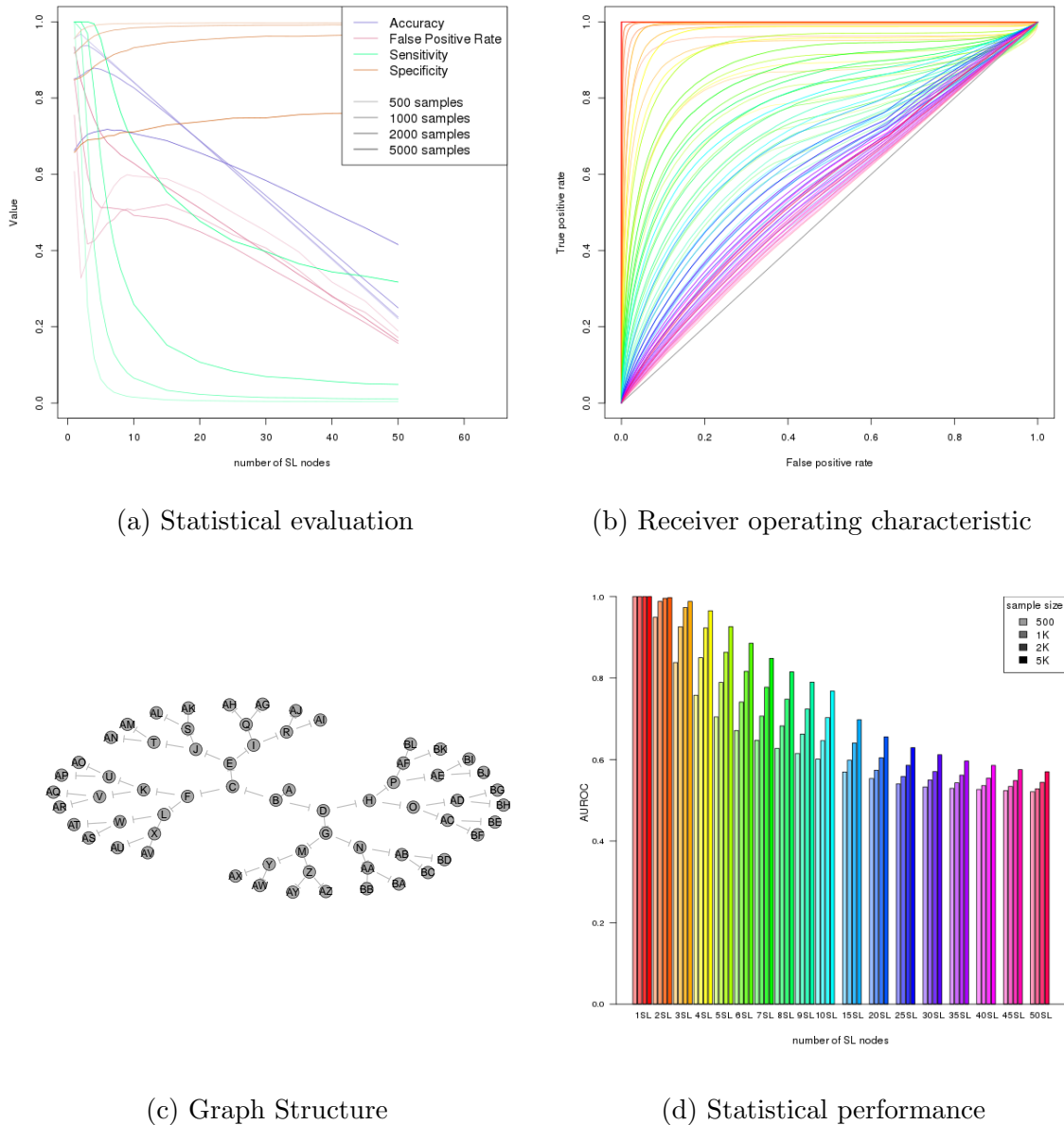
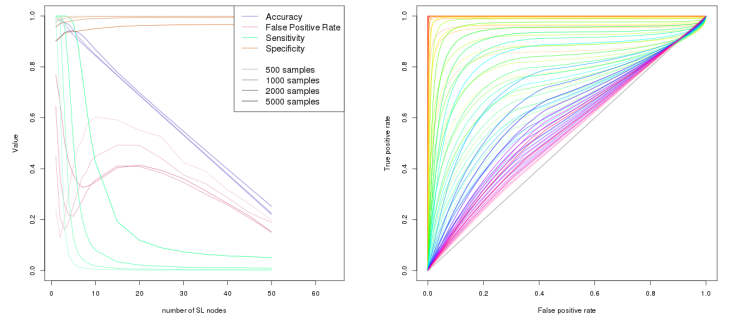
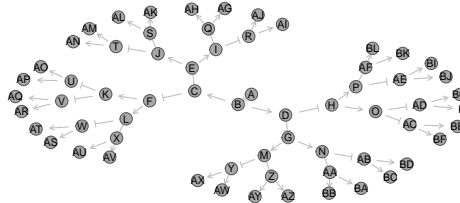


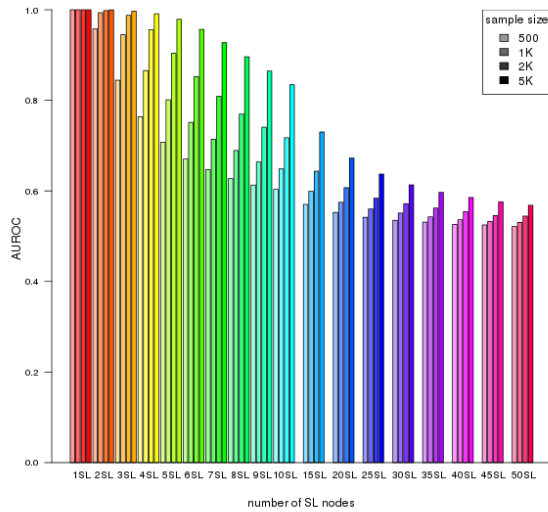
Figure K.11: **Performance of simulations on a branching graph with inhibition.** Simulation of synthetic lethality used a multivariate normal distribution from Graph6 with only inhibitions. Performance of **SLIPT** declines for more synthetic partners and lower sample sizes. For each parameter, 10,000 simulations were used.



(a) Statistical evaluation (b) Receiver operating characteristic

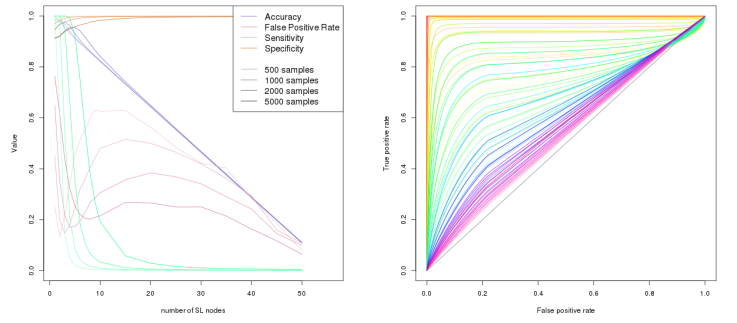


(c) Graph Structure

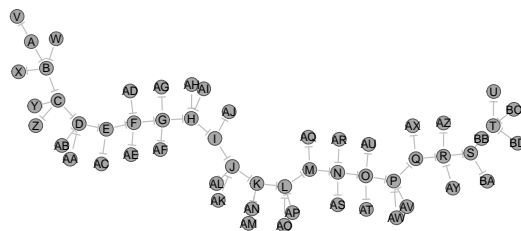


(d) Statistical performance

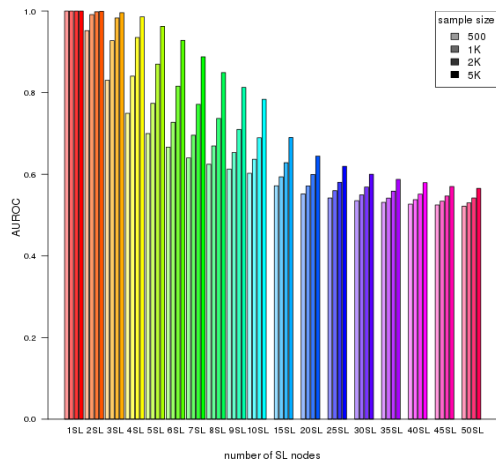
Figure K.12: Performance of simulations on a branching graph with inhibition.
 Simulation of synthetic lethality used a multivariate normal distribution from Graph6 with alternating inhibitions. Performance of [SLIPT](#) declines for more synthetic partners and lower sample sizes. For each parameter, 10,000 simulations were used.



(a) Statistical evaluation (b) Receiver operating characteristic

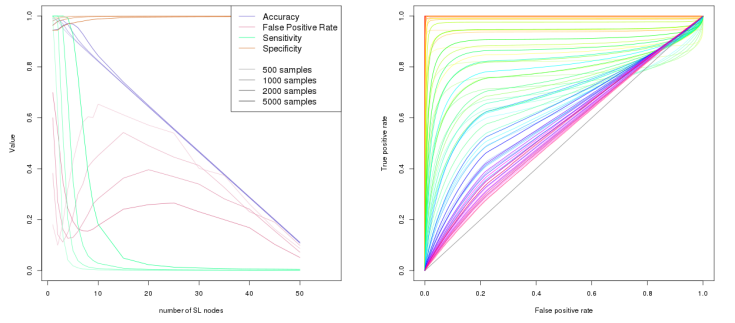


(c) Graph Structure

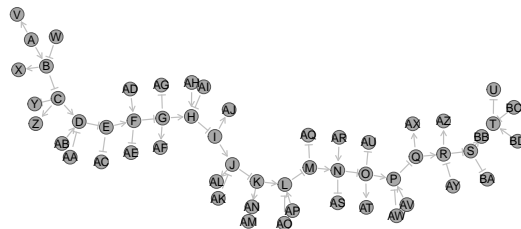


(d) Statistical performance

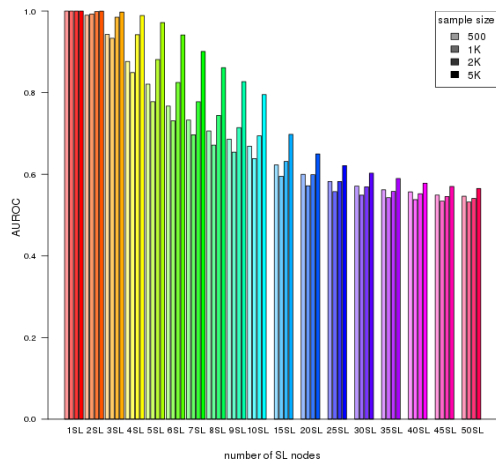
Figure K.13: Performance of simulations on a complex graph with inhibition.
 Simulation of synthetic lethality used a multivariate normal distribution from Graph7 with only inhibitions. Performance of **SLIPT** declines for more synthetic partners and lower sample sizes. For each parameter, 10,000 simulations were used.



(a) Statistical evaluation (b) Receiver operating characteristic

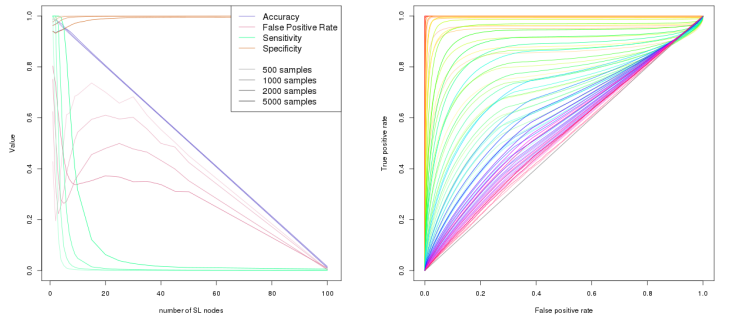


(c) Graph Structure



(d) Statistical performance

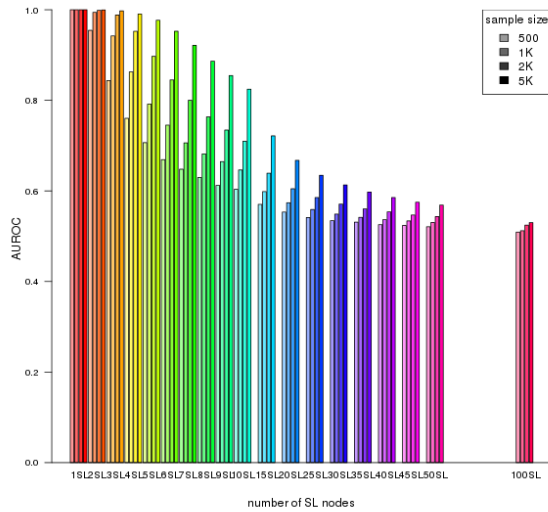
Figure K.14: Performance of simulations on a complex graph with inhibition.
 Simulation of synthetic lethality used a multivariate normal distribution from Graph7 with a combination of relationships. Performance of **SLIPT** declines for more synthetic partners and lower sample sizes. For each parameter, 10,000 simulations were used.



(a) Statistical evaluation (b) Receiver operating characteristic

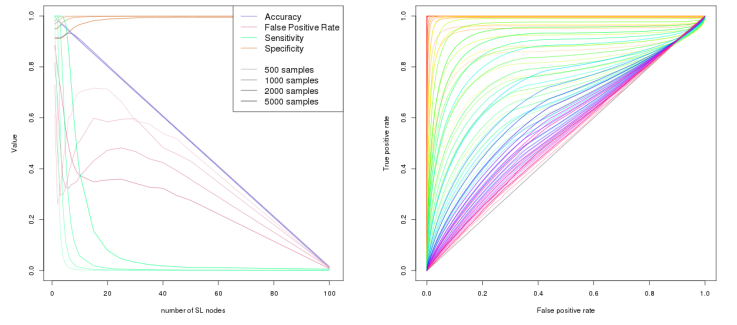


(c) Graph Structure



(d) Statistical performance

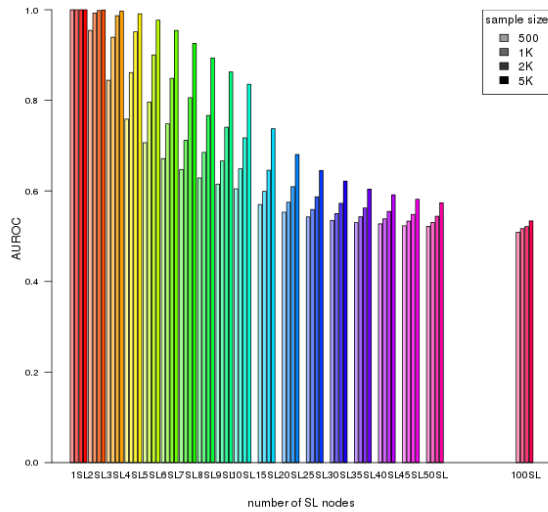
Figure K.15: **Performance of simulations on a large constructed graph with inhibition.** Simulation of synthetic lethality used a multivariate normal distribution from Graph5 with only inhibitions. For each parameter, 10,000 simulations were used.



(a) Statistical evaluation (b) Receiver operating characteristic



(c) Graph Structure



(d) Statistical performance

Figure K.16: Performance of simulations on a large constructed graph with inhibition. Simulation of synthetic lethality used a multivariate normal distribution from Graph5 with alternating inhibitions. Performance of [SLIPT](#) declines for more synthetic partners and lower sample sizes. For each parameter, 10,000 simulations were used.

K.4 Simulations from Pathway Graph Structures

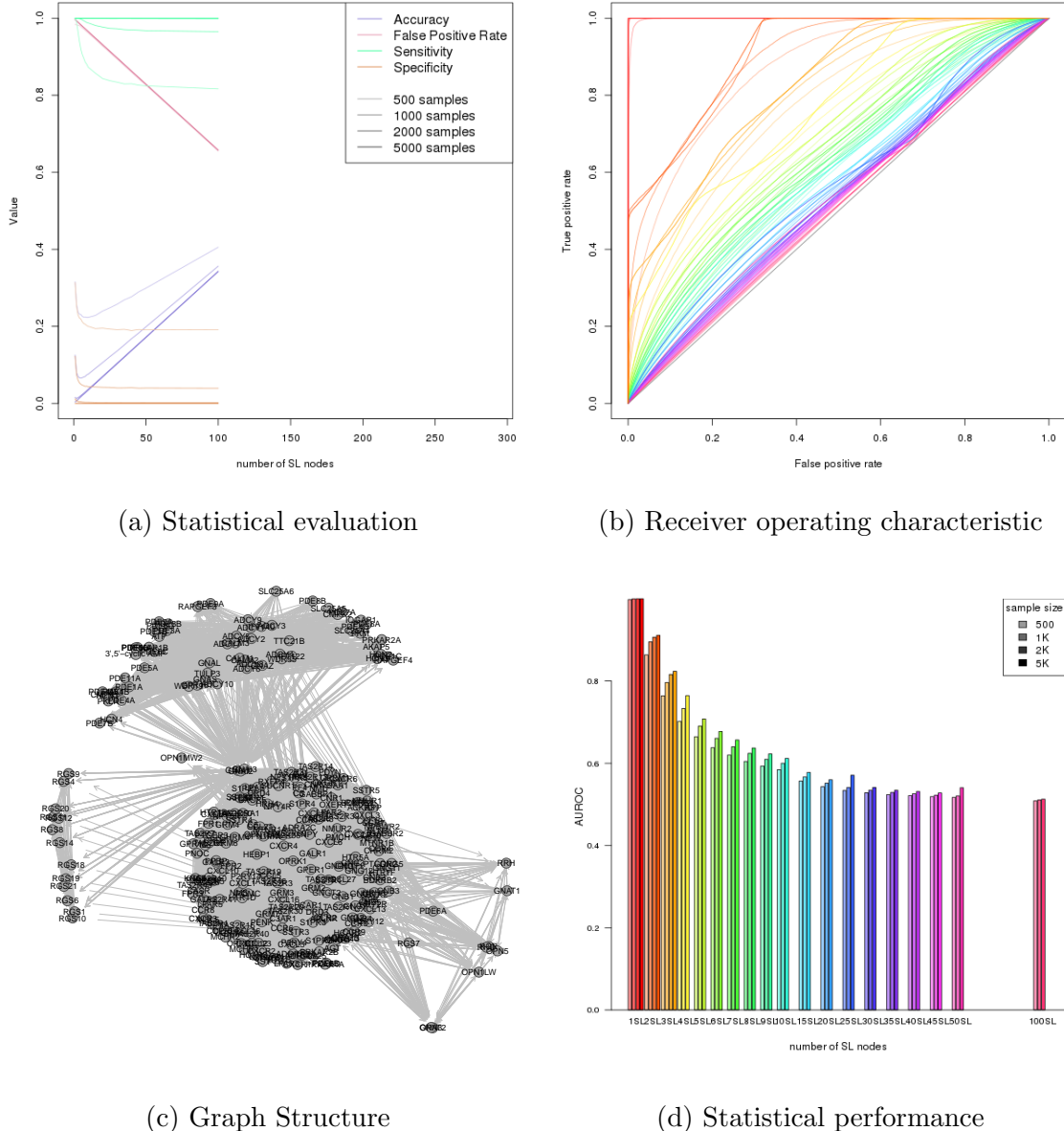
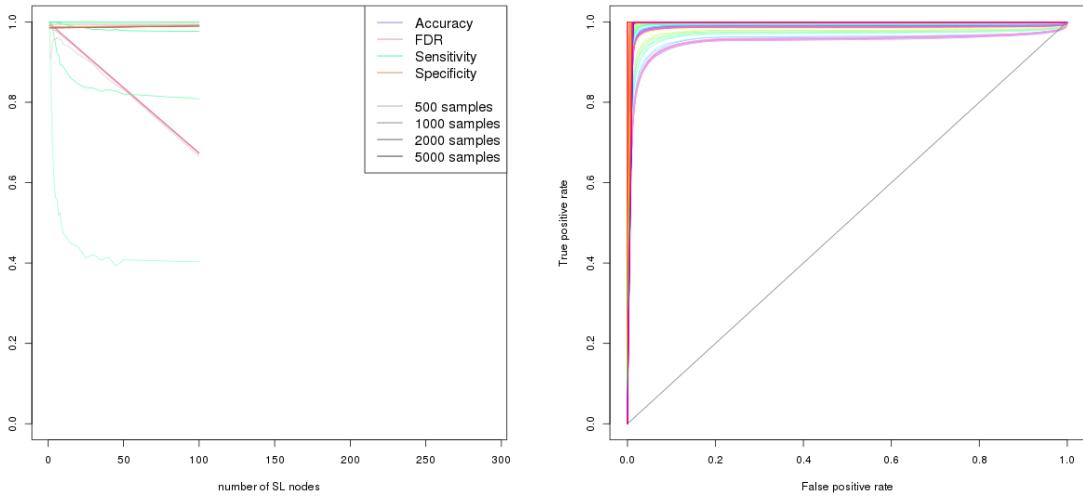
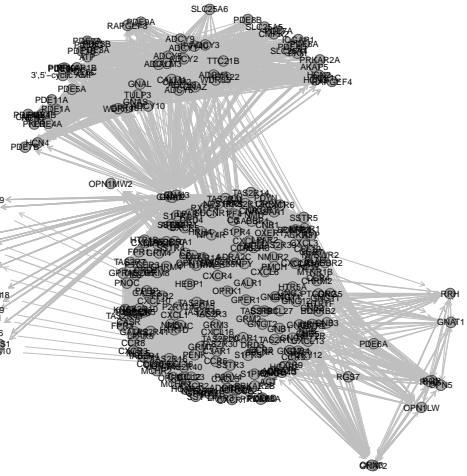


Figure K.17: Performance of simulations on the $G_{\alpha i}$ signalling pathway. Simulation of synthetic lethality used a multivariate normal distribution based on the Reactome $G_{\alpha i}$ signalling pathway. Performance of SLIPT was high across parameters for detecting synthetic lethality in the graph structure within a larger dataset. The performance decreases for a greater number of true positives to detect but the accuracy increases with a low false positive rate.

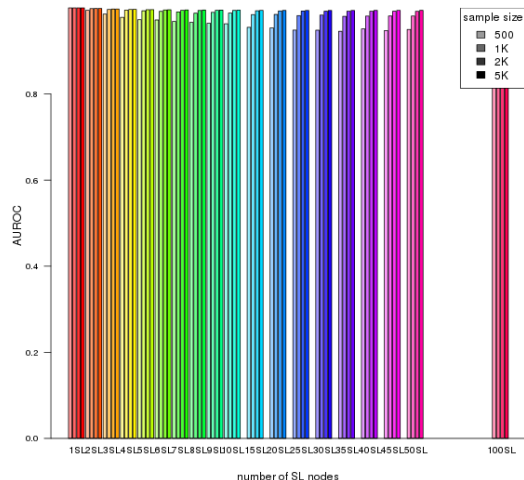


(a) Statistical evaluation

(b) Receiver operating characteristic



(c) Graph Structure



(d) Statistical performance

Figure K.18: Performance of simulations including the $G_{\alpha i}$ signalling pathway.
 Simulation of synthetic lethality used a multivariate normal distribution (without correlation structure apart from the Reactome $G_{\alpha i}$ signalling pathway. Performance of [SLIPT](#) was high across parameters for detecting synthetic lethality in the graph structure within a larger dataset. The sensitivity decreases for a greater number of true positives to detect but the specificity remains high with a low false positive rate.